SHIRA-Based River Analysis and Field-Based Manipulative Sediment Transport Experiments to Balance Habitat and Geomorphic Goals on the Lower Yuba River

Final Report

For

Cooperative Ecosystems Studies Unit (CESU) 81332 6 J002

Prepared by

Professor Gregory Brian Pasternack

University of California at Davis
Department of Land, Air, and Water Resources
(in association with the UCD Center for Watershed Sciences)

(Revised January 29, 2009)

LAND, AIR & WATER RESOURCES
UC Davis

John Muir
UCDAVIS
JOHN MUIR INSTITUTE OF THE ENVIRONMENT

TABLE OF CONTENTS

LIST OF TECHNICAL APPENDICES

Appendix 1. Gravel for Salmon in Bedrock Channels: Elucidating Mitigation Efficacy Through Site Characterization, 2D-Modeling, and Comparison Along the Yuba River, CA.

Appendix 2. Valley Width Controls on Riffle Location and Persistence on a Gravel Bed River

Appendix 3. Flow Convergence Routing on a Large Gravel Bed River, California

Appendix 4. Relationships between mesoscale morphological units, stream hydraulics and Chinook salmon (Oncorhynchus tshawytscha) spawning habitat on the Lower Yuba River, California

Appendix 5. Differences in River Ecological Functions Due to Differences in Rapid Channel Alteration Processes and Channel Morphology in Two California Rivers

Executive Summary

The 3500 km^2 Yuba River watershed in northern California has experienced extensive anthropogenic disturbance over the past 160 years due to hydraulic gold mining, dams, channelization, and flow diversions. Current dams in the system impact sedimentary and hydrological regimes on the mainstem and degrade ecological functioning, but are overlain on a complex history of channel change, yielding unique dynamics relative to other streams in the region. Many efforts have been proposed to improve the quality and quantity of habitat on the lower 37 km of the river that is accessible to anadromous salmonids. However, the large size and highly energetic character of the lower Yuba River (LYR) presents particular constraints to restoration measures. Certain restoration proposals have mistakenly assumed that (1) like many other impounded Californian systems, the LYR is a 'geomorphically fossilized' system without the potential for significant morphological adjustment and (2) due to impoundment, salmon habitats are generally degraded in the LYR and that the restoration of spawning habitat is required through-out this reach to maximize production. However, these assumptions fail to account for the unique legacy of historical and ongoing anthropogenic disturbance here.

Over a 5-year period (2003-2008), a comprehensive investigation was conducted to ascertain the linkages between hydrology, geomorphology, and ecology on two important reaches of the Lower Yuba River. State-of-the-art technologies, field methods, and analysis tools were used to characterize present and historical conditions. The resulting study presented herein could serve as a template for assessing the rest of the LYR.

The Timbuctoo Bend Reach (TBR), a 4.5-mile long gravel-bed reach from the onset of the gravel bed to highway 20 bridge, is rapidly incising as a result of a lack of incoming sediment that is blocked by Englebright Dam. From 1999-2006, 605,000 yds^3 of gravel and cobble were exported out of the TBR. All morphological units, except medial bars, are incising on average and 50% of the river in TBR has downcut by 1-6'. Nevertheless, aerial photo analysis revealed that seven riffle-pool units in the reach have persisted in their current locations for decades. Further, 2D modeling demonstrated that "flow convergence routing" is the hydrogeomorphic mechanism responsible for the observed geomorphic self-sustainability. During floods that occur every 4 years or less frequently, pools are rejuvenated and riffle-pool relief accentuated. During the intervening low-flow years, knickpoints migrate through the riffles diminishing relief. Together, these two mechanisms drive long-term incision. Chinook salmon spawning habitat in the TBR was evaluated using micro- and meso-habitat methods and found to be in excellent condition. Predictive tools are now available for evaluating future management options. No river rehabilitation actions are recommended for the TBR at this time.

The Englebright Dam Reach (EDR), a 0.89-mile long bedrock reach starting at Englebright Dam and ending at the junction with Deer Creek, was found to be devoid of habitat for spring-run Chinook salmon spawning, even though this is where many such fish come and attempt to spawn on the bedrock. The upper half of this reach lacks self-sustainable conditions and is purely governed by bedrock canyon geometry. There is an opportunity to create spawning habitat for spring-run Chinook salmon by doing a large rehabilitation project at Lander's Bar, which was impacted by shot-rock deposition in the rain-on-snow flood of 1997. Also, it is recommended that a gravel injection program be instituted at the top of the reach in the Narrows II pool in the amount of 10,000 yds^3 per year. This amount should be enough to form sustained pockets of spawning habitat behind flow obstructions in the reach and to rejuvenate a rehabilitation project at Lander's Bar.

Acknowledgements

This project involved the effort of a large number of individuals and institutions. Financial support was predominantly provided by this award, but that was leveraged by financial support from the University of California and Professor Greg Pasternack.

Graduate students Aaron Fulton, Jason White, and Marisa Escobar all used the lower Yuba River as part of their graduate educations, and their theses are integral parts of this report. Project scientist Dr. Hamish Moir and undergraduate assistant April Sawyer each made important contributions to data collection, data analysis, 2D modeling, and technical writing. Junior specialist Scott Morford led GIS-based analyses and map production for the comprehensive Timbuctoo Bend and Englebright Dam Reach efforts. Undergraduate assistants included Carlos Alvarado, Blake Andrews, Mary Berta, Mike Bezemek, Evan Buckland, Kari Fish, Dave Van Herrick, Lauren Hilliard, Ryan Keating, Cameron Poya, Davin Sanders, Carrie Simms, Dan Suderow, Nakul Thomas, Ben Torchia, Denise Tu, and Conner Voss. Two visitors from Scotland- Julie Tuck and Sophia Kellas-Mckenzie assisted with field data collection. Professor Jeff Mount, Professor Fabian Bombardelli, and Dr. Eric Larsen served on graduate thesis committees, providing valuable critique and input. Postdoctoral researchers Peng Gao and Joshua Wyrick helped with field work and provided critical thinking about the project. Staff at the UC Sierra Foothills Research and Extension Center (Chris Fedderson, Mike Connor, Art Craigmill, and Dustin Flavel) provided logistical support for site access along the north bank of the river. Diana Cummings, Ellen Mantalica, and Tania Guilfoil at the UC Davis Center for Watershed Sciences provided valuable administrative and project-management support. Kimberly Lamar in the UCD Office of the Vice Chancellor for Research provided contract and grant support.

This project would not have been possible without the collaboration and support of governmental agencies, non-governmental organizations, professional consulting firms, local land owners, and other stakeholders. At USFWS, Cesar Blanco served as the primary contact and collaborator, followed by David Hu and Beth Campbell. Curt Aikens and Steve Onken with the Yuba County Water Agency provided a lot of important and time-sensitive flow information and flow forecasts. Duane Massa, James Navicki, and Ian Drury with the CDFG provided a lot of guidance and data related to LYR fish populations. Doug Grothe and Mitch Stewart with the USACE were responsible for preparing the EIR for the gravel injection experiment and then implementing it. Tom Johnson and Paul Bratovitch provided helpful feedback on the management significance of our findings. James Kulpa did a terrific job with all of the boat-based hydrographic surveys, without which the project would not have been possible. Members of the Yuba River Preservation Foundation and local landowners (including Philip Sutherling and Ralph Mullican) were essential in helping us gain access to the south bank of the river. The diverse participants of the Lower Yuba River Technical Working Group provided a lot of useful information and feedback on the project. The editors and reviewers of several scientific journals reviewed technical appendices of this report and provided valuable feedback, criticism, and input. If I have forgotten any one else, I apologize in advance.

INTRODUCTION

This report is divided into three sections.

The first section presents overview information about the lower Yuba River (LYR). That includes three components. First, a description of the context of rivers in the Central Valley, their degradation, and the broad potential for river rehabilitation. Second, a geographical characterization of the LYR. Third, a broad hydrological analysis of the LYR.

The second section thoroughly analyzes the Timbuctoo Bend reach (TBR) on the LYR. This is the farthest-upstream gravel-bedded reach below Englebright Dam. The section includes geomorphic, hydrodynamic, and physical habitat assessments.

The third section thoroughly analyzes the Englebright Dam reach (EDR) on the LYR. This is the bedrock reach from Englebright Dam down to the junction with Deer Creek. The section includes geomorphic, hydrodynamic, and physical habitat assessments.

SECTION 1: OVERVIEW OF THE LOWER YUBA RIVER

CENTRAL VALLEY CONTEXT

Degraded Central Valley Rivers

Throughout the Pacific Northwest and California (USA) main stem rivers have been re-engineered and significantly degraded by a plethora of in-stream human activities, flow regulations, and upland land uses. Dam construction and operation, gravel extraction, historical mining, channelization, water diversion, intensive agricultural, and deforestation are specific activities that have disrupted natural hydro-geomorphic and stream ecologic characteristics of the rivers.

Some of the specific physical alterations that have resulted from all of these activities include changes to the frequency, magnitude, timing, duration, and rate of change of hydrologic events in the flow regime; a dramatic reduction in sediment supply, in particular, course sediment, gravel, and cobble; channel incision and narrowing as well as armoring (i.e. coarsening) of the channel bed; a reduction of inputs of large wood in to the rivers; the loss of riparian zone conditions; and degradation of the temperature regime.

The ecological consequences of this physical alteration include a loss of the majority of fish spawning habitat for anadromous fish, juvenile stranding problems, scour of redds, fish straying to the wrong tributaries, loss of clean gravel, riparian vegetation encroachment into channels, invasion of nonnative aquatic weeds, loss of benthic macro-invertebrate species' diversity, deficiency in spawning-size gravel, and just a general decline in the complexity of channels and habitat for many diverse species and their lifestages associated with the riverine ecosystem.

In the Central Valley, in particular, the location of dams at the line between the Sierra Mountains and the Central Valley, which basically takes place at that foothill-valley interface (i.e. where there is a line of large water-supply reservoirs that prevent anadromous fish from migrating from the Pacific Ocean and going up in to the mountains where they traditionally would have had their fresh-water reproductive life cycle) has limited fish to the stretch of channel just downstream of these dams in the lower-most foothills and in the upper Central Valley alluvial plain where there is still some remaining gravel-bed reaches that can support the reproductive life stage (Fig. 1). Typically, ~50-80% of the spawning habitat where that reproduction would take place has been lost.

The dominant approach for addressing the loss in fish populations associated with this loss of habitat has been through the production of fish at hatcheries. Unfortunately, many studies done on the genetics and behavior of hatchery fish have now shown that these hatchery fish do not have the same capabilities as wild salmon for being able to survive under natural conditions, both in the rivers as well as in the ocean. Also, hatcheries produce large amounts of chemical waste and discharge it into the rivers. This discharge appears to affect the migratory pathways fish take, drawing them into hatcheries and discouraging them from reproducing in the rivers. It is now clear that hatchery fish production is not a sustainable sole solution to the problem of the loss of populations and habitat in rivers. Hatchery production may need to be continued, but it is also extremely important to perform actions that enable fish to reproduce in rivers I a more natural way.

Degraded Central Valley Rivers

- Majority of pre-dam spawning habitat is no longer accessible.
- Hatchery fish production is a not sustainable solution because of genetic changes that are occurring.

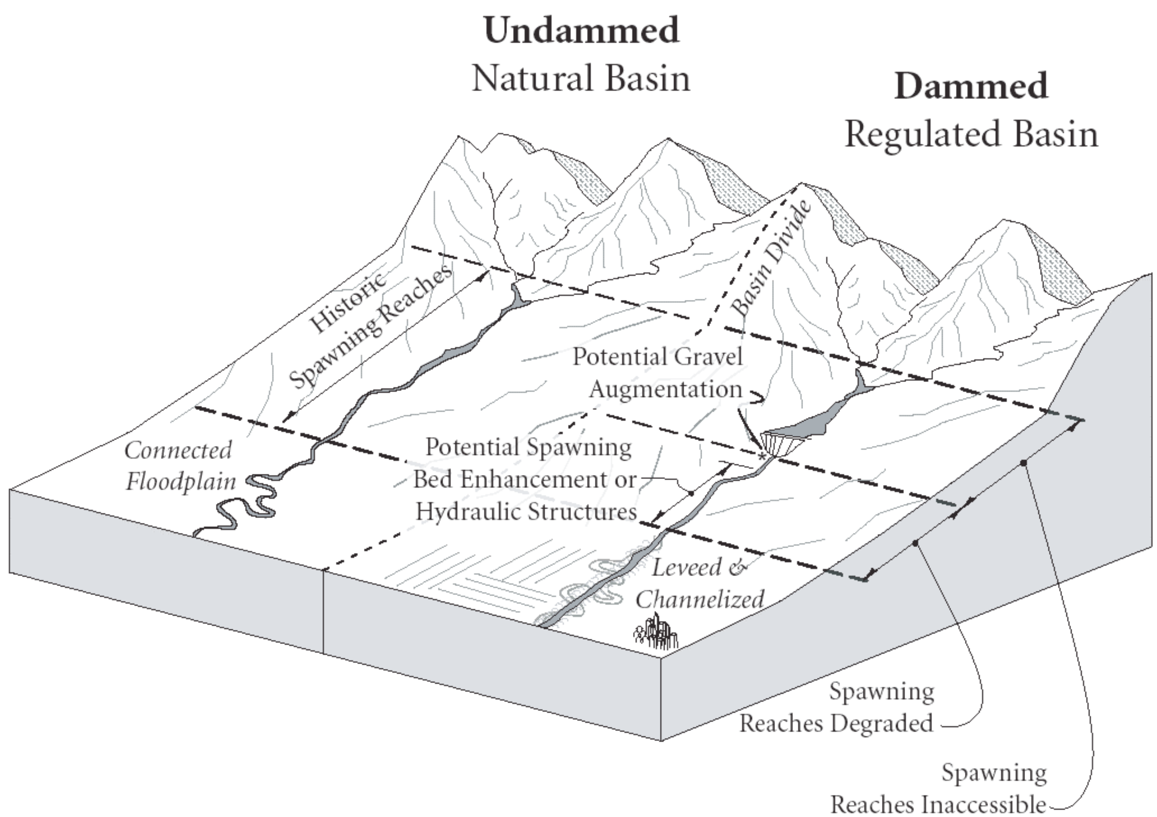

Figure 1

Regulated-River Rehabilitation

That leads to the idea that there need to be physical modifications to regulated streams as well as changes to the transport regimes of water, sediment, and wood associated with the major water-supply reservoirs in the Central Valley of California. The following definitions are helpful to bear in mind to distinguish among key activities:

River restoration- take a river that has been disturbed or degraded by a specific human action, undo that action, and alter the river back to a pre-action "natural' state. The natural state must defined by hydrogeomorphic and ecologic processes, not merely landform geometry.

River rehabilitation- change a river from a degraded state to an improved "natural" state that is unlike the pre-action condition. Again, the improved state must defined by hydrogeomorphic and ecologic processes, not merely landform geometry.

Isolated activities such as bank stabilization projects, wood removal from the channel, and river "clean ups" do not constitute either river restoration or rehabilitation, though they may be undertaken in support of societal interests.

A thorough discussion of the merits of diverse physical channel alterations and transport regime modifications is provided in Pasternack (2008), but a few key highlights relevant to this report are discussed next. Different river restoration activities can be organized according to the spatial and temporal scales at which they are effective (Fig. 2). For example, activities that are

Spatial Scales of River Rehabilitation

Hydraulic Unit Microhabitat
(10^{-1}-10^{0} Channel Widths)

Provide higher quality habitat for existing populations

Geomorphic Unit Mesohabitat
(10^{1} Channel Widths)

Provide greater quantity of habitat to increase population size

Reach Unit
(10^{2}-10^{3} Channel Widths)

Provide a mechanism for self-sustainability of the river system

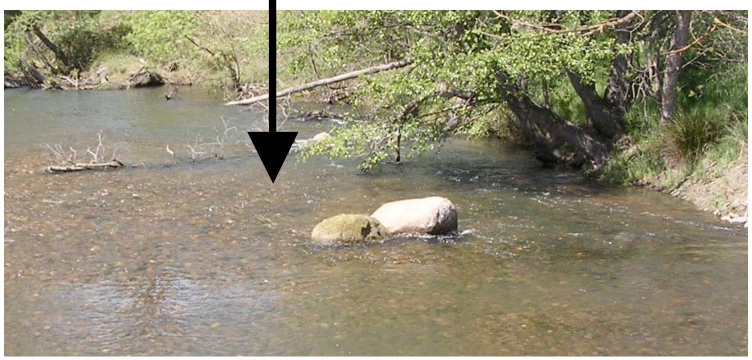

Figure 2

done at the smallest scale, what we could call the Hydraulic Unit Microhabitat scale, are technique such as putting in boulder clusters or woody debris jams, doing spawning riffle enhancement things like that. These activities provide a higher quality of habitat for existing populations because they improve the river and these are activities that tend to be done at the scale of less than one-to-one channel width if you think of the length of a river and the number of channel widths over that length. The problem with the Hydraulic Unit scale approach is that it doesn't provide long-term sustainability. The features that are created may or may not be self sustainable and will tend to wash away; because after all, the effect of the impacts of human activities on the rivers has been to degrade the natural diversity that was there in the first place. So when you rehabilitate that natural diversity without changing the underlying problems it will degrade over time again. It still has value in providing higher quality habitat to sustain the existing populations, while over a longer time horizon solutions that address the systemic problems can be worked on.

At the next scale up, the length scale of about 10 channel widths (in the length of the river), we have the Geomorphic Unit Mesohabitat scale of river rehabilitation. The goal here is to change the structure of riffles, pools, glides, runs, and so forth in the river to obtain a greater quantity of habitat to address the full range of species in their different life stages, which will result in an increase in population size. Whereas Hydraulic Unit Microhabitat rehabilitation promoted the survival of the existing populations, Geomorpic Unit Mesohabitat rehabilitation aims to increase the population size, but hereto if the flow regime and sediment supply regime remain fundamentally altered by the dam and are not addressed, then the solution will be shorter lived than ultimately desired.

The final scale of regulated-river rehabilitation is at the Reach scale, which is on the order of 100 to 1,000 channel widths. The goal at this scale is to provide a mechanism for the river to be self sustainable without doing more directed interactions. Typically that involves flow re-regulation, sediment injection, and wood injection. However, if you only provide measures at this scale, studies have shown that it is very unlikely for the river to be able to heal before populations crash below a recoverable level. We want the river to be self sustainable, but in order to do that we have to do actions at all three scales- the Reach scale, the Geomorphic Unit scale and Hydraulic Unit scale.

River rehabilitation efforts are well underway in California's Central Valley (Fig. 3). There are many examples of projects at all three scales on virtually every mainstem river and creek (e.g. Merced, Tuolumne, Mokelumne, American, Sacramento, American, Feather, and Clear Creek. Ultimately, we have to ask the question of what are these efforts going towards and the answer to that is that there are a few key outcomes (Fig. 4). People want to see want to see diverse channel features, such as riffles, pools, chutes, glides, runs, backwaters, gravel bars. They want to see that the channel is connected to the floodplain. They want to see a dynamic river corridor system that changes over time. And they want to see a diversity of in-stream wood and boulder structures thatl create a diversity of localized microhabitats. Ultimately, these goals can only be achieved in a sustainable way by figuring out the hydrogeomorphic processes that control them and developing predictive tools suitable for river rehabilitation design and evaluation. These two task- 1) figuring out hydrogeomorphic processes linked to ecological functions and 2) developing predictive tools- are the primary outcome sought for in the project reported herein.

Rehabilitation Efforts are Well Underway

Merced River

Trinity River

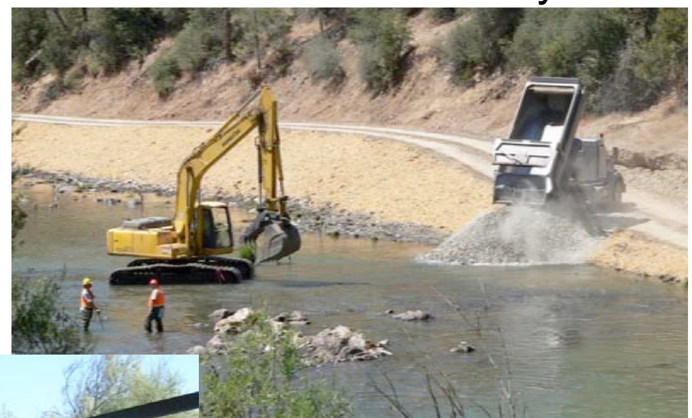

Mokelumne River

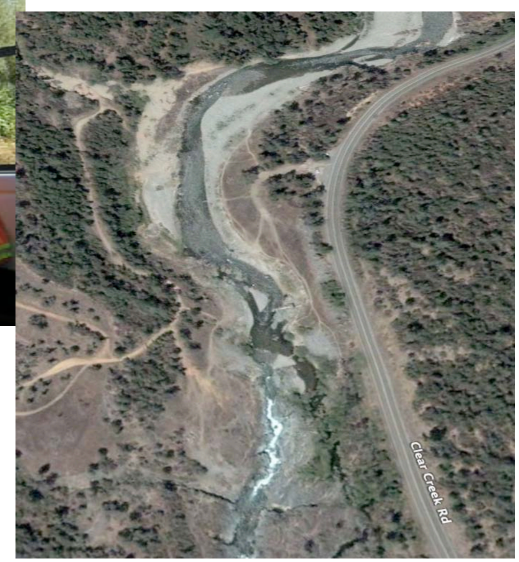

Clear Creek

Figure 3

What are These Efforts Going Toward?

Diverse channel features

Dynamic change over time

Connected floodplain

Wood

Figure 4

LYR GEOGRAPHY

In this next section, I am going to survey the geography of the Yuba River watershed and the specifics of the LYR relevant to this study. A detailed geographical description of the context of the Lower Yuba River comes from the Master's Thesis of Aaron Fulton under the supervision of the project principal investigator and it is one of the technical appendices to this report (See Appendix 1). Also, Professor Alan James from the University of South Carolina has produced many reports and scientific articles about the geography of the Yuba River.

The Yuba River Watershed has a basin area of about 3,500 km^2 (Fig. 5). There are several small dams that are located in this watershed (e.g. Spaulding, Bowman, and Jackson Meadows), but most importantly it is Englebright Dam that is the fundamental barrier for fish passage from the Central Valley up in to the foothills and the higher Sierras. Of the three forks of the river upstream of Englebright Dam (i.e. the South, Middle, and North Forks), only the North Fork has a major water-supply reservoir- New Bullards Bar. In contrast, the Middle and South Forks have long stretches of unimpeded flow, and therefore, they can generate and transport large amounts of water to Englebright Lake during early winter rainstorms. The North Fork has the majority of its water captured by New Bullards Bar.

When you look at the average annual precipitation map of California, you can see what is driving the Yuba River basin and its hydrologic functionality (Fig. 6). Specifically, the Feather and Yuba watersheds receive the highest precipitation total in the Sierra Nevada range. That’s on the order of 42-120 inches of rain per year on average. That’s a significant amount of rain and the further south you go, the less you get. Storm fronts that come off the Pacific Ocean often

Yuba River Watershed

- Basin is ~3500 km^2 (1350 mi^2)
- Englebright Dam is the primary fish barrier
- Only the North Fork has a major reservoir

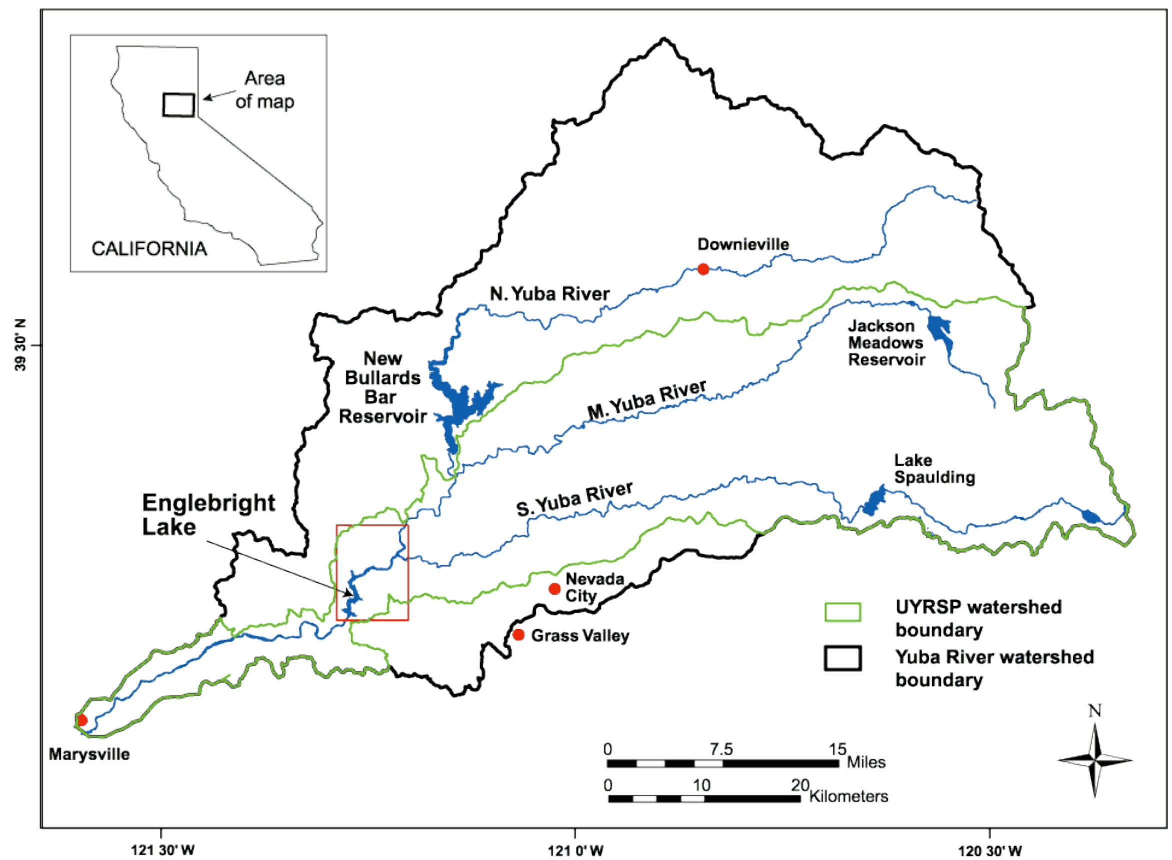

(USGS Open-File Report 2006-1346)

Figure 5

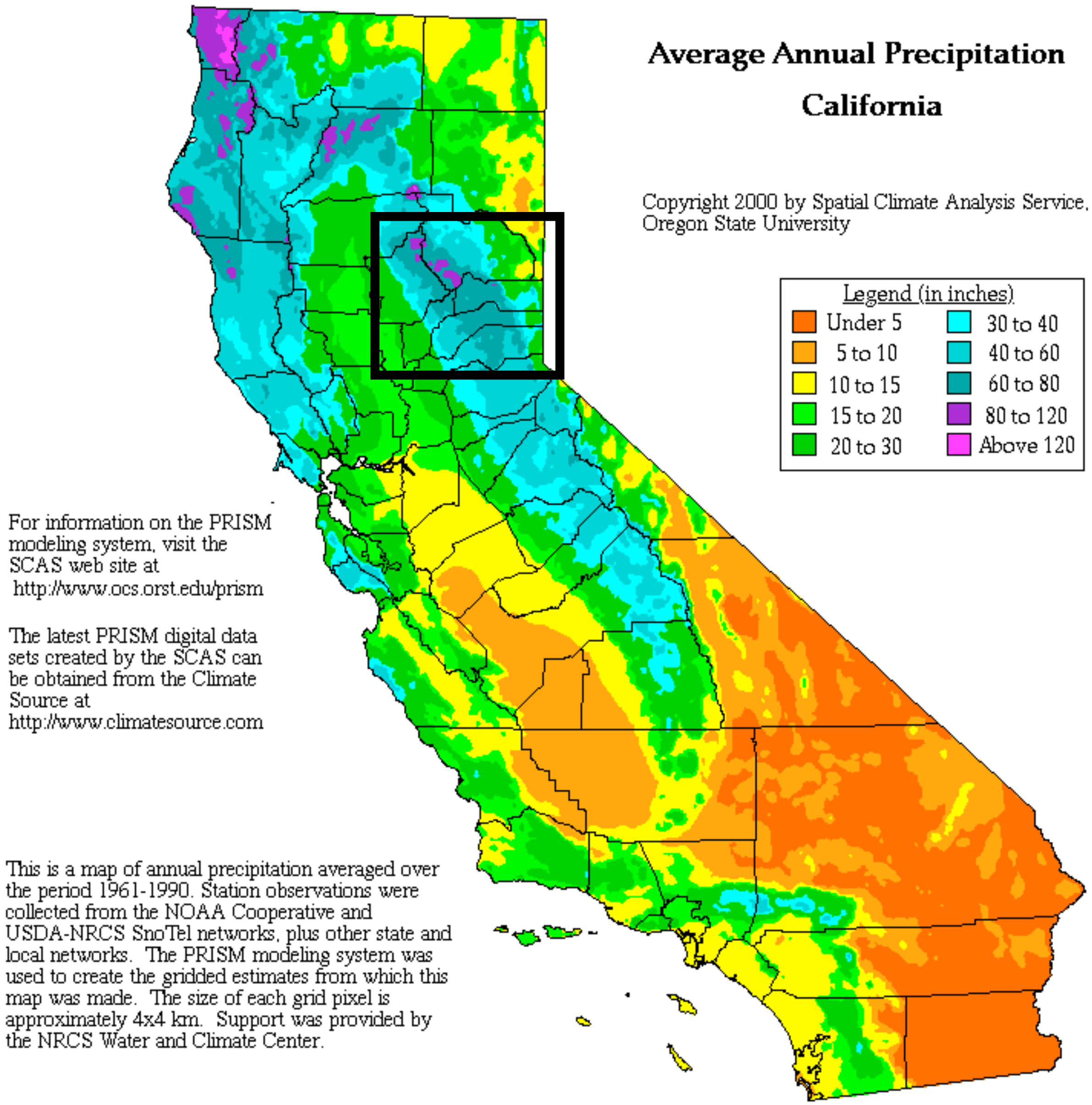

Feather and Yuba basins receive the highest precipitation total in the Sierra Nevada!

Figure 6

track right over the Yuba. This storm regime means that the Yuba has an ample water supply to help maintain a naturalized hydrologic functionality, relative to the watersheds to the south of it.

The Lower Yuba River itself is ~24 miles long from Englebright dam down to the junction with the Feather River (Fig. 7). Although previous reports by other entities provide a "geomorphic" delineation of reach for the LYR, no process basis is provided as a foundation for them. One outcome of this study has been a partial re-consideration of such reaches. However, this study only spanned from Englebright Dam down to the Highway 20 bridge, so it is beyond the scope of this study to provide a comprehensive answer. I can only warn that the pre-existing delineations appear inadequate.

For the stretch of the river evaluated in this study, the river may be functionally divided into 3 reaches (Fig. 8)- the Engebright Dam Reach (EDR), the Narrows Reach (NR), and the Timbuctoo Bend Reach (TBR). EDR is the length from Englebright Dam down to the junction with Deer Creek. It is a bedrock canyon with "shotrock" debris covering parts of the bed. The debris is from dam construction and hillside landslides during major floods. The EDR is generally a straight run, but there are a few bedrock and shotrock hydraulic controls, including one steep rapid downstream of the USGS gaging station. EDR is also influenced by a backwater effect imposed by Deer Creek, since flood pulses out of Deer Creek usually come before the larger (and more snow-covered) Yuba River. In terms of fish populations and habitat, EDR is the most heavily impacted reach. Spring-run Chinook are the fish that want to go far upstream into the mountains, so they tend to cluster in EDR, where they fail to reproduce. Our observations are that they do not turn around and head back downstream to where conditions could be more favorable in TBR. They tend to focus here and are heavily impacted by the degraded conditions in the stream here.

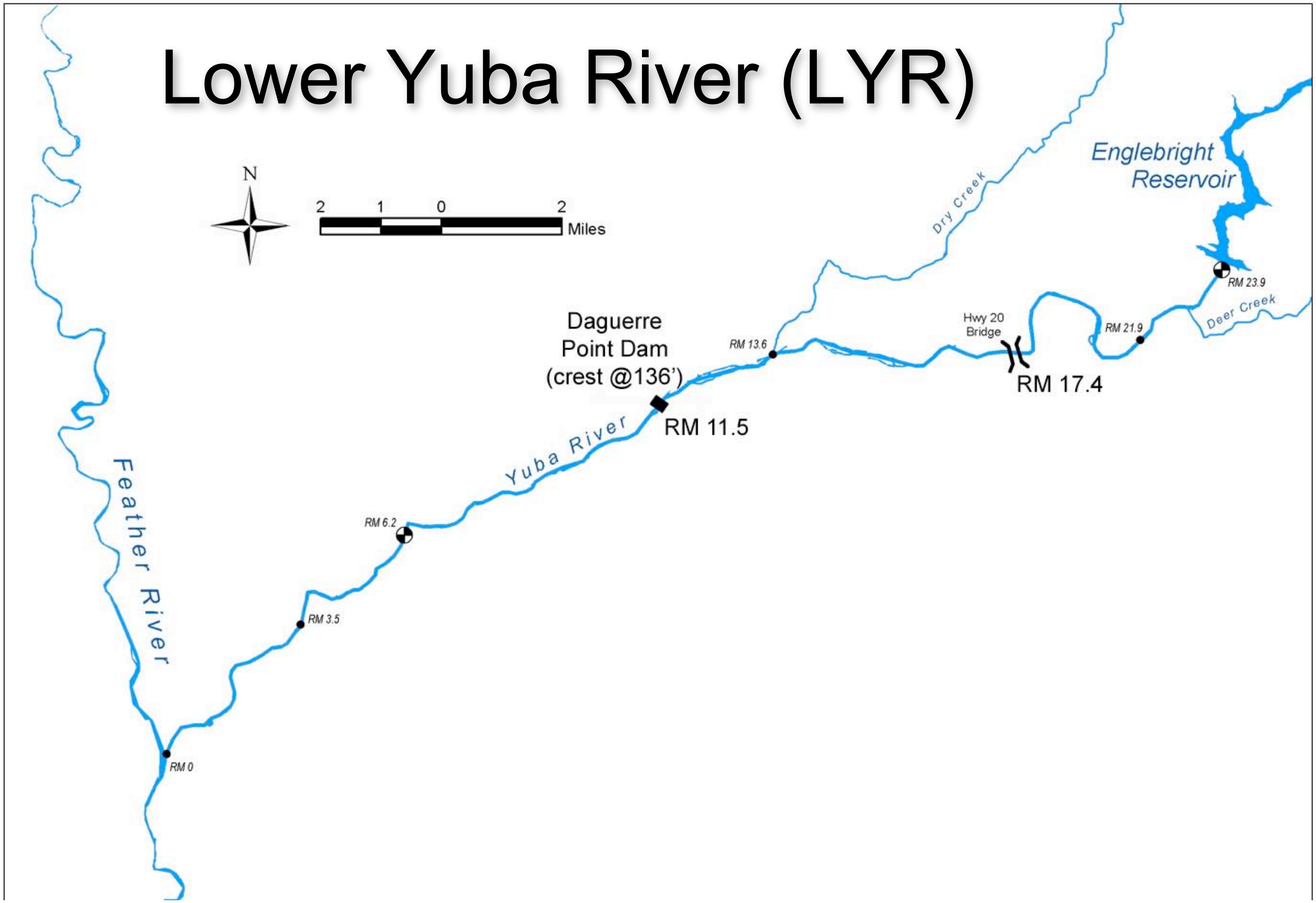
Lower Yuba River (LYR)
N
2 1 0 2
Miles
Englebright
Reservoir
Dry Creek
Deer Creek
RM 23.9
RM 21.9
Hwy 20
Bridge
RM 17.4
RM 13.6
Daguerre
Point Dam
(crest @136')
RM 11.5
Yuba River
RM 6.2
RM 3.5
RM 0
Feather River

Figure 7

UC Davis LYR Research Program

1. Research to aid fall-run Chinook and steelhead trout.
2. Research to aid spring-run Chinook salmon.

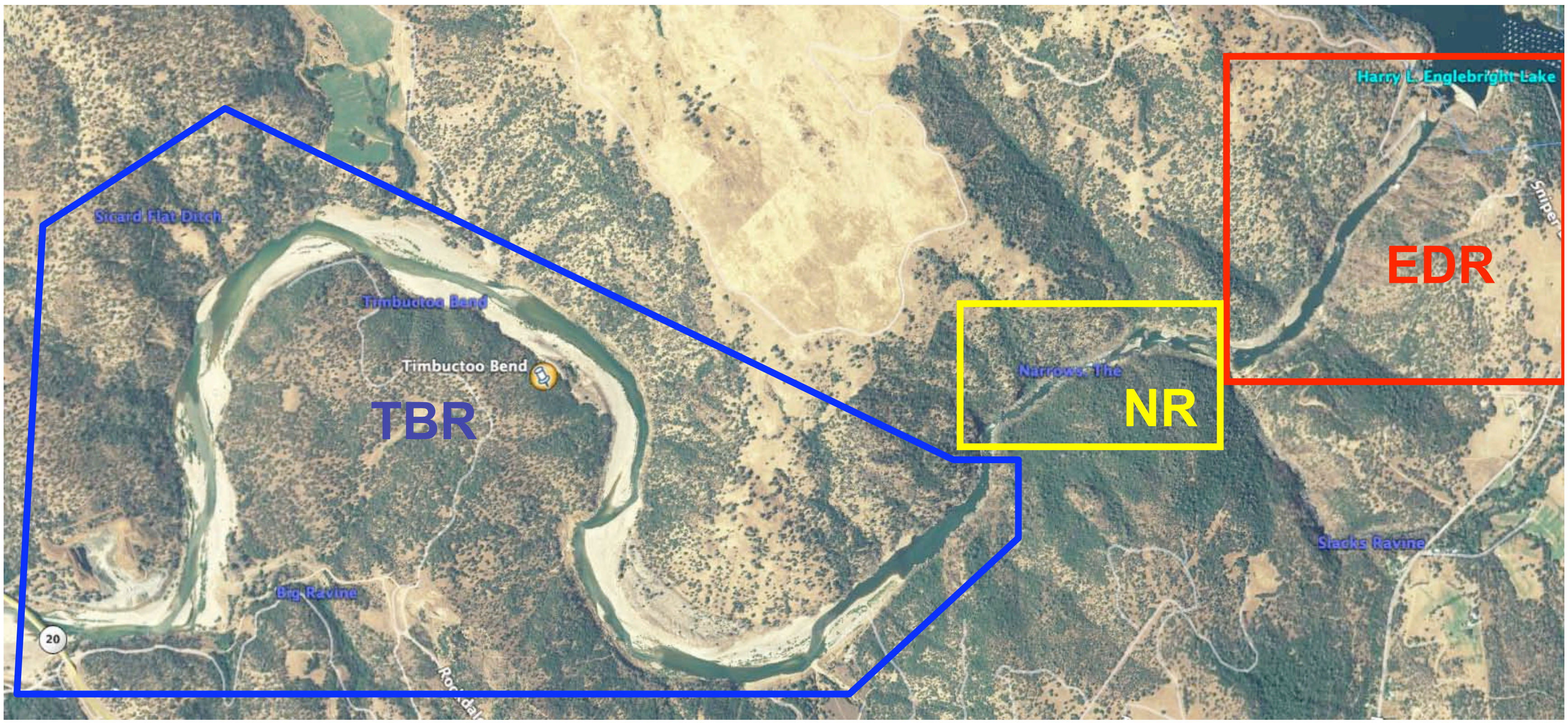

Figure 8

NR goes from the junction of Deer Creek down to a large scour pool known as Narrows Pool, which is just upstream of Blue Point Mine and Rose Bar. NR is geomorphically distinct from EDR in that it is a step-pool reach with a significant amount of alluvial sediment in it. People have considered NRto be too challenging in terms of the rapids that are present there to do much research there. Having paddled through that reach, including the one class IV rapid, I think it is possible to do research in NR. For the moment, most managers assumes that the Narrows is not a significant place for fish, and thus it has not been considered for any management or rehabilitation actions.

TBR is a gravel-bed, riffle-pool reach with a very wide, active, and unvegetated gravel/cobble floodplain. Although this study stopped at Highway 20 bridge, it is presently unknown whether the geomorphic processes and landforms reported below go beyond that arbitrary endpoint or not. One reason why it might not go further downstream is because the bridge is located at a significant bedrock valley constriction that produces a backwater effect during floods. This likely makes TBR geomorphically distinct from the next downstream reach, but that is not known at this point in time. In summary, this study focused on TBR and EDR.

The Lower Yuba River Accord is an agreement among 17 stakeholders that proposes a framework for settling various litigations over in-stream of flow requirements for the Lower Yuba River. The Yuba Accord includes not only new in-stream flow requirements aimed to increase protection of fish, but also it includes additional water to be used in dry years and in wet years to go down the river. It also includes a water “bank” for the CALFED Bay-Delta Program. Finally, it funds a river monitoring, management, and restoration program. In order for the Yuba Accord to have the most success in providing water and ecologically functional conditions in the river, there really needs to be an interdisciplinary understanding of how the Lower Yuba River works. There are several specific questions that need to be answered by a broader research effort than incorporated into the accord, which is where this project has more than academic value. Examples of important, specific questions include the following:

What is the physical structure of the LYR and how is that changing that over time?

Can we predict the spatial patterns of habitat utilization in the LYR and how that key ecological function is responding to on-going, large-scale geomorphic changes in the river, because the river is very dynamic (as will be shown later).

What specific management actions should be taken to sustain fish populations in light of an overall trajectory of rapid channel incision?

Should Daguerre Point Dam be removed or will that have too large and too adverse of an impact on the river?

There is a lot of good news for the LYR (Fig. 9). First, the river has a relatively naturalized flow regime with frequent floods that are >10,000-20000 cfs. These have now been found to be strong enough to drive significant change in the river, as reported later. Second, beginning in Timbuctoo Bend there is an incredible depth and breadth of loose sediment stored in the river corridor, because of historic gold mining that took place in the late 1800s. That sediment supplies the wetted channel, floodplains, and terraces. Consequently, unlike other degraded rivers in the Central Valley, the Yuba has the two main ingredients for Reach Scale

The Good News

(from a physical perspective)

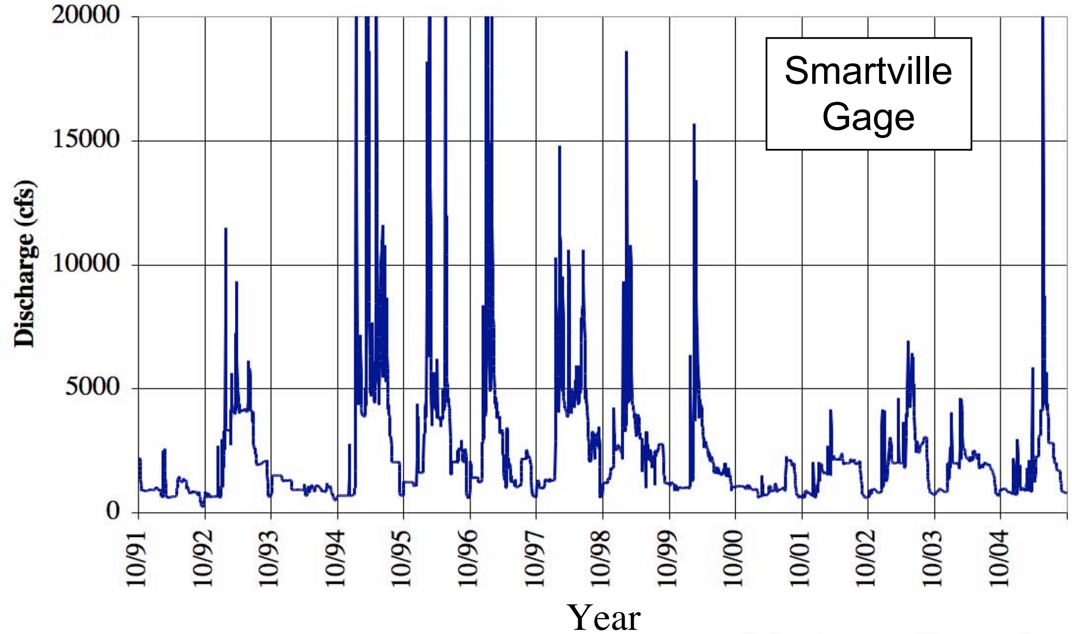

Naturalized Flow Regime

Ample Sediment Supply

Figure 9

rehabilitation; you don't have to change these two elements to restore the LYR. They are already here and that's fundamentally different from the problem on other rivers, including the Feather, American, and Mokelumne Rivers, all of which have a strong sediment deficit and highly altered flow regimes.

In summary, an understanding of fluvial geomorphology and hydrology is essential to the management of the river and the success of the Yuba Accord. All ecological dynamics, including for example competition, predation, reproduction, and migration are ultimately related to the physical conditions in the river, so physical studies are essential if the goal is to rehabilitate and maintain an ecologically functional river. That's where the UC Davis Watershed Geomorphology laboratory comes into play. This project by that group has been funded by the US Fish and Wildlife Service to look at the reach of the river from Englebright Dam down to Highway 20 bridge and to answer questions related to the status of chinook salmon and steelhead trout.

LYR HYDROLOGY

The Lower Yuba River hydrologic analysis includes a basic assessment of dams, hydrologic alteration by dams, a characterization of the flow regime, determination of geomorphically significant flows, and flood frequency analysis. A longer presentation of this information is provided in the technical appendices (Appendix 1). As I have already mentioned, the two key dams are New Bullards Bar Dam on the North Fork- completed in 1971 with a capacity of 1.2 billion m^3 of water- and Englebright Dam on the mainstem Yuba River- completed in 1941 with a capacity of 86 million m^3 (Fig. 10) Englebright Dam is tall enough

Dams and Discontinuities

Englebright Dam

Location: 32 km upstream of Marysville

Completed: 1941

Capacity: 86 million m^3

Blocks ~50% of historic spawning area

New Bullards Bar Dam

Location: North Fork Yuba (28 km upstream of Englebright)

Completed: 1969

Capacity: 1.2 billion m^3 *
(37% of Oroville, 28 % of Shasta)

Figure 10

that it blocks the entire bedrock canyon there. It is thought that it blocks ~ 50% of the historic spawning reach for the Yuba River basin.

The effect of these dams on the river has been measurable. First, the pre-Englebright median monthly discharge peaked during the snowmelt season in April at ~180-190 m^3/s (Fig. 11). After Englebright was built that dropped to ~130 m^3/s. After New Bullards Bar was built it dropped down to a peak of ~70 m^3/s. Like other regulated rivers, the LYR has a degraded monthly flow distribution in which there are the lowest flows during the late summer to early fall and then highest flows during the winter, but the lowest of the low flows are not as low as they used be and the flood peaks are curtailed.

Despite that flow regulation, the modern lower Yuba River flow regime does include geomorphically significant floods. For example, in 1997 there was a flood that produced a peak mean daily discharge of ~154,000 cfs. On New Years Eve at the end of 2005, there was a flood with a peak mean daily discharge of ~95,600 cfs. On top of each of these flows over Englebright Dam, one also has to factor in the significant contributions of Deer Creek and Dry Creek, which help to sustain the duration of the peak flood. For example, the combined hourly peak discharge for the New Years Flood at the highway 20 bridge was ~109,000 cfs.

A key goal of this study was to determine the geomorphic significance of the flood regime in TBR (Fig. 12). Before getting into the evidence underlying that determination, we found the following key flood discharges for the TBR (based on independent analyses with hydrodynamic modeling, river topographic analysis, and statistical analysis of the peak flow series):

•*A preferential riffle-scouring discharge range of <11,000 cfs,*

LYR Hydrologic Alteration 1904-2006

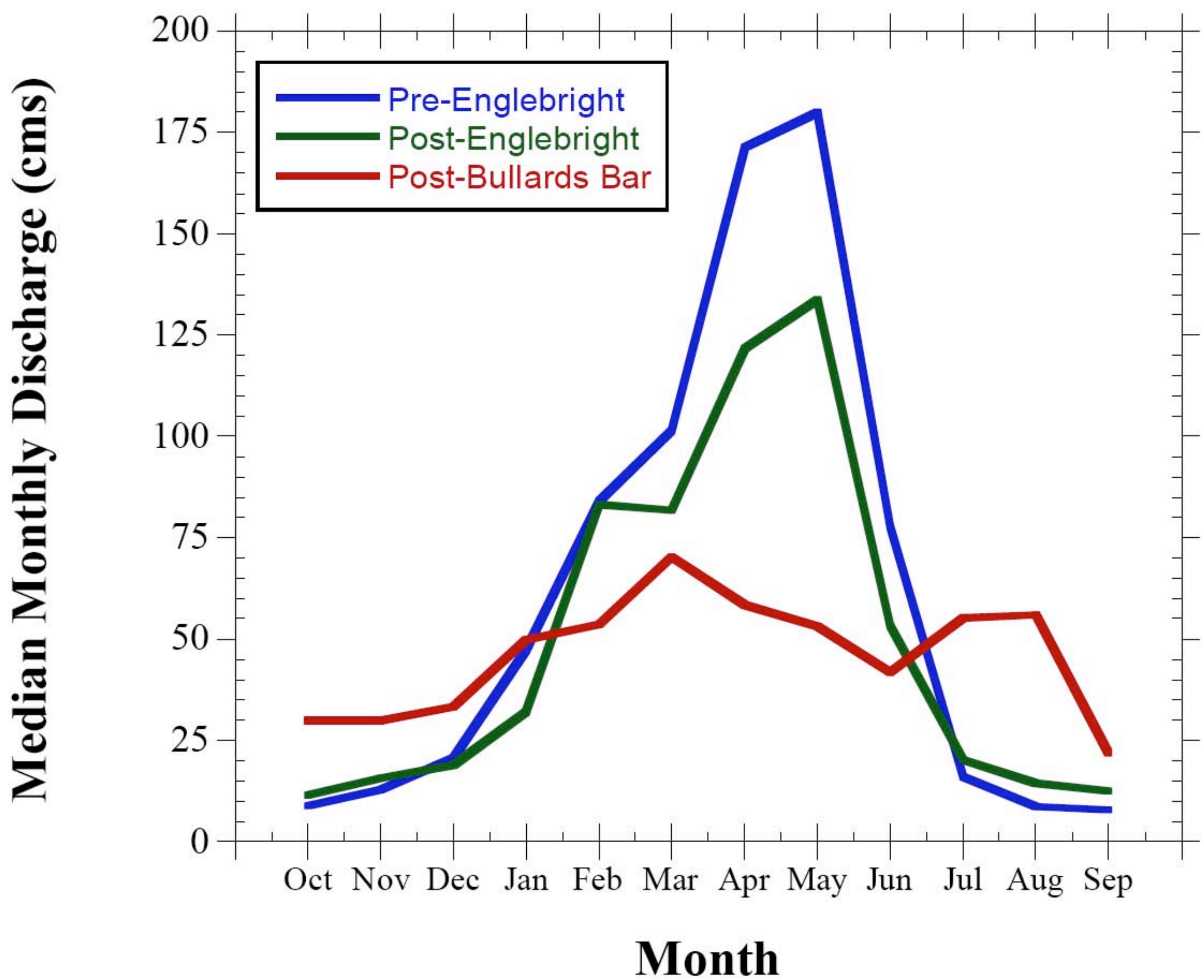

Figure 11

Modern LYR Flow Regime

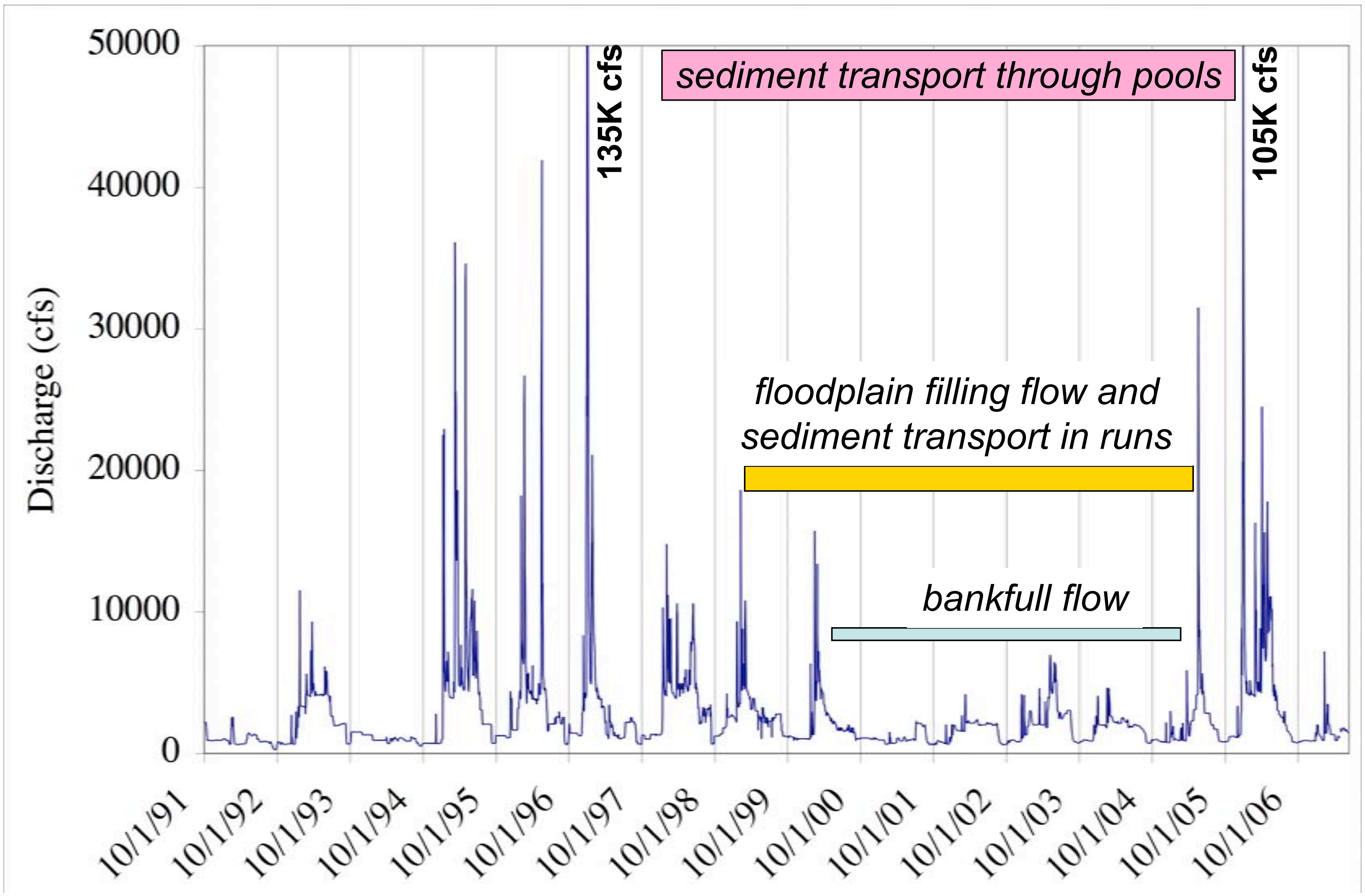

Figure 12

- *A modern bankfull discharge of ~5,600 cfs,*
- *A 1942-1971 bankfull discharge ~11,600 cfs,*
- *A preferential run-scouring discharge range of ~9,000-25,000 cfs,*
- *A floodplain-filling discharge of ~20,000 cfs,*
- *A preferential pool-scouring discharge range of >45,000 cfs.*

Details of the above information is provided below and thoroughly documented in the technical appendices. This is just a preliminary presentation of the findings suitable for the hydrology section of the report.

A LYR Flood Frequency Analysis for of the data from the USGS Smartville Gage (#11418000) found that the flows during the time of this study included some major events (Fig. 13). In May 2005 there was a flow with a mean daily discharge peak above the junction with Deer Creek of 41,300 cfs. The hourly discharge peak combined with Deer Creek outflow was 42,930 cfs through the TBR. Statistically, that event's magnitude had a 7.7 year return interval compared against the post-New Bullards Bar record (1971-2005). Using that same statistical record, the previously mentioned New Year's flood at the end of December 2005 was found to have a 24-year return interval, so very significant. Given that there are a variety of ways to do this kind of statistical analysis, the exact return-interval values are not as important as the general point that during this study two significant floods occurred, and those events provided a good opportunity to determine the flow-sediment-topography-habitat linkages for the LYR. What makes this river interesting is that unlike the majority of rivers in the Central Valley, you could monitor the LYR over any 10-year period and likely observe multiple events of this magnitude.

LYR Flood Frequency Analysis

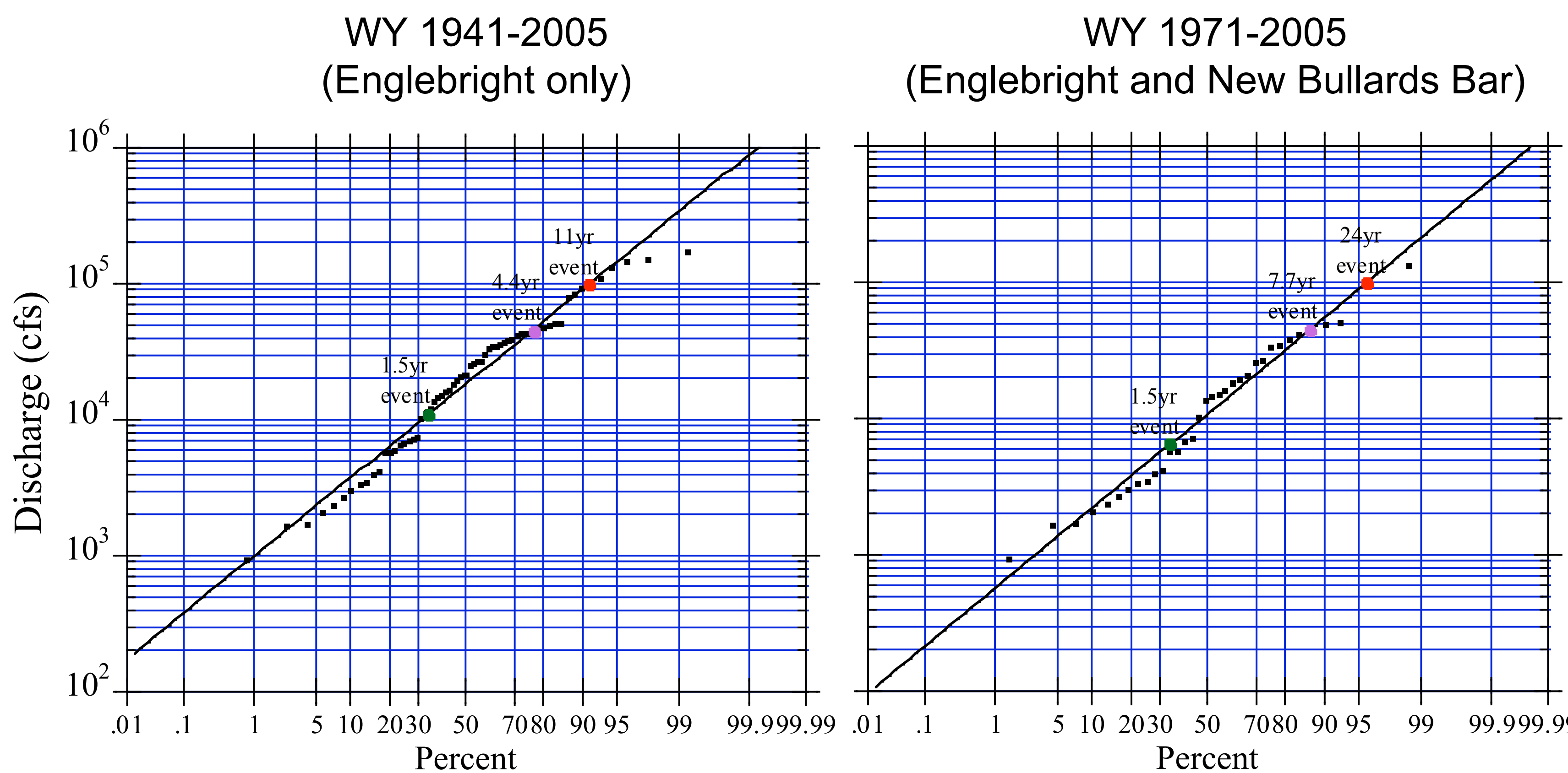

May 2005 was a 7.7-yr event; Dec 2005 was a 24-yr event

Figure 13

SECTION 2: TIMBUCTOO BEND REACH (TBR) ASSESSMENT

TBR GEOMORPHOLOGY

Next, let's look at the fluvial geomorphology of the Timbuctoo Bend Reach. This reach begins at the end of the Narrows canyon where there is a deep scour pool. It nominally at the highway 20 bridge. TBR is where a lot of research was done in this study. The key geomorphic questions that we sought to answer in this project included the following:

1) *What is the 3D topography of the TBR of the Lower Yuba River?*
2) *What morphological units exist in the TBR of the Lower Yuba River?*
3) *How persistent have the locations of riffles been during 1952-2006?*
4) *How has the topography changed 1999-2006*
5) *How does that change relate to the morphological units in the river?*
6) *How much sediment is entering and leaving Timbuctoo Bend?*

These geomorphic questions may seem academic to some resource managers and local stakeholders, but what I want to show you is that these questions are exactly the things that tell you why conditions on the LYR are what they are, and what needs to be done- if anything- in order to improve the river's ecological functionality. Wild populations of organisms are directly tied to the physical and chemical environment, and in the case of the LYR, that setting is changing very fast. Therefore, you cannot manage populations without also being aware of the trajectory of physical change for the system.

LYR Topographic Maps

The first step in understanding the geomorphology of any river is to have a high quality map of its corridor. A river corridor includes terrestrial land and submerged channel bed, and different methods are needed to map those two settings. For a system as dynamic as the LYR, you cannot assume that the topography represented in a pre-existing map is accurate after a floodplain-filling flood of >20,000 cfs. For example, we observed that the May 2005 flood of >40,000 cfs caused significant channel re-alignment.

The last time the LYR was mapped was in 1999. Terrestrial land was mapped using aerial photogrammetry. The river bottom was mapped by boat up to the Narrows Pool- no mapping was done in the EDR or NR. However, given the technology available at that time, the river bottom was only mapped with cross-sections spaced every 100-300'. Even worse, important areas with high habitat complexity and diversity were not mapped at all, because they could not be easily boated into. The 1999 map is primarily available upon request in the form of 2' contours, but that is insufficient accuracy for restoration design. For a recent USFWS "IFIM" type study, extensive mapping had to be performed at each study site, because the 1999 map was inadequate. Finally, the May 2005 and New Years' 2006 floods dramatically changed the river. The 1999 map is no longer representative, even at the scale of its lower resolution.

In this study, there was a need to map the EDR for the first time as well as to create an updated and higher resolution map of TBR. For both EDR and TBR, the terrestrial land in the river corridor was mapped this time on the ground by teams of two people using a robotic total station with both a pole-mounted reflector for manual mapping and automated reflectorless laser scanning of unvegetated surfaces. The submerged channel bed was primarily mapped by boat using a complex technological system and secondarily using robotic total station in shallow areas. QA/QC analyses were performed to make sure the two different methods provided consistent accuracy between them. Details of all of the surveying method for each survey are provided in the technical appendices. Ultimately, the 2006 map of TBR (Fig. 14) is likely the highest resolution topographic map of any shallow, gravel-bed river in the world. The 2008 map of EDR (Fig. 15) is also likely the highest resolution map of any bedrock reach. The maps show a lot of the interesting features that exist in the LYR and that make it a particularly special place.

Morphological Units

Once you have a topographic map, in and of itself, it may not tell you a whole lot, but it can tell you things when you begin to analyze it. One thing you can easily discern in the map is the bankfull channel dimensions. On the LYR, the bankfull channel is delineated by a sharp slope break across the river corridor and by the presence of a line of willows along this slope break. Based on historical aerial photo analysis reported below, lines of willows on the floodplain identify historical locations of the bankfull channel.

A key task in characterizing the river corridor is to make a map of what are called the morphological units in Timbuctoo Bend. By definition,

A morphological unit is *a discernible land form in the river valley that is typically visible at the special scale 1-10 channel widths*.

High Resolution TBR Topographic Map

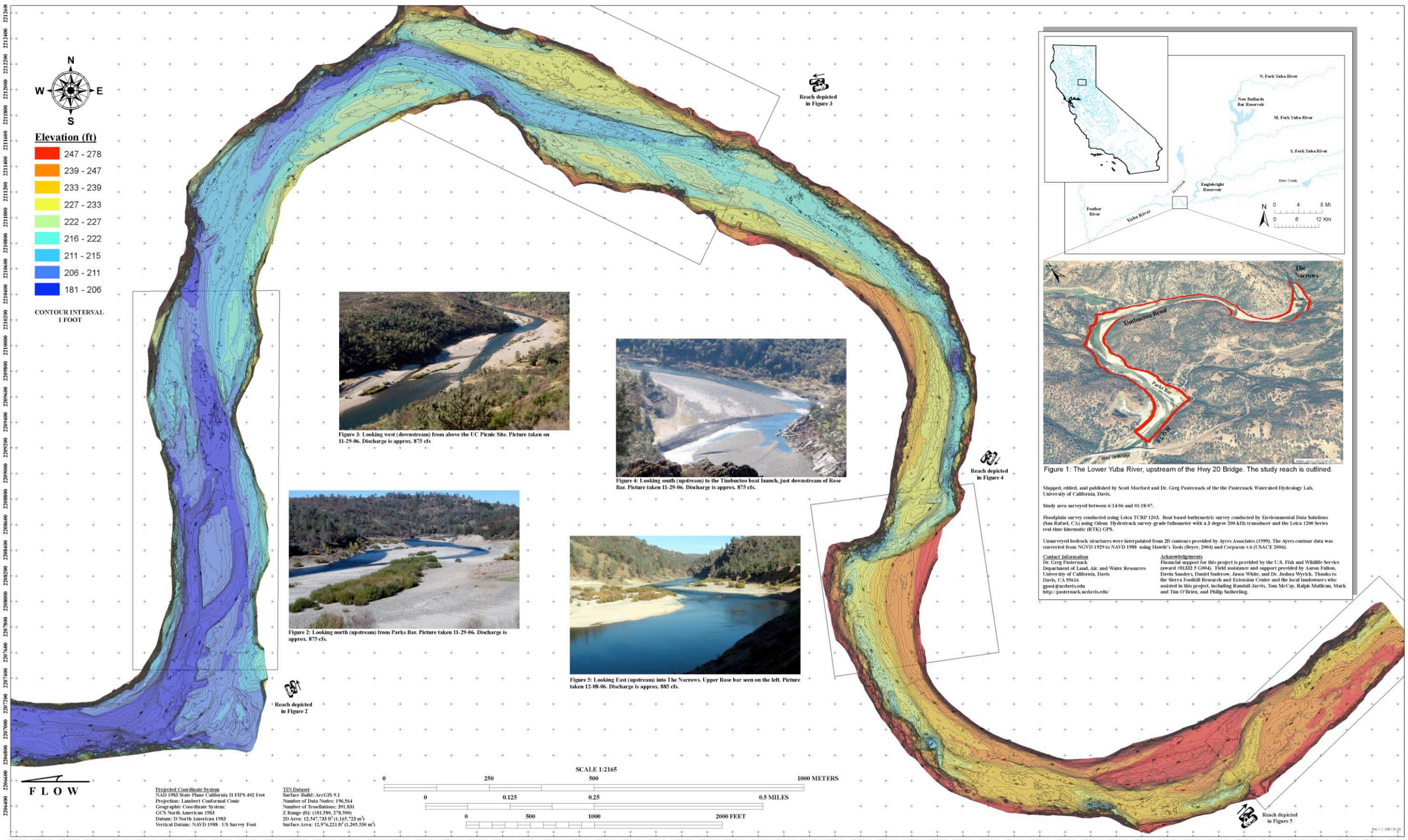

Figure 14

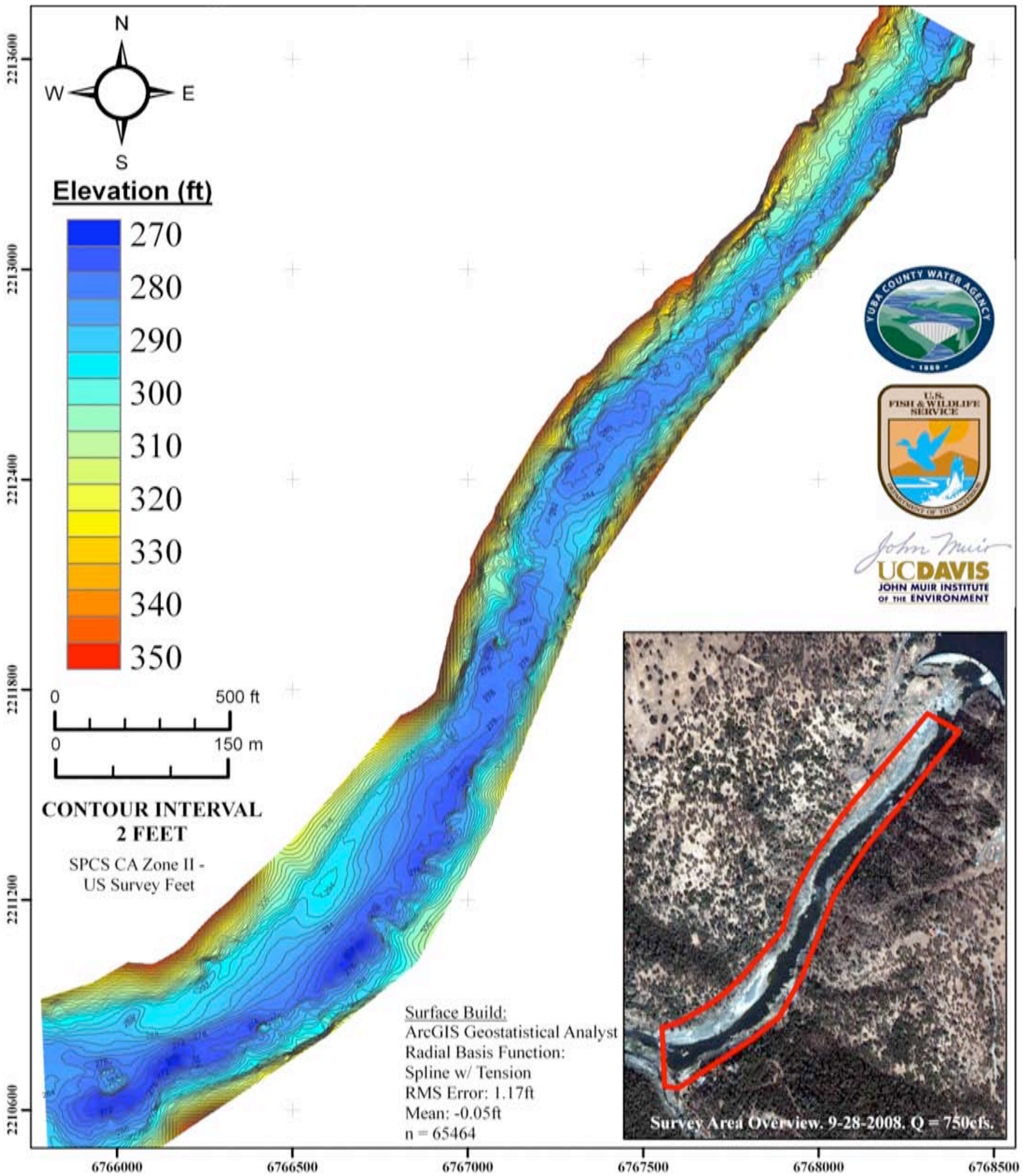

High Resolution EDR Topographic Map

Figure 15

Common examples include riffles, pools, floodplains, and gravel bars, but there are many more than those when you look closely. Aquatic ecologists refer to these features as “Mesohabitat”. Definitions of each unit suitable for each river need to clearly specified, and for the TBR those definitions are provided in Table 1.

Table 1. Metadata for the mapping of morphological units in Timbuctoo Bend on the Lower Yuba River, CA. Note that mentioned depths and velocities are those associated with a discharge of <1000 cfs, typical of the autumnal salmon-spawning flow regime.

Morphological Unit	**Description**
Forced Pool	Areas along the periphery of the channel with a water depth >4.6’ (1.4 m) and a low velocity in which the bed is “over-deepened” from local convective acceleration and scour during floods that is associated with static structures such as wood, boulders, and mostly bedrock outcrops (Montgomery and Buffington, 1997; Thompson et al., 2001).
Pool	Area with depth >4.6' (1.4 m), low velocity, and low water surface slope that was not formed by of a forcing obstruction.
Chute	Area of high velocity, steep water surface slope, and moderate to high depth located in the channel thalweg. Chutes are often located in a convergent constriction downstream of a riffle as it transitions into a run, forced pool, pool, or glide.
Run	Area with a moderate velocity and moderate water surface slope. Depth can range from ~3-8' (1-0.3-2.4 m). Runs typically occur in straight sections that exhibit a moderate water surface texture and tend not to be located over transverse bars.
Glide	Area of low velocity and low water surface slope. Depth can range from ~0.5-4.6' (0.15-1.4 m). Commonly occur along periphery of channel and flanking pools. Also exist in straight sections of low bed slope.
Riffle Entrance	Transitional area between an upstream pool and downstream riffle. Water depth is ~2.25-4.6' (0.69-1.4 m) relatively low. Velocity is low, but it increases downtream due to convective acceleration toward the shallow riffle crest that is caused by lateral and vertical flow convergence. The upstream limit is at the approximate location where there is a transition from a divergent to convergent flow pattern. The downstream limit is at the slope break of the channel bed termed the riffle crest.

Riffle	Area with depth <2.25' (0.69 m), moderate to high velocity, rough water surface texture, and steep water surface slope. Riffles are associated with the crest and backslope of a transverse bar.
Recirculation	Area of upstream-moving flow (aka "eddy") adjacent to a core of high-velocity, downstream-oriented flow and seperated from it by a sharp hydraulic shear zone (aka "eddy fence") that controls flow separation and the shedding of turbulent eddy structures. These units are usually the associated with an abrupt transition in the topography of the channel (e.g., the downstream extent of a bar feature or bedrock outcrop) that results in lateral flow separation.
Backwater	Shallow, low-velocity area adjacent to the main channel but seperated form it by a peninsula.
Medial Bar	Emerged bar surrounded by water.
Lateral Bar	Area located at the channel margins at an elevation band between the autumnal low-flow stage and bankful stage. Lateral bars are orientated parallel to the flow. The feature slopes toward the channel thalweg with an associated increase in both flow depth and velocity when submerged. Sediment size tends to be lower than in adjacent sections of the channel.
Point Bar	Area located on the inside of a meander bend at an elevation band between the autumnal low-flow stage and bankful stage. Point bars are curved and begin where there is clear evidence of point-bar deposition. The feature slopes toward the channel thalweg with an associated increase in both flow depth and velocity when submerged. Sediment size tends to be lower than in adjacent sections of the channel.
Secondary channel	A submerged channel during autumnal low flow that is adjacent to but separated from the main channel by a medial bar. It must be connected at both upstream and downstream ends to the main channel during autumnal low flow. Secondary channels incorporate a range of morphological and flow characteristics, but in order to be classified at the same absolute resolution as is necessary for the other morphological units, a single unit is defined.
Floodplain	Area located at an elevation higher than the bankful channel and lower than that of the valley toe slope break.
Tributary Delta	Alluvial fans penetrating the floodplain and main channel at tributary junctions.
Tertiary Channel	A well-defined channel on the floodplain.
Terrace	A natural alluvial deposit at an elevation higher than the floodplain surface.
Tailings	Alluvium artificially piled up to an elevation higher than the floodplain surface during historic dredging for gold.

Cutbank	Steep bank that is eroding heavily. Often located on the outside of a meander bend. Can be composed of either gravel/cobble alluvium or angular hillslode rocks and boulders, depending on the location of occurrence.
Hillside	Natural colluvium and bedrock at an elevation greater than the valley toe slope break.

Notes: High-quality bed elevation and water depth estimation is available for Timbuctoo Bend, so units that are objectively defined by depth or elevation have a high level of certainty. The delineation between glides and runs depends primarily on velocity, which was less discernable from available sources, so that delineation has more uncertainty. Similarly, many very small recirculations were not mapped, because the velocity pattern is not available in map form at this time. Where chutes overlap with pools (or forced pools), the chute was given preference. Where pools or forced pools overlapped with recirculation zones, the pools were given preference.

The TBR morphological units include three types: channel units, active bar units, and terrestrial units. The channel units include backwater, recirculation, shoot, forced pool, pool, glide, riffle entrance, riffle, run, and secondary channel. The active bar units include lateral bar, medial bar, and point bar. The terrestrial units include hillside, cutbank, terrace, tailings, floodplain, tertiary channel, and tributary delta. The spatial pattern of the TBR units shows the typical riffle-entrance-riffle-pool or riffle-entrance-riffle-run-pool sequencing, with glides flanking pools (Fig. 16).

Looking at the characteristics of the units, a few key statistics stand out. First, the three units with the most area in order of decreasing area are glide, riffle, and pool (Fig. 17). So those are three very common units that are present in any river and they are in fact the most dominant features in Timbuctoo Bend. 9.7% of Timbuctoo Bend is composed of glides, 7.32% riffles, and 5.31% pools. In terms of the bar units, the lateral bar has the largest area. For terrestrial units, 34% of the entire area of the Timbuctoo Bend is composed of floodplain, so that's a significant component of the TBR corridor.

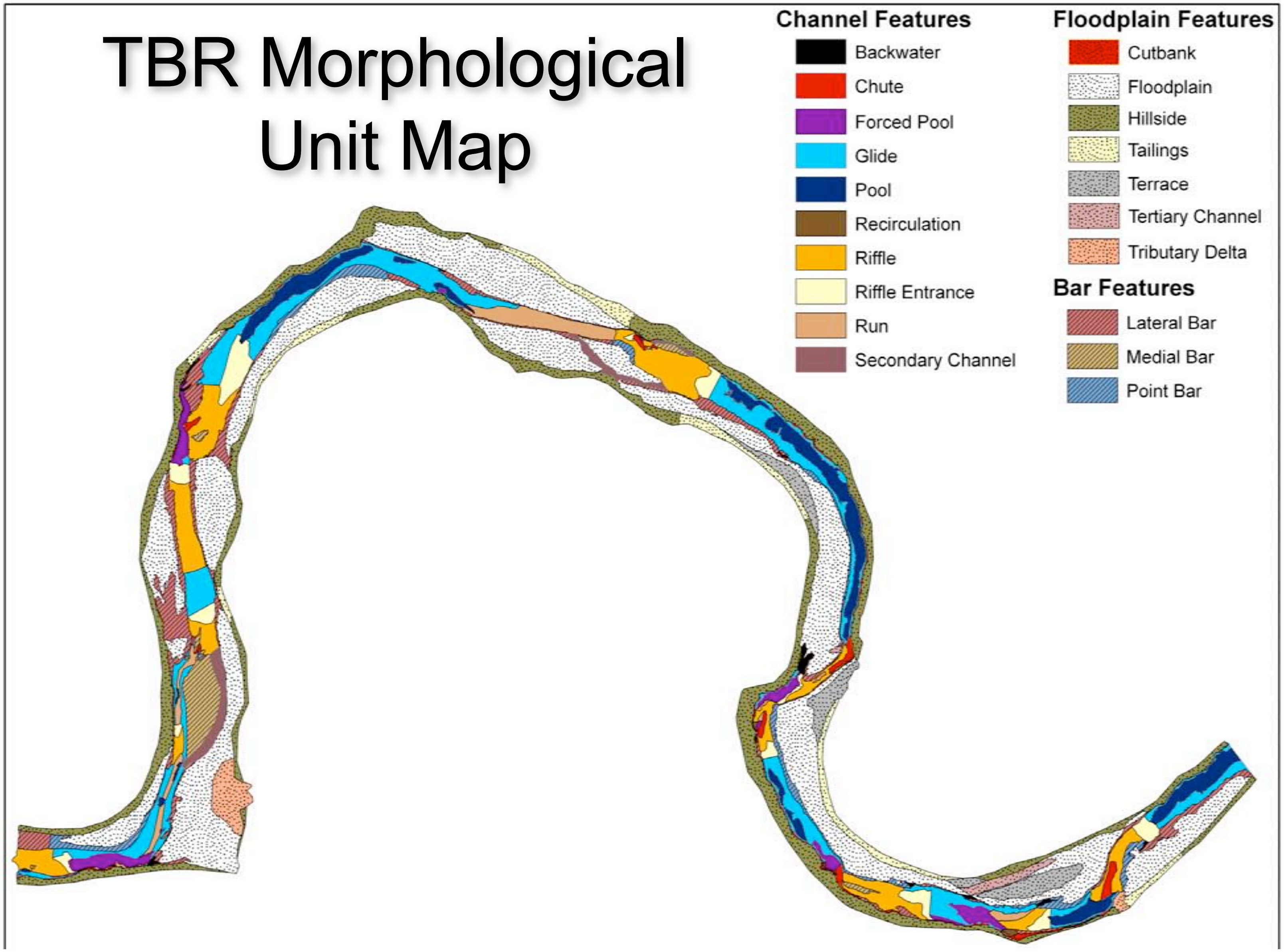
TBR Morphological Unit Map
Channel Features
Backwater
Chute
Forced Pool
Glide
Pool
Recirculation
Riffle
Riffle Entrance
Run
Secondary Channel
Floodplain Features
Cutbank
Floodplain
Hillside
Tailings
Terrace
Tertiary Channel
Tributary Delta
Bar Features
Lateral Bar
Medial Bar
Point Bar

Figure 16

Basic Characteristics of Units

Morphological Unit	Area (Ha)	% Total Area	Water Depth (m)*	StDev	Wetted Area (Ha)*
Backwater	0.35	0.30	0.48	0.37	0.16
Chute	0.68	0.58	1.04	0.66	0.67
Forced Pool	2.19	1.86	2.50	1.15	2.18
Glide	11.45	9.70	0.66	0.36	10.24
Pool	6.27	5.31	2.14	0.83	6.24
Recirculation	0.12	0.10	0.89	0.57	0.11
Riffle	8.64	7.32	0.33	0.21	6.66
Riffle Entrance	3.09	2.62	0.68	0.25	2.93
Run	2.54	2.15	0.68	0.34	2.31
Secondary Channel	1.37	1.16	0.39	0.42	0.11
Lateral Bar	6.46	5.47			
Medial Bar	2.26	1.91			
Point Bar	2.64	2.24			
Cutbank	0.67	0.57			
Floodplain	40.44	34.27			
Hillside	19.74	16.73			
Tailings	3.93	3.33			
Terrace	3.04	2.58			
Tertiary Channel	0.61	0.52			
Tributary Delta	1.49	1.26			
TOTAL	**118.00**	**100.00**			**32**

* Water depth estimated by aerial imagery overlay on DEM at 750cfs.

Figure 17

The next thing that we did is take aerial imagery of the river at 750 cfs and overlay that on to the Digital Elevation Model (DEM) of the topographic map. Using a special QA/QC procedure to account for possible error in imagery georeferencing, we were ultimately able to estimate the location of the water's edge around the channel. Then we triangulated the elevations at the water’s edge to get a water surface map and DEM. Then we subtracted the channel bed DEM from the water surface DEM to obtain the water depth at throughout TBR. What we found was that the forced pool unit is the deepest with a water depth of 2.5 m (~8.2’). Pools have a typical depth of 2.14 m (~7’), glides have a depth of 0.66 m (~2’), and riffles are the shallowest unit, with a depth of 0.33 m (~1’). In terms of the wetted area, glides have the largest wetter area followed by riffles and then pools (Fig. 17).

Historical Analysis

The historical analysis of TBR was performed by Jason White for his Master’s degree at UC Davis. His thesis is provided in Appendix 2. We obtained aerial photos going back to 1937 and up to the present, and we georeferenced them. Unfortunately, the photo sets from 1937, 1948, and 1958 were very difficult to georeference relative to the modern aerial photos for which we have really good topographic coordinates and geographical reference points. That's because back in 1937 there were very few man made structures in the river or around the hillsides, very few roads, and very few pre-existing trees that still match the conditions that we see today along the river. So the historical aerial photo analysis emphasizes the photos from 1984-2006, with an examination of the 1952 set that had an acceptable georeferencing accuracy. Appendix 2 presents the detailed historical aerial photo analysis, but here I am just going to present some of the highlights.

Four of the historical aerial images of the TBR from 1984-2002 illustrate the river's dynamism (Fig. 18). Along the N-S straight-away in the left side of each image (aka Park's Bar area), the river alternates between meandering and braided, with the configuration of medial bars changing in each image. Also, the riffle at the apex of the bend (top center) was braided in 1991, but meandering otherwise.

We delineated the wetted area of the river at each time a photoset was available, and then we documented how the area changed from one set to the next (Fig. 19). For example,from 1984 to 1991, you can see that there were islands that are no longer islands, the channel is cutting through, that the location has moved from one side of the valley to the other side of the valley. There are places where the river now bifurcates and it didn't before or vice versa. Overall, there have been significant changes to the wetted area, depending on how incised the channel is at a particular location at a particular moment in time.

We have also been able to identify the locations of all riffle crests that are present now and back to 1984 (Fig. 20). By evaluating shifts in riffle crest locations, we have been able to identify the riffles that have persisted at the same position along the longitudinal axis of the river (Fig. 21). They may be moving across the channel back and forth, but they remain at the same longitudinal position, and that's what we call a persistent riffle. There are 7 persistent riffles in the TBR. Interestingly, each of these persistent riffles is just upstream of a major valley constriction. The riffle crests are located in the widest part of the valley in between valley constrictions (Fig. 21). In the downstream straight-away of the TBR ending at the quarry on the north hillside (aka Parks Bar area) there is an undulating valley wall,so you can see the sequence

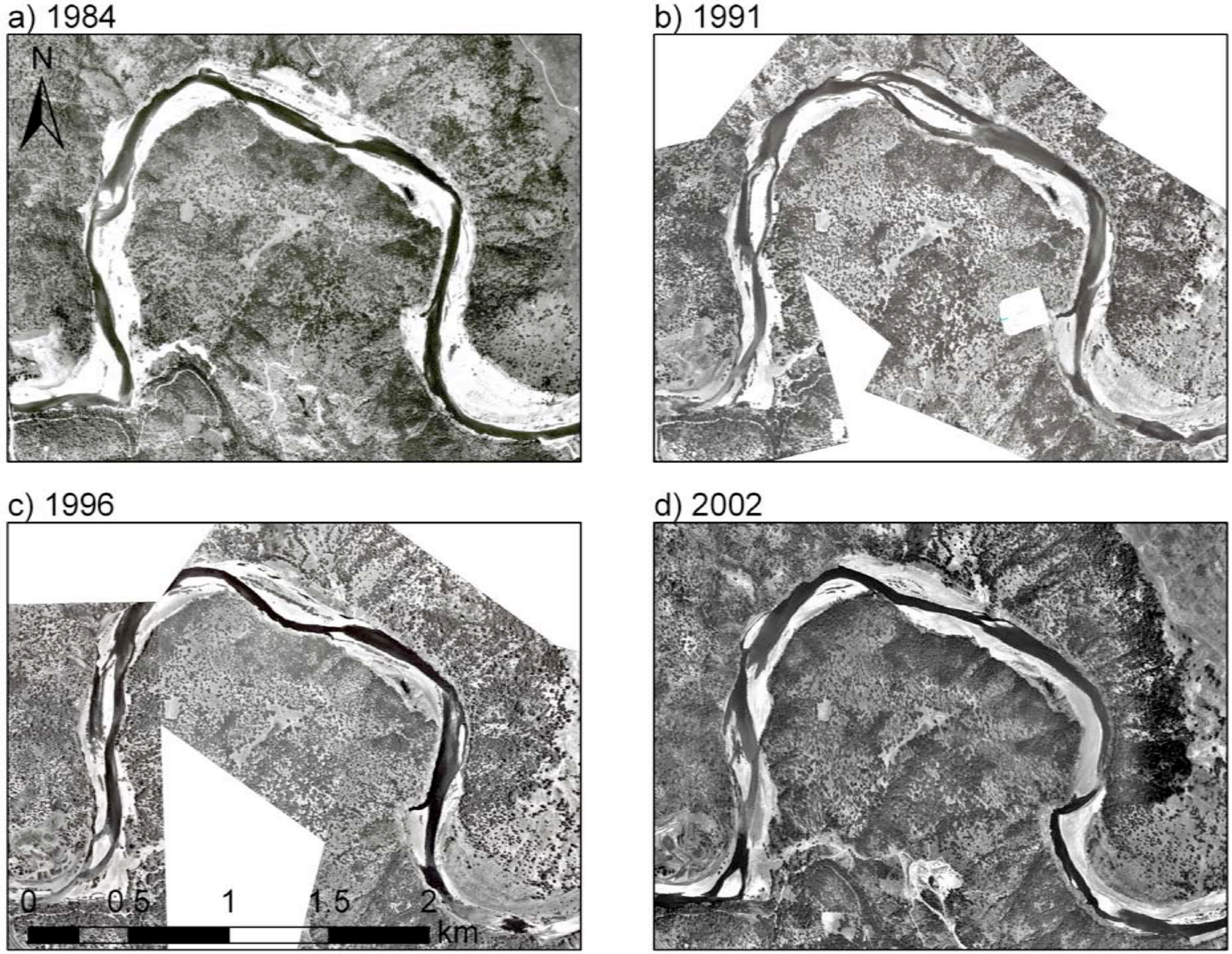

Historical Aerial Photos (1984-2002)

Figure 18

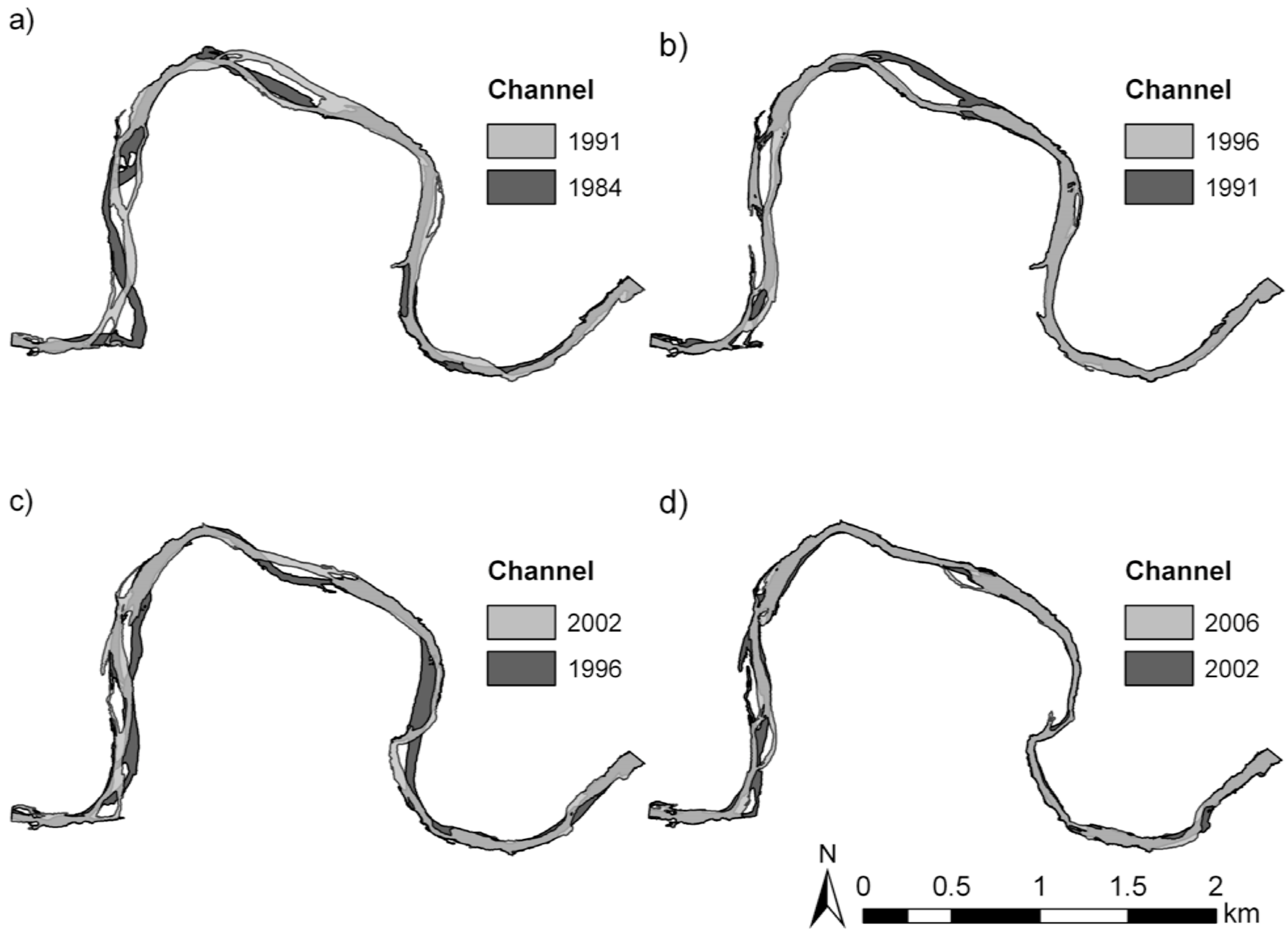

Wetted Area Channel Change

Figure 19

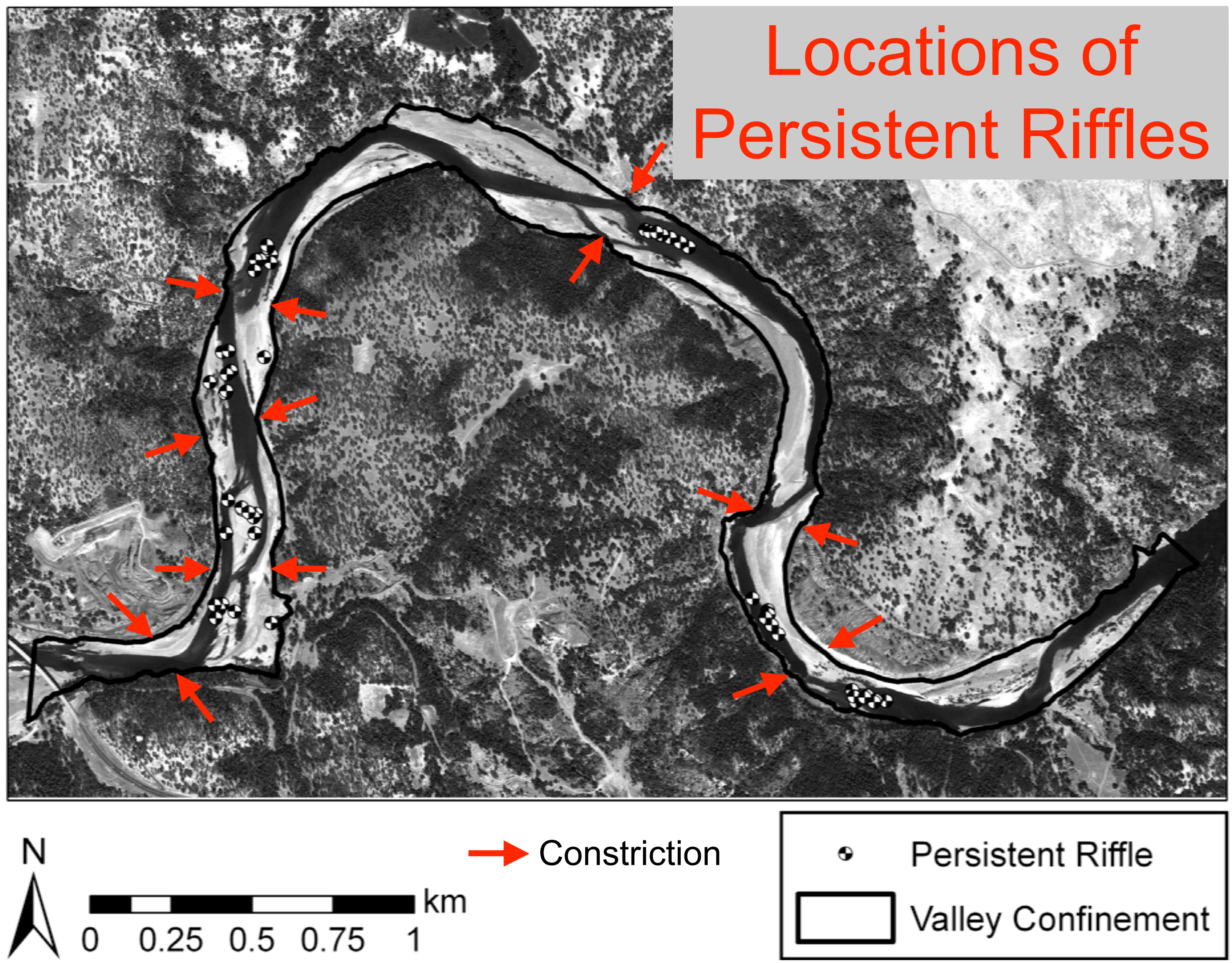
Locations of
Persistent Riffles
N
0
0.25
0.5
0.75
1
km
Constriction
Persistent Riffle
Valley Confinement

Figure 20

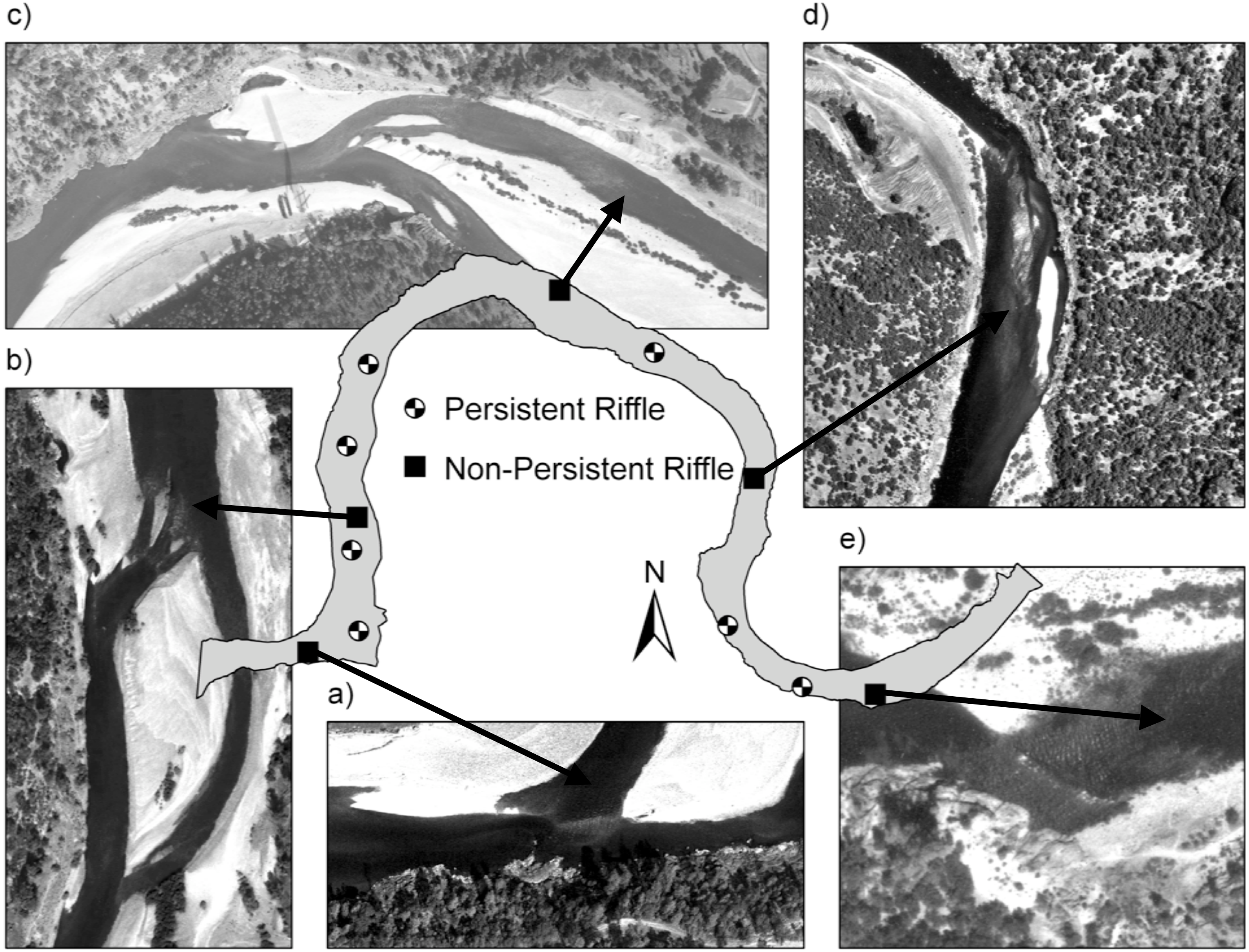

Locations of Transient Riffles

Figure 21

of persistent riffles and constricted valley walls in that area. When you look at the apex of Timbuctoo Bend, where we have what we call the Timbuctoo Bend Apex Riffle (TBAR), you can see that there too there is a bedrock outcrop on either side of the river that creates somewhat of a constriction, as well as the constriction imposed by the wide floodplain downstream of that location. There are two other constrictions further upstream in the river that plays a role in controlling the location of the two upstream most persistent riffles (Fig. 20).

In addition to the persistent riffles, there are also riffles that are transient. There are 5 of those located within TBR (Fig. 21). Commonly, these transient riffles are located in areas where there normally would be the inner point bar of a meander bend- a location where normally you have bend migration. Also, the transient riffles are located in a constriction. We conjecture that during a major flood, if the sediment was dropping out very quickly on the falling limb, then you could have the rapid formation of a transient riffle. However, on the rising limb of the next flood, then you would expect those to wash away, because scour is always focused in the constrictions during floods, as demonstrated with the hydrodynamic modeling below. So that analysis of persistence was for the aerial photos from 1984-2006. We compared mean riffle crest location for that whole set of historical aerial photos against what is evident in the older 1952 aerial photo, recognizing that the georeferencing for the 1952 aerial photo set isn't quite as good. We found that for each one of the seven persistent riffle crests, they still were present even back in 1952 (Fig. 22). There are also a few extra riffles in non-persistent locations back then, but overall this confirms the persistence of riffles in the TBR going back an additional 30 years. So now we know that over 56 years from 1952-2008, the same riffles have persisted at the same longitudinal positions, despite all of the flow changes, incision, and other processes that are going on in the river. The riffles are changing and shifting laterally, but they are persistent.

Riffle Persistence Dates Back to 1952

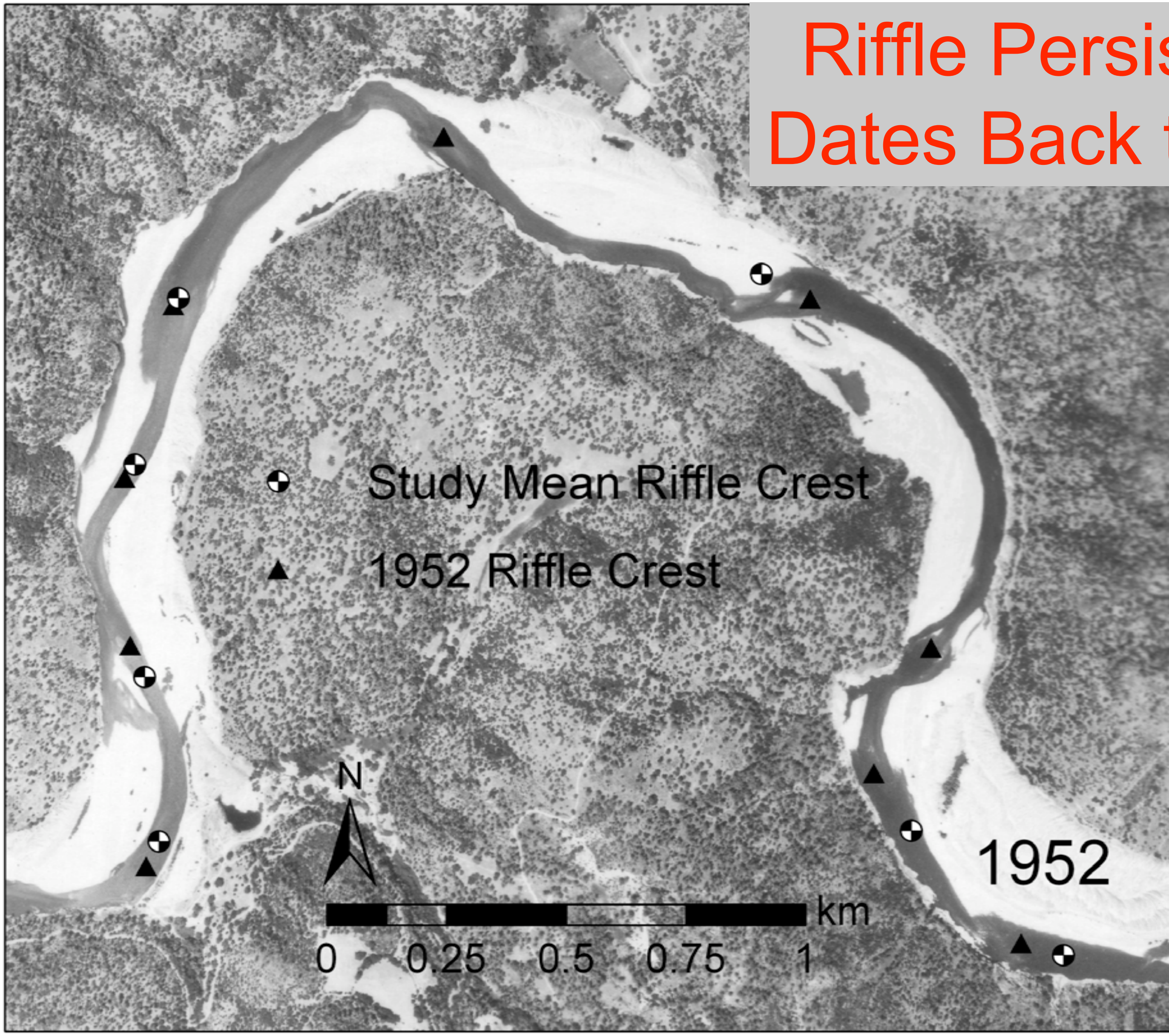

Figure 22

This is very strong evidence for a self-maintenance mechanism being active in the river, despite the overall trend of channel incision due to flow and sediment regulation. The correlation between riffle location and valley width hints at the underlying mechanism- what we have reported on before as “flow convergence routing” (MacWilliams et al., 2006), but a more complete mechanistic explanation is addressed below and in the technical appendices.

TBR Topographic Change 1999-2006

The findings of the historical analysis show both dynamism and persistence. That then leads to a desire for a more quantitative analysis to determine the rate of channel change and its spatial distribution at the point scale and relative to the pattern of morphological units. It is visually evident that the channel is changing dramatically, so that suggested that if we took the 2006 DEM of the river corridor and subtracted it from the one for 1999, using a procedure known as “DEM differencing”, then we could quantify channel change and the net export of gravel from the TBR. The 1999 DEM is not as high resolution as that from 2006- the boat-based mapping that was done in 1999 included cross sections of every 100-300’ down the river, whereas in 2006, it was more on the order of every 10-20’. However, we have done a lot of QA/QC measures to evaluate the quality of both DEMS- we are confident that the large scale of changes that we are reporting here are significant enough to really be meaningful in understanding the river. One of the ways that we have accounted for the uncertainty in the data quality is by binning the changed data to such large bins that it's not really important if there are very subtle errors associated with the different maps. For example, any change that was <1’ was considered too small to be incorporated into the analysis. Thus, even though the 1999 map isn't as good as the 2006 map, it still gives us a basis for assessing what the changes have been in the TBR.

The results from the DEM differencing analysis are startling. Over just 7 years (1999-2006), 605,000 yds^3 of sediment (primarily gravel and cobble) were exported out of Timbuctoo Bend. 50% of the river has down cut 1-6'. The majority of Timbuctoo Bend from wall-to-wall, including all morphological units, except medial bars, are incising (Fig. 23). The area that is experiencing significant deposition within TBR is the Parks Bar area (Fig. 23, left side of image). We believe that is caused by the significant channel constriction at the last bend of Timbuctoo Bend, just before the highway 20 bridge. The rbidge was build where it was, because the river is highly constricted there. The bend and constriction creates a significant backwater effect during floods that causes sediment to drop out. That explains why the channel bifurcates there and also why there is finer sediment in that area. That also helps to explain why steelhead trout prefer to spawn in that section, since the area is replenished with gravel on a regular basis.

If we take the geomorphic morphological unit map of Timbuctoo Bend and distribute the channel change from the DEM difference analysis according to the units, then we can determine the mean depth of change and the net volumetric change for each unit (Fig. 24). When we do that, we find that the units that are cutting the most include the few secondary channels and all the pools. Pools incised 1.45 m over the 7-year-period; secondary channels 1.53 m, but secondary channels don't make up a large area of the river. Pools are the third-largest aerial extent in the river and they have the deepest cutting that's going on of the major units. On the other side of it, for the in-channel units, riffles are also cutting, but they are cutting the least- at a rate of 0.54 m over the 7 years.

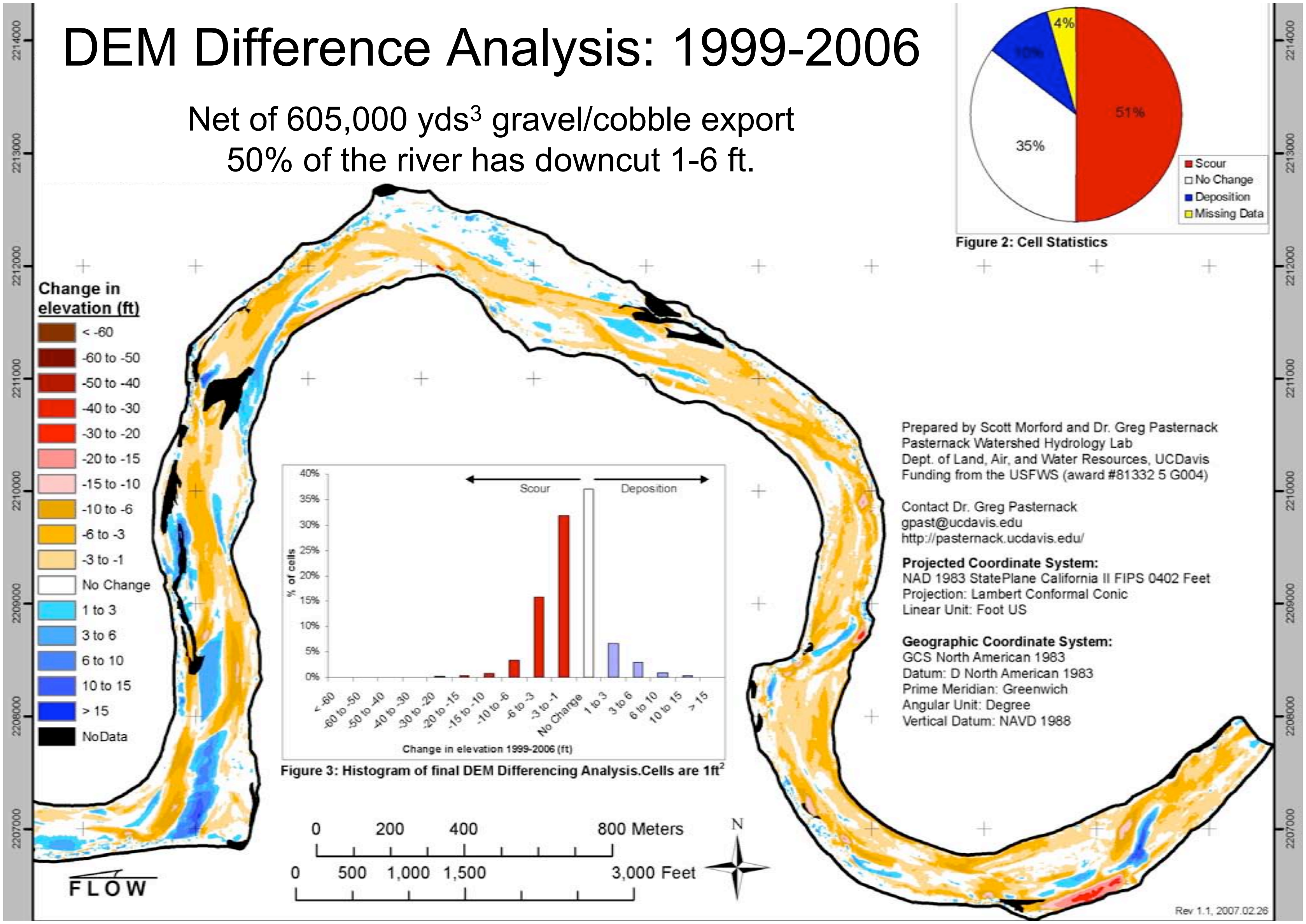
DEM Difference Analysis: 1999-2006
Net of 605,000 yds³ gravel/cobble export
50% of the river has downcut 1-6 ft.
Change in elevation (ft)
< -60
-60 to -50
-50 to -40
-40 to -30
-30 to -20
-20 to -15
-15 to -10
-10 to -6
-6 to -3
-3 to -1
No Change
1 to 3
3 to 6
6 to 10
10 to 15
> 15
NoData
FLOW
51%
35%
10%
4%
Scour
No Change
Deposition
Missing Data
Figure 2: Cell Statistics
Scour
Deposition
% of cells
Change in elevation 1999-2006 (ft)
Figure 3: Histogram of final DEM Differencing Analysis.Cells are 1ft²
0 200 400 800 Meters
0 500 1,000 1,500 3,000 Feet
N
Prepared by Scott Morford and Dr. Greg Pasternack
Pasternack Watershed Hydrology Lab
Dept. of Land, Air, and Water Resources, UCDavis
Funding from the USFWS (award #81332 5 G004)
Contact Dr. Greg Pasternack
gpast@ucdavis.edu
http://pasternack.ucdavis.edu/
Projected Coordinate System:
NAD 1983 StatePlane California II FIPS 0402 Feet
Projection: Lambert Conformal Conic
Linear Unit: Foot US
Geographic Coordinate System:
GCS North American 1983
Datum: D North American 1983
Prime Meridian: Greenwich
Angular Unit: Degree
Vertical Datum: NAVD 1988
Rev 1.1, 2007.02.26

Figure 23

Channel Change 1999-2006 By Unit

Morphological Unit	Mean Cut/Fill (m)	StDev (m)	Cut/Fill Volume (m^3)
Backwater	-1.22	0.87	-3642
Chute	-1.21	1.44	-7412
Forced Pool	-1.22	1.05	-25268
Glide	-0.78	0.84	-87641
Pool	-1.45	1.28	-90623
Recirculation	-1.03	0.65	-732
Riffle	-0.54	0.86	-39532
Riffle Entrance	-0.73	0.69	-21938
Run	-1.03	0.74	-25392
Secondary Channel	-1.53	0.73	-19667
Lateral Bar	-0.55	0.92	-32100
Medial Bar	0.40	1.00	8485
Point Bar	-0.08	0.79	-2190
Cutbank	-0.95	1.57	-5892
Floodplain	-0.15	0.76	-58288
Hillside	-0.07	0.55	-12820
Tailings	-0.64	1.03	-22737
Terrace	-0.29	0.42	-8226
Tertiary Channel	-0.73	0.46	-4448
Tributary Delta	-0.15	0.47	-1960
TOTAL			**-462022**

Figure 24

In terms of net volumetric change, the volume is found by multiplying the mean depth of cut by the total area of that unit in TBR, so the units with the largest area will tend to also have significant volumetric losses. Again, by this metric, pools are experiencing the most loss, as they very have a large extent and the deepest incision. Over 90,000 m^3 of sediment have been eroded out of pools. Then comes glides with 87,641 m^3 of loss and riffles with 39,532 m^3 of loss.

The only feature of any kind in the river corridor that is aggrading are medial bars and these are the small features that are occurring in that Parks Bar area that I mentioned earlier. Medial bars have aggraded 0.4 m over that 7- year-period, but otherwise every other landform- whether it's in the channel, on bars, or on the terrestrial features- is downcutting. For example, the floodplain is cutting 0.15 feet over the 7-year-period totaling a volume of 58,288, making it the third largest volume of cut of any of the morphological units in Timbuctoo Bend. This is important because people are interested in riparian rehabilitation, but when you look at Timbuctoo Bend, it's clear to see why vegetation cannot become established- the floodplain is incising and it is significant enough to prevent that reestablishment.

Although I prefer to look at the full DEM difference map, traditionally many people are more comfortable and familiar with looking at longitudinal thalweg profiles. The longitudinal thalweg profile for Timbuctoo Bend (Fig 25) shows that at the upstream end in 1999 the river had an elevation of 241.57’ and in 2006 it had an elevation of 235.66’. That's a change of close to 6’ over that 7-year-period, which is a significant amount of net incision. That’s roughly 1’ per year. The other thing that the longitudinal profile shows, which we have already seen in the 3D DEM difference by geomorphic unit, is that the relief between riffles and pools has been growing. So that shows that the TBR has the important characteristic of maintaining the relief between riffles and pools.

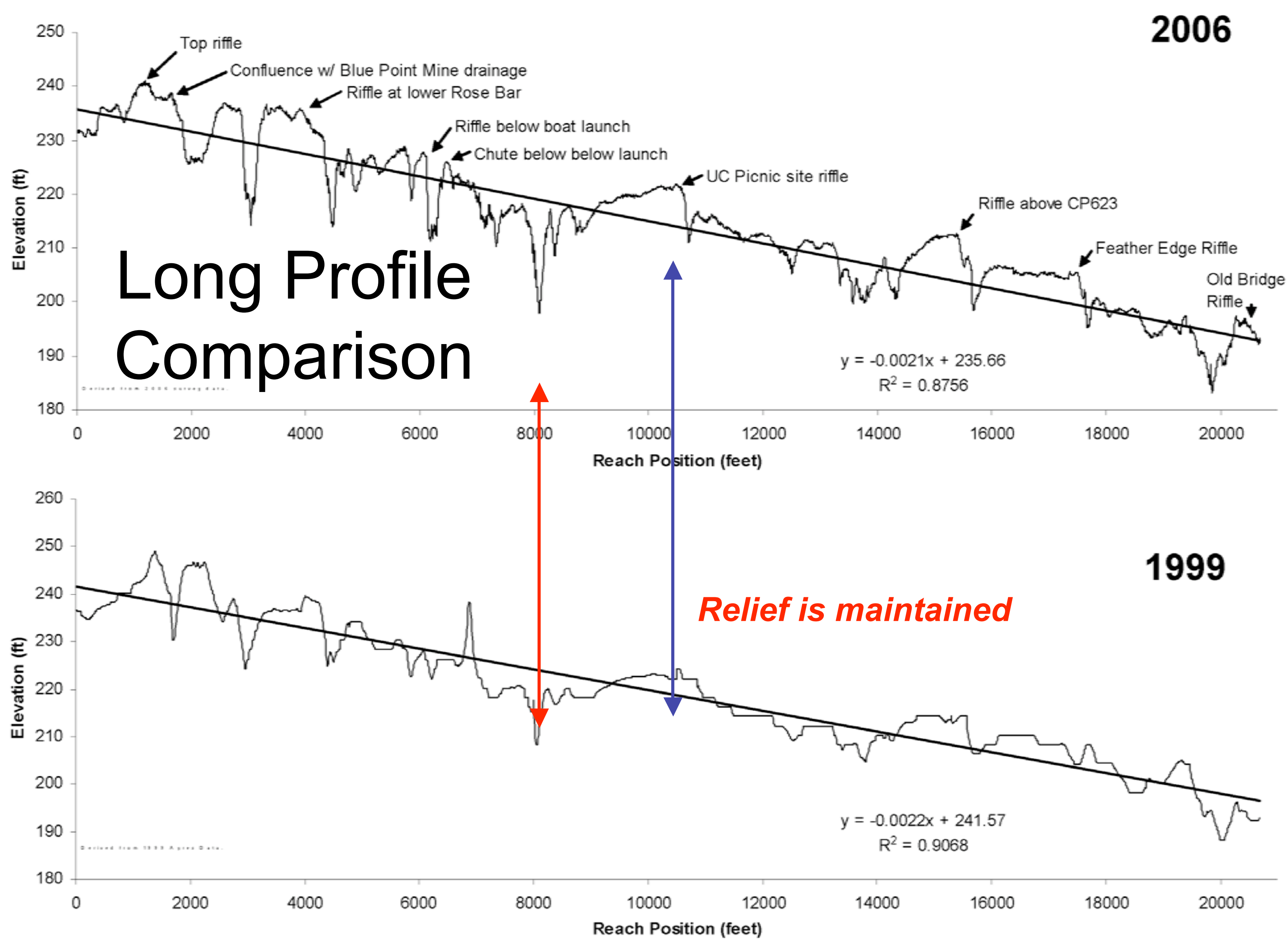

Long Profile
Comparison
2006
Top riffle
Confluence w/ Blue Point Mine drainage
Riffle at lower Rose Bar
Riffle below boat launch
Chute below below launch
UC Picnic site riffle
Riffle above CP623
Feather Edge Riffle
Old Bridge
Riffle
y = -0.0021x + 235.66
R2 = 0.8756
Elevation (ft)
Reach Position (feet)
1999
Relief is maintained
y = -0.0022x + 241.57
R2 = 0.9068
Elevation (ft)
Reach Position (feet)

Figure 25

Another way we can look at the river is by subtracting the slope of the river and just focusing on the local lateral variation of the river (Fig. 26). This provides a sense of where floodplains and terraces are sticking up the most and where the river is deepest, relatively speaking. It turns out that the river is relatively the deepest in two locations, but most importantly it's deepest at the very end of Timbuctoo Bend, which is in the constriction that I have previously mentioned as creating a backwater effect. That helps to explain that flows accelerating through that constriction scour it out and also back water up. The elevation of the river is highest around what is called Rose Bar (opposite Blue Point Mine), at the end of Rose Bar, and then just downstream of the apex of Timbuctoo Bend on the north side, where there is a large terrace. Those three terrestrial features are the main elevated surfaces in the river corridor. There is no reason to think they will remain elevated into the future, but for now they do create significant constrictions for flows in the range of 10-25,000 cfs.

Site-Scale, Event-Based River Changes

Visual and Qualitative Description

The 1999-2006 DEM difference analysis showed net change. Unfortunately, given the cost of mapping, it is not possible to re-map the whole river after every event to better understand the mechanisms of channel change. However, it was possible to do some comprehensive site-scale mapping on an event basis, and there is a lot to learn from that. So now we will shift gears and try to understand site-scale hydrogeomorphic dynamics. The key site that was the focus of this part of the study was the Timbuctoo Bend Apex Riffle (TBAR), which the USFWS Instream Flow Brach calls the “UC Sierra” riffle in its reports. TBAR was chosen for detailed

2006 3D Local Relief Analysis

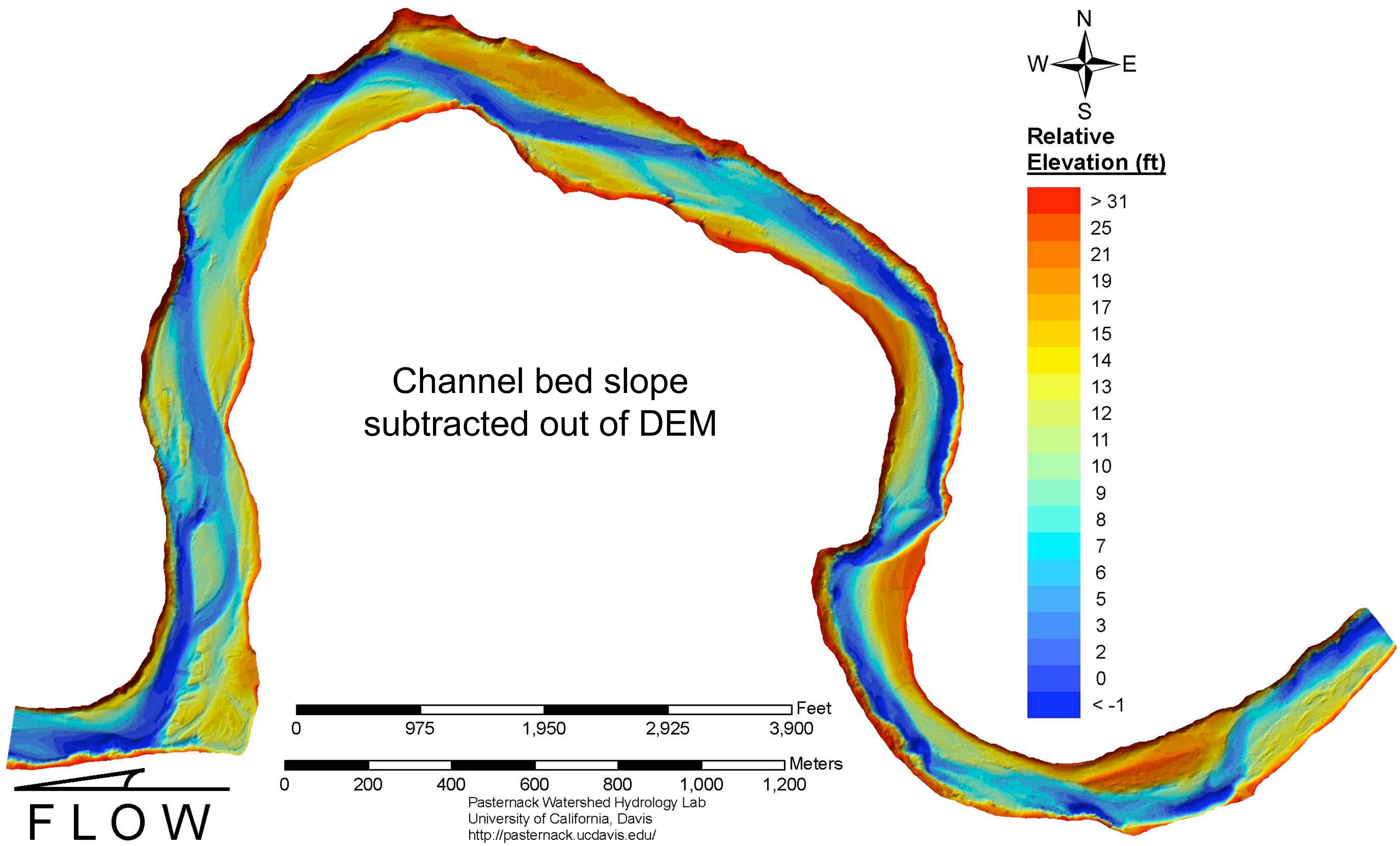

Figure 26

study because we were told that it had the highest density of fish spawning on the LYR, and that has proven to be the case during the study. We have been able to capture the changes at this site repeatedly, including a terrific series of 20 oblique site photos from the same position on the bank during 2003-2007. The complete set of photos is not presented in this report, but is available upon request.

The detailed topographic mapping of the site began in September 2004 when the flow was ~700 cfs. Under this condition, the site included the downstream end of a pool, a riffle entrance, a riffle;a chute, and then a run (Fig. 27). The site also had a medial bar and a secondary channel along the north bank. Throughout the riffle entrance and riffle units there were large transverse bars created by salmon over a few years after the 1997 flood. The ridges visually represent the location of prime salmon spawning habitat, where the fish are building redds each autumn. You can also see, and as you move downstream, a very steep riffle crest with large standing waves and what I would consider to be a class II rapid. You can see that all along the south bank, there is a large floodplain, but between the floodplain and the river is a large line of willows that are delineating the bankfull channel. You can see that very well on both sides of the river downstream in the run. The island itself is also somewhat vegetated, and it has been observed to become submerged right at the modern bankful discharge of 5620 cfs.

On May 19, 2005, there was a significant flood, and we were able to capture a photo of it on the rising limb at 26,000 cfs (Fig. 28). Two people are visible in the photo on the right side, for scale. You can see that at this flow not only is the island and floodplain fully inundated but some of the terraces are inundated too. There are only a few stalwart willows that are sticking up in the middle of the river at this flow. However, far downstream in the upper right of the photo

Apex Riffle @ UC SFREC
September 2004 (700 cfs)

Figure 27

May 19, 2005
(26,000 cfs heading to 43,000 cfs)

Figure 28

you can see that the high-relief floodplain previously discussed in relation to the 3D relief map (Fig. 26) is not submerged. That is a section where the channel is heavily incised.

After the flow came down that summer you could see that a significant knickpoint had migrated through most of the riffle forming a deep, narrow chute between the floodplain and the island (Fig. 29).

A <u>kickpoint</u> is defined as an abrupt vertical break in a river's longitudinal profile.

Also, you could see that along the south bank adjacent to the knickpoint-chute feature, there was sediment deposition, such that the willows do not demarcate the bankfull water's edge in that area any more. The island itself is much bigger and the secondary channel is much smaller. These are just qualitative descriptions that will be followed shortly by a thorough quantitatifve analysis.

Then on December 31, 2005, there was the combined Yuba River and Deer Creek peak of 109,090 cfs, termed the New Years 2006 flood (Fig. 30). The entire corridor is underwater in the photo, except for the highest terraces downstream on the north bank, which has been discussed twice earlier. After the flood when the water receded, you could see that the majority of the island was gone and that the willow line along the south bank was busted through with a large secondary channel now appearing (Fig. 31). The secondary channel actually contacts the south bank at the bedrock outcrop there and you can see some remnant willows that are now on an island in the south middle part of the river as well as just a few little pieces of vegetation on the remnant of the island along the north bank. It is highly notable that many willows survived a flood of 109,000 cfs and are thriving in the August 21, 2006 photo. There is also a

October 12, 2005 (794 cfs)

Figure 29

December 31, 2005 (109,090 cfs)

Figure 30

August 21, 2006 (1400 cfs)

Figure 31

prominent knickpoint that is present at the end of the riffle crest in the center of the channel. Upstream in the channel there are no redd dunes any more and the whole spawning area is much wider. These are the general changes that you see from over these two major events; there is knickpoint migration, island change, channel migration (Fig. 32).

We want to characterize the TBAR geomorphic changes associated with these events quantitatively, but first let's look back historically at the site based on Jason White's analysis (Fig. 33). What Jason found in the aerial photos is that a riffle crest has persisted at the TBAR site going back to 1952. However, from 1984-2006 you can see that the riffle crest has shifted upstream and downstream over a short distance of ~100-150 m, but it has persisted at this location. In comparing the wetted channel area from 1984-2002 (Fig. 33), you can see a dramatic change. In 1984 the channel was primarily along the south bank. In 2002 it was primarily along the north bank with a few islands present.

Two other important aspects of the floods observed in the TBR are worth mentioning. First, as already noted, the willows did survive the 109,000 cfs. In doing so, they captured sediment- you can see large cobbles with what we call an "imbricated" pattern of stacking on top of each other at an angle (Fig. 34). Imbrication indicates the direction of flow into and through the willows. The sediment captured into the lines of willows formed somewhat of a natural levy. Second, both at that Apex Riffle site and further downstream at the Parks Bar site, we saw new knickpoints that emerged (Fig. 35). The new features created habitat heterogeneity in terms of both hydraulic diversity and patches of different substrates. As shown later on, these knickpoints experience scour and upstream retreat during low flow, with the resulting sediment generated moving a short distance downstream and depositing to form localized, loose gravel bars.

Apex Riffle @ UC SFREC

- Knickpoint migration
- Island changes
- Channel migration
- Vegetation persistence

Figure 32

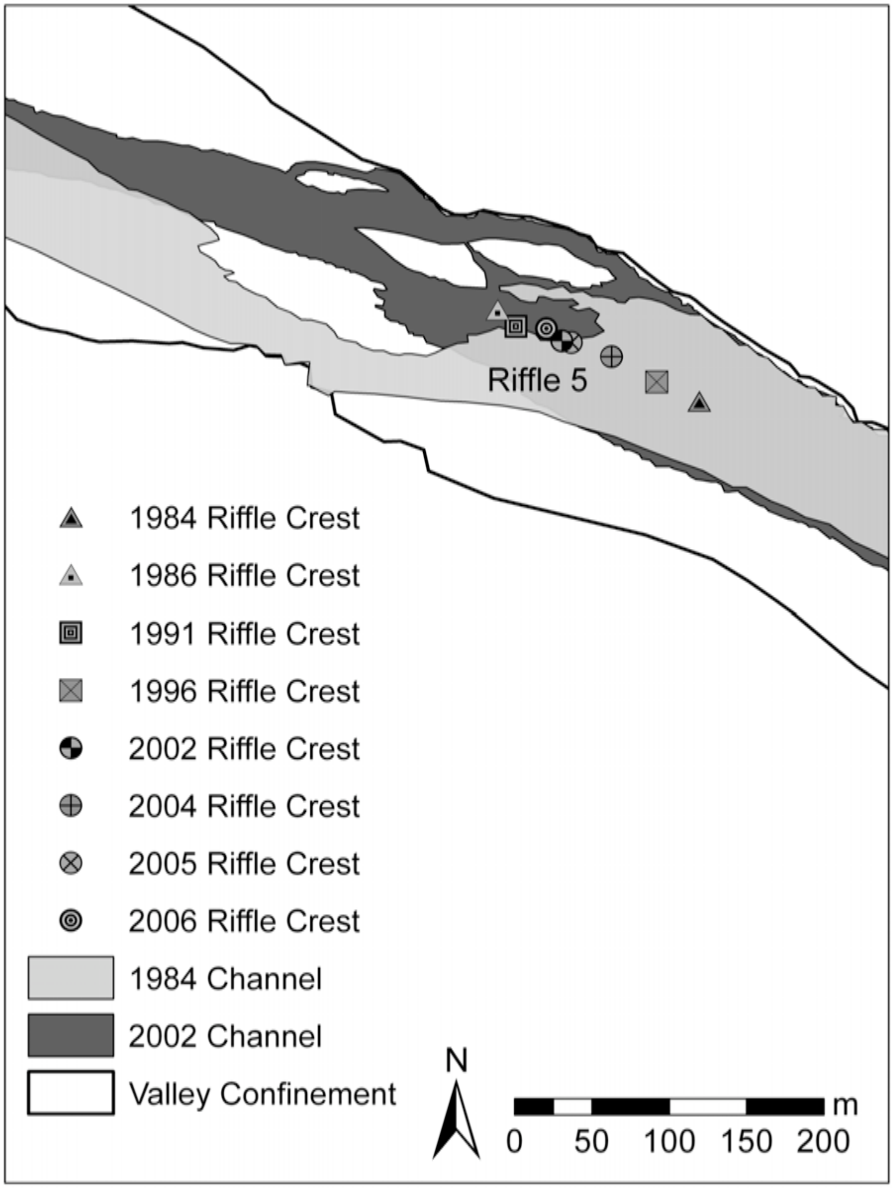

Apex Riffle Historical Riffle Persistence

Figure 33

Willows survive 109K cfs and capture sediment to form natural levees

Figure 34

New knickpoints form creating habitat heterogeneity and low-flow sediment transport

Figure 35

TBAR DEM Differencing

As detailed in the technical appendices, TBAR was topographically mapped in extremely high resolution in autumn 2004 and again in the summer and autumn of 2005. These maps were used to generate DEMs for those years (Fig. 36). Also, it was possible to extract site-scale DEMs from the 1999 and 2006 TBR maps. These 4 DEMs enabled a quantitative assessment of how the site changed over the three shorter intervals 1999-2004, 2004-2005, and 2005-2006.

From 1999-2004 there were no major floods and what you see is predominantly channel incision (Fig. 37). The incision was focused on the riffle crest, in the center of the run, and most intensely along the unvegetated bank the island, where there existed an oversteepened cutbank. Some deposition is evident on the island, but much of the island and secondary channel was not surveyed in 1999. We can infer the process underlying this pattern of change. What is happening is that the flow is being constricted laterally by the island and vertically by the upslope to the riffle crest. Very high velocities were evident on the riffle crest and through the chute downstream of it. Where the flow in the chute impinges on the edge of the island, it just scours away the unconsolidated material and then that material gets deposited downstream along the flank of the run, but in too thin of a veneer to capture accurately with the 1999-2004 DEM difference. In 2004 the substrate on the riffle crest was very coarse and became coarser toward the chute.

From 2004-2005there were areas of both scour and deposition, with little net change overall. Scour occurred in the knickpoint incision at the riffle crest, in the pool and riffle entrance upstream, and localized in the forced pool adjacent to the bedrock outcrop along the north bank (Fig. 38). In-channel deposition occurred in the secondary channel, riffle, and run units. Terrestrial deposition occurred along the willow lines and out on the floodplain. This

TBAR Site DEMs

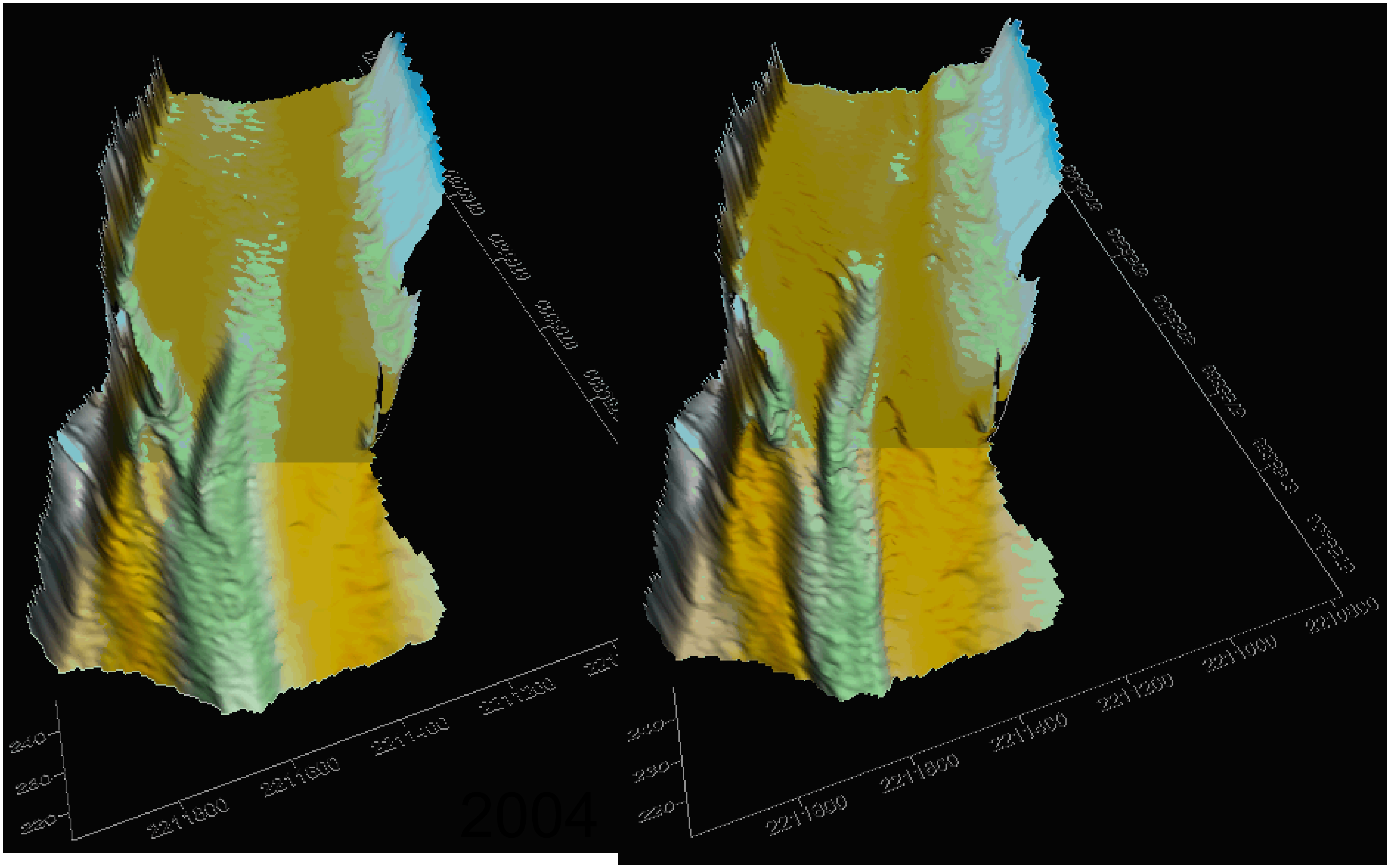

Figure 36

Apex Riffle Elevation Change 1999-2004

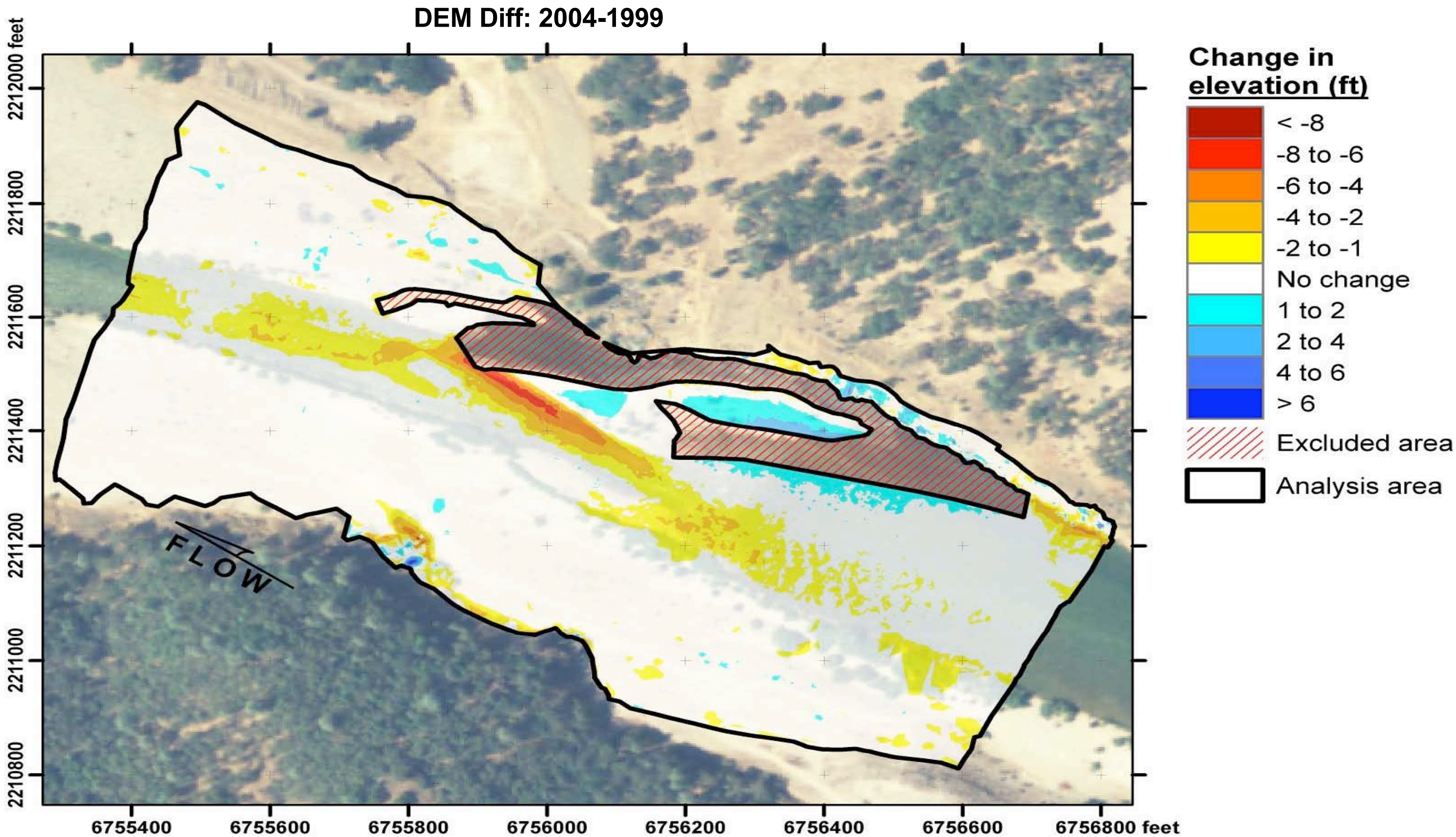

Figure 37

Apex Riffle Elevation Change 2004-2005

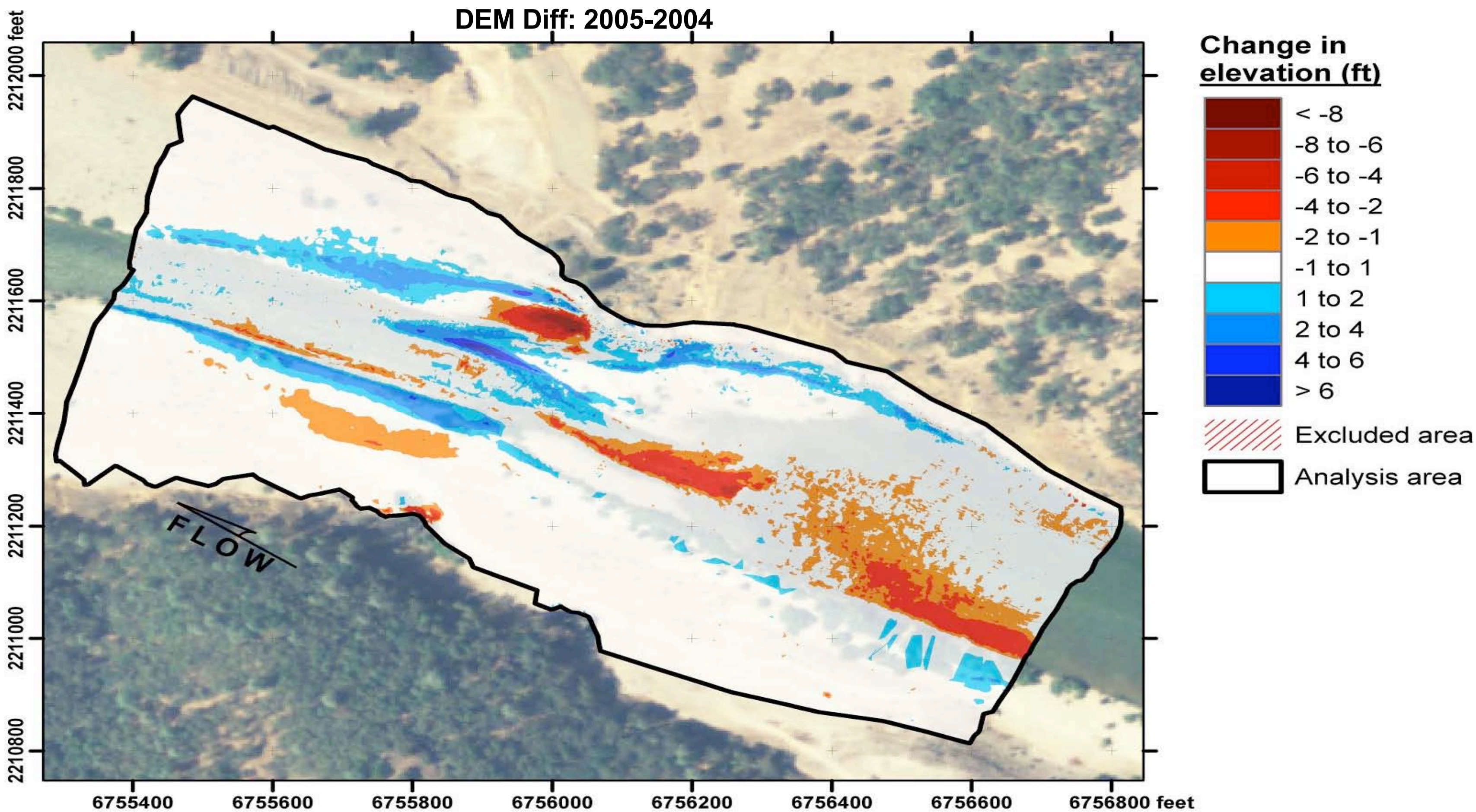

Figure 38

analysis found that sediment is moving down to the TBAR site and moving out of it in nearly equal amounts.

From 2005-2006 there was a dramatic amount of channel incision (downcutting to as much as 8' depth) as well as deposition (up to 6' of fill) (Fig. 39). The incision was all along the length of the center of the channel, but was particularly deep where the channel was constricted. Also, there was channel migration along the north bank that cut into a sizable section of the floodplain there. Also, there was scour on the floodplain itself, particularly on the south side of the river corridor. The flow followed a low swale from a pre-existing channel, eroded the vegetation blocking access to the swale, and then trenched 2-8' down cutting that swale back into an active secondary channel. This change illustrates the importance of considering event-scale change and not just decadal scale change, because from 1999-2006 the floodplains in TBAR only scouted an average of half a foot. When you look at this site what you can see is that there is scour on the floodplain, that's on the order of 2-6 times just in this one event at this one site. Thus, large floods on the LYR can and do scour new channels on the floodplain at will. That helps explain why vegetation cannot establish there other than a few resilient willows.

Although there was some deposition on the floodplain 2005-2006, the main area of deposition was in the channel itself at the riffle cross-section and just downstream of the riffle in the area that previously was a run (Fig. 39). There was also deposition in the secondary channel, but it's very important to see that the main area of deposition in the river during this large event was at the area of the riffle. That unit was observed to scour at low flow, but at the highest flow it appears to have been *growing*. That is consistent with what have seen for all of Timbuctoo Bend in what I have already presented.

Apex Riffle Elevation Change 2005-2006

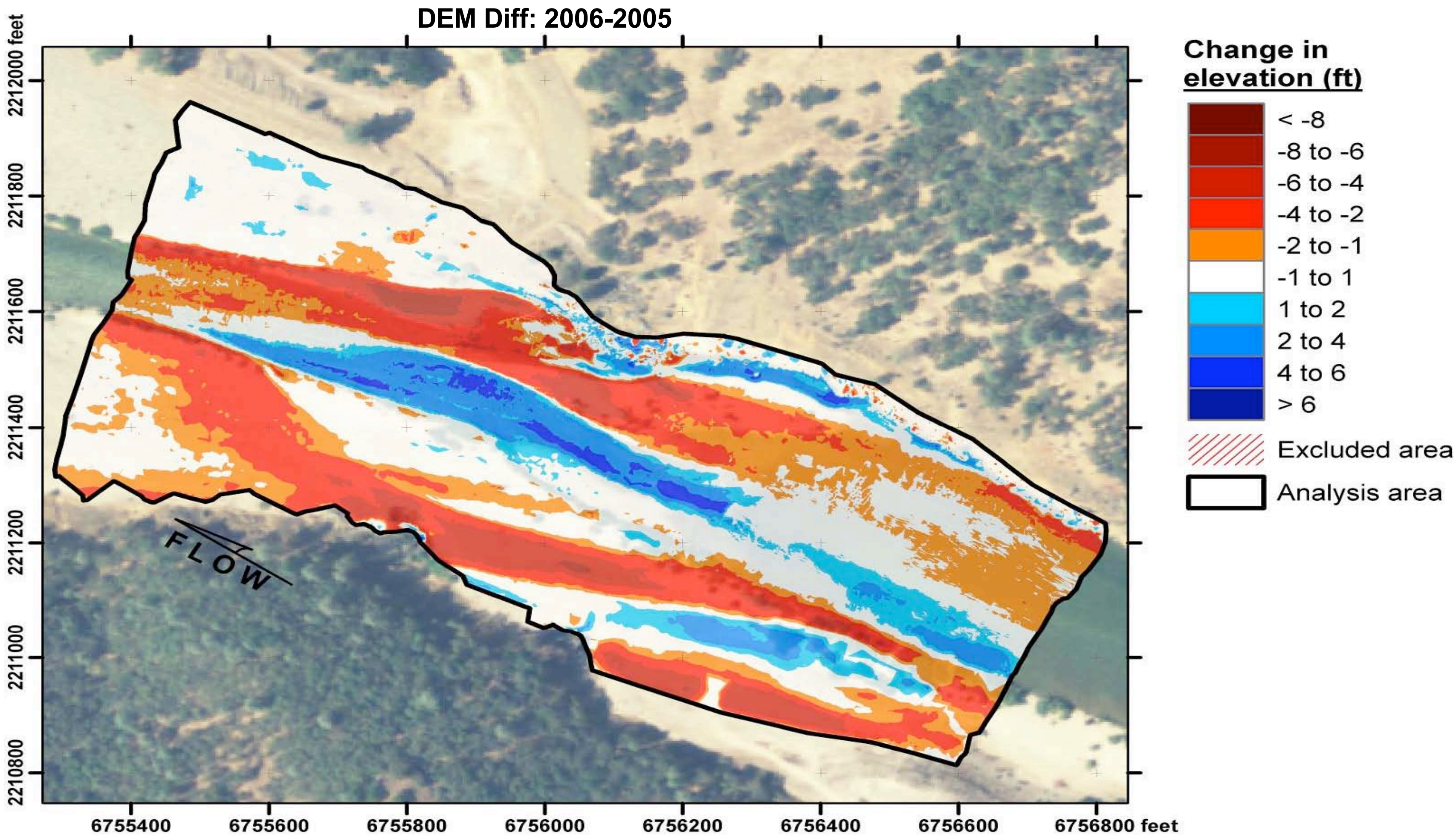

Figure 39

If we look at some of the specific statistics associated with these periods, we can determine the relative contributions of the events to the net change 1999-2006 (Fig. 40). From 1999-2004, there was a net scour of 11,046 yds^3. The May 2005 event saw both ~10,000 yds^3 of deposition and that amount of erosion, but in the net just a measly 76 yds^3 of net scour. That indicates that there was a significant sediment supply from upstream to rejuvenate the site. From 2005-2006, which included the big New Year's flood event as well as several subsequent smaller events, there was a net scour that was quite substantial- 26,138 yds^3. Whereas the 1999-2004 period encompassed 1,919 days, the period of the DEM difference from 2005-2006 was only one year (i.e. 365 days), and yet we had more than double the amount of scour in just that small period of time. In terms of the average scour intensity (yds^3/day), the 1999-2004 period had an intensity of just 5.8 yds^3/day, the May 2005 event had a intensity of 0.2 yds^3/day, and the 2005-2006 period had a scour intensity of 72 yds^3/day. Overall, there isn't a strong correlation between discharge, scour, and scour intensity, just because we only have three events and we are not looking at just events, but the time between surveys was longer than that. Most importantly, what we can see that is that the percent of change for this site for these three periods was 32% of the total change occurred in the first period, 2.5% in the second period, and 65.5% in the third period. Thus, at the site scale about two-thirds of the net scour over the 7-year-period was accounted for in just one year: 2005-2006. If we take a leap of faith and apply those above fractions to the whole of Timbuctoo Bend, for which we don't have surveys in 2004 and 2005, then we can estimate that of the total amount of scour in the TBR (605,000 yds^3), ~193,000 yds^3 scoured 1999-2004, ~15,000 yds^3 scoured 2004-2005, and ~396,000 yds^3, the vast majority of it, scoured in 2005-2006. That then brings us to the overall gravel/cobble sediment budget for the TBR.

Apex Riffle Change Summary

		Net Scour (yds3)		Scour Intensity(yds3/day)		YRS+DCS	Water
Period	# days	1999 coverage	whole area	1999 coverage	whole area	Peak Q (cfs)	volume (km3)
1999-2004	1919	11046	---	5.8	---	25635	15354
2004-2005	319	879	76	2.8	0.2	42930	575
2005-2006	365	22626	26138	62	72	105100	1560

% of change was 32%, 2.5%, 65.5% for Apex Riffle using 1999 coverage, so 2006 accounted for 2/3 of the net scour over a 7-year period

Using the above fractions and assuming it holds for the whole Timbuctoo Bend, the estimated temporal distribution of scour 1999-2006 was

1999-2004: 193419 yds^3
2004-2005: 15392 yds^3
2005-2006: 396189 yds^3

Figure 40

EDR+NR+TBR Sediment Budget

In 2004 the USGS published a study in Water Resources Research, a premier journal, that reported on the total amount of sediment stored in Englebright Dam and the relative amounts of each size fraction. Using the data from that study, we were able to establish that on an annual basis, the load of gravel and cobble- not all sediment, but of gravel and cobble- into Englebright Lake is 61,600 yds^3/yr (Fig. 41). Zero gravel and cobble gets past Englebright Lake.

We don't know how much gravel and cobble comes in from Deer Creek, but Deer Creek itself is dammed and the bottom part of the river is all bedrock, so very little gravel and cobble must be coming in from Deer Creek. Similarly numerous small tributaries (such as the Schubert Watershed draining part of the UC Sierra Foothills Research and Extension Center land) that have not been monitored do not seem to be significant contributors of sediment relative to the contributions that were already reported as coming from the channel itself (Fig. 24).

The Blue Point Mine is the north-facing hillside of Meade Hill just downstream form the Narrows Pool on river left at the upstream end of Timbuctoo Bend. This hillside was historically stripped by gold-miners using hydraulic-mining methods. The sediment from this process filled the valley by ~50-70’, depending on location. It also may have completely blocked the flow of the Yuba River at the tributary junction during the dry season while mining was on-going. A 1906 photo taken by G.K. Gilbert shows the extent of sedimentation at Rose Bar at that time. That photo has been compared to a 2006 photo taken from nearly the same vantage point. Even though the creek draining the Blue Point mine basin has a small natural contributing area for runoff, it turns out that a man-made canal, Meade Canal, runs on the South side of Meade Hill

LYR Gravel/Cobble Budget

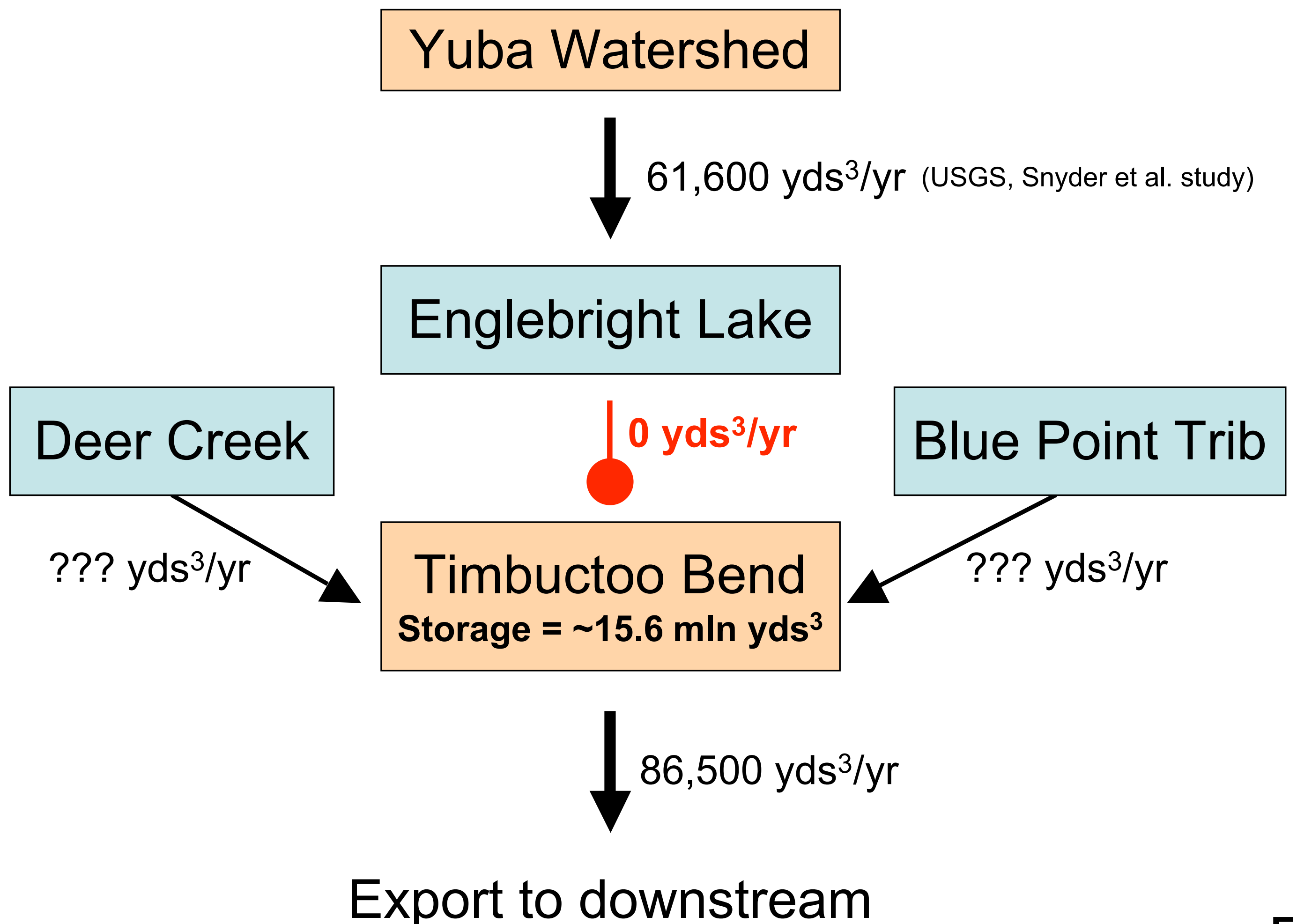

Figure 41

and contributes flow to the basin through a tunnel. During high flows the discharge can be high, though it is presently unquantified. Where the tunnel ends, scour begins. This water has created a deeply incised channel through the large hydraulic mining deposit flanking the Yuba River. The sediment load from this basin is presently unknown. Besides the erosion from the tributary, the Yuba River itself is meandering into the debris, and thus has formed a steep cutbank. This cutbank exhibited the highest rate of local erosion anywhere in Timbuctoo Bend 199-2006. It has been reported by local residents that this erosion contributes a notable amount of sand to the river during floods, but that has not been scientifically evaluated. Also, even though the local scour is intense and is visually impressive, the total volume of material liberated 1999-2006 was smaller than the total liberated by bed incision in the river itself and on the floodplain.

We know from the DEM differencing (1999-2006) that there was 605,000 yds^3 of sediment exported over that 7-year period. If you divide that volume by 7 years, then you get an average annual flux of 86,500 yds^3/yr. Also, based on observations of sediment in the bed and in cutbanks on the edges of floodplains and terraces, the majority of the sediment in the bed is gravel and cobble. Thus, you have a similar order of magnitude of material coming into Englebright Lake as it is going out of the TBR, but more is leaving the TBR. That suggests is that there is a net excess amount of sediment in the TBR associated with historic hydraulic mining. Also, it appears that the stored material is being naturally “evacuated” over a long-term period of incision, and that process is continuing right now, and will continue for a long time to come (depending on how Daguerre point Dam is managed).

Given that the TBR is incising, one wonders how long it would take to evacuate all the hydraulic mining debris stored there. That requires and estimate of the storage volume. We don't have the ability to excavate down, so an estimation method making some assumptions was necessary. To estimate the total volume of sediment stored in the TBR, we took the 3D relief map (Fig. 26) and created a horizontal plain tangent to the deepest pool in the reach. In addition, we created a deeper horizontal plane 30' below the bottom of the channel to roughly approximate the depth of fill we think is likely to be present there. These two horizontal bound what would be the likely minimum and maximum amounts of sediment fill in all of the Timbuctoo Bend underneath the river, respectively. Then we did a DEM difference between the relief map and each of the planes to determine the volume of fill, assuming vertical walls all around the edge of the valley domain. In reality, the sidewalls of the valley are sloped, so that is a source of uncertainty in the analysis. The estimate is that there is ~ 8-21 million yds^3 of sediment filling the TBR corridor. Using the best available method among all methods we have tried so far, the best intermediate estimate is 15.6 million yds^3. This estimate could be refined further by using an algorithm that tries to extrapolate the actual shape of the underlying bedrock valley, but that analysis was beyond the scope of study.

If you take the total storage estimate of 15.6 million yds^3 and divide it by 86,500 yds^3/yr, that yields an estimate of 180 years to evacuate the fill, all other things being equal and with a constant incision rate. However, that's very unlikely to happen as long as Daguerre Point Dam is present, because that dam imposes an artificial base level at a much higher elevation than the Feather River downstream would, since it is itself built on top of alluvial hydraulic mining deposits. It is not clear how much incision remains before the system is in equilibrium with the base level at Daguerre, but one key line of evidence is available in the distribution of knickpoints from the Narrows Pool down to Daguerre. Knickpoints are a key landform associated with the mechanism by which channel adjustment is occurring on the LYR. Their on-going dynamism (as report above and in more detail below) in the TBR shows that the system has not yet incised enough to reach an equilibrium slope. The number and distribution of knickpoints between the Highway 20 bridge and Daugerre are unknown.

TBR HYDRODYNAMIC STUDY

Now that we have quantified the large-scale geomorphic changes in the TBR, it is time to explain the hydrodynamic processes that control them. The key hydrodynamic questions are the flowing:

1) *What specific hydrodynamic processes are occurring at each unique range of flows?*
2) *Are there hydrodynamic mechanisms that explain why the pools are scouring the most and the riffles the least over time?*
3) *Why are medial bars growing?*

For each of these questions, I've already conjectured on the mechanisms, but in this section I demonstrate the mechanisms by using field measurements and two-dimensional (2D) hydrodynamic modeling. For example, earlier in this report, I conjectured that valley expansions and constrictions appeared to have played a role in the location and persistence of riffles. We have documented geomorphically that pools are scouring the most and riffles are scouring the least, and that everything is incising, except medial bars. So what mechanism can explain this observed geomorphic phenomenon?

In theory, the phenomenon driving riffle-pool self-maintenance in the TBR can be explained by a mechanism that my group and colleagues from Stanford University have published a study on in the journal Water Resources Research- it's called Flow Convergence Routing (Fig. 42). According to this mechanism, it is now understood that “self maintenance” of the relief between riffle crests and pool troughs through time depends on two scales of channel non-uniformity that induces flow convergence routing. During frequent low flows, when discharge is less than bankfull, longitudinal variations in the river’s bed elevation drive vertical flow convergence over riffles. That causes gradual incision, armoring, and a decrease in riffle-pool relief. Knickpoint retreat will be shown to be a prominent process under this condition. During infrequent overbank floods, lateral variation in channel and valley width drive flow convergence through pools. That causes them to scour down preferentially, thereby restoring riffle-pool relief. Forced pools associated with local non-streamlined bank protrusions (e.g. boulders, bedrock, or wood) also experience vortex shedding that causes local scour. Numerical studies that assess the presence of flow convergence routing are now being used in gravel bed river assessment and rehabilitation.

In the next part of the report I will use such methods to assess the presence of flow-convergence routing in the TBR during the May 2005 and New Year's 2006 floods. So first let's revisit the TBAR site during the May 2005 flood and look at it carefully in detail. The hourly peak discharge during the flood at the site was 42,930 cfs (combining Yuba and Deer Creek records). We have already covered the geomorphic changes associated with that event. Now we want to use field data and 2D modeling to simulate and analyze the processes that occurred and that were responsible for the changes we observed. The full detailed hydrodynamic analysis of this event was done by April Sawyer and is provided as Appendix 3.

The 2D hydrodynamic model that was used was the Finite Element Surface Water Modeling System (FESWMS) version 3.1, which was implemented within the Surface Water Modeling

Flow-Convergence Routing Hypothesis

The mechanism by which existing riffles and pools in an alluvial river maintain their relief is driven by strong channel non-uniformity that causes 2-stage scour:

1) flow converges in riffles causing them to armor, incise gradually, and diminish relief during frequent low flows;

2) flow converges in pools during infrequent floods causing rapid scour (see schematic below).

(from MacWilliams et al., 2006, WRR)

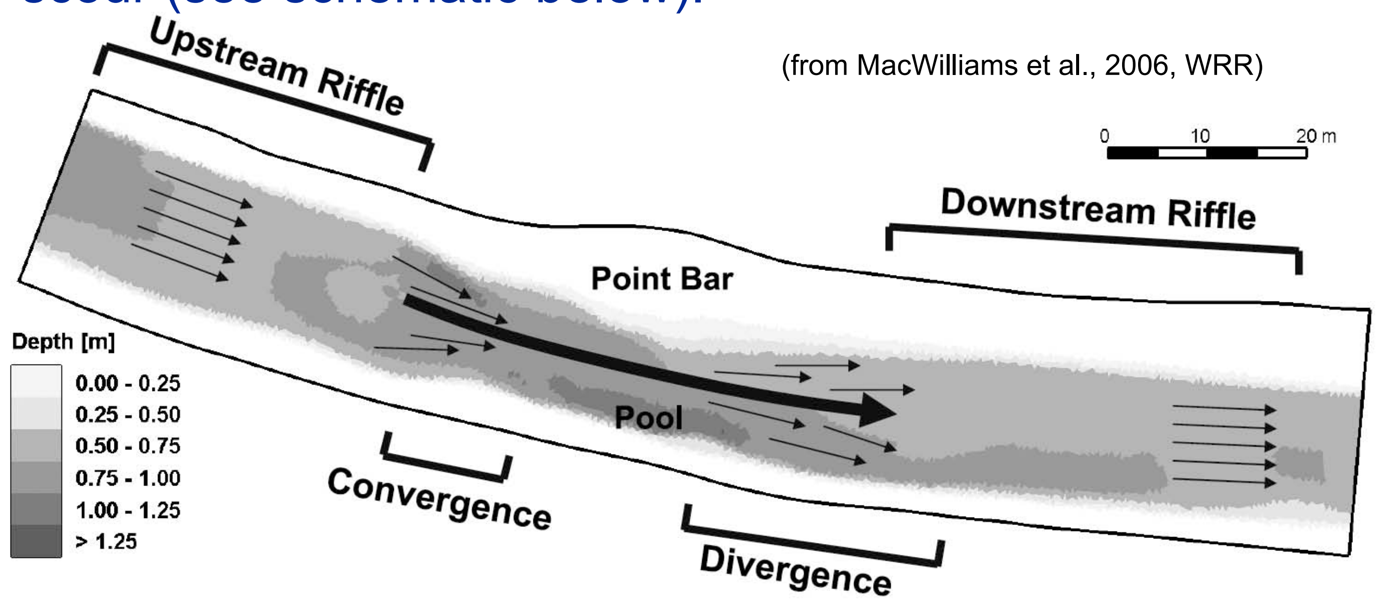

Figure 42

System (SMS) commercial software package. FESWMS assumes depth average flows and that flow is horizontal; flow can be lateral and longitudinal- you could have eddies and whirlpools, but you cannot have vertical boils of water up or whirlpools sucking down. So what the model does is it numerically solves the vertically integrated momentum and mass continuity equations using the Finite Element Method. It produces depth and depth-averaged velocity approximations for the “shallow water” (aka St. Venant) equations. FESWMS was used to predict depth and depth-averaged velocity for multiple discharges on the rising limb of the two major floods at the TBAR site.

To run the model you have to know the discharge into the upstream boundary of the site, you have to know the associated downstream water surface elevation, you have to have an estimate of the bed roughness, you have to estimate the eddy viscosity using an additional coefficient for stability of the model, and you have to have a high resolution digital elevation model of the site. All of these data were obtained as part of this project in support of the modeling effort. There are multiple detailed technical appendices in this report that present specifics of the hydrodynamic model, model set-up, and model validation.

To summarize the validation of the model, in essence, the model does extremely well at predicting water depth against observed water depth conditions (Figs. 43 and 44- top row of plots). Depth is typically within 5-10% of observed values. In contrast, the model does reasonably well (but not as good as for depth) in predicting depth-averaged velocity magnitude (Figs. 43 and 44- bottom row of plots). By reasonably well, what is meant is that the velocities are within +/- 20% of the observed values for the most part, though some spots, especially in very shallow water, can have much higher error (Pasternack et al., 2006). Observed water velocities in a river are often measured with point sensors that are heavily influenced by local

LYR 2D Model

2004 Depth and Velocity Validation

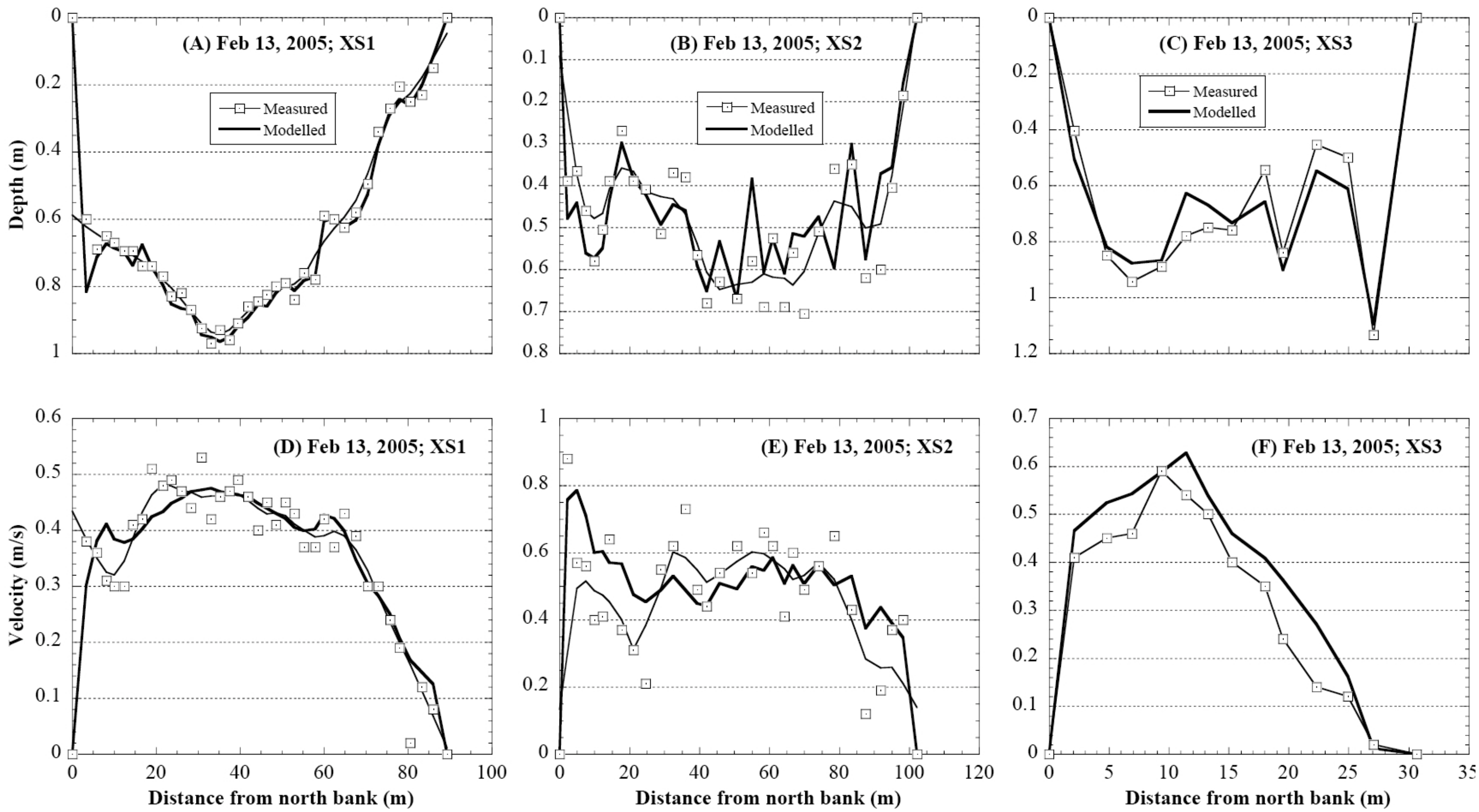

Figure 43

LYR 2D Model

2005 Depth and Velocity Validation

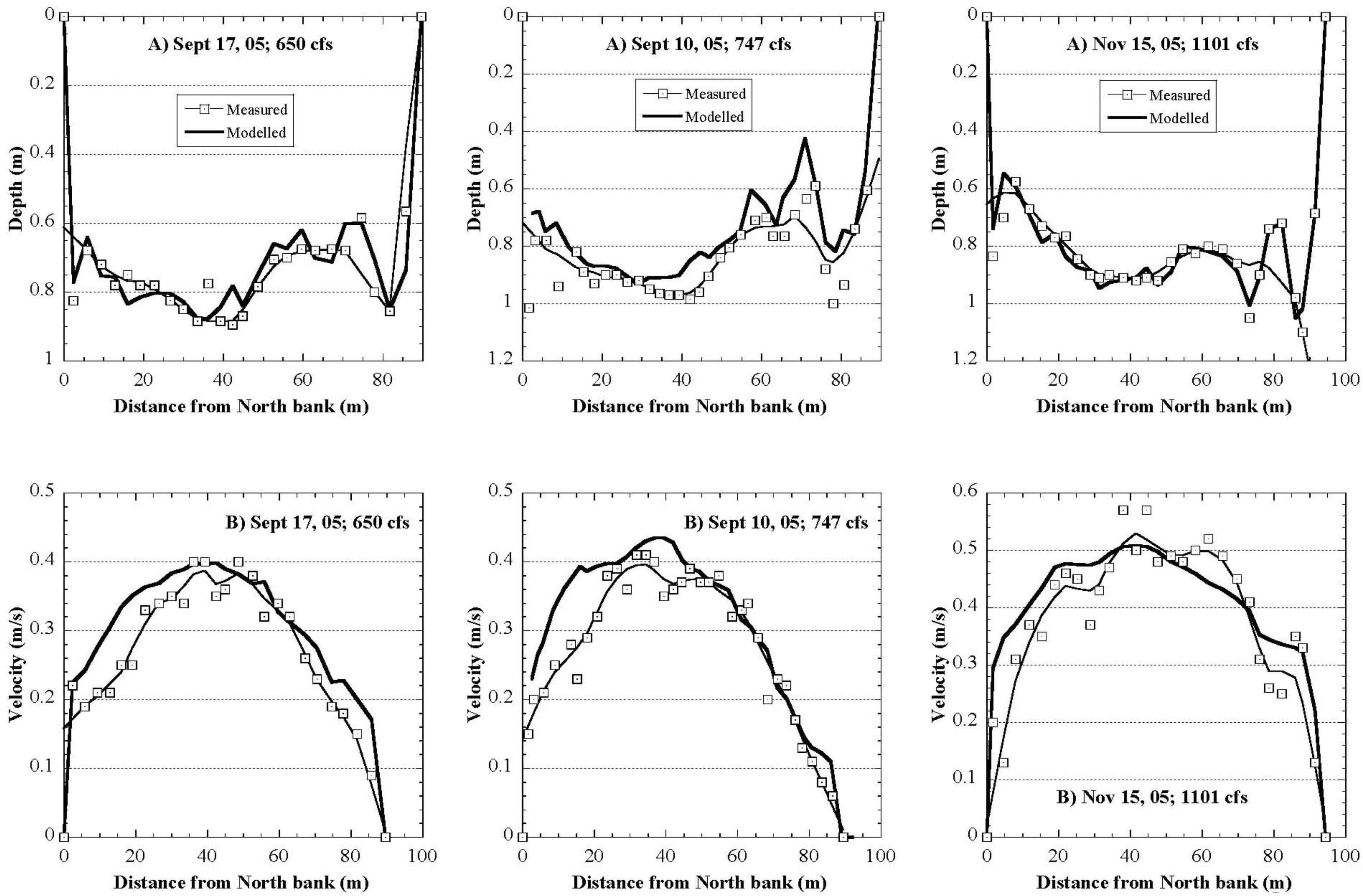

pebble clusters and other micro-scale phenomenon, what we call "sub grid scale" structures that create a lot of field noise. That kind of noise is not going to be represented in the model, so that creates the appearance of error in the validation effort. To account for that it helps to fit a smoothed curve to the field data and then compare the smoothed curve to the model predictions (Figs. 43 and 44). When you compare those, you see that the model captures the general cross-sectional flow pattern. Also, by making visual field observations, you can see that the 2D model resolves the eddies that are behind boulders and bank outcrops. Again, a highly detailed analysis of model performance is provided in Appendix 3.

May 2005 Flood Model

For discharges were modeled for the May 2005 flood. A low-flow associated with salmon spawning in autumn 2004 (830 cfs), the modern bankful flow (5620 cfs), a flow on the rising limb of the flood that was close to the pre-New Bullards Bar bankfull discharge (11600 cfs), and the flood peak (42,930 cfs). The results for the 5620 cfs are not illustrated here, but are presented in detail in Appendix 3. For the 830 cfs flow, you can see that the peak velocity occurs where the flow is constricted in the main channel at the riffle crest- where it is bounded by the island to the north and the floodplain to the south (Fig. 45). The flow width and depth decrease over the crest and a peak velocity of ~9-11 ft/s is reached there. You can see localized high velocities over the redd dunes upstream of the riffle crest. Also, the secondary channel has moderate velocities. Where the secondary channel and main channel converge downstream, two chutes crisscross and create moderate velocities through the run.

At Low Q, Scour is Focused at Riffle Crests

LOW FLOW (830 cfs)

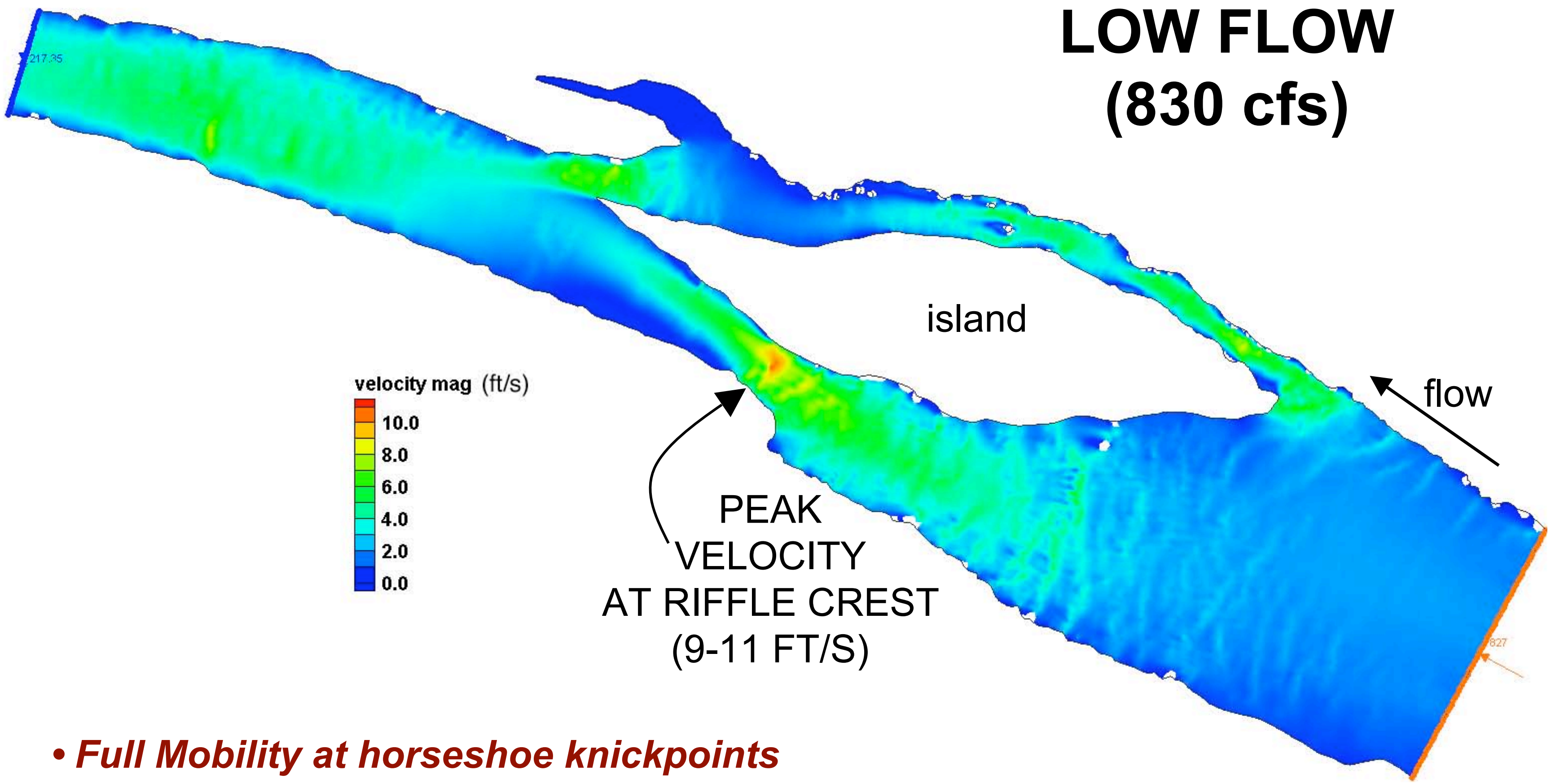

- ***Full Mobility at horseshoe knickpoints***
- ***"Partial transport" over rest of riffle--> bed armoring***
- ***No transport elsewhere***

Figure 45

In terms of the sediment transport regime (as predicted using the non-dimensional Shields stress metric- see Appendix 3 for methodology and details), the peak velocity over the riffle crest is associated with full bed mobility for a sediment mixture with a median grain size of 60 mm. That explains why the bed surface was so armored by spring 2005. Also, "partial transport" (defined as the condition in which only a portion of the grains on the bed surface ever move over the duration of a transport event) was predicted over the rest of the riffle, which was also observed to be somewhat armored. Everywhere else in the TBAR velocities were in the range of 0-4 ft/s, and therefore there was no sediment transport occurring at 850 cfs.

At 11,600 cfs the peak velocity remained in that same range (~8-10 ft/s), but it shifts its location (Fig. 46). Instead of being at what was previously a confined riffle crest, that riffle crest is no longer confined because the island is flooded and part of the floodplain is flooded there too. Now, the most constricted part of the river is downstream in the run, with the high-relief floodplain to the north and the floodplain/bedrock outcrop to the south. Now that constricted location in the run has the peak velocity and elsewhere velocity is in the range of 4-6 ft/s. Correspondingly, there is full bed mobility in the run, partial transport in the rest of the bankfull channel, and little to no transport on the floodplain.

During the peak hourly flow of 42,930 cfs, there was another shift in the location of peak velocity. Now it is located upstream in the pool and riffle entrance units (Fig. 47), though interestingly it remains ~10-12 ft/s. Down where the riffle is located and in the center of the run there are higher velocities than in those units at 11,600 cfs (~8-9 ft/s). The floodplain has velocities of 4-8 ft/s, with lower velocities in the willows. In terms of the sediment transport regime at the flood peak, there is full-bed mobility in pools and partial transport in the rest of the

At Q_{bf}, scour is focused in runs

ABOVE BANKFULL FLOW
(11600 cfs)

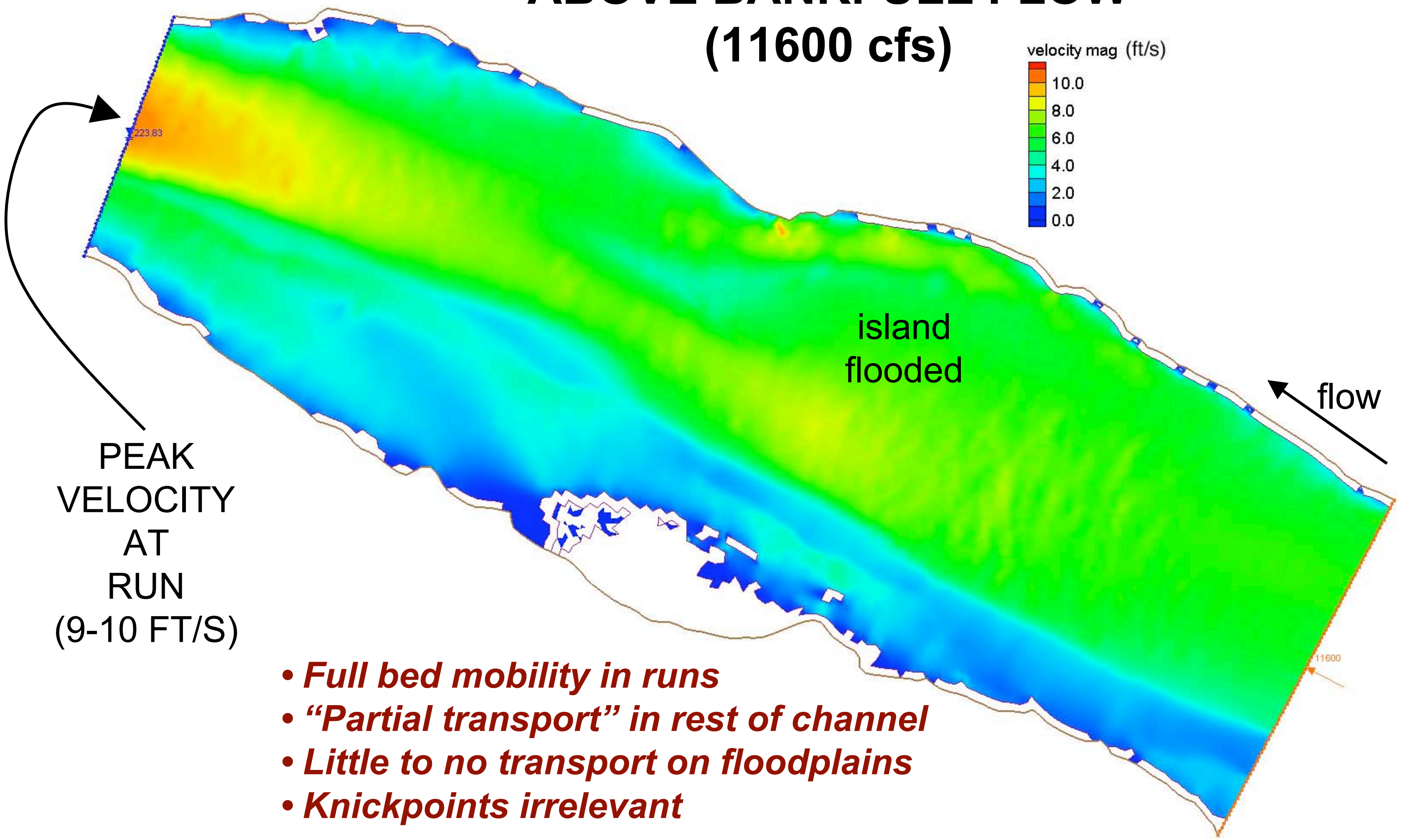

- ***Full bed mobility in runs***
- ***"Partial transport" in rest of channel***
- ***Little to no transport on floodplains***
- ***Knickpoints irrelevant***

Figure 46

In a 4.4-yr Q, Channel Relief is Rejuvenated

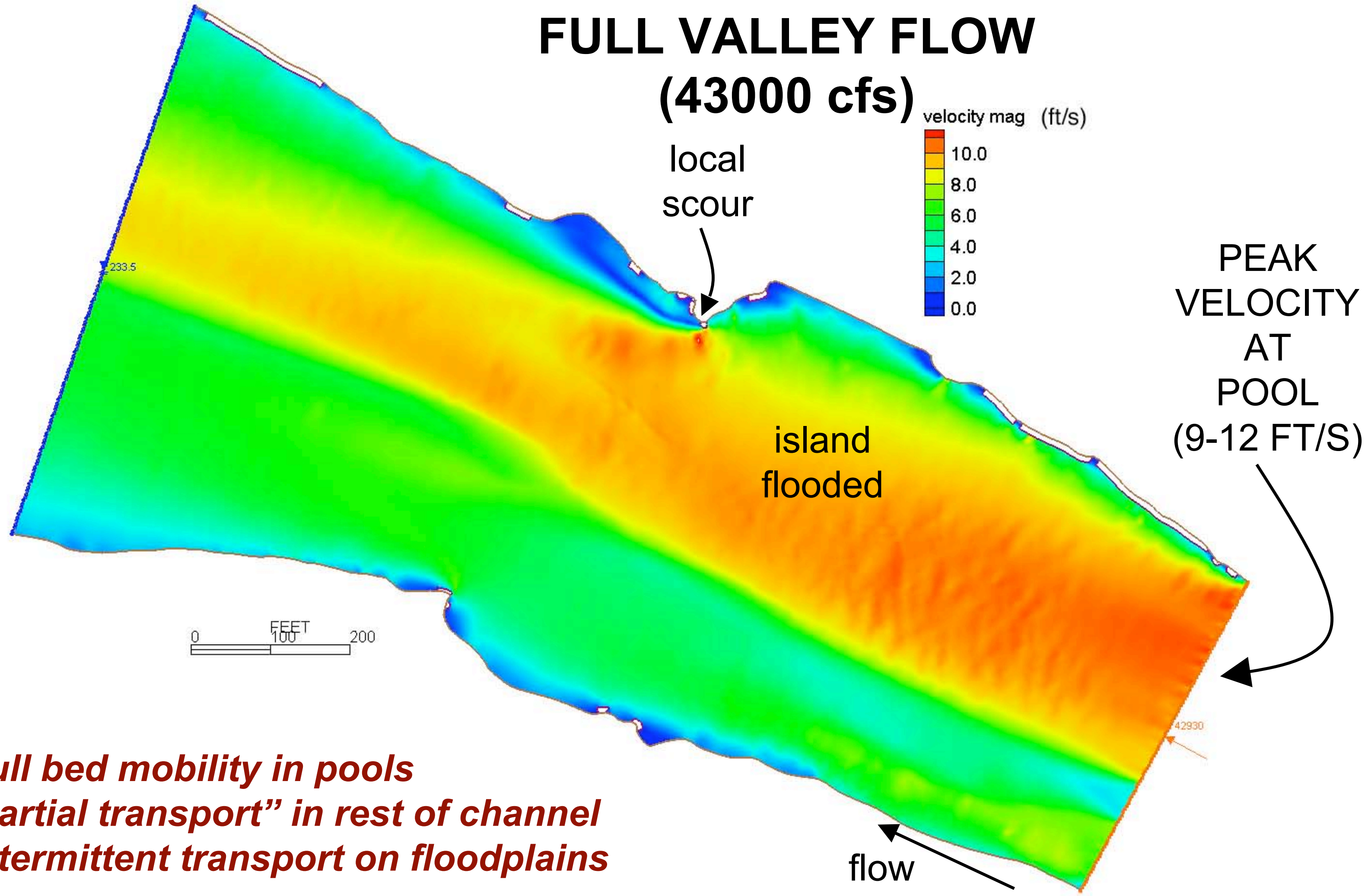

- ***Full bed mobility in pools***
- ***"Partial transport" in rest of channel***
- ***Intermittent transport on floodplains***

Figure 47

bankfull channel, with intermittent transport on the floodplains when turbulent bursts around willows and other structures cause such movement.

The above characterization of flood hydrodynamics based on 2D modeling provides detailed insight into the scour mechanisms present throughout the flood. However, in order for it to be believed, some amount of model validation associated with sediment transport is necessary. What we can do to gain confidence in the model predictions is evaluate the validity of the Shields stress predictions from the 2D model for the peak of the flood by taking advantage of the 2004-2005 DEM difference data that was already presented (Fig. 38). So when we make a plot of Shields stress on the X-axis and observed elevation change on the Y-axis, we can see whether there is an association between the model predictions and actual observed changes to the river (Fig. 48). To make this more understandable, we stratify the river according to morphological units. For example, in the pool there were two distinct zones of channel change and Shields stress (Fig. 48, upper left). There is a zone with a Shields stress greater than 0.045 in which the observed changes in elevation are all scour- anywhere from 0-1 m of scour. When the Shields stress is below 0.045 there was some deposition and some erosion. The latter was interpreted to be occurring, because during the long period of low flow, some amount of fine sediment likely settled in to the pool. Thus, there is some area in the pool and particularly along bedrock outcrops, along willows, and where there is finer sediment, where you do see some scour below 0.045. That scour does not occur when Shields stress is below 0.025. So there is a band in there where we see some transport at relatively low Shields stress. Nevertheless, the area where you have only scour and no deposition is where the Shields stress is above 0.045.

In the riffle area we have two dramatically distinct areas, there is an area where the Shields stress is above 0.045, just like in the pool, and in that area you see either no change or

Modeled Shields Stress vs. Observed Scour Depth

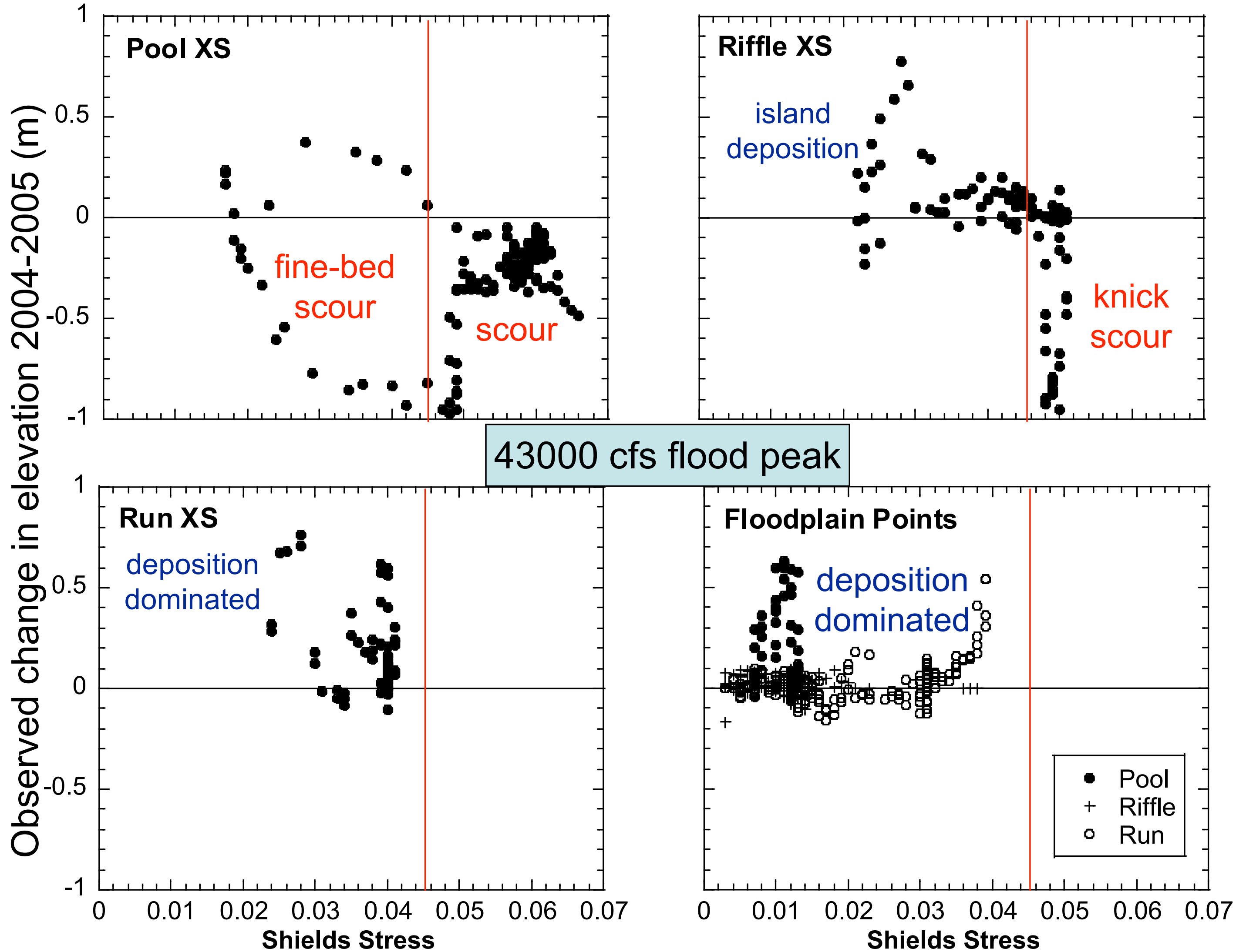

Model-predicted Shields stress value for mean channel D_{50} **Figure 48** scour up to 1 m. Then, when the Shields stress in the riffle cross-section is less than 0.03 you see that that there is deposition adjacent to or on the island or secondary channel. So the rifle shows two distinct zones where the Shields stress is predictive of the net change- either incision at very high Shields stress or deposition at very low Shields stress.

The run downstream had Shields stresses ranging from 0.02-0.04 during the flood peak. As a result it was predominantly dispositional. That is interesting, because at 11,600 cfs higher peak velocities were located at this cross-section. However, at the flood peak the velocity was lower there, causing Shields stress to be lower. The net effect over the flood hydrograph was significant deposition.

The floodplain was also predominantly depositional, although there were two distinct areas. One area was in the willows, where there was moderate Shields stress (0.034-0.04) and sediment deposition. That happens because the willows act as baffles in the flow causing significant turbulent fluctuations and rapid sediment deposition. The other area was out on the open floodplain, where Shields stress was very low (~0.01) and there was deposition.

In summary, the field observations of channel change from the May 2005 event ar ein line with the underlying mechanisms indicated by the 2D model. Where the 2D model predicted Shields stresses >0.045, scour dominated. Where the model predicted Shields stresses <0.03, deposition dominated. In between those threshold is the domain of partial transport in which both deposition or scour are possible, but in very small amounts overall. The one exception being in the lines of willows, where significant deposition will take place during partial transport. So what the model is capable of doing is predicting where there will be scour and where there will be deposition. Unfortunately, there is not a strong correlation between the magnitude of Shields stress and the magnitude of that scour or deposition. In other words, there is no simple linear relationship there, and that's because the effectiveness of a given Shields stress magnitude is different in each morphological unit. So you have to stratify the conditions by morphological unit and then you can see these outcomes popping out.

New Year's 2006 Flood Model

A 2D hydrodynamic model was made to investigate the New Year's 2006 flood, based on the 2005 river bed DEM. The full details about this model, its validation, and its results are presented in Appendix 1. The discharges that were modeled in this case were 755 cfs (21.4 m^3/s), 1223 cfs (34.6 m^3/s), 9,457 cfs (267.8 m^3/s), 23,140 cfs (655.3 m^3/s), 35,260 cfs (998.4 m^3/s), and 109,090 cfs (3089.2m^3/s). The same tools and methods were used as previously described for the May 2005 flood model, and the full details are presented in Appendix 1. The primary aim of this modeling effort was to look for further evidence of flow convergence routing and the nature of the sediment transport regime in TBR, but over a much wider range of flows than possible form the May 2005 flood. In the New Year's 2006 flood model results, we see a similar velocity pattern as in the May 2005 event for the <40,000 cfs flows (Fig. 49). Water depth and Shield's stress results for the different discharges are shown in Figures 50 and 51. As before, the peak velocity is focused on the riffle crest at the low flow and in the run at moderate flows. For the May 2005 model, there was no data to simulate flows of 15,000-40,000 cfs, but here we do have a simulation at ~35,000 cfs (Fig. 49E). At that flow, the velocity is not differentiated downstream, but is instead about the same through all of the units in the center fo the channel. The primary gradient at this flow is lateral, not longitudinal. This is a key state of the river, because in this condition all channel units are experiencing a similar sediment transport

New Year's Flood Model Results

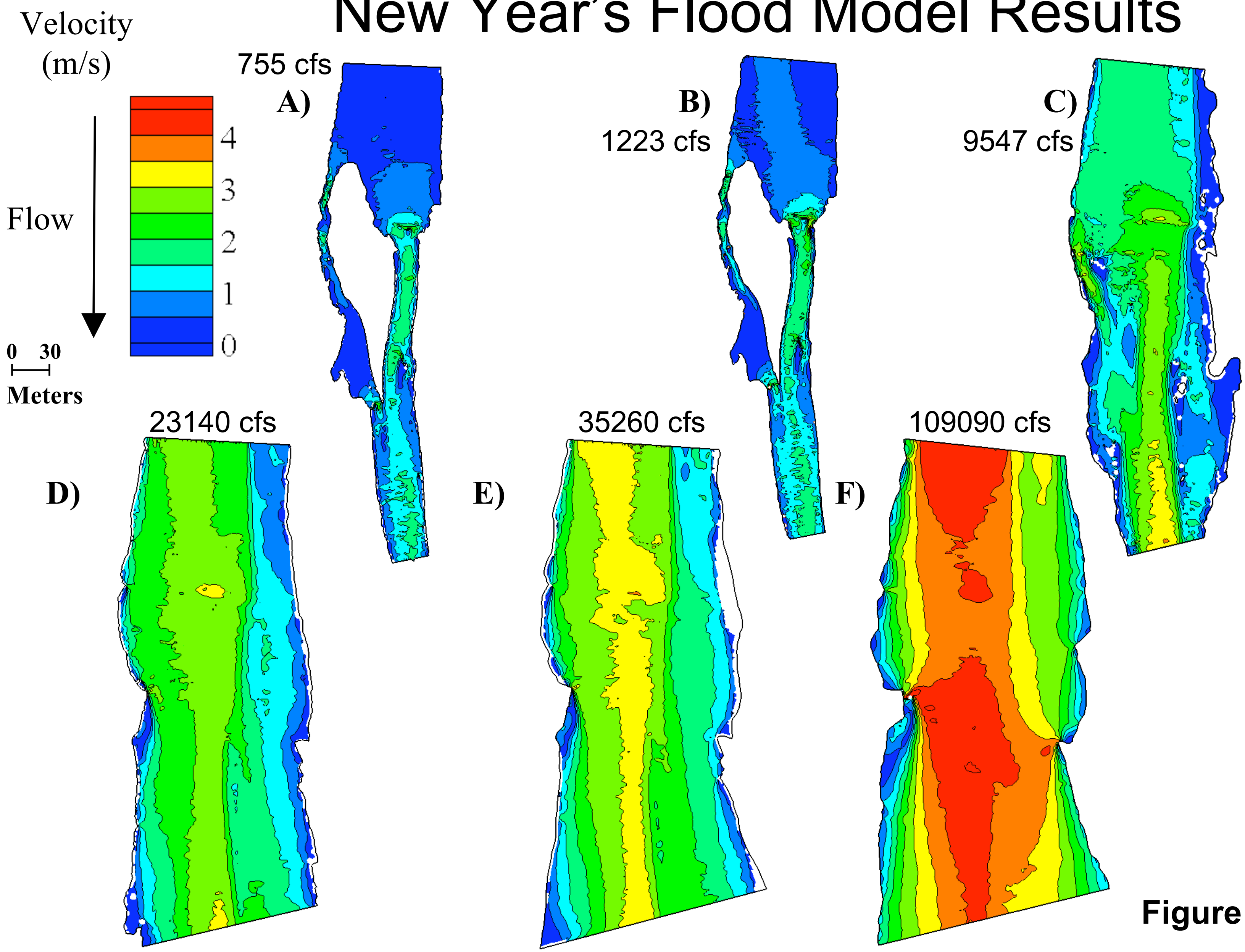

Figure 49

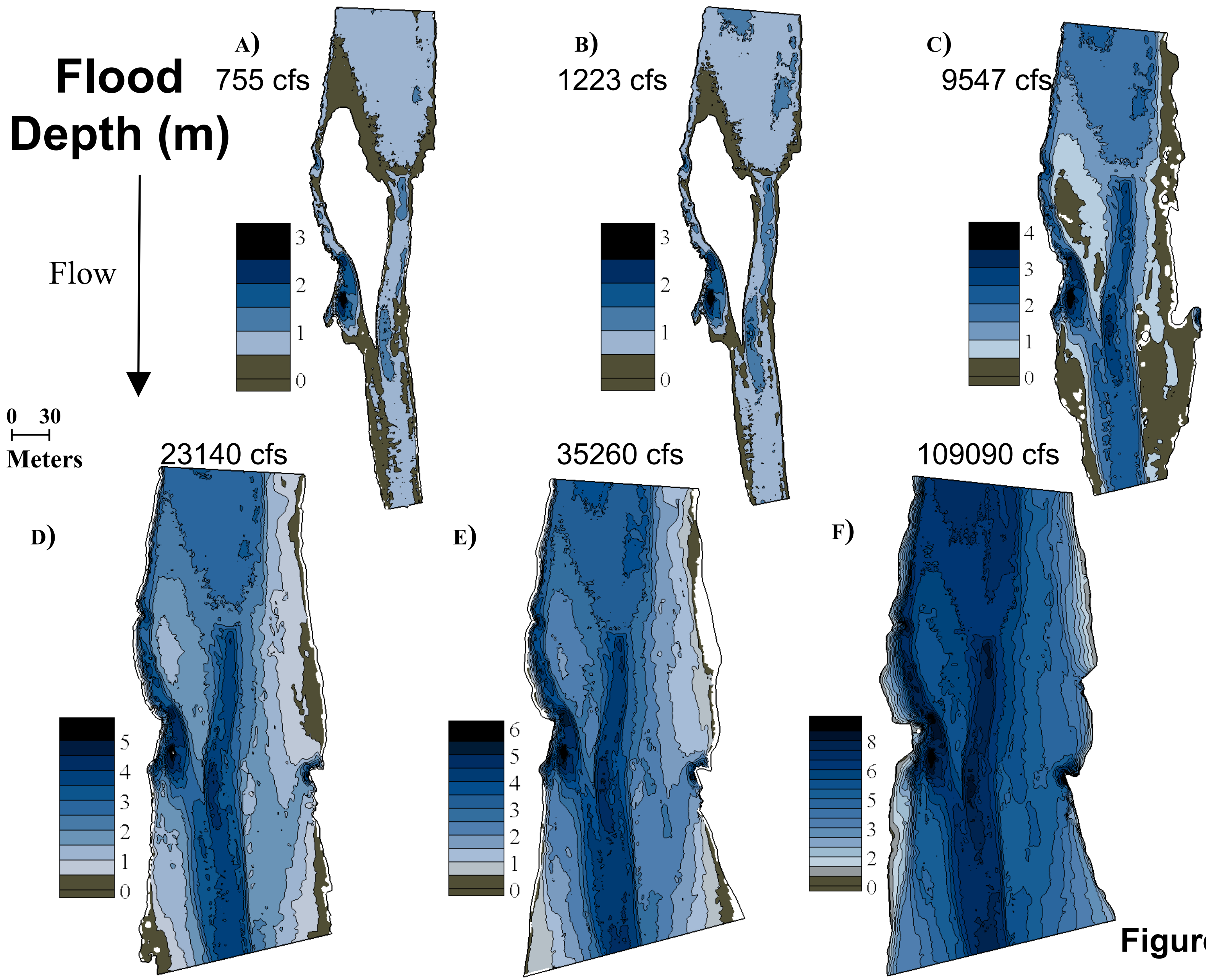

Flood Depth (m)
Flow
0 30
Meters
A)
755 cfs
3
2
1
0
B)
1223 cfs
3
2
1
0
C)
9547 cfs
4
3
2
1
0
23140 cfs
D)
5
4
3
2
1
0
35260 cfs
E)
6
5
4
3
2
1
0
109090 cfs
F)
8
6
5
3
2
0

Figure 50

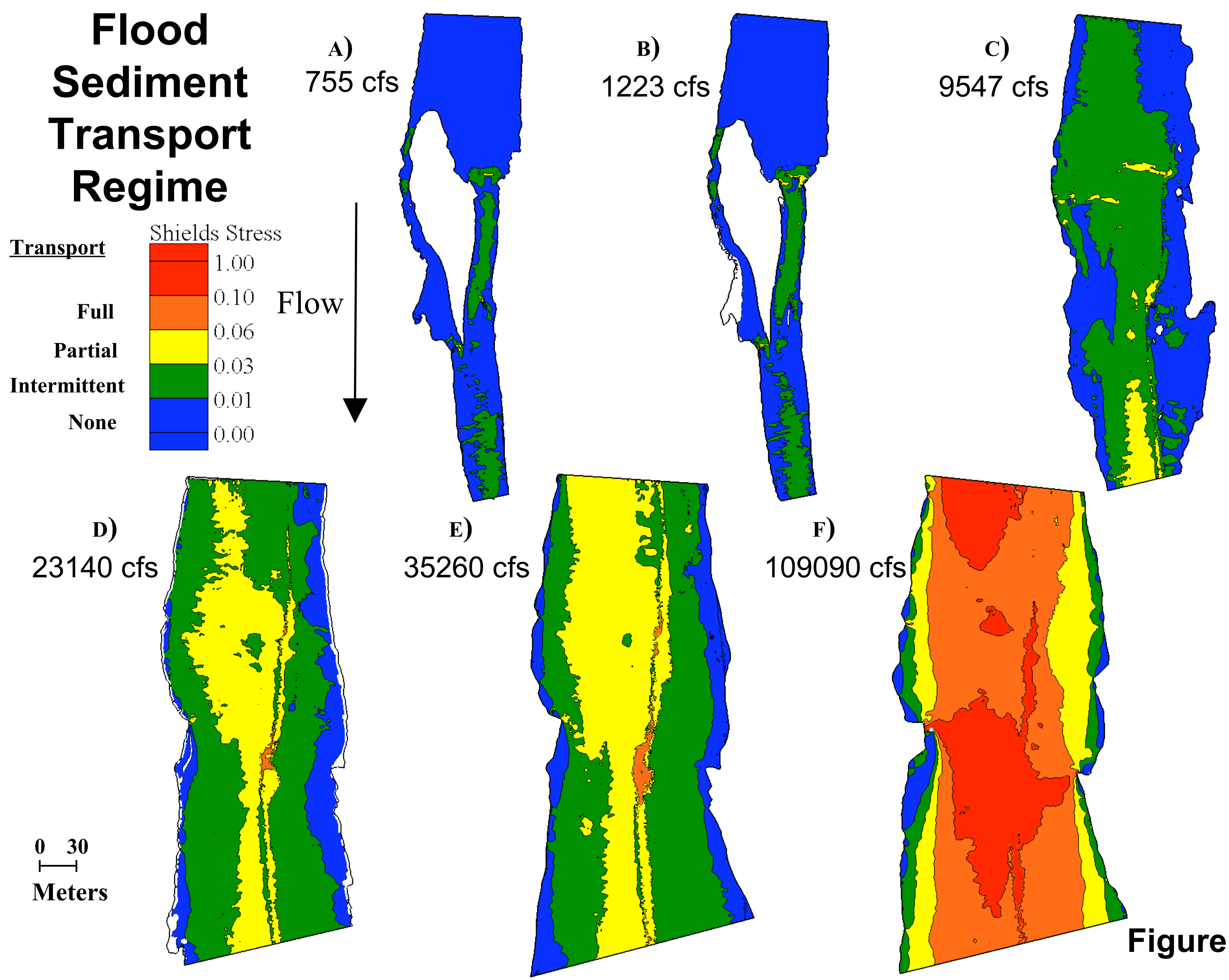
Flood
Sediment
Transport
Regime
Transport
Shields Stress
1.00
0.10
0.06
0.03
0.01
0.00
Full
Partial
Intermittent
None
Flow
A)
755 cfs
B)
1223 cfs
C)
9547 cfs
D)
23140 cfs
E)
35260 cfs
F)
109090 cfs
0 30
Meters

Figure 51

regime. There is no data to make simulations between 36,000-100,000 cfs for the New Year's 2006 flood, but we already know from the May 2005 model that at ~43,000 cfs conditions change again and peak velocities become established over the pool and riffle entrance. From the New Years 2006 flood model we can go beyond that and see that at the peak discharge of 109,000 cfs, the peak velocity is differentiated, but not as much as at 43,000 cfs. At 109,090 cfs, scour is most intense in the pool upstream, between bedrock outcrops where forced pools and chutes are located, and in the downstream run.

There is another very important result from the simulation at 109,000 cs, and that is the finding that the peak velocity is much higher than at any other discharge simulated. Whereas the peak velocity did not change over 750-43,000 cfs, it does go up to a higher magnitude by 109,000 cfs. What that means is that as discharge increases from 750 cfs to 43,000 cfs, the primary hydraulic effect is an increase in channel width and depth, with little change in the range of velocities. However, once the valley width is full of water, then the model is indicating that further increases in discharge causes a disproportionately rapid increase in velocity. That is important, because it suggests that the magnitude of sediment transport shifts sharply after the valley is full of water. Unfortunately, there is a lack of stage-discharge data for the 45,000-100,000 cfs range to enable simulations to pin down the exact nature of the increase in peak velocity.

To summarize the results of 2D hydrodynamic modeling of flood events in TBR, both models confirm that sediment transport is *always* occurring on the LYR, but that the locations and magnitudes of transport are different at different discharges: riffles scour at low flow, runs scour at intermediate flows, and pools scour at high flows. The estimated discharge ranges delineating these domains was previously reported in the hydrology section of the report. The key conclusion is that there is not a single discharge at which sediment transport begins, but that sediment transport occurs in different geomorphic units depending on the flow. Once the valley is full of water, then sediment transport in the bankfull channel appears to be at a much higher rate, but with a peak rate in pools.

Knickpoint Mechanics

According to the 1999-2006 DEM difference analysis for TBR (Fig. 24), pools preferentially scour at the highest volumetric rate of any morphological unit, while riffles incise at a much lower rate. Meanwhile, the 2D modeling studies showed that the mechanism responsible for that spatial differentiation of scour was indeed flow convergence routing with riffles scouring at low flow and pools scouring at high flow. Also, the 2004-2005 DEM difference analysis of the TBAR site captured a massive knickpoint retreating and incising through the riffle there. These three lines of evidence suggest that a special 2-stage mechanism is occurring, involving pool scour at high flows and riffle scour at low flows. Further, the riffle scour appears to involve knickpoint processes. In a regulated river such as the LYR, the absence of fresh sediment coming in from upstream due to the presence of a dam can cause waves of channel incision driven by upstream knickpoint migration. I have seen this demonstrated experimentally in large laboratory sediment flumes many times. Such migration through riffles is promoted in TBR by the extended periods of low flow when the riffle crest functions like a supercritical weir and is the focal point of extreme peak velocities.

To evaluate knickpoint mechanics, we performed comprehensive observations at two riffles in TBR during summer 2007- the TBAR site and at the Parks Bar Riffle (PBR). The discharge during this time was in the range of 1000-1600 cfs. At TBAR there was one primary horseshoe-shaped (in top view) step that was divided from the thalweg chute, and that is what we studied at that site (Fig. 52). At PBR, the knickpoint was divided into three distinct horseshoe-shaped steps across the riffle, and we investigated the one on river left the most and also the one on river right, but not the one right down the center, due to time constraints. So there were three knickpoints that were observed.

In each of these cases we took a 14-foot whitewater raft and anchored it to three rock clusters using heavy-duty rock-climbing ropes- one on river left, one in river center, and one on the river right (Fig. 53). Then we used the three long ropes to lower the raft downstream in a very controlled fashion to put the observers into the knickpoints. A Mash-McBirney velocity meter was mounted onto a specially sized and weighted prism pole to measure the velocities at the water surface, at mid-depth, and near the bed. There is no reason to expect a logarithmic vertical velocity profile under the rapids, so that is why a uniform spacing was used with these three sampling locations. By making these measurements in a pattern all around and through each knickpoint, we obtained enough data to do a spatial interpolation and arrive at velocity field maps (Fig. 54).

What we found in the velocity mapping was that the peak velocities at the surface and at the mid-column depth were in the range of ~9-12 ft/s. That is exactly the same range that the 2D models had predicted for peak velocities over other riffle crests at similar low discharges. A little bit faster at the maximum, but still right in that same range. That was a nice verification of model predictions. We also found that near the bed, the velocities were quite spotty, because it was very hard to tell if the sensor was going behind, on top of, or in front of large cobbles or gravel clusters present on the bed. Thus, there were a wide range of velocities at the bed itself.

Riffle Crests Evaluated

TB Apex Riffle

Parks Bar Right Riffle

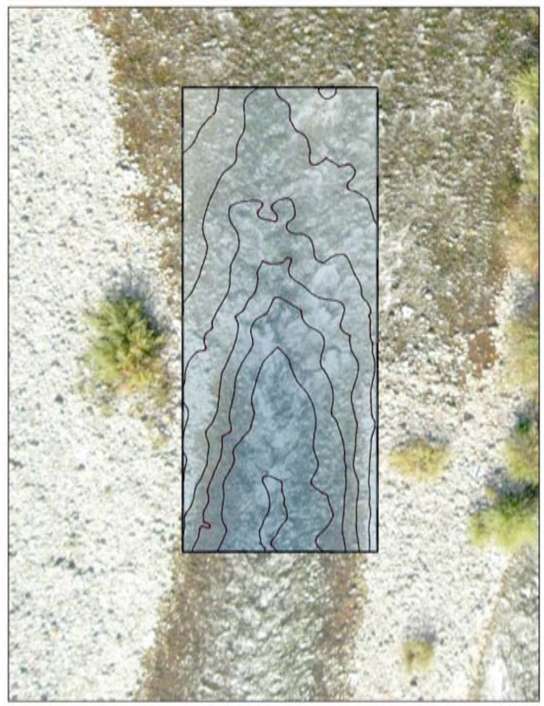

Parks Bar Left Riffle

Figure 52

Knickpoint Velocity Measurements

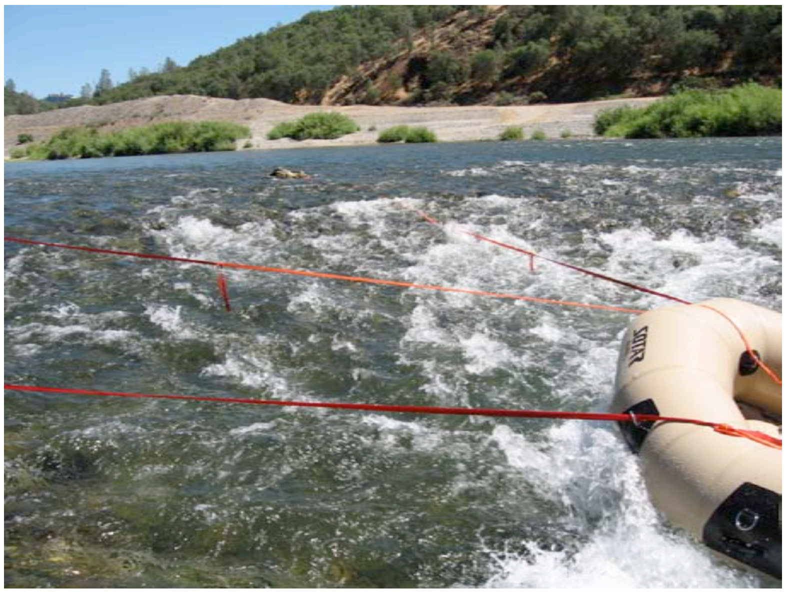

Anchored raft above riffle and used ropes to lower it downstream into knickpoint

Measured velocity at surface, mid-depth, and near-bed.

Figure 53

Knick Velocity Results

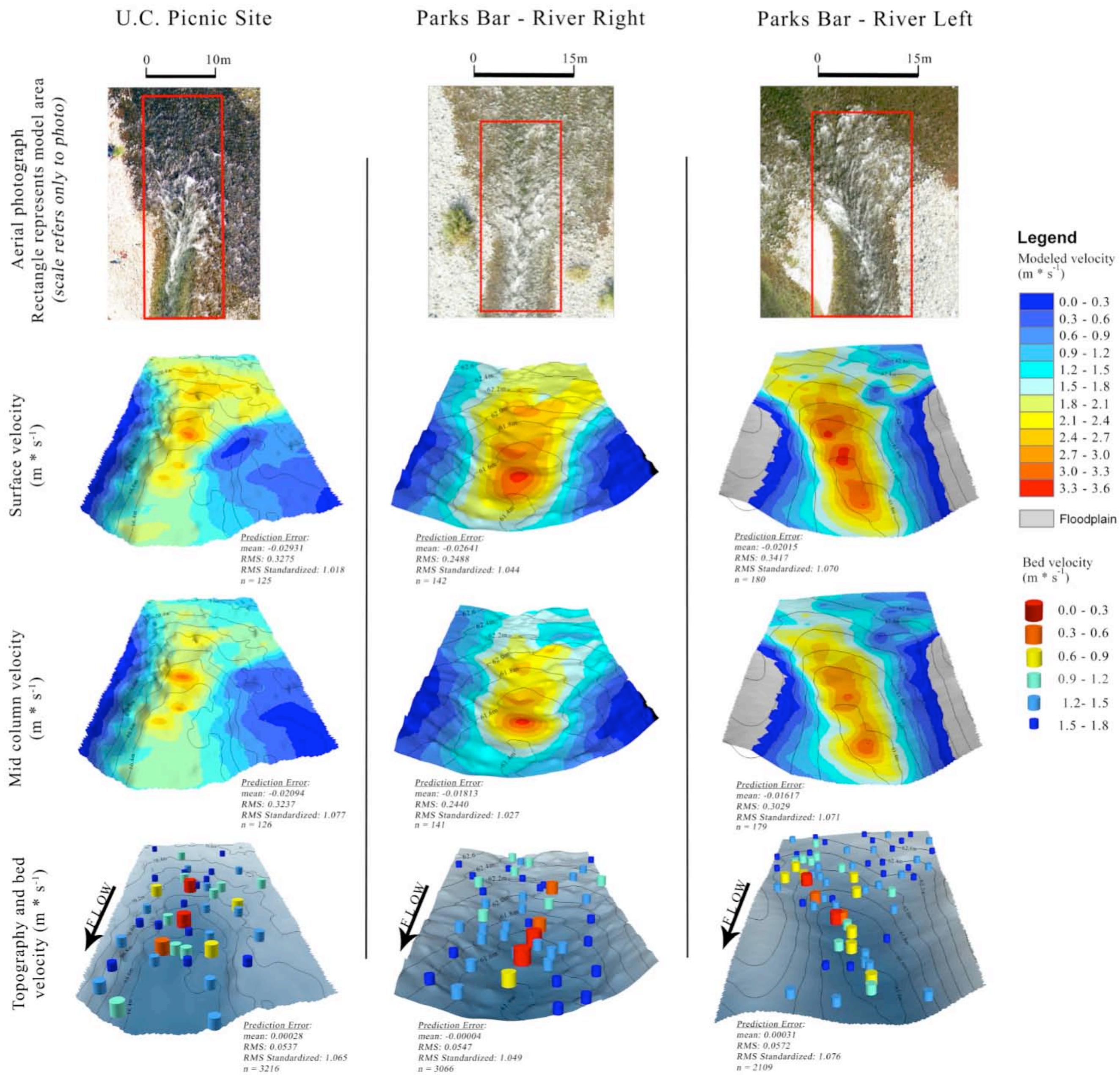

Figure 54

In addition to making velocity measurements, we were able to make very unique measurements in which we directly observed drag and lift forces on the bed in the river left knickpoint at Parks Bar Riffle. This was done using new technology and methods that I have pioneered at UC Davis in collaboration with technologists at the University of Minnesota (Pasternack et al., 2007). Originally I adapted a commercially available a six-component (i.e. 3 forces and 3 torques) strain gauge sensor used by the U.S. Navy in submarine studies to measure drag and lift forces below high-energy waterfalls. That technology was easy to re-adapt for use in determining if knickpoints in the LYR were actually experiencing erosive shear stresses on the beds at low flow, both on the knickpoint and downstream in the chute.

The details of the technology used and field methods are published in Pasternack et al. (2007). Prior to going to the river, the sensor was calibrated in the lab to yield measurements accurate to within 7% in their raw readings. Sensor accuracy increases as the applied force increases, so a lever was used with the sensor to amplify the signal. The sensor was mounted on a specially sized and weighted prism pole. I waded into the knickpoint with the sensor and made the measurements manually to obtain two longitudinal profiles. Insufficient time was available to develop a boat-mounted sensor for this study. Data were collected at 10 Hz and averaged over two minutes.

After processing the raw signals, the results of drag and lift dynamics are reported in the form of forces per unit area, in SI units of Pascals. As a reference for the magnitude of these units, the critical shear stress typically required to move a 1 m bolder in an unconsolidated bed with a friction coefficient of 0.1 and a critical shield stress of 0.03 corresponds with a drag force of about 500 Pa. So if the knickpoint experiences forces of ~500 Pa, then the flow is eroding and exporting the gravel and cobble with no difficulty. As another reference, sand moves at ~1 Pa.

The bed stress measurements at Parks Bar Riffle confirmed that river bed under the knickpoints is being actively scoured during low flows (Fig. 55). At the top of the knickpoint we observed drag stresses on the order of 340-500 pascals, so already enough to erode gravel and cobble <1 m in diameter. As the flow converges through the horseshoe knickpoint, the maximum drag stress on the backside of the riffle was 1,020 Pa. Where all the flow converges together, there was an even higher peak of 1,774 Pa. That is ~3x the drag stress necessary to move a 1-m boulder. Downstream in the chute after the flow converged and where standing waves were present we measured drag stresses of 848 and 1,166 Pa. Thus, we have directly observed the drag stress on the bed in the middle of a knickpoint at low flow on the LYR and those drag stress measurements range from ~ 300-1800 Pa. That demonstrates conclusively that there are forces strong enough at low flow to cause knickpoints to migrate.

The last piece of evidence in this part of study is the DEM differencing at knickpoints (Fig. 56). For the TBAR site, there are topographic maps in 2005, 2006, and 2007. In 2005 there was no knickpoint present at the particular location that then emerged in 2006. That new knickpoint was observed to grow in 2007 during low flows. Overall, there was a net scour of ~400 m^3 of sediment to produce the knickpoint, and then during low flows an additional ~56 m^3 of sediment was measured to be eroded out of it. In the Parks Bar knickpoints, the data is from summer 2006 and summer 2007. At those two sites, there was predominant scour of up to 0.4 m depth at the top of the knickpoint and then some scour in the center of the knickpoint with some deposition on the flanks of it.

Considering all the hydrodynamics research on the study, we can summarize the findings thusly:

Knickpoint Drag Force Results

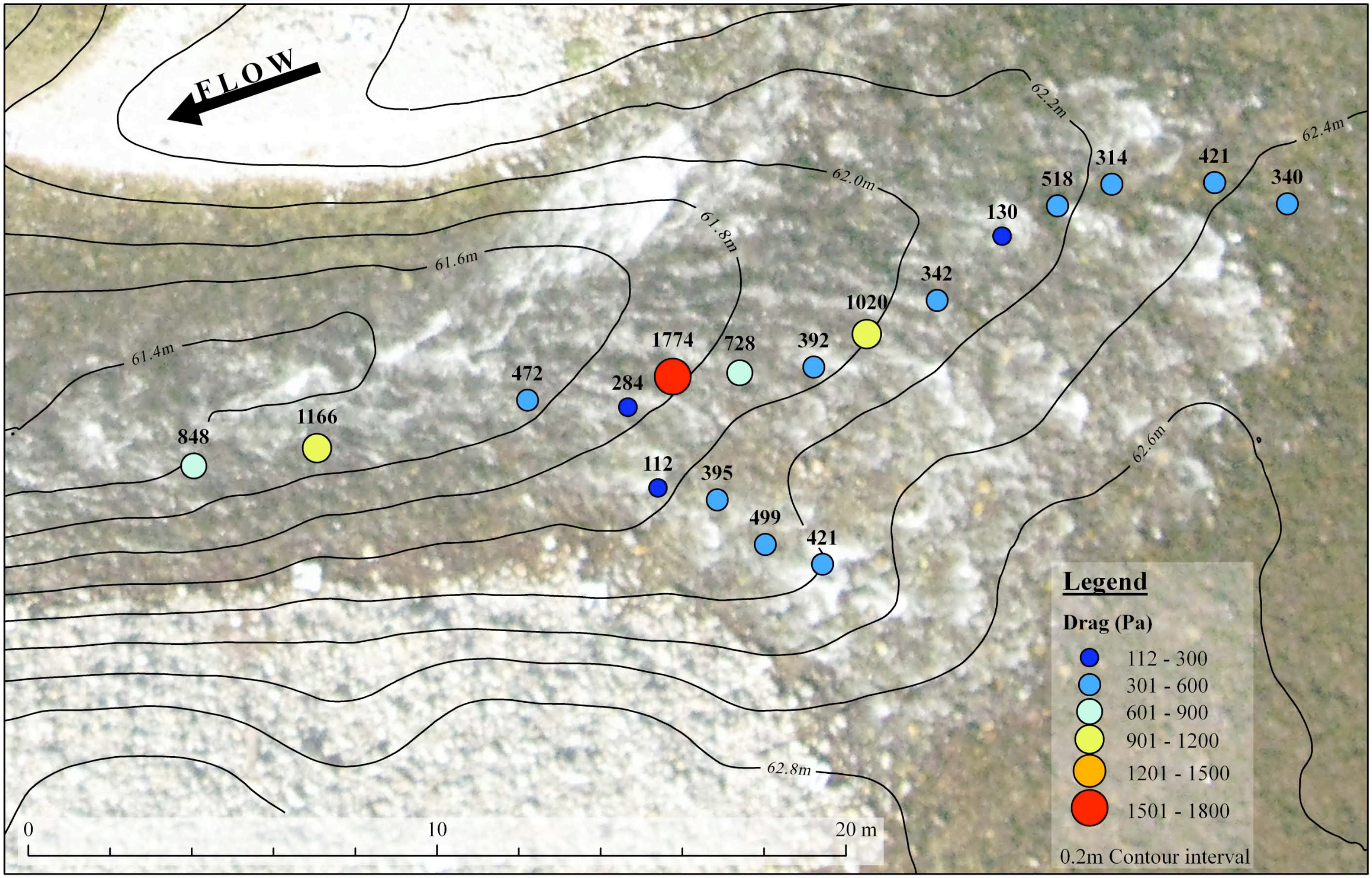

Figure 55

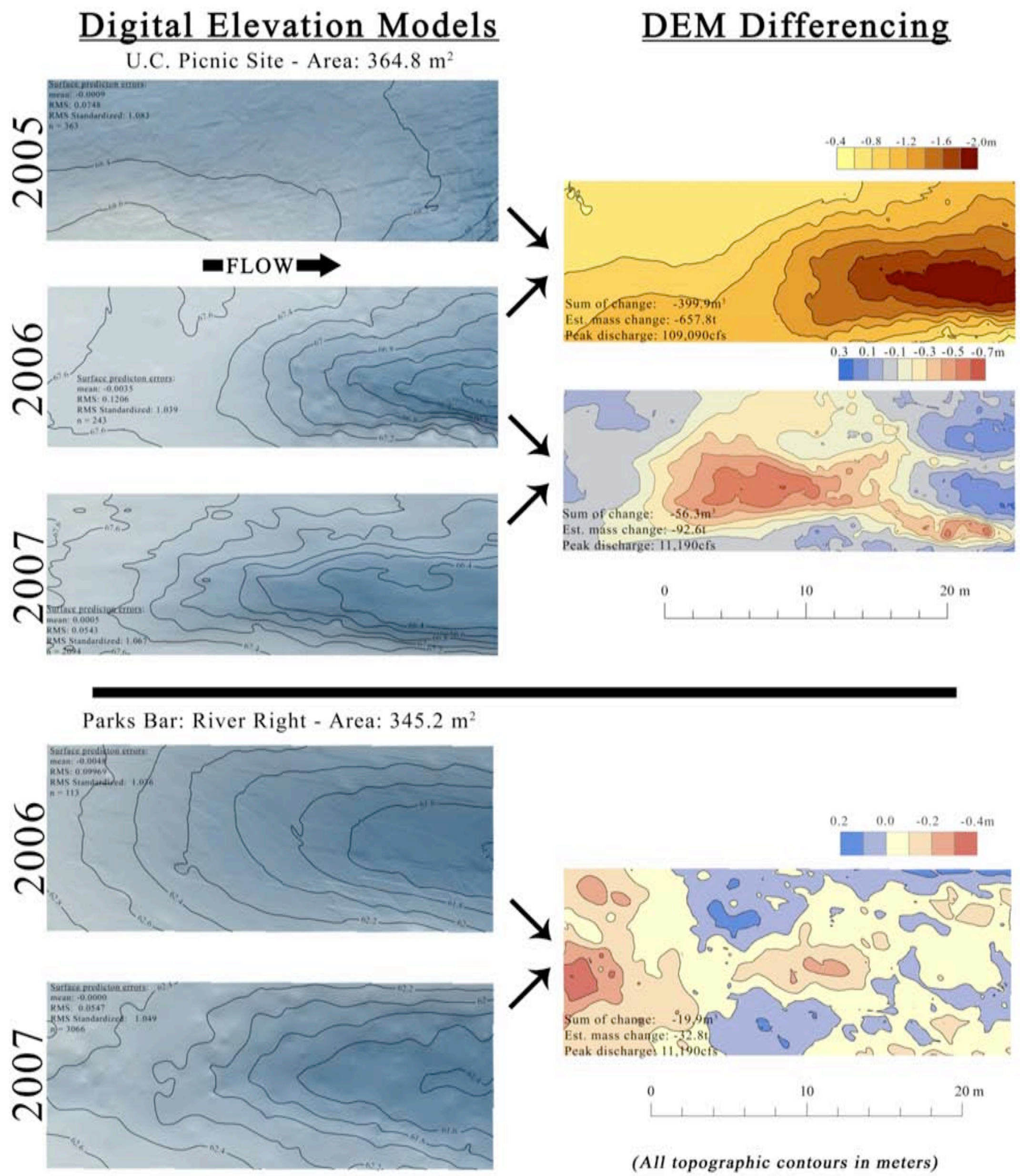

Knickpoint Topographic Changes

Figure 56

1) *2D models of two channel configurations and two flood hydrographs produced predicted low-flow peak velocities over riffle crests, and those were in the range of 9-11 ft/s. Direct observations of velocities through riffles found velocities also in the range of 9-12 ft/s- a little higher in the exact peakvalue , but in including the same range between both models and observations.*
2) *Unique, direct measurements of hydraulic stresses on the river bed through riffles demonstrated that the stresses are high enough to erode and export sand, gravel, cobble, and even boulders. Those experimental measurements are backed up by the results of DEM differencing, which showed that in fact the riffles did scour in 2007 under the same low flows as the hydraulic measurements were made.*
3) *Both 2D hydrodynamic models and geomorphic analyses of the river corridor DEM demonstrate that pools are scour ing more than riffles, with that scour primarily taking place during major floods of >40,000 cfs.*

That concludes the hydrogeomorphic analysis of the study and it leads us to an analysis of the relation between hydrogeomorphology and the freshwater reproductive life cycle of Chinook salmon in the LYR.

LINKING HYDROMORPHOLOGY AND ANADROMOUS FISH

Physical habitat units in rivers are defined as zones with characteristic physical attributes where organisms perform ecological functions, which are the ways in which organisms interact with their physical habitat. The attributes of physical habitat stem from the interaction among hydrologic, hydraulic, and geomorphic processes. These watershed and stream processes determine transient ecologic functions at the habitat-unit scale that can be characterized with observable metrics.

In this study, the primary focus was on Chinook salmon spawning habitat for several reason. First, we have conducted many studies on the lower Mokelumne River and found that this particular species' spawning lifestage is an excellent indicator of overall ecological conditions in the river. That is the case, because salmon spawning is associated with riffle crests. Riffle crest, in turn, are an expression of channel relief. If the bed relief is inadequate to produce and sustain highly functional riffle crests, then it will also fail to do the same for pools, since pools and riffles are relative to each other, by definition. Similarly, the other types of habitat heterogeneity that support many species in their diverse lifestages are also linked to the underlying hydraulic mechanisms that play a role in sustaining channel relief. So if spawning habitat is low quality, then chances are other life stages associated with pools, glides, runs, backwaters, lateral bars, etc would also be poor.

Second, this project focused on spawning habitat, becuase we were requested to do so as part of the study by the USFWS. A lot of confusion has existed among stakeholders for the LYR as to whether spawning habitat is limiting or not. At the time of this study back in 2003, ENTRIX and the USACE proposed to actively re-configure the river at Parks Bar and secondarily at Rose Bar, ostensibly to enhance spawning habitat. ENTRIX claimed that the spawner to redd ratio was ~27:1 in the TBR and that the substrate in the reach was too coarse for spawning. We sought to do a scientific study to ascertain the veracity of their unsupported claims.

The three questions we asked in relation to salmon spawning were as follows:

1) *What constitutes micro-scale habitat for spawning?*
2) *What meso-scale geomorphic features and processes control micro habitat?*
3) *Is spawning habitat availability and quality limiting the utility of Timbuctoo Bend?*

As a brief overview, Chinook salmon go through a series of freshwater lifestages when they come into California's rivers from the Pacific Ocean (Fig. 57). The overall freshwater cycle lasts anywhere from 3-7 years. It begins with adults migrating up the river and going to riffles that have the appropriate depths, velocities, substrates, and water temperatures to lay eggs into the gravel. Then they cover over those egg pockets with the gravel. The eggs become embryos that incubate for a few months. Survival is strongly influenced by intergravel water quality and dissolved oxygen flux. Embryos become Alevins, then Parr, then Smolt, and then those fish head back downriver to the ocean. The key aspect of interest here is determining the locations where fish choose to spawn, and then how successful those might be. For the LYR, there exists historical monitoring fish escapement into the river rom ~1950 to present (Fig. 58). That data shows that escapement ranges from ~1000-40,000 fish, with peaks in the early 1960s and 1980s. The pre-European estimated population is >100,000 adults in the LYR. The management goal is to have ~66,000 fish spawning in the LYR annually. However the long-term average is ~ 11,000 fish. Most recently in 2007 there were only 1,500 fish that were measured in the escapement survey.

Yuba River Chinook (*Oncorhynchus tshawytscha*)

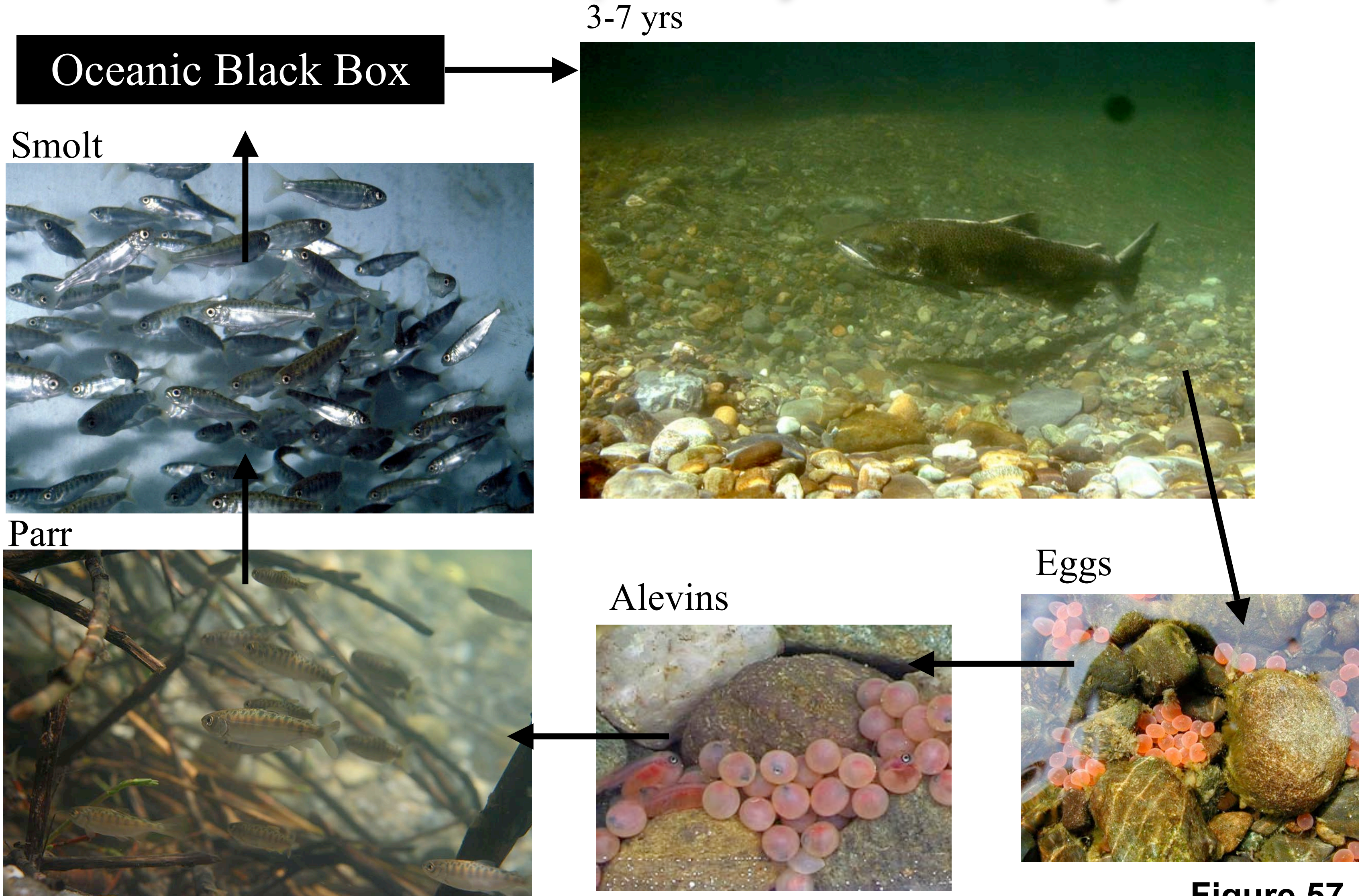

Figure 57

LYR Chinook Escapement History

- Inter-decadal Fluctuations
- Pre-European Est. Pop of >100,000 adults
- **Management Goal ~66,000/yr**

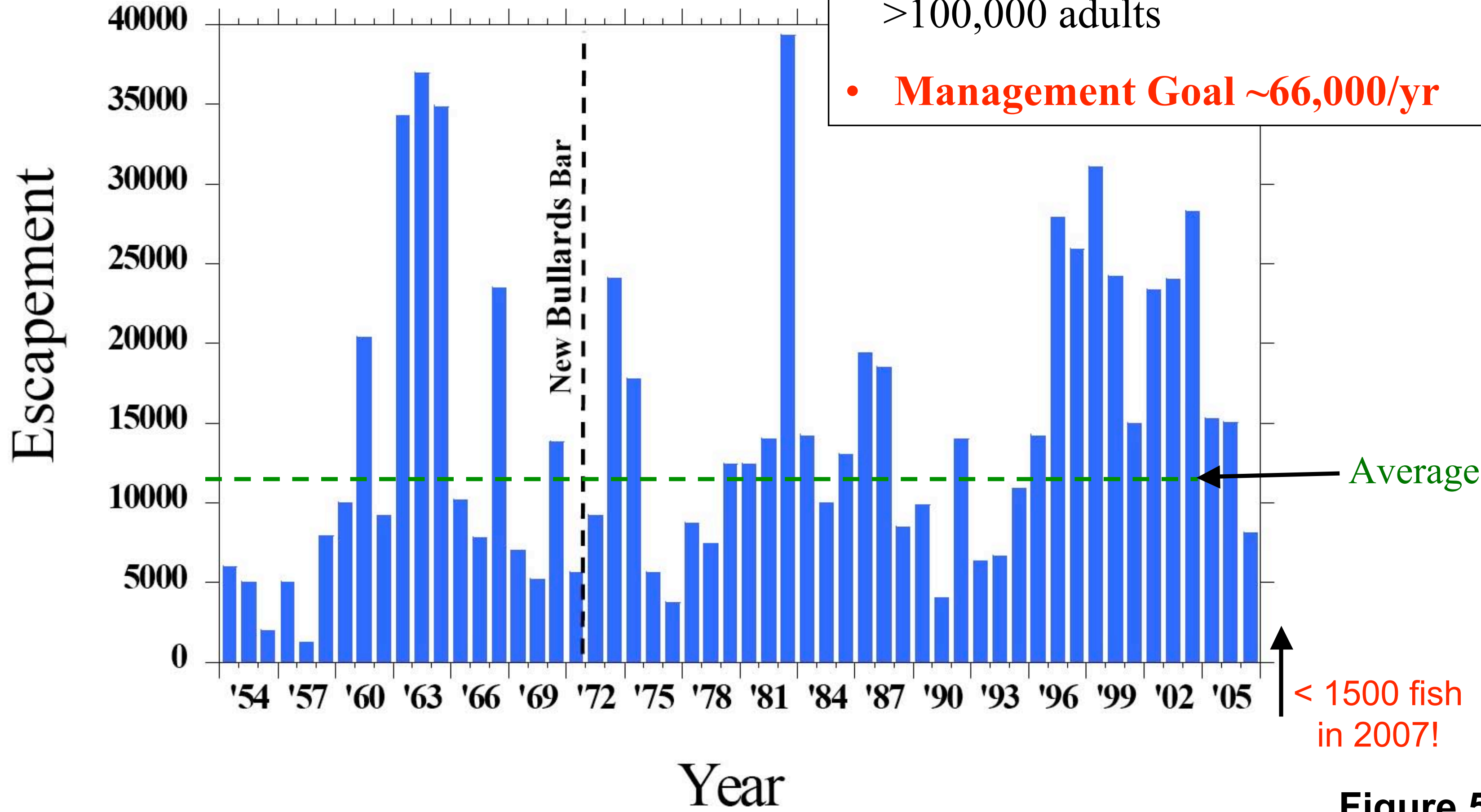

Figure 58

Our approach to determining the availability of physical habitat for Chinook salmon spawning in the TBR has been to use both microhabitat and mesohabitat methodologies. The latter was applied at two spatial scales- at the TBAR site and for the whole TBR. The two different methods show that riffles are the key morphological unit for Chinook salmon spawning.

Redd Surveys

To have a basis for testing 2D model habitat-quality predictions at the micro-habitat scale and assessing meso-habitat utilization of morphological units, redd surveys were performed in 2004, 2005, and 2006. In autumn 2007 surveys were only done at the TBAR site and at the Parks Bar site. The surveys for 2004 and 2005 used an identical approach, so it is explained in detail for 2004. The location of individual redds (cumulative total=451) were surveyed on 52 days between September 17 and November 16 inclusive during the 2004 spawning season by experienced observers (Fig. 59). The location of the deepest part of the redd "pit" was surveyed in each case using a Topcon GTS-802A robotic total station. Redds that had been previously surveyed were identified by a painted marker stone that was placed in the pit. If the marker stone was buried by subsequent redd excavation, the position of the modified pit was re-surveyed. There are 'spring' and 'fall' runs of Chinook that spawn in the LYR, with both spawning in the fall. Some local experts identify spring run fish as those that spawn September 1–30 and fall run from October 1 to December 31, while others disagree with this delineation and report overlap in timing so that it is difficult to tell with certainty that a given redd was constructed by spring or fall run fish. In relation to the period of spawning surveying undertaken in this study, the nominal "spring run" could be considered to have been sampled September 17

2004 TBAR Redd Map

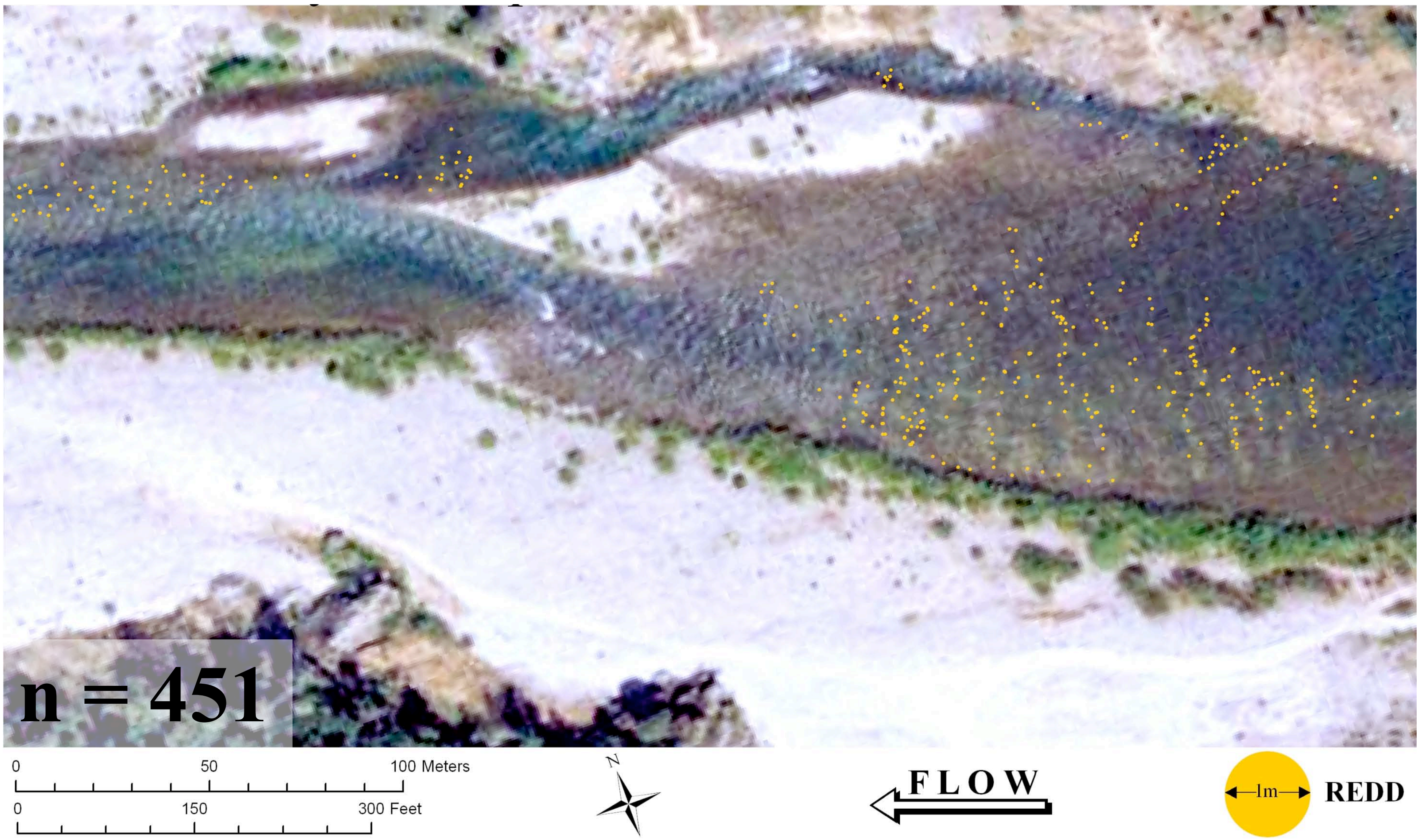

Figure 59

to 30 and the “fall run” from October 1 to November 16. However, the first survey carried out on September 17 mapped all the redds that had been constructed prior to that date. During this initial survey there were still relatively few redds at the site and it was apparent that each was a discrete feature (i.e., there was no evidence that superimposition had occurred by that point). It was therefore unlikely that many redds constructed prior to September 17 were not identified. Thus, redds were effectively mapped between the onset of the2004 spawning season and November 16. Although fall spawning is regarded to continue until December 31, the cumulative number of redds was so high in the 2004 spawning season that by mid-November it was very difficult to distinguish between new and previously constructed redds, despite the use of markers to identify previously mapped features. Therefore, to avoid bias through re-sampling, the final redd survey was conducted on November 16. The number of redds surveyed by that date (i.e. 451) was sufficient to conduct subsequent statistical analyses. Subsequent visits to the study site after November 16 revealed that no new locations had been utilized so that the spatial cover of the surveys conducted was representative.

The redd survey in autumn 2005 at the TBAR site was performe din a similar fashion as that in autumn 2004. There were two distinct discharges- ~750 cfs in early autumn and ~1150 cfs in late autumn. The redd pattern shifted through that time, so distinct 2D model runs were performed to capture that, as described below. The number of redds present at the TBAR site in autumn 2005 was 221, which was a 51% drop form the previous autumn. The distribution will be described later relative to the 2D model predictions, but is shown now in Fig 60 along with the aerial imagery of the river.

In late November and early December 2006 we did a redd survey of the entire TBR by wading and snorkeling to characterize the relative spawning density of the different

2005 TBAR Redd Map

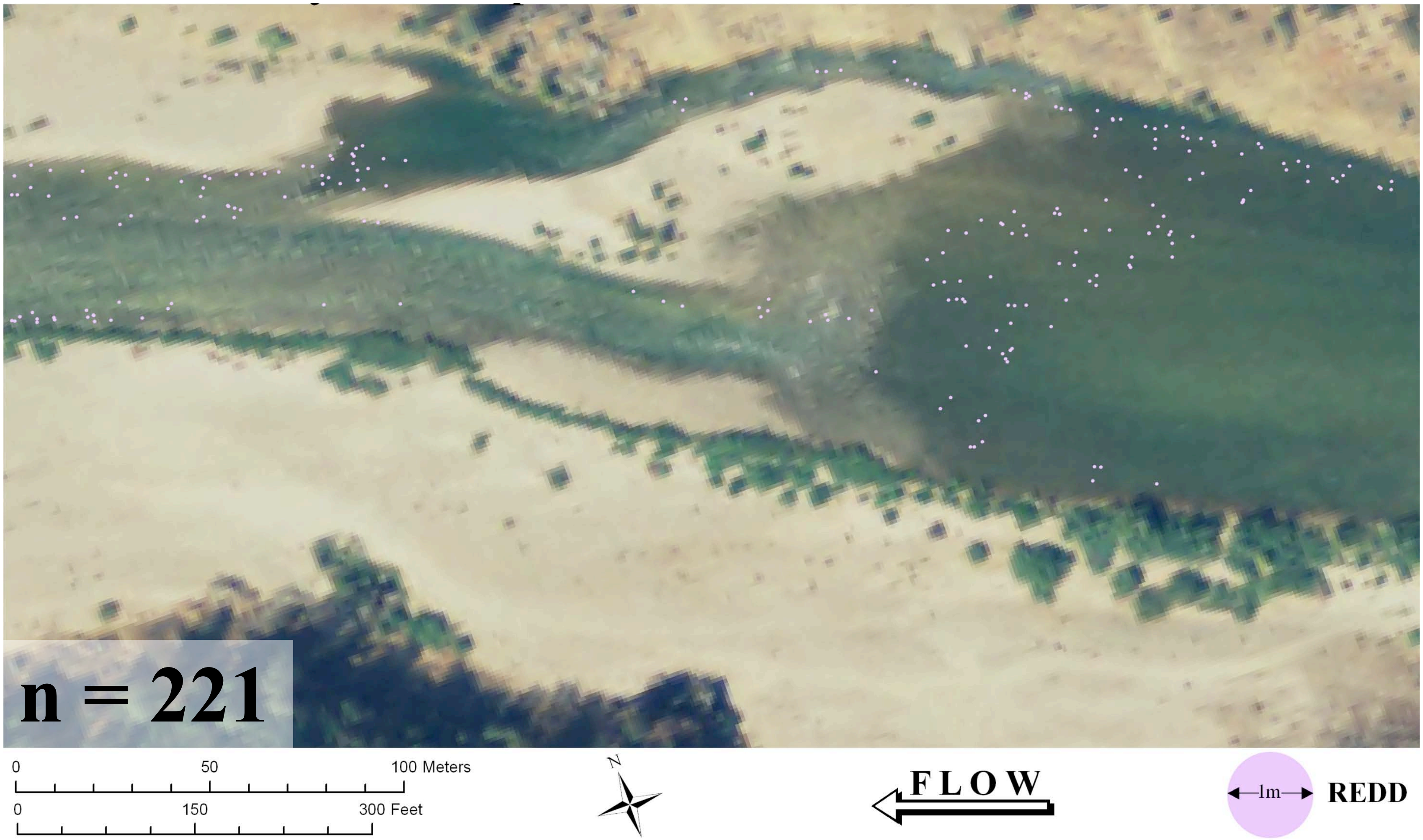

Figure 60

morphological units. The method was similar to that already described in detail fro the 2004 and 2005 surveys, but was a single pass over each location late in the spawning season and over a much larger area. The redd map for the TBAR site was isolated from the overall survey to enable interannual comparisons (Fig 61). In that case, the underlying imagery is from the tethered blimp survey, as described later. The number of redds observed at the TBAR site was only 180.

The autumn 2007 redd survey used the same approach as in 2006, but was limited to the TBAR and Parks Bar sites. At the TBAR site, only 42 redds were present (Fig. 62). Given the small number and the lack of superimposition of redds, the survey is a reliable estimate of the total number for that year.

Overall, there was a steady decline in the number of redds observed over the four years of monitoring. The decline parallels the overall decline in the number of spawners in the river over time.

Microhabitat Analysis

The term "microhabitat" is defined as the localized depth, velocity, temperature, and substrate at a point in a river without regard to surrounding conditions. Our microhabitat analyses rely on high-resolution 2D hydrodynamic modeling and habitat suitability curves (HSCs). Following standard practice, depth and velocity results from the 2D model are extrapolated into HSCs to predict the overall pattern of habitat quality (Fig. 63).

Unfortunately, prior to this study, no 2D-bioverified HSC exist for the LYR. Since 2000, the USFWS Instream Flow Branch has been developing LYR HSC for spawning and rearing

2006 TBAR Redd Map

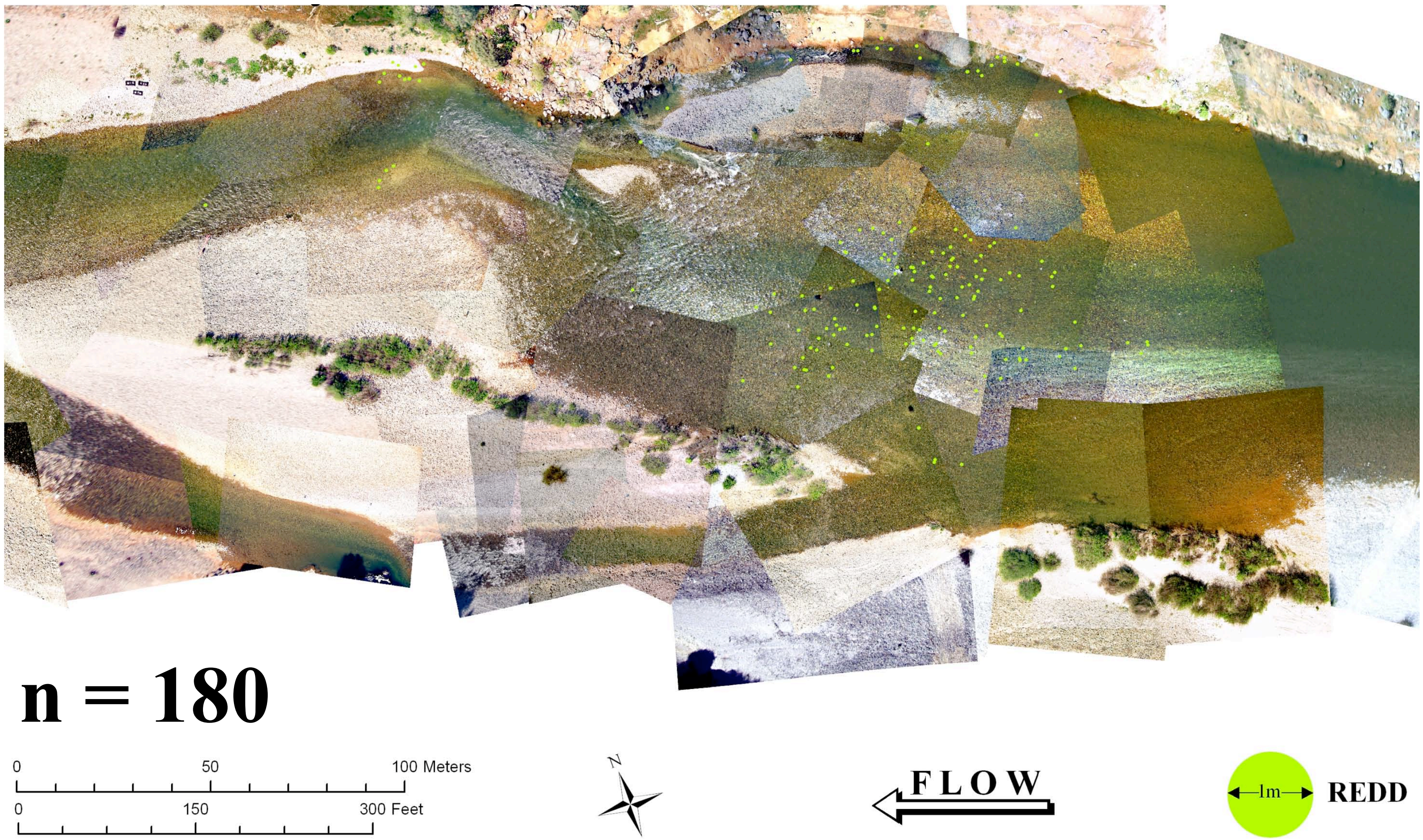

Figure 61

2007 TBAR Redd Map

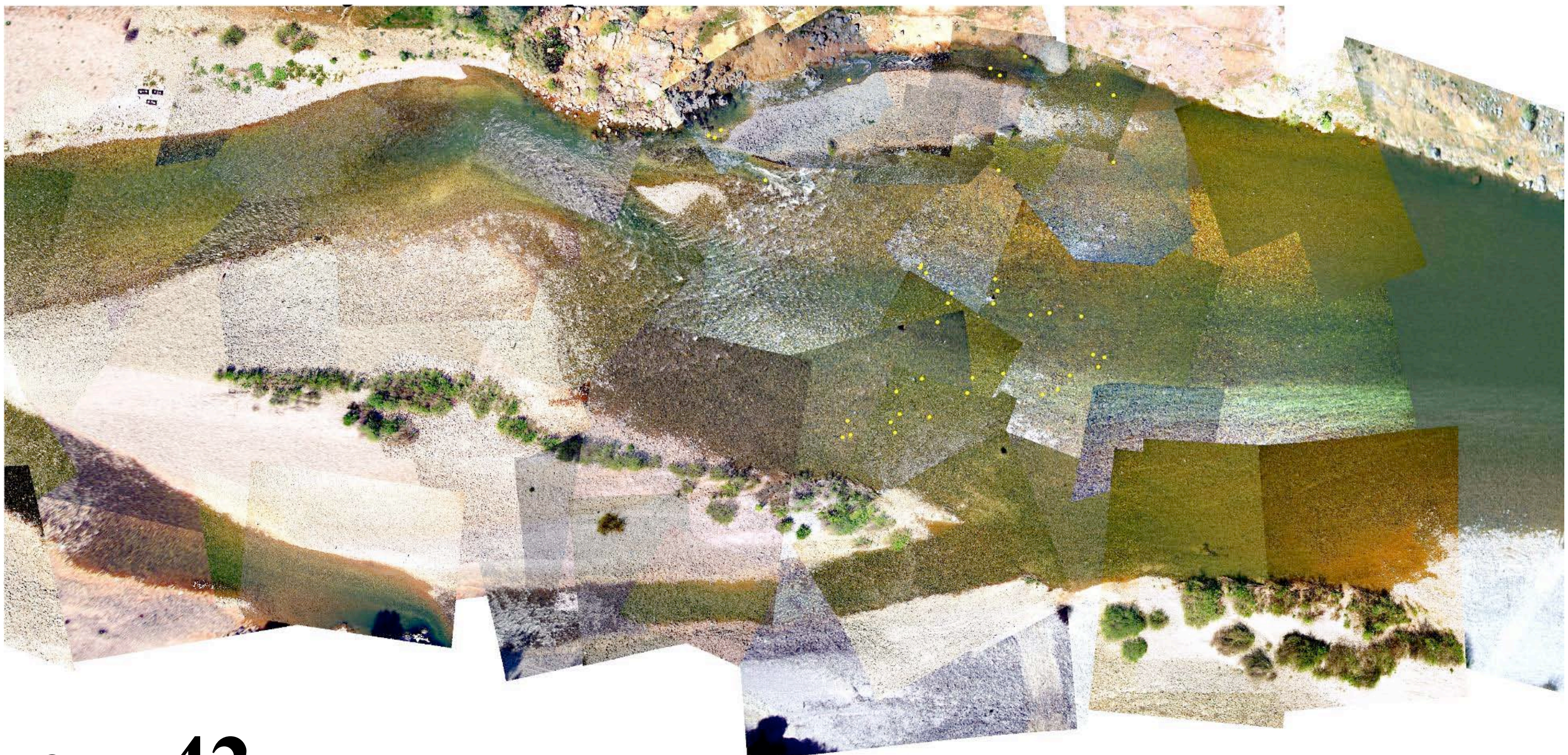

n = 42

Figure 62

2D Modeling of Physical Habitat

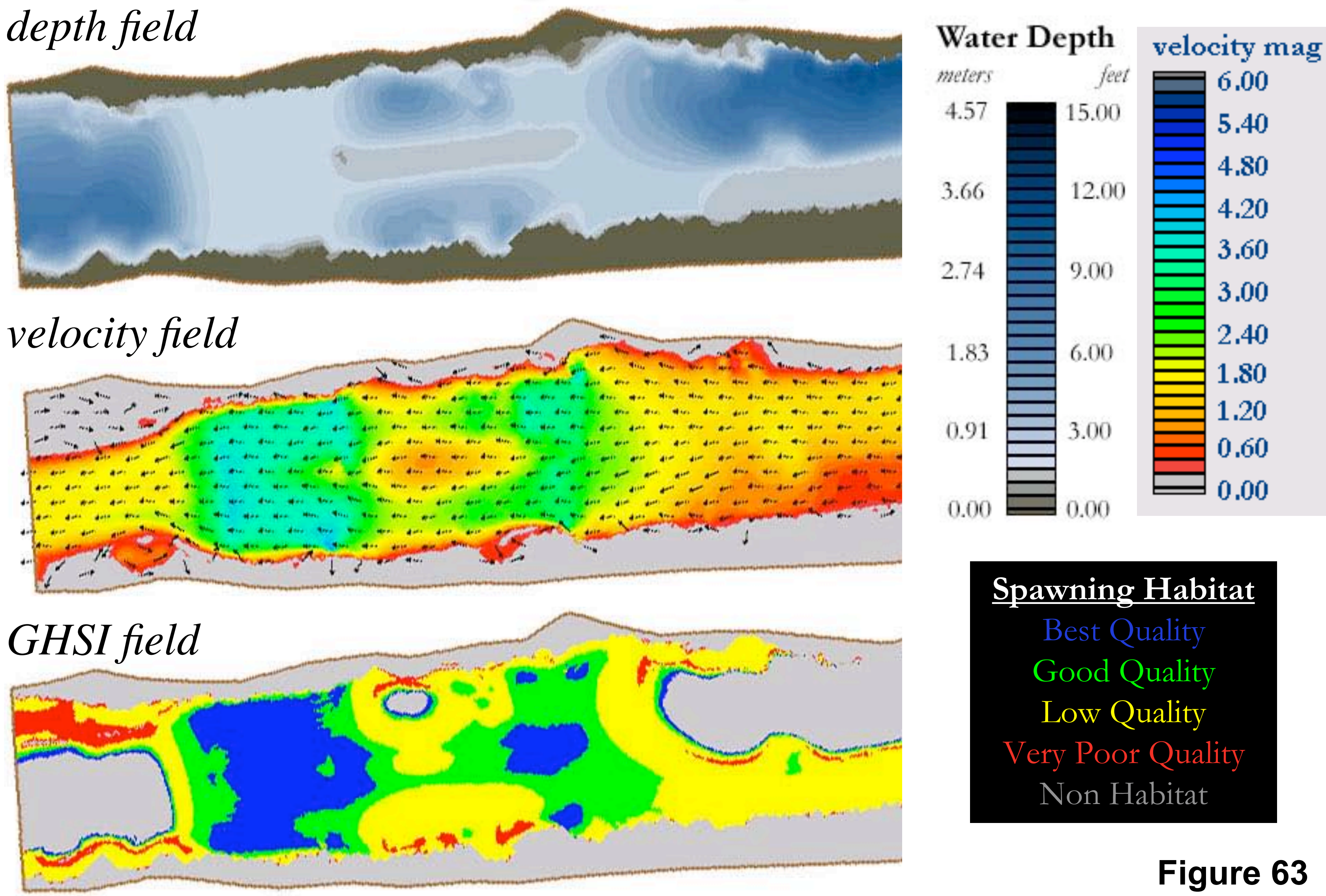

Figure 63

Chinook salmon and steelhead trout that aim to use logistic functions to account for habitat availability as well as utilization. For the duration of our 3-stage project (2003-2008) those HSC were not formally published. We were given the spawning HSC in draft form late in our project and did fully evaluate them, but because they are not published and may still change it would be unfair to publish a direct comparison in this report. I do think it is fair, objective, and necessary to report that as of January 29, 2009, none of the various fall-run Chinook HSC that the USFWS Instream Flow Branch has proposed match or outperform the predictive capability of the utilization-based HSC applied in this study in 2D bioverification tests at the TBAR site. We have shared those test results in detail on several occasions with the USFWS Instream Flow Branch and the LYRTWG. In theory, HSC that account for availability ought to outperform those that do not, but the USFWS Instream Flow Branch does not report any tests of its proposed curves against utilization curves. Objectivity requires that such tests be done and reported.

In the absence of LYR HSC, we took the bioverified Lower Mokelumne River (LMR) HSCs and bioverified them now for use on the LYR. The LMR curves come from CDFG (1991); they are derived from utilization data that are not corrected for availability (Fig. 64). Lacking direct head-to-head comparisons of the performance of utilization curves versus availability-adjusted curves for Central Valley salmonids, it is religious-like speculation to assume that the former are inferior. The bottom line is if you can take independent observations of locations of redds and show that any given HSC accurately predict the locations of redds and accurately predict avoidance where there are no redds, then those HSC are "bioverified". In hydrological language, we would say that the 2D model predicting habitat quality is "validated" under that circumstance. If the HSC cannot accurately predict both preference and avoidance, then they are falsified and should be discarded. Our study applied the strictest testing standards.

Habitat Suitability Curves

- Used Lower Mokelumne River utilization curves (CDFG, 1991) after they were bio-verified for use on the LYR- see next slide.

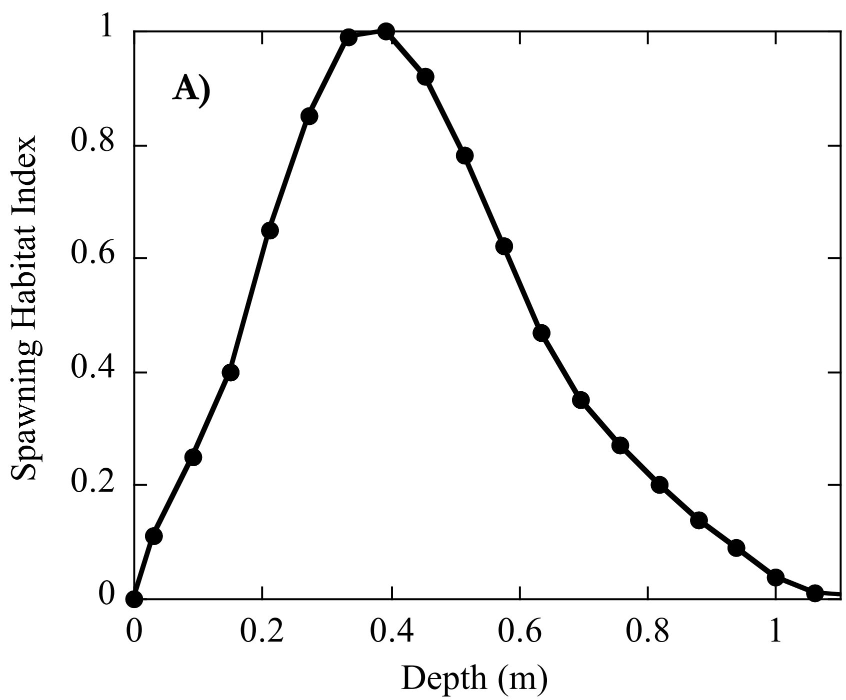

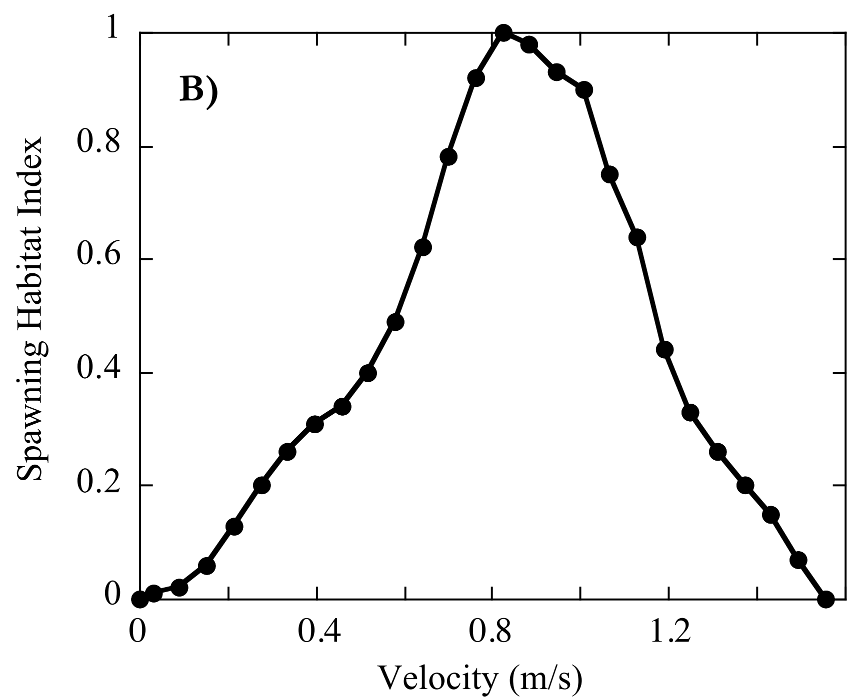

(CDFG, 1991)

Figure 64

Following this standard, we tested the predictive power of the lower Mokelumne River utilization-based HSC at the TBAR site in 2004 and 2005 (Figs. 65, 66). For each autumn, we took the 2D model results for the low-flow spawning period (827 cfs in 2004 as well as 755 and 1101 cfs in 2005), and calculated a depth habitat suitability index using the depth curve and a velocity habitat suitability index using the velocity curve. Then we took the geometric mean of those two to obtain a Global Habitat Suitability Index (GHSI). Note that we did not account for substrate as a first ordered check to see how accurately hydraulics alone could predict habitat. We did have many substrate measurements, but wanted to see how the model would perform without them.

When we compared redd observations (method as described above) against habitat quality predictions, we found that the hydraulics-only GHSI was extremely accurate at predicting where fish actually spawned (Figs. 65, 66). We found that there is a very strong preference of occurrence at the TBAR site for preferring areas with a habitat quality GHSI value of 0.6-1.0. Whereas the availability of such habitat was ~20% of total area in 2004, almost ~60% of utilization occurred in that domain. Similarly, for GHSI of 0.4-0.6, there was a slight preference. When the GHSI was 0.2-0.4 there was some avoidance, and then finally, for any value of GHSI from 0.0-0.2 there is a very strong avoidance. Another way of looking at it is to calculate an electivity index, also known as a forage ratio, by dividing the utilization percent by the availability percent for each habitat quality type. For example, for the 755 cfs test in 2005, the ratios were 3.56 and 1.61 for the two preferred GHSI bins, whereas they were 0.16 and 0.22 for the avoided ones (Fig. 66). A similar pattern of forage ratios was evident for 1101 cfs.

2004 HSC Bioverification at TBAR

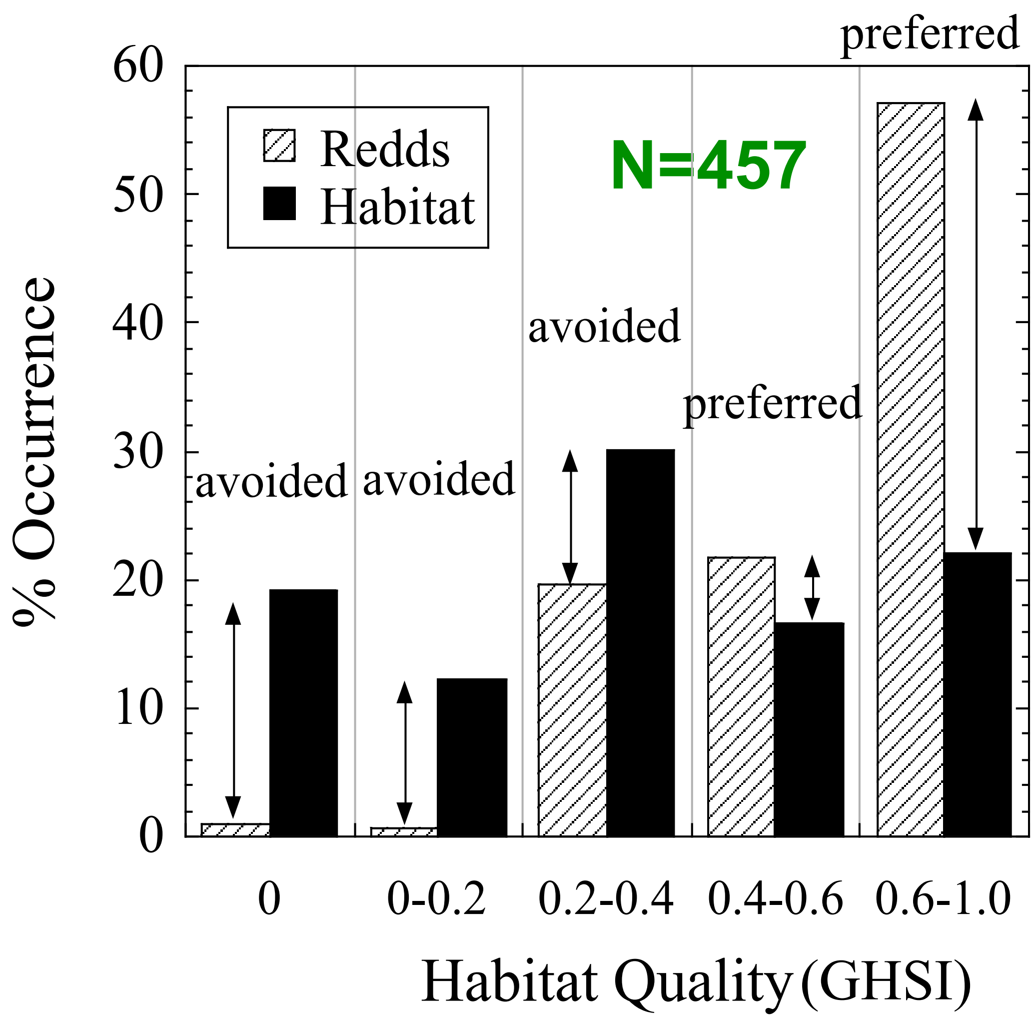

2D model predictions using lower Mokelumne River HSCs accurately predicted preference of high-quality habitat and avoidance of low-quality habitat

Figure 65

2005 HSC Bioverification at TBAR

2D model predictions using lower Mokelumne River HSCs accurately predicted preference of high-quality habitat and avoidance of low-quality habitat

755 cfs

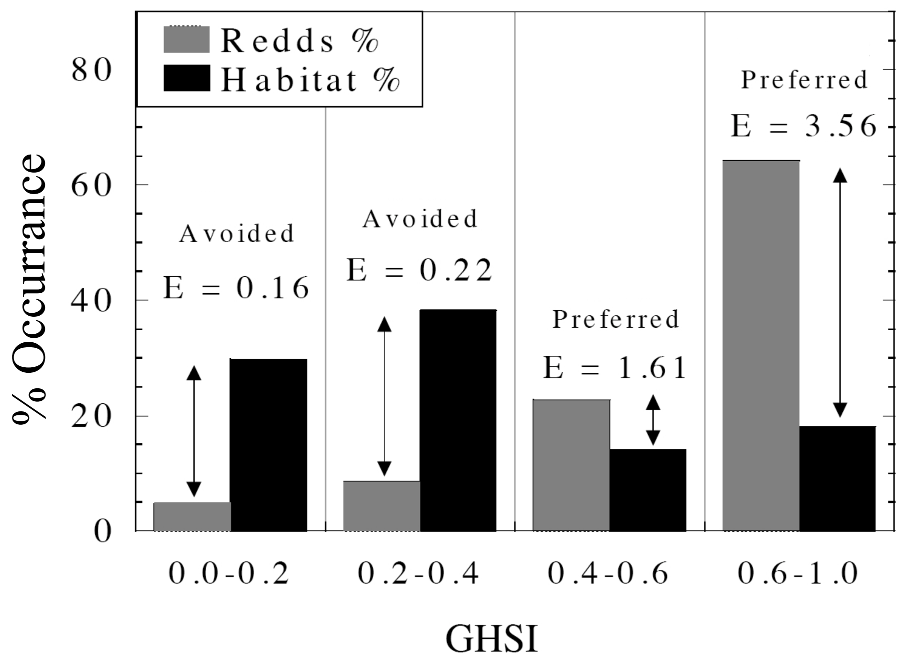

1101 cfs

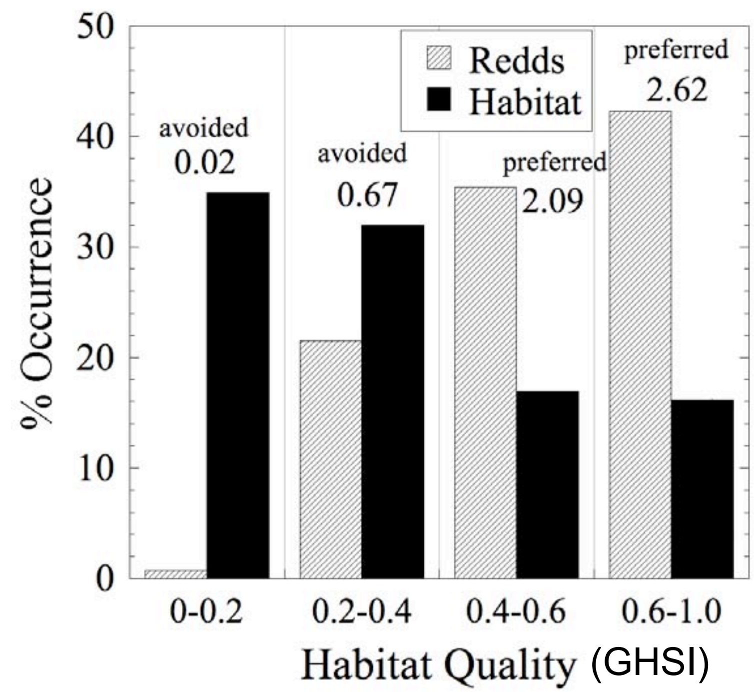

Figure 66

- *Given that they accurately predicted both preference and avoidance when accounting for availability in 3 independent tests, the Lower Mokelumne River HSC are "bioverified" for use on the LYR in TBR.*
- *Areas designated as high (0.6<GHSI<1.0) and medium (0.4<GHSI<0.6) quality habitat are the bioverified "preferred" microhabitats. High quality habitat was much more preferred than medium quality and very poor quality habitat was much more avoided than low quality habitat.*
- *Areas with GHSI<0.4 are the bioverified "avoided" microhabitats.*
- *No other HSC proposed for the LYR match the performance stated in the 2 previous bullets*

Looking at the GHSI spatial pattern for autumn 2004, there is an excellent matching of GHSI high-quality patches and the actual locations where redds were located (Fig. 67). Fish completely avoided parts of the side channel where flow was too fast or too deep. They similarly avoided the chute downstream of the riffle crest and the run downstream- both units being too fast. The areas that they primarily preferred were the riffle entrance units upstream of the secondary channel and main riffle crest. They also preferred a secondary-channel riffle crest location as well as the lateral bar downstream of the riffle in the run on the north bank, where the gravel that is eroding off the island from 1999-2004 had deposited, as reported earlier. Also, that lateral bar location had highly suitable depths and velocities. There was a band of high-quality (hydraulically defined) habitat along the south bank in the run, but when that location was ground-truthed, it turned out that the substrate quality was low. Even though the hydraulic quality was high, the bed armoring explains why the fish did not choose to spawn in that area. In summary, there appears to be no bias stemming from the HSCs not accounting for availability.

2004 TBAR Salmon Spawning Pattern

Predicted Versus Observed

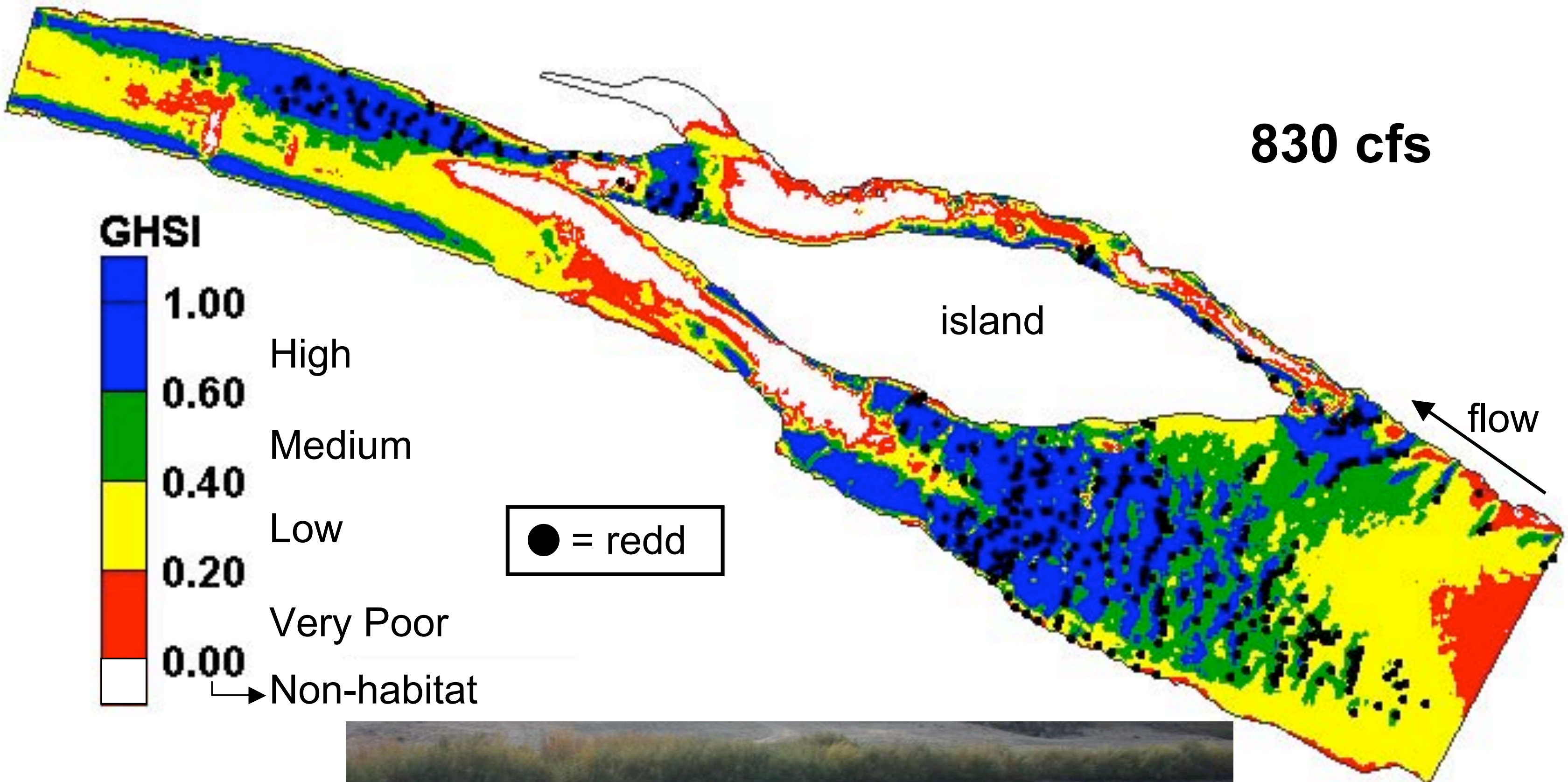

Figure 67

In 2005, spawning took place at 750 and 1100 cfs due to a change in flow out of Englebright in November. After the May 2005 flood, knickpoint migration destroyed a large area of spawning habitat on the downstream part of the riffle, while pool scour destroyed spawning habitat on the riffle entrance (Figs. 68 versus 67). Consequently, the pre-existing focal area of salmon spawning in 2004 was greatly reduced. In response, there were fewer spawners and the fish shifted their spawning down to the run, where fresh gravel had deposited and hydraulics were better. Compared with 2004, in 2005 fish spawned along both banks of the run. At 1,100 cfs more spawning took place along the upstream edge of the island (Fig. 69). Also, the quality of the habitat in the chute and run units degraded significantly due to higher velocities.

In summary, 2D hydrodynamic modeling coupled with LMR HSC performed extremely well at predicting both preference and avoidance of spawning locations at the TBAR site. Three independent tests were performed and all showed the same successful predictive outcome. These results raise serious questions about ongoing and future studies that fail to explain why these bioverified HSC should be discarded in favor of ones that perform far worse. Knickpoint migration had a detrimental effect on the riffle, but the sediment generated from that just moved downstream a short distance into the run, improving the habitat quality there.

Mesohabitat Analysis

Linking Micro and Meso Characterizations

Although it is often possible to empirically relate ecological function to microhabitat variables, as shown above, doing so provides a limited understanding of how and why fluvial–ecological linkages are spatially related. The term “mesohabitat” is defined as the

2005 TBAR Salmon Spawning Pattern

Predicted Versus Observed

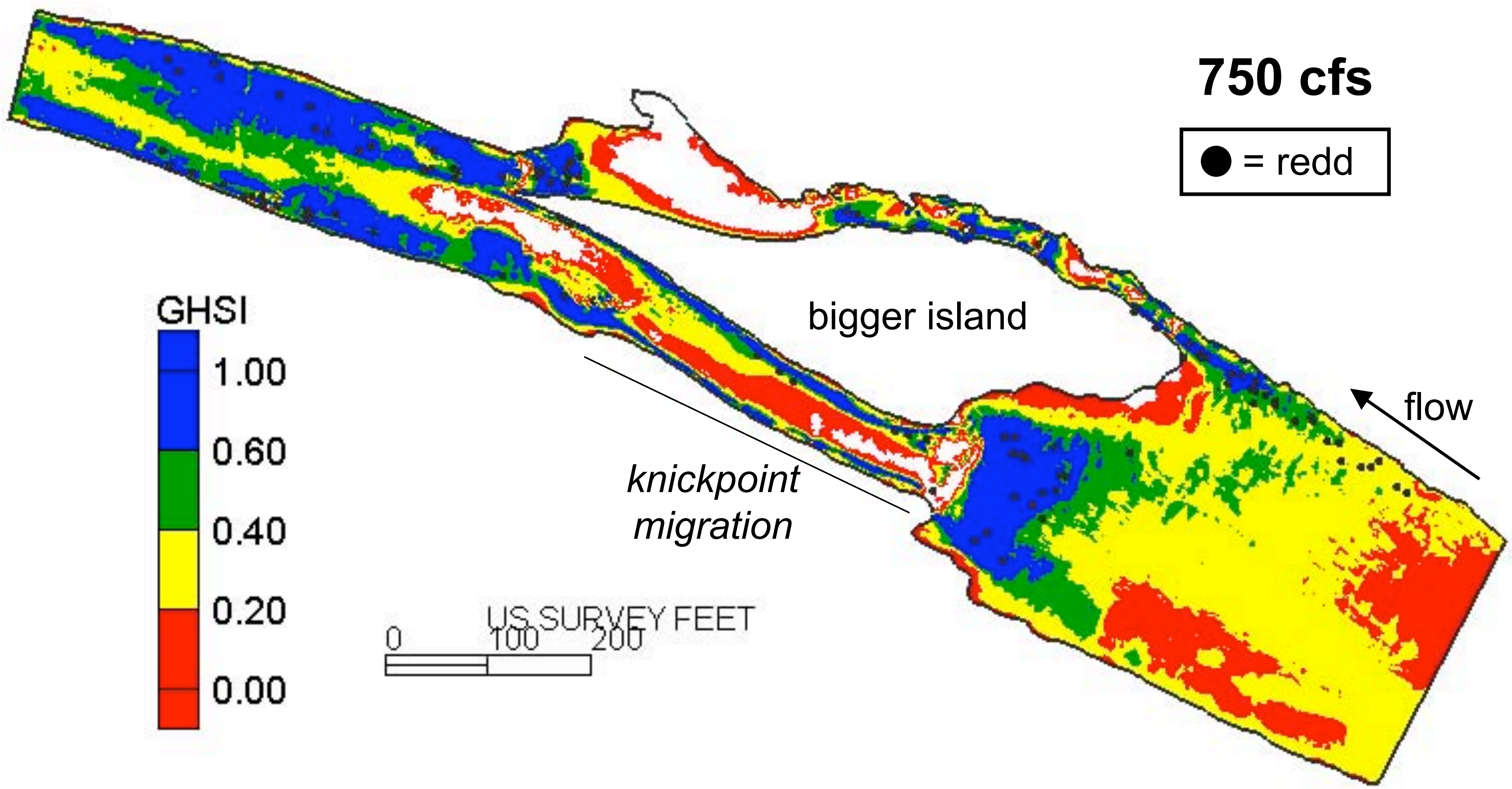

May 2005 flood dramatically reduced riffle habitat, but increased lateral bar habitat somewhat.

Figure 68

2005 TBAR Salmon Spawning Pattern

Predicted Versus Observed

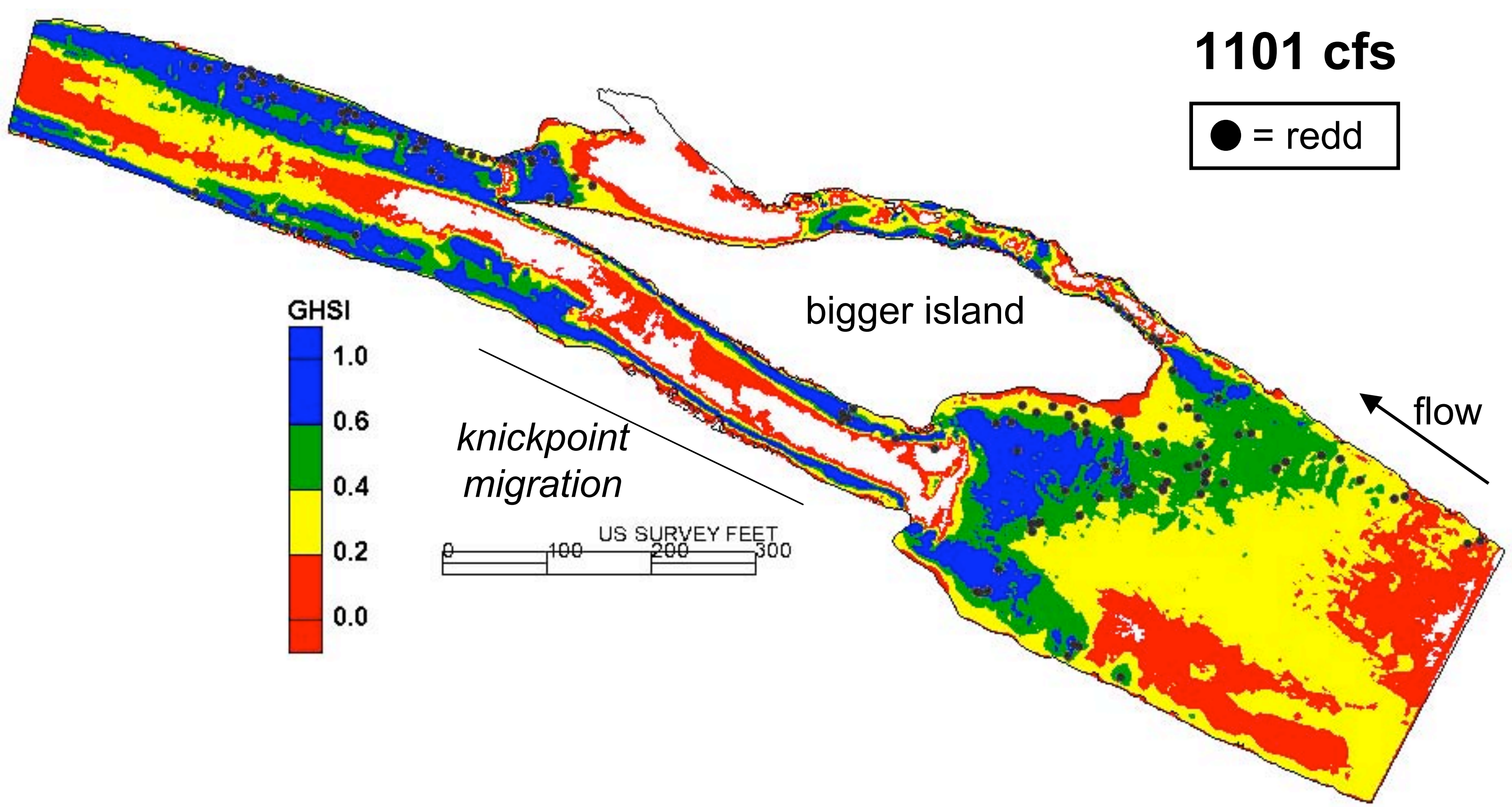

Habitat distribution shited at 1101 cfs compared with 755 cfs.

Figure 69

interdependent set of the same physical variables over a discernible landform known as a morphological unit (e.g., scour pool, riffle, and lateral bar). There is a general lack of studies that nest the microscale requirements of instream species within the mesoscale context of an assemblage of morphological units. Consequently, in this study we evaluated the hypothesis that by linking the mesoscale of morphological units to microhabitat characteristics, it would be possible to explain fluvial–ecological linkages better. This aspect of the project has already been published in a peer reviewed scientific journal, and that article is provided as Appendix 4.

In the article we used expert judgment to independently delineate the 2004 morphological units at the TBAR site graphically on an aerial photo (Fig. 70). Note that in this mapping, the "lateral bar" unit was a submerged gravel bar on the side of the run. After further studies I would now classify that unit as a run and leave the term "lateral bar" for unsubmerged gravel bars flanking the wetted channel in straight reaches. However, at that time we were trying to have a more detailed delineation of just the wetted channel and just relevant for the TBAR site. In any case, the next step was to use the micro-scale hydraulic output of the 2D model for 827 cfs make averaged hydraulic characterizations of each morphological unit. Finally, we used the 2004 redd survey and statistical methods to determine which morphological units were preferred and which avoided by salmon spawners, and we did so in relation to hydraulics, too. We found that morphological units did have distinct hydraulics, and that the ones being used as spawning mesohabitat were riffles, riffle entrances, and the lateral bar within the run (Fig. 71). In the article (Appendix 4) we explain the processes that interconnect micro- and meso-habitat.

Tethered Blimp Imagery of Riffles With Redds

Meso-scale Habitat Typing

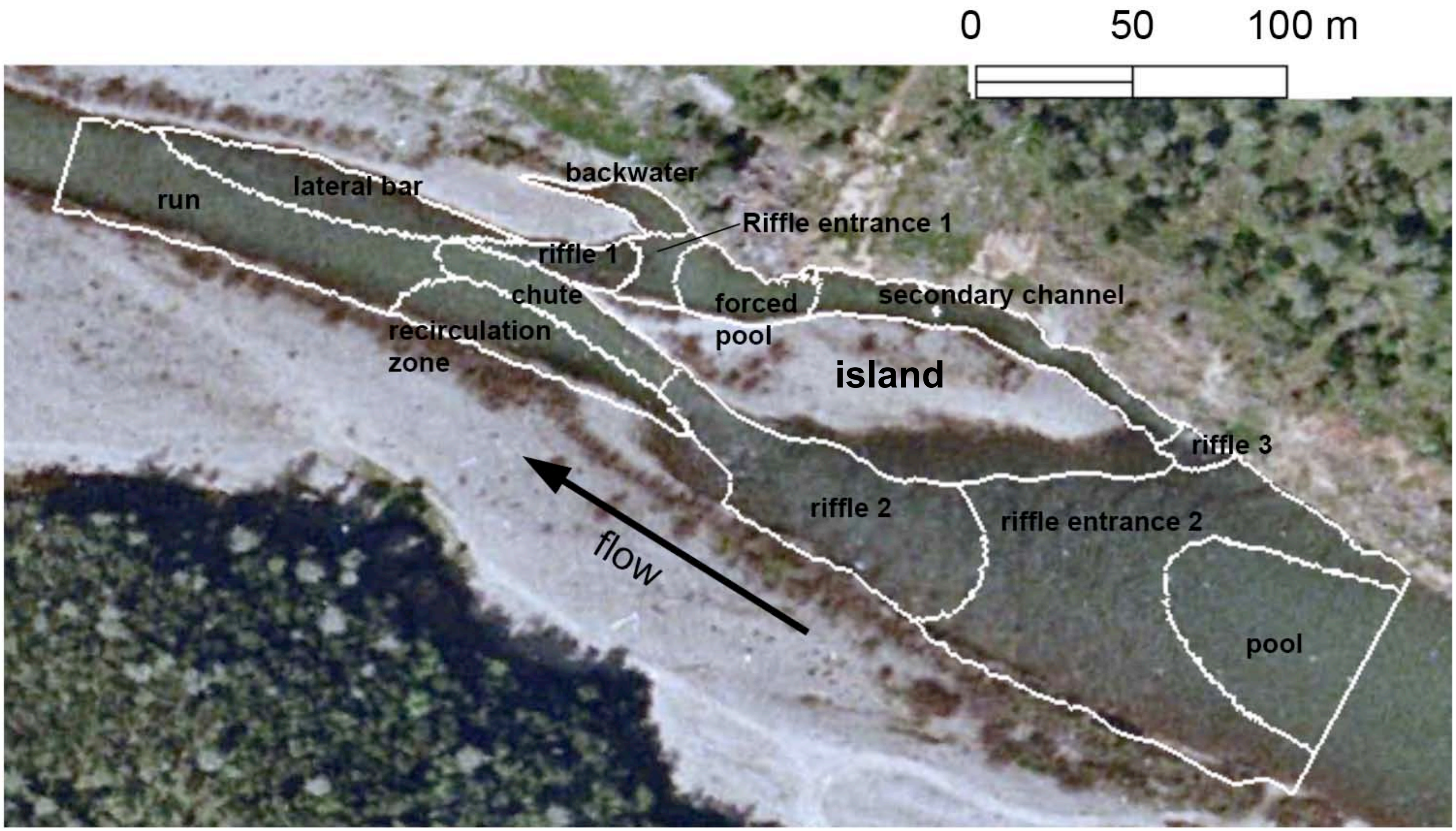

Figure 70

Preferred and Avoided Meso-Scale Hydraulics

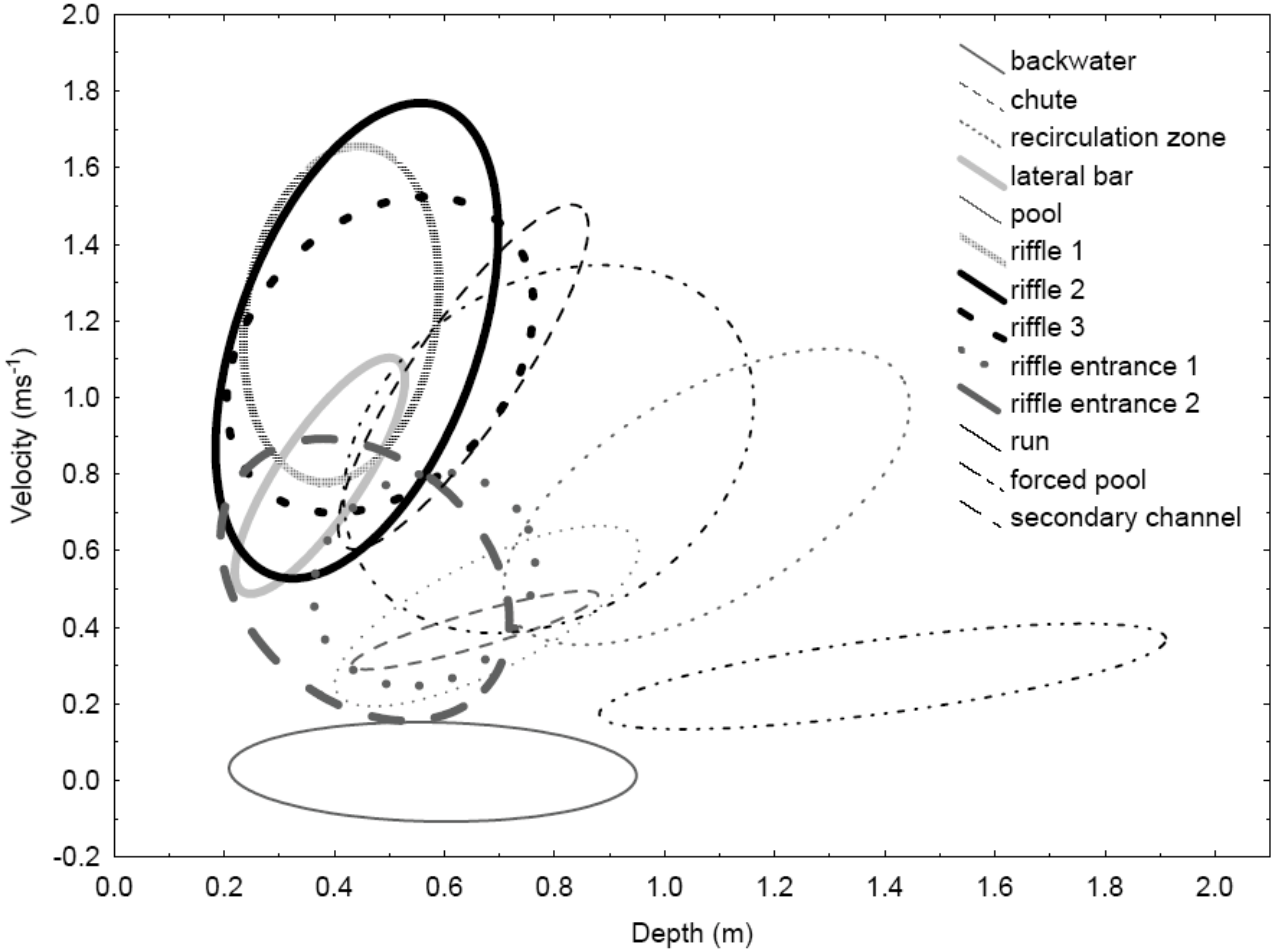

Thick ellipses are preferred conditions based on observed redds

Figure 71

Given that the LYR is so dynamic, a remote imagery method was sought to enable rapid response in capturing the state of spawning riffles after a major change. The goal was to have a method less expensive than standard aerial photography by low-flying aircraft and to have much higher resolution. The tested approach involved lofting a 3'x6' (oblong) tethered blimp with a 10 megapixel digital camera (Canon Powershot SD900). The camera was locked into a "continuous shooting" mode that took pictures automatically about every 1-3 s. The blimp was first lofted to an altitude of ~400-500' (depending on wind speed) and then it was walked down the river to capture imagery at that higher elevation. To georeference the imagery, 2'x2' square plywood sheets painted with large back-and-white numbers were located along the banks, and their geographical coordinates located with an RTK GPS. In the wetted channel, 5-gallon buckets were filled with brightly colored rocks, submerged, and located with RTK GPS to provide georeferential targets. A second pass of the blimp over a riffle was done at an altitude of ~100-150' to obtain very high resolution imagery. For reference, standard aerial photography usually has a pixel resolution of 1-3'. In contrast, the tethered blimp imagery had resolutions ranging from 0.01-0.1', so that's one to two orders of magnitude better.

An example of the tethered blimp imagery is shown for the TBAR site as it was in 2007 after a winter with no floods (Fig. 62), so it is representative of both autumns 2006 and 2007. The image looks very patchy, because it is difficult to manually adjust each component image to have the same brightness, color saturation, and contrast. Along the edges of the image is the standard aerial photo form the same time period, and you can see the dramatic difference in resolution, even at this coarse scale. Longitudinal streaks of sandier gravel are visible in the channel. Green dots on Figure 61 are redds locations observed in autumn 2006 at the TBAR site. Due to the dramatic channel change from the New Years 2006 flood, the redds were once again clustered in the riffle entrance and riffle as in 2004 and unlike in 2005. Few redds were present in the run downstream. A similar pattern was observed in 2007 as in 2006 (Fig. 62).

A close up of the imagery provides a better view of the detail visible in the blimp imagery (Fig. 72). The 2'x2' targets are visible along the north bank (top of photo), and provide a scale. Individual gravel and cobble grains are easily distinguishable. Even though redd locations are highlighted, looking at the imagery alone, some are easily distinguishable, but others not at all. The problem is that the riverbed is turned over by floods on a regular basis, so substrate brightness is not different on redds, which is usually how redds are identified in aerial imagery. However, when the full-resolution is viewed in ArcGIS, then it is possible to see many redds, even in water that is too deep to wade.

TBR Mesohabitat Utilization

In autumn 2006 redds were mapped through all of TBR (Fig. 73). Even though it was not a weekly survey, it did capture the relative distribution of redds among morphological units for the whole reach. Because we had been told by an employee of Entrix that the spawner:redd ratio for TBR was ~27, we sought to use our data to evaluate that independently. California Department Fish and Game performs annual spawner carcass surveys, so when we divided the number of redds we observed by their estimate of the spawner population from the carcass survey, we obtained a spawner to redd ratio of 4:1. California Department of Fish and Game has recommended to us that a ratio of 4:1 is a suitable ratio. For 2006 there was no lack of availability of salmon spawning habitat in the TBR. 2006 had a population of below-average size (Fig. 73), so it was necessary to evaluate the amount of available habitat to see how close to limiting spawning habitat might be.

Redds and Sediment Clearly Visible

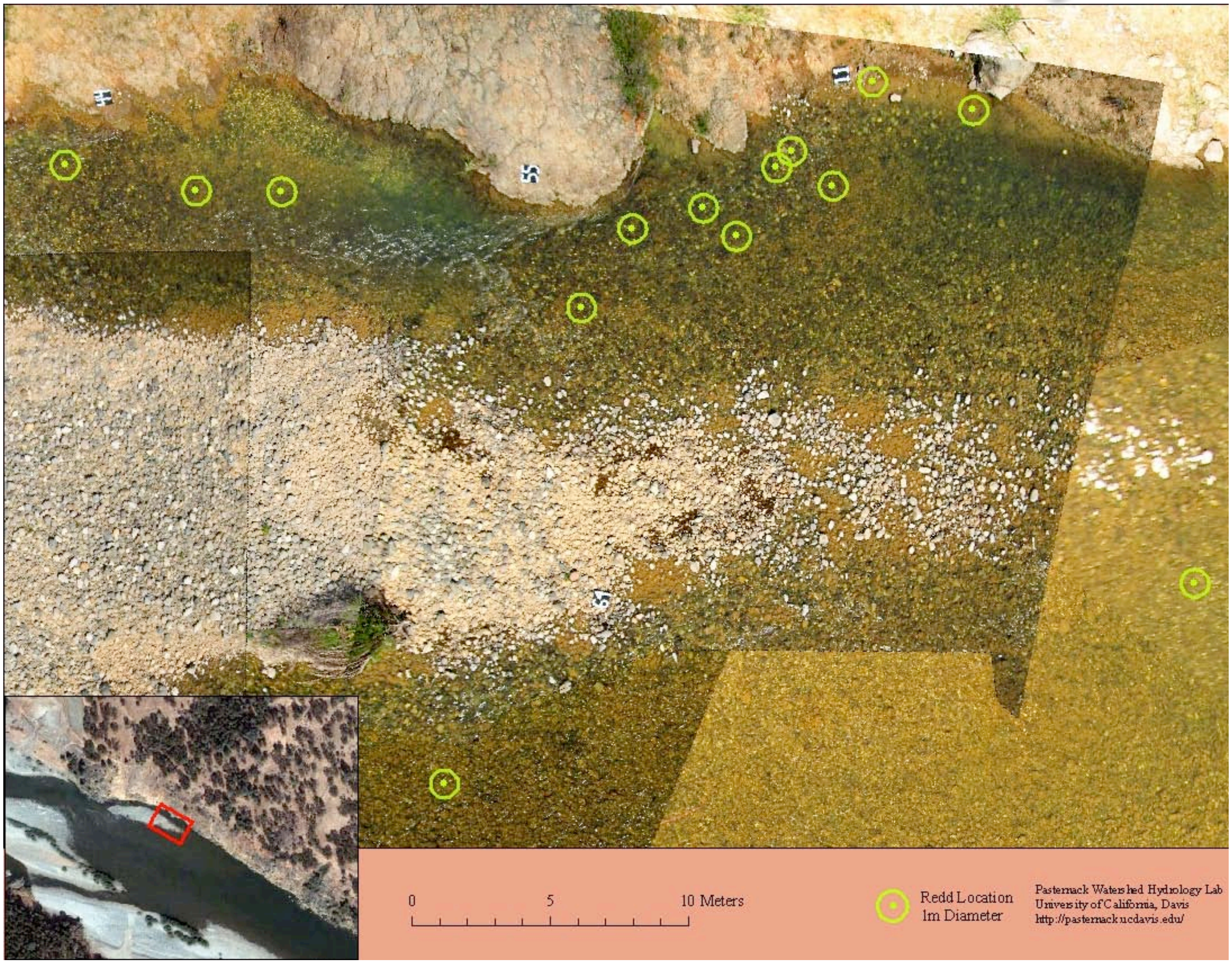

Figure 72

Timbuctoo Bend 2006 Redd Density

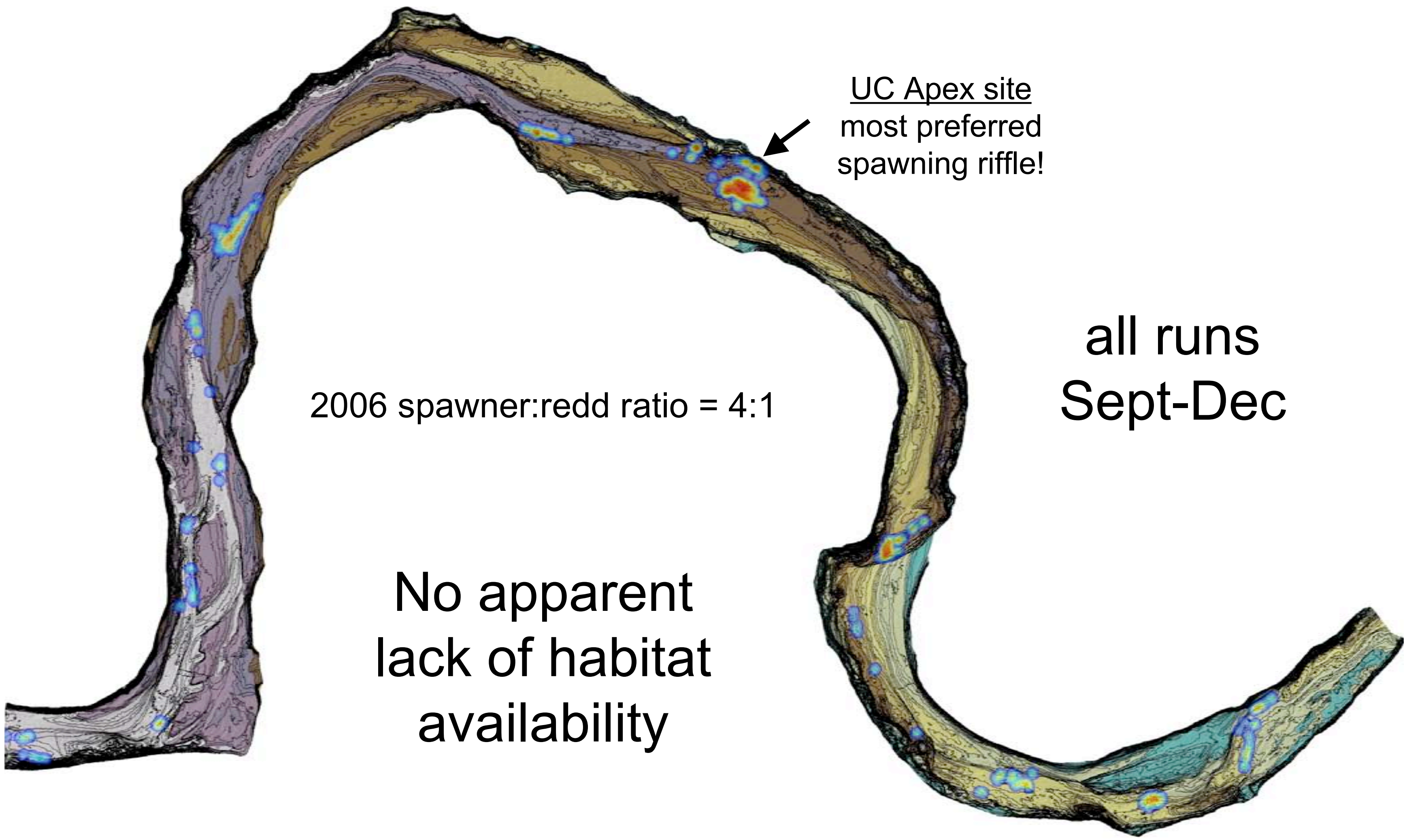

Figure 73

Using ArcGIS 9.2, we took the point shapefile of 2006 redd locations and superimposed them on the 2006 TBR morphological unit map. That enabled us to identify the number of redds located in each unit. The vast majority of redds (68.66 %) occurred on a single unit- riffles (Fig. 74). When electivity indices (i.e. forage ratios) were calculated using the known areas of each unit, the ratio for riffles was 9.38. Such an extremely high value demonstrates a very strong preference for riffles. That value is 3 times higher than that observed for the high quality GHSI class in the microhabitat analysis. Beyond riffles, we found significant preferences for riffle entrance, run, and secondary channel units, in decreasing order. Glide is a unit with a lot of area in the river and very few redds, so its ratio was only 0.48. It is not a preferred unit. The three bar features (lateral bar, medial bar, and point bar) did have minimal utilization, but again all of their electivity indices were below 1. Thus, there is a clear distinction between units- salmon are absolutely using riffle, riffle entrance, run, and secondary channel units. A few individuals are also straying into glides and bars and spawning there. Spawners are completely avoiding the use of backwaters, chutes, forced pools, pools, or recirculations.

Substrate Analysis

Substrate character is an important factor affecting salmon spawning location. When I first started working on the project in 2003, I heard claims that the substrates in TBR were too coarse for spawning, leading to proposals for river rehabilitation projects. Before Englebright dam was built, the hydraulic mining deposits that filled the entire valley were composed of a mixture of all sizes of noncohesive alluvial sediments. That mixture is still preserved in alluvial terraces on the hillsides that exist as remnant deposits. For example, at Blue Point Mine and on

Timbuctoo Bend 2006 Preferred and Avoided Morphological Units

Morphological Unit	Redds	% Redds	Electivity
Backwater	0	0.00	0.00
Chute	0	0.00	0.00
Forced Pool	0	0.00	0.00
Glide	22	4.69	0.48
Pool	0	0.00	0.00
Recirculation	0	0.00	0.00
Riffle	322	68.66	9.38
Riffle Entrance	53	11.30	4.31
Run	39	8.32	3.87
Secondary Channel	19	4.05	3.50
Lateral Bar	7	1.49	0.27
Medial Bar	4	0.85	0.45
Point Bar	3	0.64	0.29
Cutbank	0	0.00	0.00
Floodplain	0	0.00	0.00
Hillside	0	0.00	0.00
Tailings	0	0.00	0.00
Terrace	0	0.00	0.00
Tertiary Channel	0	0.00	0.00
Tributary Delta	0	0.00	0.00
TOTAL	469	100.00	

Figure 74

the east bank at the Parks Bar Riffle, you can dig into the terrace deposits and find all sizes of sediment. It is also found under the riverbed when you dig down into the submerged bed or down into the floodplains, as we have done. However, once those materials wash in to the river or are exhumed as the river incises down, silt and sand sized particles wash away, leaving local patches of fine gravel, medium gravel, and coarse gravel depending on the geomorphic unit that's present. In terms of the substrate type and quality, we have visually observed that the material in TBR includes a full range of material from sand sizes to coarse gravel and cobble (Fig. 75).

Over a 4-year period we have conducted many pebble counts and other substrate analyses to characterize conditions in TBR. During 2003-2005 (prior to the May 2005 flood), the general sedimentary characteristics across the entire TBAR site were visually assessed and mapped. This data was subsequently linked to the individual morphological units identified at the site, as reported in detail in Appendix 4. In this procedure, sediment character was defined in terms of the dominant and subdominant size classes (i.e., boulder>256 mm, cobble 64–256 mm, gravel 2–64 mm, sand and finer <2 mm, all sizes being intermediate axis diameter). Using the "Wolman-walk" procedure (Wolman, 1954), 44 pebble counts were also conducted at the study site. Although they were all carried out under low discharge, flows in the chute and run were too deep and/or fast to permit sampling using this technique. Thus, samples were not evenly distributed throughout the site or across all morphological units; they tended to be biased toward accessible channel margin locations. Therefore, only backwater, recirculation zone, riffle entrance and run units were sampled. At each location, ≥100 particles (mean=120, range=100–219) were sampled across a ~3×3 m section of the bed. The position of the center point of each sampling location was surveyed using a Topcon GTS-802A robotic total station.

TBR Substrate Types and Quality

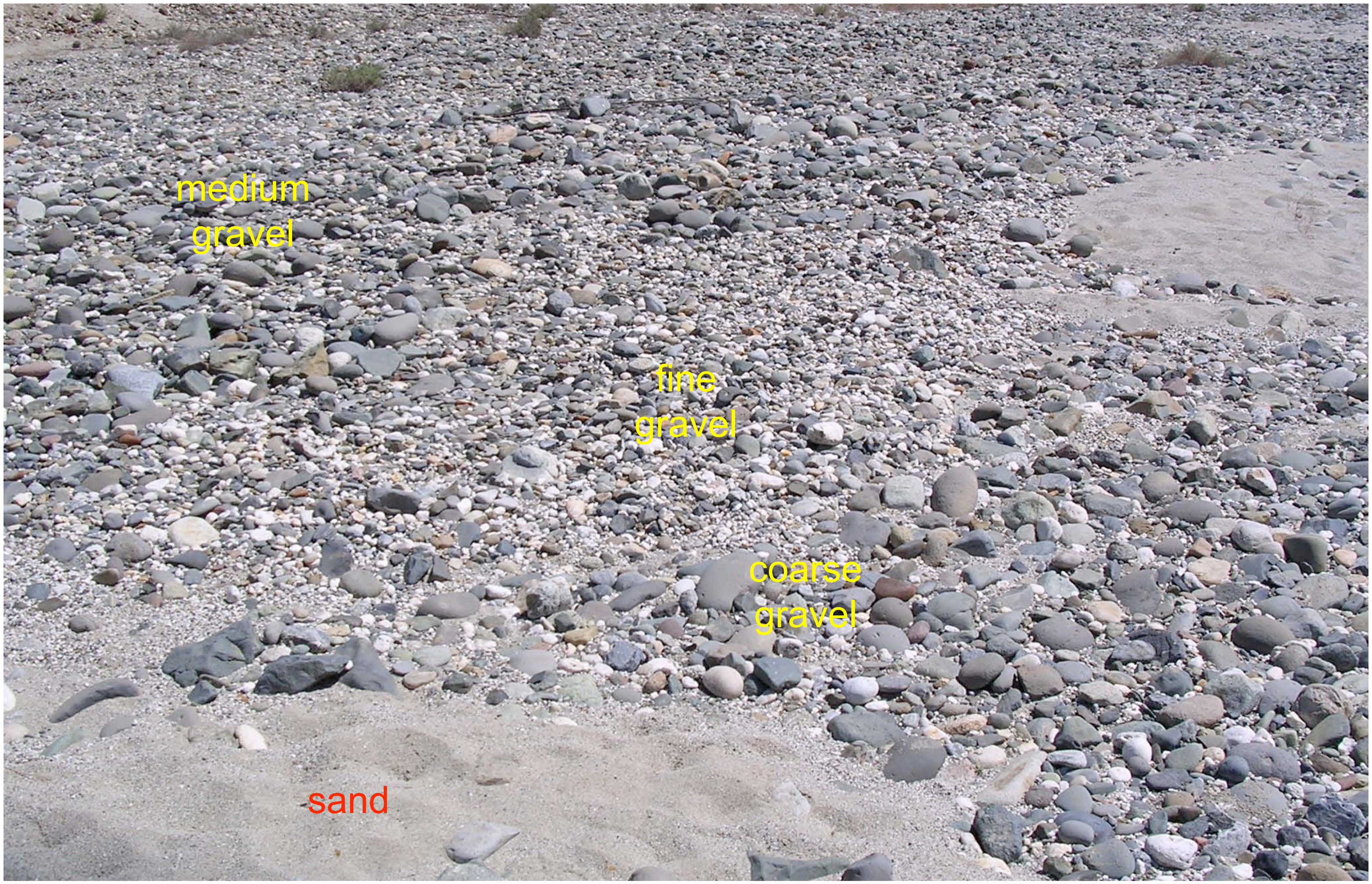

Figure 75

For this 2004 set of pebble counts, the median particle size was 62.1 mm, the D_{16} was 35.1 mm, the D_{84} was 105.8, and the D_{90} was 122.7 (where the subscript denotes the percent of particles smaller than). Consequently, we used 60 mm as the representative particle size for calculating Shields stress using 2D hydrodynamic model results to predict the sediment transport regime in the LYR.

Utilized vs Available Substrates

In autumn 2005 and 2006, we performed a study to compare and contrast utilized versus available substrates on the highly utilized riffle at the TBAR site. In September to November 2005 (after the May 2005 flood), hydraulics and sediment were characterized at redds concurrently with spawning activity. Because of the May 2005 flood, the surface that the redds were formed out of was flat and morphologically indistinguishable, so the only site differences could have been at the microhabitat level of hydraulics and substrate sizes. Individual redds (n=104) were identified by a highly experienced observer based on diagnostic macro-topography and freshly turned sediment distinct from the algae-covered, undisturbed bed material. Any redd lacking a distinct tail-spill was not sampled. Pebble counts (Wolman 1954) were taken in the redd tail-spill to characterise the size distribution of particles mobilised by spawners. Within each tail-spill >50 particles (mean = 64.0, range = 50-81) were sampled, because the area of each was small. Depth and velocity were measured at 3-6 points adjacent to and upstream of redds over undisturbed sediment; the number of sample points depended on the size of the redd. Velocity was measured with a Marsh-McBirney Flo-Mate 2000 at 30 Hz and averaged over 30 sec at 0.2 and 0.8 × depth from water surface (Byrd et al., 2000). The 0.2 × depth measurement represented the near bed interface where fish spawn. Measurement errors were ±1 cm for depth using a stadia rod and ±33 mm/s root mean square for velocity.

To characterize the un-spawned gravel bed, joint pebble counts and hydraulic measurements were taken prior to spawning in August and September 2006 at 81 locations on the riffle. Even though this sampling was done a year after redd characterization, a winter flood erased redd topography between the two sampling periods, yielding a flat, undifferentiated surface for characterizing undisturbed bed conditions. In summer 2006 (after the New Year's 2006 flood) we performed 71 pebble counts on available riffle habitat prior to spawning to characterize "available" substrates in the strongly preferred mesohabitat at the TBAR site as well as 20 other pebble conts of other morphological units at the TBAR site. At each location, >100 particles (mean = 109.9, range = 100-130) were sampled over a ~3m×3m section of the bed. Hydraulic measurements (same procedures as above) were taken at points ~1 m inside the vertices of the sample square and at its centre (n=5 per sample square).

Chinook were observed to spawn in a wider range of physical conditions than previously reported for a specific site (Fig. 76). The median grain size of fish-mobilized sediment varied from 29.2-79.9 mm (mean = 49.2 mm), depth from 0.17-0.76 m (mean = 0.37 m), mean column velocity from 0.20-1.34 m/s (mean = 0.66 m/s) near-surface velocity (i.e., 0.8×depth) from 0.24-1.72 m/s (mean = 0.82 m/s), and near-bed velocity (i.e., 0.2×depth) from 0.15-1.03 m/s (mean = 0.52 m/s). Sediment sizes for a given flow velocity tended to be smaller for the 2005 redd data than 2006 available conditions. Qualitative observations of the size of fish spawning at specific redds revealed no consistent pattern with physical conditions. Regression analysis between hydraulic and sedimentary variables revealed statistically significant relationships for the 2005 redds, but not for 2006 availability. Highest levels of significance (i.e., $P<0.001$) were obtained

Size of Sediment Moved by Spawners Is A Function of Ambient Hydraulics

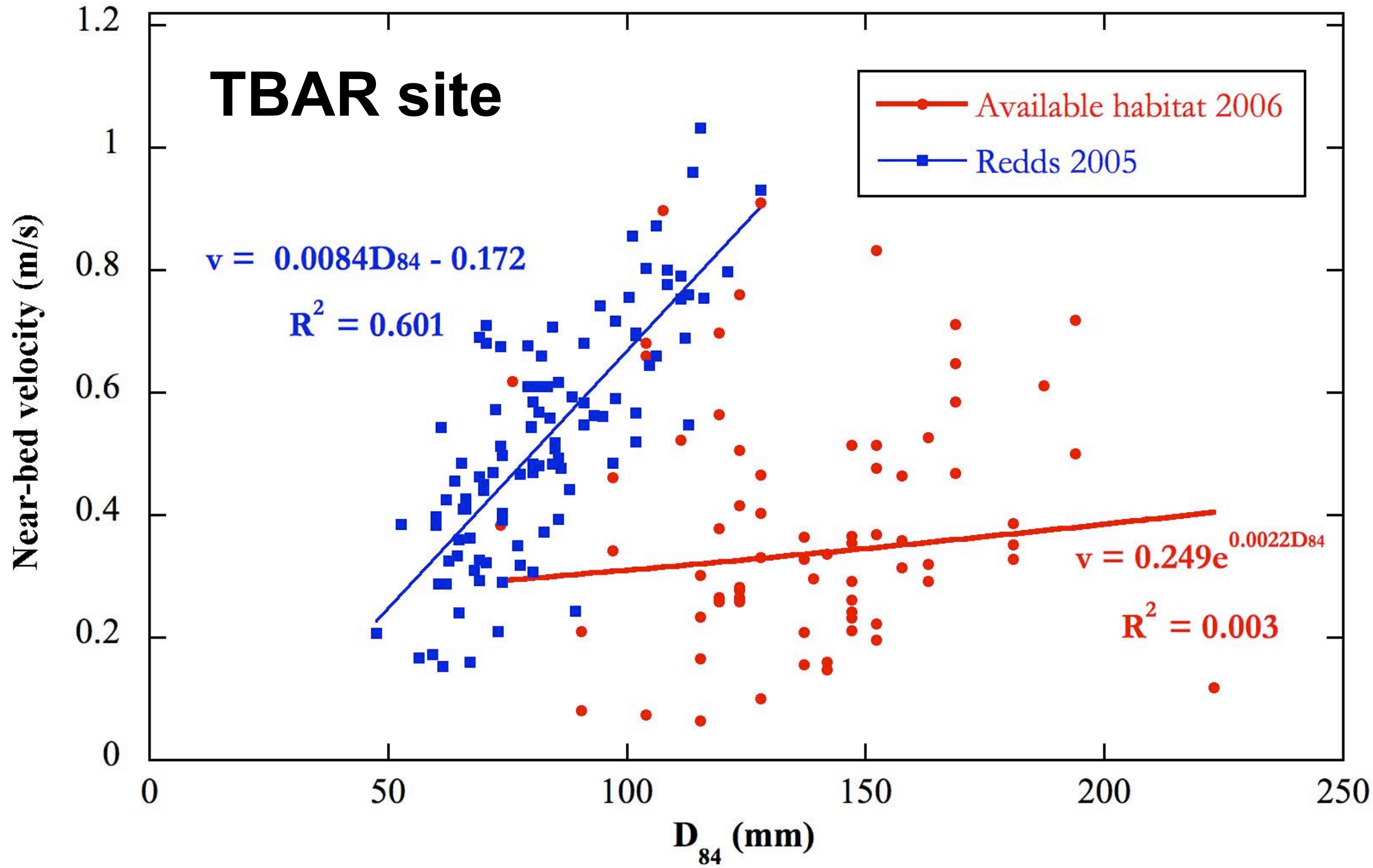

Figure 76

for all velocity variables (i.e., mean column, 0.2×depth, 0.8×depth) and the coarser fraction of sediment (i.e., D_{84}). Compared to mean column or 0.8×depth values, near-bed velocity (i.e., 0.2×depth) had consistently the highest R^2 values.

The 2005 and 2006 TBAR pebble counts demonstrated that Chinook salmon have elastic preferences for individual habitat components (i.e., depth, velocity and substrate size) governed by the relations among all characterized habitat components; spawning fish select specific combinations of micro-scale hydraulic and sedimentary variables. In other words, fish selected coarser substrate in faster flow and finer substrate if associated with velocities sufficiently low to permit the maintenance of that substrate caliber. The latter condition provided smaller values for velocity and sediment size than quoted in the literature for spawning Chinook. The data further showed that relationships between micro-habitat variables did not simply reflect available joint sedimentary-hydraulic conditions (i.e., through a hydraulic sorting mechanism); pre-spawning surveys across the entire study site showed no significant relationship between any combination of sedimentary and hydraulic descriptors. Although the utilization and available datasets were from consecutive spawning seasons separated by a major flood, the contrasting within dataset relationships are valid.

TBR Longitudinal Substrate Survey

We also did a longitudinal survey of substrate for the whole TBR in late summer 2006. Because grain size analysis is a very labor intensive activity, there is just no way we could sample every morphological unit, so what we did is we walked along the edge of the river from the top of Timbuctoo Bend all the way around to the bottom and we measured the size of sediments using Wolman Pebble Counts adjacent to each riffle and each pool and in the runs. We performed 42 pebble counts in all, with each count consisting of 100 particles. Sieve size ranges (b-axis) were determined, classified on the basis of square holes scaled at 1/2 phi intervals. At each measurement location, the geographical coordinates were measured using a real-time differential GPS (Trimble Pathfinder Pro XRS). What we found is that the substrate size distribution was normal for shallow gravel bed rivers, with a median size of 54.9 mm, a D_{16} of 22.9, and a D_{90} of 163 mm (Fig. 77). Compared with the distribution at the TBAR site in 2004 before the 2 major floods, the median is lower and the D90 higher, so that suggests that after the floods the size range is wider, reflecting the wide composition of the underlying hydraulic mining debris. When the grain size data was plotted as a function of distance downstream (Fig. 78), there was no statistically significant longitudinal trend in grain size in the river overall. One outlier in the riffle substrate data biased the riffle trend, so that should be discounted. All other samples exhibited a random distribution. Thus, there is a uniform distribution of substrate sizes down TBR with no differentiation between riffles and pools in 2006.

Knickpoint Substrate Differentiation

In summer 2007 we performed 9 pebble counts as part of the knickpoint migration study at the 3 TBAR and the Parks Bar Riffle sites. At each site, a count was made at the head of the knickpoint where flow was shallow and fast and one was made in the water on each flank of knickpoint. The median size observed at these locations was 79.9 mm and the D_{90} was 79.1 mm (Fig. 79). Thus by summer 2007 the substrates in the knickpoints had already become somewhat coarser than the size distribution observed for TBR overall in 2006. Thus, knickpoint migration is a key process responsible for differentiating substrates locally in the TBR.

2006 TBR Substrate Size Distribution

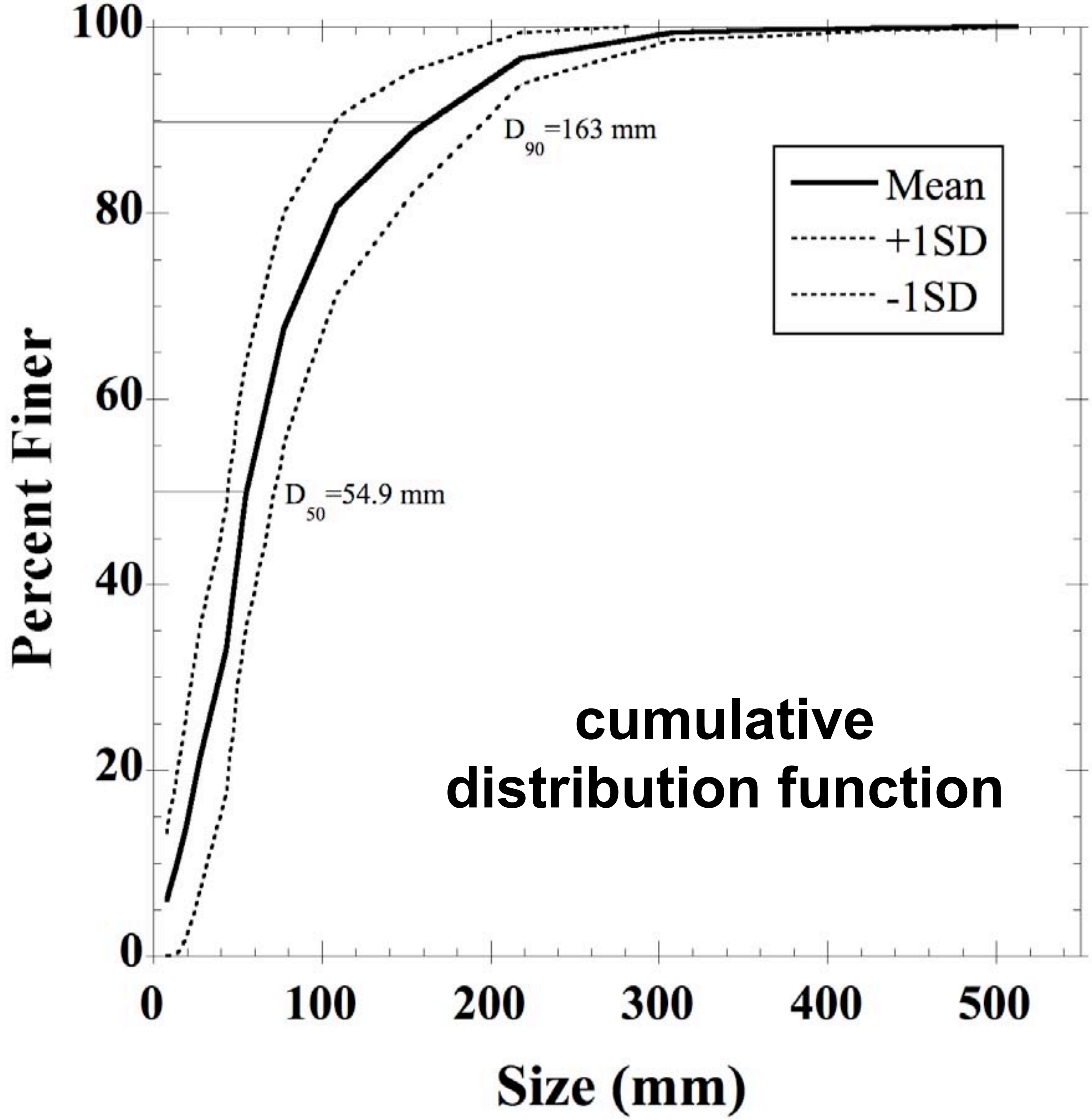

Median substrate size for TBR after the New Year's 2006 flood was 54.9 mm, which is in the highly preferred size range for salmon spawning

Figure 77

2006 TBR D_{50} Longitudinal Distribution

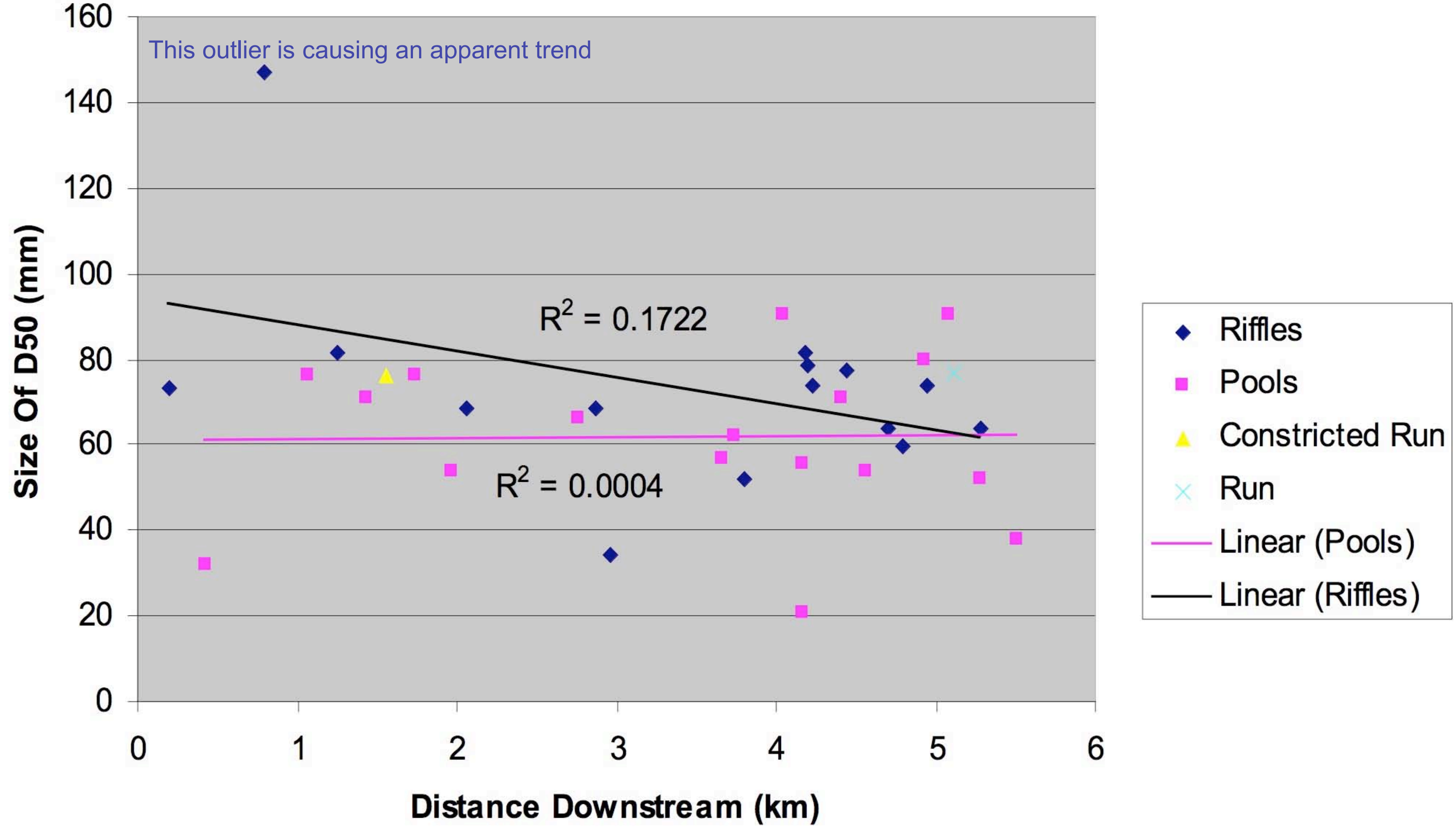

Figure 78

2007 Knickpoint Substrate Survey

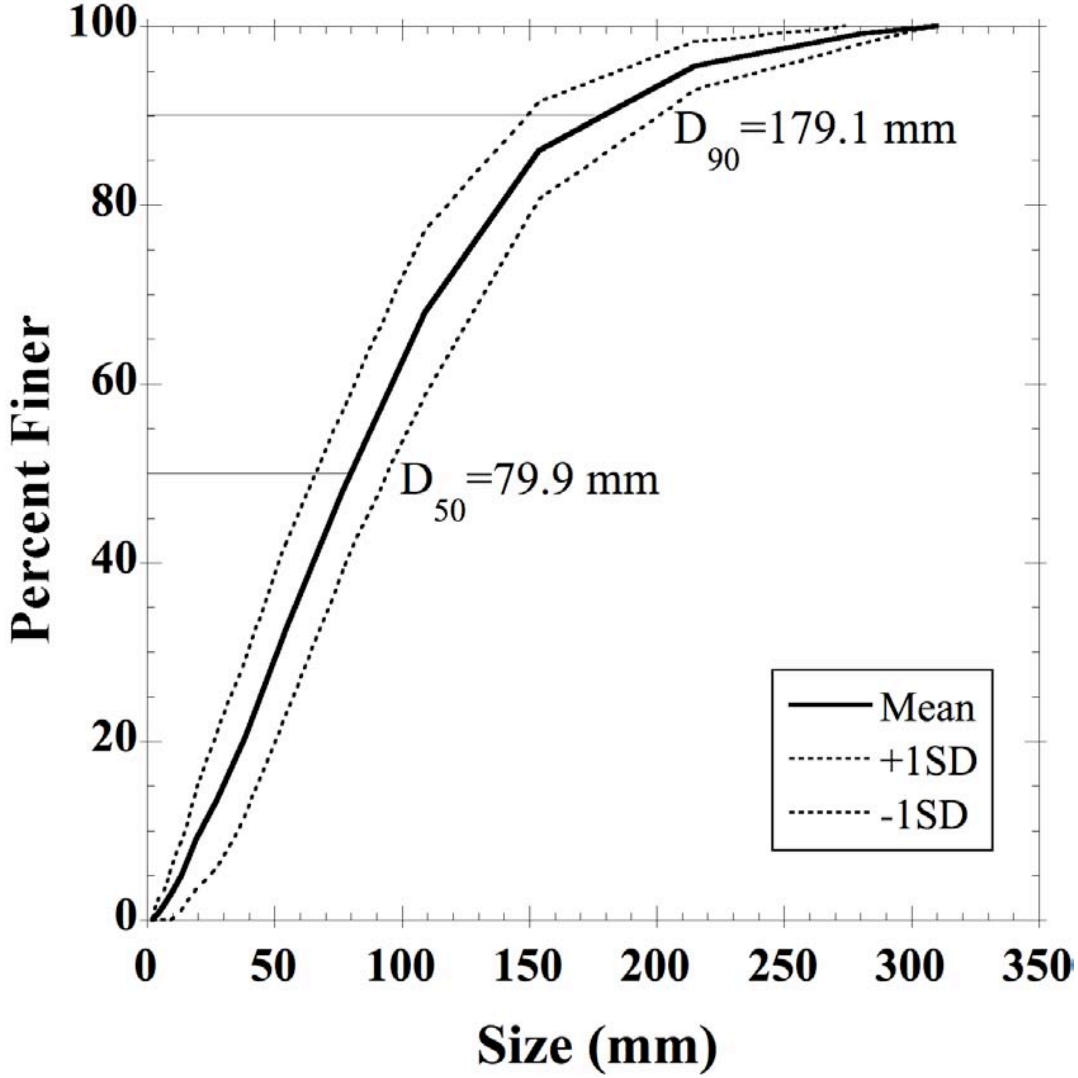

By summer 2007, the substrate median size at knickpoints was substantially coarser than the median size for TBR observed in 2006.

Figure 79

Functional Flows Model

The Functional Flows Model (FFM) was created as part of this study to integrate the role of hydrogeomorphic processes and ecological functions in riverine physical-habitat evaluations. Functional flows are discharges that serve ecological functions. In terms of the extent of in-stream habitat processes, the functional flows model is more complete than other models that assess physical habitat (e.g. IFIM, Rosgen classification, IHA, etc.), because it includes metrics of hydrologic, hydraulic, geomorphic, and ecologic dynamics (Fig. 80). FFM constitutes a robust conceptual framework to identify ecological functions and their relation to physical processes, and a coarse approach to assess functionality of habitat units that can be used at the reach and basin scales. The exploration of complex linkages among hydraulic, geomorphic, and ecologic variables constitutes the new scientific advancement of this study. Because the methods and results are quite different in what they say about a river compared to methods that managers are more used to (e.g. IFIM), only a summary of the findings is presented here, emphasizing the key conclusions. *A detailed explanation of the FFM, its assumptions, benefits, and full results related to the TBR is presented in Appendix 5.*

Events that cause rapid hydrogeomorphic changes have dramatic impacts on local habitat conditions. For example, natural floods change channel morphology, substrate composition, hydraulics, and floodplain connectivity. These alterations affect ecological functionality of physical habitat for organisms that interact with the water column and the river bed. Before a morphologic alteration, specific flow magnitudes generate certain water depths and velocities, causing specific bed mobility stages that may be functional for an organism life stage. After a morphologic alteration, the same flow magnitude may generate higher or lower water depths and

Approach	Process Considered			Spatial scale			Examples	Main characteristic
	Hydro	Geo	Eco	Habitat unit	Reach	Basin		
Biotic Integrity Indices	NO	NO	YES	X	XX	XX	Regional biotic integrity (Miller et al. 1988) Biotic integrity evaluation (Moyle and Randall, 1998)	Measures of species structure and function to monitor environmental changes
Geomorphic Classification Systems	NO	YES	NO	X	XX	XX	Rosgen classification (Rosgen, 1994) Channel morphology (Montgomery and Buffington, 1997) River Styles (Brierley and Fryirs, 2000)	Categorization framework to group morphological features
Indices of Hydrologic Alteration	YES	NO	NO			X	The Natural Flow Regime (Poff et al. 1997) IHA (Richter et al. 1996)	Statistical parameters of discharge to assess changes over time
Habitat Delineation	YES	YES	NO	X	XX		Reconnaissance survey (Thorne, 1998) Habitat mapping (Maddock, 1999)	Standard procedures to record geomorphic characteristics
Physical Habitat and Species Relations	YES	NO	YES	X	XX		Egg-to-smolt survival rates (McHugh et al. 2003) Fish guilds and hydraulics relations (Lamoroux and Cattaneo, 2006) Fish distribution from stream variables (Mugodo et al. 2006)	Statistical correlations of physical habitat parameters and biological measurements
Cross-sectional Habitat Modeling	YES	NO	YES	X	XX		PHABSIM (Bovee et al. 1998)	Analytical or 1D hydraulic modeling, cross sectional data, and habitat suitability curves to predict habitat availability
2D Habitat Modeling	YES	NO	YES	X			Numerical Habitat Model - NHM (Guay et al. 2000) FEWMS and GHSI (Pasternack et al. 2004) SHIRA (Weaton et al. 2004)	2D hydraulic modeling and topographic survey coupled to habitat suitability curves to predict habitat quality

Note: Approaches are grouped based on habitat processes and spatial scales considered. X indicates the scale at which it was developed, XX indicates other scales at which it has been applied.

Other Methods In Relation To FFM

Figure 80

velocities causing a dissimilar bed mobility stage changing its functionality. Consequently, the functionality of a specific hydrograph can change in river sections where rapid hydrogeomorphic changes occur. Likewise, sites with different morphologies may behave different in terms of their hydraulics and sediment transport stages, causing differences in ecological functionality

Assessments of flow functionality before and after changes in physical characteristics of habitat and at sites with different morphologies within a reach allow the identification of the effect of hydrogeomorphic processes and morphology on ecological functionality. The functional flows model is used to address fundamental research questions to analyze differences in habitat functionality due to gravel augmentation, natural floods, and differences in channel morphology. *The overall hypothesis of this study is that differences in hydrogeomorphic conditions due to rapid alterations in channel morphology and due to differences in channel form induce changes in ecological performance of physical habitat.*

The assessment of functional flows in locations where ecological functions occur is based on the evaluation of shear stress dynamics. For the sake of this study in the TBR of the LYR, the FFM model was tuned for fall-run Chinook salmon spawning in gravel-bed rivers. Ecological functions studied are bed occupation, or periods when the fish interact with the river bed (i.e. spawning, incubation, and emergence), and bed preparation, or periods when the river bed surface is reworked (Fig. 81). Input variables to assess shear stress dynamics are discharge (Q), depth response to incremental discharge changes (f-exponent), water surface slope (S), and median grain size (D_{50}). The analytical framework is based on the occurrence of sediment transport stages defined by threshold values of Shields stress (Fig. 82). A flow is classified as functional when it provides a sediment transport stage favorable for ecological functions (Fig. 83). Model outputs include the number of days within a water year that present functional flows,

FFM Ecological Functions Evaluated

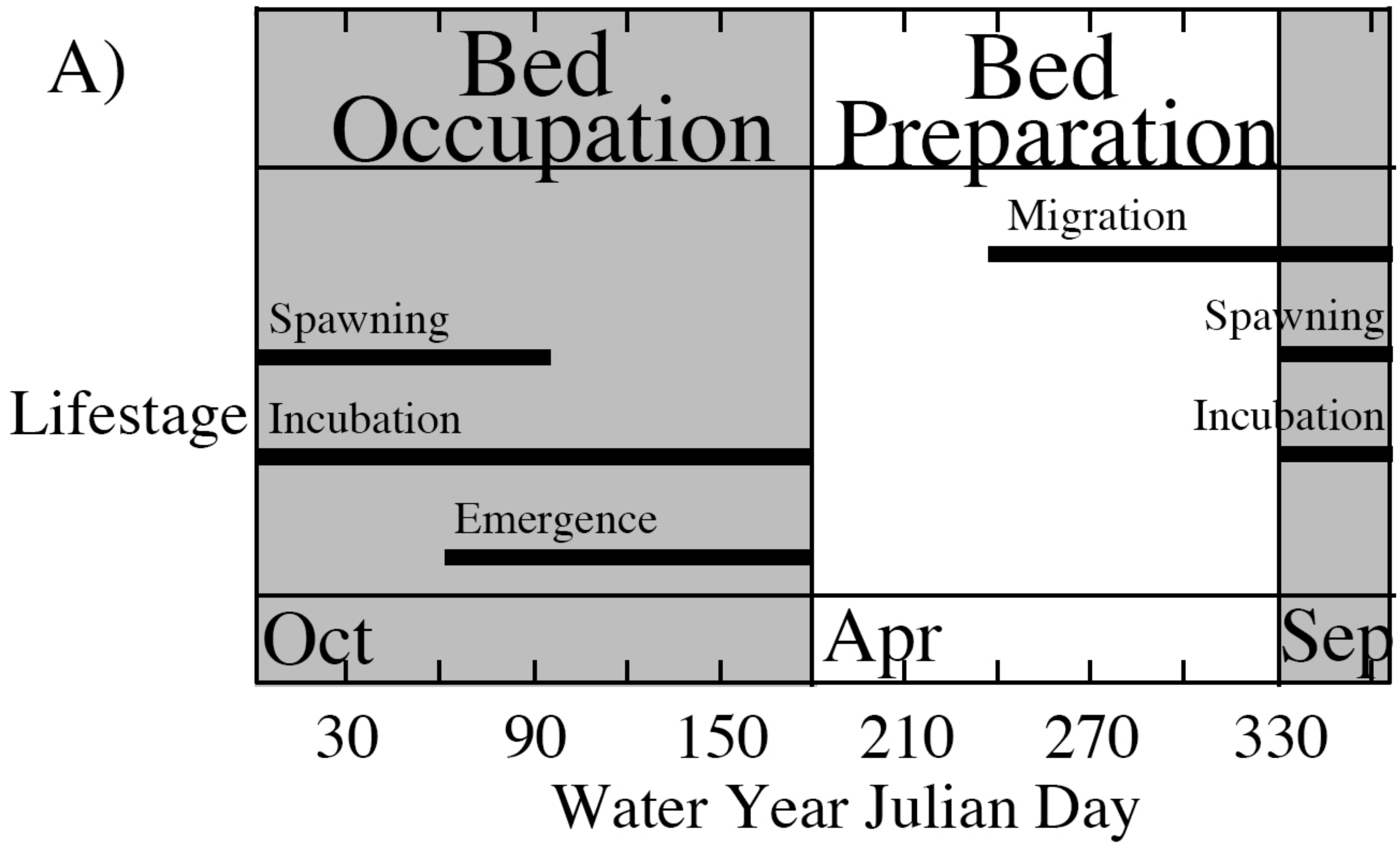

Figure 81

FFM Definitions of “Functional” Hydrogeomorphic Conditions

1	2A	2B	3	4	5	6
Flow Magnitude/	**Functional Flows Delimiters**		**Bed Occupation**			**Bed**
Bed Mobility Stage	**In terms of τ_o vs τ_{c50}**	**In terms of τ_o* vs Shields #**	**Spawning**	**Embryo Incubation**	**Emergence**	**Preparation**
High/ Full mobility (FM)	$\tau_o > \tau_{c50}$	$0.06 < \tau_o^* < 0.1$	Non-functional	Non-functional	Non-functional	Functional
Intermediate High/ Interstitial fines mobility (IFM)	$\tau_o = \tau_{c50}$	$0.03 < \tau_o^* < 0.06$	Non-functional	Non-functional	Non-functional	Functional
Intermediate Low/ Superficial fines mobility (SFM)	$\tau_o < \tau_{c50}$	$0.01 < \tau_o^* < 0.03$	Functional	Functional	Functional	Non-functional
Low/ Stable bed (SB)	$\tau_o << \tau_{c50}$	$\tau_o^* < 0.01$	Functional	Non-functional	Functional	Non-functional

Figure 82

FFM Quantitative Methodology

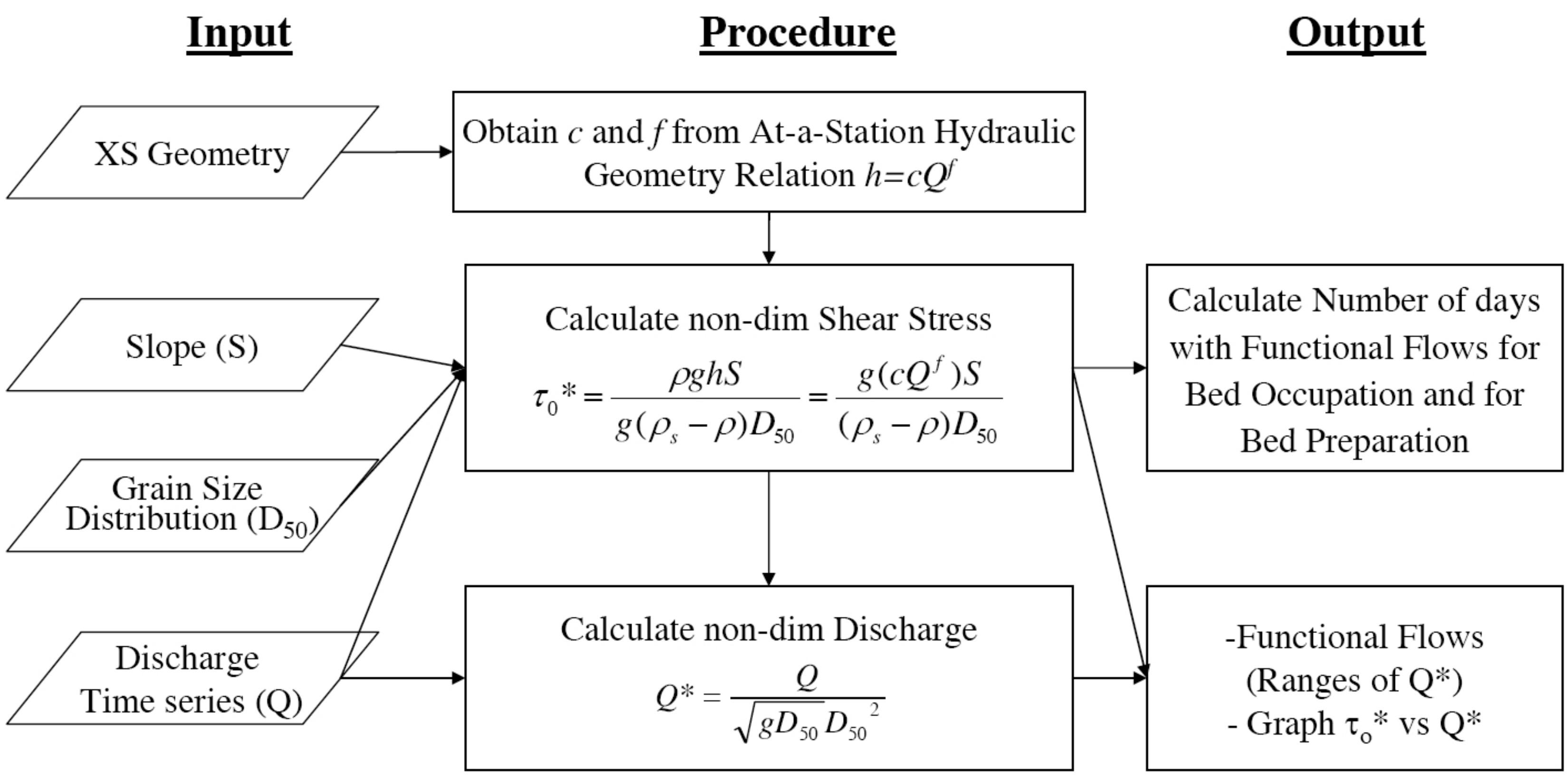

Figure 83

the ranges of functional flows that provide sediment transport stages favorable for each ecological function, and the efficiency of a site to produce functional flows from available flows. Statistical significance of the results is tested using non-parametric methods.

In the FFM analysis of TBR, 4 cross-sections were analyzed using the 2003-2004 and 2004-2005 water year daily discharge records. The results indicated that the May 2005 flood changed the geomorphology of the river such that it increased the *potential* ranges of functional flows for all cross sections for all water years (Fig. 84, top graph). Changes in hydrogeomorphic variables (S, D50, c, and f) and the functional ranges of Q* caused by the flood were statistically significant above the 97.5 % confidence level ($p<0.001$, <0.001, <0.025, <0.0025, <0.005 respectively). However, having an increase in potential for functionality only translates into actual change if the actual flows after the flood span the wider range that can yield functionality. It turns out that the actual flows after the May 2005 flood did increase the number of days with functional flows at the study sites. This can be seen in the lower graph in Figure 84, where the height of the bars for 04-05 water year are higher than those for the 03-04 water year. However, you can also see in Figure 84 that there was a high occurrence of days with functional flows before the flood, so the actual scale of the change in ecological functionality was not statistically significant. Thus, the overall effect of the flood was to create more potential functionality and some more actual functionality, but that potential was not fully realized due to the post-flood flow regime being relatively similar to the pre-flood regime, despite the flood peak itself. Full results and discussion are provided in Appendix 5, because of the unique nature of the method and findings. This study supports the hypothesis that it is possible to measure the changes in ecological functionality of the habitat by measuring hydrogeomorphic changes.

FFM Results

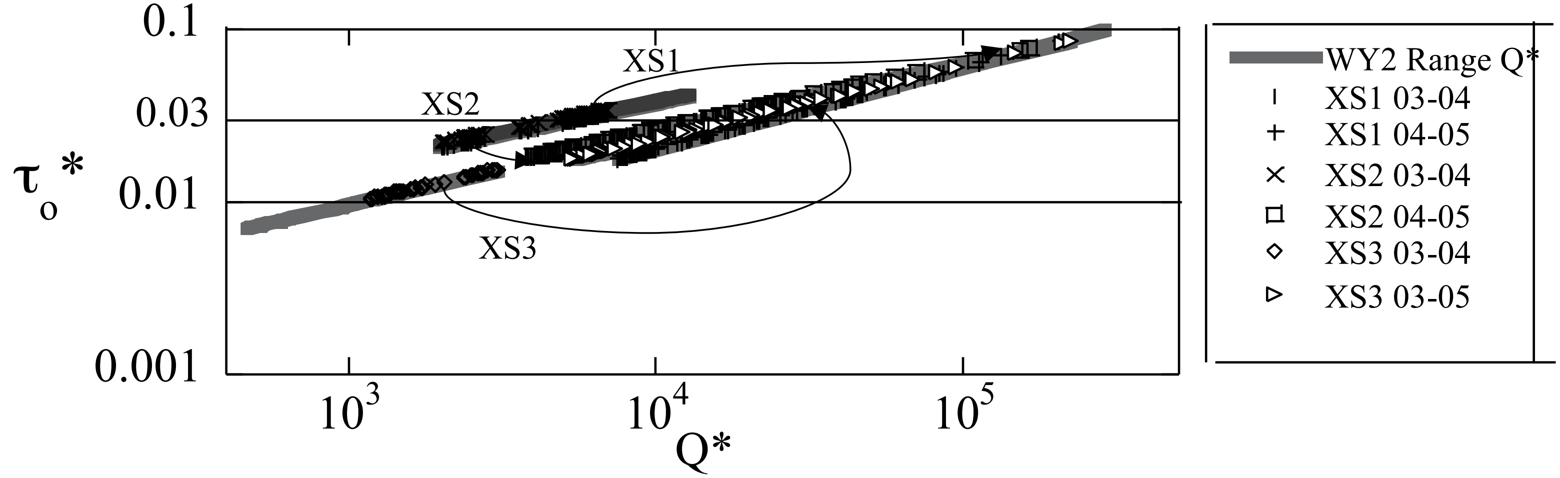

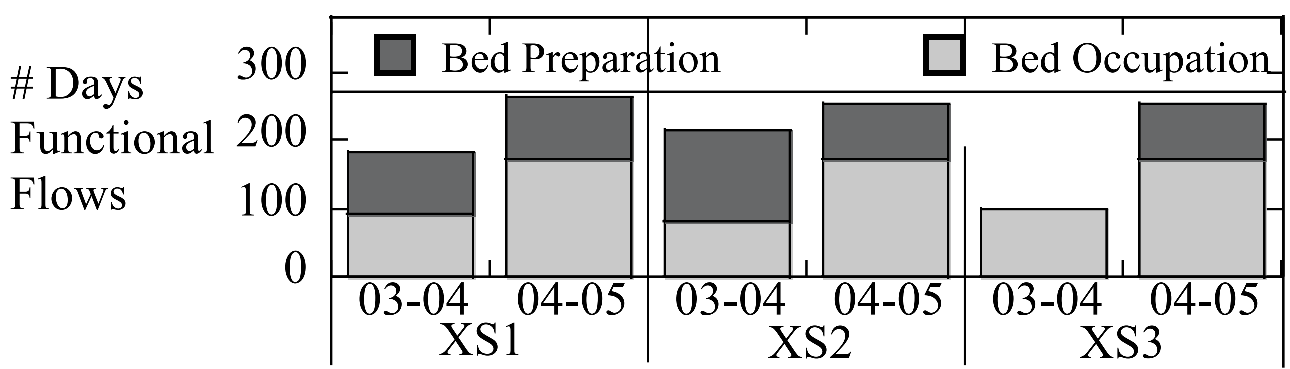

Figure 84

Comprehensive TBR Microhabitat Model

The top criticism of 2D models that is often leveled against using them is that they are too costly to create and then are limited to only small sites. The mapping effort for TBR proved that the primary data input for a 2D model- the river DEM- can be achieved at a low cost. In fact, an effort is now underway to obtain an even more detailed map and DEM of the entire LYR for under $100,000. Other data inputs for a 2D model are relatively easy to obtain by comparison.

Recently the U.S. Bureau of Reclamation has created a new 2D model called SRH-2D and made it freely available to the public. The new model is highly efficient in its computations and is also highly stable in performing wetting and drying, which is a common problem of other 2D models. The way it has been programmed, it is highly automated. Thus, it is now possible to make 2D models of dramatically larger river segments than before, while retaining the same high resolution desired for characterizing microhabitat.

As a test, I re-modeled the 2004 TBAR site spawning flow and found that the SRH model performed as well as the FESWMS model I had been using previously at the cross-sections where I had field observations of depth and velocity. SRH outperformed FESWMS in yielding highly coherent vortices and eddies behind obstructions, while FESWMS outperformed SRH in predicting the peak velocity over steep riffle crests. These difference can be traced back to the subtle differences in the fluid mechanics equations used by the models. Overall, the two models perform similarly, but SRH is dramatically more efficient. Once I was satisfied with the performance of SRH, I took advantage of its power and ran a model of the entire TBR using the 2006 topography. For this initial test I modeled a flow of 1667 cfs, which was close to the flow level at the time this report was being written. In this model, I used a 3’ internodal spacing for the perennial channel and a 3-15' internodal spacing for the rest of the river corridor. The mesh is so big and so refined that it is not possible to show the whole mesh and see its details in one view, so Figure 85 shows a small portion of the mesh just upstream of the Highway 20 bridge. You can see how small the mesh elements are in the river. Using an Intel 2.8 GHz Xeon (Harpertown) processor, SRH took 8 days to solve the computational problem, starting with a dry river bed. Subsequent runs at other discharges can start from this initial solution at 1667 cfs and go up or down from there very quickly.

The SRH-2D model of TBR at 1667 cfs shows the pattern geomorphic units in the river and how they affect channel hydraulics (Figs. 86-88). Depths range from 0-25'. Velocities range form 0-11 ft/s. The most notable finding form this comprehensive model is that when the median grain size of the river bed is used to calculate the spatial pattern of Shields stress and the sediment transport regime, then the model predicts that every riffle in TBR is experiencing widespread partial transport with focused locations of full mobility (Fig. 88). These locations of full mobility are exactly those horseshoe knickpoints that we have already confirmed to be eroding. Thus, the SRH-2D model captures the most important observed geomorphic phenomenon in the river at this discharge. It also simulates riffles that we did not take measurements on, and thus allows us to see that those riffles are also experiencing the same knickpoint process. There was not time to apply HSCs to the model results, but clearly that would be possible to do to obtain a comprehensive assessment of habitat availability in TBR.

REVIEW OF KEY TBR SCIENTIFIC FINDINGS

New SRH-2D Model of TBR

3’ internodal spacing in perennial channel, 3-15’ internodal spacing elsewhere

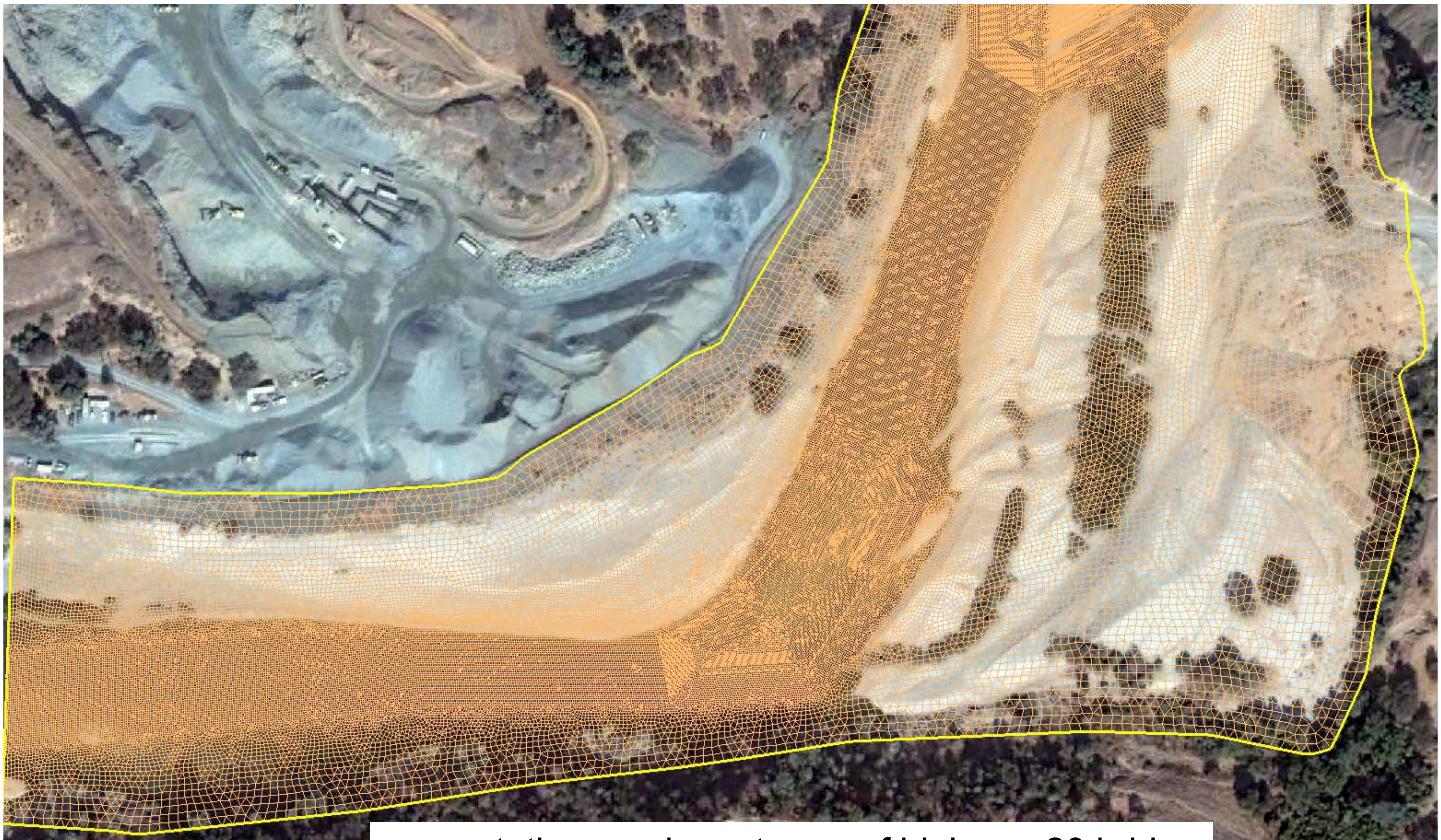

computation mesh upstream of highway 20 bridge

Figure 85

SRH-2D Depth Results

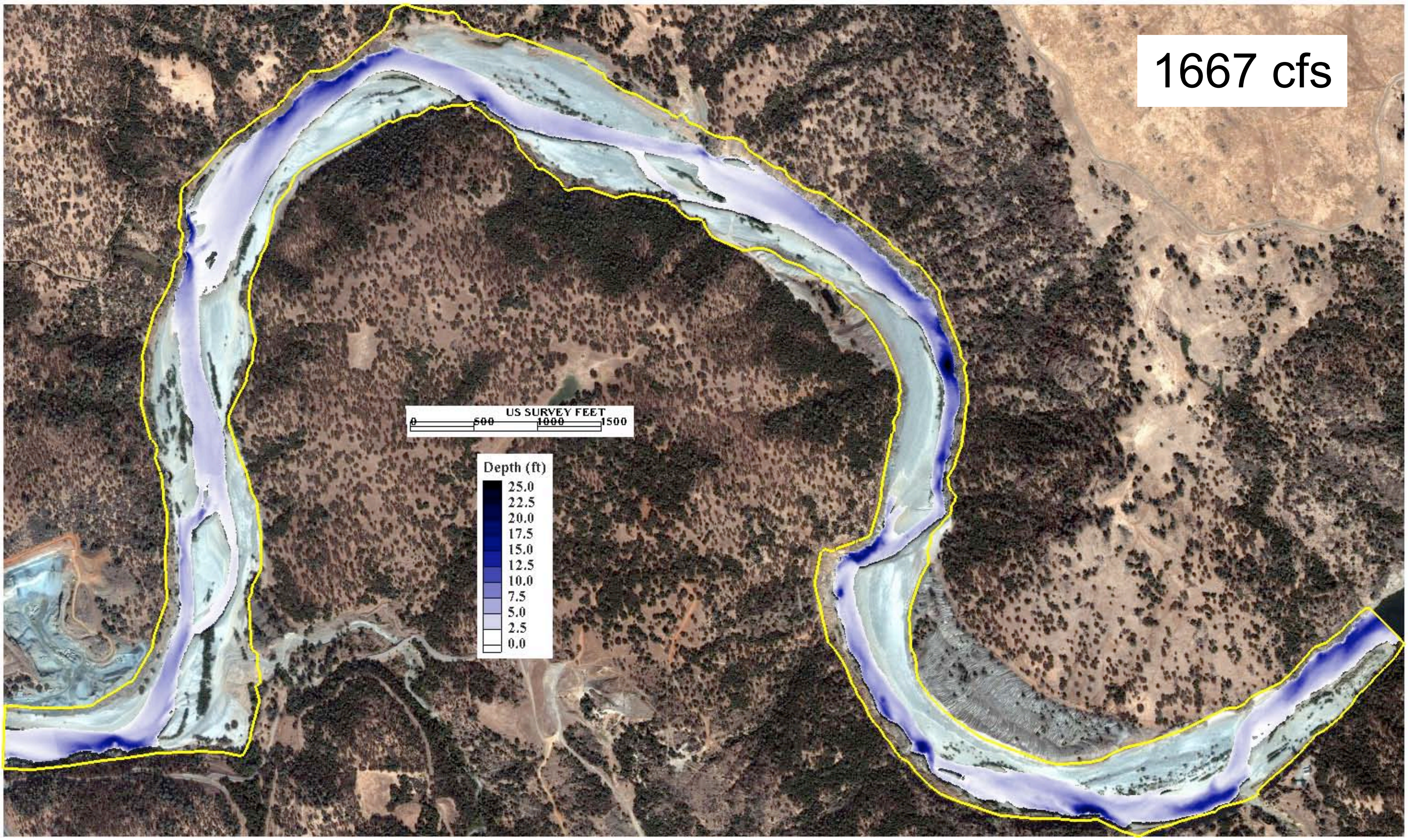

Figure 86

SRH-2D Velocity Results

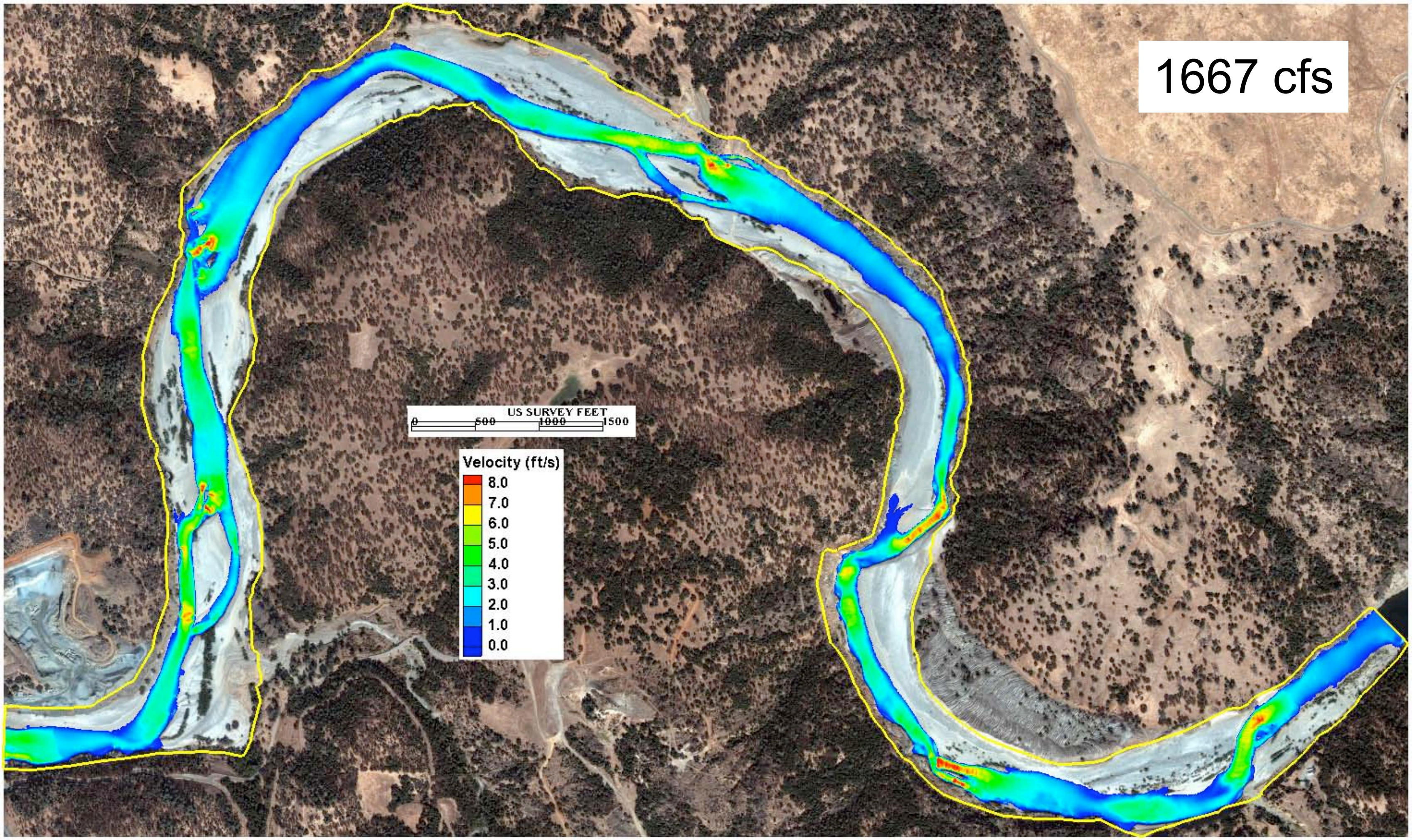

Figure 87

SRH-2D Shields Stress Results

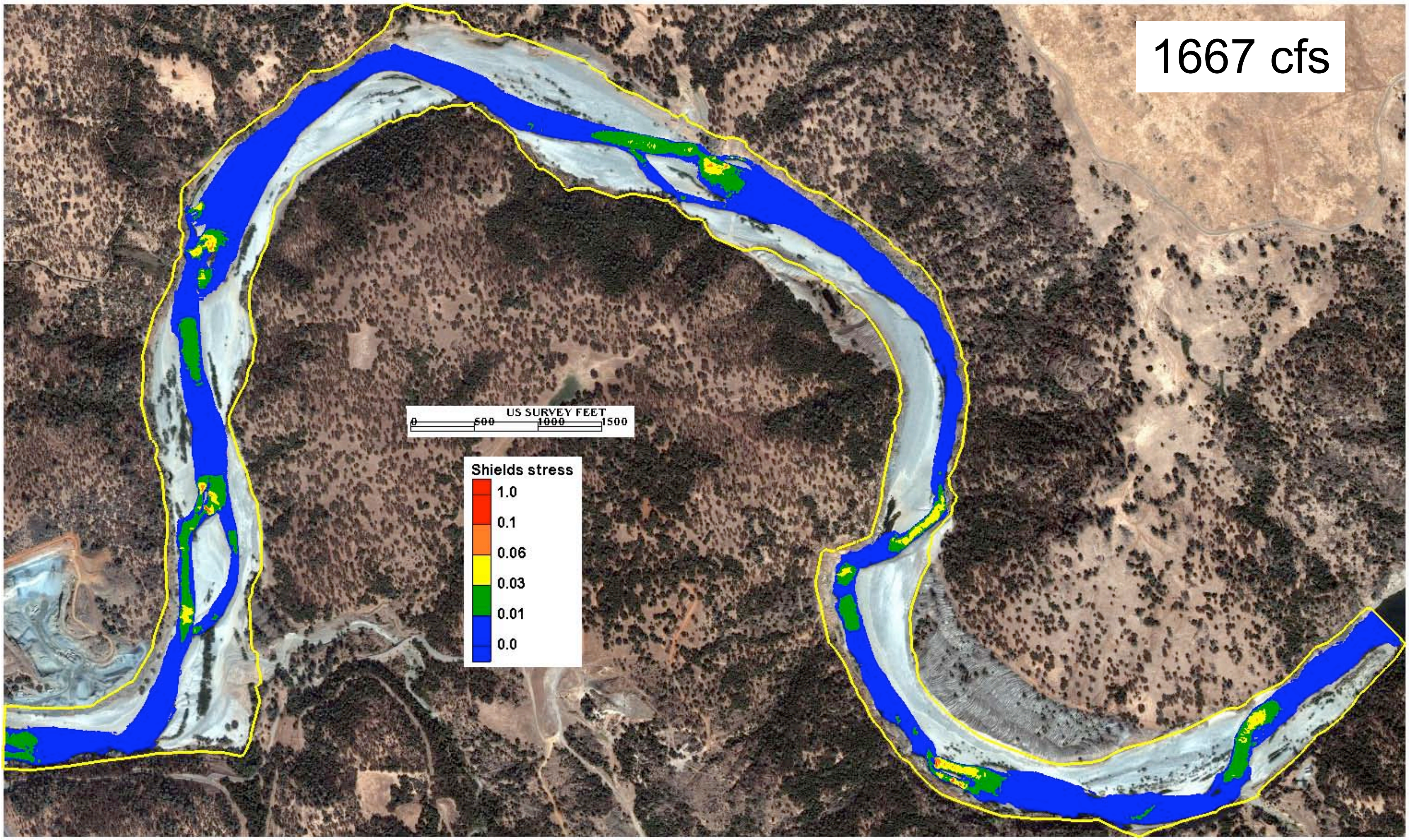

Figure 88

The Timbuctoo Bend Reach is downcutting, there is absolutely no question about that. It is systematically incising, but even though it is incising, it is self-sustaining its morphological units over decades, renewing its substrates, and maintaining its level of ecological functionality. The mechanism that explains what is happening in the river is that during short-duration floods incision is focused in pools. This serves to renew and enhance riffle-pool relief. After a flood, the accentuated riffle-pool relief yields a steep water surface slope on the back side of the riffle, including supercritical hydraulics with standing waves and localized hydraulic jumps. Those conditions cause a knickpoint to form, usually with a horseshoe or oblique planform shape. The drag stress through the knickpoint is easily storng enough to scour the bed, so such knickpoints then migrate upstream through the riffles during periods of low flow. When the low-flow periods last >4-5 years, the river bed has time to armor somewhat, but there are still large areas of unarmored bed.

When performed properly as done in this project, microhabitat simulation at a resolution of ~3' using 2D hydrodynamic models was found to accurately predict where Chinook salmon spawn in TBR. Ultimately, using microhabitat analysis for habitat assessment and flow assessment does quantify habitat, but it has no explanatory power, and thus it cannot handle or predict dynamic changes of the type that characterize the LYR. In contrast, linking microhabitat to the larger scale geomorphic processes does explain how the river functions and enables more flexibility in coping with a dynamic system. Used in conjunction, micro- and meso-habitat methods predict where salmon will spawn and explain the hydrogeomorphic foundation responsible for the habitats as they exist. The bed material size in TBR is suitable for Chinook fall-run spawning and spring-run for that matter. Thanks to knickpoint migration, there is also a lot of temporary local patches of finer gravel for steelhead spawning, although we didn't specifically analyze the microhabitat for steelhead.

TBR MANAGEMENT LESSONS

This study provides some key lessons for understanding how the LYR works. First, it is absolutely essential to appreciate the importance of what we call, "channel non-uniformity". The ratio of water depth to d_{90} (i.e. the grain size for which 90% of the material is smaller than) is a key metric for any river (Fig. 89). When this ratio is >1,000, the river is a large mainstem sand bedded river, like the Missouri or Mississippi Rivers. But as this ratio decreases, channel non-uniformity takes over as a dominant control on hydraulic, geomorphic, and ecologic processes in a river. When it is <1, the river is a steep bedrock river with enormous boulders and bedsteps that almost totally control hydraulics. The LYR falls into an intermediate zone in which the ratio is ~10. For example, if d_{90} is ~100 mm and water depth is ~1 m (i.e. 1,000 mm), then that yields a ratio of 10. Those values are typical of the LYR (Fig. 17). Consequently, any method to analyze the LYR that does not account for channel non-uniformity is going to fail. That includes widely used management tools, such as PHABSIM.

The second important lesson relates to what it takes for an incising channel, such as the LYR, to maintain its ecological functionality (Fig. 90). We have learned from this study that relief has to be maintained between riffles and pools. Associated with that relief, but at a smaller scale, you will obtain a diversity of habitats. Flow releases and channel non-uniformity were found to be the variables responsible for maintaining and rejuvenate habitat heterogeneity- not just high flows, but also low and intermediate flows, with each one serving a unique purpose, as

Lesson #1: Channel Non-Uniformity

As the water depth to bed grain size ratio decreases, channel non-uniformity takes over as a dominant control on hydraulic, geomorphic and ecologic processes in rivers.

Focus of this study

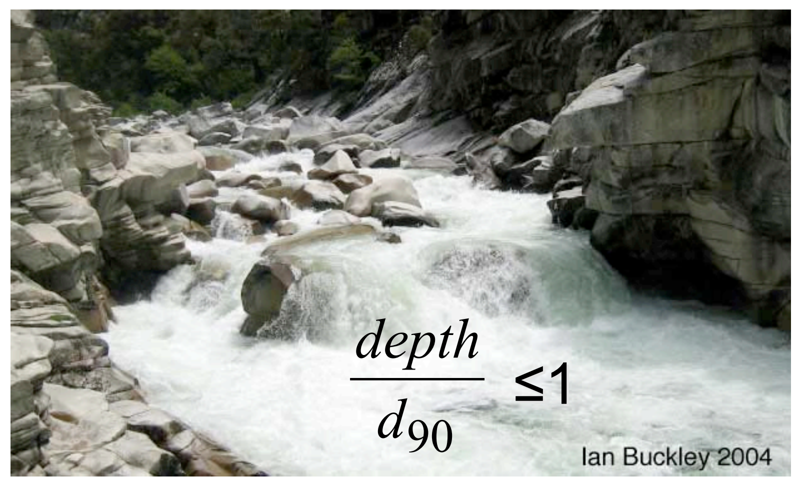

Figure 89

Lesson #2: What It Takes For An Incising Channel To Maintain Ecological Functionality

- Relief between riffles and pools must persist.
- Habitat heterogeneity needs to be rejuvenated
- Flow regime must enable channel migration to access sediment across whole floodplain
- Channel migration and overbank flooding must prevent vegetation from constraining channel dynamic.

Figure 90

outlines in the Hydrology Analysis section. For example, very low flows promote knickpoint migration that redistributes sediment locally, creating a lot of valuable diversity in substrate sizes, velocities, and depths.

The flow regime for the LYR and other Central Valley Rivers has to be dynamic enough to enable channel migration to access sediment across the whole floodplain. If that doesn't happen, then what will happen is the channel will simply incise and become trained into a very narrow, confined channel. However, that does not appear to be happening on the LYR in TBR, because the flow is accessing the whole river valley. The historical aerial photos for the LYR clearly demonstrated that the wetted channel is changing its size and shape regularly (Fig. 19). DEM differencing from 1999-2006 showed that over that 7-year-period all morphological units incised, including the floodplain, which incised an average of 15 cm. We also found that during the New Year’s 2006 flood, there were several meters of floodplain incision at the TBAR site, just as a result of that one event locally.

Finally, channel migration and overbank flooding have to be adequate enough to prevent vegetation from constraining channel dynamics. In the semi-arid climate of the Central Valley of California, many mainstem rivers are suffering from channel narrowing due to vegetation encroachment. That is not the case on the LYR. Some stakeholders are calling for riparian rehabilitation in the river corridor. However, the floodplains in the TBR are composed of lose gravel and cobble that are simply too dynamic during floods to provide a stable substrate for forest growth. It remains to be determined if that holds true for the rest of the river downstream, but the aerial photos of the river down to Daguerre Point Dam do show the floodplains submerging during floods as well as experiencing both deposition and scour. Over several years to the next few decades, the idea of trying to establish forests on these floodplains in Timbuctoo

Bend would be highly risky. It may be possible to obtain short-term benefits, if that is considered cost-effective.

In term of management recommendations for anadromous fish, this results of this study indicate that there is adequate physical habitat to support spawning of Chinook salmon and steelhead trout in their present population size. Furthermore, all of the preferred morphological units in the TBR have a lot of unutilized area and adequate substrates to serve larger populations. The best flow for providing in-channel habitat will depend on whether riffles are narrow or wide at any given time. Wider riffles will have shallower, wider, and slower conditions, and thus they will need higher flows than times when riffles are narrow. We have seen throughout history that riffle configurations have fluctuated, although the locations have persisted through time. Consequently, an IFIM study of static conditions at a moment in time has limited value for making long-term management decisions. The river has changed significant in 2005 and 2006, and will do so again every few years. It is crucial to account for the river's dynamism in management. To do that, it is best to perform predictions at both micro- and meso-scales.

SECTION 3: ENGLEBRIGHT DAM REACH (EDR) ASSESSMENT

This section of the report covers the hydraulic, geomorphic and salmon-spawning conditions in the Englebright Dam Reach of the Lower Yuba River. The EDR is defined as the LYR mainstem from Englebright Dam down to the junction with the tributary Deer Creek (Fig. 91). Technical details related to this section of the report are provided in Appendix 1.

Previously I presented the research for Timbuctoo Bend Reach which focused on fall-run Chinook salmon and steelhead trout. In contrast, the primary concern in the EDR is the apparent lack of available physical habitat for spring-run Chinook salmon. This is a section of the river in which the channel is predominantly bedrock with very little alluvial material present. Spring-run salmon that come upriver are unable to get past the dam. Observations indicate that many fish do not turn around and head back downstream to spawn in the TBR. Instead, they attempt to spawn on the bedrock and angular boulders, which has no chance of success. In addition, it is unclear if the hydraulic conditions are appropriate for spawning.

BACKGROUND

Defining A Bedrock Channel

Bedrock channels are defined as reaches along which a substantial proportion of the boundary greater than 50% is exposed bedrock or is covered by an alluvial veneer that is largely mobilized during high flows such that underlying bedrock geometry strongly influences patterns

The Spring-Run Problem

The Englebright Dam Reach (EDR) of the mainstem Yuba River is the section from Englebright Dam down to the junction with the tributary Deer Creek.

Spring-run salmon lack habitat to use for spawning or rearing in the Englebright Dam Reach.

Figure 91

of flow hydraulics and sediment movement (Fig. 92). In the Central Valley of California many of the rivers that are regulated by major dams for water supply and hydropower have bedrock sections just downstream of each dam. This include the Sacramento, Feather, Yuba, Calaveras and Stanislaus Rivers.

It's important to understand the geologic context of bedrock rivers if you want to manage and rehabilitate these sections of the rivers to support runs of fish, such as the spring-run Chinook salmon population. The Sierra mountains exist in an active tectonic setting, which means that there is rapid rock-uplift relative to what's occurring in other parts of the US. There is also orographically driven precipitation in the form of rain and snow. What that means is that when you have high mountains, wet water masses come in from the Pacific Ocean, go over the Central Valley, and then hit the Sierra Mountains. That contact forces them upward as they are pushed up against the mountains. As they go upward the air cools. That causes the wet water mass to form precipitation because of what is known as the Ideal Gas Law that relates temperature, pressure, and volume. The lower the temperature, the lower the volume and pressure. That lowering enhances precipitation. There are very high rates of precipitation in the Feather and Yuba basins (Fig. 6). So this orographically driven precipitation is occurring on a very fast uplifting mount range. The consequence of high uplift and high precipitation is that you have a very accentuated topographic relief (Fig. 93). That has features such as high drainage density and a lot of sediment transport power for mobilizing sediment and rock in the rivers. Because the Sierras are composed of granite they have a high percentage of hard exposed bedrock, especially when you get to high elevations. That means there is very thin soils and thus very low infiltration rates. As a result you can have very steep slopes. Steep slopes, thin soils, and high precipitation rates mean that the most effective geomorphic process for moving

Bedrock Channels

"Reaches along which a substantial proportion of the boundary (>50%) is exposed bedrock, or is covered by an alluvial veneer that is largely mobilized during high flows such that underlying bedrock geometry strongly influences patterns of flow hydraulics and sediment movement.

Anadromous Rivers in the Central Valley with bedrock sections downstream of dams include:

- Sacramento
- Feather
- Yuba
- Calaveras
- Stanislaus

Figure 92

Geologic Context of Bedrock Rivers

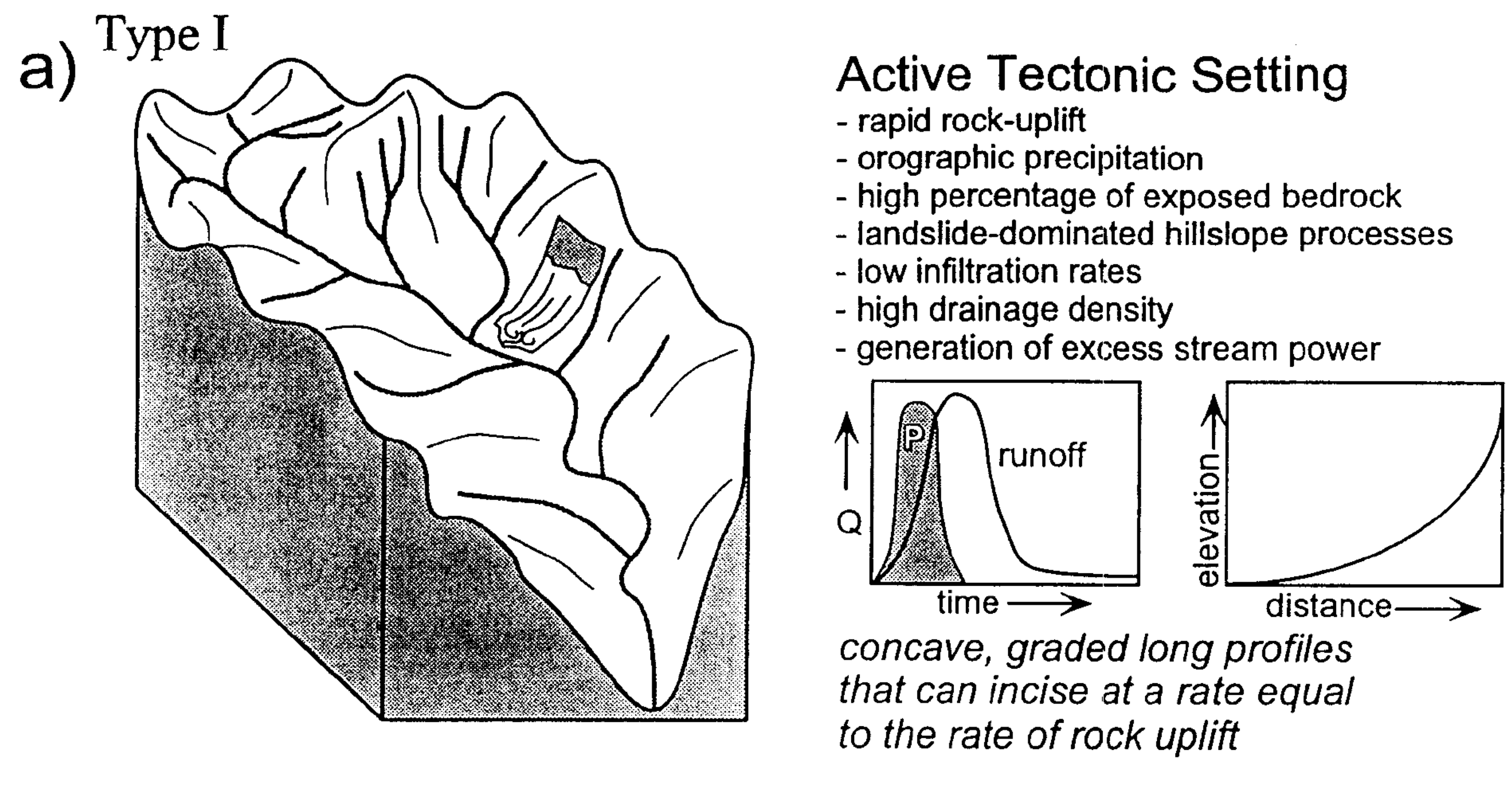

Figure 93

sediment is shallow landsliding. The net result of this active tectonic geological setting is that there are extensive bedrock reaches at relatively low elevations, downstream of where many of these water supply reservoirs that rim the Central Valley occur.

When you zoom in and look at the specific processes that are causing channel change in a bedrock channel that you actually see on the bed of the river, there are some key processes that are pretty unusual relative to what most people are familiar with in alluvial rivers (Fig. 94). These processes include abrasive blasting of bedrock and boulders by much smaller suspended sediment grains, quarrying or plucking of pieces of bedrock off the bed by rapidly fluctuating hydraulic lift, and scour under hydraulic jumps. It also includes a number of abrasive processes by which smaller particles get into cracks and holes in the bedrock and then over long periods of time chip away at them making those joints wider and cutting into the bed. For example there is a process known as potholing in which gravels spin around in a hole in the rock during high flows. Over time they abrade down deeper and deeper just like a drill. This forms a “pothole”, named thus because it looks like what you would see on a road. There is also a process known as cavitation in which very high velocities can cause very low water pressures at the bed. That causes tiny air bubbles to form. These bubbles quickly implode, damaging the river bed. This is a common occurrence on emergency spillways of dams as well as on the propellers of submarines. Overall, these are relatively small scale processes that occur, and as a result of these processes you get a variety of very unusual forms that are characteristic of the role of sediment in scouring out the bedrock in a bedrock reach. These processes create very diverse microhabitat features that could be of interest and may be necessary to consider when investigating these bedrock reaches.

Bedrock River Patterns and Processes

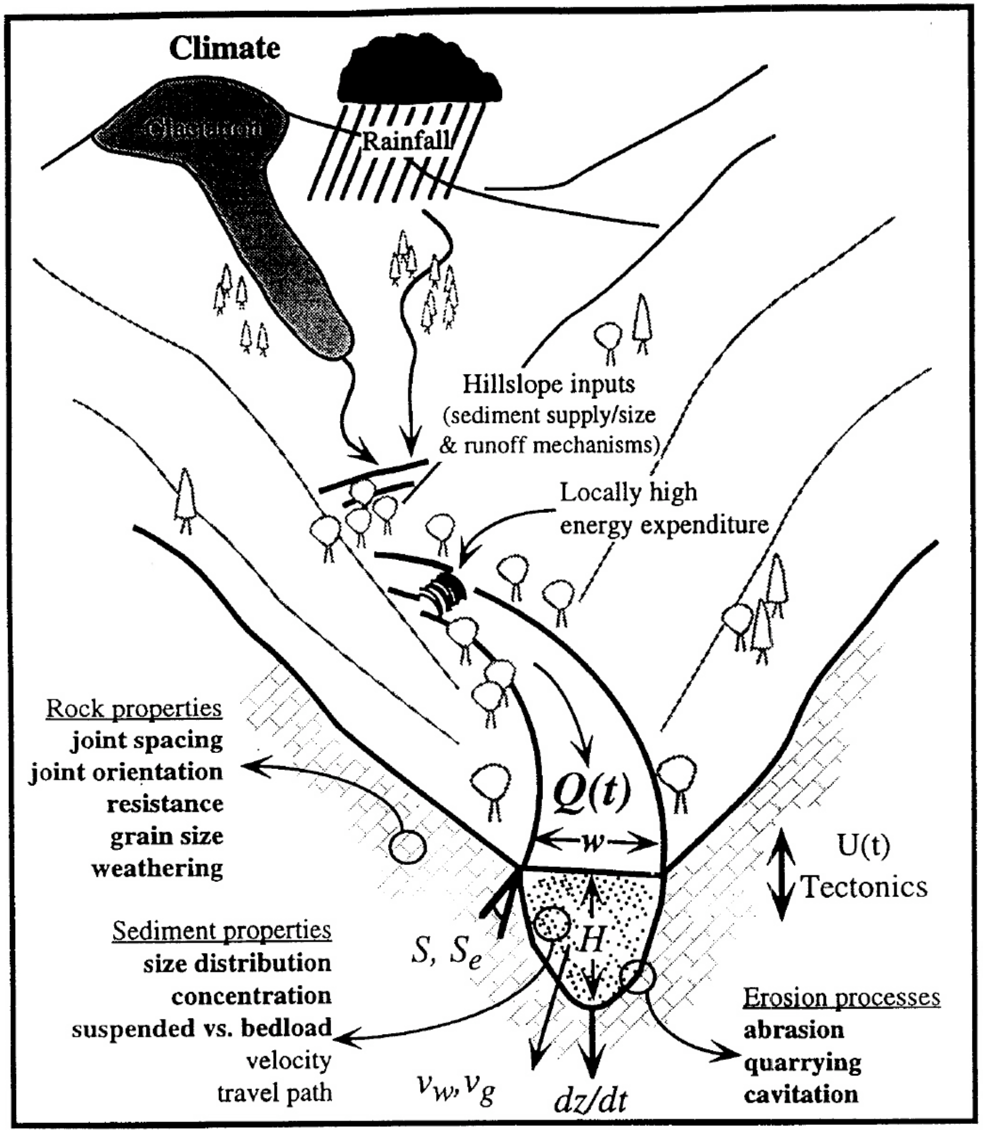

Figure 1. A schematic of a bedrock channel system, showing important variables that act to set the erosion rate, dz/dt, of the channel and terms used in the text. Channel variables are: $Q(t)$: discharge as a function of time; w: channel width; H: flow depth; v_w: water velocity; v_g: sediment velocity; A_D: drainage area; and S and S_e: channel and energy slope, respectively. Variables that are at least partially subsumed within the parameter, K, found in all reach-scale erosion rules, are shown in bold.

(Hancock et al., 1998)

Figure 94

Gravel Augmentation Defined

An important question that relates to this project is whether gravel augmentation (aka gravel injection) should be performed in the EDR. Gravel augmentation is define as the piling up of gravel within or along the channel so that future floods will entrain it and deposit it downstream, ideally yielding usable fish-spawning habitat (Fig. 95). The goal of gravel augmentation is to reinstate geomorphic continuity to get sediment transport occurring again downstream of a dam. One possible outcome of gravel augmentation is that it may reduced in-stream temperature anomalies (i.e. reduce warming of the river) if you were to put in so much gravel that a lot of water was flowing through it instead of over it. Then the water in the gravel would not be exposed to direct solar radiation or as much air-water conductive heat exchange. Another outcome is that gravel augmentation might yield more suitable substrates for downstream reaches, which may presently be okay, but may be degrading over a long time period.

The challenge with gravel augmentation is that you have to have flows that are large enough and frequent enough to redistribute that material. Then it remains unknown the extent to which the material that is entrained actually goes downstream and creates habitat. It depends on how much gravel you add and the nature of the river downstream. These are the kinds of questions that we need to answer as part of this LYR study.

When you have a bedrock canyon such as you do in the EDR, you need a method for getting gravel in that isn't particularly costly. The collaboration between UC Davis, USACE, and USFWS led to the discovery that the cheapest, fastest, and most effective way of doing that in a confined bedrock canyon with limited river access is to use a machine called the TB 105 or

Gravel Augmentation (aka Gravel Injection)

The piling up of gravel within or along a channel so that future floods will entrain it and deposit it downstream, ideally yielding usable fish-spawning habitat.

- Reinstate geomorphic continuity
- Requires flows to redistribute gravel
- 10-100 year strategy
- Shown to increase habitat availability
- May reduce in-stream temperature anomalies
- Provides substrate for downstream reaches

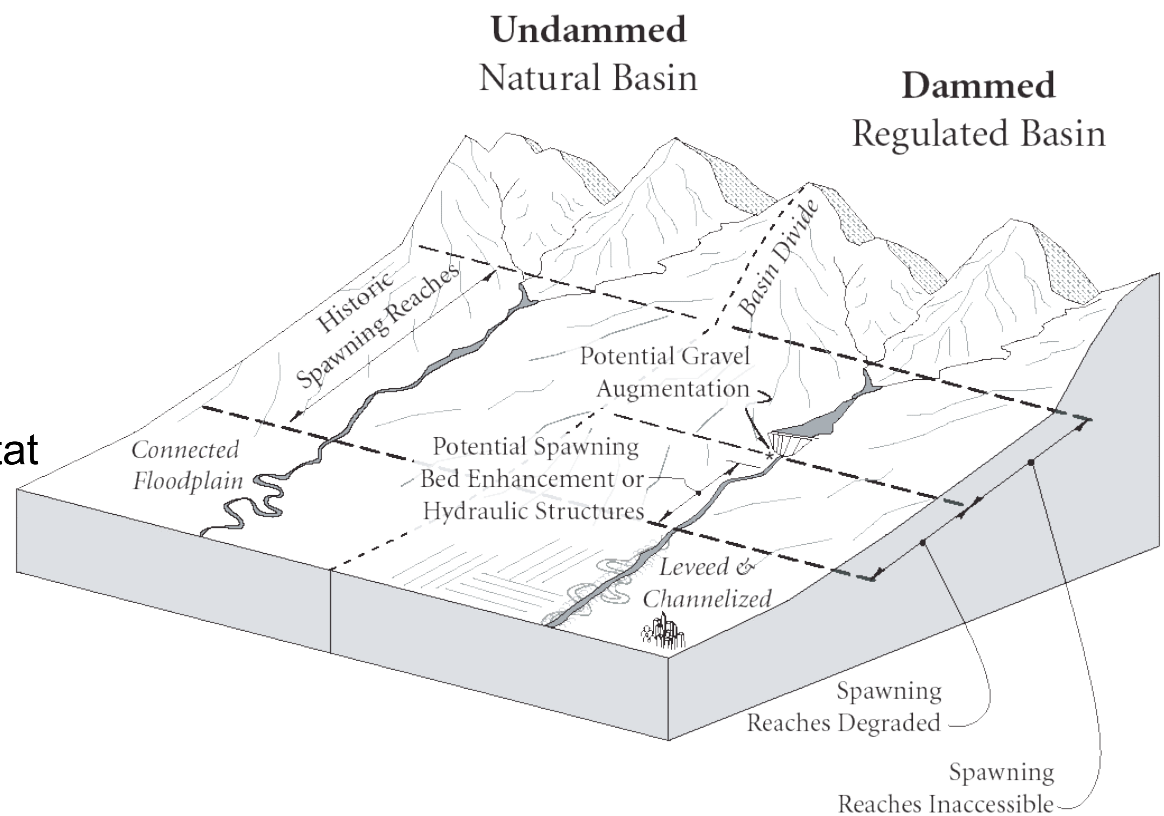

Figure 95

TB135 Belt Conveyor (Fig. 96). This machine is a truck with a conveyor mounted on it. You to park the truck adjacent to the river (but not necessary at the water surface elevation) and then use a small front loader to deposit gravel into a hopper located near the truck. The space for parking the truck only has to be ~3-4 car widths wide. It can be high above the river. Then the material in the hopper is conveyed by small motorized belt to the top of the truck and onto a larger conveyor belt. This one is extended out 105' or 135' out over the river. The material moves along this at a controllable speed to the end, where it then falls down and plunges into the water and settles into the deposit. There is an additional distance gained when the material is conveyed very fast and it projects out from the end of the belt. So gravel injection using the TB135 is possible below Englebright Dam, even with the challenging road and access conditions that exist there.

TBAR REFERENCE SITE

It is important to have a reference site so you know how the potentially degraded EDR is performing relative to a highly functional reach. Since we've already covered the Timbuctoo Bend Reach (TBR), then we are going to use that reach overall. However, since much of the evaluation of the EDR was formed at the site scale, as explained shortly, it was necessary to have a single site within TBR to use as a representative of that reach for comparison purposes. Thus, the Timbuctoo Bend Apex Riffle (TBAR) that was extensively observed within TBR was used as a high quality, gravel-bed reference site for comparison and evaluation (Fig. 97). We chose this site for several reasons, but most importantly because it is reported to have the highest fish-spawning occurrence on the LYR, according to people who have been working on the river for

Pilot Gravel Injection Method

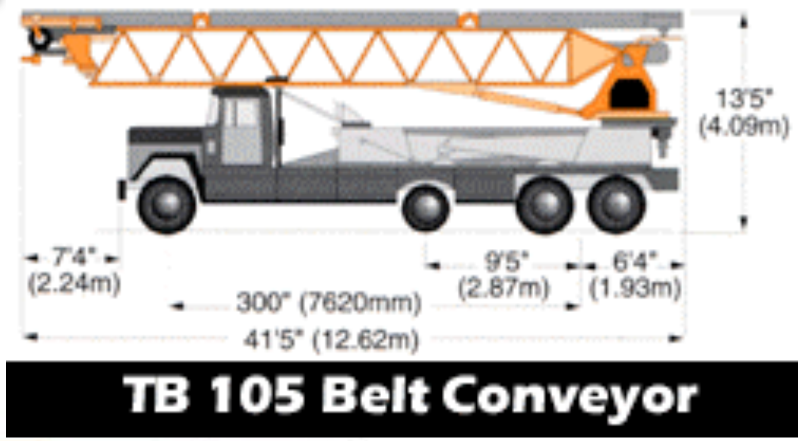

TB 105 Range Diagram

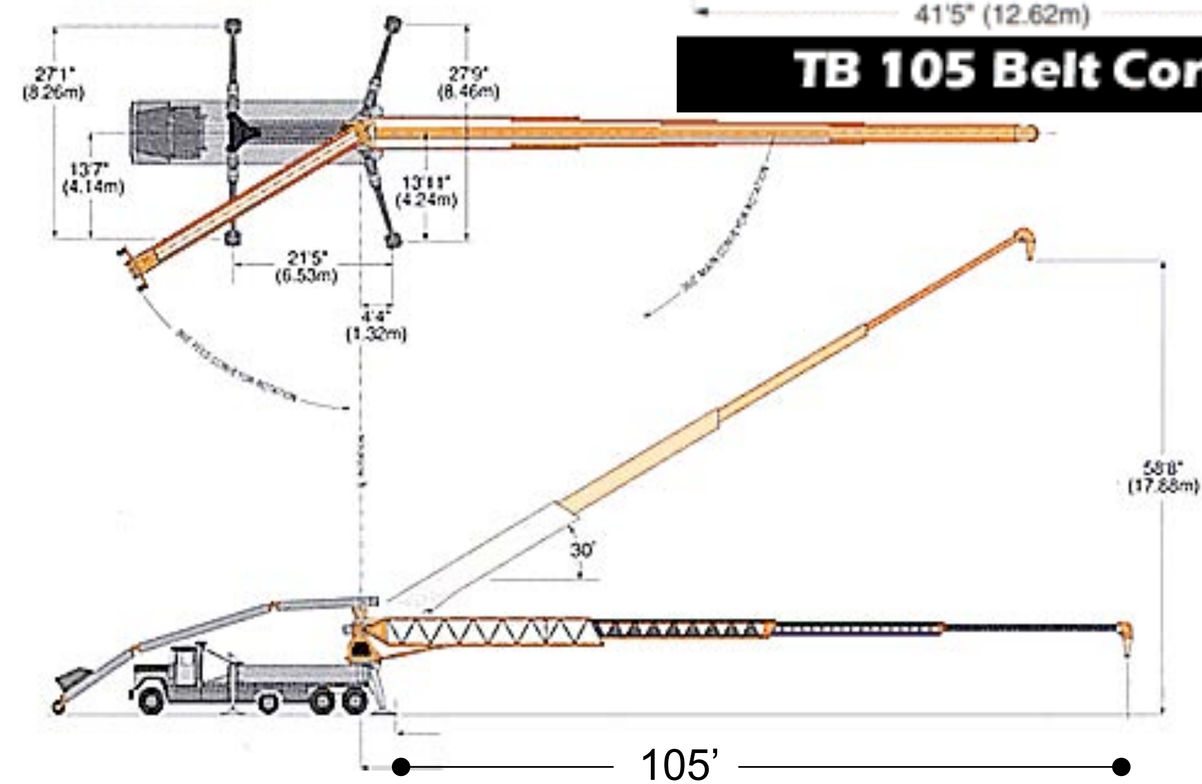

Figure 96

Timbuctoo Bend Apex Riffle (TBAR)

gravel-bed "reference" site

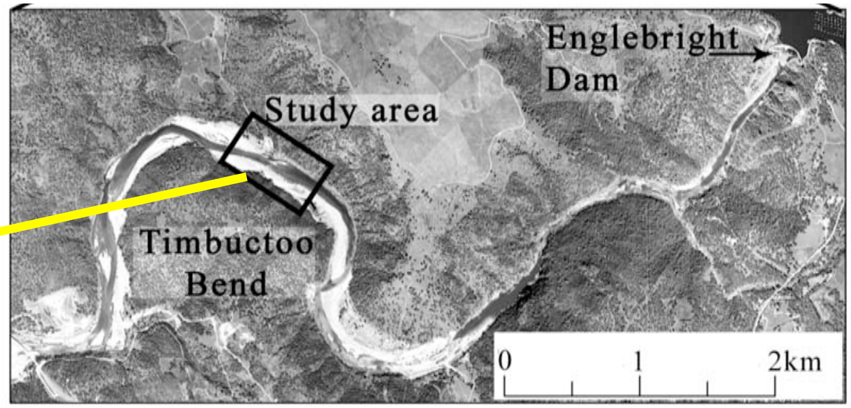

Characteristics:

- Highest fish spawning occurrence on the LYR in recent years.
- Historically persistent as a riffle 1952-2008.
- Found to have hydraulic mechanism that makes it self-sustaining.

Figure 97

many years. It is a historically persistent riffle that has been present in aerial photos from 1952 until the present. We know that a hydraulic mechanism exists at the TBAR site that makes it geomorphically self sustaining, such that the riffle crest always remains high and the upstream pool is always scouring down.

EDR TOPOGRAPHIC MAP

Obtaining a topographic map of the EDR was a major goal of and constraint against this project. Because of the challenge of mapping in the canyon, it was undertaken in three phases (Fig. 98). The 1999 US Army Corps of Engineers Map of the LYR does not contain any topographic information in the wetted channel in the EDR. Presumably that's because of the difficulty of mapping in there. All of this mapping was done by boat using an identical method as already described for the boat-based mapping in the TBR.

Our first trial of mapping in the EDR involved carrying a 14' Zodiac inflatable raft, down from the Narrows II access road to the river, and then separately carrying a 30 HP motor down. We also had to transport all the mapping equipment, set it up, and then mapping the top section. This section included the Narrows II Pool, a run and then another pool upstream of Narrows I powerhouse (Fig. 98- red box, Fig. 99). This initial effort was done in the late summer of 2005. The region encompassed in this survey was called the Englebright Dam Site (EDS), because it is closest to the dam, and thus is the farthest upstream area that fish might hold and spawn. The reason why we focused on EDS so much was simply because we had this data in 2005 and this is the area where gravel would be injected, if indeed gravel were to be injected at Englebright Dam. So it became very important to understand what the conditions were between Narrows II and

3 Phases of EDR Mapping

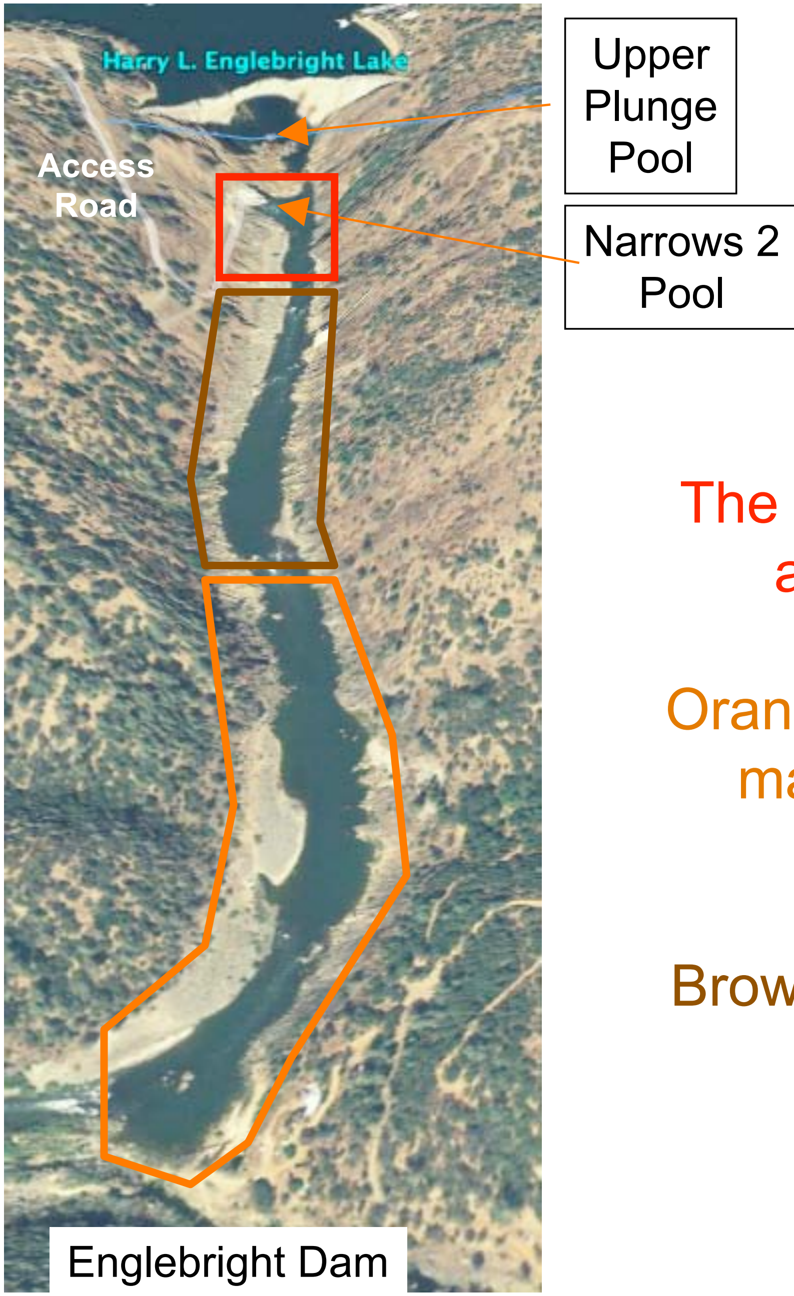

The red box denotes the pool-run-pool area that was mapped in 2005.

Orange box denotes pool-run-pool area mapped in December 2006; study pending.

Brown box denotes run-pool-rapid area mapped in Autumn 2007

Figure 98

Englebright Dam Site (EDS)

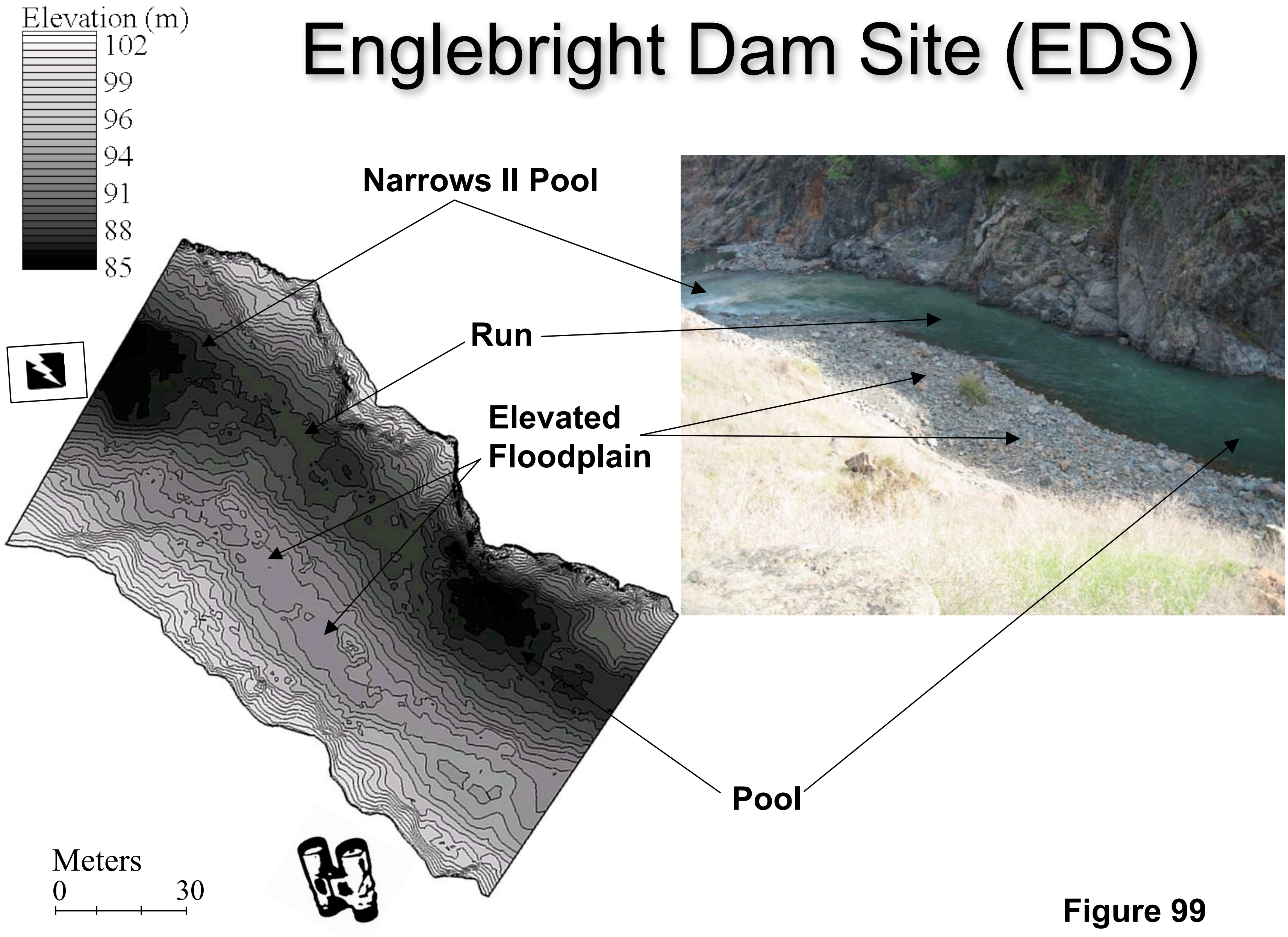

Figure 99

Narrows I powerhouses where the gravel was injected and where it might potentially create some problems between the two powerhouses. One of the concerns raised in planning gravel injection was that if gravel was to deposit between the two powerhouses in the run, then during the September period when Narrows II is turned off for maintenance you might dewater the gravel in the run (Fig. 99) and therefore dewater any fish embyros that salmon might have places into the deposited gravel there. So it was important to make an assessment about whether it would be possible for gravel to deposit in the run between Narrows II and I. That is why we did a lot of work, including extensive 2D hydrodynamic modeling at the EDS. It was not until autumn of 2007 that we had the entire river surveyed and then not until early 2008 that we had all of that data checked for quality and processed to produce a map.

In December 2006 an opportunity arose to do more mapping, and so in this case we chose to do the next segment that was relatively easy to do, which was the section from the Deer Creek junction all the way up to the bottom of the one rapid that exists in the EDR, which is just downstream of the USGS Smartville gaging station, and thus we're just going to call it the USGS Gaging Station rapid (Fig. 98- orange polygon). To access this section, we brought the Zodiac in by trailer down to a boat-launch location on the property at the Yuba junction with Deer Creek with the permission and assistance of property-owner Ralph Mullican.

The final area that was mapped was the remaining middle section that went from just upstream of Narrows I down through the USGS Gaging Station rapid (Fig. 98- brown polygon). That was mapped in August 2007 using the same boat-based method and boat access point as in December 2006.

Besides all of the boat-based surveying, all of the terrestrial land in the canyon was mapped using the robotic Leica total station by teams of 2 people. Also, the Leica was used to map canyon walls using its reflectorless red-light scanning capability. The Leica was also used to do some infil in the wetted channel along both banks and in the USG Gaging Station rapid.

The completed EDR topographic map is show in Figure 100.

EDR STUDY OBJECTIVES

There were 4 scientific objectives to the research in the EDR. First, to investigate the hydraulics and sediment transport regime in that EDR over a wide range of flows. Second, to investigate the historical presence and fate of alluvium in the EDR, which is a significant geomorphic question. Third, to evaluate spring-run Chinook salmon spawning habitat quality in the EDR. Fourth, to evaluate if, how, and where gravel should be added to provide the necessary habitat for salmon spawning and embryo incubation.

The baseline research components in the study involve mapping the wetted flow area in the EDR; mapping the channel bathymetry and terrestrial topography (as described above), performing 2D hydrodynamic modeling for habitat and sediment transport regime, performing some sediment transport experiments with tracers, and making habitat quality observations. Such observations included spawning observations in early autumn during the spring-run spawning season as well as hydraulic and sedimentary microhabitat measurements and analyses.

We articulated 9 specific hypotheses to assess the conditions in the EDR (Fig. 101). A hypothesis is a statement that can be tested with specific metrics. It is nothing more than a statement. It must be posed either in the affirmative or negative, but it really does not match which, because then we can test it. We have not specifically pre-cooked the statements to be one way or other, we just wrote them down and then they can either be affirmed or rejected in the

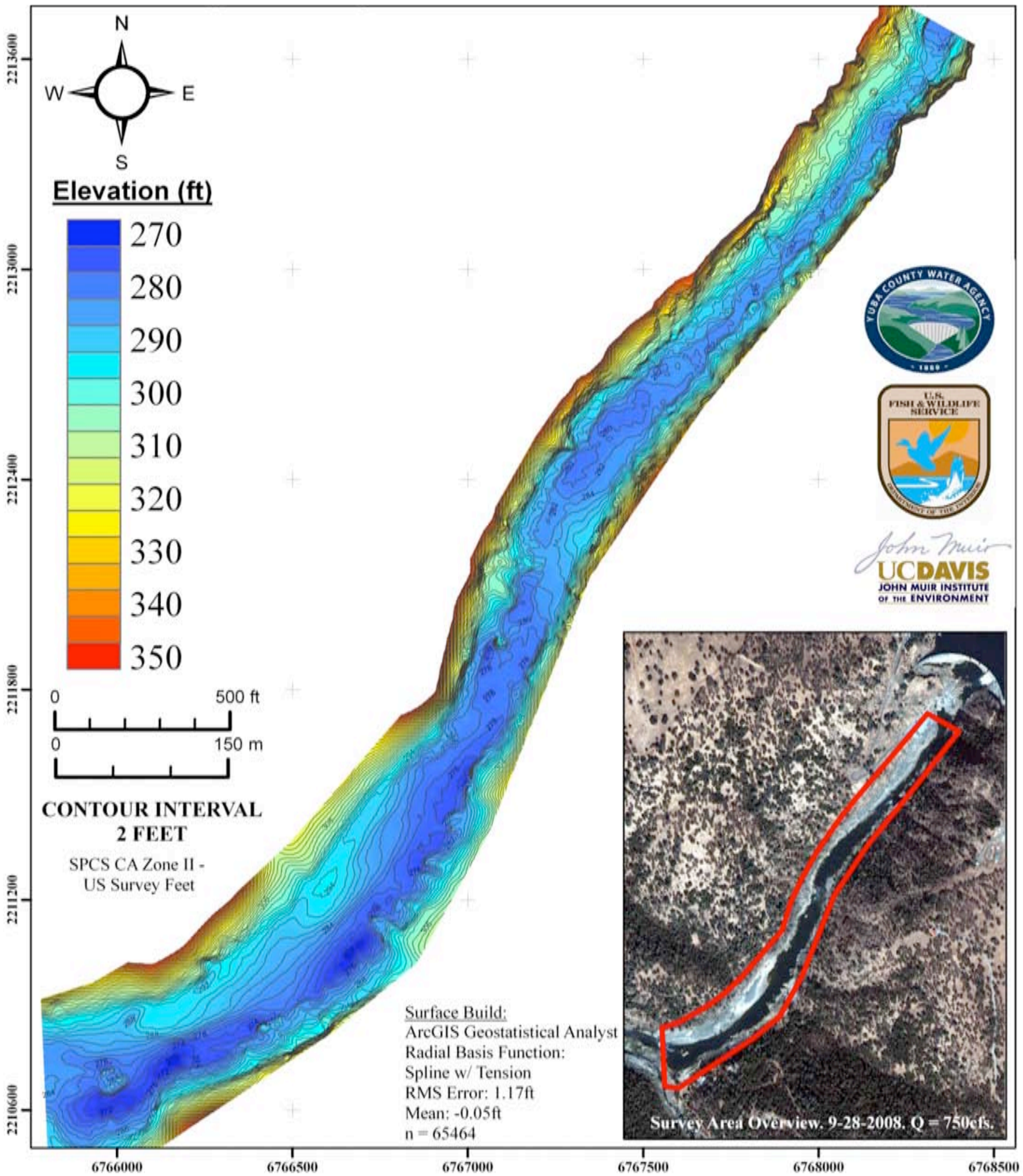

High Resolution EDR Topographic Map

Figure 100

EDR Scientific Hypotheses

A hypothesis is a statement that can be tested with specific metrics.

Hyp.	Statement	Test Metrics *
H_1	Sediment characteristics at the EDR and TBAR are comparable and suitable for spawning.	PC, VC, LR
H_2	Flow convergence routing will produce alluvial geomorphic features (riffles, pools, glides) at the EDR and TBAR study sites.	HM, SS
H_3	Injected gravels at the EDR will be stable during spawning flows.	HM, SS
H_4	Injected gravels at the EDR will be stable during 273.2 m^3/s discharges (2-year event).	HM, SS
H_5	Injected gravels at the EDR will be stable during a 900.5 m^3/s discharge (~5-year event).	HM, SS
H_6	Injected gravels at the EDR will be stable during a 2588.2 m^3/s discharge (~24-year event).	HM, SS
H_7	Gravel augmentation will aggrade the EDR and produce extensive cross channel habitat that is susceptible to scour.	HM, SS HI, DR
H_8	Historically, the EDR supplied ample spawning habitat for chinook salmon.	HI, LR, HOS, ROS
H_9	Current spawning habitat at the EDR and TBAR is not limited.	HM, HSC

* DR = Discharge Record Analysis, HI = Historical Imagery, HM = Hydraulic Modeling, HSC = Habitat Suitability Curves, LR = Literature Review, PC = Pebble Counts, HOS = Historical Observations of Spawning, SS = Shields' stress predictions, ROS = Recent Observations of Spawning, VC = Visual Comparisons

Figure 101

testing. The test metrics that were used in this investigation included pebble counts, hydraulic modeling, and historical imagery- these are some of the essential methods that were also used to study the TBR. In this case, the most important of these tools is 2D hydrodynamic modeling, because it provides a mechanistic explanation of what is occurring at the EDS and the EDR overall.

EDS AND EDR 2D MODELS

Two different 2D models were built for this part of the study. The EDS modeling was done at the site scale and relied on the program, Finite Element Surface Water Modeling System 3.1 (FESWMS). A complete model of the whole EDR only became possible at the very end of the study, and it was done using the program, Sedimentation and River Hydraulics 2D (SRH). FESWMS and SRH numerically solve the vertically integrated momentum and mass continuity equations. These models produce depth and velocity approximations for the shallow water equations. They assume horizontal flow, so the flow is depth averaged. What that means is that the models do not account for vertical upwelling and downwelling in the river that can occur over very steep rapids and at very small scales. The two models do use slightly different forms of the governing equations, with each one have merits. In head-to-head comparisons I found that SRH outperformed FESWMS in yielding highly coherent vortices and eddies behind obstructions, while FESWMS outperformed SRH in predicting the peak velocity over steep riffle crests. These difference can be traced back to the subtle differences in the fluid mechanics equations used by the models. Overall, I have concluded that the models are interchangeable for use at EDS and EDS, but since SRH is so much more efficient, it is the preferred one.

2D models require information about boundary conditions, input conditions, and model parameters. The first thing you need is a high resolution topographic map and digital elevation model of the river, which we have already presented. You have to know the inflowing discharge, which we have from Englebright Dam and the USGS Smartville gaging station. You also have to know the downstream water surface elevations at the end of the model domain, which was surveyed in the field at different stages using the Leica total station or a Trimble 5700 RTK GPS. You also need an estimate of the bed roughness. That can be predefined or it can be calibrated, and in this study we did both. Finally, you need an estimate of the eddy viscosity parameter for turbulence closure or you have to use an equation to calculate it, and both of those methods were used here.

In terms of validating the depth and velocity predictions of the 2D FESWMS model, I already presented two sets of validation results from 2004 and 2005 at the TBAR site (Figs. 43 and 44). Those validation efforts demonstrate the model's capability in predicting gravity-driven flow in the LYR. There is absolutely no reason to think that model performance would be any different in the EDR, because the laws of physics are the same upstream as they are downstream; there is no fundamental difference. The depths and velocities are all similar in both of those areas. Just because the river is bedrock in the EDR and gravel-bedded in the TBR really doesn't matter, because the model is not a mobile bed model anyway; it assumes a rigid bed. So the fact that it is bedrock makes no difference.

One thing we did do to evaluate model performance was to look at observed versus predicted water surface elevations at all the flows we modeled for the EDS. It is very difficult in a bedrock river that is as confined as this is to go out and wade in relatively fast flow with poor footing to make detail depth and velocity measurements, but you can go along the edge and map the water surface elevation and compare observations against model predictions. For example, when you look at the WSE profiles for 1190 and 31800 cfs, you can see that although different roughness values are used for each of these models, the matches are very close (Fig. 102). There is no systematic trend where one is higher all the time or lower all the time; there is a mixture of places where there are some deviations between the two and those deviations tend to be a small fraction of the water depth. The deviations are on the order of 2-4 cm for 1190 cfs and 5-15 cm for 31800 cfs. At higher discharges, there is more error in the field observations, because the water is bouncing up and down as it smashes against the rocks. So it's not clear that that error is entirely due to the model, but also due to uncertainty in the measurements. Overall, what you can see is that the model does match the observations very well.

HYPOTHESIS 1

The first hypothesis that we tested is the assessment of the statement that sediment characteristics at the EDS and TBAR sites are comparable and suitable for spawning. The testing method in this case involves analyzing empirically derived diameter statistics and observations of particle shape in terms of their roundness to determine if sediment conditions are within the known preference range of 12-80 mm for Chinook salmon spawning at the EDS. If particle size at the EDS is substantially coarser or sharper than at the TBAR site or if a significantly smaller fraction of particles fall within the limits of Chinook preference, then Hypothesis1 will be rejected.

The results of grain size analysis show that a median grain size in EDR is 143.6 mm compared with 54.9 m at TBR from the longitudinal survey performed in 2006 (Fig. 103). We

EDS Water Surface Profile Validation

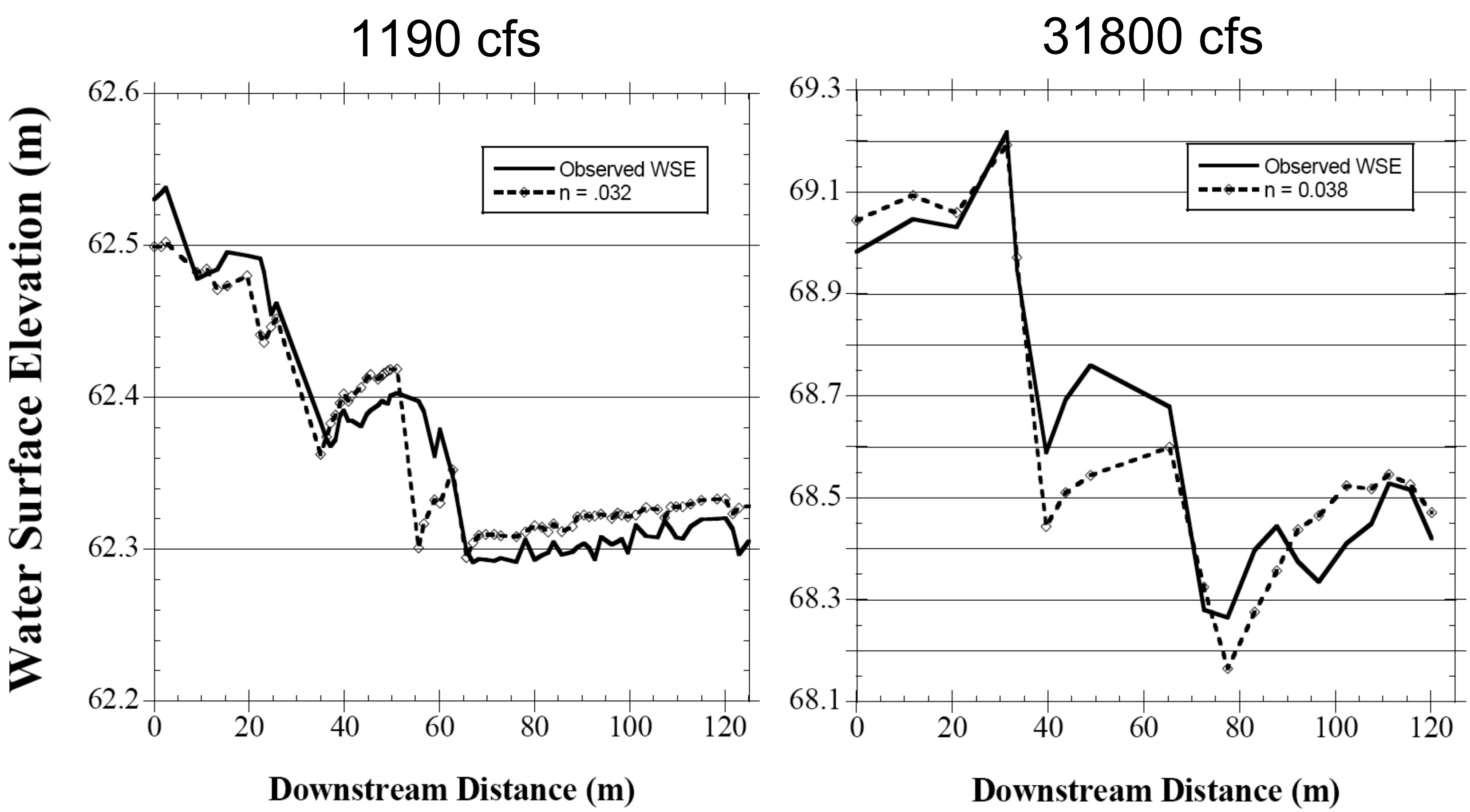

Figure 102

H_1 Rejected

EDR bed material is too coarse, too few, and too angular to support salmon spawning and embryo incubation.

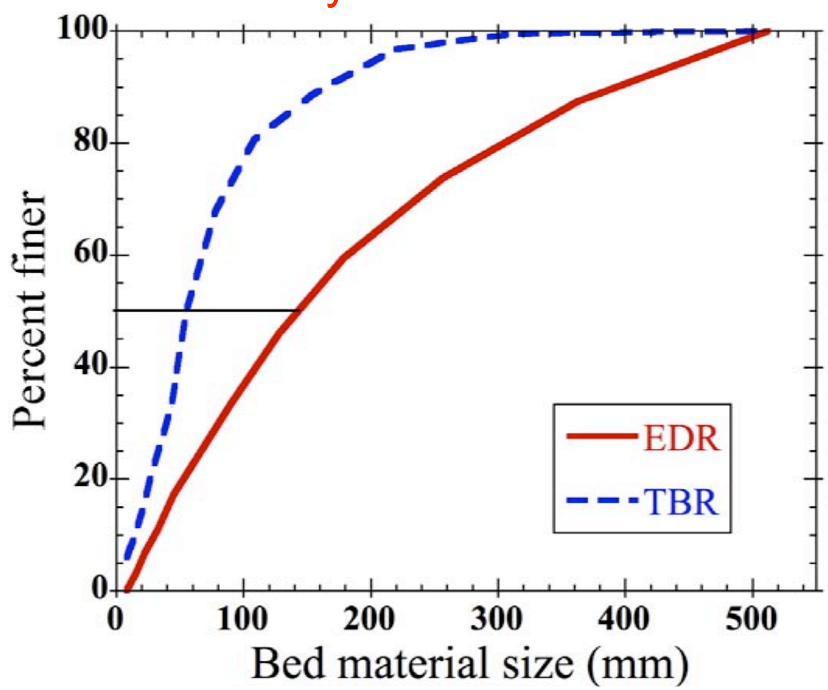

TBR (2006)

- D_{16} = 22.9 mm
- D_{50} = 54.9 mm
- D_{90} = 163 mm

EDR

- D_{16} = 42.8 mm
- D_{50} = 143.6 mm
- D_{90} = 395.7 mm

EDR

TBAR

Figure 103

observed a range of median grain sizes over the years at the TBAR site, but that was always between 50-65 mm, which is about one-third the size that has persisted in EDR. D_{90} for EDR is 395.7 mm compared with 163 m for TBR. At the smaller end of the spectrum, D_{16} equaled 42.8 mm for EDR and 22.9 m for TBR. So for all 3 of these metrics EDR values are 2-3 times that for TBR. You can also see that in the entire cumulative distribution function where the blue line for TBR is far to the left of that for EDR which is a red line off to the right at the higher Bed material sizes systematically (Fig. 103). Looking at the roundness of the particles, you can see in photos that the sediments at the TBAR site and throughout Timbuctoo Bend Reach are well rounded and include a wide range of sizes. On the other hand, in the EDR all the particles are highly angular and are pretty coarse (Fig. 103). In conclusion, we can *reject* Hypothesis 1- EDR bed material is too coarse, too few, and too angular to support salmon spawning and embryo incubation.

HYPOTHESIS 2

Hypothesis 2 states that flow convergence routing does exist at the EDS. Thus, if gravel and cobble were injected there, it would produce self-sustainable, alluvial geomorphic features and associated spawning habitat at the EDS just like it does at the TBAR site.

Flow Convergence Routing Revisited

That brings us to the topic of flow convergence routing. In the TBR section of the report, I went to extensive detail about this mechanism called flow convergence routing (Fig. 42). In summary, the flow convergence routing mechanism explains the process by which pools and riffles rejuvenate the relief between them. At low flow, high velocities converge over riffles causing them to armor, incise gradually and diminish the relief over the long periods of time that you do have these low flows. On the other hand, at high flows the highest velocities converge in pools, because of the lateral construction associated with the valley width in those pools in Timbuctoo Bend. As a result of that, during those infrequent floods the convergence of high velocities in pools causes rapid scouring and restores the relief between riffles and pools. So these are the stages of low-flow and high-flow scour that cause pools and riffles to persistently incise over decades, but retain riffle-pool relief, and this was demonstrated to exist in the TBR.

To review what we observed at the TBAR site, we found that at low discharges the highest velocities occurred over the riffles (Fig. 104). At the highest discharges the highest velocities occurred over the pool. So we did see flow convergence routing at the TBAR site. The question is whether a mechanism like this is present in the EDR, and that is critical because that determines whether any injected gravel would deposit on high areas and form riffles or whether it would just fill in pools.

EDS Flow Convergence Routing Assessment

The method to test Hypothesis 2 involved predicting depth and velocity fields per six discharges using FESWMS at the EDS and then analyzing whether flow convergence routing is evident in the model results. The absence of a velocity reversal at high discharges would suggest that habitat formation and preservation is unlikely at the site. If it is not observed then the hypothesis has to be rejected.

TBAR Site Has Flow Convergence Routing

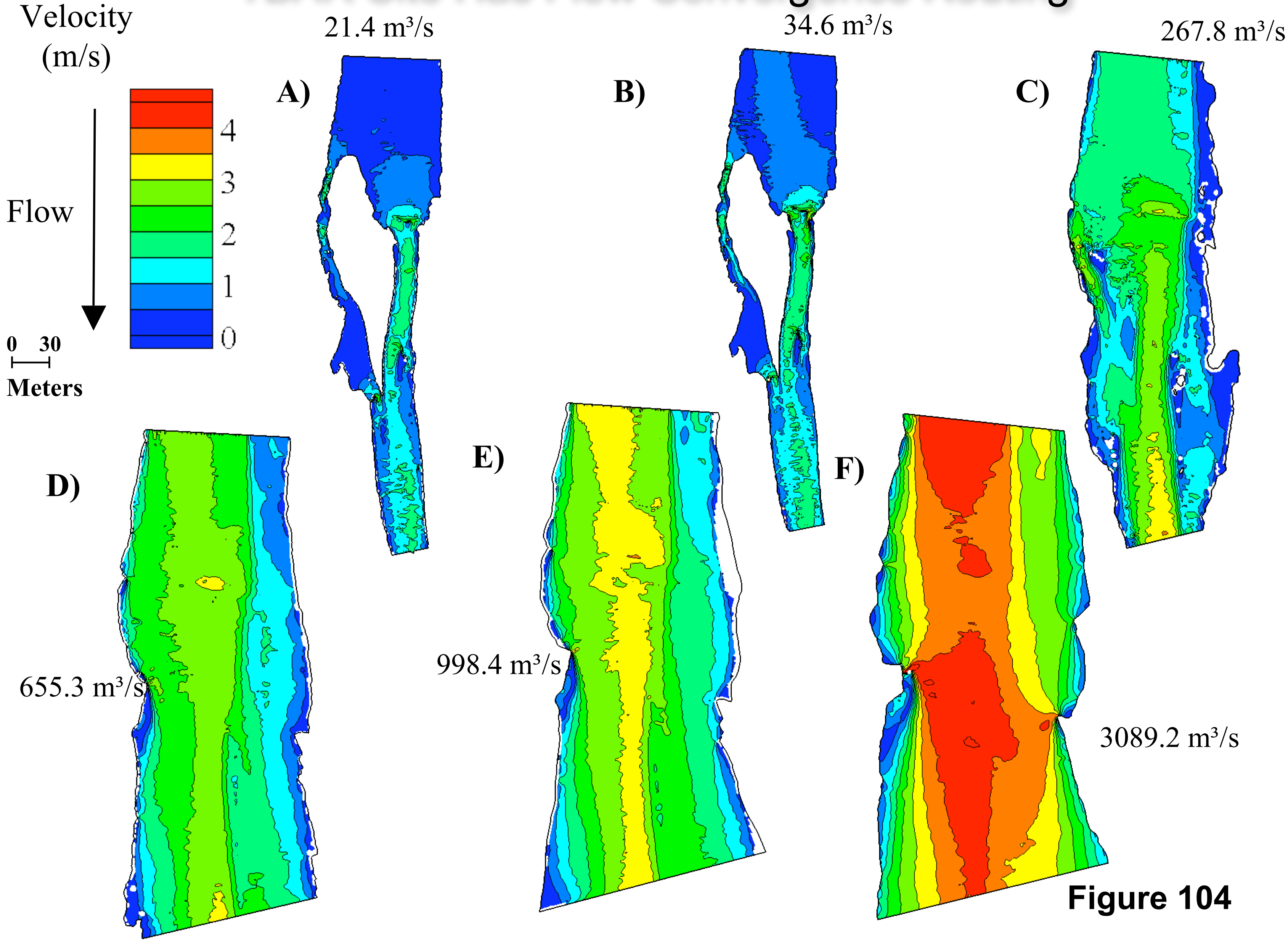

Figure 104

The velocity results for discharges ranging from 22.7-2588.2 m^3/s (800- 91,400 cfs) shows that there is no velocity reversal present (Fig. 105). At low discharge the lowest velocities are in the upstream and downstream pools. The highest velocity is in the run in the center of the site. As discharge increases, the magnitude of the velocity-difference remains high. By 271.3 m^3/s the velocity in the run, in the most constricted area, is about 4 m/s, while in the pool it's only 1-2 m/s. When you get to 2588.2 m^3/s (91,400 cfs), there velocities on the pool are up to 6 m/s; that is on the order of 18 ft/s. So very, very fast, but in the pools it is relatively sluggish. So there is no evidence of flow convergence routing at the EDS when we look at the velocity results. We can conclude that there is a static location of maximum predicted velocity at the EDS. Also, we can conclude that it is caused by the localized vertical and lateral constrictions imposed by the bedrock walls as well as the bed plateau that the run is located over. This illustrates the strong control of bedrock channel form in determining the presence and role of flow convergence routing in creating and maintaining alluvial habitat features. In contrast, the dynamic location of maximum velocity at the TBAR Site supports flow convergence routing there.

HYPOTHESES 3-6

The next four hypotheses relate to whether injected gravels dropped into the riverbed right below Englebright Dam would be stable there and not transport downstream during specified different flows. There is one hypothesis for each specified flow, and the flows evaluated span a wide range. For Hypothesis 3-6, the question is whether injected gravels would be stable during spawning flows (22.7 (800 cfs) and 33.7 m^3/s (1190cfs)) , during 273.2 m^3/s

H_2 Rejected at EDS Site

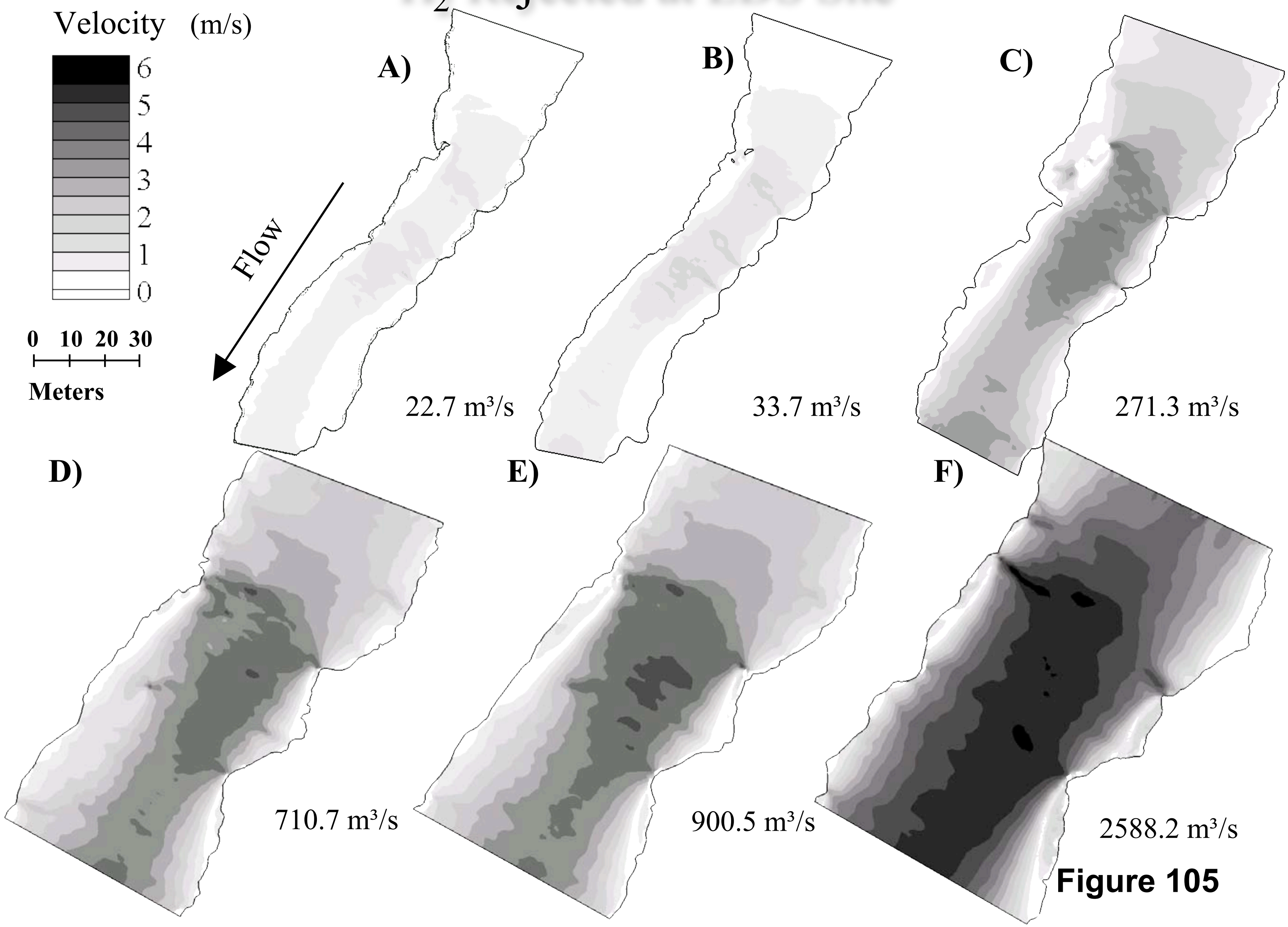

Figure 105

(9,580 cfs); 900.5 m^3/s (31,800 cfs), or 2588.2 m^3/s (91,400 cfs), respectively. The 3 higher values correspond with 2-year, 5-year and ~24-year return interval events, when you look at it from the statistical perspective of flood frequency analysis. So these are significantly different magnitude events. The method used to test these hypotheses was to determine the likelihood of gravel mobilization by evaluating the proportion of wetted channel that had a Shields' Stress that indicated full channel mobility. Each hypothesis is rejected if a significant proportion of the channel, which was set at a threshold value of 10%, registered in the full transport regime.

Shields' stress is a non-dimensional metric that looks at the pressure or stress on the bed of the river relative to a characteristic grain size of sediment that might be on the bed (Fig. 106). You begin by taking the depth and roughness of the bed and using those to calculate a drag coefficient. Next, you take that drag coefficient, put it together with the local velocity at a point in the river to get an estimate of the bed shear stress. Finally, you non-dimensionalize the bed shear stress using a reference grain size of interest that characterizes conditions on the river bed. In this case the reference size was taken as the salmon-spawning gravel size that has a median value of ~60 mms. Shields stress is then binned into ranges corresponding with different sediment transport domains, including none, intermittent, partial transport and full mobility. These Shields' stress domains have already been described in the TBR section of the report and are also explained further in Appendix 1.

The results for these four hypotheses are shown in Figures 107 and 108. You can see that at the low discharges of 22.7 and 33.7 m^3/s (800 and 1190 cfs), the majority of the EDS experiences no transport. Once you get to 271.3 m^3/s (9,580 cfs)you have a mixture of intermittent and partial transport, with the partial transport focused over the run where the lateral and vertical constrictions are. At 710.7 m^3/s (25,100 cfs) you do have some amount of full

Sediment Transport Regime Assessment

Use drag-force method to calculate Shields' stress

Model predicted depth, Manning's n → $$Cd = \frac{9.81 n^2}{H^{1/3}}$$

Model predicted velocity → $$\tau = \rho_w C d U^2$$

Spawning gravel size (60 mm) → $$T^* = \frac{\tau}{(\gamma_s - \gamma_w) D_{50}}$$

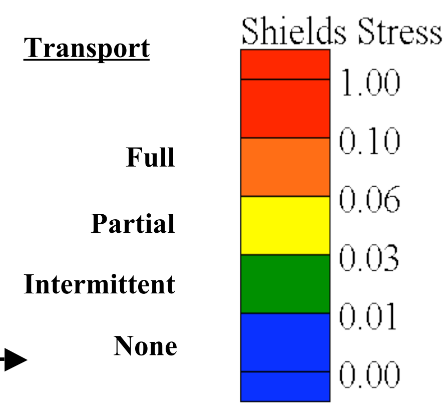

After Lisle (2000)

Figure 106

Results H_3-H_6

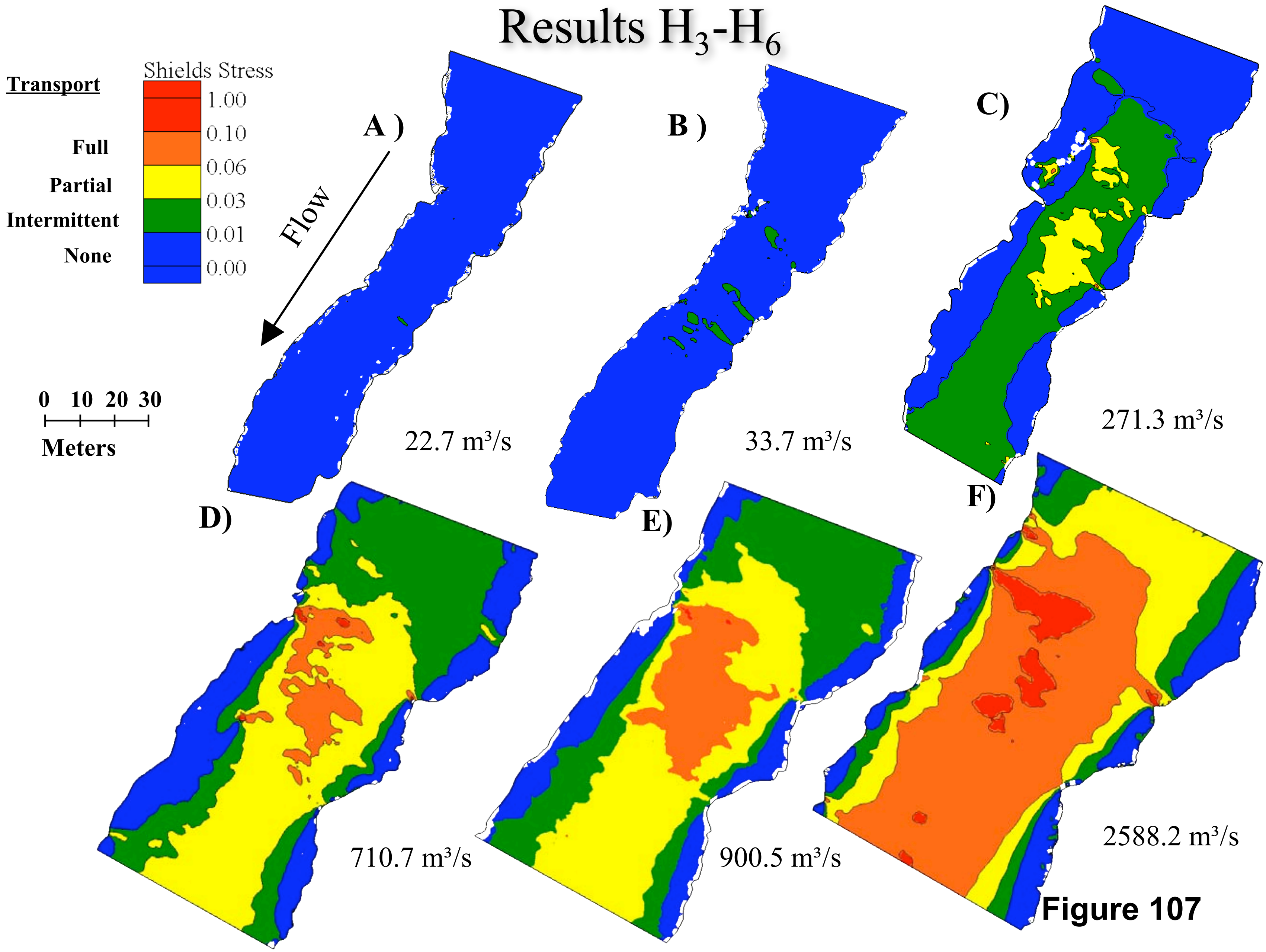

Figure 107

More Results H_3-H_6

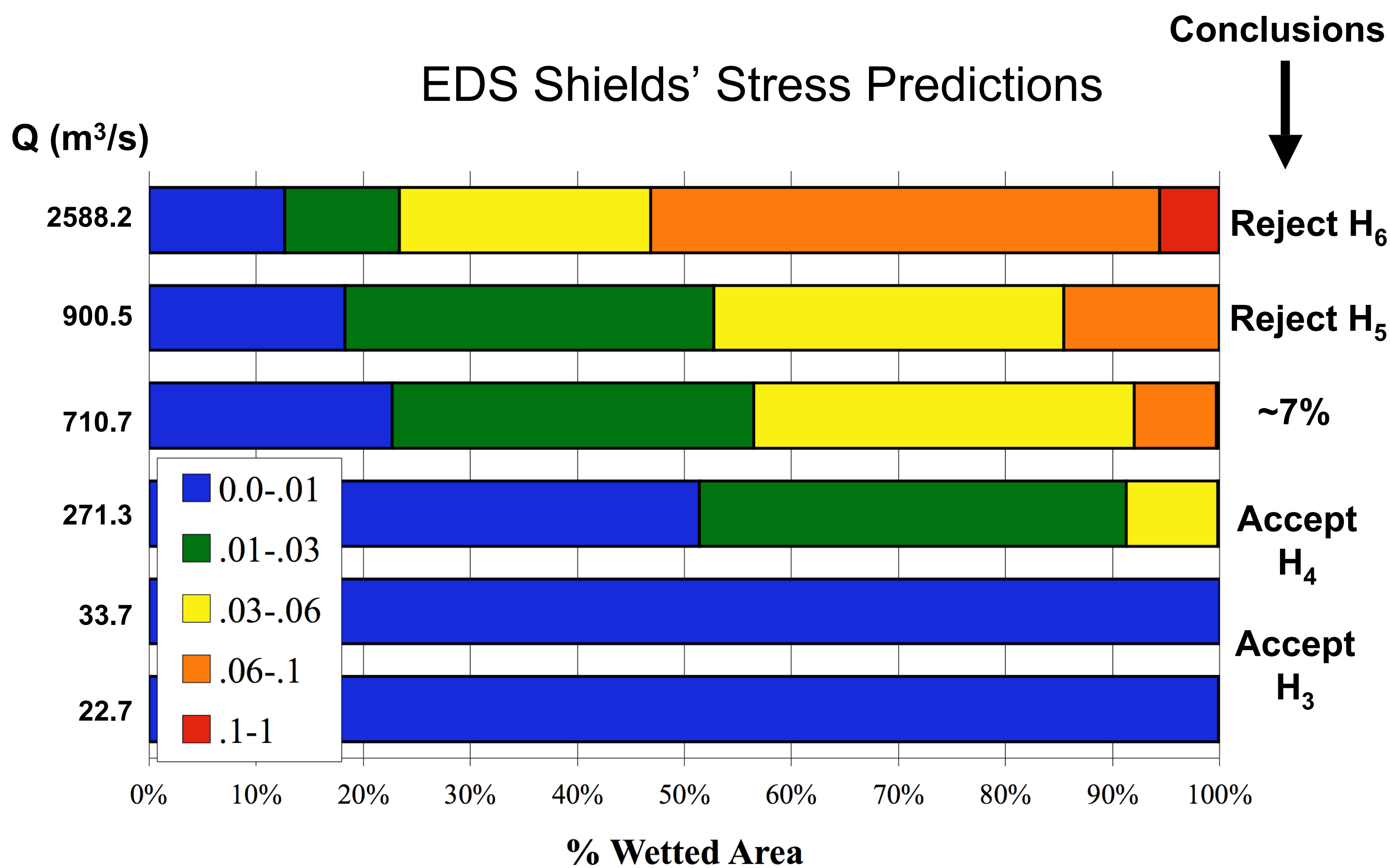

Figure 108

mobility, and then that increases until at 2588.2 m^3/s (91,400 cfs), there is a lot of area of full mobility (Fig. 107). To quantify those percentages, we calculated Shields' stress distributions based on the maps, and what we found is that at 22.7, 33.7 and 271.3 m^3/s, we can accept the stated hypothesis that the river is stable, because there is no full mobility at all at those three discharges. At 271.3 m^3/s there is ~8-9% of the channel experiencing partial transport, but looking at the map you can see that the area of partial transport is not where the gravel will be injected, so there will be no gravel available to be moving there. By the time you get to 710.7 m^3/s (25,100 cfs), ~7% of the channel is experiencing full mobility, but again that is limited to the run in the constricted section where no gravel is being injected or is otherwise available. So we can still accept the hypothesis there, although we are closed to the threshold. At 900.5 m^3/s (31,800 cfs), there is 13-15% of the channel experiencing full mobility and thus we must reject the hypothesis, in that case the fifth hypothesis. Even at that flow the full mobility is focused over the run. There is some partial transport occurring in the upper pool and a lot of partial transport in the lower pool. Only at 2588.2 m^3/s (91,400 cfs), do you have a huge amount of full mobility in the channel with >50% of the channel experiencing full mobility. The upper pool is still primarily in a partial transport domain though. So you are not going to be picking up a lot of material out of the pool, and anything you do will definitely pass through the constricted run between the Narrows II and I powerhouses, because that whole domain is in full mobility. In summary, significant mobilization of gravel out of the Narrows II pool where it could be injected easily is not predicted to occur until discharge >710.7 m^3/s (25,100 cfs). Most likely above 800 m^3/s, but certainly by 900 m^3/s (31,800 cfs), you will have instability beginning where you have sediment transport of injected gravel. So if gravel is injected into the Narrows II pool, then do not expect short-term increases in habitat any where downstream until you have a flow that is more than 710.7 m^3/s (25,100 cfs). Also, sediment transport in all modeled scenarios is greatest in the run. Any time you have sediment transport occurring in the Narrows II pool where gravels being injected, you are guaranteed to have that material transport through the run and downstream to the next pool.

Overall the flow regime does provide sufficiently dynamic floods, with Q > 700 m^3/s occurs every 2-5 years, that you can redistribute gravel, if it were available. In other rivers there are cases where gravel has not been redistributed as well, because such dynamic flows never come. That leads to the question of how may gravels be retained in the channel given the Shields' Stress patterns and static location of the maximum velocity in the run?

To address that question, we have to look at two related conceptual models: One by McBain and Trush called nested depositional features and another from Wohl called gravel beaches (Fig. 109). These concepts are also similar to a third concept by Prof. Leonard Sklar, who also has looked at the issue of sediment transport in bedrock rivers with nested dispositional features. All of these concepts describe a channel in which you have a complex mosaic of resistant bedrock, large boulders, and then smaller boulders, cobbles, and wood structures within the larger bedrock channel. These nested features create localized areas of upwelling, flow separation, and lateral vortices that facilitate alluvial deposition behind them. Also, and of great significance, nested features tend to be along the channel margins, because that is where they can lodge against bank vegetation and rock outcrops. It is behind these nested features that is know to typically be where gravel deposition would occur. Thus, if you look at the spatial of Shields' Stress, it is important to note that the values are indeed lowest along the channel margins at the EDS (Fig. 107). That means that if you do have gravel that is transporting, it is possible that some grains will deposit behind big obstructions, such as boulders along the margins of the run.

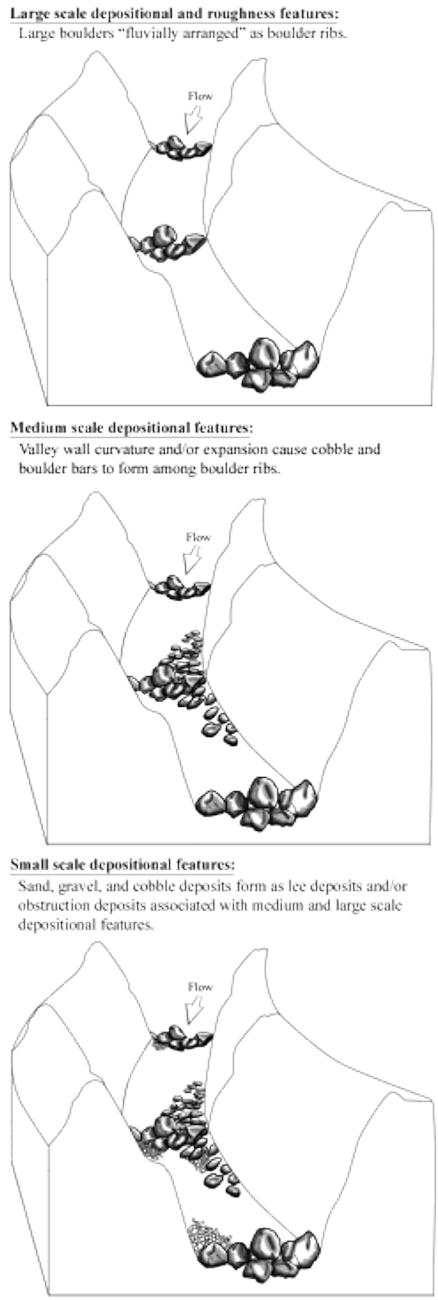

Alluvial Deposition in Bedrock Channels

1. McBain & Trush (2004) "nested depositional features."
2. Wohl (1998) "gravel beaches."

Both concepts describe a complex mosaic of resistant bedrock and large boulders within bedrock channels that create localized areas of upwelling, flow separation, and lateral vortices that facilitate alluvial deposition.

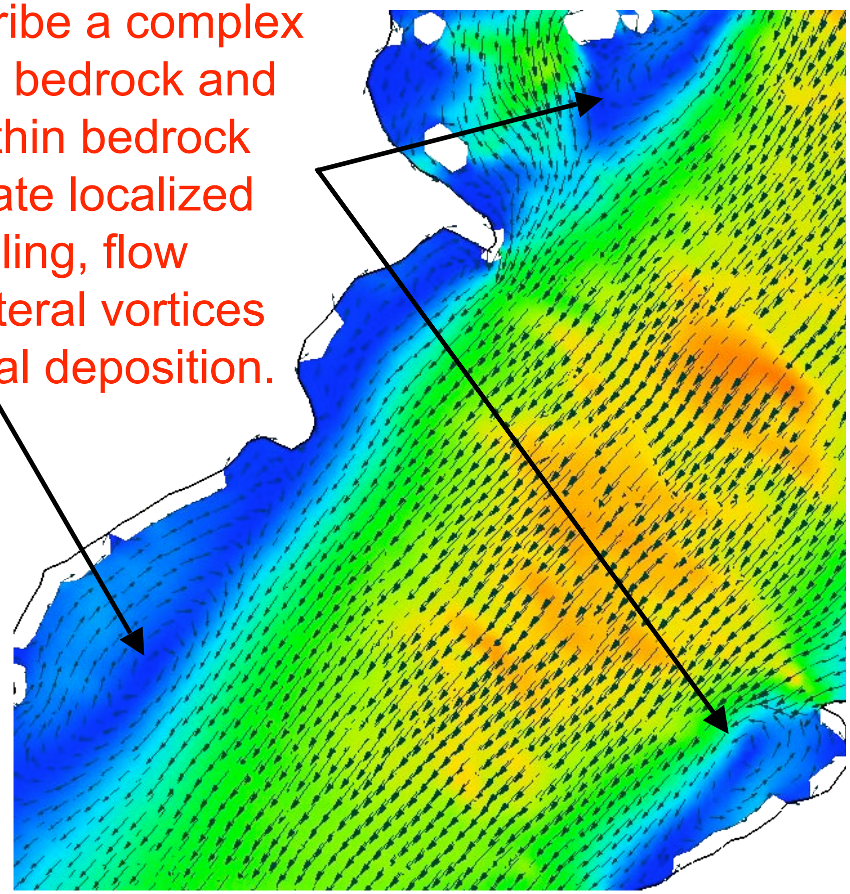

Figure 109

From: McBain and Trush (2004)

However, the amount of gravel that can squeeze into that type of location is small, given the extreme Shields' stresses and rapid turbulent fluctuations that are in the channel at higher flows. Only through field observation of a test gravel injection could we see exactly how much might collect in this way.

HYPOTHESES 7 AND 8

Hypothesis 7 posses that if a sustained and substantial gravel augmentation program was implemented in the EDR that gravel will transport down river and deposit in the channel, thereby producing extensive channel-spanning gravel forms with suitable salmon-spawning habitat. Hypothesis 8 poses that historically, the EDR had ample spawning habitat for Chinook salmon. These hyptheses go beyond the EDS location where gravel would directly injected and tries to get at what the fate of such injected gravel would be and whether gravel should be there at all. Because fish can no longer get past the EDR, due to the height and design of Englebright Dam, it must be recognized that even if the reach did not historically provide salmon-spawning habitat, it may need to do so now under the present dam regime. Still, it is worthwhile to evaluate the history of the EDR and determine what was going on there in the past.

To test these hypothesis, the primary tools used were historical oblique and aerial photographs that visually recorded reach morphogenesis in the EDR. These photographs depict the pattern and nature of alluvial deposits in the reach, and how they changed over time. Based on observed changes, it is possible to infer the likelihood of aggradation of any injected gravels in the EDR as well as where such material would deposit, why those locations would be the key ones, and what the character of deposition patterns would be. Hypothesis 7 has to be rejected if the underlying response of the system is to evacuate the injected gravels over the whole range of the dynamic flow regime. Hypothesis 8 has to be rejected if the EDR never had any gravel deposits in it that were large enough to form channel-spanning geomorphic features, such as riffles and bars.

We are very fortunate to have ground-based oblique photos of the LYR that was taken by G. K. Gilbert, an early physical geography professor at UC Berkeley, between 1905 and 1910. These high-quality photos show conditions in the LYR in the EDR as well as downstream to Marysville. In 2006-2008 we went out and took comparable photos of the similar locations as they are today. In addition, the USACE has ground-based oblique photos from before, during, and after the construction of Englebright Dam. Finally, there are historical aerial photos of the LYR maintained in various libraries in the region that were pulled together by Prof. Allen James, who researches the geography of hydraulic mining for gold in the region. He shared the digital versions of the images with us, and then we georeferenced them by rubbersheeting onto the modern imagery, as detailed in Appendix 2. The georeferenced imagery enables us to do comparisons of what is going on in the EDR from 1937-2006.

First, consider the USACE photo of the pre-Englebright Dam canyon (Fig. 110). This is upstream of the dam location and looking upstream. It is important, because you can see that in this photo from the 1930's that in fact in this section there is a gravel riffle in the river. It looks like there probably was a cofferdam or some other kind of temporary dam downstream of this location, because you can see a water line high on the hill side. The gravel that is deposited here may be associated with that cofferdam or just with the high load associated with upstream hydraulic mining. Either way, you can see a gravel riffle present in the bedrock reach before Englebright Dam was built. Consequently, hypothesis 8 must be accepted, because the reach did

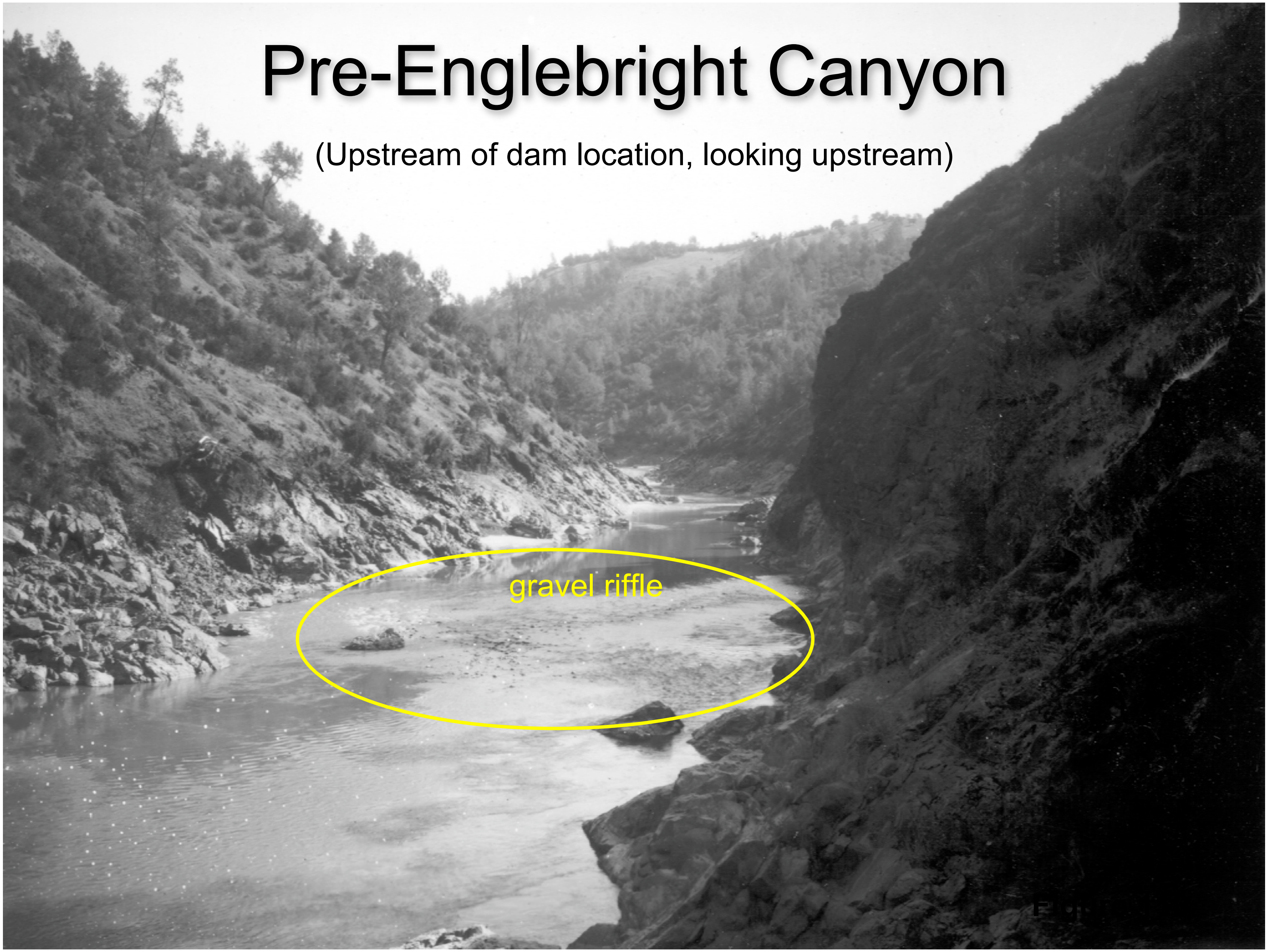
Pre-Englebright Canyon
(Upstream of dam location, looking upstream)
gravel riffle

have at least one substantial gravel riffle that would have provided salmon spawning habitat. Further analysis of hypothesis 8 is present next, along with results for hypothesis 7.

Landers Bar Shot Rock Deposit

One of the big issues in managing the EDR right now is to decide what to do if anything about “shot rock deposits” in the canyon (Fig. 111). Shot rock is defined as blasted rock. In the EDR, it was generated by two processes. First, construction of Englebright Dam. Second, floods that overtop the dam, intensively scour the hillside, and cause landslides of the steep sideslope.

There are three shot rock deposits in EDR (Figure 111). First, an extremely coarse and thin veneer at the upper end of the reach on river right. Second, angular cobble forming a bar just upstream of the USGS Gaging Station rapid that impacts the gaging station every time there is a flood. Third, a mixture of angular gravel, cobbles, and boulders primarily deposited in 1997 flood that is upstream of the junction with Deer Creek on river right. This deposit is called Lander’s Bar. Thus, there are two big deposits on river right and one small deposit on river left.

We can make a direct comparison of the ground-based photos of Lander’s Bar between the 1909 and 2008 photos (Fig. 112). In the 1909 photo you can see a very large point bar that was deposited on river right and is composed of a mixture of well rounded gravel, cobble and sand from the hydraulic mining upstream. You can also see a lot of hydraulic mining debris in the junction with Deer Creek where it imposes onto the Yuba River. There are also two riffles that are evident in the river- one at the bedrock outcrop near the apex of this point bar and another one farther downstream. An important aspect of the 1909 photo is that when you look

Shot Rock Deposits

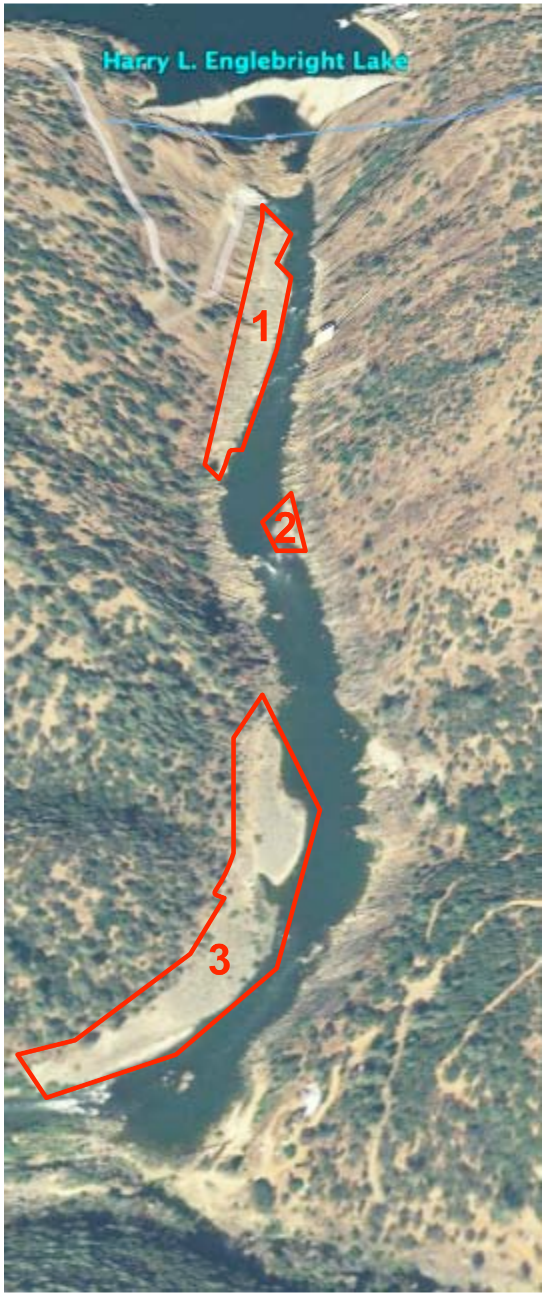

"Shot Rock" is defined as blasted rock.

In EDR it was generated by 2 processes:
1) Construction of Englebright Dam
2) Floods that overtop the dam, intensively scour the hillside, and cause landslides of the steep sideslope.

There are 3 shot rock deposits in EDR, as shown to the right.
1) Extremely coarse and thin veneer,
2) angular cobble bar impacting gaging station,
3) mixture of angular gravel, cobbles, and boulders primarily deposited in 1997 flood.

Figure 111

History of 1997 Shot Rock Deposition Site

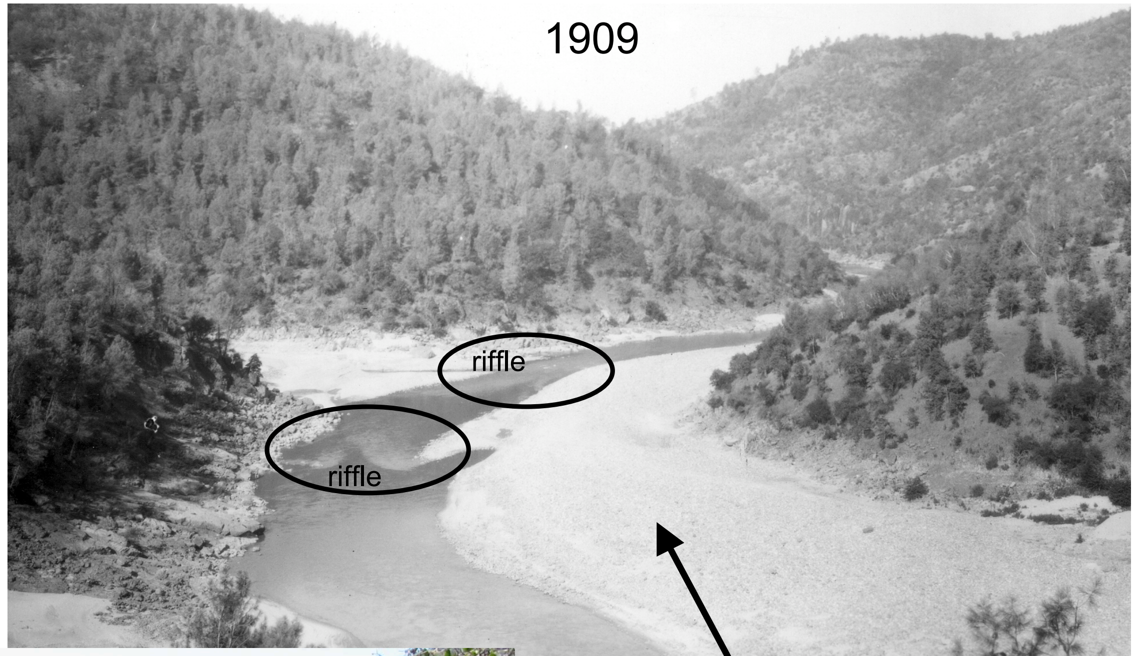

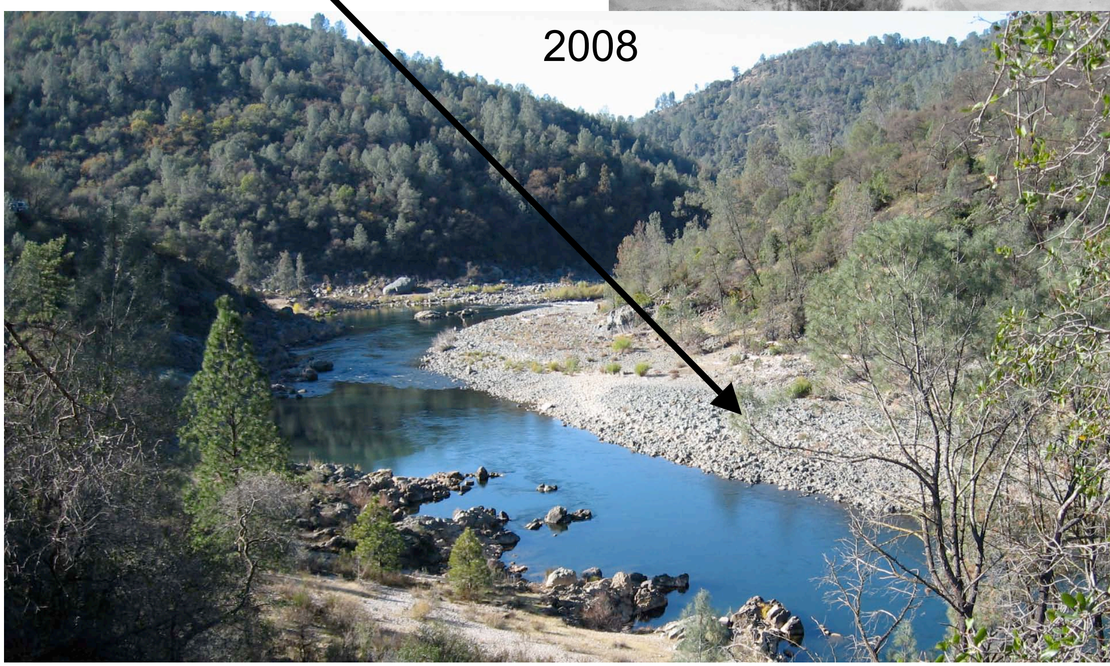

2008 photo shows loss of mine tailings and presence of blast rock

1909 photo by G.K. Gilbert shows riffles and a point bar composed of a mixture of well-rounded gravel, cobble, and sand from hydraulic mining.

Figure 112

across the channel, the channel looks relatively flat. The canyon looks like it is relatively well filled in with this material and the water looks relatively shallow all down through the section.

Contrast that with the 2008 photo where you can see a lot of coarser boulders and cobbles, mixture of different sizes, and a lot of angular material (Fig. 112). There are still two riffles that are present in 2008, but the upper one is not composed of gravel and cobble. When you actually go out to the river there, you can see that the bed is very coarse, with bedrock exposure that wasn't so exposed before. The downstream riffle is still present, but it has steepened to form a rapid and it is composed of much coarser material. Thus, in 2008 you can see the blast rock that is there as a result of the 1997 flood.

To gain an understanding of the history of how Lander's Bar evolved from 1909-2008, we can look at the aerial photos that we have georeferenced. The method of aerial photo analysis was already covered in the TBR section of and is also detailed in Appendix 2. The first aerial photo is from 1937 (Fig. 113). You can see the hydraulic mining sediments on the entire point bar as well as in the mouth of Deer Creek. You can also see the two riffles that were visible in the 1909 oblique photo. The water itself looks very turbid; it is hard to tell if this is just as a result of the camera technology at the time. It would make sense for the water to be turbid, since this photo is from before construction of Englebright Dam. Overall, in this photo you see the same conditions that were present in 1909 persisting to 1937, because the dam still is not present and you still have a large amount and a wide mix of sedimentary material coming down from large upstream deposits of hydraulic mining debris as well as directly off of exposed and abandoned hillsides.

Unfortunately, the 1947 photo, which is the next one available, is relatively blurry and low resolution (Fig. 114). There is not a whole lot to get out of it. You can still see the

Yuba River At Deer Creek

1937

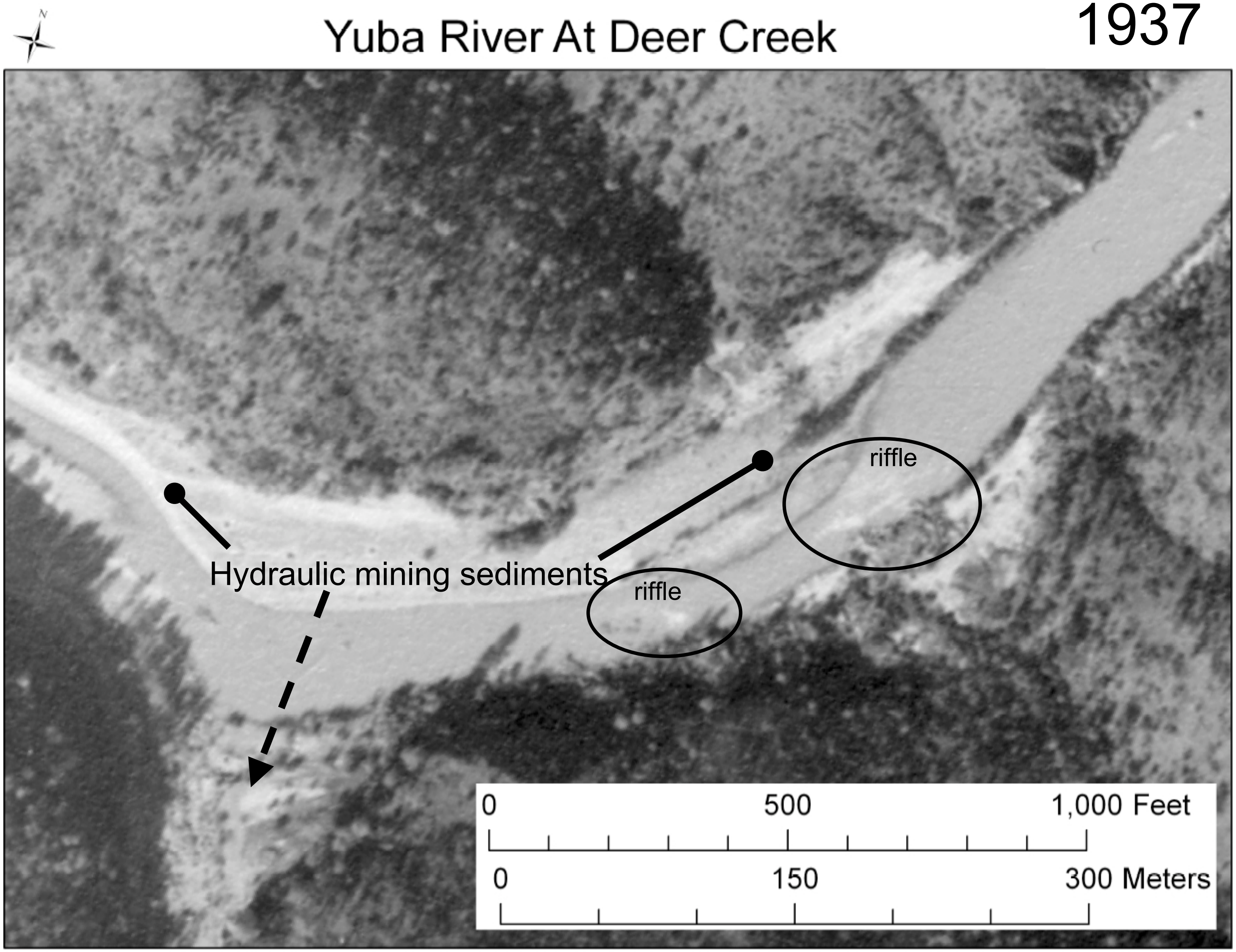

Yuba River At Deer Creek

1947

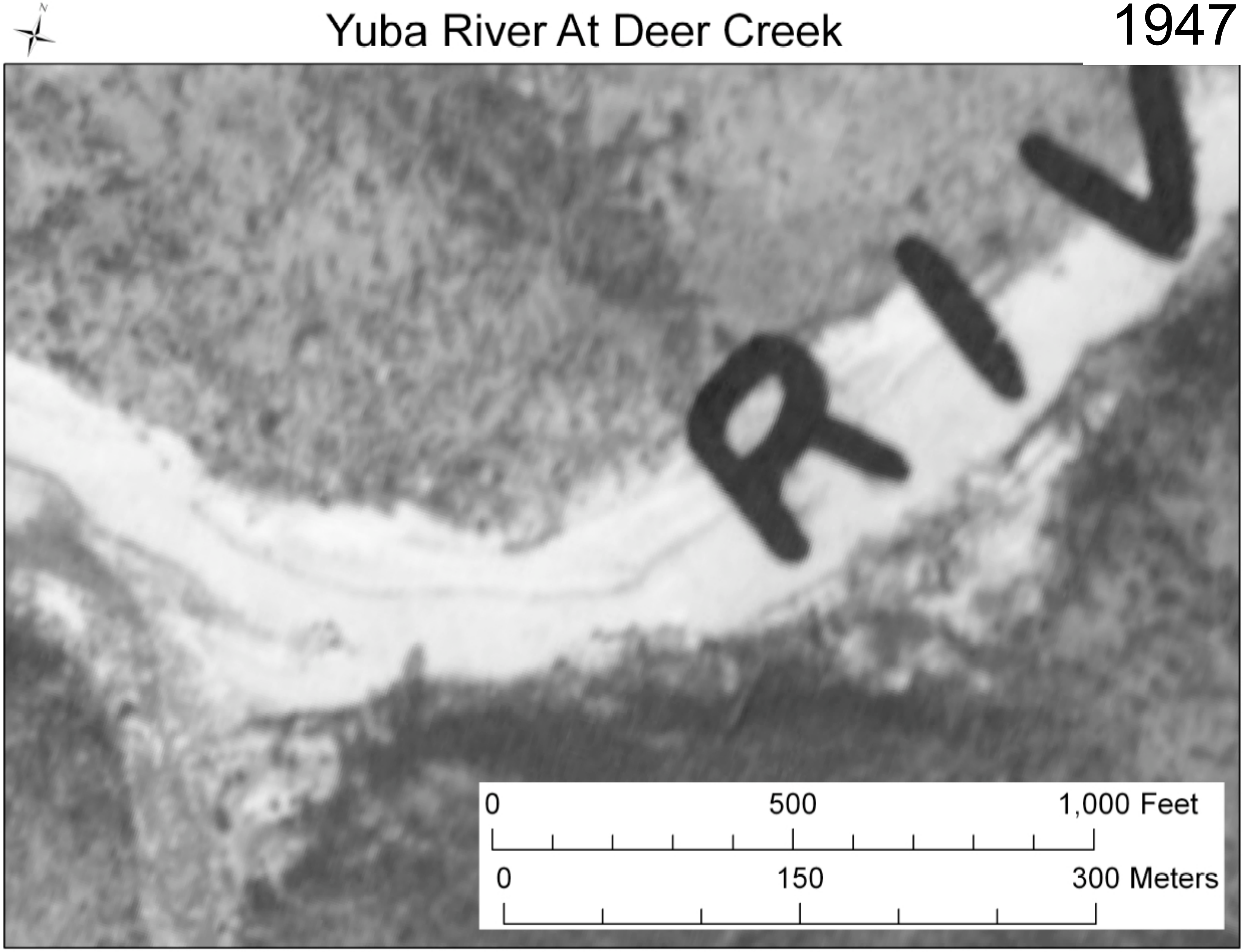

hydraulic mining debris on both sides of the river. The water still looks pretty turbid although this is after the dam was built. It is hard to know exactly what the conditions are. This photo is not particularly useful.

In 1952, we do have a good quality aerial photo (fig. 115). The water is now darkly colored, which indicates that it is clear. First, it does not have much sediment in to it compared with the earlier photos. Second, a lot of the mining debris is gone. Third, there are now three riffles that are present. These riffles still look like they consist of fine sediment. Some of the material in the Deer Creek junction is gone. You can see Deer Creek itself off to the left side, Deer Creek's river left, meandering through a substantial bar that is present mostly on its river right.

There is a big gap in the aerial photo record we have from 1952-1986. There are photo series in 1957 and 1984, but we could not get the photo that included Lander's Bar. From 1952 to 1986 there is a significant change (Fig. 116). There is still a large residual mining sediment bar on river right, but when you look at the mouth of Deer Creek, all of that alluvial material has gone, and in fact in its place there is an in-stream pit. I think this is due to gravel mining. Also, further upstream on river right there is a smaller in-stream gravel mining pit present, and you can tell it is an artificial pit, because of the square shape of the wetted area in the hole. That is definitely unnatural for unconsolidated alluvial sediment. In terms of riffles, the area has gone from two riffles to one riffle, in part because of the in-stream gravel mining, but also further upstream you can see that the channel is entrenching along the south bank and that the riffle is now being strongly influenced by the bedrock outcrop on the south bank. The downstream riffle though is still quite wide and gravel dominated.

Yuba River At Deer Creek

1952

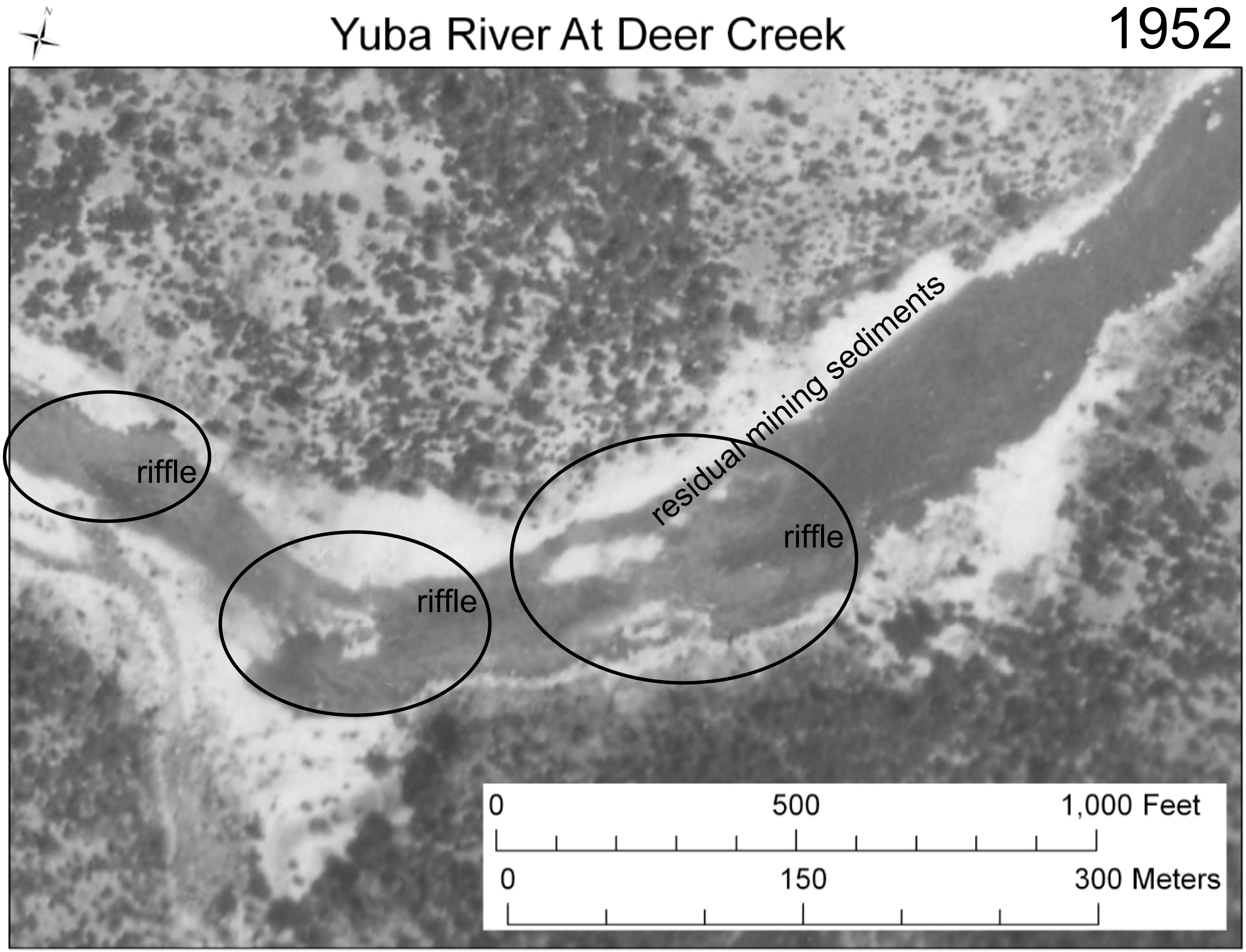

Yuba River At Deer Creek

1986

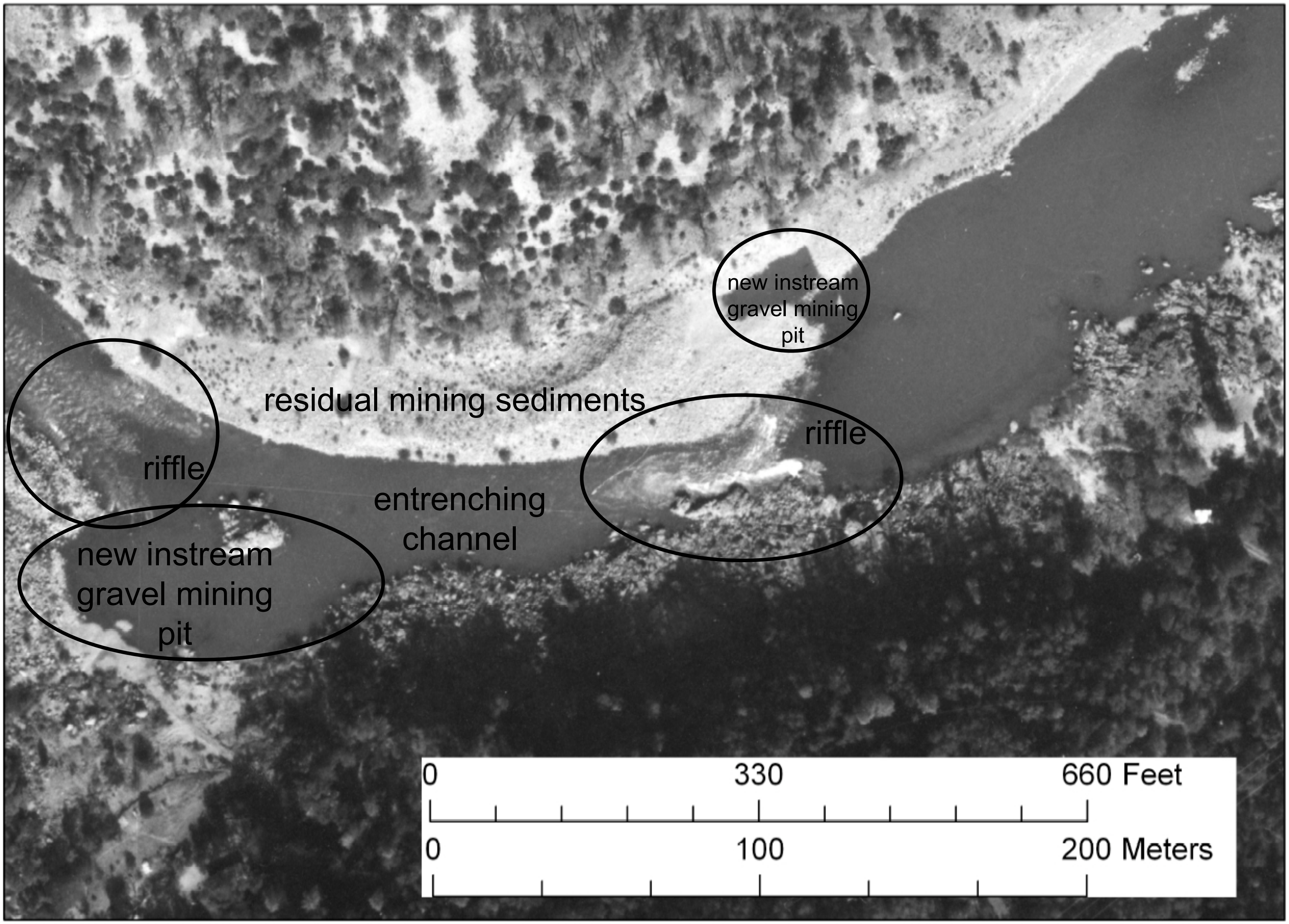

In 1996, you still see that entrenched channel, but you also now see that the in-stream gravel mining has eaten away on the point bar over to the river right (Fig. 117). Also, you can see that there are still the two riffles that are present as in 1986. Overall, the sediment on Lander's Bar is still discernible in this photo and does not look particularly course.

Then we have the rain-on-snow flood of January 1997 which had a very large discharge. We don't have a photo immediately after that. The next photo is a very high quality photo taken in 2002, and this is the photo where you can see all the new shot rock debris that's been deposited on Lander's Bar (Fig. 118). Because the deposit is so fresh, it looks relatively fine in this photo, but it is actually quite coarse. You can see that it has buried a lot of the vegetation that was evident earlier. It is very helpful to compare and contrast the 1986, 1996 and 2002 photos. In the 2002 photo, not only do you see new material, but the upstream riffle has been degraded to a chute, because of the intense scour through there. Also, the downstream riffle became heavily armored and more like a rapid at this point. It probably received a lot of coarse boulders and cobble that replaced the finer gravel that was there.

After 2002, there are photos in 2004, 2005 and 2006. (Figs. 119-121). There is not much change evident in these annual photos. In the 2006 photo (Fig. 121) the discharge is noticeably lower. There may have been some adjustment to the material as a result of the New Years 2006 flood, but overall there is still a lot of the 1997 shot rock debris that is present in 2006.

In summary, the 1909 photo shows that hydraulic mining debris filled in the canyon. It also shows the mixture of sizes, including a lot of small particles. The 2008 photo shows very coarse cobbles and boulders on the same bar, and that bar rises high above the wetted channel, due to long-term channel incision. It also shows more bedrock outcropping into the channel where incision has hit the underlying valley floor. The 1937 to 2006 set of aerial photos show

Yuba River At Deer Creek

1996

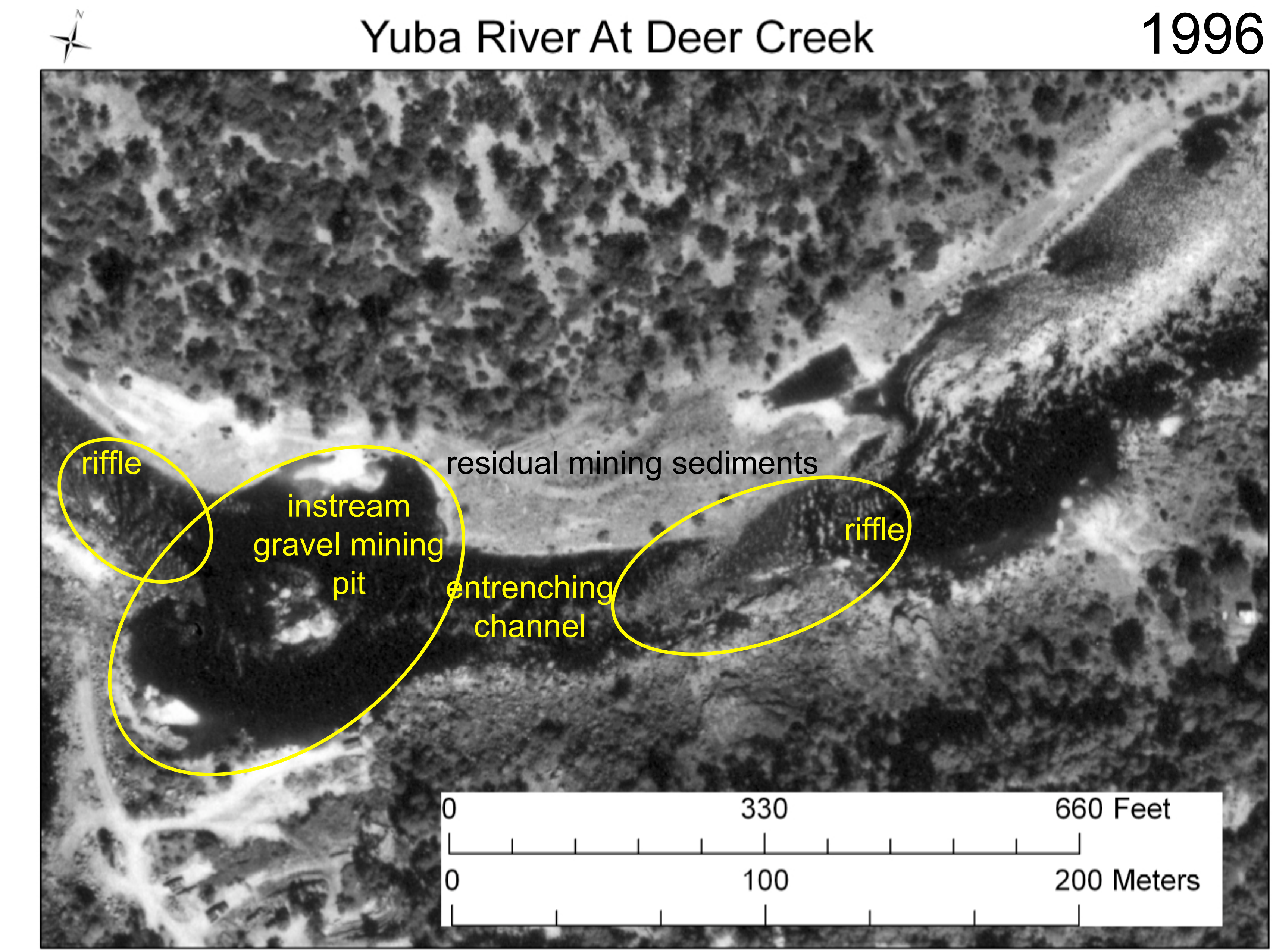

Yuba River At Deer Creek

2002

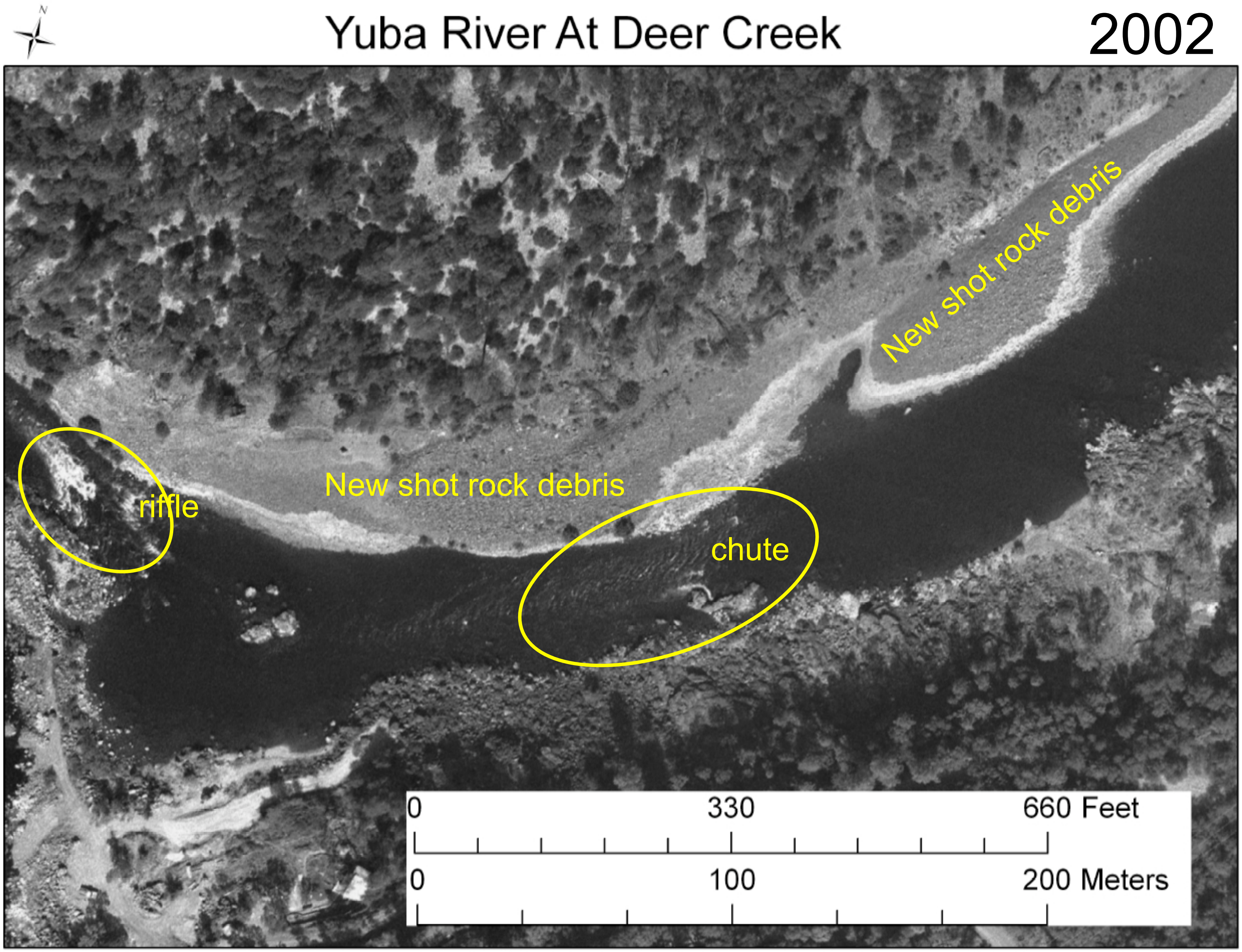

Yuba River At Deer Creek 2004

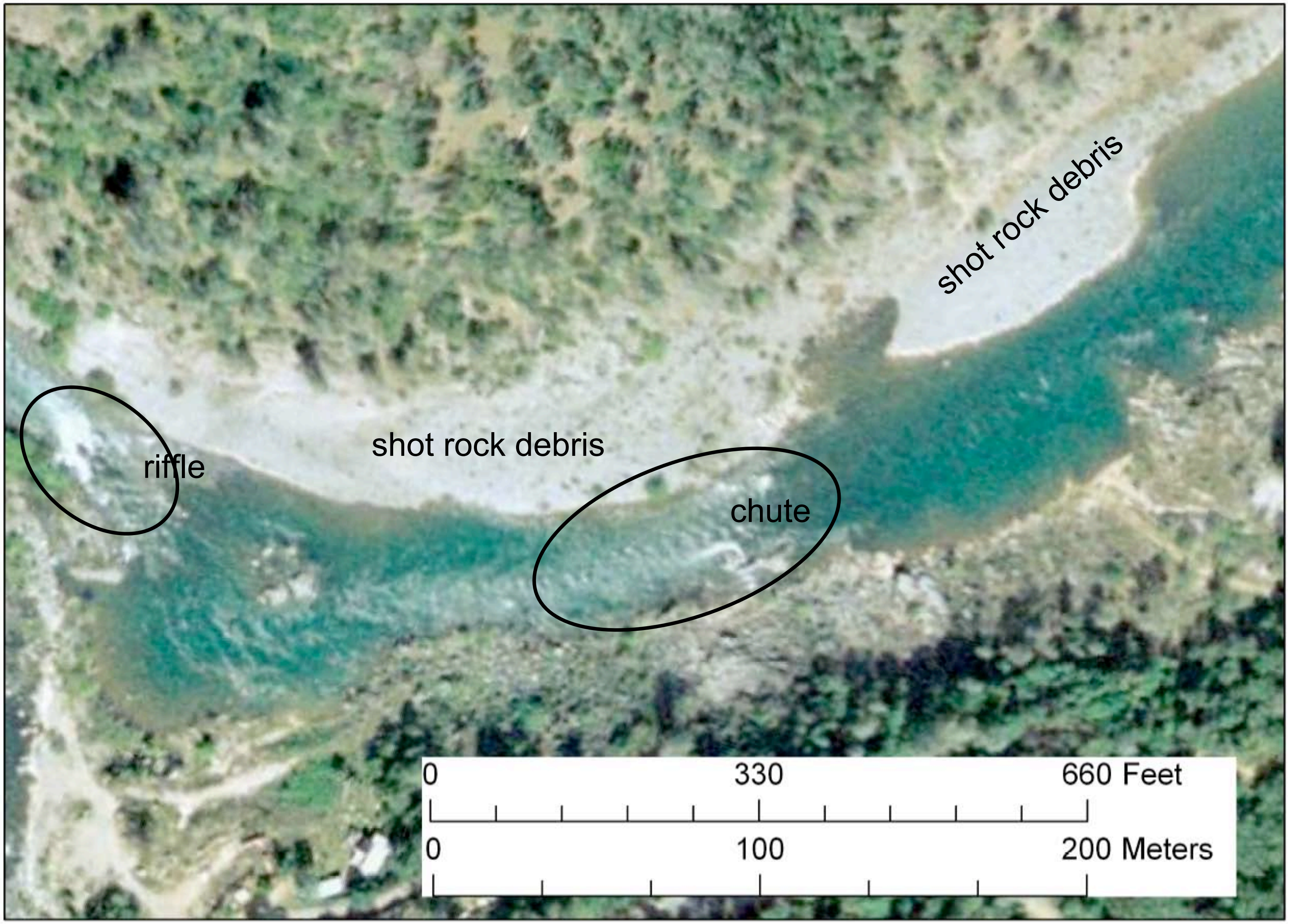

Yuba River At Deer Creek

2005

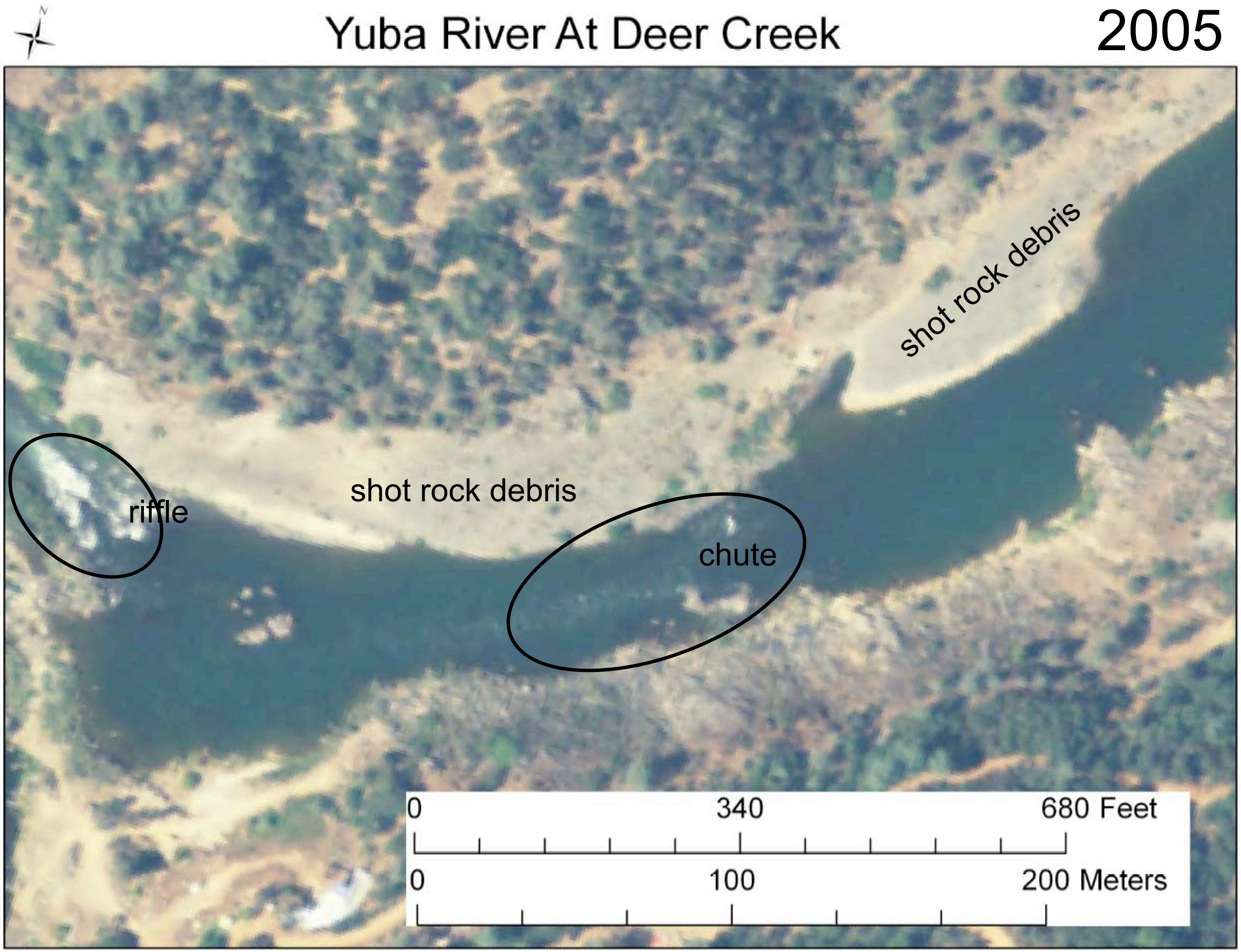

Yuba River At Deer Creek

2006

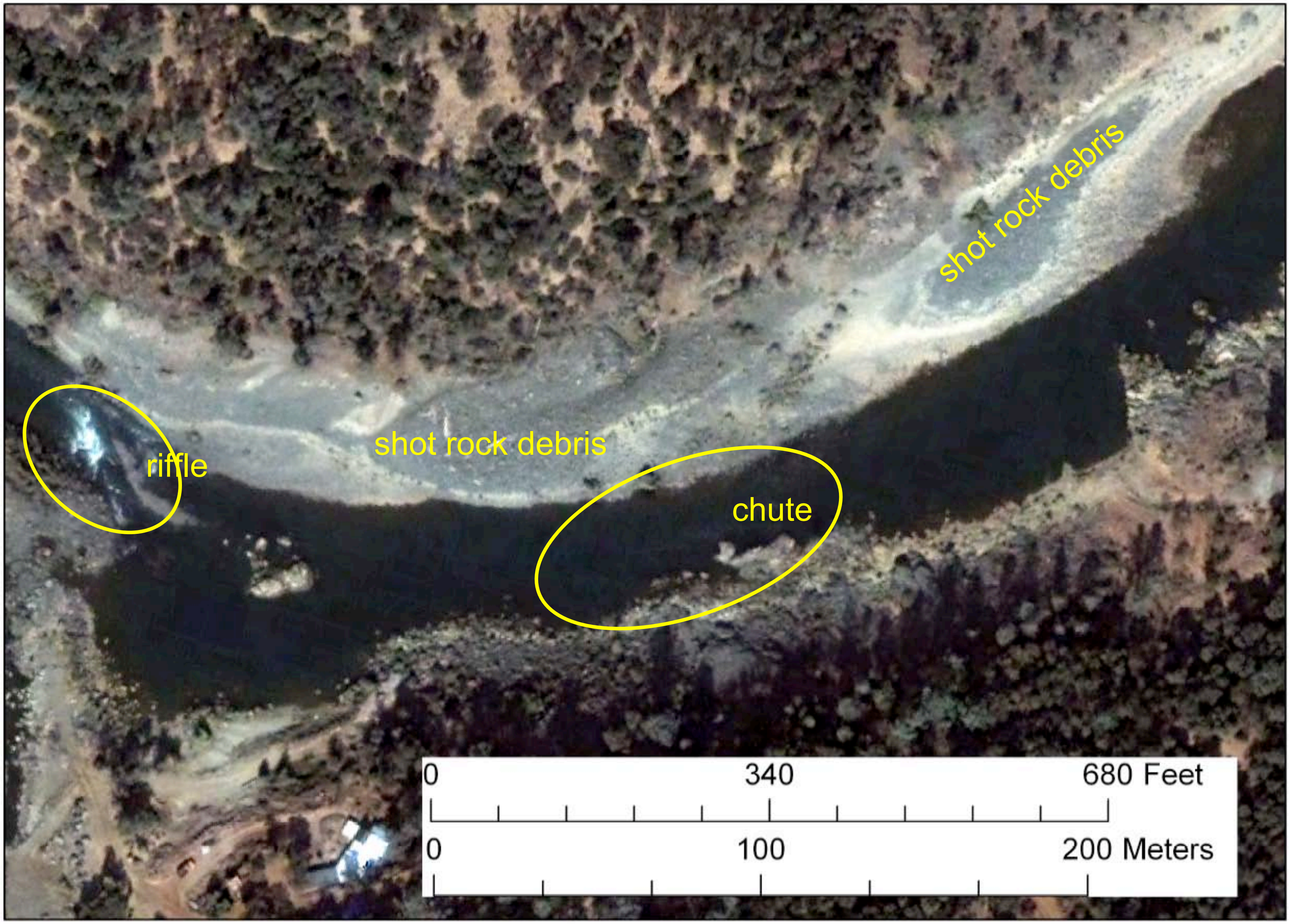

persistence of hydraulic mining debris, active mining in that sediment, and deposition of new shot rock sediments over the mining debris. Riffles are present in every photo of the site. The main gravel riffle opposite the bar has been degraded to a deep fast chute controlled by bedrock on the south bank and lacking gravel.

As a result of all of this evidence, it appears that the EDR locations where shot rock deposited in the past provides a key natural "experiment" in and of itself. This natural experiment indicates the likely location where any gravels injected right below Englebright Dam as part of future management activities will now deposit. Even though the shot rock does take up some of the, what sedimentary geologists call, "accommodation space" where that gravel might go, there is still ample room in EDR such that during a high event, injected gravel could simply deposit on Lander's Bar or in the mining pits on and near it.

If we look at the whole EDR and we evaluate where gravel injection at the dam might go, it's going to go places where the river is wide and relatively deep, with some form of obstruction downstream that dams up the water to some extent. There are three locations and each location is just upstream of a bedrock hydraulic control (Fig. 122). The first possible location is a wider glide-pool unit that is just upstream of the USGS Gaging Station rapid. That rapid is located at a significant narrowing of the river, due to both vertical and lateral constriction. Velocities are lower in this glide-pool, meaning that there is a chance for deposition there. Deposition in the glide-pool would be upstream of the gaging station cross-section, so it would not influence or impact the rating curve for that station, unless the glide-pool was completely filled in and gravel also was so abundant as to then also change the rapid itself. The fact that the rating curve at the USGS Gaging Station has changed so many times, essentially after every flood, proves that there is both deposition and erosion occurring at the rapid that is the hydraulic control. Also, since the

Gravel Placement Point and Where Will it Go

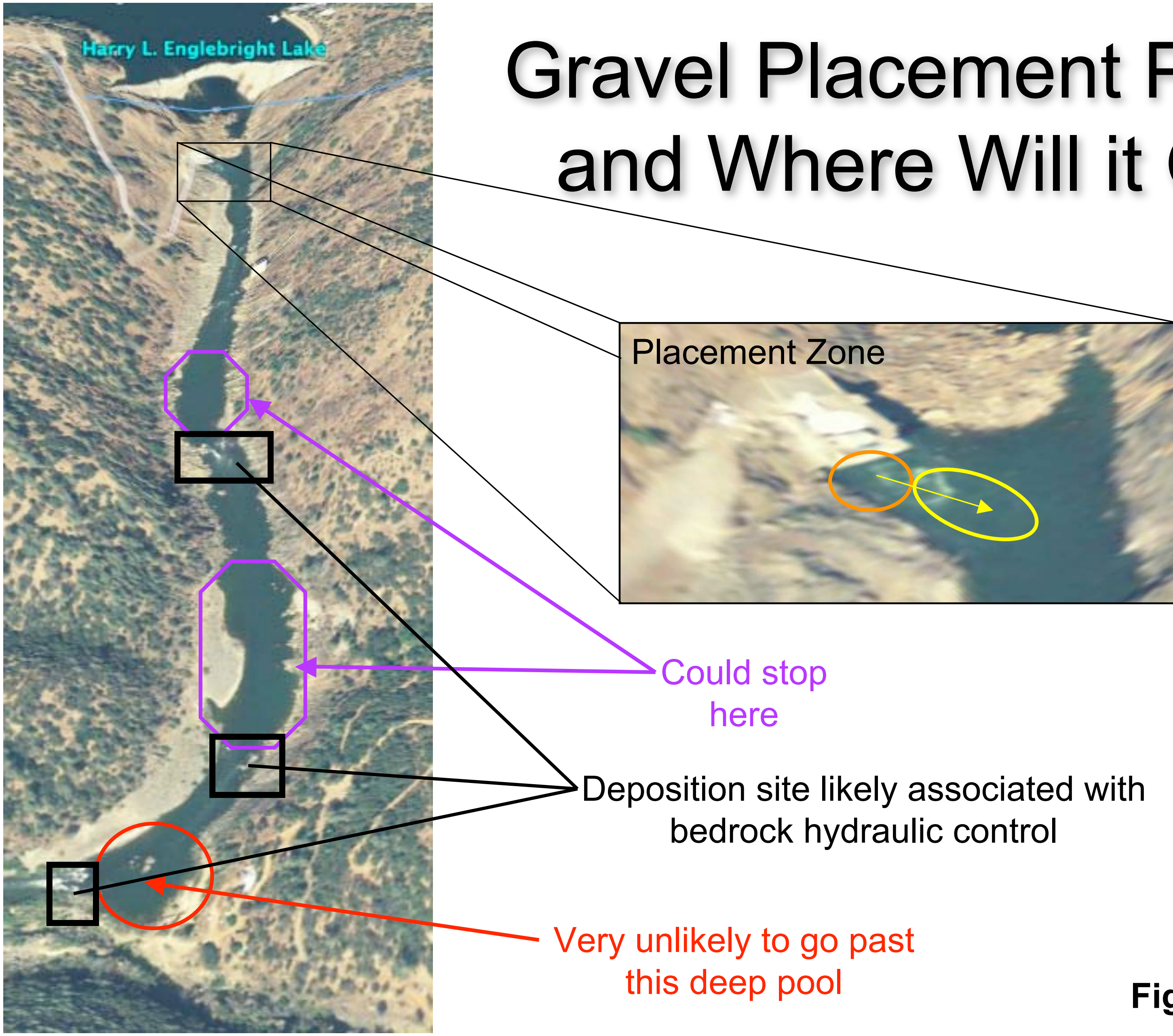

Figure 122

rating curve is already being changed by the frequent floods, there is no fair argument that gravel augmentation should be restricted or prevented due to the desire to have a stable rating curve-there is no stable rating curve at this site. If the operators of the gaging station want a stable rating curve, then they should propose actions in the river to promote stability of the rapid. Deposition of gravel in the glide-pool upstream will not affect the rating curve.

As you go downstream from the USGS gaging station rapid, the channel continues to widen and there is another bedrock hydraulic control where, in the historical photos, there used to be a riffle (Fig. 122). Upstream of that, in the upper third of Lander's Bar at river right, is the second location where injected gravels could deposit. This hydraulic control does not appear as strong as the USGS gaging station rapid, but it would take 2D modeling of the EDR to determine that. The third and final location in the EDR is in the large in-stream mining pit right at the junction with Deer Creek and just upstream of that. At ~1600 cfs, the mining pit has a maximum depth of 16' and widespread depths of 8-10'. Hydraulics in this pit are controlled by a bedrock-boulder-cobble rapid. Also, the boulder-cobble sedimentary fan prograding out of Deer Creek provides somewhat of a lateral constriction at this point. Thus, in the EDR there are 3 hydraulic controls and 3 potential deposition sites. The fact that the majority of the 1997-flood shot rock made it pass the first one and deposited in the second and third locations is the best real evidence that we have to suggest where any injected gravels would go. The majority of the material deposited on Lander's Bar.

Based on all of the historical imagery of the EDR, hypothesis 8 must be accepted, because over the last 100 years there were multiple gravel riffles in the EDR. We have no imagery from before hydraulic mining, but there is no question that since hydraulic mining has been going on, there have been riffles in the EDR. Based on the size and shape of the riffles evident in the imagery, they would have provided salmon-spawning habitat. Thus, even though the reach is bedrock controlled, it does have ample gravel and spawning habitat for Chinook salmon.

Regarding hypothesis 7, the evidence from both the EDS 2D model and the historical imagery demonstrates that there are locations in the river where injected gravel would deposit. However, in order for the deposits to form extensive cross-channel bars and riffle, there would have to be a sizable gravel augmentation program. Just how big that program would have to be is uncertain. Based on my experience with gravel augmentation over the last decade, any amount less than 5,000 yds^3 of gravel per year would be too small to yield benefits. I conjecture that 5,000-10,000 yds^3, would promote sustainable deposition behind flow obstructions that would be large enough to support a small population of spawners. To determine how many could be supported by this size of injection program, it would be necessary to use a 2D model to perform an instream flow assessment of the spatial pattern, size distribution, and number of flow obstructions present in the EDR for flows ranging from 800-2000 cfs. I think that a gravel augmentation program of 10,000-20,000 yds^3 would likely be large enough to yield sustainable gravel bars in the river that could form riffles. Recall from the earlier sediment budget analysis that the load of gravel and cobble- not all sediment, but of gravel and cobble- into Englebright Lake has been 61,600 yds^3/yr from 1942-2004. So we know for certain that a load of that magnitude would yield sustainable riffles in the EDR, because we saw them in the river from 1909-1937 when the yield was about that magnitude. However, a magnitude of that sie might impact the river downstream of the Narrows, so that is not recommended.

Finally, there is the alternate option of doing a gravel placement and spawning habitat rehabilitation project in the river at Lander's Bar. To yield high quality Chinook spawning habitat such a project must do two things. First, it must remove the massive amount of shot rock off of Lander's Bar, returning that entire point bar to the elevation of the water 's surface at ~800 cfs. Second, it must place suitable spawning gravel into the river filling in the present channel substantially and changing the flow to a new suitable pattern. It is highly recommended that such a project be designed using the Spawning Habitat Integrated Rehabilitation Approach (SHIRA) that is in use on the Feather, American, Trinity, and Mokelumne Rivers. For details, see the website at http://shira.lawr.ucdavis.edu. Using SHIRA would ensure that a project of this magnitude would immediately yield spawning habitat, as has been documented thoroughly on the Mokelumne and Trinity Rivers so far. It would also check to see the effect of large floods on project alternatives. Once spawning habitat rehabilitation is performed at the site, if such action was chosen by the river's management team, then it would be possible to sustain the project using gravel injection at the dam or by doing additional gravel placement at the site.

HYPOTHESIS 9

The final hypothesis states that current spawning habitat conditions at the EDS and TBAR sites are not limiting. The testing method involves looking at the percentage of channel in the very poor, low, medium and high quality habitat bins. To get those quantities, micro-habitat distribution at each site was estimated for a flow of ~800 cfs using autumn 2005 DEM, the FESWMS 2D model, and the bioverified HSC (given in TBR section of report). The results were analyzed in ArcGIS 9 using the classification and zonal statistics tools in the spatial analyst toolbox. If the proportion of channel in the medium and high quality habitat bins is below 5% of the wetted channel area, then Hypothesis 9 must be rejected.

The results for the EDS at 800 cfs show that the site has no unsuitable spawning habitat. In terms of hydraulic conditions, there is only a tiny amount of suitable area (Fig. 123). Most of the flow is too deep and fast. There are a few peripheral spots that have adequate hydraulics responding, but field observations revealed that these spots are devoid of the suitable gravel and cobble bed. Almost the entire EDS is devoid of spawning gravel. Thus, in the typical range of spawning discharges of 700-1200 cfs, there is really no habitat present in the EDS. You can contrast that with what was observed at the TBAR site (Fig. 124), as was already described in the TBR section of the report. There were no redds observed during the 15 site visits over two spawning seasons (2005 and 2006) at the EDS, but there have been many redds observed at the TBAR site.

2007 PILOT GRAVEL INJECTION EXPERIMENT

All of the hypotheses put forward in this report have now been evaluated. On the basis of the preliminary findings of this project, UC Davis, USFWS, and USACE collaborated on an experimental gravel injection below Englebright Dam in November 2007. The purpose of this experiment was to determine the efficiency of gravel injection as a habitat enhancement tool for spring-run Chinook salmon in the EDR. The idea was to inject the gravel during low flow in autumn of 2007, and then hopefully we would have some high flows in 2008 or 2009. Then we would then be able to track where those materials went. No flow >10,000 cfs occurred in winter 2008, so such monitoring was not possible as part of this contracted project.

The TB 135 that was previously described (Fig. 96) was used to reach out over the river and inject a few hundred yds^3 of gravel into the Narrows II pool (Fig. 125). 500 short tons of

Results H_9

Chinook Spawning Hydraulic Habitat Quality Predictions

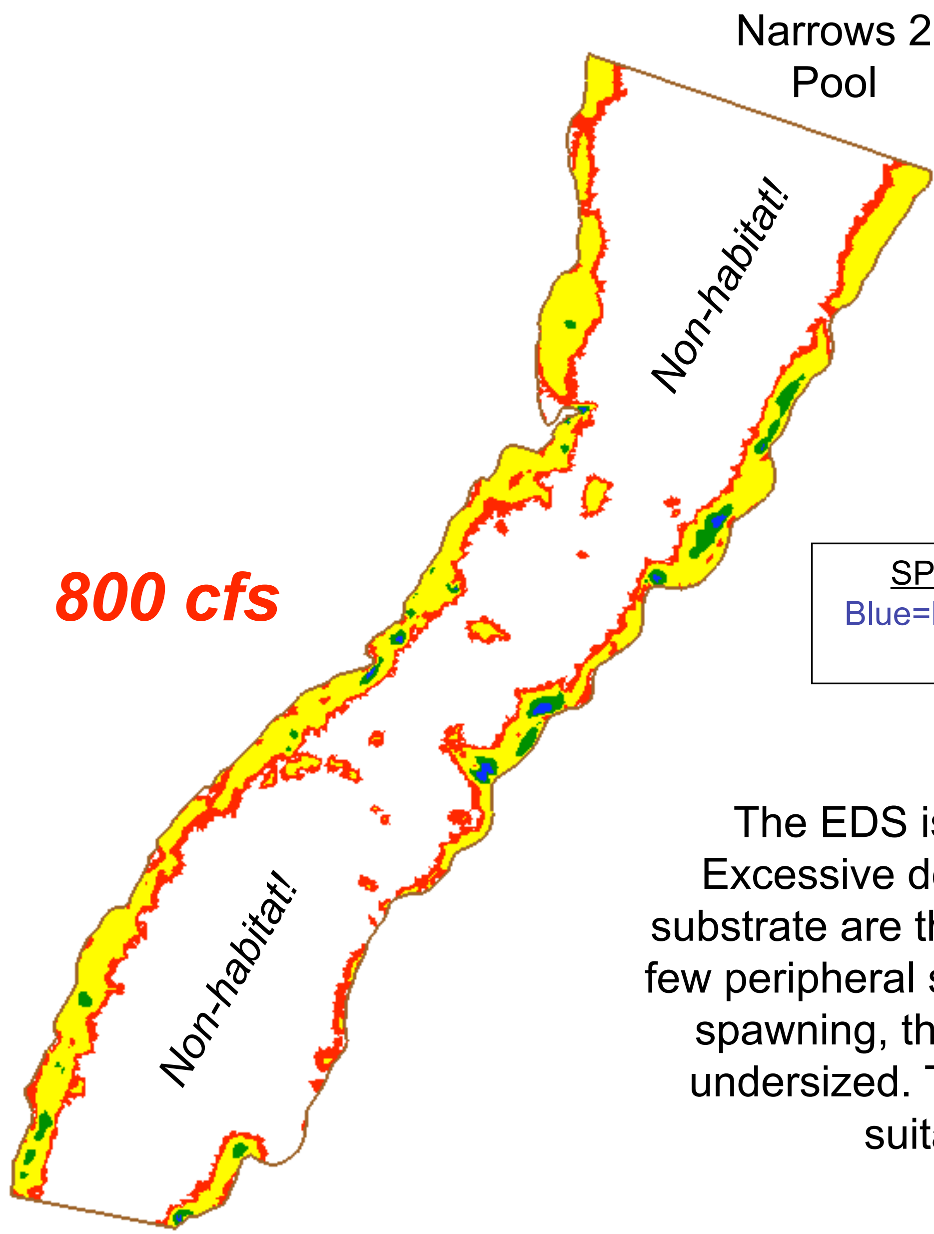

SPAWNING HABITAT QUALITY LEGEND
Blue=high, green=medium, yellow=low, red=very poor, white=non habitat

The EDS is unsuitable spawning habitat. Excessive depth and lack of a gravel/cobble substrate are the causes of inadequate habitat. A few peripheral spots have adequate hydraulics for spawning, these spots are disconnected and undersized. These areas are also devoid of a suitable gravel/cobble bed.

Figure 123

Results H_9: 2005 EDS vs TBAR

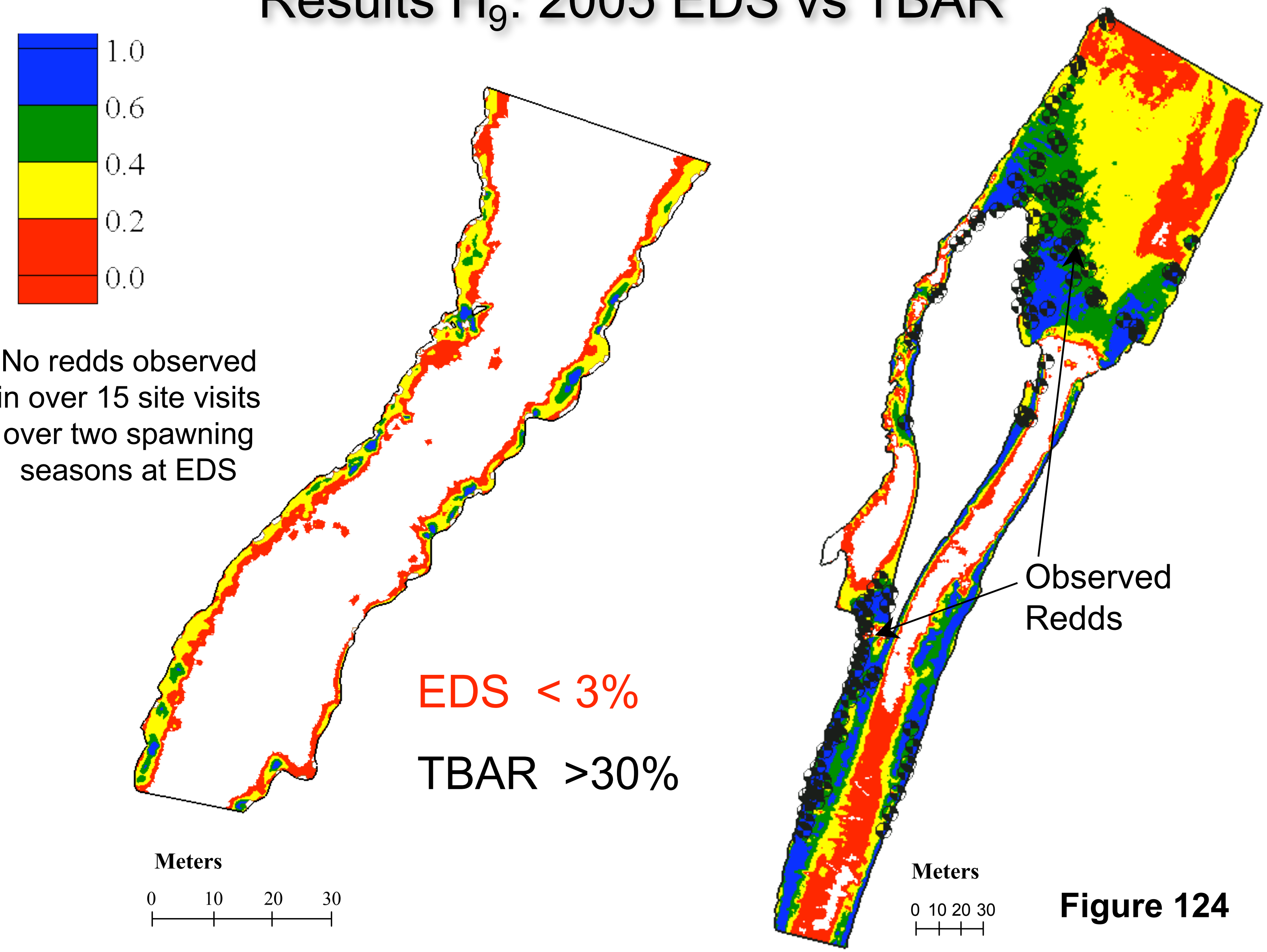

Figure 124

Experiment Implemented on 11/29/07

Elucidate the efficacy of gravel injection as a habitat enhancement tool for spring-run Chinook salmon in the EDR of the Yuba River, CA.

rock tracers

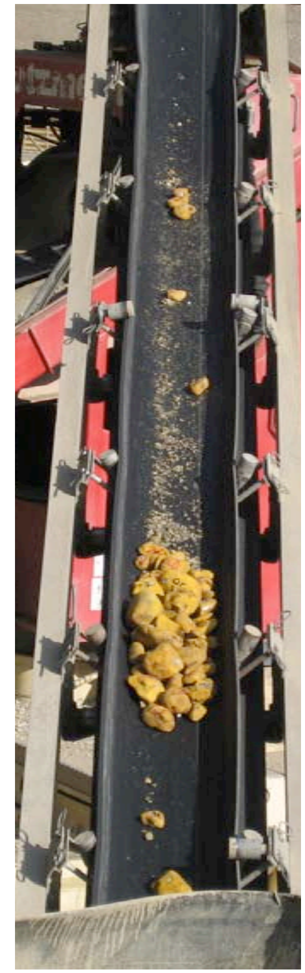

Figure 125

triple washed river gravel was purchased from a nearby quarry downstream. The material was trucked in ahead of time and piled on top of the gravel parking lot at the Narrows II powerhouse. Gravel injection took place on November 29, 2007 beginning at 9:30 am and finishing by 3:00 pm. A single small loader was used to transfer piled gravel into the hopper, but it turned out that not all the gravel could be fully injected during the single allotted day. Consequently, an unknown small amount ended up being incorporated into the parking lot, instead of going into the river. That suggests that in the future 2 loaders be used per 500 short tons of gravel placed per day. Nevertheless, a substantial amount of gravel was placed into the river and we were able to get it all in and begin to track to see what would happen. As the material was being placed into the river, we also put ~400 painted, magnetized tracer stones into the hopper (Fig. 125). Those tracers are thus integrated all throughout the in-river gravel pile. Those stones will be easy to track, but really any gravel that you find downstream in the EDR must be coming from this source, because there is no other rounded river gravel in this reach.

It also turned out that there was a fair amount of finer material in the gravel, even though the gravel had been washed multiple times at the quarry. The permit for the project required that turbidity be monitored upstream and downstream of the injection spot. We chose to do monitoring and sampling on an hourly basis from 9 am to 3 pm at three locations. Because the injection site was at the upstream limit of the river below the dam, the “upstream” reference sampling location was taken to be along the edge of the Narrows II pool away from where the injection was occurring. Sampling was also performed 300’ downstream as well as 3.84 miles downstream at the TBAR site.

Table 2 below presents the results of turbidity monitoring, with values in NTUs. These data were collected using a Hach Model 2100P turbidity meter in the 0-10 NTU range with a stated resolution of 0.01 NTU. The background turbidity of the river was in the range of 1.3-2.2 NTU. The highest value observed during the project was 4.24 NTU, which was in the injection pool. The rate of injection was slowed thereafter and the turbidity never exceeded 2.75 at that location, which is within 1 NTU of background. At the location 300' downstream, the peak was 3 NTU, also in the first hour. At the key habitat location 3.84 miles downstream, there was no significant increase in turbidity observed. No tributaries bring significant flow into the river, so this effect must be due primarily to mixing over time. At all three sites, the average of turbidity values shows that the average increase over background was ~1 NTU or less right at the project area and insignificant far downstream.

Table 2. Tubidity monitoring results for the 2007 gravel injection experiment.

Sampling time	Pool	300' downstream	3.84 miles downstream
pre	2.17	1.38	1.36
10:00 AM	4.24	3.00	1.03
11:00 AM	2.19	2.64	1.12
12:00 PM	2.75	2.57	1.63
1:00 PM	1.97	1.98	1.35
2:00 PM	2.69	2.17	1.67
post	1.55	1.55	1.43
clean avg	1.86	1.47	1.40
project avg	2.77	2.47	1.36

avg increase	0.91	1.01	-0.03

Two 5-gallon bulk samples of the gravel were taken at random from the gravel piles. One of those was processed to determine the amount of silt and clay in the material. The material was wet sieved to separate out gravel and cobble. A sediment dispersant (Sodium Hexametaphosphate) was used to keep the fine sediment from forming aggregates. Then the residual material was wet sieved again to remove all sand sizes. The final residual bath with fines was allowed to settle, and then a lot of the water was decanted off. Then the sample was homogenized and subsampled to determine the mass of fines (silt + clay), which turned out to be 49.85 g of fines per 5-gallon bucket. 5 gallons equals 0.6684 ft^3 equals 0.02476 yd^3. This equals a concentration of 2.013 kg per yd^3. Also, from research done on the Mokelumne River, it is estimated that there are 0.722 yd^3 per short ton of gravel delivered, so the maximum amount of gravel ijected into the river was 361 yd^3. Putting these numbers together reveals that the total fines content of the injected gravel was ~726.7 kg of silt and clay. Grain size analysis using a laser granulometer revealed that 81.8 % of the fines (by volume) was silt and 18.2 % was clay. There were two peaks in the size distribution, with the larger peak at 15.651 μm. The secondary peak was at 33.008 μm. Unfortunately, the sand fraction of the 5-gallon bulk sample was accidentally spoiled and could not be analyzed.

Overall, the gravel injection pilot experiment using ~361 yds^3 of material was smooth to implement. One lesson learned was that 2 loaders should be used. A second lesson learned was that triple washing river gravel does not yield a "clean" pile of gravel. However, the TB135 conveyor trickles the sediment out into the river at a reasonable rate that is slow enough to limit any harmful turbidity plume from this dirt. No perceptible change in turbidity was detectible 3.84 miles downstream at the TBAR site. Because the flow never got high enough in the 2008 water year to yield any gravel movement, it remains to be seen what the fate of the injected material will be.

EDR 2D MODEL

The last scientific results to be presented and discussed is that most recently we have been able to perform a comprehensive model simulation of the entire EDR. Originally we only had that 2005 EDS map and we only had the FESWMS program, which has a relatively limited size of river that it can model in the full microhabitat resolution that we want to do. However, using the newer SRH model previously described, we were able to make a model that had a computational mesh spanning the entire EDR canyon. The model had a resolution of 3' internodal spacing in the wetted low-flow channel and then anywhere from 3-10' resolution out on the bedrock floodplain and the canyon sidewalls. This new model is suitable to investigate how the canyon as a whole functions, both in terms of spawning habitat conditions and flood-flow hydrogeomorphology.

The new SRH model of the entire EDR was done initially at 855 and 1600 cfs, because those were discharges for which we had really good WSE data to run the model. Looking at the results from the higher of those two discharges, for the entire reach depths range from 0-16' and velocities range from 0-14 ft/s (Fig. 126). The peak velocities of ~12-15 ft/s occur over that USGS Gaging Station rapid. That is the one dominant hydraulic feature in the river, and it

New SRH-2D Model Simulations

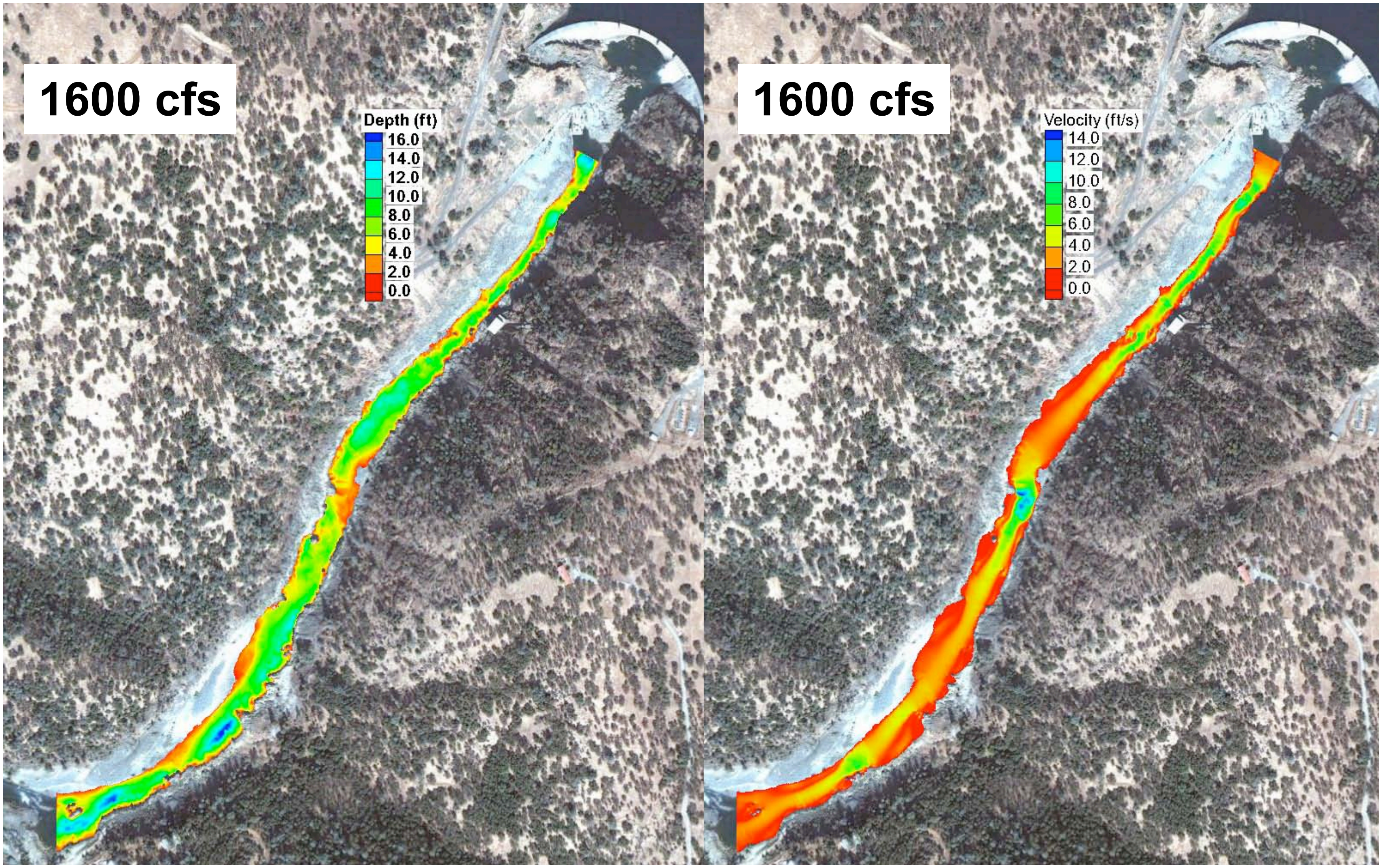

Figure 126

probably should be subjected to further scientific investigation, because of its importance to the USGS gaging station. Between Narrows II and I powerhouses we can see that where we had been running the EDS model that the downstream run continues all the way down to Narrows I and even beyond that a little bit farther. That demonstrates how constricted the upper part of the EDR is, which expands the evidence in favor of limited deposition potential for such a narrow canyon in that section of the EDR. Only once you get to the wider glide that is present upstream of the USGS Gaging Station is there a chance for sediment deposition to occur. Another thing evident in the EDR 2D model velocity results is that through that glide and then downstream through the rest of the reach there is a thalweg right in the center of the channel with higher velocities in the range of 2-6 ft/s. Along the margins there are lower velocities in the range of 0-2 ft/s. So even though these results are for a low discharge, it does confirm the evidence earlier presented suggesting that you are not going to have cross-channel deposition or sizable gravel features in the center of the channel when you do gravel augmentation, because there is a high velocity in the thalweg, even at a low flow. This project was not contracted to do more models with SRH-2D, we just had the opportunity, but in the future it would be possible to simulate discharges up to 87,800 cfs, which the highest flow for which we have WSE data down at the end of the model domain.

EDS SITE-SCALE CONCLUSIONS

The conclusions for the EDS follow:

1. A 4-year flow event of about 710 m^3/s (25,100 cfs) is required to initiate gravel movement in the Narrows II pool within the EDS.

2. The flow convergence routing mechanism that sustains the TBR does not exist in the EDS or beyond that downstream to the Narrows I Powerhouse.

3. Scour is always focused in the center of the channel, regardless of discharge. That prevents cross-channel gravel riffles from forming, and would do so even if there was a large gravel augmentation program.

4. Deposition of augmented gravels, information of alluvial habitat features is only possible along channel margins and recirculation zones where nested dead features impact local hydraulics and promote local deposition in the ED.

EDR CONCLUSIONS

The conclusions for the whole EDR follow:

1. Spawning habitat for spring-run Chinook salmon is almost nonexistent in the EDR, because velocities are too high, water is too deep, and there is no substrate of rounded gravel in the reach.

2. Historically, floods deposited hydraulic mining debris and shot rock debris just upstream of the USGS Gaging Station rapid and down at Lander's Bar. These are locations where there exist notable bedrock hydraulic controls. These features are inferred to explain the observed pattern of deposition in EDR.

3. The fact that shot rock and hydraulic mining debris deposited in the EDR indicates that gravels injected at Englebright Dam can be expected to deposit in the EDR too, and at those same locations. In light of the strong bedrock control at the three key depositional locations in the reach, it is unlikely that injected gravel would move downstream into the Narrows Reach. If it did, the enormous pool at the end of that reach would trap it.

4. An experimental gravel injection was performed on November 29, 2007, but no high flows occurred in the 2008 water year, so the material remains where it was placed. That material did have some silt and clay in it, but not enough to create a significant turbidity plume.

5. Because the shot rock in the EDR is taking up a lot of the depositional space where there used to be a large point bar composed of spawning gravel, it will be worthwhile to consider removing the shot rock debris and directly placing spawning gravel across the channel there. Such a projects should be designed using the Spawning Habitat Rehabilitation Approach.

REFERENCES

MacWilliams, M. L., Wheaton, J. M., Pasternack, G. B., Kitanidis, P. K., Street, R. L. 2006. The Flow Convergence-Routing Hypothesis for Pool-Riffle Maintenance in Alluvial Rivers. Water Resources Research 42, W10427, doi:10.1029/2005WR004391.

Pasternack, G. B. 2008. Chapter 18. Spawning habitat rehabilitation: advances in analysis tools. In (D. A. Sear and P. DeVries, Eds) Riverine salmonid spawning habitat: physical controls, biological responses and approaches to remediation. American Fisheries Society, Bethesda, Maryland.

Pasternack, G. B., Gilbert, A. T., Wheaton, J. M., Buckland, E. M. 2006. Error Propagation for Velocity and Shear Stress Prediction Using 2D Models For Environmental Management. Journal of Hydrology 328:227-241.

Snyder, N.P. 2004. Estimating accumulation rates and physical properties behind a dam: Englebright Lake, Yuba River, northern California. Water Resources Research, 40(W11301): 1-19.

APPENDIX 1

Gravel for Salmon in Bedrock Channels: Elucidating Mitigation Efficacy Through Site Characterization, 2D-Modeling, and Comparison Along the Yuba River, CA

By

AARON ANDREW FULTON
B.S. (University of California, Davis) 2005

Thesis

Submitted in partial satisfaction of the requirements for the degree of

Master of Science

in

Hydrologic Sciences

in the

OFFICE OF GRADUATE STUDIES

of the

UNIVERSITY OF CALIFORNIA

DAVIS

Approved:

Gregory B. Pasternack, Professor of Hydrologic Sciences

Jeffrey Mount, Professor of Geology, Director of the Center for Watershed Sciences

---

Hamish J. Moir, Phd., Macaulay Institute, Aberdeen, UK

Committee in Charge

2008

(Page Intentionally Left Blank)

Aaron Andrew Fulton
October 2008
Hydrologic Sciences

Gravel for Salmon in Bedrock Channels: Elucidating Mitigation Efficacy Through Site Characterization, 2D-Modeling, and Comparison Along the Yuba River, CA

ABSTRACT

Aside from blocking upper watershed spawning areas, dams degrade in-stream aquatic habitat conditions by reducing or halting the transport of alluvial sediments that some species like salmon require for spawning. Gravel augmentation (GA), the technique of adding gravels to regulated rivers directly below impoundments, attempts to restore alluvial sediment inputs and has produced high quality interim spawning habitat in many gravel-bed channels since the 1970s. In the future, as Federal Energy Regulatory Commission permits are reissued, GA could be used as mitigation for upstream habitat loss and as a way to bolster declining populations. Although a significant effort has been made to develop channel rehabilitation programs that include GA on low gradient gravel-bed channels, no previous studies have investigated the role and applicability of GA in bedrock channels.

In this study, we evaluated the efficacy of GA in a bedrock channel below Englebright Dam on the Yuba River, CA using historical imagery, surface grain measurements, 2-D hydrodynamic modeling, habitat suitability curves, sediment transport analyses, and inter-site comparisons. Overall we tested nine hypotheses related to sediment characteristics, hydraulics, geomorphology, and spawning habitat to elicit controls on GA in bedrock channels.

The sediment size distribution at the Englebright Darm Reach (EDR) is significantly coarser than the highly utilized Timbuctoo Apex Reach (TBAR) and can be improved through GA. While a velocity reversal and flow convergence routing promote riffle pool maintenance at the alluvial TBAR, no reversal was observed at the EDR. Instead, lateral and vertical constrictions associated with the underlying bedrock morphology at the EDR create convergence along topographical highs and divergence within pools for all discharges. Therefore, flow convergence routing at the EDR will tend to fill existing pools with augmented gravels or lead to particle accumulation along channel margins where depositional features impact local hydraulics. Shields stress predictions at the EDR suggest the entire channel is stable during spawning flows and that full transport of augmented gravels can be expected in the channel center at discharges above 900.5 m^3/s (5-yr event). A consistent pattern of maximum velocity and Shields stress in the channel center will prohibit the formation of cross channel alluvial habitat. Overall, small scale GA in bedrock channels similar to the EDR will lead to small improvements in suitable habitat instead of macro-scale spawning beds and riffles constructed in regulated gravel bed channels. The greatest increase in habitat quality will occur along channel margins where roughness features in the channel promote deposition.

ACKNOWLEDGEMENTS

First, I would like to thank Gregory Pasternack and his previous graduate students Chien Wang, Joe Merz, Joe Wheaton, Eve Elkins, Rocko Brown, and Marisa Escobar. Their efforts and additions to the methodologies employed herein made this project possible. Funding was provided by the U.S. Fisheries and Wildlife Service (Award # 113323J011 and 813325G004) while Diana Cummings and Tania Guilfoil of the UC Davis Center for Watershed Sciences provided administrative support. Extensive site access was granted by Curt Aikens and staff at the Yuba County Water Agency, Doug Grothe of the U.S. Army Corps., Ralph Mullican, and the University of California Browns Valley Research Station. Field and technical support was provided by James Kulpa of Environmental Data Solutions and Scott Morford. I would also like to thank Greg Pasternack, Jeff Mount, Hamish Moir, and Peter Moyle for stimulating my interest in geomorphology and salmonid ecology and providing inspiration for my own research. Finally, I am indebted to my family, Harold and Tish Fulton, Deborah and Kevin Kalkowski, Frank and Barbara Caliva, Shannon Fulton, and Dana Jewell for their unwavering support and patience.

1. INTRODUCTION

Dams throughout California and the Pacific Northwest suppress anadromous salmonid populations by blocking access to historic spawning areas and severing the hydrologic, geomorphic, and ecologic continuity that river ecosystems require (Baxter, 1977; Brandt, 2000; Bunn and Arthington, 2002; Collier et al., 1996; Graf, 1999; Ligon et al., 1995; Poff et al., 1997; Power et al., 1996; Williams and Wolman, 1984). The initial tool for mitigating the effects of dams on fisheries was grounded in an industrial/agricultural vision that embraced fish hatcheries as a technology that could produce water, power, agriculture, and salmon from the worlds' rivers (Lichatowich 1999). Despite a federally supported hatchery program, the decline of Pacific salmon stocks continued and fueled further investigation and development of mitigation measures like fish ladder/transport systems (Cada and Sale, 1993), sub-thermocline water releases (Crisp, 1987), re-regulated flow regimes (Richter, 2007; Ward and Stanford, 1995), and spawning habitat rehabilitation projects (SHR) that use channel design in combination with gravel augmentation (GA) to increase spawning habitat (Bunte, 2004).

GA entails adding spawning sized gravels to degraded channels to improve aquatic habitat. It can be effective at increasing the quantity and quality of physical habitat for multiple salmonid life stages on highly regulated, low gradient, gravel-bed rivers where physical habitat quality is defined as the degree of suitability of local depth, velocity, and river-bed substrate size in a stream to support a particular ecological function (e.g., spawning, rearing) (CDWR, 1992; Elkins et al., 2007; Merz, 2006; Merz et al., 2004; Mesick, 2002). Using GA to shift physical habitat quality from poor to high has been tested experimentally and found to increase fish utilization of previously degraded aquatic channels (Elkins et al., 2007).

However, the effectiveness of GA has not been investigated below dams in bedrock channels, where the character and pattern of ongoing physical processes are substantially different from low gradient gravel-bed rivers. In particular, bedrock channels often have high transport capacity and low sediment supply which promote redd scour or may limit the production of suitable spawning habitat within a reach. If GA is selected as mitigation for habitat loss upstream of dams or used to increase in-stream habitat quality to meet fisheries goals in bedrock channels, the overall effectiveness must be determined before widespread adoption in the public and legal arena transpires.

To bridge the void between GA in alluvial and bedrock channels this study set out to determine the potential benefit of GA by characterizing and comparing the substrate, depth, velocity, and sediment transport regimes of two study sites; (1) a bedrock channel, and (2) an alluvial reach, both on the lower Yuba River (LYR), CA. The study uses established empirical, numerical, and analytical methods to predict the overall efficacy of an established rehabilitation tool in a novel environment.

1.1. Bedrock Channels

Of the ten large anadromous fish bearing tributaries in the Sacramento/San Joaquin Delta system, the Stanislaus, Sacramento, Feather, Yuba, and Calaveras Rivers contain a continuous stretch (>0.5 km) of bedrock channel below an impassable barrier. Bedrock channels have been loosely defined as those with >50% exposed bedrock and include reaches with a hydraulic and morphologic character controlled by resistant underlying geologic formations (Wohl and Tinkler, 1998). In reality, the number of anadromous rivers in California that experience some form of bedrock control at higher discharges is much greater, as bedrock reaches also occur on the Tuolumne and Merced Rivers.

Differences in physical processes between bedrock and gravel-bed channels must be considered prior to GA. Bedrock channels are more efficient at moving sediment because they typically exhibit a reduced valley width, high gradient, and higher average velocity than their lowland alluvial counterparts (Wohl and Tinkler, 1998). In general, transport capacity generally exceeds sediment supply in bedrock channels (i.e. they are supply limited) which suggests that bedrock reaches function as sediment routing units and have limited capacity to retain coarse sediments. This differs significantly from alluvial channels where coarse sediments compose the entire channel bed. The response to discharge in alluvial and bedrock channels is also different. Alluvial channel morphology is controlled by more frequent events with a one to five year return interval that rearrange the water-sediment boundary (Emmett and Wolman, 2001), but bedrock channel morphology is controlled by lower frequency events that create the hydraulics and grain ballistics necessary to lift bedrock slabs, abrade bedrock, and move boulders and wood through the channel (Whipple, 2001)

These disparities suggest that the observed processes and outcomes associated with GA efforts in alluvial channels should be carefully evaluated for the potential effectiveness in bedrock channels. For example, MacWilliams (2006) proposed that flow convergence over riffles in alluvial channels during long periods of low flow causes armoring, gradual incision, and diminishing relief. However, during high magnitude and infrequent floods flow convergence shifts to pools, causing pool scour, deposition near riffles, and enhancement of overall relief. This proposition is based on Keller (1971), who observed higher near bed velocities and shear stress in pools than riffles during high flows. It is unclear whether flow convergence routing in bedrock channels is responsible for observed patterns of thin alluvial deposits there, and thus salmon habitat distribution.

Because an understanding of geomorphic processes in bedrock channels is required for GA, further investigation into the dominant mechanisms of habitat formation is warranted and should be based on previous research. McBain (2004) proposed that "nested depositional features", including large immobile boulders, channel spanning bedrock formations, and large wood, control gravel deposition in bedrock channels at multiple scales. In another study Wohl (1998) coined the term "gravel beaches" which referred to the depositional environments behind large boulders and topographic highs. Overall, these studies provide a conceptual basis for predicting bedrock channel response to GA and its potential use as a sustainable river rehabilitation tool.

1.2. Gravel Augmentation

GA introduces coarse gravels within or along a channel with the intention that future flows will entrain, transport, and deposit sediments downstream: ideally to yield some form of usable habitat for spawning salmonids. It first surfaced in late 1960s as a tool for the rehabilitation of salmonid spawning habitat and replenishment of coarse sediment deficiencies below large dams that cut off sediment inputs (Kondolf, 2004). In fact, since 1968 over 380,000 m^3 of gravel have been added to California rivers in projects of varying success (Minear and Kondolf, 2006). Overall, this method of habitat rehabilitation is more conducive for rivers with high bed slopes and periodic overbank flows capable of reworking coarse sediment annually or biennially. Therefore, an understanding of hydraulics and sediment transport is required in GA projects because the hydrogeomorphic regime determines the fate of introduced gravels.

GA attempts to re-instate geomorphic continuity and mitigate for some of the physical channel modifications linked to dams. This includes incision, substrate coarsening, bank stabilization, habitat homogenization, channel narrowing, and a lack of spawning gravels for anadromous species (Brandt, 2000; Friedman et al., 1998; Kondolf, 1997; Williams and Wolman, 1984). The damming of rivers also endangers salmonids through flow and temperature regime alterations, dissolved oxygen reductions, loss of in-stream wood habitat, vegetation encroachment, and abrupt changes in macro invertebrate assemblages (NMFS, 2006). As a habitat rehabilitation tool GA aims to alleviate sediment deficiencies, reduce incision, promote floodplain connectivity, increase hyporheic flow and dissolved oxygen content, increase interstitial habitat for benthic macro invertebrate populations, and provide substrate for redd construction (Merz, 2005). For instance, after studying the gravel bed Clackamas River in Oregon, Grant (2006) showed that bars formed by augmented gravels promoted lateral hyporheic flow and reduced diurnal temperature extremes experienced by salmonids.

GA involving annual injections in perpetuity is a decadal to centennial scale rehabilitation tool because the passive creation of habitat and associated geomorphic features (riffles, pools, bars, lateral shear zones) may take a long time to occur. GA relies on flows to redistribute sediments and create such features and therefore, increases in habitat quantity and quality are unlikely to result if flows do not redistribute gravels, if the amount of introduced gravel is less than channel deficits, or if annual transport exceeds augmentation rates. GA is unique in that a design based on a specific flow or channel prototype (Rosgen, 1985) is not used. Instead, GA reinstates sediment supply and relies on the remaining dynamism of a regulated system to mimic process rather than form (Stanford et al., 1996; Wohl et al., 2005). It is uncertain whether sufficient dynamism remains in a degraded river to achieve the desired goals or whether GA could be yet another harmful ecological disturbance.

1.3. Spawning Habitat Rehabilitation

Spawning habitat rehabilitation (SHR) is a sub-type of GA that includes direct manipulation of channel morphology via design and modeling programs to create specific areas of high quality spawning habitat and/or jumpstart geomorphic processes that cleanse gravels (Wheaton et al., 2004a; Wheaton et al., 2004b). Therefore, the persistence and success of SHR projects is highly dependent on design considerations and geomorphic thresholds that when exceeded may change a rehabilitation site or scour redds during embryo development (Kondolf, 1998; Merz, 2006). SHR, which includes riffle construction, hydraulic structure placement, and slope creation, is the primary management tool for quickly mitigating geomorphic and hydrologic discontinuities in regulated rivers and increasing the quality and quantity of spawning habitat in the near term (Elkins et al., 2007; Kondolf, 2004; Wheaton, 2004). Projects have been completed on rivers throughout California and the Pacific Northwest, including the Sacramento, Mokelumne, Stanislaus, Tuolumne, Merced, and Trinity Rivers in California, and the Clackamas River in Oregon (Grant et al., 2006). SHR has been implemented internationally with projects in Newfoundland (Scruton, 1996), the United Kingdom (Harper et al., 1998), and Germany (Zeh and Donni, 1994).

1.4. Habitat Rehabilitation Constraints

GA and SHR projects face the same constraints that fish hatcheries contended with in the 1900s. A lack of funding for pre and post-project evaluations that test project objectives clouds the overall understanding and applicability of these projects (Kondolf, 1998; Kondolf, 2001). The most scientifically valuable studies are those with clear objectives and testable hypotheses. For example, Merz (2005) analyzed measurable habitat characteristics such as dissolved oxygen, inter-gravel flow, invertebrate populations, and substrate conditions before and after a rehabilitation project on the Mokelumne River, CA. Two testable hypotheses in GA projects include (1) was suitable habitat created over the time scale of interest? and (2) was habitat sufficiently used by salmon to warrant expenditures? Tests of the two hypotheses would include measuring the areal extent of habitat following transport events and annual redd surveys downstream of gravel injection sites to monitor habitat utilization. Pre-project data synthesis and post-project analysis would provide an appropriate arena for evaluating GA studies that try to elucidate patterns of gravel transport, morphologic change, habitat formation, possible redd scour, and overall effects on the freshwater life stages of anadromous fish. However, given cost constraints and shifting priorities of many rehabilitation programs, the post-project monitoring necessary for testing hypotheses is often not prioritized

Based on a national survey of 37,099 projects, Bernhardt et al. (2005) estimated that over $1 billion/yr is spent on restoration projects of varying objectives. Kondolf (1998) suggested that objectives based on an ecologic and geomorphic understanding at the reach and basin scale are essential for project success. This parallels the view of Ebersole (1997) who proposed that habitat expression is a complex function of stratified systems spanning four and seven orders of magnitude in spatial and temporal processes, respectively. An attempt to understand the processes controlling habitat formation and rehabilitation should consider these scales and begin with a historic and contemporary biogeomorphic analysis of the targeted watershed (Kondolf, 1995). This includes evaluating basin hydrologic events with available streamgage data, estimating sediment transport, and accounting for anthropogenic forcing due to mining, road building, agriculture, etc. Important reach-scale processes and characteristics include the quantity, quality, and spatial distribution of sediment, channel form, mass wasting, valley confinement and expansion, channel response (depth, width, velocity, bed shear stress) to increasing discharge, and anthropogenic boundary controls (Brown and Pasternack, 2008). When combined, these processes and characteristics determine the physical habitat encountered by a target species such as Chinook salmon (*Oncorhynchus thyswatcha*) and Steelhead trout (*Oncorhynchus mykiss*).

The underlying goal of anadromous habitat rehabilitation projects, whether SHR or GA, is to increase escapement. Therefore, a full understanding of life history characteristics and habitat requirements of the target species is critical. An evaluation of species population history, type, run timing, lotic habitat requirements, and possible physical limitations to biologic productivity is essential. For example, if pre-project studies suggest available spawning habitat is not limiting at a site, then habitat restoration targeting juvenile rearing habitat may be more appropriate than GA or hydraulic structure placement. If pre-project analysis and modeling show unsuitable combinations of substrate size, flow velocity, and depth, GA directed at spawning habitat improvement may be beneficial. In other words, habitat rehabilitation will be most successful when watershed managers approach projects with both ecologic and geomorphic information in hand.

To generate this information and overcome rehabilitation constraints for the case of bedrock channels, this study combines a traditional geomorphic approach with 2-D numerical simulations of channel hydraulics that have been used to test channel designs, conceptualize ongoing physical processes, and select appropriate sites for GA in numerous SHR projects (Bunte, 2004; Wheaton et al., 2004a; Wheaton et al., 2004b). For example, when combined with high quality digital elevation models (DEMs), sediment transport, habitat suitability, and overall site hydraulics can be approximated with widely available hydraulic models (e.g. MIKE-21, RMA2, UnTRIM, FESWMS, SHR-2D, and TELEMAC) to determine where GA might be effective (Rathburn and Wohl, 2003).

2. OBJECTIVES

The overall goal of this study was to elucidate the efficacy of GA as a habitat mitigation tool in the bedrock Englebright Dam Reach (EDR) of the LYR, CA by characterizing and comparing it against a highly utilized spawning reach in the alluvial portion of the same river. The specific objectives were to: 1) quantify bed material and local hydraulic patterns with traditional sediment characterization protocols and a 2-D hydrodynamic model, 2) assess the historic and current hydrogeomorphic regimes by analyzing hydrologic patterns, historical imagery, approximating sediment transport patterns, and modeling contemporary instream Shields stress, and 3) map the current spatial pattern of spawning habitat with habitat suitability curves for each site. Comparisons of qualitative and numerical data at each site were used to test specific hypotheses related to GA efficacy in bedrock channels **(Table 1)**. The significance of this study is that it provides a process-based approach for determining the applicability of an increasingly popular regulated river rehabilitation tool in bedrock channels. A secondary yet important benefit of this approach is the substantive baseline information required for adaptive management and determination of gravel augmentation project success.

3. STUDY SITE

3.1. Watershed Attributes

The Yuba River watershed, located northeast of Sacramento on the western flank of the Sierra Nevada, encompasses 3480 km^2 of topographically diverse vegetated landscapes **(Fig. 1)**. In the upper watershed bedrock lined canyons drain glacially cut granitic plutons formed as the Pacific plate subducted the North American plate approximately 80 million years ago. The geology of the lower watershed is more heterogeneous, including overlapping belts of shale, sandstone, metavolcanics, and highly metamorphosed combinations thereof (Hill 2006). The watershed experienced three late Pleistocene glacial episodes, each depositing significant amounts of cobble and gravel along the Sierra Nevada front where reduced slopes promoted deposition (James, 2002). These transitional and highly active meandering river environments were exploited by numerous species of Pacific salmon as they evolved in a rapidly changing geologic environment (Montgomery, 2000).

The current Mediterranean climate, with precipitation exceeding 1500 mm in higher elevations and 500 mm in the lower watershed, controls basin hydrology. Winters are cool and wet with an occasional tropical influence, while summers are dry and hot. Ambient air temperatures frequently exceed 35ºC (95 ºF) during the summer months and fall below freezing (0 ºC) in many parts of the upper watershed during the winter. A combination of a cooling gradient towards higher elevations and an orographic effect causes most precipitation to fall in the upper watershed as snow between the months of December and April. This spatial diversity of geology, precipitation, and temperature regimes has sustained mixed coniferous forests (*Pinus, Calocedrus, Abies*) at high elevations (>1000 m) , and oak (*Quercus spp.*) woodlands, chaparral (*Ceanothus spp., Chamise spp.*), Manzanita (*Arctostaphylos spp.*), willow (*Salix spp.)*, alder (*Alnus spp.*), and cottonwood (*Populus spp.*) populations along the Sierra front where the study site is located.

With an average annual unimpaired run-off of 3.02 km^3 (2.25 maf), the Yuba basin is a snowmelt system that historically peaked between the months of April and July. Together the north (1270 km^2), middle (543 km^2), and south (1010 km^2) fork drainages have experienced significant human alterations, including projects by local irrigation districts, Pacific Gas and Electric, and the Yuba River Development Project administered by the Yuba County Water Agency. The cumulative effects of five dams, water diversions, logging, mining, and other land use changes have drastically altered the physical, chemical, and thermal habitat characteristics of the basin's lotic systems.

However, water temperatures in the main stem of the Yuba are cool enough, due to sub-thermocline reservoir releases, to sustain one of the last remaining hatchery-free runs of Chinook salmon (spring and fall runs) and Steelhead trout in California. This unique natural assemblage of anadromous salmonids, a vestige of a once prolific annual ecologic cycle that connected ocean productivity to inland food webs, supplemented First Peoples' diets and later supported an influx of miners after the discovery of gold in 1848 (Yoshiyama et al., 1998).

Gold mining in the Yuba watershed completely altered geomorphic processes with additions of hydraulic mining debris, channel obstructions, and increased fine sediment loads (Mount 1995; James 1999; James 2005; Snyder 2006). Early miners relied heavily on panning and sluice box sorting to locate gold within and adjacent to stream channels. However, as these surficial placer deposits waned a new method called hydraulic mining was employed to target tertiary gravels in ancient riverbeds. Hydraulic mining leveled hillsides and deposited far more sediment into Yuba River tributaries than stream networks could transport. The single largest delivery of sediment to the Sacramento River watershed, (~522 million m^3), originated in the South Fork of the Yuba River where hydraulic mining was particularly extensive (Gilbert 1917 quoted in (James, 2005)). The resulting channel aggradation, of up to 40 m, impacted river morphology and continues to control lotic community composition more than a century after hydraulic mining was discontinued.

In 1884 the Sawyer Decision temporarily terminated large scale hydraulic mining in the Yuba Basin and across California. The law aimed to reduce flood damage to crops and personal property caused by hydraulic mine debris that reduced levee system capacity in the farming communities of Yuba City and Marysville to the west. However, 9 years later, the Caminetti Act re-authorized this devastating technique through a permit and inspection program loosely administered by federal government. James (2005) investigated the historical influx of hydraulic mining debris in the Yuba Watershed before and after the Sawyer Decision. This work suggests the effects of historic hydraulic mine operations have been largely misunderstood and concealed by erroneous and inadequate record keeping. In reality, large-scale damage to Yuba River fisheries continued into the 1950s, well after public outcry inadvertently provided environmental protection. Unfortunately fisheries endured further stress with the construction of sediment barriers and reservoirs for California's growing water demand.

3.2. Dams and Discontinuities

Englebright Dam, with a capacity of 86 million m^3, was completed in 1941 to halt hydraulic mining sediments, reduce levee infilling, and mitigate flood levels for farmers in the rapidly growing agricultural communities to the west. At 81 m high, the concrete arch structure with an ogee crested spillway has caused both ecologic and physical system discontinuities. The dam currently blocks anadromous fish access to historic upper-watershed spawning areas and limits habitat to the LYR, a 39 km stretch between Englebright and the Feather River confluence.

Englebright Dam physically separates the Yuba River basin into two geomorphically independent units. The transport of coarse sediment from the upper watershed is completely blocked from the LYR. Suspended silt and clay as well as wood can float over Englebright Dam, but these mostly flush out to the Feather River. A bathymetric survey of Englebright reservoir by Snyder (2004) estimated that 24,000,000 metric tons of total sediment, including 4,728,700 metric tons of coarse cobble and gravel, has accumulated between 1941 and 2004 and reduced reservoir capacity by almost 25%. These coarse sediments, a combination of natural load and hydraulic mining debris, are presently locked within the reservoir creating a major geomorphic discontinuity. Although significant in-channel, bar, and remnant dredge tailing gravel sources exist within 3 km of Englebright Dam, near complete cessation of gravel recruitment to the EDR has occurred; gravel that is key for salmon survival.

Englebright Dam is situated below the largely unregulated south and middle forks of the Yuba, provides minimal flood protection, and is designed to overtop in most years. Given the small capacity of the lake, Englebright Dam was unable to attenuate major floods in 1950, 1986, and 1997 for the communities of Marysville and Yuba City. Englebright reservoir is home to a small year round house boat and small summer recreational boating community and produces $10 million in hydropower each year (Pejchar 2001). These varying anthropocentric benefits are far reaching, but have impacted anadromous salmonid populations throughout the watershed by cutting off key upper-watershed habitat of the threatened spring run Chinook salmon.

Damming of the middle and south forks of the Yuba River above Englebright reservoir has created numerous small reservoirs at the highest elevations in these sub-basins. The reservoirs have small contributing areas and influence summer flows and water temperatures during dry years. Spaulding reservoir (92.6 million m^3) is larger than Englebright and was completed in 1913 at an elevation of 1528 m by Pacific Gas & Electric for hydropower production on the Yuba's south fork. In 1927 Canyon Creek, a small tributary of the South Fork of the Yuba, was dammed by Nevada Irrigation District (NID) for drinking and irrigation purposes, forming Bowman reservoir at an elevation of 1642 m with a capacity of 84.5 million m^3. Jackson Meadows, the fourth largest dam upstream of Englebright at 77 million m^3, was completed in 1965 by NID at an elevation of 1840 m. Many other minor dams dot the Yuba watershed but their small size has a minor influence on hydrology relative to New Bullard's Bar Dam.

New Bullards Bar Dam was completed in 1969 and is situated 28 km upstream of Englebright on the North Fork Yuba. With a capacity of 1.2 billion m^3, its completion marked a shift in hydrograph properties of the basin **(Fig. 2)**. Long term USGS records for Smartville gages (#11418000 and #11419000) located approximately 500 m downstream of Englebright Dam allow an analysis of hydrologic alterations attributed to New Bullards bar using the non-parametric form of Indicators of Hydrologic Alteration (IHA) (Richter et al., 1996; Richter, 1997). Numerous deviations in biologically relevant hydrograph parameters include increased base flows, spawning flows, fall rates, and the number of discharge reversals **(Fig. 3)**. Flows in July, August, September, October, and November, corresponding to when adult salmon typically inhabit the Yuba, are between 1.5 and 2 times larger after New Bullards Bar was constructed. Increased fall rates, where discharge drops rapidly, and discharge reversals can cause juvenile stranding, redd drying, and sufficiently alter hydraulic conditions for both juveniles and adults such that survival can be compromised.

The hydrologic alterations suggested by IHA are consistent with flood frequency analysis comparing pre and post Bullards Bar flood regimes. Discharge records at the Smartville gage show that, typical of many regulated rivers, flood-peak dampening is greatest for small events **(Fig. 4)**. Bullards Bar caused a 71% decrease in statistical bankfull discharge ($Q_{1.5}$) at Smartville from 590 m^3/s to 170 m^3/s. However, flows exceeding 590 m^3/s have occurred in 13 of 34 years since construction; suggesting a moderate dynamism (flood regime) still exists in the system. As demonstrated by morphological changes evident in the sequence of available historical photos and repetitive topographic surveying to be presented later, geomorphically significant flows capable of transporting and reworking remnant hydraulic mine deposits that once filled the river valley still occur.

3.3. Lower Yuba River

The first 3 km of the LYR is a bedrock dominated reach, while the lower 36 km is composed of a gravel-cobble bed channel. Historic additions of hydraulic mine debris significantly aggraded the entire LYR and since the construction of Engebright, an overall pattern of incision prevails throughout the LYR. Two small regulated tributaries, Deer and Dry creeks, join the Yuba 1.5 km and 16 km downstream of Englebright, respectively, and support small steelhead and Chinook salmon populations in their lower reaches. The hydrograph response to rainfall events is rapid in Deer and Dry Creeks, with flow event peaks occurring well before peaks in the mainstem Yuba.

The LYR has been delineated into 6 reaches based on dominant channel morphology and importance to spawning salmonids- Englebright Dam, the Narrows, Timbuctoo Bend, Highway 20, Daguerre Dam, and Simpson lane reaches **(Fig. 1)**. The EDR includes the 1.5 km of river between the Narrows II powerhouse (39º14’23.95”N, 121º16’08.48”W) and Deer Creek (39º13’47.75”N, 121º16’45.24”W) where bedrock constrained and supply limited channel morphology prevails **(Fig. 1F)**. This section contains the GA site detailed in this study. The Narrows extends for 1.5 km below Deer Creek and is characterized by steep adjacent valley walls, significant bedrock control, rapids, large boulders, and deep pools **(Fig. 1E)**. After exiting the Narrows, the river flows 6 km in the Timbuctoo Bend Reach (TBR), an active gravel bed zone with an abundant supply of coarse substrate from adjacent dredge tailing and hydraulic mine deposits **(Fig. 1D)**. Alternating bar, island, side channel, and pool complexes dominate the river from the Narrows exit, through the TBR to the Hwy 20 Bridge. The Hwy 20 reach begins at the bridge and extends 10 km to the Daguerre Point diversion dam **(Fig. 1C)**. Throughout the Hwy 20 reach, valley width is generally wider than portions of the river upstream of Hwy 20, thus the river is less confined by adjacent hillsides. Similar to TBR, the Hwy 20 reach contains numerous side channels and island complexes that transition into a divided morphology upstream of Daguerre Dam. Within the Hwy 20 reach the Yuba River is still adjusting to the elevation control imposed by Daguerre with numerous riffle knickpoints evident. However the exact boundary between the adjusted and unadjusted reach has not been delineated. The Daguerre Dam reach **(Fig. 1B)** contains numerous elongated lateral bars and limited side channels before transitioning into a deep, fine grained, levee constricted channel known as the Simpson Lane reach **(Fig. 1A)**, 11 km below Daguerre Dam. Willow species are the dominant vegetation type along channel edges throughout the TBR and Daguerre Dam reaches and provide essential habitat for beavers, salmonids, amphibians and a host of other aquatic and terrestrial species.

Typical spawning habitat along the main-stem Yuba is situated around pool exits/riffle entrances, side channels, and along margins near flow separation features (Moir and Pasternack, 2008). Site visits throughout the TBR section have demonstrated the ability of Chinook salmon to use very small areas (<1 m^2), however the majority of observed redds are clustered near pool exits and riffle entrances. Spawning habitat is most limited between Englebright Dam and the Deer Creek confluence where bed coarsening from dam construction and scour associated with significant floods (>2830 m^3/s) in 1963, 1965, 1986, 1997, and 2005 has likely occurred. The highest quantity of habitat is found within TBR and Hwy 20 reaches while the Daguerre Dam reach has slightly less area due to fewer riffles and side channels.

Two persistent anthropogenic structures inhibit adult and juvenile salmon populations on the LYR. The first is the Yuba Goldfields, a complex mosaic of active and historic gold/gravel dredge tailings and pools that pose a significant challenge to system management (Brown et al., 1998). This prevalent feature extends adjacent to the river from Browns Valley to 5.5 km beyond Daguerre Dam **(Fig. 1)**. Hyporheic flow between tailing pools and the river network complicate discharge analysis and alter water temperatures within the river. In the past, large floods have reconnected the channel to the Yuba Goldfields, allowing anadromous juveniles to stray into deep tailings pools where invasive warm-water species including black bass (*Micropterus salmoides)*, channel catfish (*Ictalurus punctatus)*, black crappie (*Pomoxis nigromaculatus*) and other centrarchid species are prevalent. When adult salmon and steelhead return from the ocean they negotiate the 2nd important structure. The 8.5 m high Daguerre Point Dam is a sediment detention and water diversion structure that has two inadequately designed fish ladders that fail to attract migrating adults. Furthermore, during out-migration juveniles can become disoriented as they plunge over the structure into a large pool where invasive warm water piscivores are abundant. Recent progress has been made to construct barriers to cease juvenile straying into the goldfields and a passage system at Daguerre has been under consideration since 1988 (Talbert, 1999).

3.4. Yuba River Salmonids

Steelhead trout and Chinook salmon utilize the Yuba River for spawning, rearing, and migration. The life history characteristics of Pacific salmonids are extremely variable, dynamic, and dependent on geographic location (Groot and Margolis, 1991; Yoshiyama et al., 1998). Four distinct races of Chinook occupy the Sacramento river system although only two, a spring run and a fall run, utilize the Yuba River today (Banks et al., 2000). Annual escapement on the Yuba is dominated by the fall run and has averaged ~ 14,000 Chinook/yr with observable inter-decadal fluctuations between 1953 and 2006 **(Fig. 5)**. The fall run enters freshwater between mid September and November and spawns within weeks of arriving at spawning grounds. The spring run, a federally threatened species, enters freshwater between April and June and over-summers in cool pools before spawning in August and September. Before dams were constructed and migration routes severed, this life history strategy enabled the spring run to penetrate deep into the watershed when high flows from snowmelt made it possible to pass natural hydraulic structures that impeded the fall run.

A dramatic decline in spring run populations throughout California has been attributed to dams which block up to 80% of historic spawning sites. On the Yuba, although Englebright and New Bullards Bar restrict access to 73 % of upper watershed spawning areas, a remnant population of less than 1000 spring salmon persists and must spawn within the lower limits of its historic extent. The resulting loss of geographic isolation has likely caused genetic mixing and most certainly increased the relative competition between the two stocks as observed on the Sacramento river by Slater (1963).

From a fisheries management perspective, the population and life history characteristics of spring run salmon on the Yuba are not well documented and pose a major challenge to management decisions in the basin. On-going screw-trap studies by the California Department of Fish and Game and United States Fish and Wildlife Service near Daguerre Dam are expected to produce key information about age, size, and timing of juveniles during outmigration. For the purposes of habitat rehabilitation and GA, the instream requirements (temperature, dissolved oxygen, depth, velocity, substrate conditions, large wood structure) of spring run are assumed to parallel that of the fall run however differences in feeding habits, habitat preferences, and movements likely exist. Despite these uncertainties, habitat rehabilitation based on an understanding of fall run habitat is a suitable approach, especially given its numerical robustness.

3.5. Study Reaches

3.5.1 Englebright Dam Reach

The EDR begins at the Narrows II powerhouse pool at the uppermost section of the LYR **(Fig. 1)**. The EDR extends for 135 m in a narrow supply limited bedrock canyon of relatively low slope (avg. 0.18%, 0.0018 m/m). The upper pool is a release bay for water used in hydroelectric power generation and provides important spring and fall run adult salmon holding habitat during the late summer months **(Fig. 6A)**. The channel is constrained by steep sparsely vegetated canyon walls and bordered by a narrow, elevated, unnatural floodplain on the western edge. Substrate in the floodplain and within the channel is composed of bedrock and large irregular boulders (> 256 mm intermediate axis diameter) blasted from surrounding hill-slopes during the construction of the dam. Limited pockets of angular gravel and cobble sized particles exist within boulder crevices and boulder shadows and deter riparian shrub colonization. Overall, channel morphology is bedrock controlled, valley confined, and exhibits significant substrate alteration from human construction activities.

3.5.1. Timbuctoo Bend Apex Riffle: Functional Spawning Segment

The highly functional salmon-spawning reach in this study is located ~5 km downstream of Englebright Dam along the active gravel/cobble TBR reach of the LYR **(Fig. 6B)**. Available historic aerial photographs and recent topographic surveys after significant floods of the site, called the Timbuctoo Bend Apex Riffle (TBAR), depict a dynamic morphology dominated by a persistent pool/island/riffle complex. Willow species line the bank, corresponding to the water surface elevation at ~1600 m^3/s. A large dredge tailing pile abuts the active floodplain on the uppermost southern side of the river. The well connected floodplain extends to the valley walls and contains numerous secondary channels active during large flow events. The site is dominated by cobble (64-256 mm) and gravel (2-64 mm) sized sediments. Additionally, there are a few large boulders associated with two exposed bedrock features opposite one another in the middle of the site. No SHR projects have occurred at the site and natural Chinook spawning activity is extensive.

3.6. Gravel Augmentation and the Yuba River

Despite recent interest in dam removal across the Pacific Northwest and California, the hydrologic and geomorphic dominance exerted by hydropower facilities similar to Englebright are likely permanent controls on salmonid populations. If salmon populations are to persist, resource managers must continuously mitigate for habitat loss and degradation in channels directly below dams (CDWR, 2006). The process of organizing mitigation plans will occur over the next 20 years as the Federal Energy Regulatory Commission reviews operation contracts and stipulates the mitigation measures to be invoked. For example, Englebright Dam enters review in 2013 and some form of gravel augmentation will likely be required.. During the relicensing process mitigation for spawning habitat loss in sediment starved bedrock controlled channels will be a topic of debate with no proven mitigation strategy or system for evaluating overall efficacy.

GA has been proposed as a mitigation measure below Englebright Dam on the Yuba River, CA where Chinook salmon habitats have declined due to a combination of dam construction, hydraulic mining, logging, road building, urbanization, and hydropower development. In the fall of 2007, the United States Army Corps of Engineers (USACE) performed a small (629 metric tons) pilot gravel injection intended to provide data to guide a future mitigation plan aiming to increase spring-run Chinook spawning habitat in the 1.5 km length of river between the Narrows powerhouse II and Deer Creek confluence.

4. METHODS

To provide a baseline habitat, hydraulic, and geomorphic characterization for testing the hypotheses in **Table 1**, field data was acquired between August 2005 and 2007 at the EDR and TBAR. Substrate, topographic, hydraulic, biological, and visual data was collected for 2D hydraulic modeling, validation, and subsequent biogeomorphic analyses. Historical photographs, stream-gage measurements, field reconnaissance, government documents, and previous geomorphic studies of the basin provided further background data to guide a historical and contemporary hydrologic and geomorphic assessment of each site. Previous salmon habitat restoration projects have focused on gravel-bed channels and the wealth of information available on hydrogeomorphic and ecologic processes in that stream type. The data collected in this study supported a comparative analysis aimed at determining if the same processes exist in bed-rock channels.

Overall, six discharges of comparable magnitude were evaluated at both sites using a standard 2D (depth averaged) hydraulic model that estimated the spatial distribution of depth and velocity at the ~1-m scale. The flows modeled at the EDR were the 22.7, 33.7, 271.3, 710.7, 900.5, and 2588.2 m^3/s. TBAR model simulations were completed for the 21.2, 34.6, 267.8, 655.3, 998.4, and 3089.2 m^3/s events. Required model inputs for the six comparable discharges at the EDR and TBAR are provided in **Table 2**. Two extra model runs, in addition to the 21.2 m^3/s event, were completed for evaluating model performance at 18.4 and 31.2 m^3/s at the TBAR. Overall, a total of fourteen flow scenarios were modeled between the two sites. Model predictions were used to estimate spawning habitat quality and Shields stress distributions at each discharge, and thus represent spawning and sediment transport regimes. Although 2-D models have not been tested much in bedrock channels, the bed slope in this case was suitably low (0.18%) and allowed the model to illuminate river processes relevant to proposed mitigation strategies.

4.1. Topography

Topographic data of the channel and floodplain constrains DEM formulation and subsequent 2-D hydraulic modeling. The number of bed elevation points required within deeper parts of the channel to accurately represent the sites challenged traditional surveying methods that are limited by the depth and velocity that a surveyor can wade. Therefore, a combination of boat-based bathymetric and robotic total station surveys was employed to provide the site characterization required by the models used in this study. Bathymetric surveys were conducted on August 27, and June 10, 2005 for the EDR and TBAR, respectively. Robotic total station surveys were conducted before and after the bathymetric surveys to fully characterize areas the boat could not access. Water surface elevation data, composed of projected coordinates and elevation values, was recorded for a range of flows during the 2006 water year (i.e. October 2005-September 2006) as boundary conditions for the hydraulic model used.

4.1.1. Bathymetric and Total Station Surveys

A bathymetric survey was conducted by a professional hydrographer (Environmental Data Solutions, San Rafael, CA) on a customized 4.2-m long Zodiac raft in accordance with U.S. Army Corps of Engineers' rigorous Class 1 standards. Geographic positioning (± 1 cm) was attained with a Trimble 5800 Real-Time Kinematic (RTK) base station and 5700 series rover mounted to the customized vessel. Depth was measured using an Odom Hydrotrac Fathometer (3°, 200-kHz transducer, ± 2 cm vertical accuracy), a TSS 335B motion sensor that adjusted for roll/pitch of the vessel, and Max 4.3 Hydrographic Survey Software (Hypack, Inc., Middletown, CT) that accounted for water surface elevation changes across the site (Kulpa, 2006). Although discharge was essentially constant during bathymetric surveying (~34.3 m^3/s for the EDR and varied somewhere near ~158.6 m^3/s at the TBAR), the water surface profile was monitored through time using Insitu LevelTroll 500 pressure transducers (In-situ, Inc., Fort Collins, CO) positioned and surveyed for elevation along channel margins. In post-processing, a radial filter was applied to the bathymetric data to obtain a 0.61-m spacing between points. Quality assurance and quality control information beyond the scope of this summary can be retrieved from the contractor.

A permanent control network consisting of brass pins and masonry nails was established at each site with the Trimble RTK GPS. The control network enabled repeated channel margin, riffle crest, floodplain, and water surface elevation surveys using a Leica TPS 1200 robotic total station to supplement the bathymetric data. All total station surveying efforts were conducted using a grid approach with higher-density sampling where topographic complexity (slope breaks, drop-offs, and large boulders) necessitated more detail. Filtered bathymetric bed elevations were combined with total station data. Where the two datasets overlapped, geospatial (in a x,y,z coordinate system) comparisons showed consistency in the disparate measurement techniques and validated the combination of the two approaches. A total of 15,705 and 47,765 points were mapped within the 2,588 m^3/s and 3,089 m^3/s channel margins (i.e. the lateral extent of inundation at each measured discharge) for the EDR and TBAR, respectively. Overall surveying density was 0.49 pts/m^2 at the TBAR and averaged 0.29 pts/m^2 in the floodplain and 1.07 pts/m^2 in the channel. Point density at the EDR was 0.94 pts/m^2 in the floodplain, 1.64 pts/m^2 in the channel, and 1.13 pts/m^2 overall.

4.1.2. Digital Elevation Model (Triangular Irregular Network)

DEMs represent topographic variation and, in this application, provide a surface for routing channel flow within a 2-D hydraulic model. In this study the DEM was created from the high resolution bathymetric and total station data acquired in the field. Total station and bathymetric survey data points were imported into ArcGIS 9.2 with 3D-Analyst for surface creation. Although a modified grid surveying technique was applied, a triangular irregular network (TIN) scheme was needed for interpolation to exploit the varied sampling density (Heil and Brych, 1978; Lee, 1991). Preliminary TIN surfaces were visually checked for topographic errors, compared to field reconnaissance notes, and modified with removal or addition of survey points to better characterize observed topography for both sites. Augmented and original data points were exported for mesh generation within the Surface-water Modeling System (SMS) graphical user interface.

4.2. Substrate Characterization and Analysis

Substrate conditions at each site were qualitatively and quantitatively characterized using photographs, maps, visual assessments, and pebble counts following the methods of Wolman (1954) and Kondolf (1992). Pebble counts consisted of approximately 100 randomly sampled bed particles from 9 m^2 (3 m x 3 m) sections in the active channel and surrounding floodplain at each site. Pebble count samples within the channel were limited to accessible areas and did not include the high velocity thalwegs at the TBAR and EDR. The intermediate axis size classes of sediment particles were determined using a sediment template and tallied to characterize size distributions for each sample. At the TBAR 87 pebble counts (avg. 120 pebbles per count) were completed in varying hydraulic conditions, while 5 counts (average of 123 particles) were conducted at the EDR in the summer of 2006. The small number of pebble counts at the EDR does not limit substrate characterization due to the homogenous nature of limited sediment deposits, which was validated by high-resolution aerial photographs and field notes. Despite initial qualitative differences observed between EDR and TBAR, the non-parametric Wilcoxon-Mann-Whitney Rank Sum test was used in Kaleidograph 4.0 (Synergy Software, Reading, PA) to determine if the D_{16}, D_{50}, D_{84}, and D_{90} size classes were statistically different. This method tests the hypothesis that two samples come from the same population. When reported alpha values are less than 0.05 this test suggests a statistically significant difference between two datasets.

4.3. Hydrodynamic Modeling

Hydraulic models like the Finite Element Surface Water Modeling System 3.1 (FESWMS) are frequently used to predict the spatial distribution of physical variables including velocity, depth, and shear forces along bridge structures, estuaries, coastlines, and habitat rehabilitation sites (Froehlich, 2002; Moir and Pasternack, 2008; Wang et al., 2004). FESWMS is a two-dimensional (depth averaged) hydrodynamic model best used as a conceptual guide to depict river hydraulics. It assumes a horizontal water surface and negligible vertical velocity and acceleration components. The model was applied using the commercial graphical user interface Surface-Water Modeling System 9.2 (SMS) (Environmental Modeling Systems, Inc., South Jordan, UT), which greatly expedited the lengthy process of data pre-processing, modeling, visualization, and interpretation. Depth and velocity values at computational mesh nodes can be analyzed to predict potential spawning habitat and sediment entrainment, and therefore promote a conceptual understanding of ongoing hydrogeomorphic processes (Brown and Pasternack, 2008; Elkins et al., 2007; Ipson, 2006; MacWilliams et al., 2006; Moir and Pasternack, 2008; Pasternack et al., 2006).

4.3.1. Model Calculations

The FESWMS model was developed by the U.S Department of Transportation's Federal Highway Administration to solve steady and unsteady 2-D flow problems using the finite element method (FEM). The FEM is a numerical procedure for solving partial differential equations like those governing the equations of motion and mass continuity in river networks. This method breaks a modeled area into a mesh of triangular and quadrilateral elements, and then solves the set of applicable equations for nodes spaced along each element within the mesh. FESWMS solves the vertically integrated equations of motion in the x and y directions (equations 1 and 2 respectively) and mass continuity (3) for each node using the method of weighted residuals. Residuals are forced to vanish by numerically substituting values of dependent variables (depth and velocity) into the governing equations yielding a numerical approximation of depth and velocity that is interpolated over the entire modeled mesh. For more information on how FESWMS obtains nodal solutions and interpolates depth and velocity values across the finite mesh see Froehlich (2002).

$$\frac{\partial}{\partial t}(HU)+\frac{\partial}{\partial x}(\beta_{uu}HUU)+\frac{\partial}{\partial y}(\beta_{uv}HUV)+gH\frac{\partial z_b}{\partial x}+\frac{1}{2}g\frac{\partial H^2}{\partial x}$$
$$+\frac{1}{\rho}[\tau_x^b-\frac{\partial}{\partial x}(H\tau_{xx})-\frac{\partial}{\partial y}(H\tau_{xy})]=0 \quad \textbf{(1)}$$

$$\frac{\partial}{\partial t}(HV)+\frac{\partial}{\partial x}(\beta_{vu}HVU)+\frac{\partial}{\partial y}(\beta_{vv}HVV)+gH\frac{\partial z_b}{\partial y}+\frac{1}{2}g\frac{\partial H^2}{\partial y}$$
$$+\frac{1}{\rho}[\tau_y^b-\frac{\partial}{\partial x}(H\tau_{yx})-\frac{\partial}{\partial y}(H\tau_{yy})]=0 \quad \textbf{(2)}$$

$$\frac{\partial H}{\partial t}+\frac{\partial}{\partial x}(HU)+\frac{\partial}{\partial y}(HV)=0 \quad \textbf{(3)}$$

H = water depth
U = depth-averaged velocity component in the horizontal x direction
V = depth-averaged velocity components in the horizontal y coordinate direction
z = the vertical direction
z_b = the bed elevation
u = the horizontal velocity in the x direction at a point along the vertical coordinate
v = the horizontal velocity in the y direction at a point along the vertical coordinate
$\beta_{uu},\beta_{uv},\beta_{vu},\beta_{vv}$ = momentum correction coefficients that account for the variation of velocity in the vertical direction
g = gravitational constant
ρ = water density (assumed constant)
τ^b_{x},τ^b_{y} = bottom shear stresses acting in the x and y directions, respectively
$\tau_{xx},\tau_{xy},\tau_{yx},\tau_{yy}$ = shear stresses caused by turbulence where, for example, τ_{xy} is the shear stress acting in the x direction on a plane that is perpendicular to the y direction

4.3.2. Model Inputs

FESWMS uses field data to quantify input variables, boundary conditions, and model parameters. The four primary inputs are: 1) discharge, 2) downstream water surface elevation 3) channel margin boundaries 4) and a topographic boundary surface.

Discharge data for the Smartville and Deer Creek gages was collected from the California Data Exchange Center. Downstream water surface elevations were measured in the field for six discharges and combined with stream-gage data to compile a rating curve for each site. The only model run lacking measured downstream water surface data (the EDR 22.7 m^3/s) was approximated using the EDR rating curve. Channel margin locations were obtained from water surface edge surveys completed at specific discharges. For each model run a map delineating channel boundaries including upstream, downstream, and channel edges was constructed. In areas of greater hydraulic complexity (around boulders and channel margins) node spacing within the map was reduced to capture localized hydraulics where topographic survey resolution permitted. The map was used to generate a 2-D finite element mesh using the TIN paving scheme of SMS's mesh module. The resulting field of triangular and quadrilateral elements with equidistantly spaced nodes along their edges were checked for errors and corrected before topographic survey data were interpolated to mesh nodes. The resulting mesh yielded a complete lower boundary surface for routing channel flow.

Secondary inputs include user specified bed roughness and eddy viscosity parameters. Bed roughness was adjusted within SMS's mesh module interface to capture energy dissipation and resistance along the water/bed substrate boundary. As explained in Horritt (2006), roughness parameters for 2-D models can be broken into two components; one representing roughness below the scale of the DEM, and roughness associated with processes below the scale of the computational mesh. Extensive survey resolution was achieved in this study to reduce roughness effects of the former and Manning's *n* was used in model calculations to represent the latter. For practical purposes Manning's *n* for each site was selected as follows. A roughness value for incised irregular bedrock channels similar to the EDR was absent from the literature and was at first estimated through expert opinion. During modeling an attempt was made to calibrate Manning's *n* by minimizing the deviations between modeled and observed water surface profiles. Five water surface surveys were conducted at the EDR, yet only two, the 33.7 m^3/s and 900.5 m^3/s discharge events, provided adequate reach length data for this analysis. Waves that surged against channel boundaries created water vapor that inhibited accurate total station measurements at higher discharges. Surveyed points were imported to the SMS scatter module where nearest node predictions of water surface elevation (±0.003 m) were extracted from the model. Overall, two Manning's *n* values were used at the EDR, one corresponding to discharges less than 710.7 m^3/s (n = 0.032) and one for discharges equal to and exceeding 710.7 m^3/s (n = 0.038). Although studies suggest that roughness is spatially complex and stage dependent, a constant Manning's coefficient was used for all model runs at the EDR.

For the TBAR model runs below 267.8 m^3/s a Manning's coefficient of 0.030 was used to capture channel roughness. At discharges exceeding this value, where willow patches along channel margins were inundated, an attempt to incorporate the increased roughness was made following the methods of Freeman (2000). A roughness value of 0.052 was attributed to elements that coincided with inundated willow patches at these increased discharges. The roughness coefficient used in model calculations for the TBAR is consistent with those reported values for cobble and gravel streams (Chow, 1959).

Eddy viscosity, a parameter used to capture transverse mixing associated with turbulent flow, is a sensitive variable in 2-D model applications in bedrock channels (Miller and Cluer, 1998). FESWMS uses the Boussinesq eddy viscosity method which assumes that turbulent stress terms in the governing equations are proportional to local velocity gradients (Miller and Cluer, 1998). This treatment of turbulence closure is included in the system of model equations explained above and allows a more representative prediction of transverse velocity gradients than methods which hold E constant. In FESWMS, node value eddy viscosities are calculated using equations 4 and 5 where u* is shear velocity, Cd is a coefficient of drag represented by equation 6, and E_o is a minimized empirical constant of 0.033 m$^2 s^{-1}$. Eddy viscosities set too high reduce transverse mixing and cause models to underestimate turbulent eddy features, lateral velocity variability, and mid channel velocity, while extremely low eddy viscosities promote model instability.

$$E = 0.6H \cdot u* + E_o \tag{4}$$

$$u* = U\sqrt{Cd} \tag{5}$$

$$Cd = \frac{9.81n^2}{H^{1/3}} \tag{6}$$

4.3.3. Model Performance

Although the FESWMS model has been thoroughly validated on the gravel-bed Mokelumne (Elkins et al., 2007; Wheaton et al., 2004a) and Trinity (Brown and Pasternack, 2008) Rivers, an investigation of its relevance along the Yuba River was still warranted for this study. Recently, Moir and Pasternack (2008) reported a FESWMS modeling and validation study at the TBAR using data from 2004-2005, prior to a large flood that yielded the morphology investigated in this study. For this new morphology, depth and velocity were recorded at three cross sections during the 18.4, 21.2, and 31.2 m^3/s low flow events at the TBAR and compared against modeled predictions by surveying (±2cm) the locations of depth and velocity measurements with the Leica 1200 system described above. Velocity was measured at 60% of water column depth using a depth setting rod and Marsh McBirney electromagnetic flow meter averaged for 30 seconds at 30 Hz to approximate average column velocity. The coordinates of depth and velocity measurements were imported to the SMS mesh where the nearest depth and velocity node predictions were used to test the model. A best fit curve was applied to modeled and measured datasets to ascertain the predictive capabilities of the model across the channel.

Performance of the model at the EDR was evaluated by plotting the field measured and final modeled water surface profiles across the site for the 33.7, 271.3, and 900.5 m^3/s discharge events. For each event, the most upstream water surface elevation point was used as the datum. Although a cross-sectional comparison of depth and velocity similar to the TBAR would be a more robust test of model capability at the EDR, logistical and field constraints prohibited the use of this method. For example, much of the EDR cannot be waded and precludes any direct measurement of depth and velocity at a cross section. Even access by boat is a difficult task to achieve and requires a portage of a shallow rapid downstream of the EDR.

4.4. Shields stress Calculations

Shields stress is a common dimensionless parameter used to predict sediment entrainment in gravel-bed rivers (Elkins et al., 2007; Lisle et al., 2000). It is the ratio of shear stress (τ) to the submerged weight of a sediment particle of a specific grain size. To get an approximation of Shields stress the drag coefficient method of calculating shear stress was employed, where shear stress is equal to the product of water density (ρ_w), a drag coefficient (Cd), and velocity squared **(**Eqn. 7**)**. Water density was assumed constant and velocity values were exported from model predictions. As outlined above, the drag coefficient (Cd) was approximated as a function of Manning's *n* and channel depth; the former fixed in each model scenario and the latter exported along with velocity values for each node in the mesh. Overall, depth and velocity predictions were used to calculate drag coefficients **(Eqn. 6)**, shear stress **(Eqn. 7)**, and Shields stress **(Eqn. 8)** at each mesh node where γ_s and γ_w are the specific weight of sediment and water, respectively, and D_{50} is the median sediment particle size in mm. Shields stress values were calculated within SMS in a stepwise fashion and adjusted by a factor of 0.51 to account for lower real-world near bed velocities (MacWilliams et al., 2006; Pasternack et al., 2006).

$$\tau = \rho_w CdU^2 \qquad \textbf{(7)}$$

$$\tau^* = \frac{\tau}{(\gamma_s - \gamma_w)D_{50}} \qquad \textbf{(8)}$$

Shields stress values of τ^* <0.01, 0.01< τ^*<0.03, 0.03< τ^*<0.06, and τ^*>0.06 correspond to no transport, intermittent transport, partial transport, and full transport regimes, respectively, as defined by (Lisle et al., 2000). These ranges helped to account for uncertainty in depth and velocity predictions. The Shields stress classes adopted here provide a conceptual understanding of sediment transport, but it is important to appreciate that transport is a probabilistic phenomenon and not governed by strict thresholds. For example, Paintal (1971) showed that even though shear stress values are below the critical value required for “insipient motion”, some form of transport is likely to occur, which corresponds to the intermittent transport class used in this study. Overall the qualitative definitions of the Shields stress classes are as follows: no transport corresponds to a stable bed, intermittent transport corresponds to minimal transport associated with turbulent bursts, partial transport suggests that particle entrainment will occur for a specific sediment size class if it is in relative abundance on the bed (compared to other particle sizes), and full transport suggests a carpet of sediment moving along the boundary.

The method of Shields stress calculation outlined above makes explicit assumptions about the relationship between Shields stress and various physical variables. For instance, τ^* is proportional to both velocity and Manning’s *n* to the second power, suggesting that Shields stress increases with channel roughness and velocity in a nonlinear fashion. Model predicted Shields stress values were exported from SMS and spatially analyzed within ArcGis 9.2.

4.5. Habitat Modeling

FESWMS provides depth and average velocity predictions central for describing potential spawning habitat within a rehabilitation site. Habitat suitability curves (HSCs), polynomial regressions between key spawning variables (e.g., depth, velocity) were used to relate predicted hydraulic variables and available physical habitat. For this study a depth and velocity HSC developed for the Mokelumne river fall run Chinook salmon was used to predict physical spawning habitat quality from model solutions (CDFG, 1991). Various field studies have shown that habitat suitability curves vary not only by species, but may also vary by watershed, fish size, and specific physical conditions including temperature and hyporheic upwelling (Giest and Dauble, 1998). Thus, the Mokelumne River HSCs were tested and validated for use on the Yuba River as described below. Predicted node depths and velocities were exported and entered into the Mokelumne River depth and velocity HSCs, which produced a measure of habitat quality for each node between 0 (no habitat) and 1 (highest quality). The contribution of depth and velocity to overall habitat suitability were evenly weighted and used to create an index defined as the geometric mean of the two independent depth and velocity functions **(Eqn. 9)**. V(x) and D(y) represent the velocity and depth suitability functions (HSCs) formulated for the Mokelumne River fall run Chinook. The combined habitat suitability metric, denoted the geometric habitat suitability index (GHSI), was calculated at each node and interpolated over the modeled area giving a spatial distribution of predicted habitat that was compared across sites. GHSI values were broken into four classes that qualitatively represent poor (0.0-0.2), fair (0.2-0.4), good (0.4-0.6), and excellent (0.6-1.0) habitat.

$$GHSI = \sqrt{V(x) \bullet D(y)} \qquad \textbf{(9)}$$

4.5.1. Habitat Model Performance

To evaluate the performance of Mokelumne River HSCs, salmon redd locations were surveyed on fifteen days between September 7th and November 15th 2005 at the TBAR and overlaid onto the model predicted GHSI mesh. Observed redds were divided into two groups based on the dominant measured discharge. The first represented redds observed while flows were approximately 22 m^3/s and the second represented redds observed at 34 m^3/s. Redds were identified in the channel by expert observers that keyed in on disturbed sediment patches, pit and tailspill morphology, and direct observations of spawning salmon. The location of each redd pit was surveyed with the Leica 1200 system described above while weighted tags were placed adjacent to each pit to reduce repetitive sampling. Tags that were buried or moved suggested a new spawning event occurred and the redd structure was surveyed again. Overall, survey procedures provided ± 0.02 m horizontal accuracy for comparing locations of redds against model predicted GHSI values.

An electivity index was constructed to test the Mokelumne River HSC's ability to capture observed habitat preferences. First, a raster data set of model predicted GHSI values in ArcGIS 9.2 for the 21.2 m^3/s model run was created. The total channel area in each GHSI class was exported using the zonal statistics tool in spatial analyst and raster values (GHSI) at redd locations were extracted. The percent of channel area and observed redds within each GHSI class was calculated and plotted. Following the work of Ivlev (1961), the electivity index method was used, where E is the ratio of the proportion of redds observed to the proportion of channel area within a GHSI class **(Eqn. 10)**. Values less than one (<1) suggest fish use a specific habitat less than its availability (avoidance) while values greater than one (>1) suggest a particular habitat class is used more often than its availability (preference). The electivity indices for each of the four habitat suitability classes were calculated and analyzed for preference and avoidance phenomena.

$$E = \frac{\%Redds_{GHSI}}{\%Habitat_{GHSI}} \qquad \textbf{(10)}$$

4.6. Imagery

Historical photographs and aerial imagery are fundamental tools for characterizing channel form, sediment deposits, and reconstructing site morphogenesis. Research at the turn of the century (ca. 1909) by G.K. Gilbert and USACE photographs of the LYR between the current locations of Englebright and Daguerre Dams were obtained from the USGS (2006) photographic library and government agencies respectively. Aerial images were available from James (2007) and Terraserver® (2007) for 1937, 1947, 1952, 1958, 1984, 1986, 1991, 1996, 2002, 2004, 2005, and 2006. Although aerial imagery was not used for detailed analysis in this study, it provided a depiction of system evolution.

4.7. Sediment Transport Analysis

A vital component of restoration efforts aimed at ameliorating sediment discontinuity below dams is an estimation of sediment transport to the project reach. Although current delivery to the EDR is negligible, two broad quantitative estimates of sediment transport within the LYR were made based on (1) swath bathymetry and sediment core data acquired by Snyder (2004), and (2) repetitive topographic surveys of the TBAR as described above.

Using the conservative variable layer method of calculation reported in Snyder (2004), percent gravel in sampled cores was multiplied by total mass of sediment for each layer area and summed for the entire lake deposit. The resulting number represents the total mass of gravel locked behind Englebright. Total volume of gravel detained by Englebright was estimated by dividing total gravel mass with an average bulk density of 1.65 kg/m^3. An assessment of average annual load was made by equally distributing the total volume of gravel over the 61 years since Englebright was completed, providing an average annual load that would have reached the EDR without the dam upstream.

A secondary, event specific, approximation of transport for the LYR was conducted through DEM differencing methods by surveying bed topography at the TBAR before and after the December 2005 3,089 m^3/s (24-yr) flood event. This method quantifies changes in the storage component of a sediment budget, an overall accounting of inputs, outputs, and sediment storage in a channel. Topographic points from the pre and post flood survey were used to create separate DEMs using the TIN interpolation method described above. DEMs were rasterized to cells of 0.023 m^2 within ArcGIS 9.2 3D Analyst and the 2005 raster was subtracted from the 2006. This produced a new raster representing elevation deviations attributable to the flood. To account for bed elevation variability and sub resolution noise, elevation deviations of $\pm$ 0.051 m were filtered out and not considered in the differencing analysis. Volumetric estimations of transport at the site were produced by multiplying elevation deviations by the appropriate cell size.

5. HYPOTHESIS TESTING

Empirically and numerically generated data streams were used to reject or accept the hypotheses presented in **Table 1**. The general testing methodology for each hypothesis is presented below and the relevancy to GA efficacy at the EDR will be discussed.

5.1. Bed Material

***H*$_1$**: *Sediment characteristics at the EDR and TBAR are comparable and suitable for spawning.*

A sediment characterization, represented by empirically derived diameter statistics and observations of particle shape (roundness, sharpness), was used to determine if sediment conditions were within the known preference range (12-80 mm) of Chinook salmon at the EDR (Kondolf, 1993). If sediment particles at the EDR are substantially coarser or more angular than TBAR sediments or if a significantly smaller fraction of particles fall within the limits of Chinook preference curves, then hypothesis H_1 will be rejected. The former was tested by comparing the D_{16}, D_{50}, D_{84}, and D_{90} size classes at each site using the Wilcoxon-Mann-Whitney Rank Sum test mentioned above with an alpha value of 0.05. A qualitative test of the latter was completed by comparing particle roundness through field observations and imagery of the two sites.

5.2. Hydraulics

***H*$_2$**: *Flow convergence routing will enable the injection of small doses of gravel to produce alluvial geomorphic features (riffles, pools, glides) that accentuate the existing pattern of topographic highs and lows at the EDR and TBAR study sites.*

Model predicted velocity fields for the six comparable discharge events were analyzed for flow convergence effects. The presence of a velocity reversal, associated with confinements upstream of pools at high discharges would suggest that deposition of augmented gravels will occur downstream of pools on topographical highs (sills) and maintain site morphology. The absence of a velocity reversal at either site would suggest that alluvial deposition on bedrock sills and riffle-habitat formation is not likely to occur. In that case, the injection of small doses of gravel would only serve to fill in pools or accumulate along channel margins. If a velocity reversal is not observed at the EDR, H_2 will be rejected.

5.3. Geomorphology

***H_3**: Injected gravels at the EDR will be stable during spawning flows.*

***H_4**: Injected gravels at the EDR will be stable during a 271.3 m^3/s discharge (2-year event).*

***H_5**: Injected gravels at the EDR will be stable during a 900.5 m^3/s discharge (~5-year event).*

***H_6**: Injected gravels at the EDR will be stable during a 2588.2 m^3/s discharge (~24-year event).*

To determine the likelihood of gravel mobilization the proportion of wetted channel within each Shields stress class was calculated to test hypotheses H_3-H_6. Each hypothesis will be rejected if a significant proportion of the channel (10%) registers in the full transport regime.

***H_7**: GA will aggrade the EDR and produce extensive cross channel habitat that is susceptible to scour.*

Historical images depicting site morphogenesis, an estimation of sediment transport, and Shields stress in the spawning channel of the EDR were used to infer the likelihood of scour and deposition patterns. H_7 will be rejected if the underlying response of the system is to rapidly evacuate injected gravels and produce heterogeneous depositional patterns.

5.4. Habitat

***H_8**: Historically, the EDR supplied ample spawning habitat for Chinook salmon.*

Historical images, observations of spawning behavior at the EDR, and a literature review provided a means for testing H_8. Overall, H_8 will be rejected if historical evidence suggests that salmon spawning at the EDR was limited in spatial extent and frequency.

***H_9**: Current spawning habitat at the EDR and TBAR is not limited.*

The percentage of channel in the poor, fair, good, and excellent quality habitat was calculated with HSCs and ArcGIS 9.2 for the 33.7 m^3/s EDR and 34.6 m^3/s TBAR and compared. If the proportion of channel in the medium and high quality class is below 5% of the wetted channel area H_9 will be rejected.

6. RESULTS

6.1. Topography

DEMs of the two project sites are presented in **Fig. 7** to highlight topographical diversity and facilitate general morphologic comparisons. The EDR exhibits a pool/run/pool sequence with near vertical canyon walls confining the single channel on the south and inhibiting lateral channel migration. To the north, a 20 m wide by 40 m long deposit of blast rock bolsters the channel edge before adjacent hillsides impinge the irregular elevated floodplain. Topographic variability of the bed is pronounced, influenced by the character (slope, curvature) of surrounding hill-slopes, and controls hydraulic variables within the channel. For example, hillsides on the northern edge of EDR are more gradual than on the south, resulting in shallower depths for a given discharge along the northern channel edge. Further topographic control is evident between the head and tail of the run where two bedrock features jut into the channel from the southern hillside forming shallow shelves (aka "sills"). During spawning flows (22-34 m^3/s) the channel is widest in the Narrows pool (~40 m), constricts through the run (~20 m), and expands slightly below the 2nd bedrock feature (~28 m) before reaching the Narrows I powerhouse 600 m downstream of Englebright Dam. At a discharge of 2588.2 m^3/s, channel width is uniform throughout the 135 m reach and averages ~64 m.

The TBAR exhibits gradual slopes along channel margins and is less influenced and constrained by surrounding hillsides than the EDR. A highly connected floodplain and adequate sediment supply allows significant channel migration during extreme events along the pool/island/riffle sequence. Two topographic lows in the middle of the site represent the main and highly complex side channel that merge downstream of a depositional mid-channel island bordering the main riffle on the north. During spawning flows the main channel constricts from ~100 m at the head of the island to ~ 45 m at the riffle crest before transitioning to a narrow (~22 m) thalweg that cuts across the tail of the island. Topographic variation at the subunit scale (10^{0}) is extensive near two bedrock outcrops that promote pool formation downstream and along island margins. This topographic heterogeneity provides an array of physical habitat types including pools, riffles, recirculating eddies, shallow margin zones, and cut banks for differing life stages of salmonids (Moir and Pasternack, 2008).

6.2. Roughness Calibration

Initial efforts were made to calibrate the model by adjusting Manning's *n* values to attain convergence between predicted and observed water surface profiles. **Table 3** provides the results of calibration using the 75 and 20 field measured water surface profile points acquired in the field for the 33.7 m^3/s and 900.5 m^3/s discharges, respectively. To avoid closure errors, eddy viscosity values were altered to attain model convergence in accordance with Rameshwaran (2003) who found that eddy viscosity had little effect on channel roughness calibration. Overall, changing Manning's *n* from 0.022 to 0.040 causes an average absolute profile deviation of 0.007 m or 0.41 % of mean channel depth for the 33.7 m^3/s event. Calibration efforts altered average absolute errors for the 900.5 m^3/s model run by 0.08 m or 0.43% of channel depth.

6.3. Model Performance

6.3.1. TBAR Hydraulics

Model predictions and field measurements of depth and velocity for 83 points along three cross sections at the TBAR are presented in **Fig. 8** for validation purposes. At cross section 1 with a discharge of 18.40 m^3/s, the average absolute depth and velocity errors were 0.05 m and 0.04 m/s. At a discharge of 21.15 m^3/s the model under predicted depth for the entire length of cross section 2 and over-predicted velocity along the northern side of the channel with average absolute errors in depth and velocity of 0.08 m and 0.04 m/s. At a discharge of 31.18 m^3/s at cross section 3, absolute errors in modeled versus measured predictions were 0.03 m and 0.05 m/s for depth and velocity. Despite these inaccuracies, raw comparisons of all modeled and observed values provided a coefficient of determination of 0.929 and 0.768 for depth and velocity, respectively. Overall, depth and velocity predictions for each cross section have a mean error of ±10% for depth and ±22 % for velocity.

6.3.2. EDR Water Surface Profiles

Surveyed water surface elevation data along the channel edges provided a means to assess model predictions of water surface elevations for the 37.7, 271.3, and 900.5 m^3/s discharges at the EDR. For the 37.7 m^3/s event, a channel roughness coefficient of n = 0.032 caused the model to over predict water surface elevation through the majority of the site with an average absolute error of 1.1 % of channel depth **(Fig. 9)**. Although modeled water surface elevation deviated from the measured locations, the coefficient of determination for raw differences was 0.89. The model predicted water surface elevation for the 271.3 m^3/s discharge was less accurate and had an error of 6% of average channel depth. Overall, there was a parallel between the two sets with the model consistently over-predicting water surface elevation in a downstream direction. The coefficient of determination between modeled and measured data points for the 271.3 m^3/s discharge was 0.76 using a Manning's *n* of 0.032. At the highest analyzed discharge of 900.5 m^3/s and using a Manning's roughness value of 0.038, an error of 1.57% of average channel depth (0.08 m) was observed with a coefficient of determination registering at 0.89.

6.3.3. Habitat Suitability Curve Performance

Two hundred and forty redds were mapped at the TBAR during the two spawning discharges. Model predicted GHSI values and the 110 observed redds for the 21.2 m^3/s event are presented in **Fig. 10**. Predictions for the higher spawning flow are similar but left out for sake of brevity. Redds and model predicted good and excellent habitat classes are clustered around the island head and downstream of the island tail. Some redds and high quality habitat areas are located in very narrow zones along the side channel. The results of the electivity analysis, including the percent of channel area and percent of observed redds in each of the habitat suitability bins, are presented in **Fig. 11**. Electivity values for the poor, fair, good and excellent habitat suitability classes were 0.16, 0.22, 1.61, and 3.56, respectively. Overall, poor and fair quality habitat covered ~ 67 % of the channel area while good and excellent habitat amount to ~32 % of the channel.

6.4. Bed Material

6.4.1. Hypothesis H_1

Sediment size distributions based on five pooled bed samples at EDR validated field observations on the coarseness of the heavily altered channel **(Fig. 12)**. Average D_{16}, D_{50}, D_{84}, and D_{90} values were 50.0, 144.3, 327.9, and 382.5 mm for the EDR, respectively. Obvious intra-site variation was absent although a limited sample size may have obscured patterns that visual assessments had indicated. For example clast size appears to increase moving away from the channel. Overall only ~25 % of sampled particles at the EDR were within the size limits of spawning gravels reported in the literature and all were highly angular.

At the TBAR 87 pebble counts were pooled to obtain reach average values; cumulative frequency plots depict a site dominated by cobble and gravel with computed D_{16}, D_{50}, D_{84}, and D_{90} values of 36.7, 74.2, 138.9, and 162.3 mm, respectively **(Fig. 12)**. General patterns of intra-site variation were evident and controlled by local hydraulic conditions. Overall a significant portion (~50%) of the sampled area at the TBAR contained gravels of appropriate size and character for Chinook salmon. The alpha values for the Wilcoxon-Mann-Whitney rank sum test were 0.057, 0.00054, 0.00018, and 0.00018 when comparing the D_{16}, D_{50}, D_{84}, and D_{90} size classes at the EDR and TBAR.

6.5. Hydraulics

6.5.1. Hypothesis H_2

The spatial distribution of depth and velocity for the six EDR modeled discharges are presented in **Fig. 13 & 14** respectively and are dominated by local bedrock topography. For all model runs depth is greatest in the Narrows II pool afterbay. There was a general longitudinal pattern of depth decreasing downstream of the Narrows pool, staying consistent in the run section, and increasing again downstream of the second bedrock constriction **(Fig. 13)**. At the two modeled spawning flows, depth at the exit of the Narrows pool and throughout the channel is consistently >1 m except along channel margins. A maximum velocity of 1.5 m/s occurred near two bedrock features that laterally constricted and accelerated flow **(Fig. 14A)**. For the lowest two discharges velocity decreased between the bedrock features before accelerating over the second shelf and into the lower pool **(Fig. 14 A & B)**. For discharges above 33.7 m^3/s deceleration in the run was less pronounced and the location of maximum velocity swelled to incorporate the entire mid-section of the modeled reach **(Fig. 14D, E, & F)**. A maximum velocity of 6 m/s was predicted in the 2588.2 m^3 discharge scenario where velocity in the entire run was above 5 m/s. The location of maximum velocity showed little variation across discharges and coincided with the two constriction points denoted in the DEM.

The spatial distribution of depth and velocity at the TBAR for all modeled discharges is presented in **Figure 15** and **16** respectively. Depth was greatest in the main channel thalweg downstream of the riffle crest and along the side channel in the forced pool complex. During spawning flows at the TBAR, depths across the riffle ranged from 0-1 m. Velocity at the TBAR was more variable than the EDR for the low (21.2 m^3/s) spawning flow **(Fig. 16A)**. Maximum velocity (~3 m/s) occurred downstream of the main riffle crest where lateral convergence accelerated flow and directed it through the narrow thalweg. Spatial patterns of velocity were similar for the 34.6 m^3/s discharge event **(Fig. 16B)**, but as discharge increased to 267.8 m^3/s **(Fig. 16C)**, the model predicted an increase and shift in maximum velocity (4 m/s) to the run 60 m downstream of the island tail. Interestingly, more than doubling the discharge to 655.3 m^3/s had little effect on maximum velocity, yet the region that exhibited > 3 m/s increased dramatically and covered ~75% of the site **(Fig. 16D)**. For discharges exceeding 998.4 m^3/s, velocity increased towards the channel center, and reached a maximum value of 4.5 m/s in the upstream pool and over the island tail for the 3089.1 m^3/s event. Overall, velocity variation was dampened at higher discharges and a velocity reversal was detected.

6.6. Geomorphology

6.6.1. Hypotheses H_3-H_6

The spatial distribution of Shields stress was calculated using the D_{50} of spawning sized sediments for the six EDR flows **(Fig. 17)**. Intermittent transport was predicted from the run entrance throughout the entire mid-channel for the 271.3 m^3/s EDR discharge **(Fig. 17C)**. A localized patch of partial transport was also predicted in the center of the run between the two topographic features constricting the channel. Except for margin areas, the entire channel was under intermittent transport at a discharge of 710.7 m^3/s while partial transport extended mid-channel from the run entrance through the downstream boundary **(Fig. 17D)**. Between the 710.7 m^3/s and 900.5 m^3/s discharge events, full transport in the run increased by 7% of channel area and partial transport expanded laterally and upstream into the Narrows II pool exit **(Fig. 17D & E)**. At 2588.2 m^3/s, the entire mid-channel section of the EDR was under full transport with localized areas within the run registering in the highest of Shield stress values **(Fig. 17F)**.

For the 900.5 m^3/s and 2588.2 m^3/s events, the model predicted Shields stress values corresponding to “full transport” in 15% and 54% of the wetted channel area, respectively **(Fig. 18)**. Significant full transport was not predicted for the spawning (22.7 and 33.7 m^3/s) flow or 2-year event (271.3 m^3/s) discharge. Overall, Shields stress for all modeled discharges was at a maximum in the run between the two topographic boundary controls and minimized along channel margins.

Unlike the EDR, intermittent transport was predicted at the TBAR below the riffle crest, through the narrow thalweg, and in the run section downstream of the island for the two modeled spawning flows **(Fig. 19A & B)**. At a discharge of 267.8 m^3/s, intermittent transport was predicted throughout the TBAR with a section of partial transport near the downstream boundary corresponding to the velocity increase in that area **(Fig. 19C)**. Aside from a small zone of full transport associated with increased element roughness in the willow margin, significant full transport was not predicted in the channel until discharge exceeded 998.4 m^3/s **(Fig. 19D & E)**. During the 3089 m^3/s flood event at the TBAR Shields stress values above 0.1 are predicted throughout the channel center, and peak in the pool upstream of the main riffle and at the valley constriction evident in the DEM. Overall, approximately 1% and 46% of the channel were in the full transport regime for 998.4 m^3/s and 3089 m^3/s respectively at the TBAR.

6.6.2. Hypothesis H_7

Numerous historical photos helped characterize the Yuba River around the EDR and provided a conceptual understanding of ongoing geomorphic processes and system evolution. An image taken 0.4 km upstream of the EDR by G.K. Gilbert in 1909 facing upstream is the earliest available high quality photo of the Yuba river near the project site **(Fig. 20)**. Although the picture was taken 400 meters upstream of the EDR, the morphology pictured is representative of conditions throughout the narrow bedrock lined reach at that time. Steep canyon walls border the channel on both sides and extensive bedrock control is evident. Interestingly, a deposit of hydraulic mining debris remains in the channel forming a small riffle complex on river left (right in picture). Gravel deposits are also present behind protruding bedrock features upstream and along channel margins. Overall, the channel is confined and dominated by angular resistant bedrock features that protrude into the channel and allow deposition of cobble and gravel size material in their lee.

During the construction of Englebright Dam substrate conditions at the EDR were highly manipulated. Dynamite was used to raze weathered rock from surrounding hillsides while steam shovels and dump trucks moved large quantities of rubble around the site **(Fig. 21)**. Angular blast rock was built up on river left and formed a large terrace bordering the southern channel margin. The blast rock terrace has since been removed by numerous flood events and transported downstream. The volume of rock removed from surrounding hillsides is unknown yet its effect on channel substrate is documented by field mapping of continuous blast rock deposits from the EDR to downstream of Deer Creek.

A 1909 image provided by G.K. Gilbert 0.5 km downstream of the EDR overlooking the Deer Creek confluence depicts a bedrock channel inundated with large quantities of hydraulic mining debris **(Fig. 22A)**. The bar on river right extends past the Deer creek confluence and bedrock features within the channel are completely covered. A recent photo of the Deer creek confluence from about the same location clearly shows the amount of sediment removed in the 98 years since Gilbert's photo through incision processes **(Fig. 22B)**. Cobbles and hydraulic mine debris are virtually absent, and the large bar on river right has been replaced with resistant blast rock washed down from the construction of Englebright. The lateral bar on river right no longer extends beyond the

Deer Creek confluence and all remaining coarse hydraulic mine sediments are greater than 30 m above the low flow water surface elevation.

As reported by Snyder (2003), over 25% of Englebright Reservoir's initial capacity has be filled with ~26 x 10^6 metric tons of sediment consisting of silt, sand, gravel, and organic material. Of this, the approximate mass of gravel retained by Englebright is ~ 4.73 x 10^5 metric tons. With an assumed bulk density of 1.65 kg/m³, this is equivalent to a volume of 2.86 x 10^5 m³ of gravel. Distributing the total mass and volume over the 61 years since Englebright was completed produces an estimated annual load of 77520 metric tons/yr or 47124 m³/yr of gravel that would have entered the EDR.

The DEM differencing analysis at the TBAR provided the spatial distribution of cut and fill attributable to the December 2005 24-year flood event, and an approximate estimate of transport **(Fig. 23)**. A net loss of 19,984 m³ cubic meters occurred at the site with 30,057 m³ and 10,073 m³ of scour and deposition respectively. Topography was completely reworked and channel morphology changed dramatically. The location of the island moved downstream towards river left and a new side channel formed along the southern valley margin. Maximum scour and fill within the reach was ~ 2.4 m and 2.25 m respectively with a negligible change in average channel elevation. Overall, the volume of sediment removed from the TBAR represents a lower bound estimate of transport, as much more material could have moved through the site during the event and subsequently replaced by sediments from upstream.

Model predicted Shields stress values for the 2-yr, 5-yr, and 24-yr events were overlain on the area of channel inundated at spawning flows for the EDR. The resulting map represents the spatial distribution of probable scour and deposition within the spawning channel area for the modeled events at the EDR **(Fig. 24)**. For a typical 2-year event partial transport will occur in the narrowest section of the spawning channel but as the channel expands laterally moving downstream, velocity decreases and Shields stress was reduced **(Fig. 24A)**. During a 5-yr event, significant full transport on the along the northern channel boundary was predicted with most of the spawning channel in partial transport **(Fig. 24B)**. During the 24-year event, full transport dominated the spawning channel **(Fig. 24C)**. Results show that for all discharges Shields stress was lowest along channel margins and specifically downstream of major bedrock/topographic features that protrude into the channel. For all discharges a relatively stable environment occurs along the southern side of the channel at the tail of the Narrows pool afterbay.

6.7. Habitat

6.7.1. Hypotheses H_8

Gilbert's 1909 image **(Fig. 20)** also provides some information about the character of spawning habitat that may have formed in this active supply limited channel. The small riffle present in the foreground and channel margin/boulder deposits of sediment in the background show that despite the transport dominated regime, gravel and cobble-sized material (presumably hydraulic mining debris) was deposited and may have provided suitable sediments for spawning salmonids. It is difficult to predict, but sediment input to the channel prior to hydraulic mining may not have filled the channel to the same extent, however some deposition of suitable gravels likely occurred. Regardless, the image clearly shows that significant lateral bars and riffle features do not exist at a time of extreme sediment supply and that the spatial pattern of deposition in the channel is not continuous.

Field observations and historical accounts provide meaningful clues about the magnitude and extent of historical spawning habitat at the EDR. For example, multiple pairs of salmon were observed spawning near the Narrows I powerhouse throughout the 1970s and early 1980s (Mullican, 2007). Although the location of the observed spawning activity is roughly 200 m downstream of the EDR, substrate conditions were likely comparable. On two other occasions, (October 10^{th} 2005 and September 25^{th} 2007), the author observed large (~800 mm) female salmon "testing" sediments along channel margins at EDR by turning horizontal in the water column and attempting to dislodge particles from the bed through body flexing. In both cases, female salmon were unable to mobilize sediments and successful spawning was not observed.

6.7.2. Hypotheses H_9

Medium and high quality habitat predictions at the EDR, based solely on hydraulic variables, were limited to small (< 0.5 m^2) strips along channel edges while habitat associated with pool exits/riffle entrances was nonexistent. Overall, 87%, 10%, 2%, and <1% of the wetted channel was in the poor, fair, good, and excellent quality habitat classes at the EDR for the 33.7 m^3/s spawning flow **(Fig. 25A)**. At a discharge of 21.2 m^3/s FESWMS predicted extensive medium and high quality habitat at the pool exit/riffle entrance and forced pool/riffle complex adjacent the to the island tail at the TBAR **(Fig. 10)**. Results for the higher (~34.6 m^3/s) discharge were similar but left out for sake of brevity. Localized areas of margin habitat exist, and predictions are substantiated by observed redds within the side channel. The proportion of channel in the poor, fair, good, and excellent quality habitat were approximately 36%, 29%, 18%, and 15% respectively at the TBAR.

A decomposition of the geometric habitat suitability index into its component depth and velocity functions within the modeled mesh provided an areal distribution of depth and velocity habitat suitability for the EDR 33.7 m^3/s spawning flow **(Fig. 25B &C)**. While velocity is suitable throughout the channel center, depth is adequate only along channel edges. At the pool exit, the most frequently utilized location of spawning activity in the LYR, depths are greater than those preferred by Chinook salmon (given the HSCs employed) and averaged between 1 and 2 m. Although not provided, habitat predictions for the 22.6 m^3/s EDR spawning flow provide the same spatial patterns of habitat.

7. DISCUSSION

For organizational purposes the following section has been separated into two parts. The first three divisions (7.1-7.3) are directed towards methodological issues such as roughness calibration, model behavior (hydraulics) and habitat validation. The second part (divisions 7.4-7.7) discusses results directly related to the stated hypotheses.

7.1. EDR Roughness

Roughness calibration results at the EDR suggest that in bedrock channels the 2-D model FESWMS was rather insensitive to Manning's *n* when it comes to matching observed and modeled modeled water surface profiles. Changing Manning's *n* from

0.022 to 0.040 in the 33.7 m^3/s run altered average absolute errors by only 0.41% of channel depth **(Table 3)**. Ghanem (1996) found similar results after calibrating a 2-D model in which changing roughness by 100% caused an 8% increase in channel depth.

Model insensitivity in the roughness parameterization scheme can be attributed to the scale of dominant roughness elements in the channel and their accurate representation in the DEM. The DEM in this study consisted of high density (1.44 points/m^2) survey data that resolved the dominant roughness features like lateral bedrock constrictions, resistant inundated boulder clusters, and overall bed-form irregularities. Previous 2-D model applications have shown significant model sensitivity to the representation of topographic complexity. Detailed survey procedures increased the resolution of roughness characterization and implicitly incorporated it into the surface over which flow was routed. In effect, this increased the overall proportion of roughness accounted for in model simulations. Furthermore, unlike gravel-bed streams where roughness associated with individual grain diameters may be quite important, channel roughness in bedrock channels is dominated by larger scale features best characterized through the direct intensive surveying methods employed here. Overall, the insensitivity of water surface deviations to Manning's *n* suggests that the topographic characterization of the EDR adequately describes a high proportion of roughness elements in the channel.

All three of the modeled water profiles at the EDR followed the general form of measured water surface elevation and are comparable to errors reported in other studies. For instance, the maximum observed error of 6% of channel depth for the 271.3 m^3/s event is within the 0.11 m and 0.23 m range (5.1%-15.4% of channel depth respectively) reported by Miller (1998). Both the 33.7 m^3/s and 900.3 m^3/s event registered errors smaller than the lower limit of 0.11 m referenced above. The largest error for the 33.7 m^3/s occurs at the location of a channel protruding bedrock outcrop 60 m from the upstream datum and was likely caused by the model's inability to capture vertical accelerations that result from the constriction and associated vertical momentum flux that occurred at this location. Unlike Miller (1998), a correlation between water surface errors and discharge was not observed, further suggesting the adequacy of the constructed DEM. Overall, a general agreement is observed between model predicted and measured water surface profiles with errors equal to or below previous studies in bedrock channels. Further investigation into the ability of FESWMS to capture spatial patterns of velocity and depth is warranted.

7.2. TBAR Hydraulics

The three cross-sectional comparisons of measured and modeled depth and velocity at the TBAR validate FESWMS's ability capture channel hydraulics in gravel bed channels. As reported in Moir and Pasternack (2008), the model accounts for a large proportion of the observed hydraulic variability with errors comparable to other 2-D model studies. Given the uncertainty associated with survey procedures (±0.02 m) and field velocity measurements, the errors of 0.05, 0.08, and 0.03 m depth and 0.04, 0.04, and 0.05 m/s velocity at the three low flow TBAR cross sections depth and velocity at the TBAR are considered adequate **(Fig. 8)**.

7.3. Habitat Modeling

Model predictions of habitat suitability at the TBAR were substantiated by redd surveys. Redds are consistently located near predicted good and excellent habitat zones throughout the site and areas predicted to have poor habitat suitability lack any significant number of redds **(Fig. 10)**. Where the model predicts small areas (<1m²) of habitat along the complex side channel, salmon redds were observed. This suggests salmon can locate and utilize extremely localized hydraulic conditions and that the HSC methodology is capable of resolving such features. Therefore, the model was able to capture both wide scale patterns of habitat suitability associated with meso-scale features (e.g. riffle entrances) and smaller micro-scale conditions along the complex side channel. Results from the electivity calculations further support the use of Mokelumne River HSCs **(Fig. 11)**. The low electivity values for poor and fair habitat suggest an overabundance of poor and fair habitat at the TBAR with only minor utilization. The values of 1.61 and 3.56 for the good and excellent habitat classes suggest utilization proportionally exceeds availability and that a preference for these GHSI values was observed. Overall, the Mokelumne River HSC model accurately predicted both the pattern of habitat suitability and the observed preference and avoidance behaviors of spawning Chinook salmon at the TBAR.

7.4. Bed Material

7.4.1. Hypothesis H_1

Although not accounted for in the habitat suitability indices in this study, sediment size distributions are key selection variables for spawning salmonids. The suitability of gravels is a function of species, fish size, and specific hydraulic conditions including upwelling near the bed where female salmon interact with the substrate (Giest and Dauble, 1998; Kondolf, 1993). For instance, higher near-bed velocities enable anadromous fish to excavate larger particles by using the increased momentum of the flow. The basic analysis and comparison provided does not account for this dynamic relationship between velocity, upwelling, and other parameters on the suitability of gravel at each site. Instead the analysis assumes a suitable gravel size defined by past studies.

At the EDR, Englebright Dam has blocked off all coarse sediment input. This caused what Kondolf (1997) termed "hungry water", where suitable spawning gravels are winnowed away leaving only coarse, resistant particles. The remaining bed consists of stable blast rock and resembles rip rap used to bolster eroding levees and seashores. Only 25% of bed particles are within the reported suitable range of 12-80 mm for spawning Chinook salmon at the EDR compared to nearly 50% at the TBAR. Although one quarter of sediments at the EDR might be available to salmon, this value masks the fact that all recorded gravels were highly angular and thus less suitable for spawning salmonids. All comparisons of sediment classes using the Wilcoxon-Mann-Whitney test had alpha values below 0.05 except for the D_{16} analysis. The reported alpha value was slightly higher than the threshold for rejection (0.057 versus 0.05). Overall, H_1 is rejected due to statistical differences between the study sites and the reduced quantity and quality of spawning gravels within the known preference range of Chinook salmon at the EDR.

The rejection of H_1 suggests that if mitigation goals are to increase habitat in the 1.5 km reach between Englebright and Deer Creek, the issue of sediment deficiency must be resolved. GA will alter the sediment size distribution at the site through direct injection of size sorted gravels from quarries nearby. In this respect GA is a direct manipulation of a channel input that will skew the sediment component of habitat. However, as mentioned above, the simple injection of gravels does not guarantee that habitat conditions will improve; ultimately the in-stream geomorphic processes of entrainment and deposition determine where gravels deposit and whether they form usable spawning habitat.

7.5. Hydraulics

7.5.1. Hypothesis H_2

H_2 is rejected because a velocity reversal associated with an upstream constriction is not observed at the EDR **(Fig. 14)**. Flow convergence routing is focusing high Shields stress over the constricted run across all discharges and keeping Shields stresses over the pools lower. Consequently, injected gravel would never deposit on the high bedrock shelves directly below the two pools in the DEM. These results show that for all modeled flows valley constriction is the dominant geomorphic factor controlling hydraulics and sediment transport in the EDR, and that was also found to be the controlling factor at the TBAR. The lateral constriction at the EDR causes the location of maximum velocity to change little with increasing discharge and produces significant differences in sediment transport between the EDR and TBAR. For example, valley constriction causes Shields stress values in the full transport range (0.06-0.1) to occur at a discharge of 710.7 m^3/s at the EDR but not until somewhere between 998 m^3/s and 3089 m^3/s for the TBAR **(Fig. 17 & Fig. 19)**. From the perspective of GA, the effect of valley constriction on hydraulics and transport at the EDR will cause gravels mobilized upstream of the run to be transported over the topographic controls identified in the DEM and through the run with only minor deposition in micro-scale depositional environments (e.g., boulder shadows).

7.6. Geomorphology

7.6.1. Hypothesis H_3-H_6

In general, Shields stress values above 0.06 ($\tau^* > 0.06$) represent full transport of the channel bed and are expected to produce considerable morphologic change. A significant portion of the channel is not in the full transport regime for the 22.6, 33.7 or 271.3 m^3/s events: H_3 and H_4 are accepted. For the spawning flows, scour and evacuation of particles does not occur and habitat features formed via GA and high-flows will be stable. A biologically important consequence is that redd scour and reduced survival of embryos during frequent low intensity events should not be a management concern. However, morphologic change resulting from GA will alter the location and percent of channel experiencing full transport. Therefore, velocity and Shields stress values after gravel augmentation should be recognized as important factors to consider when limiting the loss of eggs and developing embryos.

Although significant full transport was not predicted for the EDR 271.3 m^3/s event, partial transport covered ~10% of the wetted channel. At this discharge mid-channel habitat will start to degrade under current conditions. Intermittent and partial transport in the run could potentially scour redds in the channel center and poses a major restriction on GA efficacy to be discussed later. To determine the potential risk for redd scour, an investigation that blends the conceptual understanding of Montgomery (1996) and

FESWMS's sediment transport module could provide typical scour depths for any flow and better quantify the effects on salmonids if GA led to mid-channel habitat formation.

Stability of the channel bed during low flows does not infer rehabilitation success and instead brings up the issue of temporal efficacy. If GA proceeds and is followed by extensive low flow periods, habitat features will not form. For instance, current logistical constraints limit gravel additions to the tail of the Narrows II afterbay where intermittent transport is not predicted until discharge exceeds 271.3 m^3/s. This suggests a characteristic lag between the time of investment (injection of gravels) and entrainment that can be approximated by investigating Shields stress in the Narrows pool at lower frequency (higher discharge) events.

During the 900.5 m^3/s (5-year) event, more than 10% of the channel was in the full transport regime. At this discharge, velocities in the Narrows II afterbay are large enough to entrain and transport particles downstream. Therefore, a rough estimate for the lag between injection and significant entrainment is 5 years. Overall, H_5 is rejected at the EDR with the primary location of full transport corresponding to the run section of the channel. Similar to the 271.3 m^3/s discharge, a 5-year event will tend to degrade channel morphology and scour redds in the run. Although H_5 is rejected, full transport is highly localized, and the no, intermittent, and partial transport regimes predicted along channel edges suggests margin areas are less susceptible to scour.

With over 52% of the channel in the full transport class at a discharge of 2588.2 m^3/s (24-year event), H_6 is rejected. The consequences to habitat are more extreme than the 5-year event and overall augmented gravels can be expected to move as a carpet along the resistant bed. An event equal or exceeding this magnitude would pose a serious concern for incubating eggs or larval fish residing within gravel interstices. The rejection of H_5 and H_6 suggest spawning habitat formed in the channel center should not be a rehabilitation priority.

7.6.2. Hypothesis H_7

Historical photos near EDR before the construction of Englebright Dam elicit valuable information about the underlying geomorphic character of the site and provide a starting point for evaluating system response to GA. For instance, although a large amount of sediment, ~522 million m^3 from the South Yuba alone, was forced into the Yuba as a consequence of hydraulic mining, the site lacks large deposits or bars of exposed gravel and cobbles in the 1909 photo **(Fig. 20)**. This suggests transport capacity at the EDR was not lacking before the construction of Englebright and that the reach was supply limited even with the flux of hydraulic mine debris. The hydrologic event analysis furnished above **(Fig. 4)** and the corresponding Shields stress predictions for the modeled discharges suggest the EDR will continue to operate as a supply limited reach.

The sediment deposition patterns depicted in **Fig. 20** have profound consequences on GA efficacy in at the EDR and other bedrock channels. Instead of widespread aggradation in riffle and run sequences, gravel deposition will preferentially occur in conjunction with resistant bed-forms and boulder particles. For example, at the EDR the underlying topography and roughness elements create localized areas of upwelling and lateral vortices that facilitate deposition much like the site shown in Gilbert's 1909 image. This finding agrees with the concept of "nested depositional features" proposed by McBain (2004) and "gravel beaches" by Wohl (1998). Originally, McBain (2004) suggested these features were deterministically organized by the dominant flow regime, however in reality stochasticity likely plays a larger role. Overall, the available historical images indicate that heterogeneous patterns of deposition and habitat, correlated to underlying topographical control, will occur after GA.

Comparing historical and current images can further clarify the possible response of the channel to GA. **Figure 22A** and **22B** represent ~100 years of change in the reach directly below EDR. Prior to the completion of Englebright, coarse substrate was ubiquitous between what is now the Narrows I powerhouse and Deer Creek. A large pool and riffle sequence with underlying gravel substrate dominateed the Deer Creek confluence. Despite an increase in valley width downstream of the EDR, which may have contributed to aggradation, the comparison suggests an underlying behavior of the channel. As upper watershed sediment inputs were cut off, the remaining stream power of the Yuba River gradually evacuated hydraulic mine sediments from the site. The entrainment and deposition of blast rock depicted in **Fig. 21** over the time period signifies an innate high transport capacity that will certainly distribute augmented gravels downstream.

The post Englebright estimated sediment transport numbers for the EDR and TBAR provide another insight regarding system response to GA. The estimations should not serve as goals for mitigation efforts that if reached will elicit permanent habitat improvements at the site. The EDR gravel budget of 47124 m^3/yr and volumetric differencing at the TBAR of 19984 m^3 for the 24-year event reflect inputs of hydraulic mine debris that increased delivery of sediments to channels throughout the Sierra Nevada. Consequently each number is likely an overestimation of natural sediment delivery. Instead the numbers should serve as reference for overall channel transport capacity to conjure and analyze mitigation objectives. For example GA on the scale of 47124 m^3/yr would cost roughly 1.2 million dollars annually in washed gravel assuming the same material and delivery price of $14/ton as projects on the Mokelumne River, Ca. This high cost, (especially since it does not include transportation and injection) suggests that matching augmentation to pre-dam volumetric delivery would be a costly objective to pursue given the risk of gravels vacating the site in a single year.

The cost of matching channel inputs to sediment transport estimations underscores the importance and necessity of pilot gravel injections and adaptive management. Small GA projects like the one completed in the fall of 2007 at the EDR can test modeling predictions of transport and deposition against habitat development through pre and post project assessments. For instance, although Shields stress predictions suggest that mid-channel habitat will preferentially deteriorate at the EDR, subsequent deposition on riffle sequences downstream of the study site might create habitat over longer temporal scales that only continuous monitoring can capture. If this is the case, the investment of 1.2 million dollars per year may be a viable option to pursue.

A final comparison of Shields stress values in the EDR spawning channel against transport processes at the TBAR provides further evidence that extensive cross channel habitat will not develop at the EDR. Shields stress patterns in **Fig. 24** show the channel mid-section is the most active part of the site and that for all flows, once entrainment begins in the pool, particles will funnel through pool tail and run sections. Without an upstream sediment source and dynamic Shields stress distribution, riffle habitat that forms at the tail of the Narrows II pool and in the channel center will not be stable and will rapidly degrade. This is in sharp contrast to the TBAR, where a significant source of sediment for maintenance of topographical relief exists and dynamic transport process scours pools and deposits sediments near the riffle crest during high flows. This fundamental difference suggests that habitat formation at the EDR is not dominated by flow convergence routing and an associated velocity reversal. Therefore, the transport dominated character of the bedrock EDR will prohibit large scale aggradation in the spawning channel and H_7 is rejected.

From a management perspective two broad conclusions regarding GA efficacy can be drawn from these results. First, mitigation measures aimed at increasing spawning habitat at the EDR should focus on channel margin areas and the depositional features where natural processes promote gravel deposition. The second conclusion is that habitat formed via GA will be spatially limited due to the patchy and heterogeneous character of depositional features in bedrock canyon channels.

7.7. Habitat

7.7.1. Hypothesis H_8

Historical data of spawning on the Yuba river includes the general locations and physical barriers to migrating salmonids (Yoshiyama et al., 1998). Although extremely valuable, the literature provides little information about specific spawning activity at the project site investigated in this study. In general, salmonids prefer to spawn in homogeneous lower gradient gravel-bed channels, however, micro scale heterogeneity (10^0-10^1 channel widths) is important and provides a range of hydraulic conditions for spawning, resting, and juvenile rearing. Kondolf (1991) investigated the spawning habitat of brown trout (*Salmo trutta*) and rainbow trout (*Onchorhynchus mykiss*) in boulder-bed channels of the eastern Sierra Nevada. Although the research was not on Chinook salmon habitat, the conclusions drawn from that study are similar to those encountered at the EDR. Kondolf (1991) found that highly localized patches of habitat formed near natural hydraulic controls or roughness elements in the channel that promoted sediment deposition. Given the distribution of sediment particles in historical images and Shields stress predictions, spawning at the EDR was likely limited to similar highly localized areas. Therefore, both the geomorphic and ecologic evidence suggests widescale spawning at the EDR did not occur; H_8 is rejected.

The observations of successful Chinook spawning near the EDR in the 1970s and 1980s and of brown and rainbow trout by Kondolf (1991) both represent the ability of salmonid species to locate and utilize patchy habitat features in bedrock systems. In the Yuba River example, hydraulic mining provided ample sediments to fill localized depositional zones and likely increased habitat suitability. Successive flood events have since degraded the depositional features and explain the complete lack of observed redds in over fifteen visits to the EDR spanning the 2005 and 2007 spawning seasons. GA will reconnect the sediment component of channel inputs, and restore some of the patchy depositional features in the channel.

7.7.2. Hypothesis H_9

Model predicted habitat at the two project sites differed quantitatively and qualitatively. The large proportion of good and excellent quality areas at the TBAR (~34% of area) and a lack of redd superposition issues suggests that spawning habitat is not limiting there. However, at the EDR less than 3% of the channel was within the same good and excellent quality suitability classes (based on hydraulics alone) and therefore H_9 is rejected; spawning habitat at the EDR is severely limited. Given the vast differences of channel response to increasing discharge, bed mobility (Shields stress), sediment input, and large scale topographic control between the EDR and TBAR, one cannot assume that the proportion of suitable habitat should be similar at the two sites (Buffington et al., 2004). The quantitative comparison is most useful in that it shows the differing capacity of each site to harbor spawning and serves as a baseline value of habitat at the EDR prior to any rehabilitation efforts.

By breaking spawning habitat into two general groups at each site, one associated with riffle entrances and the other with margin habitat, a distinct difference in the proportion of habitat types is apparent. Good and excellent habitat at the TBAR is dominated by riffle entrances while at the EDR all good and excellent quality habitat can be attributed to margin zones parallel to the channel edge where the combination of edge topography and water depth create suitable hydraulic conditions. Depths within the channel center and pool exits are too great given the low velocity values predicted with the model. Therefore, suitable spawning habitat was only predicted within two meters of the channel margin. Shields stress predictions suggest that alluvial deposition is most likely to occur along and adjacent to these channel margins where depth is currently limiting spawning habitat. Any alluvial deposition that occurs along channel margins may increase overall spawning habitat via a decrease in depth and increase in velocity at the EDR. Interestingly, similarly sized (<1m) strips of margin habitat exists at the TBAR where riffle entrance habitat is not limiting and redd surveys have confirmed the ability of Chinook salmon to utilize these narrow strips. This suggests that if the issue of sediment size and depth limitations within margin zones at the EDR could be resolved, spawning activity would be promoted on a localized scale.

8. CONCLUSION

The precipitous decline of anadromous fish species throughout the Pacific Northwest is widely attributable to hydrologic, geomorphic, and ecologic discontinuities. GA has been a successful rehabilitation technique in many regulated gravel bed rivers and its extension to bedrock canyon channels has been investigated herein. The efficacy of GA is a complex function of channel hydraulics, sediment supply/transport, local topographic control, and high flow events in regulated systems.

For the bedrock canyon channel at the EDR, the underlying transport dominated character, as evidenced through Shields stress predictions and the remaining dynamic flow regime, will have two overarching impacts on augmentation efficacy. First, it guarantees augmented gravels will be distributed downstream with intermittent transport of particles predicted near the 5-year event discharge. Second, and most importantly, valley wall constrictions and depositional features dominate deposition processes and force velocity and Shields stress values to their maximums near the channel thalweg for all modeled scenarios. This will suppress the formation of cross channel gravel riffles that begin to scour during relatively frequent (Q_2 and Q_5) events. Instead of creating riffle spawning habitat, GA in the bedrock canyon channel at the EDR will likely produce patchy heterogeneous habitat along channel margins and recirculation zones where depositional features impact local hydraulics.

Overall, small scale GA at the bedrock dominated EDR is not expected to significantly increase the proportion of channel available for spawning salmon despite the small (1 m^2) localized zones of habitat that are likely to form. Unlike gravel-bed rivers directly below impoundments, where the creation of macro-scale bed features such as riffles and spawning beds have been highly successful, such features are not promoted in the active bedrock channel investigated here. However, small scale habitat features that result from gravel augmentation may be disproportionately important to the endangered spring-run Chinook salmon that have had historic spawning areas cut off by impoundments. To determine if augmented gravels increase spawning habitat at the EDR or form macro-scale habitat features (e.g., riffles) outside of the EDR domain, the continued monitoring of injected gravels and salmon utilization along the 1.5 km reach below Englebright Dam is recommended.

9. REFERENCES

Banks, M.A., Rashbrook, V.K., Valavetta, M.J., Dean, C.A. and Hedgecock, D., 2000. Analysis of microsatellite DNA resolves genetic structure and diversity of chinook salmon *(Oncorhynchus tshawytscha)* in California's Central Valley. Canadian Journal Fisheries and Aquatic Sciences, 57: 915-927.

Baxter, R.M., 1977. Environmental Effects of Dams and Impoundments. Annual Review of Ecology and Systematics, 8: 255-283.

Bernhardt, E.S. et al., 2005. Synthesizing U.S. River Restoration Efforts. Science, 308.

Brandt, S.A., 2000. Classification of Geomorphological Effects Downstream of Dams. Catena, 40: 375-401.

Brown, A.V., Lyttle, M.M. and Brown, K.B., 1998. Impacts of Gravel Mining on Gravel Bed Streams. Transactions of the American Fisheries Society, 127: 979-994.

Brown, R.A. and Pasternack, G.B., 2008. Engineered Channel Controls Limiting Spawning Habitat Rehabilitation Success on Regulated Gravel-bed Rivers. Gemorphology, 97: 631-654.

Buffington, J.M., Montgomery, D.R. and Greenberg, H.M., 2004. Basin-scale Availability of Salmonid Spawning Gravel as Influenced by Channel Type and Hydraulic Roughness in Mountain Channels. Canadian Journal Fisheries and Aquatic Sciences, 61: 2085-2096.

Bunn, S.E. and Arthington, A.H., 2002. Basic Principles and Ecological Consequences of Altered Flow Regimes for Aquatic Biodiversity. Environmental Management, 30(4): 492-507.

Bunte, K., 2004. State of the Science Review, Gravel Migration and Augmentation Below Hydroelectric Dams : A Geomorphological Perspective, USDA Forest Service, Fort Collins, CO.

Cada, G.F. and Sale, M.J., 1993. Status of Fish Passage Facilities at Nonfederal Hydropower Projects. Fisheries, 18(7): 4-12.

CDFG, 1991. Lower Mokelumne River Fisheries Mangement Plan, California Department of Fish and Game. Resource Agency, Sacramento, California.

CDWR, 1992. Project Report: Sacramento River Spawning Gravel Restoration Phase 1, California Department of Water Resources. Northern District.

CDWR, 2006. Upper Yuba River Watershed Chinook Salmon and Steelhead Habitat Assessment Technical Report. Upper Yuba River Studies Program Study Team.

Chow, V.T., 1959. Open-channel hydraulics. McGraw-Hill, New York, 680 pp.

Collier, M., Webb, R.H. and Schmidt, J.C., 1996. Dams and River: Primer on the Downstream Effects of Dams. Circular 1126, U.S. Geological Survey, Menlo Park, CA.

Crisp, D.T., 1987. Thermal ' Resetting ' of Streams by Reservoir Releases with Special Reference to Effects on Salmonid Fishes. Regulated Streams: Advances in Ecology. Plenum Press, New York, p 163-182 pp.

Ebbersole, J.L., Liss, W.J. and Frissell, C.A., 1997. Restoration of Stream Habitats in the Western United States: Restoration as Reexpression of Habitat Capacity. Environmental Management, 21(1): 1-14.

Elkins, E.M., Pasternack, G.B. and Merz, J.E., 2007. Use of Slope Creation for Rehabilitating Incised, Regulated, Gravel Bed Rivers. Water Resources Research, 43(W05432): 16.

Emmett, W.W. and Wolman, G.M., 2001. Effective Discharge and Gravel-Bed Rivers. Earth Surface Processes and Landforms, 26: 1369-1380.

Freeman, G.E., Rahmeyer, W.H. and Copeland, R.R., 2000. Determination of Resistance Due to Shrubs and Woody Vegetation, U.S. Army Core of Engineers Technical Report. ERCD/CHL TR-00-25.

Friedman, J.M., Osterkamp, W.R., Scot, M.L. and Auble, G.T., 1998. Downstream Effects of Dams on Channel Geometry and Bottomland Vegetation:Regional Patterns in the Great Plains. Wetlands, 18(4): 619-633.

Froehlich, D.C., 2002. Finite Element Surface-Water Modeling Systems: Two-dimensional Flow in a Horizontal Plane--Users Manual. Federal Highway Administration Report FHWA-RD-88-177, pp. 285.

Ghanem, A., Steffler, P., Hicks, F. and Katopodis, C., 1996. Two-Dimensional hydraulic simulation of physical habitat conditions in flowing streams. Regulated Rivers:Research and Management, 12: 185-200.

Giest, D.R. and Dauble, D.D., 1998. Redd Site Selection and Spawning Habitat use by fall Chinook salmon: the importance of Geomorphic features in large rivers. Environmental Management, 22(5): 655-669.

Graf, W.L., 1999. Dam Nation: A geographic census of American dams and their large-scale hydrologic impacts. Water Resources Research, 35(4): 1305-1311.

Grant, G., Burkholder, B., Jefferson, A., Lewis, S. and Haggerty, R., 2006. Hyporheic Flow, temperature anomalies, and gravel augmentation: Preliminary findings of a field investigation on the Clackamas River, Oregon, Pacific Northwest Research Station (USFS) and Oregon State University.

Groot, C. and Margolis, L., 1991. Pacific salmon life histories. University of British Columbia Press, Vancouver, Canada.

Harper, D., Ebrahimnezhad, M. and Cot, F.C.I., 1998. Artificial riffles in river rehabilitation: setting the goals and measuring the successes. Aquatic Conservation-Marine and Freshwater Ecosystems, 8(1): 5-16.

Heil, R.J. and Brych, S.M., 1978. An approach for consistent topographic representation of varying terrain, American Society of Photgrammetry: Digital Terrain Models Symposium, St. Louis, Missouri, pp. 397-411.

Horritt, M.S., Bates, P.D. and Mattinson, M.J., 2006. Effects of mesh resolution and topographic representation in 2D finite volume models of shallow water fluvial flow. Journal of Hydrology, 329(1-2): 306-314.

Ipson, M.K., 2006. Analysis of the Sediment Transport Capabilities of FESWMS FST2DH. Maters Thesis, Brigham Young University, Provo.

Ivlev, V.W. (Editor), 1961. Experimental Ecology of the feeding of fishes. Yale University Press, New Haven, 302 pp.

James, A., 2002. Late Pleistocene Glaciations in the Northwestern Sierra Nevada, California. Quaternary Research, 57(3): 409-419.

James, A., 2005. Sediment from hydraulic mining detained by Englebright and small dams in the Yuba basin. Geomorphology, 71(1-2): 202-226.

James, A., 2007. Yuba River Aerial Imagery 1937-1952. Personal Communication.

Keller, E.A., 1971. Areal Sorting of bed-load material: the hypothesis of velocity reversal. Geological Society of America Bulletin, 82: 723-756.

Kondolf, G.M., and Li, S., 1992. The Pebble Count Technique for Quantifying Surface Bed Material Size in Instream Flow Studies. Rivers, 3(80-87).

Kondolf, G.M., and M.G. Wolman, 1993. The sizes of salmonid spawning gravels. Water Resources Research, 29: 2275-2285.

Kondolf, G.M., and M.G. Wolman, 1998. Lessons learned from river restoration projects in California. Aquatic Conservation: Marine and Freshwater Ecosystems, 8: 39-52.

Kondolf, G.M., Cada, G.F., Sale, M.J. and T., F., 1991. Distribution and Stability of Potential Salmonid Spawning Gravels in Steep Boulder-Bed Streams of the Eastern Sierra Nevada. Transactions of the American Fisheries Society, 120(2): 177-186.

Kondolf, G.M., Larson, M., 1995. Historical channel analysis and its application to riparian and aquatic habitat restoration. Aquatic Conservation: Marine and Freshwater Ecosystems, 5(2): 109-126.

Kondolf, G.M., M.W. Smeltzer, Railsback, 2001. Design and Performance of a Channel Reconstruction Project in a Coastal California Gravel-Bed Stream. Environmental Management, 28(6): 761-766.

Kondolf, M.G., 1997. Hungry Water: Effects of dams and gravel mining on river channels. Environmental Management, 21(4): 533-551.

Kondolf, M.G., 2004. Coarse sediment augmentation on the Trinity river below Lewiston dam: Geomorphic perspectives and review of past projects.

Kulpa, J., 2006. Environmental Data Solutions. Personal Communication.

Lee, J., 1991. Comparison of existing methods for building triangular irregular network models of terrain from grid digital elevation models. International Journal of Geographic Information Systems, 5(3): 267-285.

Ligon, F.K., Dietrich, W.E. and Trush, W.J., 1995. Downstream Ecological Effects of Dams. Bioscience, 45(3): 183-192.

Lisle, T.E., Nelson, J.M., Pitlick, J., Madej, M.A. and Barkett, B.L., 2000. Variability of bed mobility in natural, gravel-bed channels and adjustments to sediment load at local and reach scales. Water Resources Research, 36(12): 3743-3755.

MacWilliams, M.L., Wheaton, J.M., Pasternack, G.B., Street, R.L. and Kitanidis, P.K., 2006. Flow convergence routing hypothesis for pool-riffle maintenance in alluvial rivers. Water Resources Research, 42(W10427).

McBain, S. and Trush, B., 2004. Attributes of Bedrock Sierra Nevada River Ecosystems. U.S. Department of Forest Service.

Merz, J.E., Chan, Leigh H. Ochikubo, 2005. Effects of gravel augmentation on macroinvertebrate assemblages in a regulated California river. River Research and Applications, 21(1): 61-74.

Merz, J.E., Pasternack, G. B., Wheaton, J. M., 2006. Sediment Budget for Salmonid Spawning Habitat Rehabilitation in the Mokelumne River. Geomorphology, 76(1-2): 207-228.

Merz, J.E., Setka, J.D., Pasternack, G.B. and Wheaton, J.M., 2004. Predicting benefits of spawning-habitat rehabilitation to salmonid (Oncorhynchus spp.) fry production in a regulated California river. Canadian Journal of Fisheries and Aquatic Sciences, 61(8): 1433-1446.

Mesick, C., 2002. Knights Ferry Gravel Replenishment Project. Project # 97-N21, Cal Fed Bay Delta Program.

Miller, A.J. and Cluer, B.L., 1998. Modeling considerations for simulation of flow in bedrock channels. In: Rivers over rock: fluvial processes in bedrock channels. American Geophysical Union Monograph #107, Washington, DC.

Minear, T.J. and Kondolf, G.M., 2006. Gravel Augmentation for Salmon Habitat Below Dams in Northern California. Presentation.

Moir, H.J. and Pasternack, G.B., 2008. Relationships between mesoscale morphological units, stream hydraulics and Chinook salmon (Oncorhynchus tshawytscha) spawning habitat on the Lower Yuba River, California. Geomorphology.

Montgomery, D.R., 2000. Coevolution of the Pacific Salmon and Pacific Rim Topography. Geological Society of America Bulletin, 28(12): 1107-1110.

Montgomery, D.R., Buffington, J.M., Peterson, P.N., Schuett-Hames, D. and Quinn, T.P., 1996. Stream-bed scour, egg burial depths, and the influence of salmonid spawning on bed surface mobility and embryo survival. Canadian Journal Fisheries and Aquatic Sciences, 53: 1061-1070.

Mullican, R., 2007. Personal Communication, Private Landowner and Yuba County Resident.

Paintal, A.S., 1971. Concept of critical shear stress in loose boundary open channels. Journal of Hydraulic Research, 9(1): 91-113.

Pasternack, G.B., Gilbert, A., Wheaton, J.M. and Buckland, E., 2006. Error Propagation for velocity and shear stress prediction using 2 D models for environmental management. Journal of Hydrology, 328(1-2): 227-241.

Poff, L.N. et al., 1997. The Natural Flow Regime: A paradigm for river conservation and restoration. Bioscience, 47(11): 769-784.

Power, M.E., Dietrich, W.E. and Finlay, J.C., 1996. Dams and downstream aquatic biodiversity: potential food web consequences of hydrologic and geomorphic change. Environmental Management, 20: 887-895.

Rameshwaran, P. and Shiono, K., 2003. Computer modelling of two-stage meandering channel flows, Proceedings of the Institution of Civil Engineers - Water and Maritime Engineering, pp. 325-339.

Rathburn, S. and Wohl, E., 2003. Predicting fine sediment dynamics along a pool-riffle mountain channel. Geomorphology, 55: 111-124.

Richter, B.D., and G. A. Thomas, 2007. Restoring environmental flows by modifying dam operations. Ecology and Society, 12(1): 12.

Richter, B.D., Baumgartner, J.V., Powell, J. and Braun, D.P., 1996. A Method for Assessing Hydrologic Alteration within Ecosystems. Conservation Biology, 10(4): 1163-1174.

Richter, B.D., Baumgartner, Jeffrey V., Powell, Jennifer, and Braun, David, P., 1997. How much water does a river need? Freshwater Biology, 37: 231-249.

Rosgen, D.L., 1985. A Stream Classification System, First North American Riparian Conference, Tucson, AZ, pp. 91-95.

Scruton, D.A., 1996. Evaluation of the construction of artificial fluvial salmonid habitat in a habitat compensation project, Newfoundland, Canada. Regulated Rivers-Research & Management, 12(2-3): 171-183.

Slater, D.W., 1963. Winter-run Chinook salmon in the Sacramento River, California with notes on water temperature requirements at spawning., U.S. Fish and Wildlife Service, Washington, D.C.

Snyder, N.P. and Rubin, D.M., 2004. Estimating accumulation rates and physical properties of sediment behind a dam: Englebright Lake, Yuba River, northern California. Water Resources Research, 40.

Stanford, J.A. et al., 1996. A general protocol for restoration of regulated rivers. Regulated Rivers:Research and Management, 12: 391-413.

Talbert, T., 1999. Yuba Goldfields Fish Barrier Project:Preliminary Engineering Report, California Department of Water Resources, Yuba County, CA.

USGS, 2006. U.S. Geological Survey Photographic Library, http://libraryphoto.cr.usgs.gov/photo_all.htm.

Wang, C.L., Pasternack, G.B. and Merz, J.E., 2004. Application of a 2-D Hydraulic Model to Reach-scale Spawning Gravel Rehabilitation. River Research and Applications, 20(2): 205-225.

Ward, J.V. and Stanford, J.A., 1995. Ecological connectivity in alluvial rivers and its disruption by flow regulation. Regulated Rivers:Research and Management, 11: 105-119.

Wheaton, J.M., Pasternack, G.B. and Merz, J.E., 2004a. Spawning Habitat Rehabilitation-II. Using Hypothesis Testing and Development in Design, Mokelumne River , CA USA. International Journal of River Basin Management, 2: 21-37.

Wheaton, J.M., Pasternack, G.B., Merz, J.E., Garcia de Jalon Lastra, D. and Martinez, P.V., 2004b. Use of habitat heterogeneity in salmonid spawning habitat rehabilitation design, Fifth International Symposium on Ecohydraulics, Aquatic Habitats: Analysis & Restoration, Madrid, pp. 791-796.

Wheaton, J.M., Pasternack, G.B., Merz, Joseph, 2004. Spawning habitat rehabilitation-1 Conceptual approach and methods. International Journal River Basin Management, 2(1): 3-20.

Whipple, K.X., 2001. Fluvial landscape response time: How plausible is steady-state denudation? American Journal of Science, 301(4-5): 313-325.

Williams, G.P. and Wolman, G.M., 1984. Downstream effects of dams on alluvial rivers. U.S. Department of the Interior, Geological Society, Professional Paper #1286.

Wohl, E. et al., 2005. River Restoration. Water Resources Research, 41.

Wohl, E. and Tinkler, K.J., 1998. A Primer on Bedrock Channels. In: Rivers over rock: fluvial processes in bedrock channels. Geophysical Monograph Series #107

Wolman, M.G., 1954. A Method of Sampling Coarse River-bed Material. Transactions of the American Geophysical Union, 35: 951-956.

Yoshiyama, R.M., Moyle, P.B. and Fisher, F.W., 1998. Historical Abundance and Decline of Chinook Salmon in the Central Valley Region of California. North American Journal of Fisheries Management, 18(3): 487-521.

Zeh, M. and Donni, W., 1994. Restoration of Spawning Grounds for Trout and Grayling in the River High-Rhine. Aquatic Sciences, 56(1): 59-69.

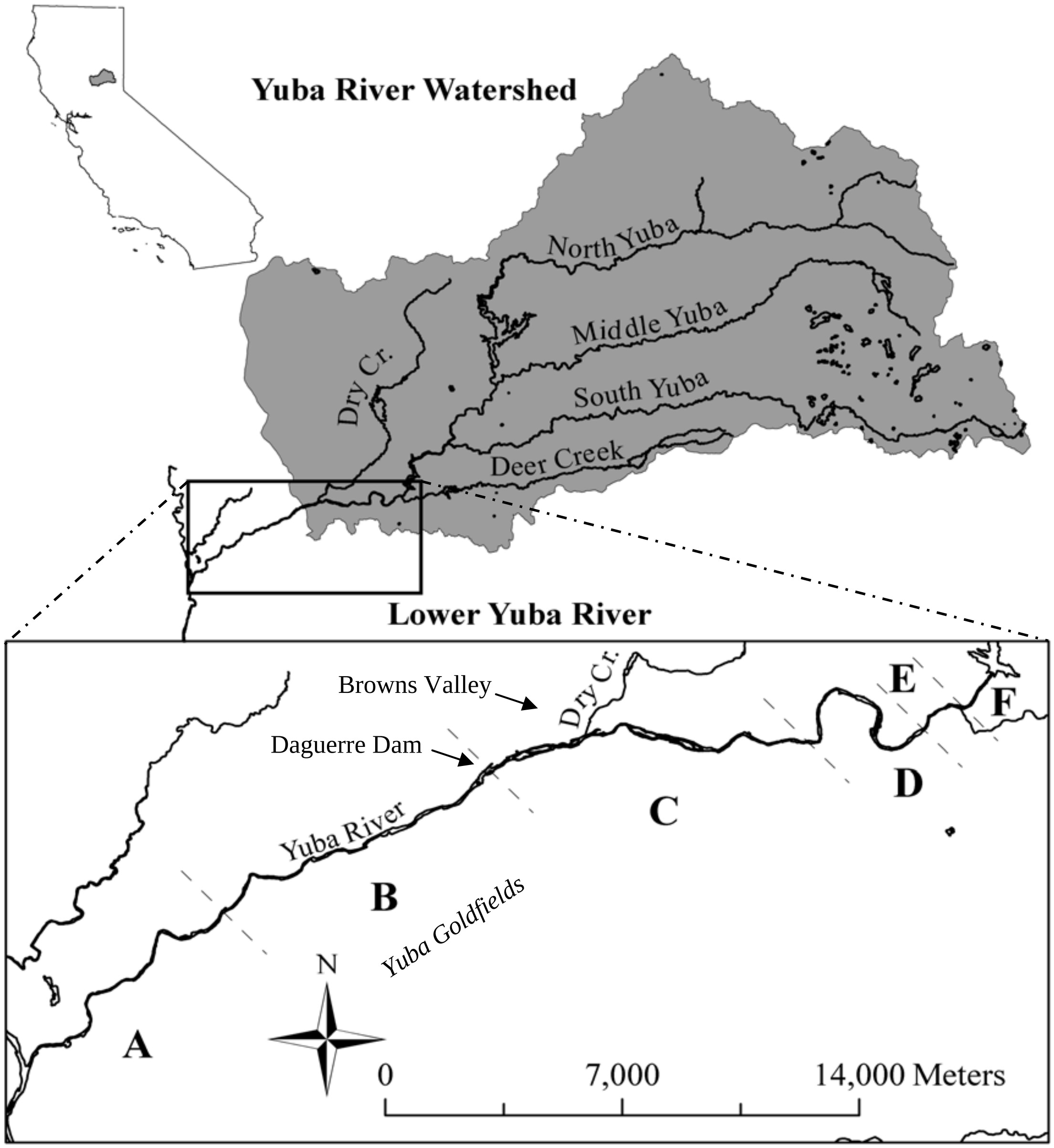

Figure 1. The Yuba River watershed and its tributaries are located on the western slope of California's northern Sierra Nevada Mountain Range (top). The six sections of the Lower Yuba River include A) the Simpson Lane, B) Daguerre Dam, C) Highway 20, D) Timbuctoo Bend, E) Narrows, and F) Englebright Dam reaches (bottom).

Hydrograph Alterations of the Yuba River, CA

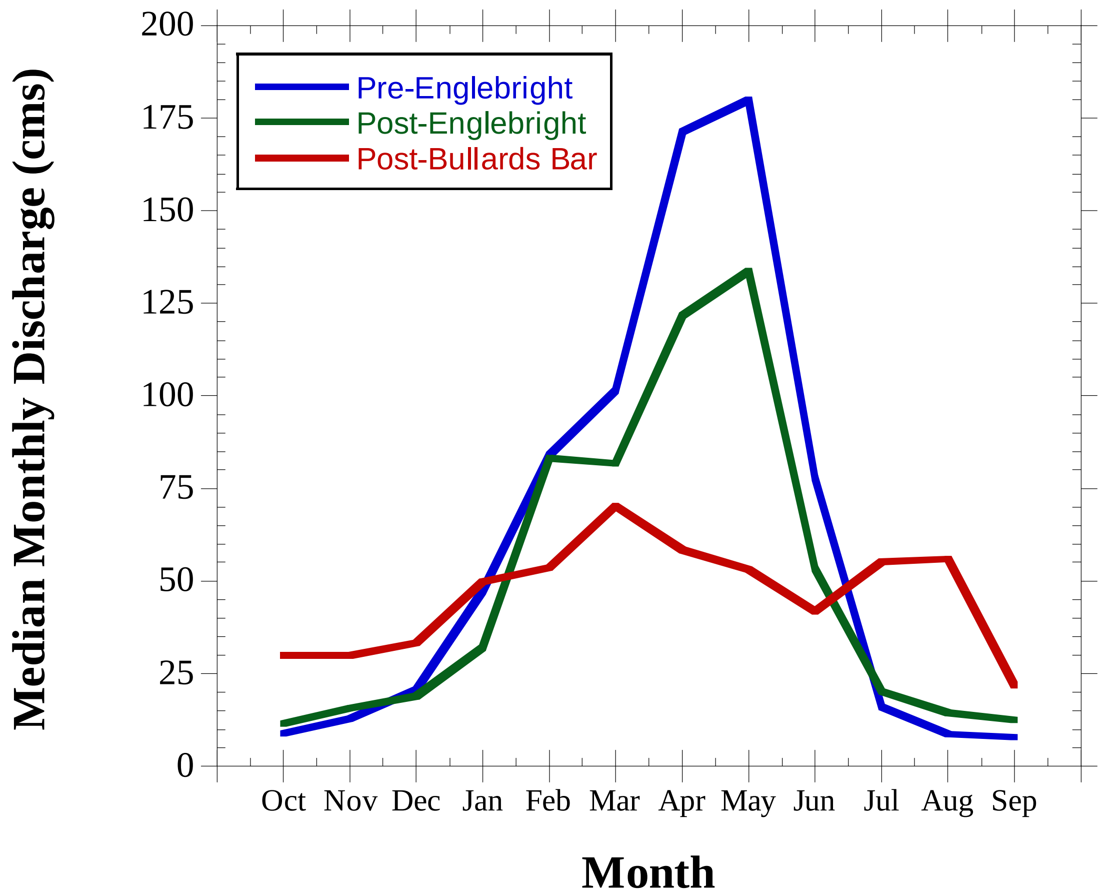

Figure 2. Median monthly discharge for the Smartville gages (#11418000 and #11419000) during the three major hydrologic periods spanning 1904-2006.

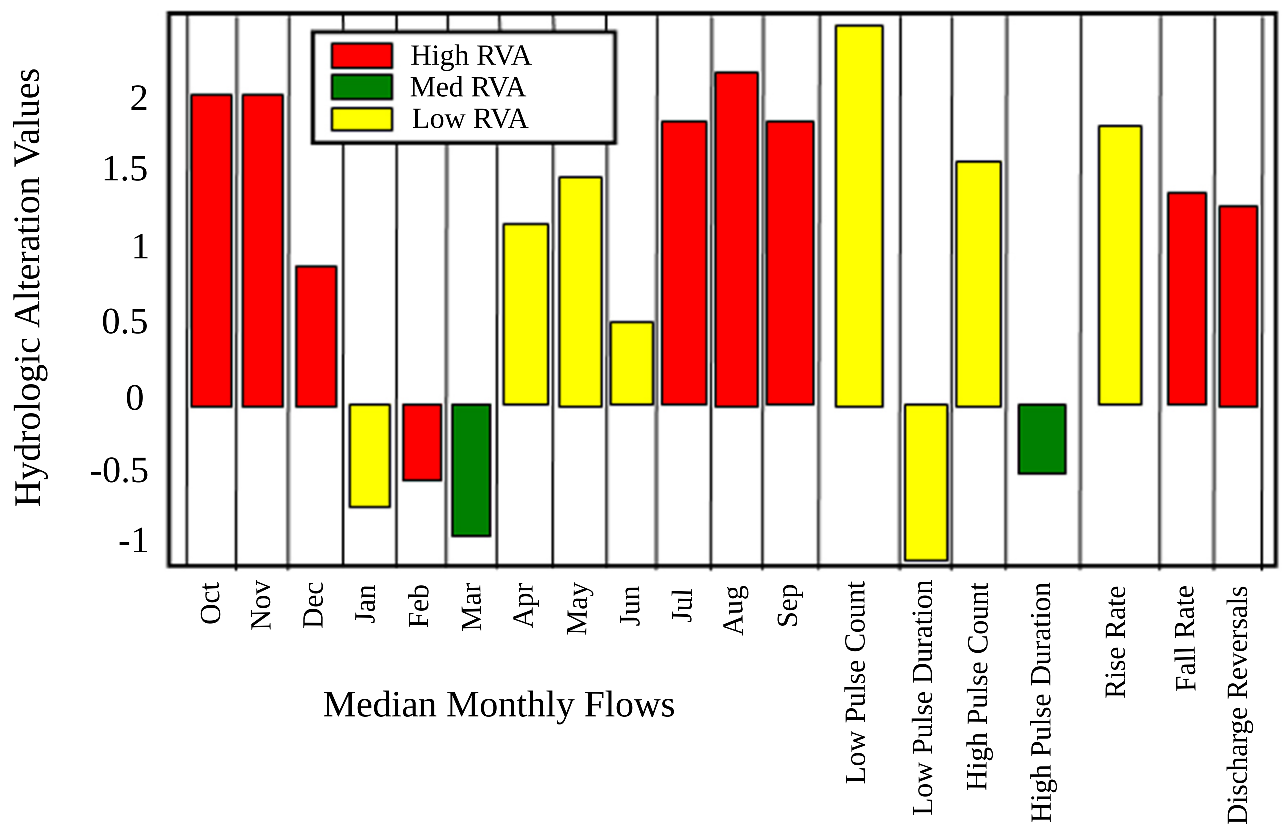

Figure 3. Output from the non-parametric form of Indicators of Hydrologic Alteration (Richter, 1996) using Yuba river discharge data before and after the construction of New Bullards Bar Dam.

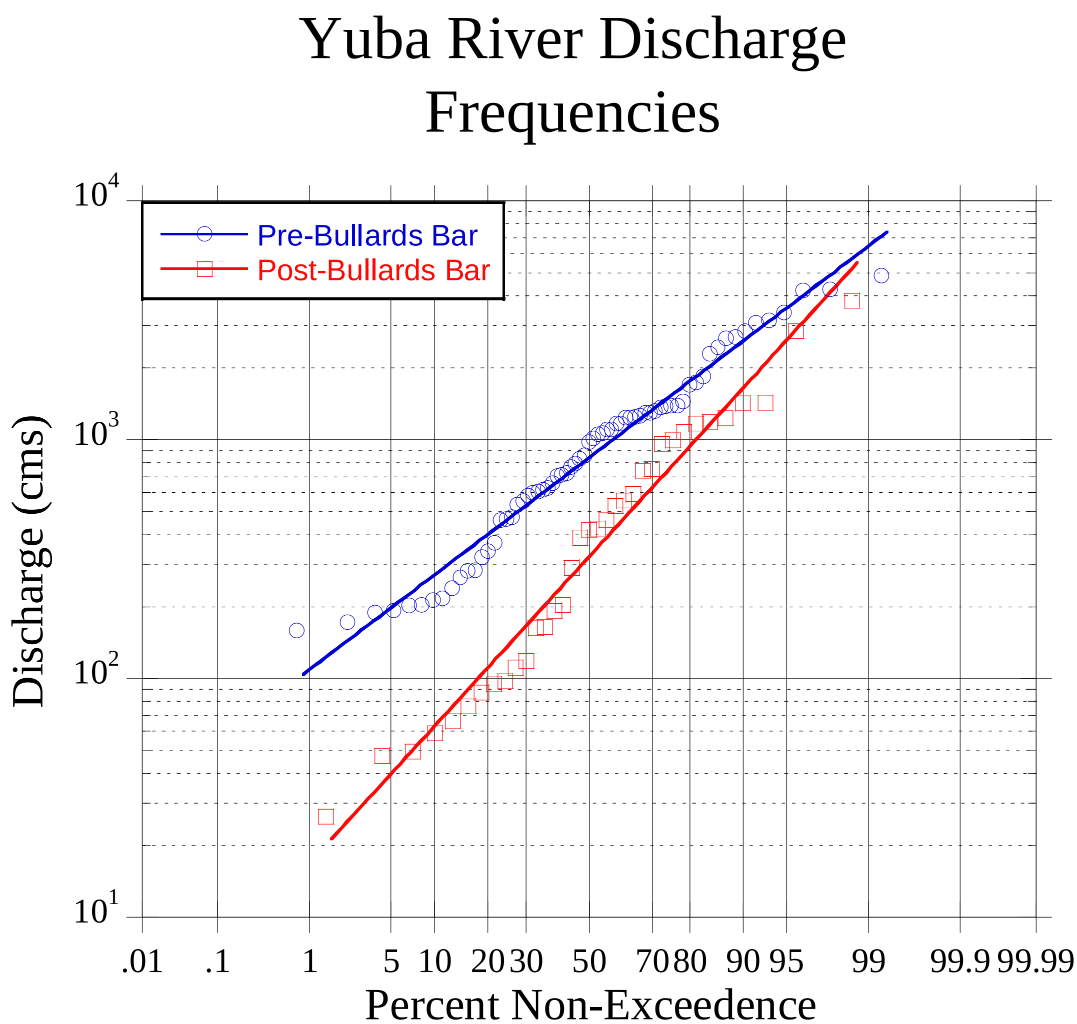

Figure 4. Reduction in annual peak discharge frequencies following the construction of New Bullards Bar Dam.

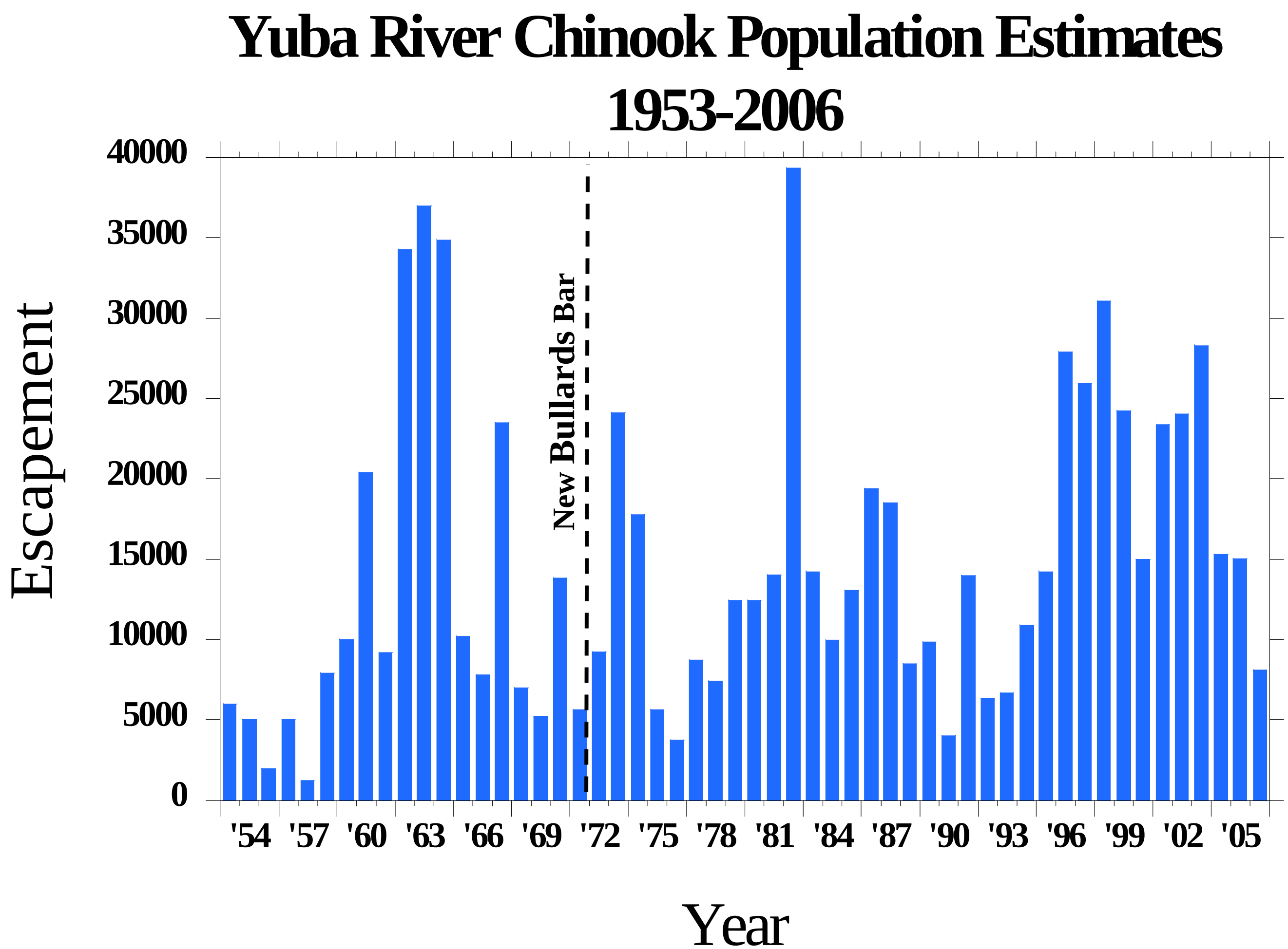

Figure 5. Inter-decadal fluctuations of Chinook salmon escapement on the Yuba River, CA between 1953 and 2006.

A)

B)

Figure 6. The bedrock channel EDR below Englebright dam at ~33.7 cms (A) and the gravel-bed TBAR reach at a discharge of ~22.5 cms (B). The coarse floodplain at the EDR is composed of rock blasted from surrounding hillsides during the construction of Englebright. The gravel bed TBAR site lacks large clusters of blast rock and is composed of alluvial hydraulic mine debris.

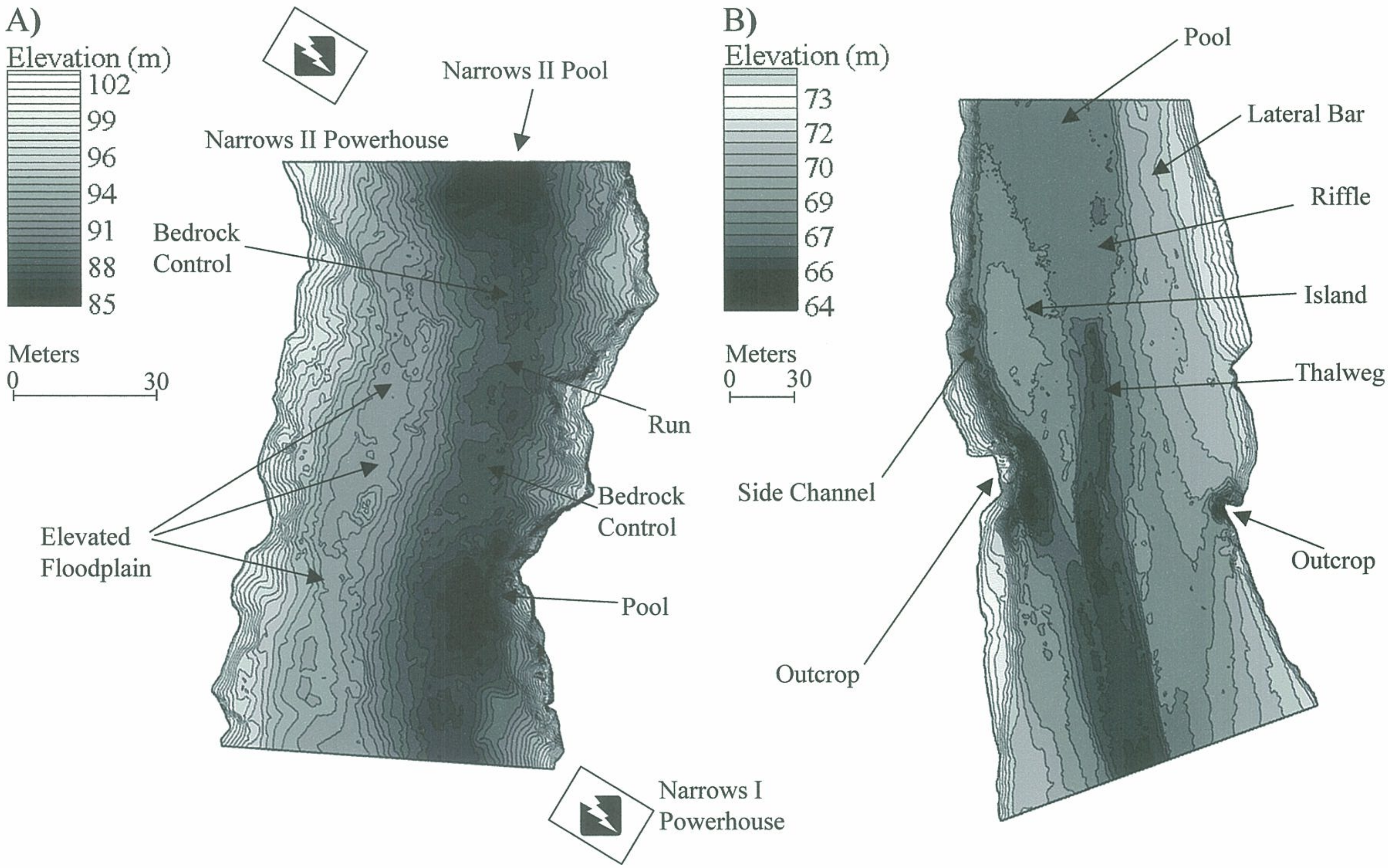

Figure 7. Digital elevation maps of A) the confined bedrock channel at the EDR and B) the alluvial TBAR on the Yuba River, CA. Contour intervals represent 0.5 meters.

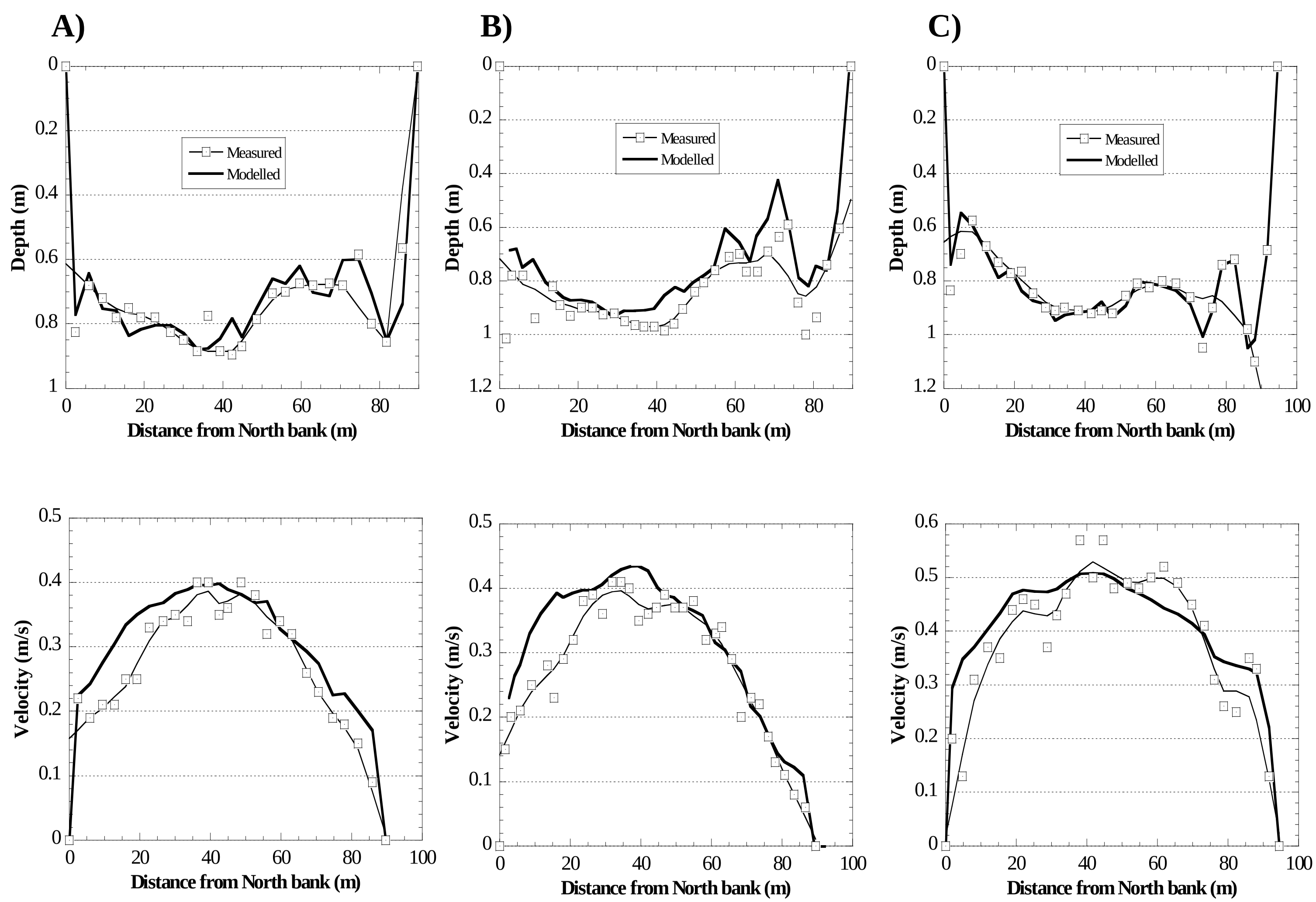

Figure 8. Field measurements and model predictions of depth and velocity at three cross sections during an A) 18.40 cms, B) 21.15 cms, and C) 31.18 cms discharge event at the TBAR site.

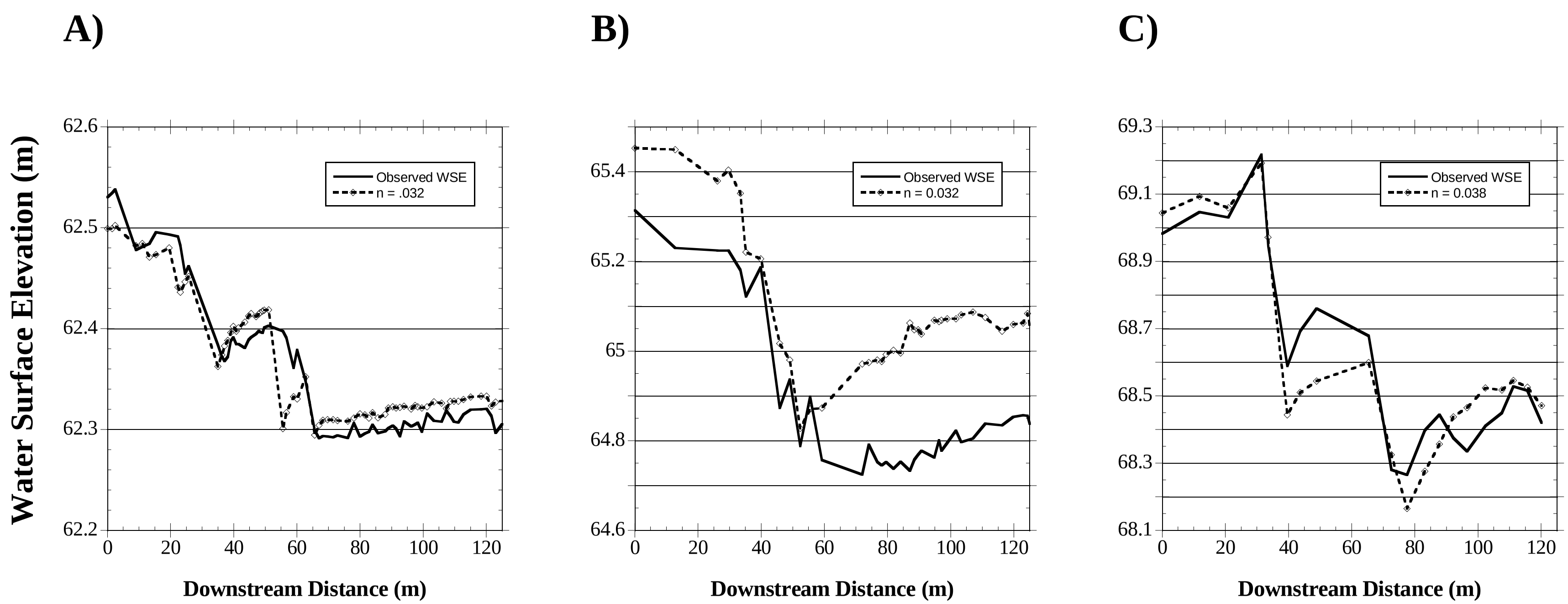

Figure 9. Measured and modeled water surface profiles for the A) 33.7 cms B) 271.3 cms, and C) 900.5 cms discharge events at the EDR. Datum corresponds to most upstream water surface elevation point measured in the field.

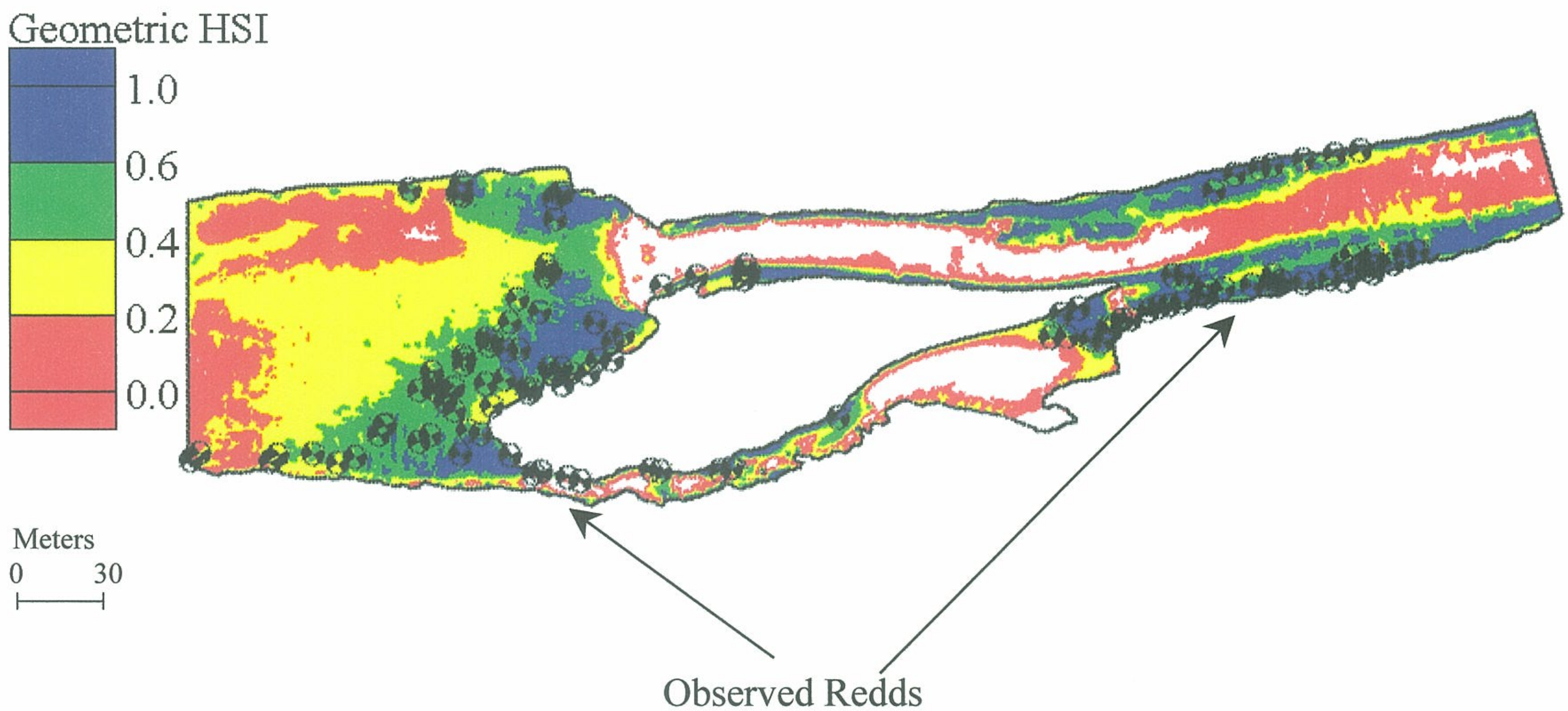

Figure 10. The spatial distribution of model predicted GHSI values and field observed redds for the 21.1 cms discharge at the TBAR.

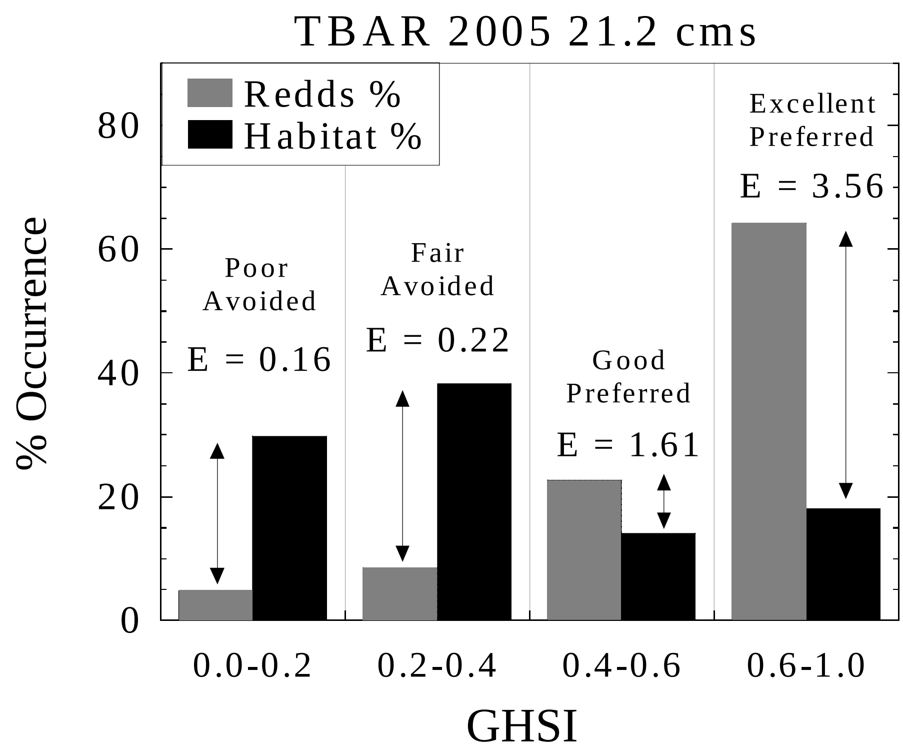

Figure 11. The percent of observed redds and model predicted habitat in each of the GHSI classes at the 2005 TBAR. Redds were observed at flows near ~22 cms and the modeled discharge for habitat predictions was 21.2 cms.

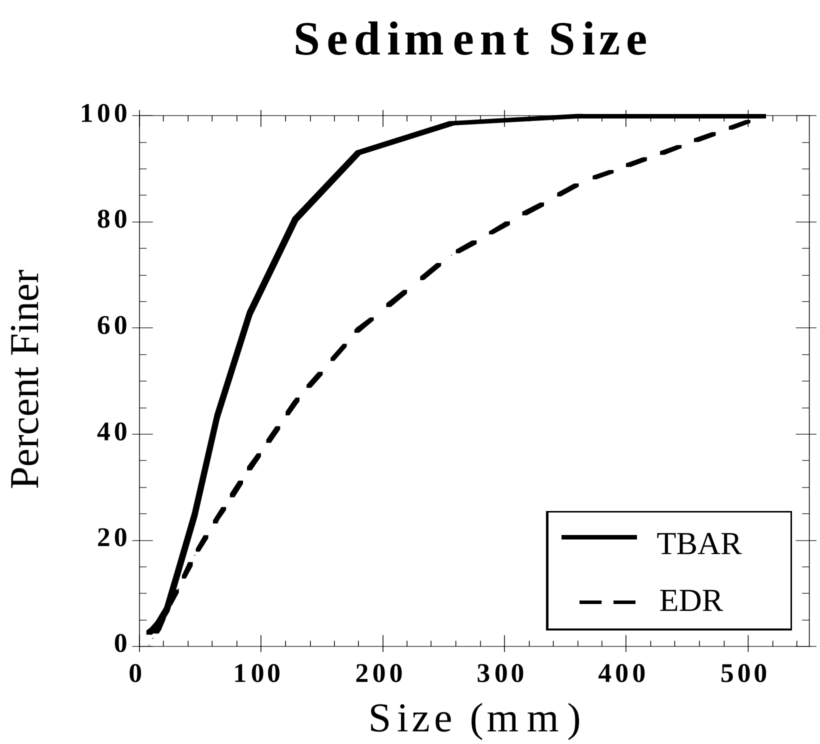

Figure 12. Cumulative frequency plot of pebble counts at the TBAR and EDR.

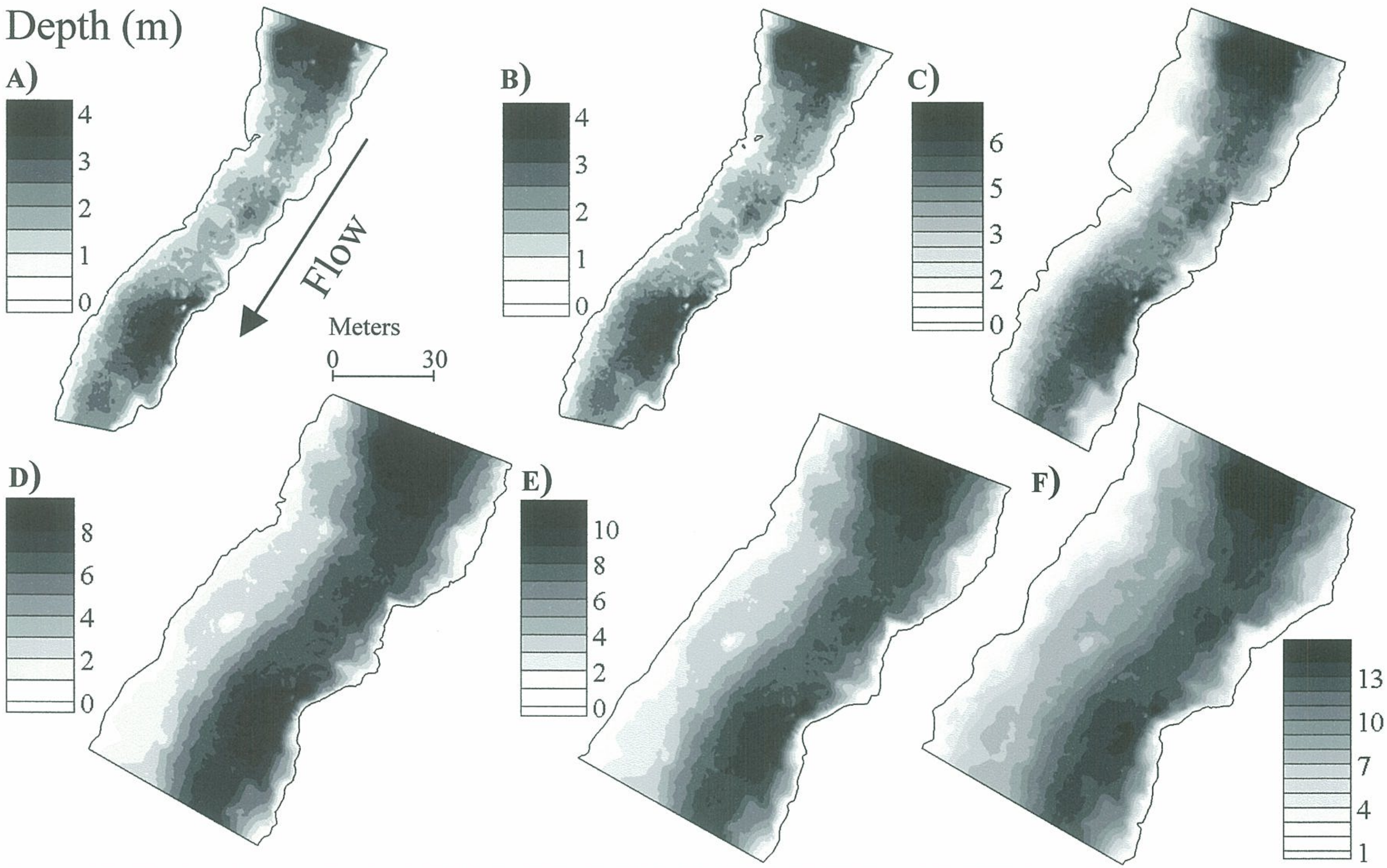

Figure 13. Depth predictions for the A) 22.7, B) 33.7, C) 271.3, D) 710.7, E) 900.5, and F) 2588.2 cms discharge events at the EDR.

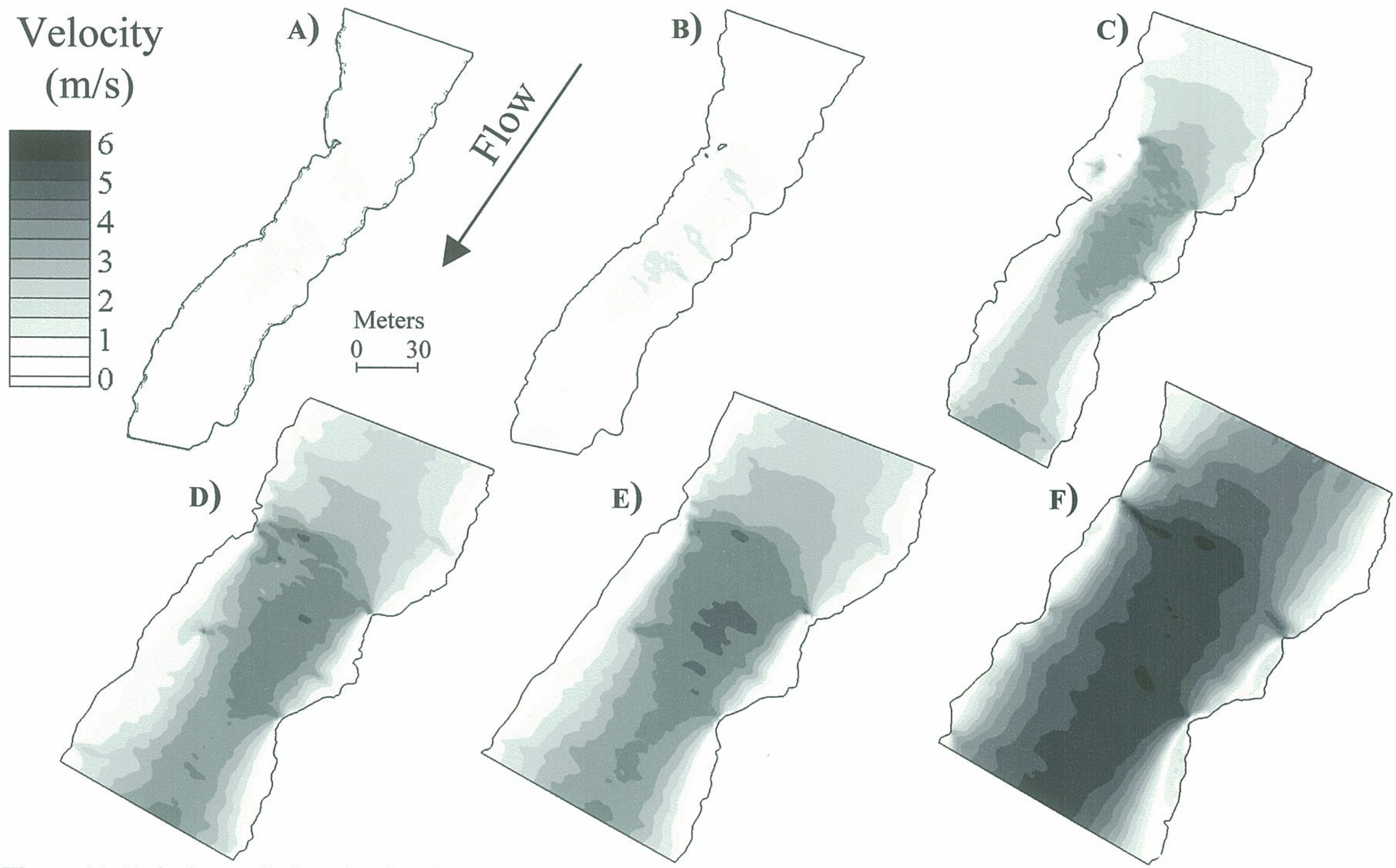

Figure 14. Velocity predictions for the A) 22.7, B) 33.7, C) 271.3, D) 710.7, E) 900.5, and F) 2588.2 cms discharge events at the EDR.

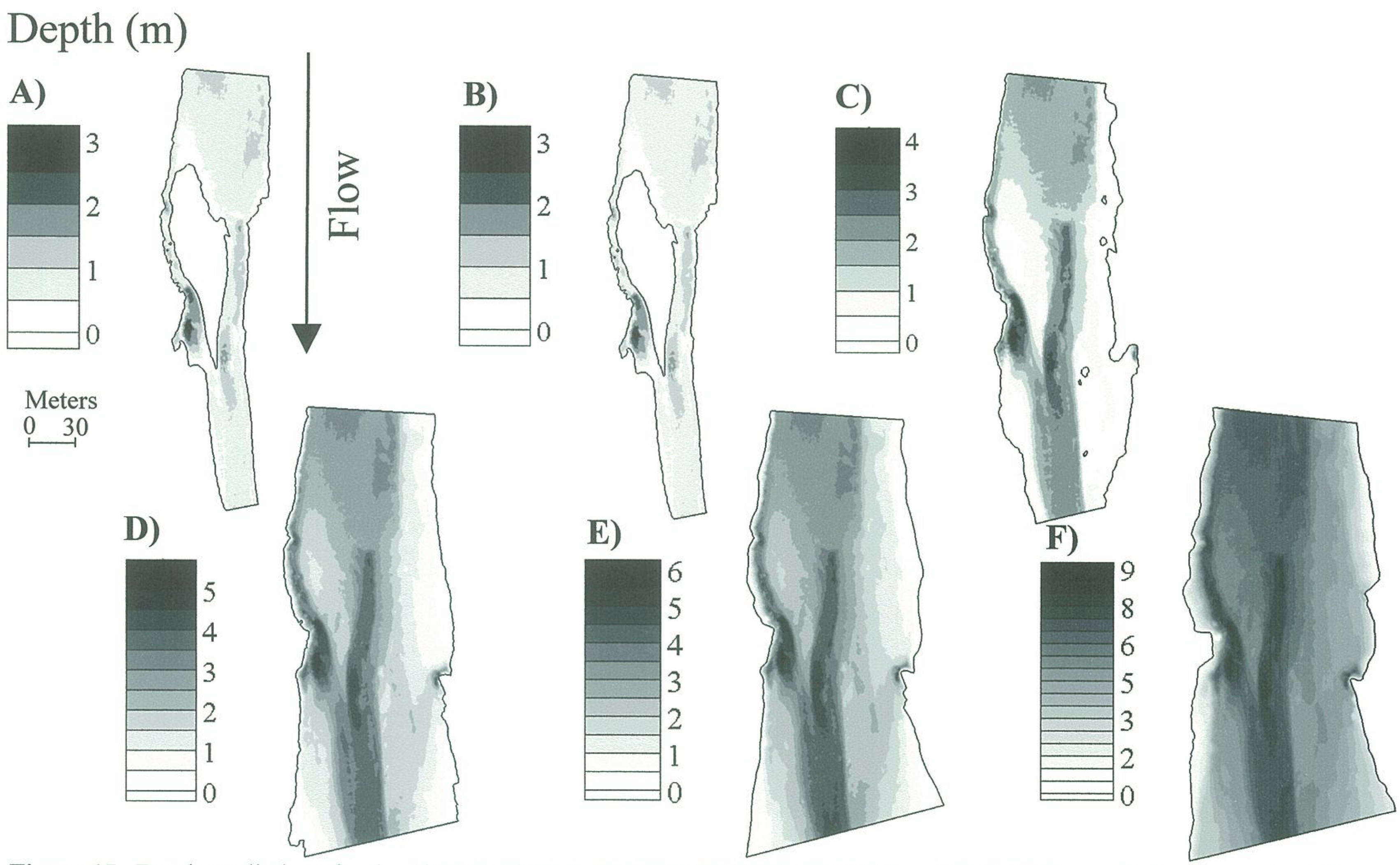

Figure 15. Depth predictions for the A) 21.2, B) 34.6, C) 267.8, D) 655.3, E) 998.4, and F) 3089.2 cms discharge events at the TBAR.

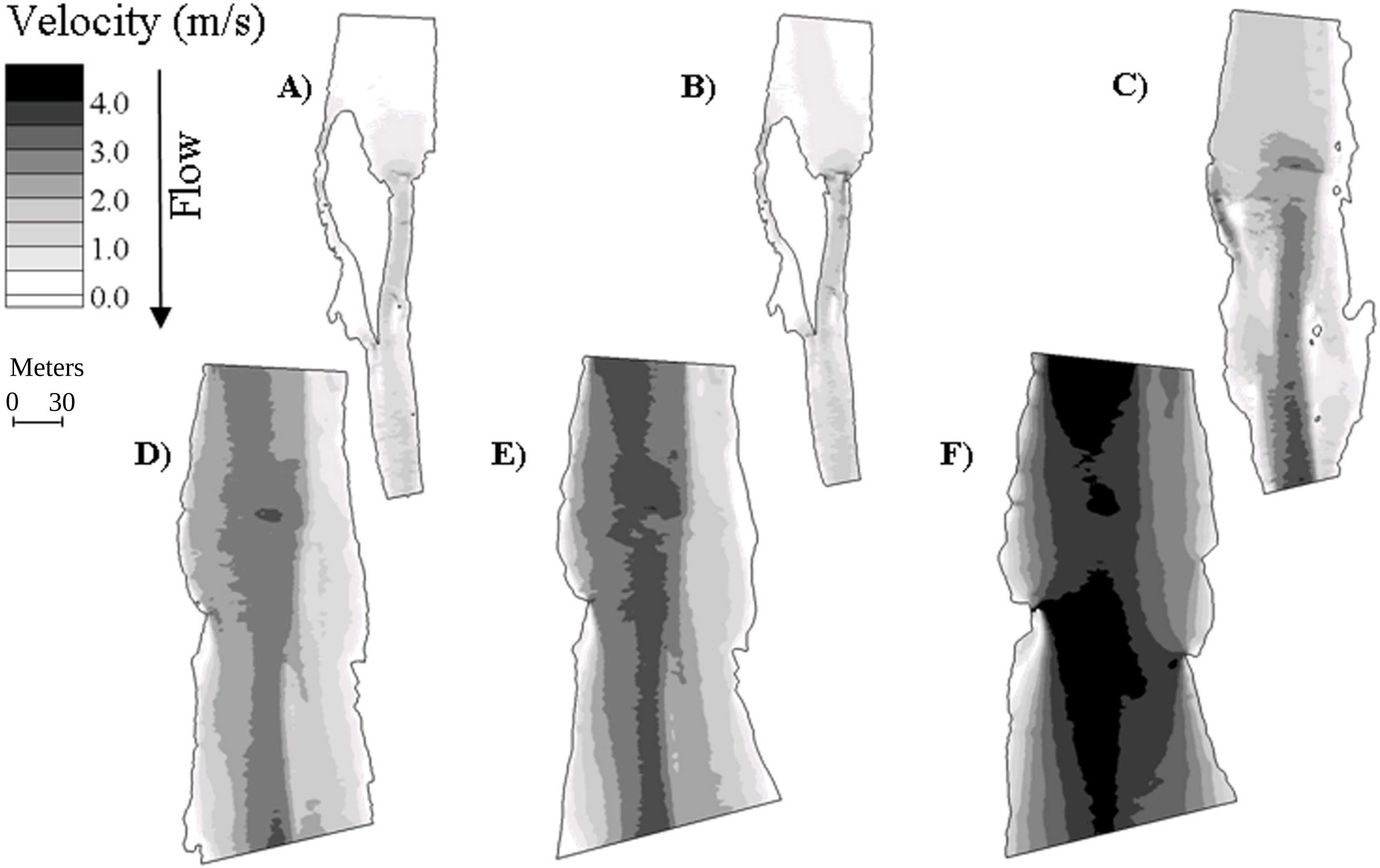

Figure 16. Velocity predictions for the A) 21.2, B) 34.6, C) 267.8, D) 655.3, E) 998.4, and F) 3089.2 cms discharge events at the TBAR.

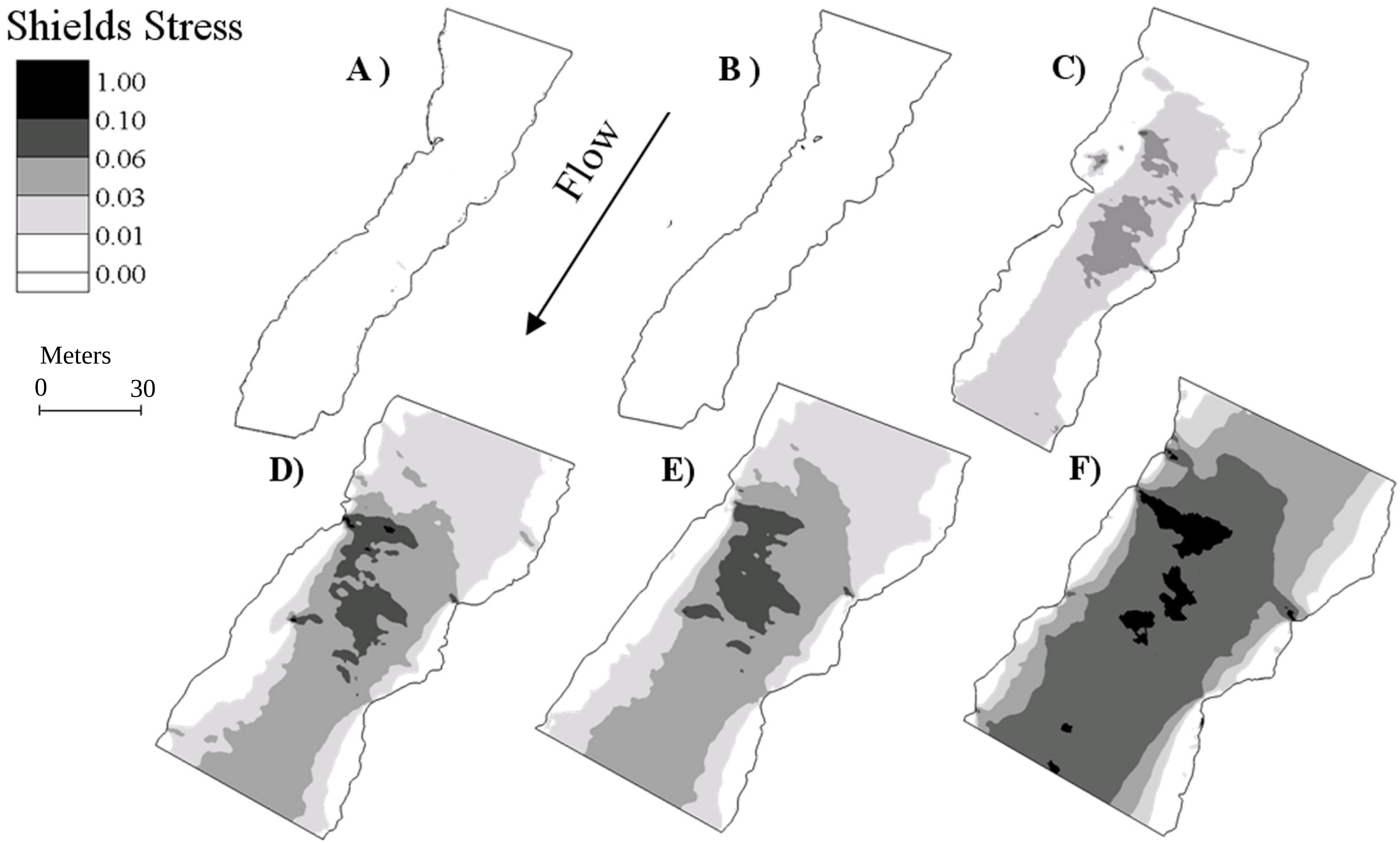

Figure 17. Shields stress predictions for the A) 22.7, B) 33.7, C) 271.3, D) 710.7, E) 900.5, and F) 2599.2 cms discharge events at the EDR.

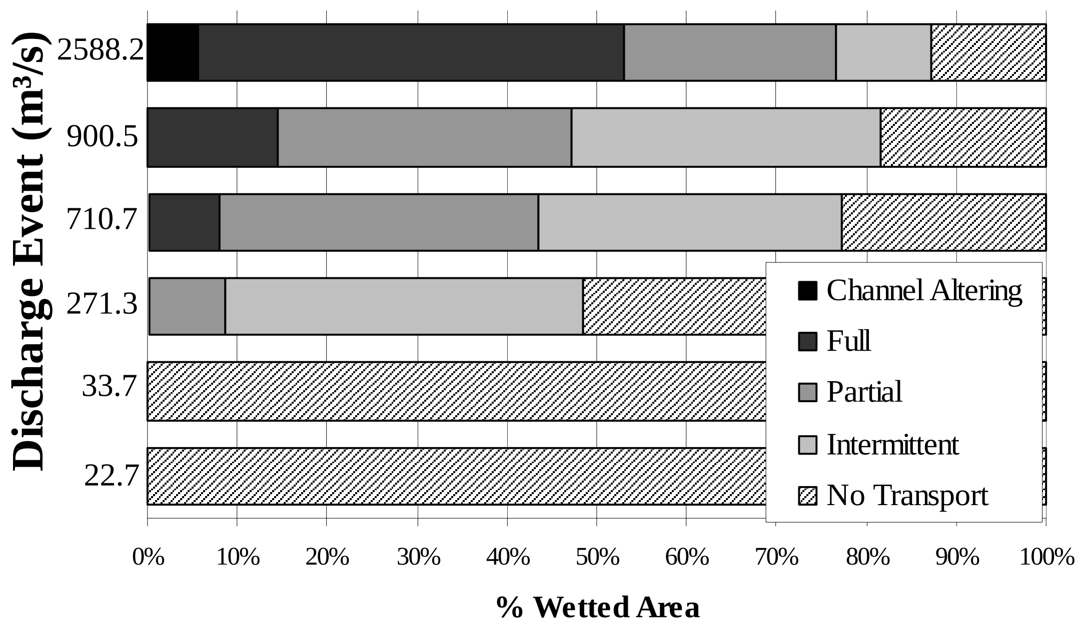

Figure 18. Percent of wetted channel area in representative Shields stress classes at the EDR for all modeled flow scenarios.

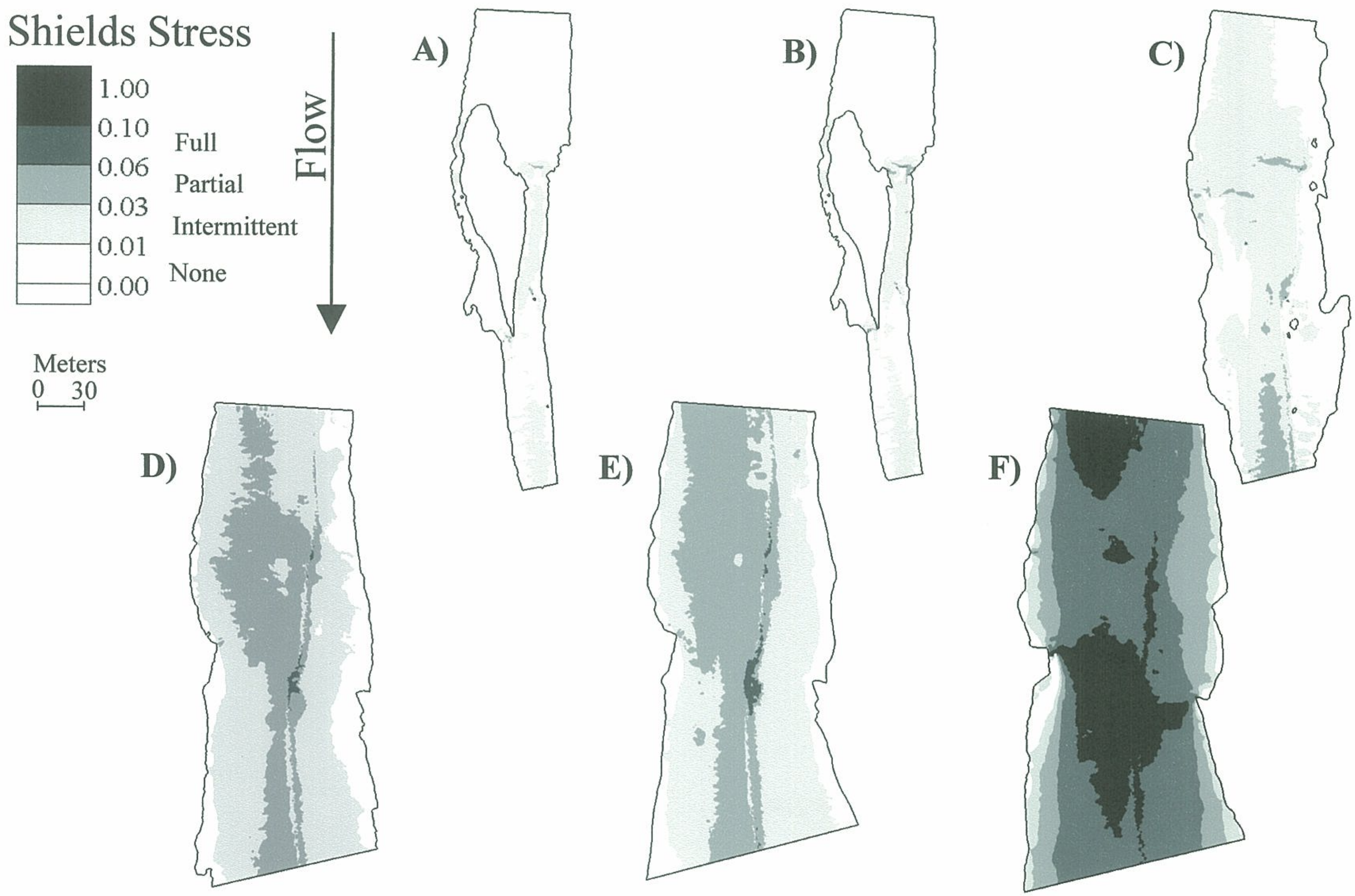

Figure 19. Shields' stress predictions for the A) 21.2, B) 34.6, C) 267.8, D) 655.3, E) 998.4, and F) 3089.2 m³/s discharge events at the TBAR.

Figure 20. Historical photograph of the main-stem Yuba River 0.4 km upstream of the EDR study site (G.K. Gilbert; *USGS, 1909)*. Note presence of small riffle on river left, and localized deposits of sediment clustered near bedrock and roughness elements along channel margins (river right).

Figure 21. A steam shovel, dump truck, and five wagon drills razed the weathered canyon hillsides on July 25th 1939 at the EDR. Large quantities of rock were stockpiled to support construction roads along channel margins and were later transported during high flow events (Courtesy: USACE, 2006).

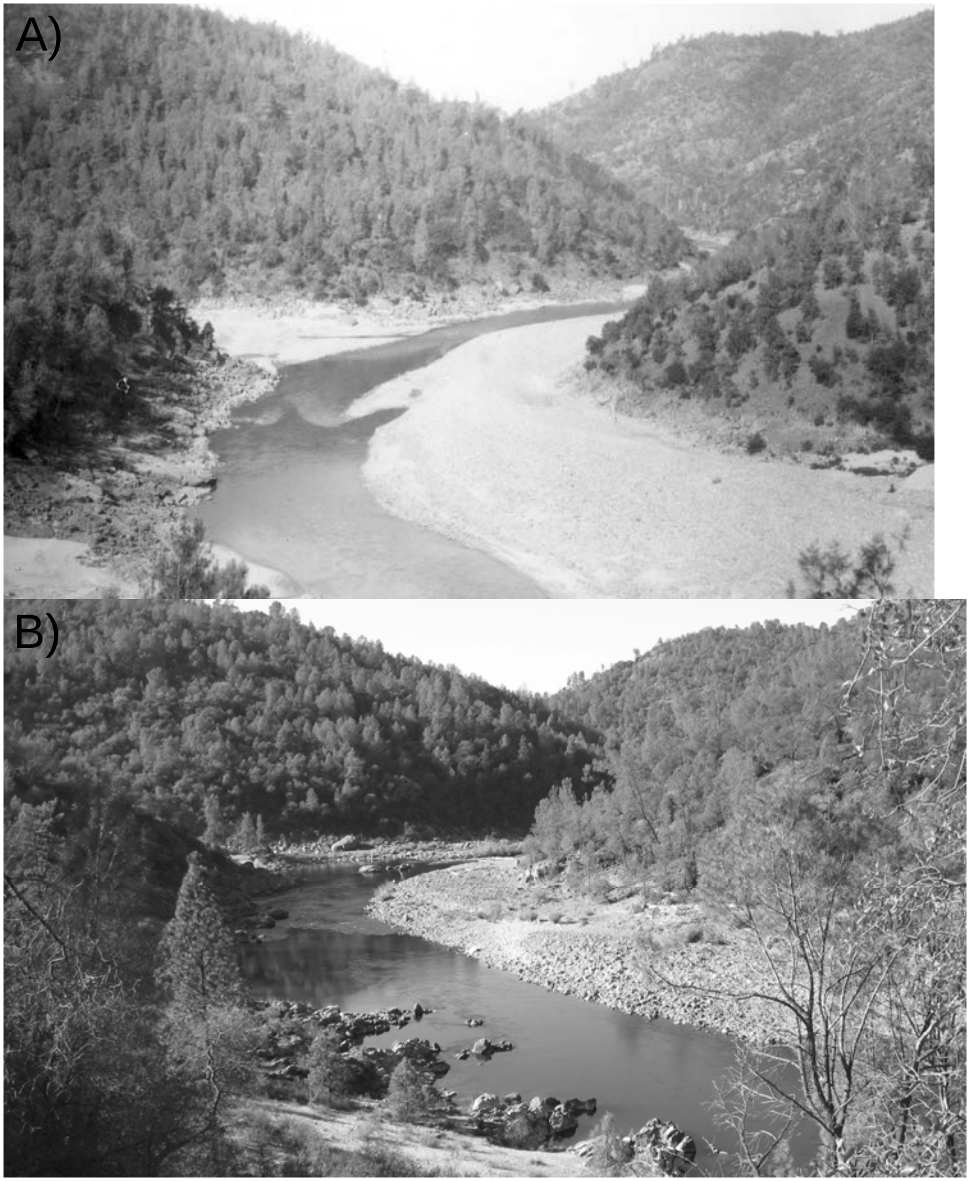

Figure 22. Imagery obtained by G.K. Gilbert of the Deer Creek confluence in 1909 (A) and a recent photo in 2006 (B) of the same location. Both images are located ~ 0.5 km downstream of the EDR where Deer Creek joins the mainstem Yuba River.

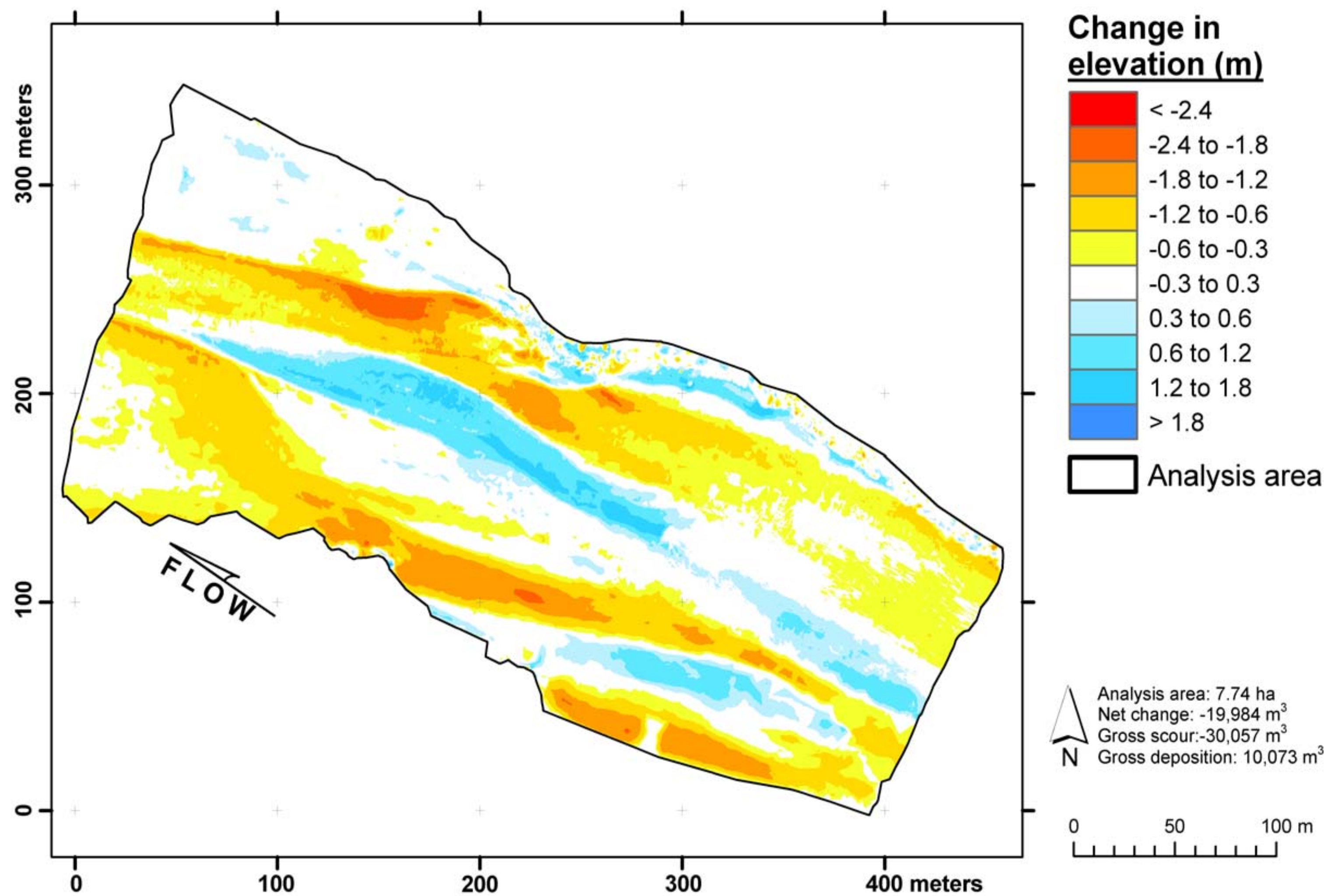

Figure 23. Patterns of scour depths (negative values) and fill heights (positive values) at the TBAR following the 3089 cms event. (Figure produced by S. Morford)

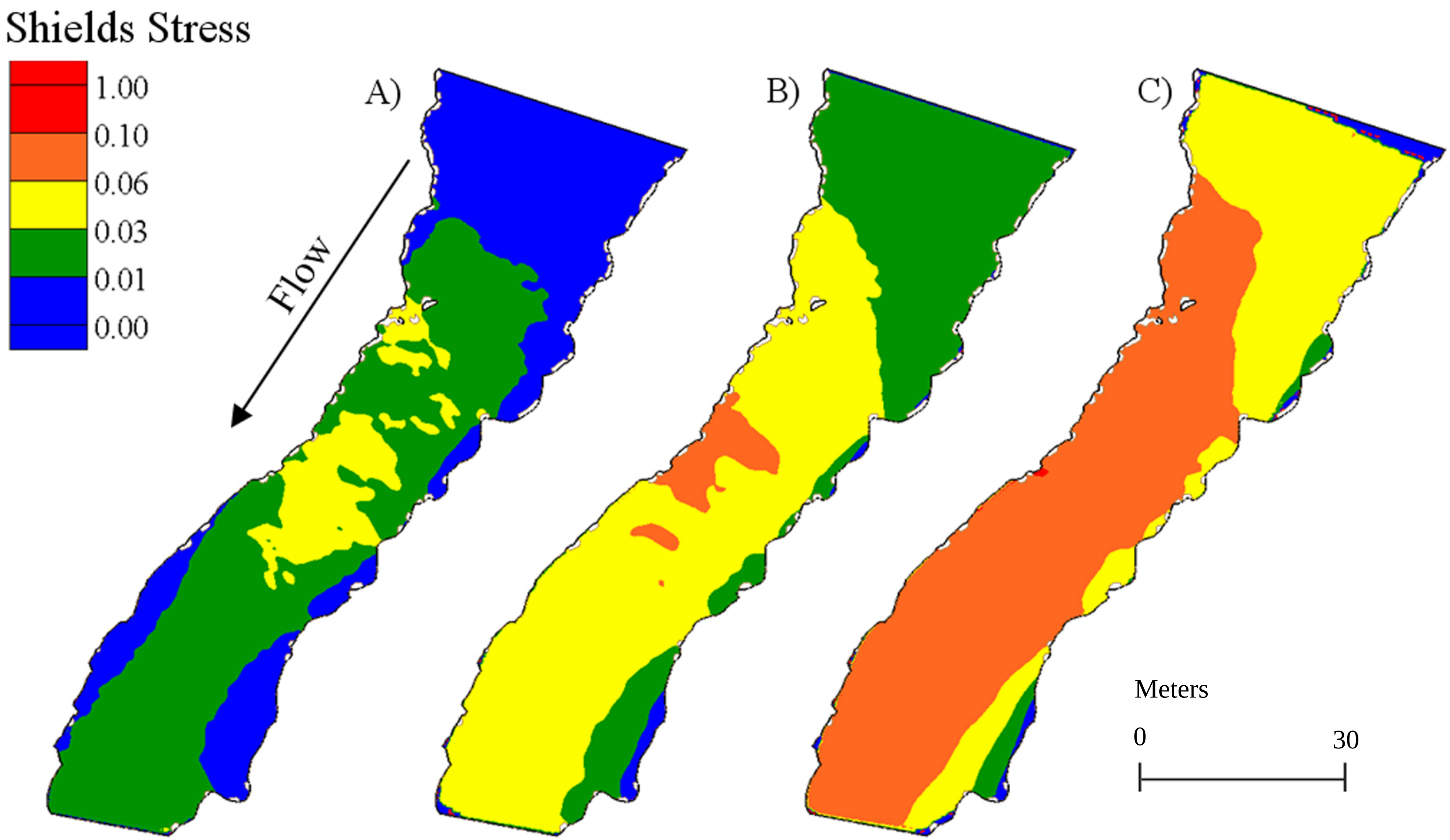

Figure 24. Shields stress predictions for a discharge of A) 271.3 cms (2-yr event), B) 900.5 cms (5-yr event) and C) 2588.2 cms (24-yr event) in the EDR spawing channel (33.7 cms wetted channel area).

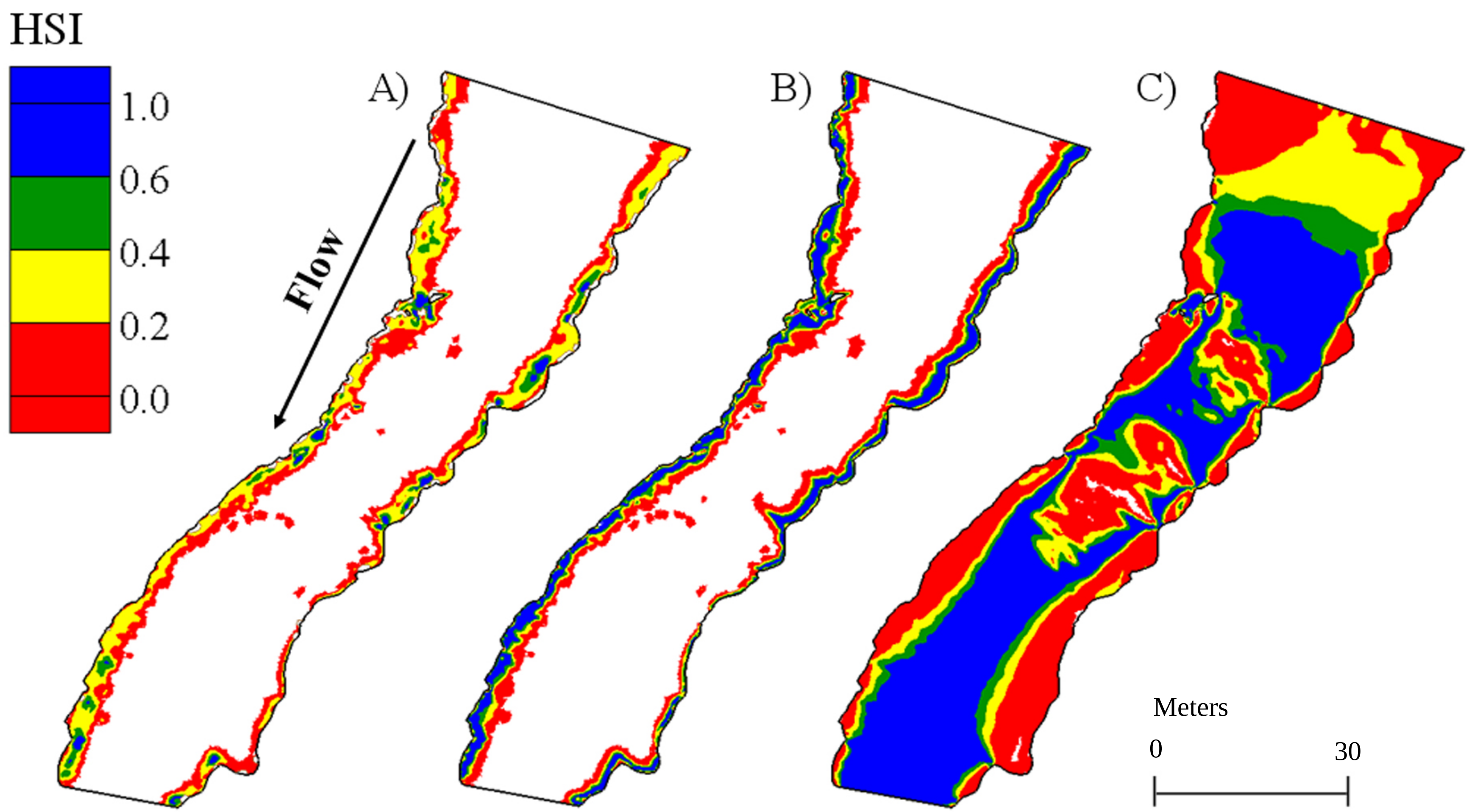

Figure 25. Model predictions of the A) geometric habitat suitability index (GHSI), B) depth habitat suitability index (DHSI), and C) velocity habitat suitability index (VHSI) for the 33.7 cms spawning flow at the EDR.

Hyp.	Statement	Test Metrics *
H_1	Sediment characteristics at the EDR and TBAR are comparable and suitable for spawning.	PC, VC, LR
H_2	Flow convergence routing will produce alluvial geomorphic features (riffles, pools, glides) at the EDR and TBAR study sites.	HM, SS
H_3	Injected gravels at the EDR will be stable during spawning flows.	HM, SS
H_4	Injected gravels at the EDR will be stable during 273.2 m^3/s discharges (~2-year event).	HM, SS
H_5	Injected gravels at the EDR will be stable during a 900.5 m^3/s discharge (~5-year event).	HM, SS
H_6	Injected gravels at the EDR will be stable during a 2588.2 m^3/s discharge (~24-year event).	HM, SS
H_7	Gravel augmentation will aggrade the EDR and produce extensive cross channel habitat	HM, SS, HI, DR
H_8	Historically, the EDR supplied ample spawning habitat for chinook salmon.	HI, LR, HOS, ROS
H_9	Current spawning habitat at the EDR and TBAR is not limited.	HM, HSC

* DR = Discharge Record Analysis, HI = Historical Imagery, HM = Hydraulic Modeling, HSC = Habitat Suitability Curves, LR = Literature Review, PC = Pebble Counts, HOS = Historical Observations of Spawning, SS = Shields Stress Predictions, ROS = Recent Observations of Spawning, VC = Visual Comparisons

Table 1. Hypotheses and test metrics used for evaluating the efficacy of gravel augmentation at the bedrock channel EDR.

Location	Discharge (m^3/s)	Downstream WSE (m)	Manning's *n*
TBAR	21.2	66.35	0.03
	34.6	66.53	0.03
	267.8	67.95	0.03
	655.3	69.51	0.03 & 0.052
	998.4	70.22	0.03 & 0.053
	3089.2	72.83	0.03 & 0.054
EDR	22.7	62.20	0.032
	33.7	62.30	0.032
	271.3	64.82	0.032
	710.7	67.32	0.038
	900.5	68.45	0.038
	2588.2	72.83	0.038

Table 2. FESWMS model inputs for the six comparable flows included downstream water surface elevation, Manning's *n* , and gaged discharge at the EDR and TBAR sites.

Discharge (m^3/s)	33.7 m^3/s (n=75)			900.5 m^3/s (n=20)		
Manning's n	Mean Error (m)	σ	Ev (m^2/s)	Mean Error (m)	σ	Ev (m^2/s)
0.022	0.028	0.020	0.8	-	-	-
0.024	0.022	0.024	0.8	-	-	-
0.026	0.021	0.021	0.8	-	-	-
0.028	0.022	0.021	0.8	-	-	-
0.03	**0.020**	0.018	0.8	0.103	0.088	2.5
0.032	**0.020**	0.015	0.4	0.097	0.086	2.5
0.034	**0.020**	0.013	0.4	0.086	0.082	2.5
0.036	0.022	0.013	0.4	0.085	0.077	2.5
0.038	0.025	0.013	0.4	**0.081**	0.056	2.5
0.04	0.028	0.013	0.4	0.086	0.063	2.5

Table 3. Mean errors, standard deviation of errors, and corresponding eddy viscosity values for Manning's n calibration scheme at the EDR. Bold values represent the smallest absolute error obtained in the analysis.

APPENDIX 2

Valley Width Controls on Riffle Location and Persistence on a Gravel Bed River

Valley Width Controls on Riffle Location and Persistence on a Gravel Bed River

Author: Jason Q White

Department of Land, Air, and Water Resources, University of California, One Shields Avenue, Davis, CA 95616-8626, USA.

Key Words: gravel-bed river, confined river, velocity reversal, flow constriction, valley width, fluvial geomorphology

Abstract

It has been hypothesized that flow boundary width variation causes variation in flow velocity, shear, and sediment transport capacity influencing channel morphology. Studies have observed width variation controls on channel morphology in a variety of forms including point bars, alluvial fans, boulder obstructions, bedrock outcrops, sharp bedrock beds, and wood. On confined rivers, such as de-glaciated or leveed rivers, during infrequent events, overbank flows may extend out and interact hydraulically with confining valley walls. In such circumstances, can variation in valley width influence sediment transport capacity and channel morphology, forcing riffle location and persistence? To address this question research was performed on a valley-confined wandering gravel-bed reach of the regulated lower Yuba River, CA. Hydraulic gold mining caused deep alluvial infilling of this 6-km reach from 1853-1941 with mixed coarse sediment creating a confined, dynamic, fluvial landscape with many riffles and pools. The study assessed stream planform and elevation change over 22 years (1984-2006) using eight aerial photo sets and two digital elevation models, and then examined relations between locations of persistent riffles and valley-wall constrictions. Analysis revealed that over the past 22 years, the river has undergone significant incision and planform change in response to frequent floods, yet seven of the ten riffles persisted in the same location. Persistent riffle crests were located close to the widest point between downstream and upstream constrictions. The results show that valley width plays a significant role in controlling riffle locations and persistence for confined rivers.

1. Introduction

It has been proposed that width variations of channel boundaries play a significant role in riffle-pool formation and maintenance in alluvial streams. Experiments using 1-D, 2-D, 3-D, and physical models have shown that channel width variation can cause sediment transport capacity to vary, influencing channel sedimentation processes and patterns. Channel width variation controls on bedform pattern have been observed in a variety of forms including point bars at pool heads in free-forming riffle-pools, and boulder obstructions, bedrock outcrops, sharp bedrock beds, wood, and alluvial fans in forced riffle-pools. One possible form of width variation control on riffle-pool formation is river-confining walls.

1.1 Riffles and Pools

Two elements make up alluvial stream beds: discrete particles (grains) and aggregates of particles in the form of definite (bedform) structures (Leopold et al., 1964). A common aggregate structure found in alluvial gravel-bed rivers is the riffle and pool sequence (Leopold et al. 1964). Riffle-pool sequences are longitudinally undulating surfaces in stream beds with high and low relief deviations from the average bed slope (Richards, 1976). Riffles are accumulations of coarse sediment having a steep water surface slope and shallow fast flowing water at below bankfull flow (Keller, 1971). Pools are scour features with a low water surface slope and relatively deep slow moving water at below bankfull flow (Keller, 1971).

1.2 General Process of Riffle-Pool Formation

It has been a commonly held theory that the riffle-pool sequence is maintained through a “reversal” in near-bed velocity or bed shear stress as a function of stage (Keller, 1971; Lisle, 1979). The reversal hypothesis proposes that as flow stage increases, bed velocity increases at a higher rate in pools than riffles, such that at approximately above bankfull stage, near-bed velocity, bed shear stress, and bed material scour rate become greater in pools than in riffles (Leopold et al., 1964; Keller, 1971; Lisle, 1979). Thus, stage-dependent shifts in the location of peak sediment transport capacity are conjectured to maintain riffle-pool relief (Keller, 1971; Lisle, 1979).

Some studies have corroborated the existence of velocity reversal for riffle-pool units (Jackson and Beschta, 1982; Keller and Florsheim, 1993), while others have reported the absence of velocity reversal at riffle-pool units (Bhowmik and Demissie, 1982; Carling, 1991; Clifford and Richards, 1992; Clifford, 1993a,b; Sear, 1996). Despite observing a reversal in bed shear stress at high discharges for the deepest part of pools, Booker et al. (2001) concluded velocity reversal was not significant because sediment routing bypassed the deepest portion of pools. Ultimately, the velocity reversal hypothesis has not provided a sufficient general mechanism to explain formation and maintenance of all riffle-pool sequences (MacWilliams et al., 2006).

Flow convergence routing has been proposed as a more general mechanism to the process of riffle-pool maintenance (MacWilliams et al., 2006). Converge of flow in this context is the funneling or focusing of flow (MacWilliams et al., 2006). Under low-flow conditions, vertical variations in topography along the length of a river control channel cross-sectional area and hydraulics, thus determining sediment transport capacity; pools having slow, divergent flow and low transport capacity, determined by a low water-surface slope; and riffles having faster, convergent flow and moderate transport competence due to a steep water surface slope (Clifford and Richards, 1992; Brown and Pasternack, 2007). Under high-flow conditions, longitudinal variations in channel width control channel cross-sectional area and hydraulics, driving flow divergence over riffles and convergence over pools. Flow convergence over pools creates a zone of high velocity and shear stress at the pools (Carling, 1991; Booker et al., 2001; Cao et al., 2003, MacWilliams et al., 2006). These high velocity zones cause mobilized sediment to be routed through pools and deposited as riffles downstream where flow diverges and velocity, shear, and transport capacity reduces (Leopold et al., 1964; Keller, 1971; Lisle, 1979, Booker et al., 2001; Repetto et al., 2002; MacWilliams, 2006). As discharge increases the effect of flow convergence on velocity and shear stress increases (MacWilliams et al., 2006). MacWilliams et al. (2006) used 2-D and 3-D models to confirm the presence of flow convergence routing at the classic Dry Creek study site upon which the velocity reversal was proposed by Keller (1971), and previously modeled in 1-D (Keller and Florsheim, 1993). In reviewing past literature, MacWilliams et al. (2006) found that most studies of velocity reversal (both for and against) provided results and discussion that indicated support for flow convergence routing (see Table 1 of MacWilliams et al., 2006).

Varying channel width, the driver of flow convergence routing at high flow, has been shown to influence sediment depositional patterns. Studies by Repetto et al. (2002) and Wu and Yeh, (2005), on channel bifurcation and midchannel bar formation, used 2-D and 3-D models, as well as flume experiments to demonstrated the influence of varying channel width on sedimentation patterns. With the 2-D and 3-D models and flume experiments, a sediment depositional pattern was observed in which relative highs lined up with the widest portion of the channel and the relative lows lined up in the narrowest portion of the channel, resulting in channel width oscillations in phase with bed undulations (Repetto et al. 2002; Wu and Yeh, 2005).

1.3 Free Forming Riffle-Pool Channels

Riffle-pool sequences not forced by stable elements, are considered free forming (Montgomery and Buffington, 1997). Free formed riffle-pool sequences typically are found on purely alluvial streams with beds and banks composed of unconsolidated materials (Keller and Melhorn, 1978). In free forming riffle-pool channels, riffle and pool locations have been found to typically correlate with meander geometry (Leopold et al., 1964; Keller and Melhorn, 1978). Pools are located at bends and riffles are located at meander inflection points (Leopold et al., 1964; Yang, 1971; Karasev, 1993).

Free-forming riffle pools are believed to be self-formed through bedform feedback. Constricting bedform shape at the head of pools create zones of high flow velocities and bed shear stress away from the deepest parts of the pool, near the inside of the meander bend (MacWilliams et al., 2006). Sediment bypasses the deepest parts of pools, remaining on the inside of bends, depositing a lobate shoal longitudinally, which forms point bars lateral to pools and riffles at meander inflection points (Keller, 1972; Thompson, 1986; Booker et al. 2001; MacWilliams et al., 2006). As mentioned, the deposited point bars promote flow constriction and convergence at the head of pools, closing the loop on the free-forming feedback.

Sediment routing that bypasses the deepest portion of the pool is enhanced by secondary transverse flow created by lateral shear between non-uniform flows from flow convergence at the head of pools (Booker et al., 2001; MacWilliams et al., 2006). Meander bends experience converging secondary transverse flow circulation cells, while diverging secondary transverse flow occurs between meander bends as secondary flow cells from upstream and downstream pools overlap (Leopold et al., 1964; Keller 1972; Deitrich et al., 1979; Thompson, 1986). Hence at the bed surface transverse flow is constantly toward the inside bend, helping to maintain sediment routing through the inside of the meander bend. At higher discharges secondary flow cells increased in length and overlap due to increased secondary velocities and flow depth (Thompson, 1986).

1.4 Forced Riffle-Pool Channels

Typical pool and riffle locations found in free forming alluvial channels may not be applicable where forcing elements exist (Lisle, 1986; Thompson, 2001). Pools have been observed to form in alluvial and semi-alluvial streams around forcing elements such as alluvial fans, wood, boulders, and bedrock outcrops (Lisle, 1986; Miller, 1994; Montgomery et al., 1995; Thompson, 2001). These obstructions cause abrupt changes in channel width, creating flow constriction and local convective acceleration (Lisle, 1986; Miller, 1994; Thompson, 2001). Such constrictions create deep, slow backwater formation upstream, and steep water-surface slopes with shallow fast flow acceleration through constrictions, creating a zone of high velocity, shear, and sediment transport capacity (Keiffer, 1989; Thompson, 2005; MacWilliams et al., 2006). In effect, this is another example of flow convergence routing. However, in the case of forced pool-riffle units, the abruptness of the channel change also causes localized, high-frequency vortex shedding around the constricting elements. In turn, that yields turbulent fluctuations in velocity, lift, and drag that are all thought to be capable of scouring and routing sediment (Woodsmith and Hassan, 2005; Thompson, 2006). Thus, in contrast to free-forming units where sediment routes around pools, with forced units sediment routes through pools, depositing downstream in lower flow competence zones (Thompson, 2001, MacWilliams et al., 2006). Additionally, forced pools are shortened and deepened by the re-circulating eddies, vortices, and boils caused by flow separation at the non-streamlined forcing elements (Woodsmith and Hassan, 2005; Thompson, 2006).

Bedform forcing elements have been studied in a variety of forms at a local geomorphic unit scale. Montgomery et al. (1995) observed scoured pools around wood on the Alaskan and Washington streams, with 82% of pools formed near wood or other obstructions. Additionally, they found 40% of the in-channel wood influenced pool location (Montgomery et al. 1995). A study by Lisle (1986) documented that 85% of pools on Jacoby Creek, California were next to large obstructions or bedrock bends, and 92% of large obstructions or bends had pools (Lisle, 1986). Those obstructions or bedrock bends without pools were closely spaced to other obstructions or bends, suggesting minimum spacing requirements for pool formation (Lisle, 1986). Extensive field research in New England also showed that a majority of pools were associated with “pool-forming elements” such as bedrock outcrops and boulders (Thompson, 2001).

1.5 Confining Valley Walls and Channel Morphology

Valley confining walls are one possible forcing element that may play significant role in forcing riffle-pool formation during big floods on larger reach or segment scales (Karasev, 1993). A confined alluvial river is one in which valley width is equal to or less than the width of the meander belt (Alabyan and Chalov, 1998). Confining valley walls of confined rivers include hillslopes, canyon walls, abandoned terraces, or anthropogenic structures such as mine tailings or levees (O'Conner et al, 1986; Grant and Swanson, 1995). On confined rivers, during large infrequent flows that exceed bankfull and flood the entire valley, flows may interact hydraulically with valley walls potentially causing valley walls to function as physical constrictions to flow (Jacobson and Gran, 1999). The effects of such hydraulic-channel interactions are not thoroughly understood. Based on the flow convergence routing hypothesis, it may be possible varying valley width flow could cause flow velocity and bed shear stress to vary enough to influence sediment transport and bedform morphology. On the Cascapedia and Bonaventure Rivers, in Quebec Canada, Coulombe-Pontbriand and Lapointe (2004) found that valley width had an influence on riffle substrate size. Jacobson and Gran (1999) found that in certain reaches of the Current River, Missouri, gravel peaks could be associated with wider valleys. McKenny (1997) found on confined rivers, a significant relationship between riffle spacing and valley width.

Studying riffle-pool patterns on Boulder Creek, Utah, O'Conner et al. (2006) found relation between confining walls and boulder riffle location in a narrow canyon setting. The study hypothesized that during large infrequent events large riffle forming boulders deposited in areas of lowered sediment transport capacity from canyon expansion (O'Conner et al, 1986). This hypothesis was tested by mapping riffle locations on 5.9 km of Boulder Creek (O'Conner et al., 1986). Eighty-six riffles were identified, of which 65 were located at canyon expansions (O'Conner et al., 1986).

1.6 Study Objectives

Width controls on bedform morphology had been observed for a variety of channel features: wood, boulders, bedrock outcrops, point bars, and narrow canyon walls. The next logical test of width control on sediment deposition was deemed to be larger scale valley walls of valley-confined rivers.

The goal of this study was to test the role of valley width variations in controlling riffle location and persistence. The hypothesis tested was that in a valley-confined, dynamic fluvial landscape, riffles persist in the same longitudinal position due to forcing imposed by valley width variation on sediment depositional patterns during large infrequent flooding events. The benefit gained from this research is a further understanding of the influence river confinements have on bedform structure. Such knowledge may prove useful in restoring bedform and lotic habitat complexity in confined (i.e. leveed) streams with little to no bedform structure.

To test this hypothesis, research was performed on the valley-confined wandering gravel-bed lower Yuba River. The specific objectives of the study were to (1) demonstrate that the study reach is a dynamically changing landscape at the inter-annual time-scale (and are not features inherent from antecedent conditions), (2) determine the persistence of all study reach riffles, and (3) examine quantitative and qualitative relations between persistent riffle locations and valley width.

2. Study Area

Wandering gravel-bed rivers with mixed coarse sediment and a high likelihood of flooding have a dynamic fluvial landscape ideal for studying floodplain and channel change. Recently, floodplain and channel change has been studied on wandering gravel bed-rivers in Washington, Alaska, Canada, Scotland, England, France and China (Desloges and Church, 1987; Marston, 1995; Xu, 1996; Bryant and Gilvear, 1999; Winterbottom, 2000; Passmore and Macklin, 2000; Parsons and Gilvear, 2002; Burge, 2005; Burge and Lapointe, 2005; Froese et al., 2005; Beechie et al., 2006). Conditions required for wandering gravel-bed rivers include high seasonal and annual variation in discharge, and a large quantity of bed load (Xu, 1996). The conditions that form wandering gravel-bed rivers result from mountain valleys filling with cobble (64-256 mm) and gravel (2-64 mm) sized sediment, typically from deglaciation (Nanson and Croke, 1992). Return intervals of floodplain erosion for wandering gravel-bed rivers fall between meandering and braided rivers (Beechie et al. 2006). Additionally, on wandering gravel-bed rivers, the confinement of the channel may limit the production of multiple channels (Burge and Lapointe, 2005).

The lower Yuba River, CA from the Narrows Pool (39°13'20"N, 121°17'40"W) downstream to the Highway 20 bridge (39°13'13"N,121°20'7"W), a wandering gravel-bed reach, provided the ideal conditions for this study, because of its thick mixed coarse sediment alluvial fill, proximal confining valley walls, and significant variations in valley width. The Yuba River is part of the Feather River basin, which in turn empties into the Sacramento River (Fig. 1). It drains the western slope of the temperate Sierra Nevada Mountains of Northern California with headwaters originating nearly 3000 meters above sea level. The study site is ~38 km upstream of the Yuba River-Feather River confluence, with a basin area of ~3480 km^2 (Fig. 1). Deer Creek, a regulated tributary with a basin area of ~220 km^2, joins the Yuba River just upstream of the study reach. Inflow to the study reach is a combination of the two basins.

The Yuba River study reach has a well connected floodplain, partially vegetated islands, abandoned channel accretion, mixed coarse sediment, and a single dominant channel with irregular sinuosity of 1.1 - all features of a wandering gravel-bed river (Nanson and Croke 1992). In the case of the Yuba River the cause of sediment filling was anthropogenic. During 1853-1884, many hillslopes in the Yuba River watershed were subjected to intensive hydraulic gold mining (James, 2005). Halted in 1884 due to a court injunction, hydraulic mining supplied large quantities of sediment to downstream reaches of the Yuba, Feather and Sacramento Rivers through to San Francisco Bay, causing problems for agriculture, navigation, and flood management (James, 2005). Based on detailed topographic mapping and an assumed underlying valley shape, it is estimated that the 6-km reach investigated in this study is presently filled with ~9-18 million m^3 of mixed coarse sediment (Pasternack and Morford, unpublished data).

Constructed in 1941, Englebright Dam was built 3.1 km upstream of the study reach to retain sediment supplied from upstream anthropogenic sources (James, 2005). Standing 85 m high, Englebright Dam is a concrete, arch, ogee-crested dam with flow discharging from the bottom through a retro-fitted hydroelectric plant (James, 2005). Its reservoir is estimated to contain 21.9 million m^3 of sediment, 25.5% of its original capacity (Childs et al., 2003). New Bullards Bar Dam most influences flows on the lower Yuba River. It was constructed in 1970, and captures the entire North Fork Yuba River.

Spaulding Dam and Jackson Meadows Reservoir Dam are smaller structures, and both located high in the watershed on the South and Middle Fork respectively (Moir and Pasternack, 2008).

Annual precipitation for Marysville, CA along the lower Yuba River is ~500 mm, 85% of which falls between November and April (Curtis et al., 2005). In the upper regions of the catchment, the annual precipitation is >1500 mm, most of which accumulates as snow pack contributing to spring runoff, April–July. Due to the ogee-crest design of Engelbright Dam, during large precipitation events, water spills directly into the channel, allowing the Yuba River to exhibit a closer to natural flood hydrograph below the dam. Flow is recorded for the Lower Yuba River at the U.S. Geological Survey (USGS) Smartville gage (#11418000), 0.5 km downstream of Englebright Dam. Following the construction of New Bullards Bar dam (1970), there have been over one hundred uncontrolled flow events overspilling Englebright Dam, many of which exceeded bankfull conditions downstream. Since 1971, bankfull discharge is 160 m^3/s (the 1.5-yr event for this reach of the Yuba River), and visually corresponds to the willow vegetation bordering the channel (Fig. 2). It is estimated that the majority of the floodplain is inundated at ~540 m^3/s. Visual observations (Fig. 3) determined that the entire floodplain of the study reach is definitely inundated at a flow of 736 m^3/s, which has a recurrence interval of 2.5 years (1971-2004). Discharges associated with the 5-, 10-, and 50-yr recurrence intervals for 1971-2004, are 1050, 1450, and 4025 m^3/s respectively, providing sufficient flows to regularly rework the gravel valley fill of the study site (Moir and Pasternack, 2008). Figures 4a-c shows significant floodplain and channel change due to a 41-yr event.

3. Methods

The objectives of this study were accomplished through the use of aerial photo analysis and digital elevation model (DEM) analyses using ArcGIS 9 (ESRI, Redlands, CA). A number of studies have found GIS useful in analyzing river morphology and tracking planform change in aerial photographs (Gurnell et al., 1994; Gurnell, 1997; Winterbottom and Gilvear; 1997; Winterbottom, 2000). Winterbottom and Gilvear (1997) showed that aerial photos can be used to accurately quantify channel bed elevation, and Winterbottom (2000) found GIS an effective and accurate tool in quantifying medium- and short-term channel changes on a wandering gravel-bed river from survey maps and aerial photos.

3.1 Aerial Photo Registration

Aerial photos were obtained from a number of sources in either hard copy or digital format for the following years: 1937, 1947, 1952, 1958, 1984, 1986, 1991, 1996, 2002, 2004, 2005, and 2006. The hard copy aerial photo scales ranged from 1:6000 to 1:32 000. Aerial photo sets for 1937, 1947, 1952, 1958, were scanned at 400 or 600 dpi using 216 x 279 mm flat bed scanner. The 1984, 1986, 1991, and 1996 photo sets were scanned using a 310 x 437 mm flatbed color scanner using a resolution of 1200 dpi. Digital aerial photos existed for 2004, 2005, and 2006. A digital orthophoto was obtained for 2002. Orthophotos are digital aerial photos that have been geometrically corrected for relief and photographic tilt effects (Lo and Yeung, 2007). Spatial resolution of digital aerial photos ranged from 0.3 m to 1.0 m. All digital imagery was referenced horizontally in the Projected State Plane Coordinate System, California Zone 2, with a reference datum of North American Datum of 1983 (NAD83).

Scanned hard copy images required co-registration. Co-registration is the conversion of digital photo sets to a common projection and coordinate system (Hughes et al., 2006). All images were co-registered through georectification in ArcGIS 9 using the 2002 digital orthophoto as the base image. Geo-referencing is lining up the image to be co-registered to a base image, typically an orthophoto, through common points, known as ground control points (GCP). Between twelve and fifteen GCPs were located for georeferencing each photo for improved accuracy (Hughes et al. 2006). GCPs, no greater than 8 m in planview dimensions, were identifiable for photo sets 1984, 1986, 1991, and 1996 at 10 to 20 times zoom. Ground control points included soft points such as trees and bushes as well as hard points such as bedrock outcrops. Soft points used in combination with hard points do not significantly change the overall georectification accuracy (Hughes et al., 2006). The GCPs were selected solely from the floodplain to increase the accuracy in the vicinity of the targeted area (Hughes et al. 2006). A spline (rubbersheeting) transformation was chosen for rectifying each photo set rather than a first, second, or third order transformation, so that each image was most accurately fit in the vicinity of the GCPs, in this case the floodplain. By choosing a spline transformation the areas outside the floodplain did not affect accuracy of the area inside the floodplain. Photo sets from 1937, 1947, 1952, 1958 were found to be of too low resolution and too old to provide a sufficient number of identifiable GCPs for a spline transformation (10 GCPs required). Thus, these were rectified using between 5 and 10 GCPs and a second order transformation, providing lower accuracy than the photosets from 1984-2006. Due to the lower accuracy and lower resolution of the 1937-1958 photo sets, these where omitted from much of the analysis, only to be used to examine riffle persistence rather than precise location. Each photo set was rectified as a TIFF format file using cubic convolution and 0.3 m pixel size. Cubic convolution was chosen because it smoothes out jagged edges along boundaries making it best suited for floodplain interpretation (Hughes et al., 2006).

3.2 Digital Elevation Model Construction

The 1999 DEM was provided by the US Army Corp of Engineers, Sacramento District and developed by Ayres Associates as part of Sacramento and Feather River Basins topographic and bathymetric surveys. The terrestrial survey of the Yuba River floodplain and terraces from the Yuba-Feather confluence to Englebright Dam was conducted by aerial photogrammetry with flight elevations of 3000 meters above the mean terrain surface. The vertical accuracy of this survey was ~0.2 m, with 1.2-m contours provided. The bathymetric survey of the Yuba River was done by boat using a dual frequency GPS receiver, fathometer, and sonar transducer mapping system. Cross-sections were made ~50-100 m apart. This survey had a vertical resolution of 0.6 m for the floodplain and 0.3 m for the river bed, with 0.6-m contours provided. The 1999 DEM used the same horizontal coordinate system and datum as the aerial photos, along with the National Geodetic Vertical Datum of 1929 (NGVD29) Vertical Datum, which was later converted to the North American Vertical Datum of 1988.

The 2006 DEM was generated through terrestrial and boat-based survey as part of an overall Yuba River research program that included this study. The terrestrial survey was done April through December 2006 using a Leica TPS1200 robotic total station, with the prism-pole operator walking an ~3x3 m grid. Hard to reach and steep areas were surveyed using the reflectorless capability of the total station. Shallow, wetted channel areas such as riffle crests that were unreachable by boat were surveyed by wading with the prism pole. The control network for the total station survey was professionally surveyed using real-time kinematic (RTK) GPS. After quality checks, the survey yielded 66 531 points. The mean sampling density in the relatively flat floodplain was 0.107 points/ m^2. Surveying accuracy was assessed using control network checks and was found to average 0.013 m in the horizontal and 0.011 m in the vertical, which is significantly smaller than the natural error induced by the bed material, typically ranging in size between 0.05-0.2 m.

A private hydrography firm (Environmental Data Solutions, San Rafael, CA) was contracted to partner in this effort to produce a bathymetric map meeting U.S Army Corps of Engineers' rigorous Class 1 standard (±0.15m vertical accuracy; USACE, 2002). The boat-based survey was performed June 9-21, 2006 when the flow was 85.5-126.6 m^3/s. A customized 4.23-m long Zodiac inflatable raft was fitted with an Odom Hydrotrack survey-grade fathometer with a 3°, 200-kHz transducer. Position data for the fathometer were collected using a Leica GPS 1200 RTK GPS receiving corrections by radio from an on-site base station located on one of the pre-established benchmarks from the terrestrial survey. Both streams of data were recorded onto a laptop running Hypack Max 4.3 (Hypack, Inc., Middletown, CT). Where depth permitted, the boat made cross-sections on an ~3-m interval and did six longitudinal transects approximately evenly spaced across the channel. To account for the water surface slope and its changes through time, four Mini Troll 400 vented pressure transducers (In-situ, Inc., Fort Collins, CO) were placed in the river along the study site and their elevations were surveyed using a total station. An algorithm within Hypack (tide adjustments) was used to interpolate water surface elevation values based on distance between the pressure transducers. In post-processing, a radial filter was applied to the boat-based data to ensure a 0.25-m spacing between points; this yielded 114 681 points at a density of 0.267 points/m^2 in the channel.

The 2006 DEM was constructed in ArcGIS 9 using a triangular irregular network (TIN). A total of 180 612 survey points were used, with an overall point density of 0.164 points/m^2. Rigorous quality control procedures were followed to integrate the boat-based and total station datasets to produce a high quality DEM. Quality assurance and quality control information beyond the scope of this summary is on file with the contractor and author.

3.3 Channel Change Quantification

Planform channel change was quantified in ArcGIS 9. Using the georectified scanned aerial photos sets for 1984, 1986, 1991, and 1996 along with the georeferenced digital photo sets for 2002, 2004, 2005, and 2006, the wetted channel was delineated in ArcGIS at 3-6 times zoom, using polygon shape files. The daily mean flow at the time of the photo was also obtained from U.S. Geological Survey (USGS) Smartville gage (#11418000) to ensure flows at the time photos were taken were comparable, and that measured channel change was not due to merely a difference in stage. Aerial photo sets for 1937, 1947, 1952, and 1958 were not included in this analysis due to their low georectification accuracy and low quality resolution. For each year's photo set, the boundary of the wetted channel was delineated as a polygon shape file. Mid-channel bars (islands) were clipped from the polygon shape file, leaving only the wetted channel area to be represented by the polygon shape file. For consecutive photo sets, the surface area of channel fill and channel cut was determined. The channel fill was defined as the area of previously wetted channel that was later dry surface. The channel cut was defined as the area of previously dry surface that was later wetted channel. A channel fill polygon shape file was created by clipping the previous photo set's wetted channel polygon shape file from the following year's wetted channel. And conversely, a channel cut polygon shape file was created by clipping the following year's wetted channel polygon shape file from the previous year's wetted channel. The area of cut and fill were measured in ArcGIS 9, and summed to determine the area of planform channel change. Values of planform channel change area were later reported as a percentage of the total area within the confining valley boundary in order to place into context the change of wetted surface area with respect to total valley confined area. It has been suggested that when measuring planform channel change from georectified aerial photos, a lateral buffer of 5 m should be applied (Hughes et al. 2006). Based on this value planform channel change less than 3% of the confined area was considered no change.

Flow data was acquired as part of the channel change assessment. Flow data post-New Bullards Bar dam (1971) from the U.S. Geological Survey (USGS) Smartville gage (#11418000) was provided along with a flood frequency analysis from concurrent Yuba River studies (Moir and Pasternack, 2008). Peak daily flows occurring between photo sets and their respective recurrence intervals were determined. Peak flows were paired with channel change for their respective time interval providing insight into the quantity of channel change occurring for a given flow magnitude.

Vertical channel change was examined and quantified using longitudinal profiles constructed from the 1999 and 2006 DEMs. In ArcGIS 9, thalwag centerlines for the DEMs were drawn as polyline shape files. Points were created on the thalwag centerlines at 3 m intervals. Each DEM was converted to a raster digital elevation model. Elevations at each point along the profiles were extracted from the raster DEMs and plotted versus distance upstream. A mean change in elevation was determined from the plotted points for the reach to determine in general if the reach overall is aggrading or incising.

3.4 Riffle Persistence Assessment

For this study, riffle locations were defined by their respective riffle crests. Riffle crests were identified for the 1937, 1947, 1952, 1958, 1984, 1986, 1991, 1996, 2002, 2004, 2005, and 2006 photo sets in ArcGIS 9. Riffles were identified by their shallow depth, high surface slope, high flow velocity, and, most importantly for plan-view identification, disturbed surface (Keller, 1971; Emery et al., 2004). Picturing a pool-riffle sequence as an undulating surface, the riffle crest would be the relative peak in relief. Each location was assigned a single point in a point shape file corresponding to the center position laterally on the riffle crest. Giving each riffle crest a discrete location allowed for ease of identification, statistical analysis, and comparison to valley width. For each identified riffle crest, the distance upstream from the Highway 20 bridge on the valley centerline was determined.

The process of identifying riffle crest locations improved with practice, which required continual adjustments in previously identified riffle crest locations. A number of factors played into identifying riffle crest locations. Riffle crests were first identified for the 2006 aerial photo set, with the aid of the 2006 contour map and extensive field knowledge of the study site. The contour map was most useful in locating the local topographic peak of the riffle crest. This allowed for a precedent to be set in identifying riffle crests of earlier photo sets. In general, riffle crests were clearly identified in the aerial photos at the upstream edge of a disturbed water surface section. In cases when disturbed surfaces were washed out due to sunglint off water surfaces, riffle crests could be estimated at the widest point of the channel. Typically, riffle crests occur upstream of channel width increases (Richards, 1976). Some riffles were identified at sudden bends in the channel. For the color digital photos, the transition from deep pools to shallow riffles was visible through improved bottom reflectance, allowing for further ease of riffle crest identification.

Riffle crests for the 1984-2006 photo sets were separated into two categories: persistent and non-persistent. Persistent riffle crests were defined as those that clustered in the same general locations for the entire duration of the study. The causes of non-persistent riffle formation were examined.

Basic statistical analyses were performed to determine the level of riffle crest persistence from 1984-2006. In Microsoft Excel 2003, mean, range and standard deviation of riffle crest position at each location was calculated. All values were later reported as a non-dimensional percentage of their respective distance between upstream and downstream constrictions (d_c), to place into context the distribution of riffle crests between constrictions. Additionally, upstream or downstream longitudinal riffle migration between one photo set to the next was determined.

Persistent riffles also assessed at the smaller spatial scale of the geomorphic unit (10^0-10^1 channel widths) and compared with lateral channel migration patterns. Riffle locations identified in the earlier photo sets of 1937, 1947, 1952, 1958 were compared with mean persistent riffles locations for 1984-2000.

3.6 Riffle Persistence and Valley Width Relations

Valley width was quantified using ArcGIS 9 to allow comparison with riffle persistence. The 2006 DEM made the 2006 aerial photo the logical choice for the initial delineation of the valley width in ArcGIS. The 2006 aerial photo was also color, further aiding in valley width delineation. Comparing the 1999 and 2006 DEMs showed an overall lowering of valley fill elevation due to net sediment export from the reach (Pasternack and Morford, unpublished data). With sloping valley walls, floodplain incision over decades should cause valley width to decrease. However, due to the relatively steep slopes of valley walls and moderate width of the valley, changes in valley width due to incision of sediment are negligible relative to total valley width. After a visual comparison of 2006 valley width to that for the 1984, 1986, 1991, 1996, 2002, 2004, and 2005 photo sets, it was deemed unnecessary to delineate and measure the valley width for each photo set.

The boundary between the valley wall and alluvial sediment was defined as the location where the steep natural sloping, grassy hills are met by the relatively flat and unvegetated alluvial floodplain surface. This abrupt transition was highly visible on the

2006 aerial photo, since the floodplain gravel was brightly colored, while hillslopes were dark. Also, first-hand knowledge of the study reach and valley-floodplain boundary was obtained while performing the ground-based terrestrial topographic survey. However, the 2006 DEM visualized with 1.5-m contours provided the most accurate and useful resource in delineating the slope break at the valley border. A boundary polygon shape file was delineated in ArcGIS 9 at 3-6 times zoom. Next, a centerline polyline was drawn by visually estimating the center between the valley boundaries on either side of the river down the length of the boundary polygon. The centerline was smoothed and stationed every 3 m, with cross-sections perpendicular to the centerline at each station. The high resolution of cross-sections, one every 3m for a total of 2000 cross-sections compensated for lost accuracy in measuring valley width due to the angle of cross-section. For the set of cross-sections, an attributes table was created with the following fields: distance upstream from the Highway 20 bridge, valley width moving upstream, and location of identified riffles.

An analysis was done to determine if a relationship existed between persistent riffle crest locations for 1984-2006 photo sets and the 2006 valley width. For each persistent riffle crest the associated downstream valley wall constriction, associated upstream constriction, and the widest valley point between the two constrictions was located. Constrictions and widest points were identified as reach maximum and minimums of oscillating valley width. All locations were reported as distances upstream of the Highway 20 bridge on the valley centerline. The distance from persistent riffle crests to their associated widest point, the distance from persistent riffle crest to their associated constriction and distance between constrictions (d_c) were calculated and reported as a non-dimensional percentage of d_c.

The channel longitudinal profiles constructed from the 1999 and 2006 DEMs were converted to slope subtracted profiles. This was done by fitting a trend line to each profile and obtaining the overall slope for the 6 km reach for each year. Then each year's trend line was subtracted from its raw profile to obtain slope-subtracted profiles that highlighted the relief between riffles and pools. Persistent riffle locations and the slope-subtracted bed elevations for 1999 and 2006 were plotted with valley width versus distance upstream to allow comparison between riffle persistence and relative relief to valley width.

4. Results

Over the 22 years studied, the site has experienced significant planform change, however seven of ten riffles persisted in the same location. A close relation found between persistent riffle crest location and the widest point of the confining valley between valley constrictions.

Examples of georectified photos sets for 1984, 1991, 1996 along with the 2002 orthophoto are shown in Figure 5a-d. The DEM constructed from the terrestrial and boat-based surveys for 2006 is shown in Figure 6.

4.1 Planform Channel Change

Channel change is illustrated in Figure 7 over four time intervals: 1984-1991, 1991-1996, 1996-2002, 2002-2006. In Figure 7a (1984-1991) the main channel shifted from one side of the valley to the other at three locations, and the channel bifurcated at the northern apex of the valley bend. Channel change for 1991-1996 showed main channel abandonment at the northern apex, shifting to a single main channel pushing against the southern valley wall (Fig. 7b). The single main channel at the northern apex moved to the center of the valley confinement 1996-2002, and further upstream the channel shifted from the left center to the right on the outer bend (Fig. 7c). Channel bifurcation occurred just upstream from the Highway 20 bridge in Figure 7d (2002-2006) and a secondary channel was cut at the northern apex (also depicted looking downstream in Figures 4a-c).

The area of channel change from period to period ranged from 12 758 m^2 (4% of the confined area) to 133 867 m^2 (34% of the confined area). The area of the wetted surface ranged from 389 466 m^2 to 467 397 m^2, on average 42% of the confined area (1 009 978 m^2). Flows at the time the photos were taken ranged from 19 m^3/s to 62 m^3/s (Table 1). Peak flows ranged from 203 m^3/s to 3823 m^3/s from 1984 to 2006 (Table 1). Flows for each photo set were of the same magnitude (10^1 m^3/s) while flows ranged in magnitude from 10^0-10^3 m^3/s for the duration of the study, meaning that differences in stage from one photo set to the next were effectively negligible. Peak daily flows, the recurrence interval of that peak flow, and flow at the time of the photo are also reported below with their respective channel change time interval.

Based on the estimate for floodplain inundation (~540 m^3/s), the entire floodplain was flooded for more than 100 days over the period 1984-2006 (Table 1). The most significant change in wetted area, a 34% change, occurred between 1984 and 1986 due to a 24-yr event of 2832 m^3/s, occurring February 19, 1986 (Table 1). The largest event of the study, a 42-yr event with a discharge of 3823 m^3/s, occurring January 2, 1997, caused a change in wetted area of 29%. Another 24-yr flow event of 2815 m^3/s occurring between 2005 and 2006 (December 31, 2005) caused only a 14% change in wetted area, topped by a change in area of 17% occurring between 1991 and 1996 due to 8-yr event of 1228 m^3/s, May 1, 1995 followed by a 9-yr event of 1427 m^3/s, May 18, 1996. An 8% change in wetted area was experienced for both a 4-yr event between 1986 and 1991and an 8-yr event between 2004 and 2005. The least significant event was from 2002 to 2004, at 203 m^3/s, just above bankfull, caused a 4% in area change.

Vertical channel change for the study reach was mostly in the form of incision (Fig. 8). Eighty-three percent of the thalwag was incised. Over the entire reach the mean vertical channel change was an incision of 0.78 m, an incision rate of 0.11 m/yr. Areas of significant deposition occurred at ~1700 m, ~4300 m, and ~5500 m upstream from the Highway 20 bridge due to downstream migration of riffle crests (Fig. 8). Over the 83% of the reach that incised, the average incision was 1.11 m, a rate of 0.16 m/yr.

4.2 Riffle Persistence

Eight riffle crests were determined to be persistent out of on average ten riffle crests. These eight riffle crests were clustered in the same locations over the 6 km study reach for the entire 22 years (Fig. 9). The persistent riffle crest formed at the most upstream end of the sediment fill was omitted from further analysis because its formation was known not to relate to valley width, narrowing the analysis down to seven persistent riffle crests.

Non-persistent riffle crests appeared in particular locations for anywhere between 1 to 6 photo sets, with an average of 3 photo set appearances. The number of non-persistent riffle crests for given photo set ranged from 1 to 4 with an average of 3. Non-persistent riffle crests occurred due to low flow competence at channel confluences (Fig. 10a), lateral channel cutting at channel bifurcation (Fig. 10b), mid-channel bar high relief (Fig. 10c), lower flow competence due to sudden bend in valley (Fig. 10d) and local bedrock channel constriction (Fig. 10e).

The average standard deviation of the seven persistent riffle crest locations was within 9% of d_c (Table 2). The largest persistent riffle crest location standard deviation was 15% of d_c, with the tightest persistent riffle crest location standard deviation 4% of d_c. The range of riffle locations varied from 8% of d_c to 45% of d_c with an average of 25% of d_c. Riffle migration was 53% downstream and 45% upstream with 2% no migration.

Examining the persistent riffle locations for 1984-2006 at the finer resolution of the geomorphic unit (10^0-10^1 channel widths) showed that as the channel shifted laterally from one side of the confining valley to the next, riffle crests continued to persist in the same longitudinal position. At persistent riffle crest 1, the center of the channel migrated laterally ~150 m from 1984-1991, yet the persistent riffle crests remained in the same general longitudinal location (Fig. 11a). At persistent riffle crest 2, the center of the channel migrated laterally ~100 m with the same results as persistent riffle crest 1 (Fig. 11a). For persistent riffle crest 3, two riffle crests, 1995 and 2005, were located at the same distance upstream despite their respective main channels being located on opposite sides of the valley confinement (Fig. 11b). For persistent riffle crest 4 (Fig. 10b), the riffle crests cluster tightly in the same general location for all 7 years depicted (standard deviation of 7% of d_c) even though the channel flows toward opposite valley walls for different years (1996 and 2005). Figure 11c illustrates that the channel shifts from one valley wall to the other, and the riffle crests have the largest longitudinal spread in distribution for any persistent riffle crest (standard deviation of 15% of d_c). Riffle crests for persistent riffle crest 6 (Fig. 11d) remain transversely center between valley walls despite the channel shifting from the left center to the far right bank. Persistent riffle crest 6 appears to also have a tight distribution (standard deviation of 7% of dc) and there does not appear to be much lateral channel migration.

Visual inspection of older aerial photos showed a number of the seven persistent riffles from 1984-2006 present in 1937, 1947, 1952, 1958 aerial photo sets. For reference, bankfull flow pre-New Bullards Bar (1971) has been estimated at 330 m^3/s (Moir and Pasternack, 2008). The 1937 aerial photo set was taken Oct. 21 of that year, and had a flow of 8.8 m^3/s with muddy water, indicated by the high reflectance of the water surface. Heavy machinery is evident still mining the gravel fill adjacent to persistent riffle 7. Riffle crests in the same location as persistent riffle crests 5 and 6 were apparent in the presence of mid-channel bars. The 1947 photo set (Feb. 22) had a flow of 42 m^3/s, also with muddy waters as well. It appeared that riffle crests were present in the same general location as persistent riffle crests 3, 4, and 6, and it was certain that a riffle crest was located in the same general location as riffle crest 5. The 1952 photo set (Jul. 16) had a flow of 82 m^3/s, and followed spring runoff that exceeded bankfull for ~30 days over the months of May and June of that year. Riffle crests were present in the 1952 photo set in the same general location as all seven persistent riffle crests for 1984-2006 (Fig. 12). The 1958 photo set (Aug. 31) had a flow of 20 m^3/s, and had riffle crests present in the same general locations as persistent riffle crests 2, 5, 6, and 7. Riffle crests were present for all photo sets at persistent riffle crests 5 and 6 locations.

4.3 Riffle Persistence and Valley Width Relations

Valley width over the entire 6-km segment ranged from 102 m to 314 m with a mean of 164m (Fig 13a). For the 7 persistent riffle crests, their respective mean constriction width was 143 m, and the mean widest point was 209 m. The mean longitudinal distance between constrictions (d_c) for the 7 persistent riffle locations was 425 m, ranging from 320 m to 515 m.

Persistent riffles were located closest to the widest point between constrictions (Table 3). The average longitudinal distance from riffle crest to widest valley point was within 16% of d_c, and with 1 outlier removed (persistent riffle crest 6), 10% of d_c. Persistent riffle crests 1-4 were closest to their respective widest point. The distance between the mean persistent riffle crest and the downstream and upstream was 52% and 48% of d_c respectively. The outlier (persistent riffle crest 6) was 50% of d_c to the widest point, 75% of d_c to the downstream constriction, and 25% of d_c to the upstream constriction.

Plotted in Figure 15a-c is valley width, persistent riffle locations, and slope-subtracted longitudinal bed elevations for 1999 and 2006 versus distance upstream. This visually illustrated that persistent riffles tended to cluster at the widest point between constrictions. For slope-subtracted bed elevations (Fig. 13b-c), areas of high relief corresponded to riffle crests, and areas of low relief corresponded to pools. Comparing valley width (Fig 13a) to slope-subtracted bed elevations for 1999 and 2006 (Fig. 13b-c), areas of high relief tended to line up with the widest points between constrictions, and areas of low relief coincided with constrictions. The undulation of the bed appeared to be somewhat in phase with the oscillation of valley width. From about 3700 m upstream to 4100 m upstream there was a long pool that existed for both 1999 and 2006, which appeared to be associated with a long constriction.

5. Discussion

The valley confined wandering gravel-bed reach of the Yuba River from the Narrows Pools to the Highway 20 bridge is unquestionably a dynamic fluvial landscape. Channel change ranged from 4% to as much as 34% of the confined area over the 22-years. Based on the criterion set for planform channel change (3%), planform channel change occurred over every time interval. Additionally, the majority of the reach has been incising at a rate of 0.16 m/yr. With frequent floodplain inundation, and planview and vertical change occurring over every time interval, it is clear that riffles did not persist due to a lack of system dynamism.

Non-persistent riffles crests that occurred were vulnerable to large floods. A number of non-persistent riffle crests formed when large mid-channel gravel bars were deposited (Fig. 10). However, these large mid-channel gravel bars proved unstable and were frequently destroyed and re-formed (Fig. 7). A non-persistent riffle crest that did persist for 3 of the 7 time intervals due to a sudden bend in the valley (Fig. 10d) was removed by a 41-year event of 3823 m^3/s. A non-persistent riffle crest that persisted due a local bedrock outcrop (Fig. 10e) for 5 of the 7 time intervals was removed by a 7.7-yr event of 1218 m^3/s in 2005.

Over the 22 years spanned by the study, seven riffles clustered in the same locations (Fig. 9), with a tight distribution along the distance from the downstream to upstream constrictions (the average standard deviation being 9% of d_c). These riffle locations were not random, nor did they show a tendency to migrate upstream or downstream; they were persistent. Many of the same riffle crests that persisted over the study period were also evident in the 1937, 1947, 1952 (Fig. 12), and 1958 photo sets, suggesting their persistence over many decades. Figures 11a-d show the channel migrated laterally from one side of the valley to the other, islands formed and were removed, secondary channels were cut and filled, yet these seven riffles clustered in the same general location over the 22 years of the study.

The fact that riffles had persisted in the same general location despite significant planform change, indicated some stable forcing factor, unsusceptible to large floods, controlling riffle location. The study revealed a close relationship of persistent riffle crest location to the widest point of the confining valley between valley constrictions. The average distance of riffle crests to the widest point was 16% of d_c, in contrast to the average distances to downstream and upstream constrictions of 52% and 48% of d_c respectively. Persistent riffle crest 6 (Fig 11d) appeared to be an outlier, located upstream of the widest point at a distance of 50% of d_c. A possible reason for this might be that it was located on a bend in the valley, or perhaps due to the drastic change in valley width. Additionally, persistent riffle crest 7 does not appear to form in as wide of a valley expansion as the other 6 persistent riffle crests. Persistent riffle crest 7 may be influenced by a more local channel constriction. All other persistent riffle crests are located on relatively straight sections of the reach (Fig. 9), that exhibit large oscillations in valley width (Fig. 13).

The strongest evidence of the relationship between riffle locations and valley width is provided by the 1999 and 2006 slope-subtracted bed elevation plots (Fig. 13). Figure 13 shows areas of high relief (i.e. riffles) aligned with the widest points of the confining valley and areas of low relief (i.e. pools) aligning with valley constrictions. The oscillation in bed relief appears to be in phase with valley width, suggesting a geomorphic relationship between these two variables. Flume experiments along with 2- and 3-D models resulted in similar undulating bedform depositional patterns in phase width oscillation, with relative highs lined up with the widest portion of the channel and the relative lows lined up in the narrowest portion of the channel (Repetto et al. 2002; Wu and Yeh, 2005).

5.1 Process of Confining Valley Width Control on Riffle Location

Smaller scale elements such as boulders, bedrock outcrops, and point bars all were shown to influence bed morphology by creating zones of high velocity, shear, and sediment transport capacity (Thompson, 2006, MacWilliams et al., 2006). This general process has been termed flow convergence routing (MacWilliams et al., 2006). This general process may apply to the valley-confined Yuba River from the Narrows Pool to the Highway 20 bridge during times of complete floodplain inundation. It may be possible that when the floodplain is inundated, flows interact hydraulically with the valley walls, and the oscillations in the valley width may cause increase flow velocities, shear and transport capacity at constrictions, and decreased flow velocities, shear and transport capacity at the widest points of the valley width. Consequently, sediment is routed through constrictions maintaining pools, and is deposited at the widest point forming riffle crests. Thus a bedform morphology is created that is in phase with channel width oscillations, as can be seen in Figure 13.

5.2 Implications of Valley Width Control on Riffle Location

The implications of this study apply to confined river systems, such as glacial outwash filled valleys or highly leveed rivers. In confined rivers, understanding width-variation controls on forming key riverine features such as riffles and pools may assist in understanding the long-term evolution of morphological diversity and distribution of aquatic habitats. In terms of river management, the results have potentially important implications for stream restoration activities, such as predicting the redistribution of injected gravel or inducing morphological heterogeneity in uniform channels and maintaining constructed features. When constructing instream habitat features, it would be important not to place an artificial riffle in an area that would have constricted flow during times of inundation. If the goal were to improve gravel bar sustainability in leveed rivers, it may be useful to oscillate the width between the levees. Also, understanding width controls on sediment deposition and scour will aid in determining where injected gravel may deposit and form riffle features. Considering the number of confined systems due to levees and topographic controls, the implications of this study may be very useful in future restoration efforts.

6. Conclusion

This study showed that the Yuba River from the Narrows Pool to the Highway 20 bridge is a dynamic fluvial landscape, confined by valley walls. The results suggest that riffles persist in the same location longitudinally due to the stable controls of varying valley width, with areas of high relief aligning with the widest portion of the valley. This study suggests large scale width variations of valley walls play a role in forcing bedform depositional pattern and provide long-term controls of stream bed heterogeneity. The mechanisms behind this may be explained by flow convergence routing causing sediment to deposit in the widest portion of the confining valley due to reduced flow velocities, shear and bedload transport capacity.

Acknowledgements

Financial support for this work was provided by the United States Fish and Wildlife Service Anadromous Fish Restoration Program (Agreement #113323J011). Aerial photos were obtained from Professor Allan James (University of South Carolina), the University of California at Davis Shields Library, DigitalGlobe, Incorporated (Longmont, CO), Jones and Stokes (Sacramento, CA), Globe Xplorer NAIP, and Airphoto USA Archives. Boat-based surveying was conducted by James Kulpa, Environmental Data Solutions (San Rafael, CA). Ground-based surveying was conducted by Aaron Fulton, Scott Morford, and Jason White with the assistance of Davin Sanders, Daniel Suderow, Crystal Replogle, and Michael Catania. Survey data processing and ArcGIS assistance provided by Scott Morford.

References

Alabyan, A.M., and Chalov, R.S., 1998. Types of River Channel Patterns and Their Natural Controls. Earth Surface Processes and Landforms 23, 467-474.

Beechie, T.J., Liermann, M. Pollock, M.M., Baker, S., and Davies, J., 2006. Channel Pattern and River-Floodplain Dynamics in Forested Mountain River Systems. Geomorphology 78, 124-141.

Bhowmik, N. G., and Demissie, M., 1982. Bed material sorting in pools and riffles. J. Hydraul. Div. Am. Soc. Civ. Engr., 108, 1227-1231.

Booker, D. J., Sear, D.A., and Payne, A.J., 2001. Modeling three-dimensional flow structures and patterns of boundary shear stress in a natural pool-riffle sequence. Earth Surface Processes and Landforms 26(5), 553-576.

Brown, R. A. and Pasternack, G. B., 2008. Engineered Channel Controls Limiting Spawning Habitat Rehabilitation Success on Regulated Gravel-bed Rivers. Geomorphology 97:631-654.

Bryant, R.G., and Gilvear, D.J., 1999. Quantifying Geomorphic and Riparian Land Cover Changes Either Side of a Large Flood Event Using Airborne Remote Sensing: River Tay, Scotland. Geomorphology 29, 307-321.

Burge, L.M., 2005. Wandering Miramichi Rivers, New Brunswick, Canada. Geomorphology 69, 253-274.

Burge, L.M. and Lapointe, M.F., 2005. Understanding the Temporal Dynamics of the Wandering Renous River, New Brunswick, Canada. Earth Processes Landforms 30, 1227-1250.

Cao, Z. X., Carling, P., and Oakey, R., 2003. Flow reversal over a natural pool-riffle sequence: A computational study. Earth Surface Processes and Landforms 28(7), 689-705.

Carling, P. A., 1991. An Appraisal of the Velocity-Reversal Hypothesis for Stable Pool Riffle Sequences in the River Severn, England. Earth Surface Processes and Landforms 16(1), 19-31.

Childs, J.R., Snyder, N.P., Hampton, M.A., 2003. Bathymetric and geophysical surveys of Englebright Lake, Yuba-Nevada Counties, California. U.S. Geological Survey Open-File Report, 03–383.

Clifford, N. J., 1993a. Differential bed sedimentology and the maintenance of a riffle-pool sequence, Catena, 20, 447-468.

Clifford N. J., 1993b. Formation of riffle-pool sequences: field evidence for an autogenetic process, Sediment. Geol., 85, 39-51.

Clifford, N. J., and Richards, K. S., 1992. The Reversal Hypothesis and the Maintenance of Riffle-Pool Sequences: A Review and Field Appraisal, in Lowland Floodplain Rivers: Geomorphological Perspectives, edited by P. A. Carling and G. E. Petts, pp. 43-70, John Wiley & Sons, Chichester.

Coulombe-Pontbriand, M. and Lapointe, M., 2004. Geomorphic Controls, Riffle Substrate Quality, and Spawning Site Selection in Two Semi-Alluvial Salmon Rivers in the Gaspe Peninsula, Canada. River Research and Applications 20, 577-590.

Curtis, J.A., Flint, L.E., Alpers, C.N., Yarnell, S.M., 2005. Conceptual model of sediment processes in the upper Yuba River, Sierra Nevada, CA. Geomorphology 68, 149-166.

Desloges, J.R. and Church, M., 1987. Channel and Floodplain Faces in a Wandering Gravel-Bed River. The Society of Economic Paleontologists and Mineralogists 6, 99-109.

Dietrich, W.E., Smith, J.D., and Dunne, T., 1979. Flow and Sediment Transport in A Sand Bedded Meander. Journal of Geology 87, 305-315

Froese, D.G., Smith, D.G., and Clement, D.T., 2005. Characterizing Large River History with Shallow Geophysics: Middle Yukon River, Yukon Territory and Alaska. Geomorphology 67, 391-406.

Emery, J.C., Gurnell, A.M., Geog, C., Clifford, N.J., and Petts, G.E., 2004. Characteristics and Controls of Gravel-Bed Riffles: An Analysis of Data From the River-Habitat Survey. The Journal 18, 210-216.

Grant, G.E. and Swanson, F.J., 1995. Morphology and Processes of Valley Floors in Moutain Streams, Western Cascades, Oregon 89, 83-101

Gurnell, A.M., Downard, S.R., Jones R., 1994. Channel planform change on the River Dee meanders, 1876-1992. Regulated Rivers: Research and Management 9, 187-204.

Gurnell, A.M., 1997. Channel change on the River Dee meanders, 1946-1992, from the analysis of air photographs. Regulated Rivers: Research and Management 12, 13-26.

Hughes, M.L., McDowell, P.F. and Marcus, W.A., 2006. Accuracy Assessment of Georectified Aerial Photographs: Implications for Measuring Lateral Channel Movement in a GIS. Geomorphology 74, 1-16.

Jackson, W.L. and Beschta, R. L., 1982. A model of two-phase bedload transport in an Oregon coast range stream, Earth Surf. Processes Landforms, 7, 517-527.

Jacobson, R.B. and Gran, K.B., 1999. Gravel Sediment Routing From Widespread, Low-

Intensity Landscape Disturbance, Current River Basin, Missouri. Earth Surface Processes and Landforms 24, 897-917.

James, L.A., 2005. Sediment From Hydraulic Mining Detained by Engelbright and Small Dams in the Yuba Basin. Geomorphology 71, 202-226.

Karasev, I.F., 1993. Regularities of Channel Formation and Contradictions of its Concepts. Gidrotekhicheskoe Stroitel'stvo 4, 18-24.

Keller, E.A., 1971. Pools, Riffles, and Meanders: Discussion. Geological Society of America Bulletin 82: 279-280.

Keller, E.A. 1972. Development of alluvial stream channels, a five stage model. Geological Society of American Bulletin 83: 1531-1536.

Keller, E.A. and Florsheim, J.L. 1993. Velocity-reversal hypothesis: a model approach. Earth Surface Processes and Landforms 18, 733-740.

Keller, E.A., and Melhorn, W.N., 1978. Rhythmic Spacing and Origin of Pools and Riffles. Geological Society of American Bulletin 89, 723-730.

Kieffer, S.W., 1989. Geologic Nozzles. Reviews of Geophysics 27, 3-38.

Knighton, D. 1998. Fluvial Forms and Processes: A New Perspective. New York, Oxford University Press Inc.

Lo, C.P. and Yeung, A.K.W., 2007. Concepts and Techniques of Geographic Information Systems. 2nd Ed. New Jersey, Pearson Prentice Hall.

Leopold, L.B., Wolman, G.M., and Miller, J.P. 1964. Fluvial Processes in geomorphology. San Francisco, W. H. Freeman. 522 pp.

Lisle, T.E., 1979. A sorting mechanism for a riffle-pool sequence. Geological Society of American Bulletin 90, 1142-1157.

Lisle, T.E., 1986. Stabilization of a Gravel Channel by Large Streamside Obstructions and Bedrock Bends, Jacoby Creek, Northwestern California. Geological Society of America Bulletin 97, 999-1011.

MacWilliams, M.L., Jr., Wheaton, J.M., Pasternack, G.B., Street, R.L., and Kitanidis, P.K., 2006. Flow convergence routing hypothesis for pool-riffle maintenance in alluvial rivers. Water Resources Research 42, W10427, doi:10.1029/2005WR004391.

Marston, R.A., Girel, J., Pautou, G., Piegay, H., Bravard, J.P., and Arneson, C., 1995. Channel Metamorphosis, Floodplain Disturbance, and Vegetation Development: Ain River, France Geomorphology 13, 121-131.

McKenny, R. 1997. Formation and Maintenance of Hydraulic Habitat Units in Streams of the Ozark Plateaus, Missouri and Arkansas, unpublished PhD dissertation, Pennsylvania State University, 347 pp.

Miller, A. J., 1994. Debris-fan constrictions and flood hydraulics in river canyons: Some implications from two-dimensional flow modeling, Earth Surface Processes Landforms 19, 681–697.

Moir, H.J., Pasternack, G.B., Relationships between mesoscale morphological units, stream hydraulics and Chinook salmon (Oncorhynchus tshawytscha) spawning habitat on the Lower Yuba River, California, Geomorphology (2008), doi:10.1016/j.geomorph.2008.02.001

Montgomery, D.R. and Buffington, J.M., 1997. Channel-reach morphology in mountain drainage basins. Geological Society of America Bulletin 109 (5), 596-611.

Montgomery, D.R., Buffington, J.M., Smith, R.D., Schmidt, K.M., and Pess, G, 1995. Pool Spacing in Forest Channels. Water Resources Research 31, 1097-1105.

Nanson, G.C. and Croke, J.C., 1992. A Genetic Classification of Floodplains. Geomorphology 4, 459-486

O'Conner, J.E., Webb, R.H., and Baker, V.R., 1986. Paleohydrology of pool-riffle pattern development: Boulder Creek, Utah. Geological Society of America Bulletin 97, 410-420.

Parsons, H., and Gilvear, D., 2002. Valley Floor Landscape Change Following Almost 100 Years of Flood Embankment Abandonment on a Wandering Gravel-Bed River. River Research and Applications 18, 461-479.

Passmore, D.G. and Macklin, M.G., 2000. Late Holocene Channel and Floodplain Development in a Wandering Gravel-Bed River: The River South Tyne at Lambley, Northern England. Earth Surface Processes and Landforms 25, 1237-1256.

Pasternack, G. B. 2007. The importance of flow-convergence routing for maintaining riffles and pools on large, regulated, gravel-bed rivers. Geological Society of America Abstracts with Programs 39:6:34.

Repetto, R. Tubino, M., and Paola, C., 2002. Planimetric Instability of Channels with Variable Width. Journal of Fluid Mechanics 457, 79-109.

Richards, K.S., 1976. The morphology of riffle-pool sequences. Earth Surface Processes 1, 71-88.

Sear, D. A., 1996. Sediment Transport Processes in Pool-Riffle Sequences, Earth Surf. Processes Landforms, 21(3), 241-262.

Thompson, A., 1986. Secondary flows and the pool-riffle unit: a case study of the processes of meander development. Earth Surface Processes and Landforms 11, 631-641.

Thompson, D.M. 2001. Random Controls on Semi-Rhythmic Spacing of Pools and Riffles in Constriction-Dominated Rivers. Earth Surface, Processes, and Landforms 26, 1195-1212.

Thompson, D.M., 2006. The Role of Vortex Shedding in the Scour of Pools. Advances in Water Resources 29, 121-129.

Winterbottom, S.J., 2000. “Medium and Short-Term Channel Planform Changes on the Rivers Tay and Tummel, Scotland. Geomorphology 34, 195-208.

Winterbottom, S.J. and Gilvear, D.J., 1997. Quantification of Channel Bed Morphology in Gravel-Bed Rivers Using Airborne Multispectral Imagery and Aerial Photography. Regulated Rivers: Research & Management 13, 489-499.

Woodsmith, R.D., and Hassan, M.A., 2005. Maintenance of an obstruction-forced pool in a gravel-bed channel: stream flow, channel morphology, and sediment transport. Catchment Dynamics and River Processes: Mediterranean and Other Climate Regions 10, 69-196.

Wu, F.C. and Yeh, T.H., 2005. Forced Bars Induced by Variations of Channel Width: Implications for Incipient Bifurcation. Journal of Geophysical Research 110, 1-22 (F02009)

Xu, J., 1996. Wandering Braided River Channel Pattern Developed Under Quasi-Equilibrium: An Example From the Hanjiang River, China. Journal of Hydrology 181, 85-103.

Yang, C.T., 1971. Formation of Riffles and Pools. Water Resources Research 7, 1567-1574.

Table 1. Change in wetted area from one photo set to the next along with the peak daily flow occurring over the time interval.

water year	1984	1986	1991	1996	2002	2004	2005	2006
date of photo	4/24/84	10/6/86	7/2/91	7/16/96	9/30/02	4/1/04	9/23/05	9/28/06
daily flow at time of photo (m^3/s)	42	35	37	58	19	62	23	21
date of largest daily flow for time interval		2/19/86	3/25/89	5/18/96	1/2/97	5/8/03	5/20/05	12/31/05
largest daily flow for time interval (m^3/s)	n/a	2832	742	1427	3823	203	1218	2815
recurrence interval of largest daily flow (yr)	n/a	23.8	4.1	9.1	41.7	1.6	7.7	24.0
number of complete flooding events		21	4	43	25	0	4	26
area of planform change[a] (%)	n/a	34%	8%	17%	29%	4%	8%	14%

[a] Area of Planform Change = {[(Area of Cut)+(Area of Fill)]/(Valley Confined Area)}x100%

Table 2. Results of persistent riffle crest statistical analysis.

riffle crest ID	1	2	3	4	5	6	7	mean
mean riffle crest posititiion distance upstream (m)	652	962	1407	1775	3197	4577	4971	
range in riffle crest position (% of dc)	12%	30%	30%	21%	45%	26%	22%	26%
standard deviation in riffle position (% of dc)	4%	10%	12%	7%	15%	8%	7%	9%

Table 3. Results of persistent riffle crest location and valley width relations quantitative analysis.

riffle crest ID	1	2	3	4	5	6	7	mean
mean riffle crest location distance upstream (m)	652	962	1407	1775	3197	4577	4971	
associated widest point distance upstream (m)	616	975	1436	1756	3164	4340	4913	
associated downstream constriction distance upstream (m)	329	844	1195	1628	3036	4231	4694	
associated upstream constriction distance upstream (m)	844	1195	1628	2039	3356	4694	5179	
d_c: distance between constrictions distance upstream (m)	515	351	433	411	320	463	485	425
distance from mean riffle crest to downstream constriction (% of dc)	63%	34%	49%	36%	50%	75%	57%	52%
distance from mean riffle crest to widest point in the valley (% of dc)	7%	8%	11%	6%	13%	51%	12%	16%[a]
distance from mean riffle crest to upstream constriction (% of dc)	37%	66%	51%	64%	50%	25%	43%	48%

[a] With the outlier riffle crest 6 removed this value becomes 10%

Figure 1. The lower Yuba River, CA from the Narrows Pool (39°13'20"N, 121°17'40"W) downstream to the Highway 20 bridge (39°13'13"N,121°20'7"W).

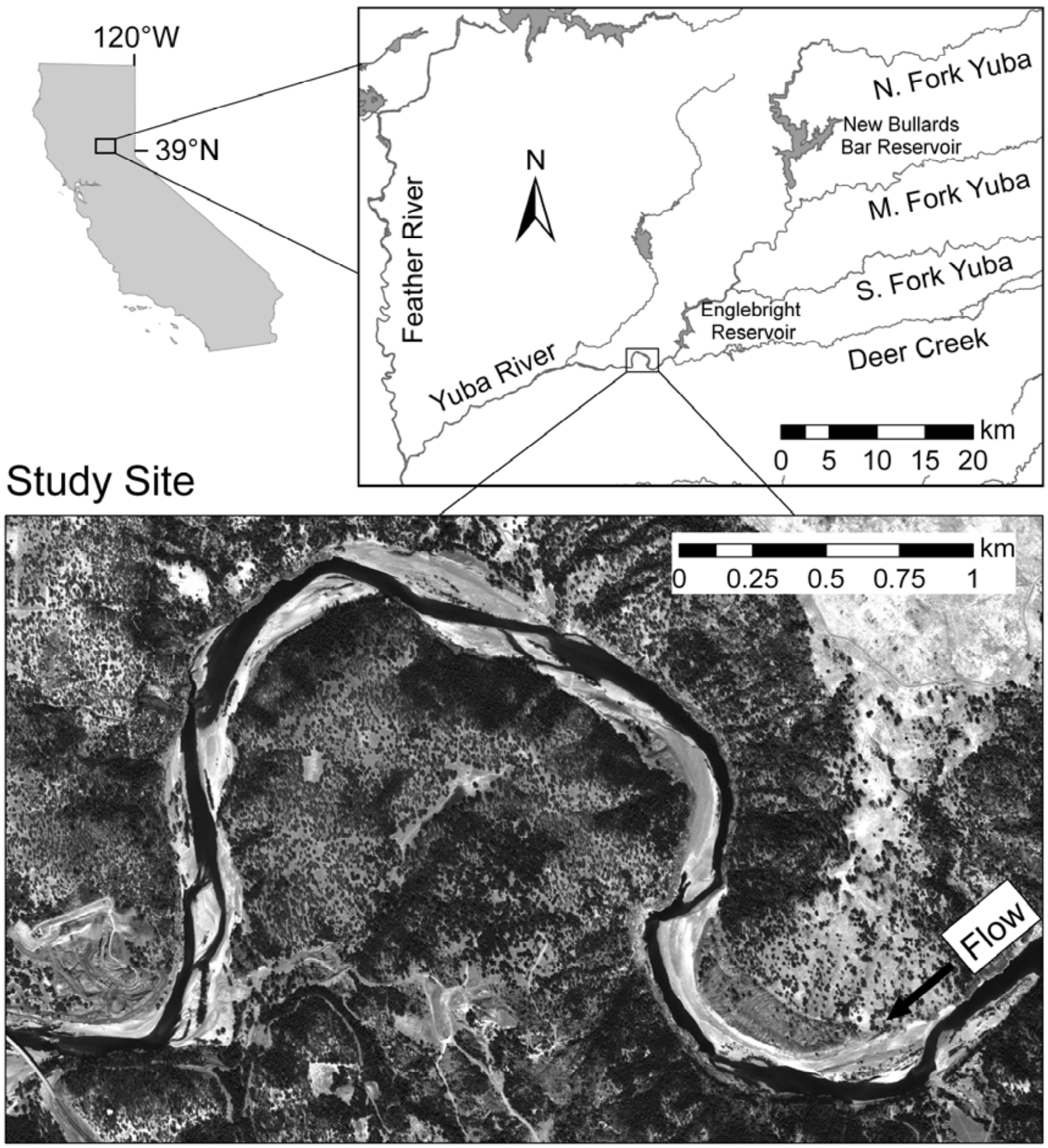

Figure 2. A nearly bankfull flow of 142 m^3/s on the lower Yuba River. Note the willows growing at the slope break that delineates the bankfull channel from the floodplain.

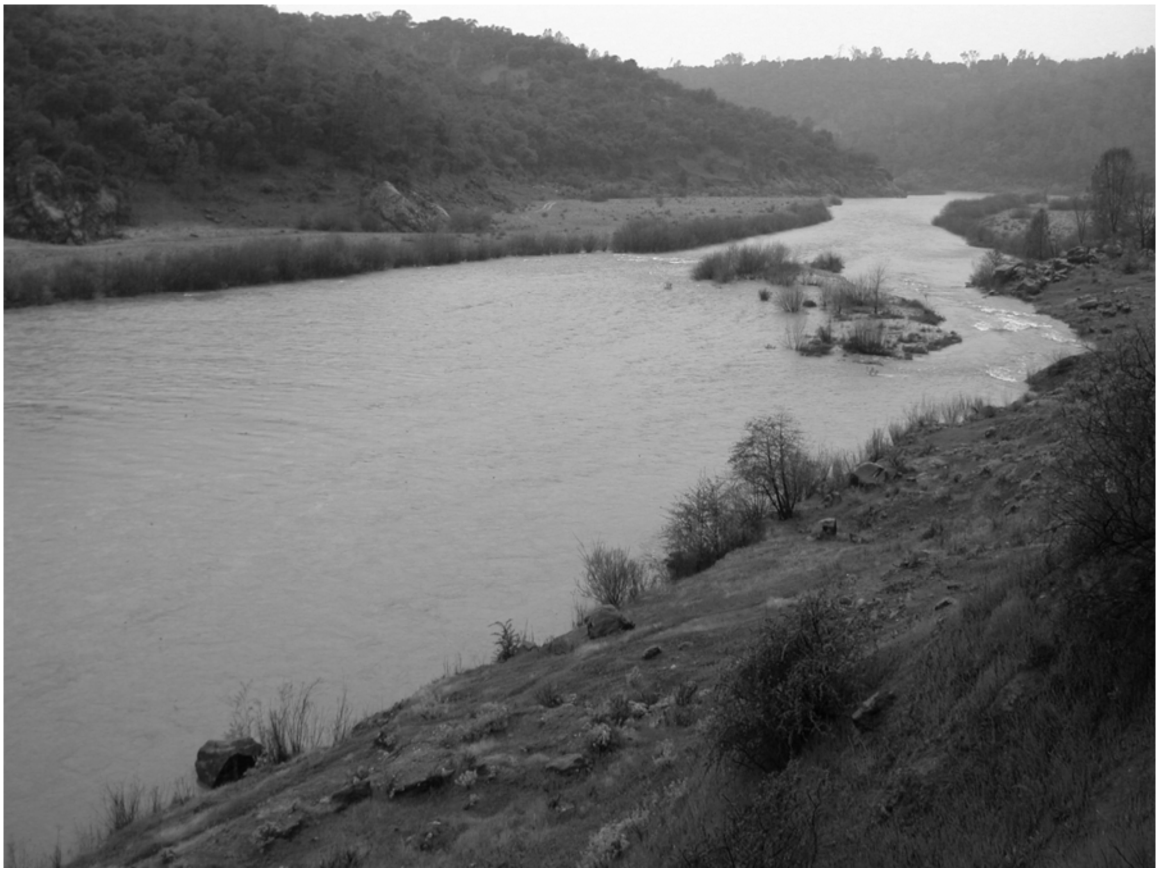

Figure 3. Valley-wide inundation of the lower Yuba River's floodplain at a flow of 736 m^3/s.

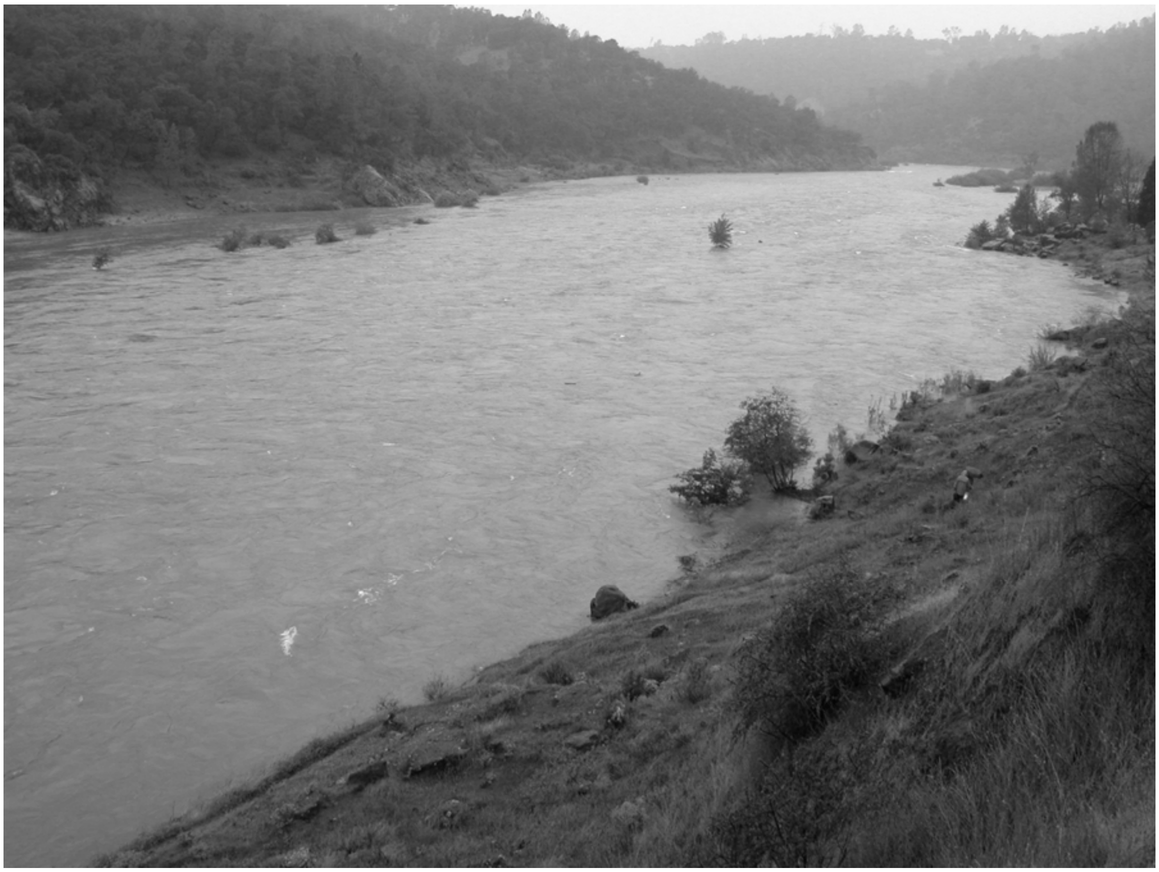

Figure 4. The lower Yuba River a) before, b) during, and c) after a 24-yr flood event. The photo time series shows willow removed, a secondary channel formation, and partial removal the of the mid-channel bar.

a) October 12, 2005: 22 m^3/s

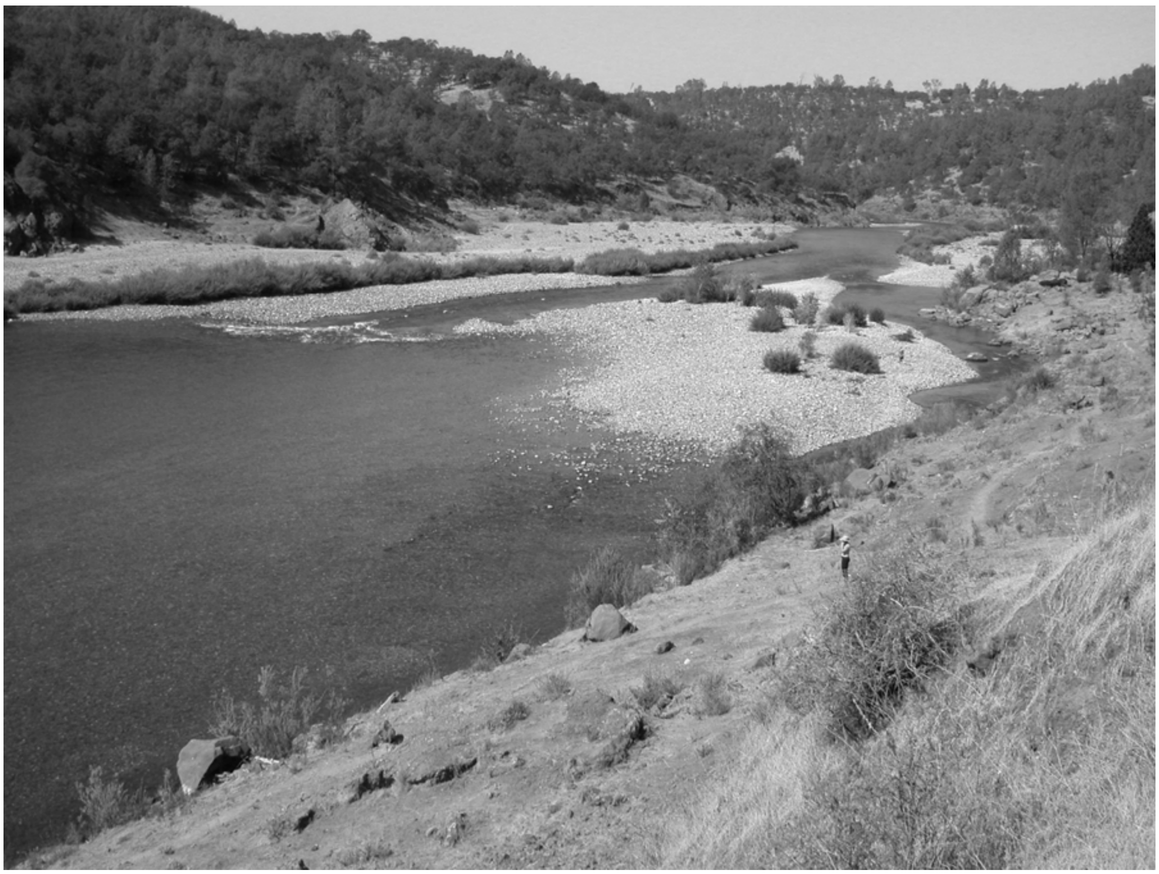

b) December 31, 2005: 2996 m^3/s

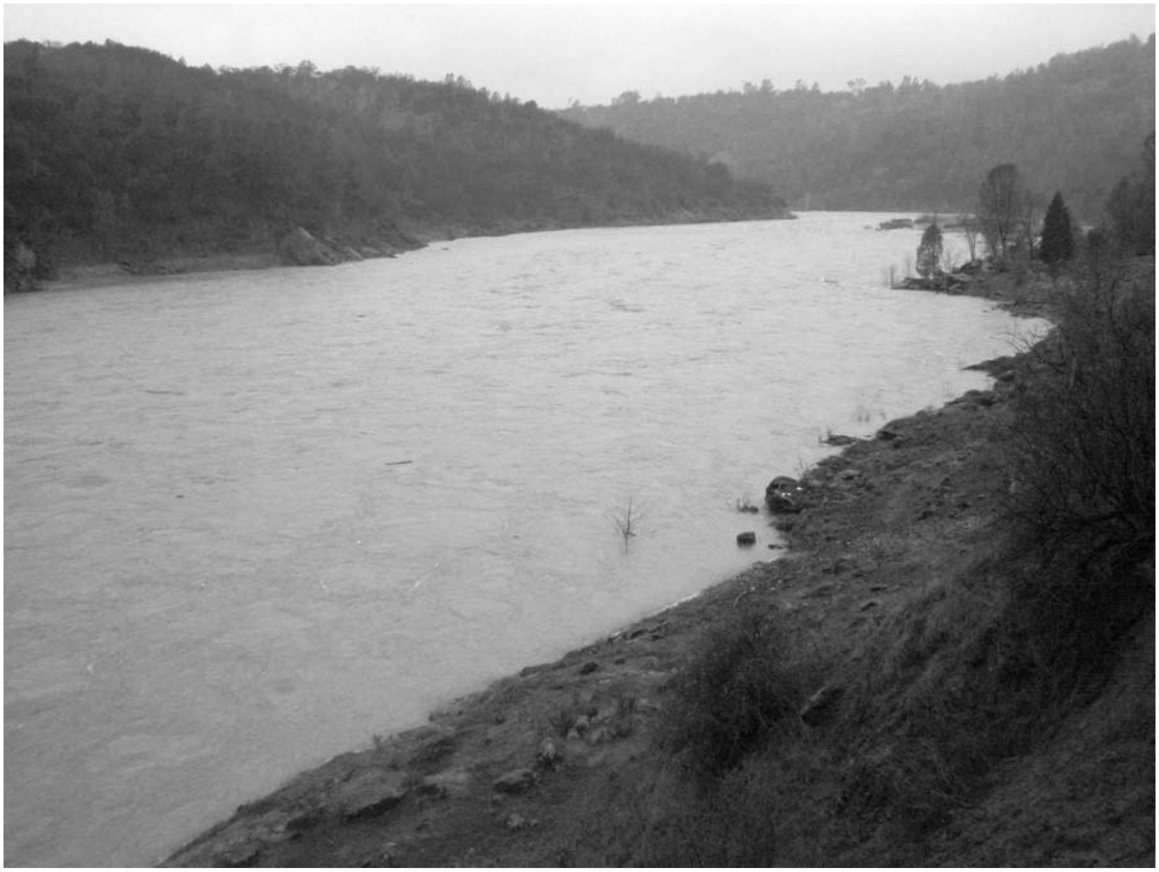

c) August 21, 2006: 39 m^3/s

Figure 5. Georectified photos for a) 1984, b) 1991, c) 1996, and the orthophoto for d) 2002.

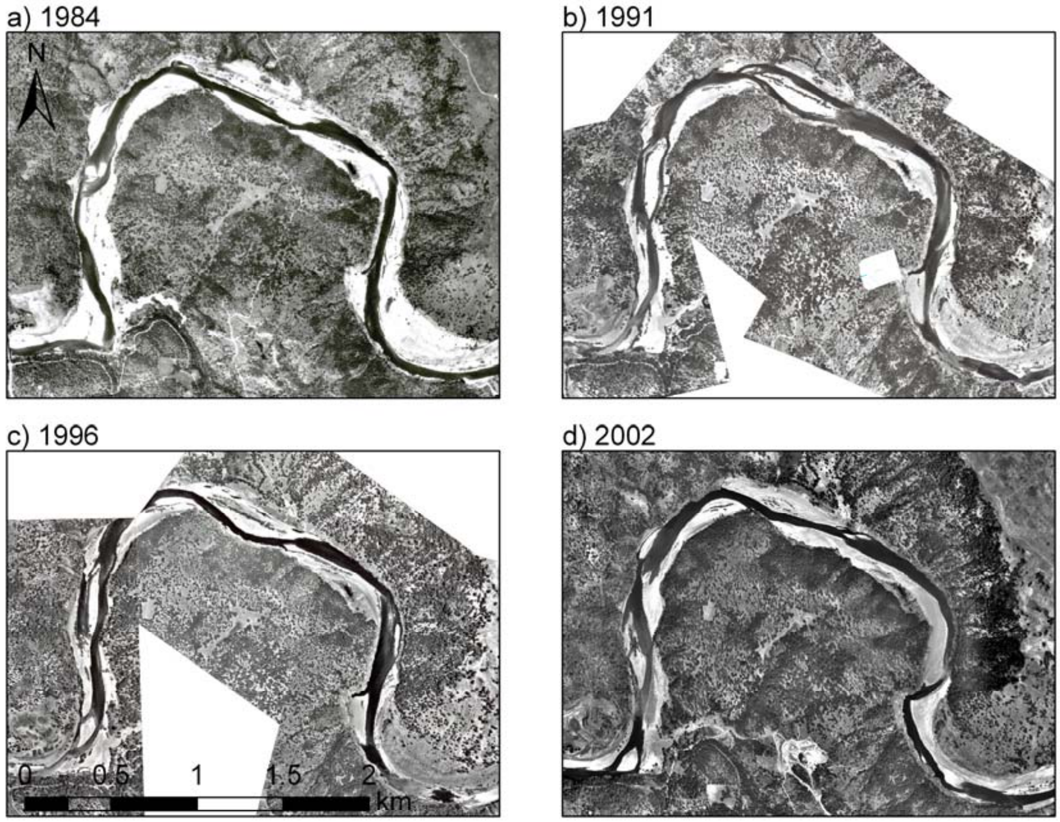

Figure 6. The 2006 DEM constructed in ArcGIS from the land-based total station and boat-based fathometer survey.

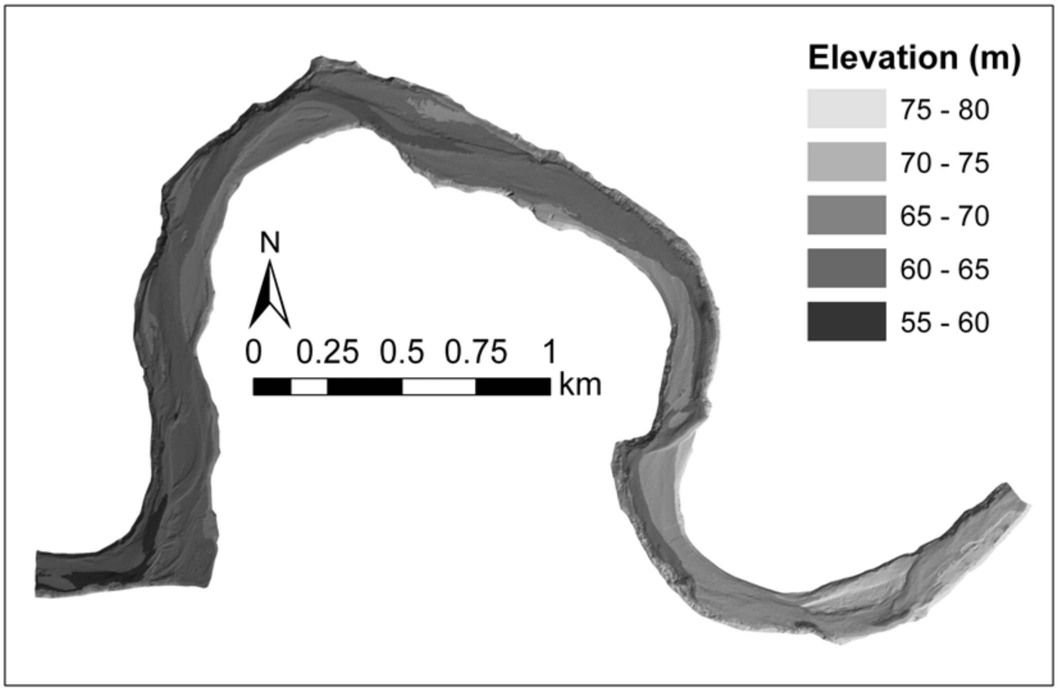

Figure 7. An illustration of wetted channel change over four time intervals: a) 1984 to 1991, b) 1991 to 1996, c) 1996 to 2002, and d) 2002 to 2006.

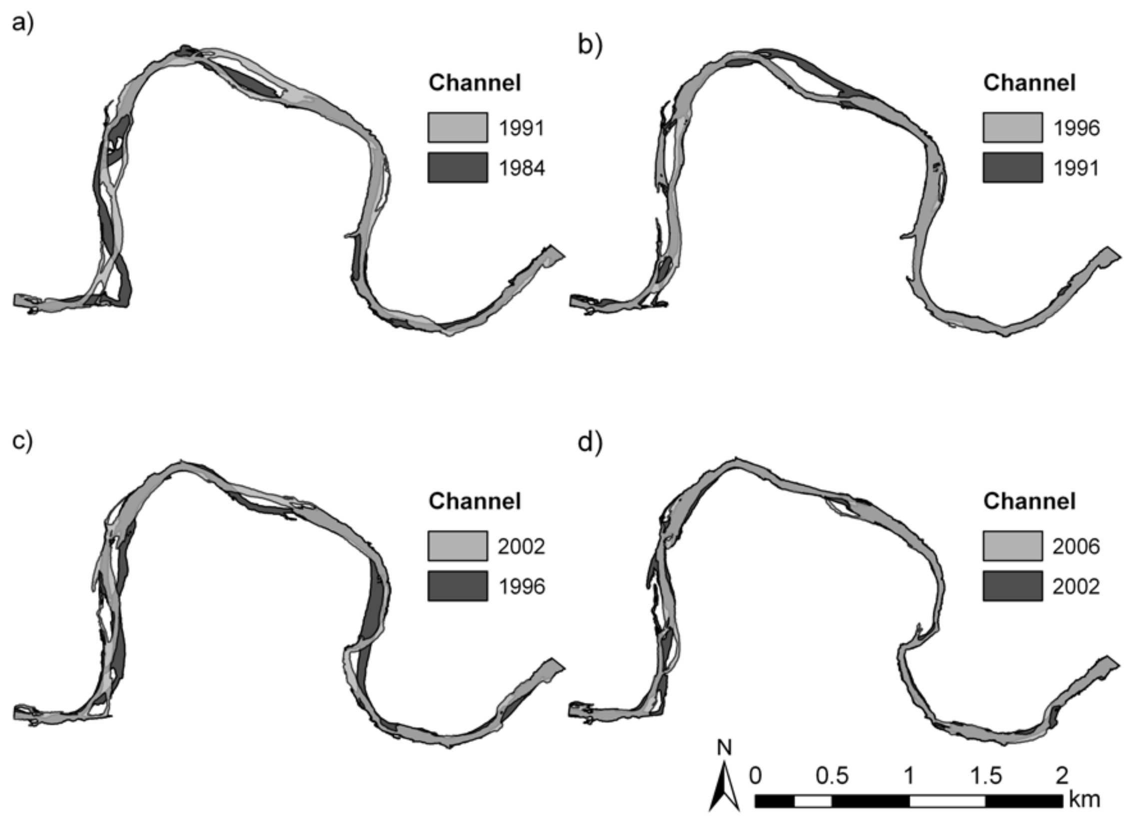

Figure 8. Channel thalwag bed elevations for 1999 and 2006 starting at the Highway 20 Bridge traveling upstream. Plots show overall incision of the channel from 1999 to 2006.

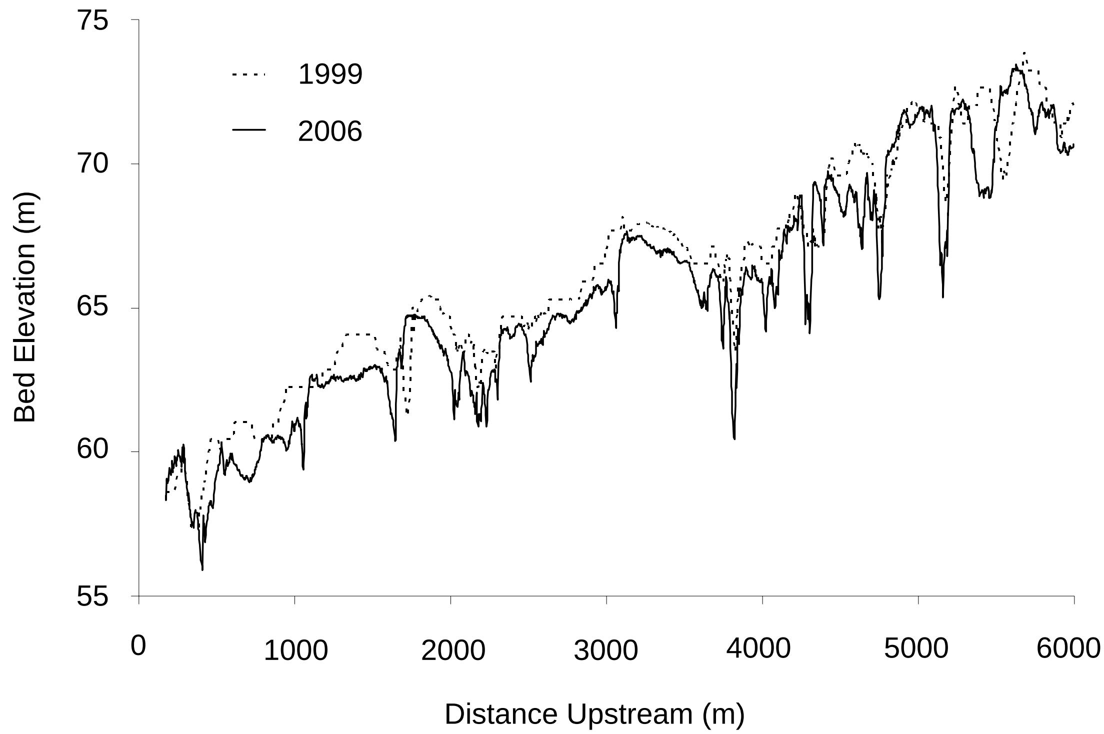

Figure 9. 2006 aerial photo of the study reach with the confining valley border delineated and persistent riffle crests identified.

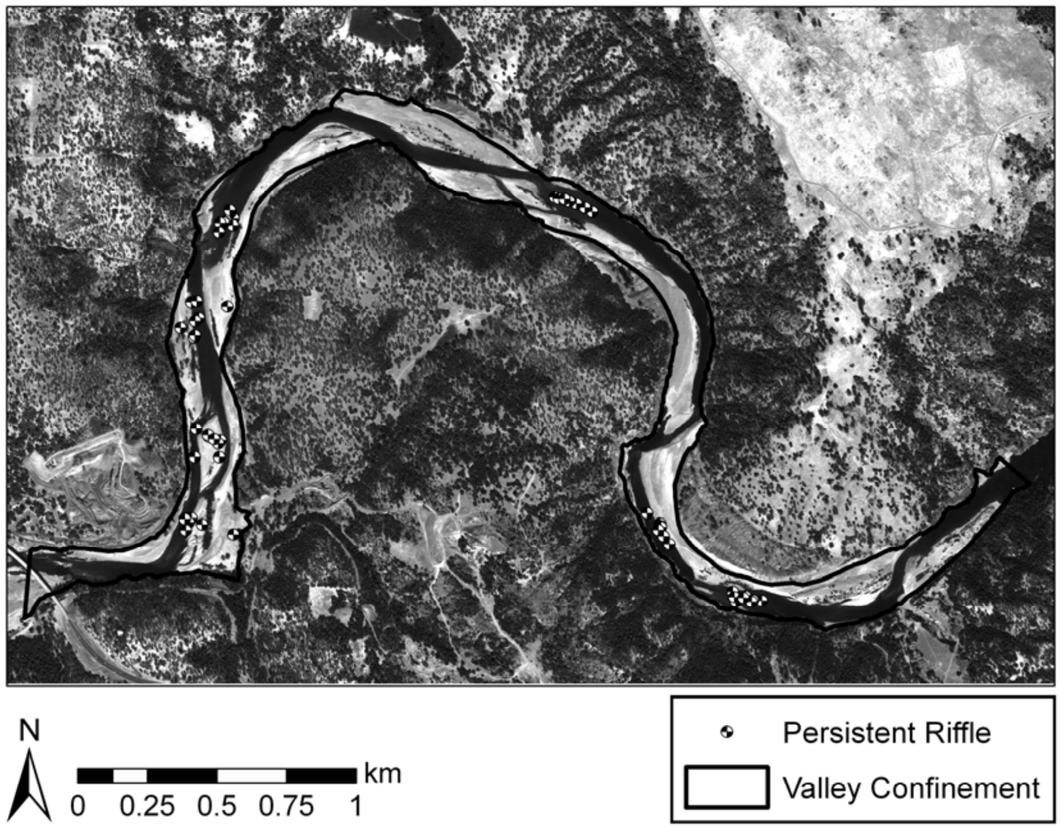

Figure 10. Non-persistent riffle crests occurring due to a) low flow competence at channel confluences, b) lateral channel cutting at channel bifurcation, c) mid-channel bar high relief, d) lower flow competence due to sudden bend in valley, and e) local bedrock channel constriction.

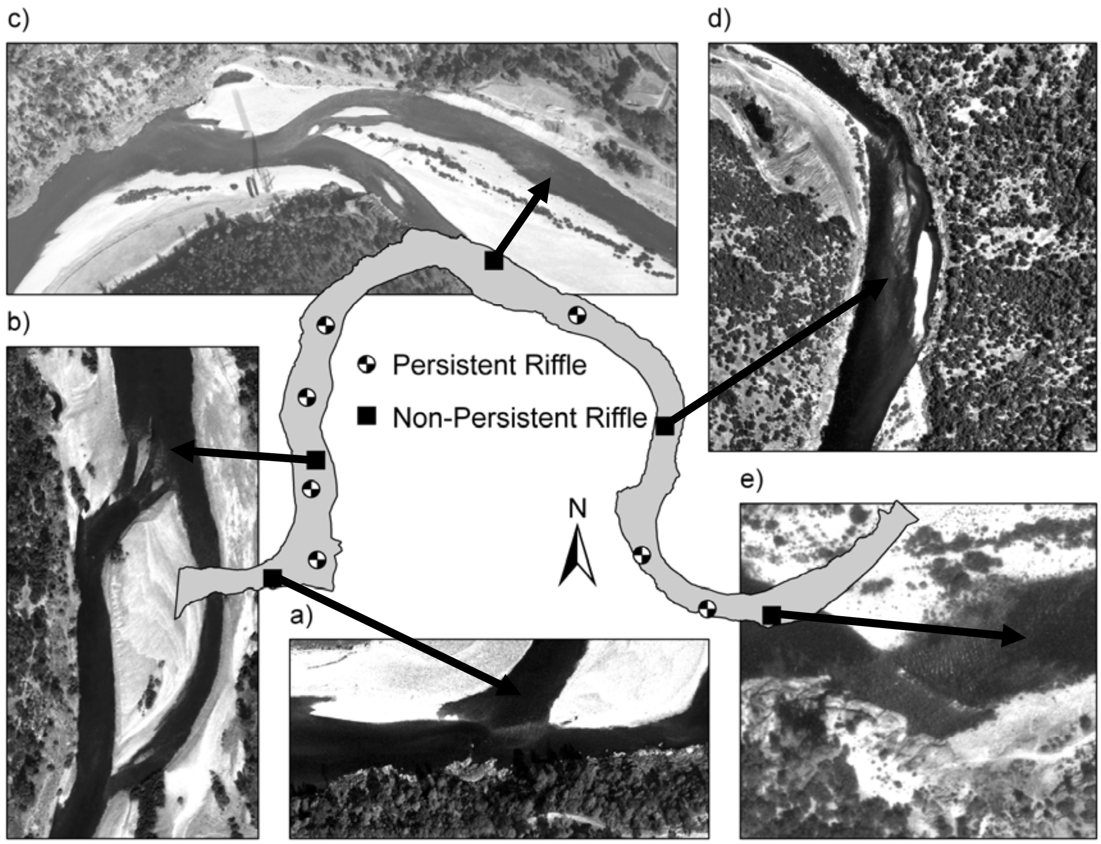

Figure 11. A close up of persistent riffle crests a) 1 and 2, b) 3 and 4, c) 5, and d) 6 and 7. The illustrations show the channel the channel migrates, mid-channel bars are removed and formed yet the riffle crests have remained clustered in the same general location.

a)

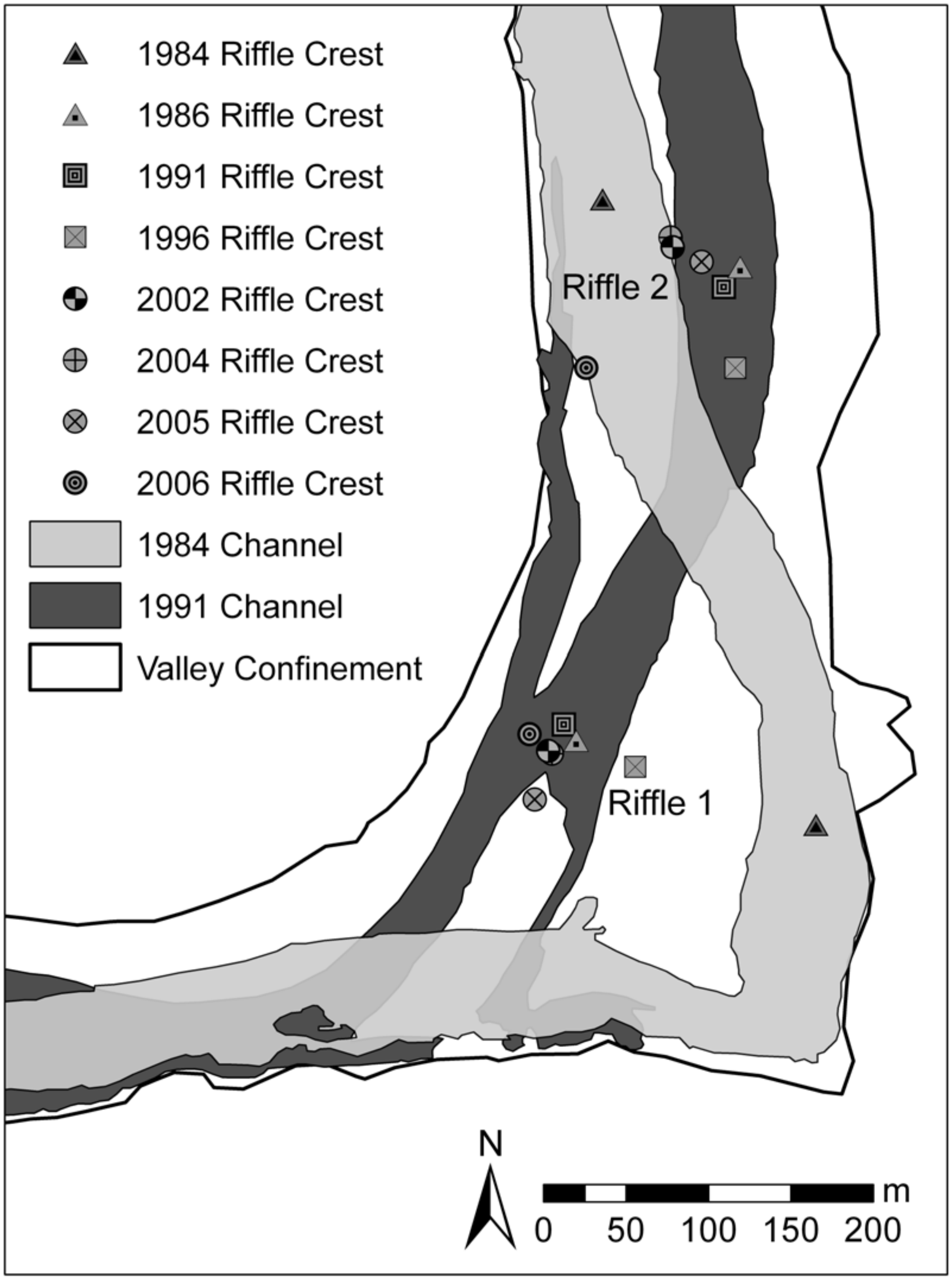

1984 Riffle Crest
1986 Riffle Crest
1991 Riffle Crest
1996 Riffle Crest
2002 Riffle Crest
2004 Riffle Crest
2005 Riffle Crest
2006 Riffle Crest
1984 Channel
1991 Channel
Valley Confinement
Riffle 2
Riffle 1
N
m
0
50
100
150
200

b)

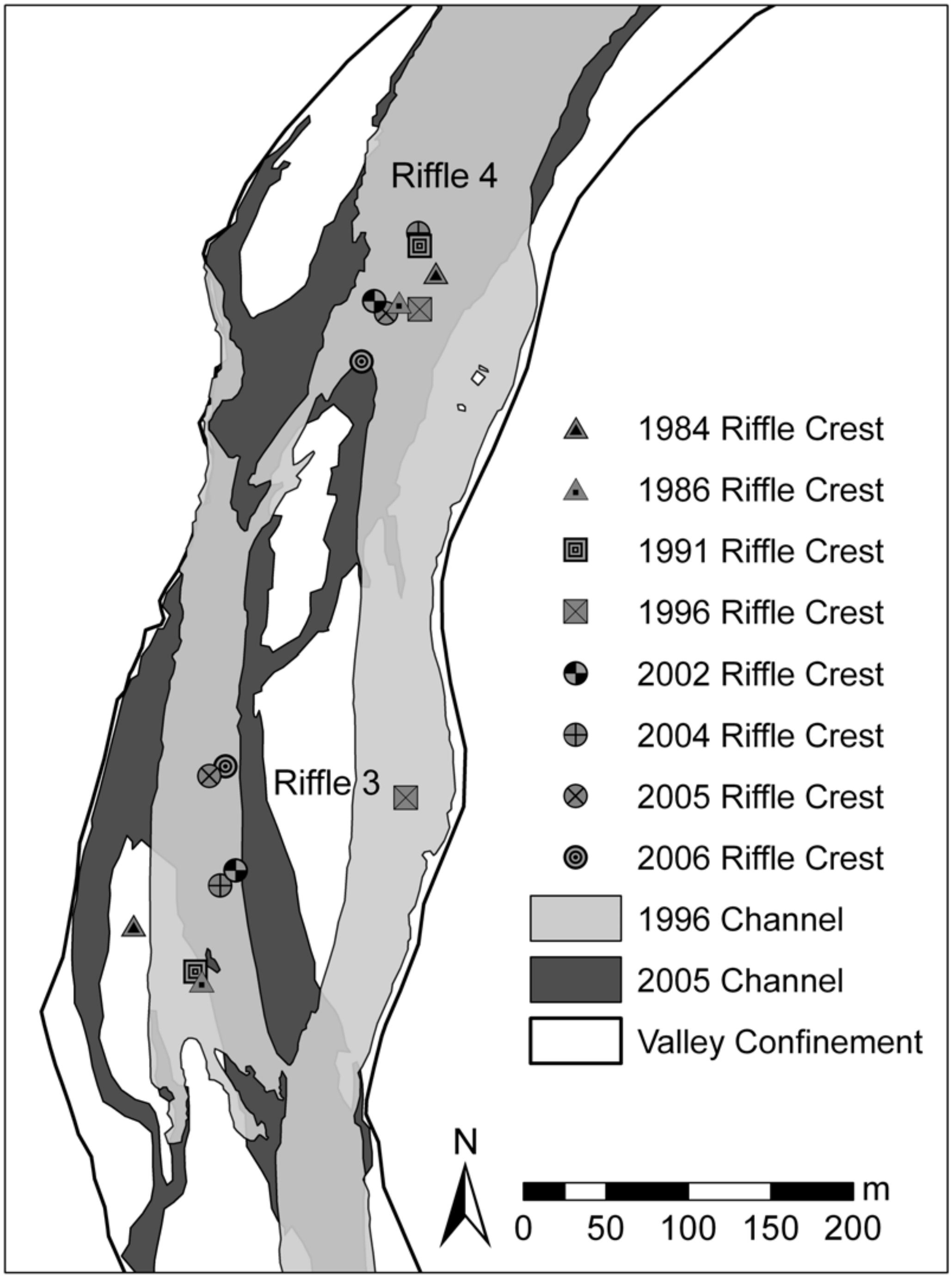

Riffle 4
Riffle 3
1984 Riffle Crest
1986 Riffle Crest
1991 Riffle Crest
1996 Riffle Crest
2002 Riffle Crest
2004 Riffle Crest
2005 Riffle Crest
2006 Riffle Crest
1996 Channel
2005 Channel
Valley Confinement
N
m
0
50
100
150
200

c)

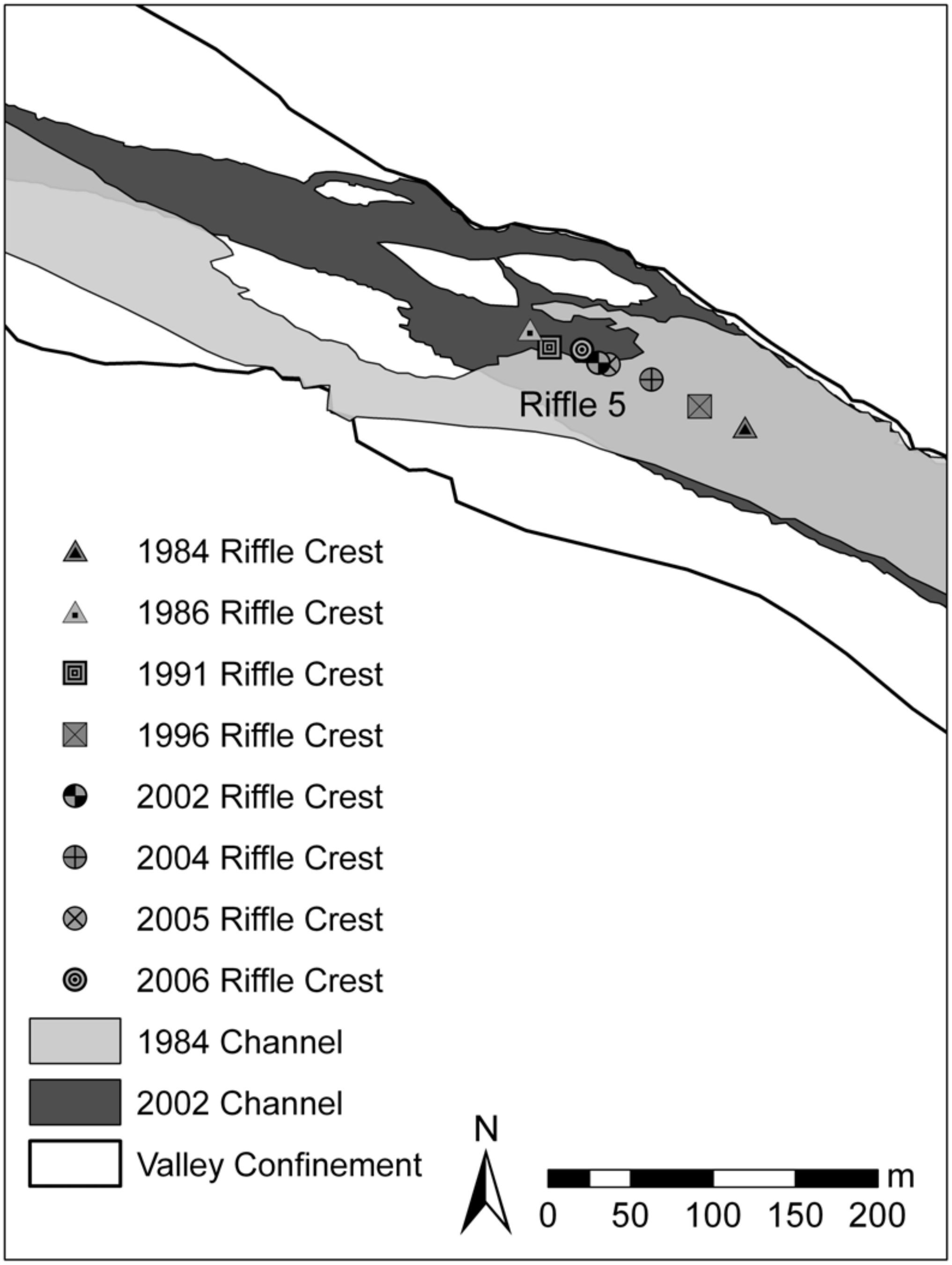

Riffle 5
1984 Riffle Crest
1986 Riffle Crest
1991 Riffle Crest
1996 Riffle Crest
2002 Riffle Crest
2004 Riffle Crest
2005 Riffle Crest
2006 Riffle Crest
1984 Channel
2002 Channel
Valley Confinement
N
0 50 100 150 200 m

d)

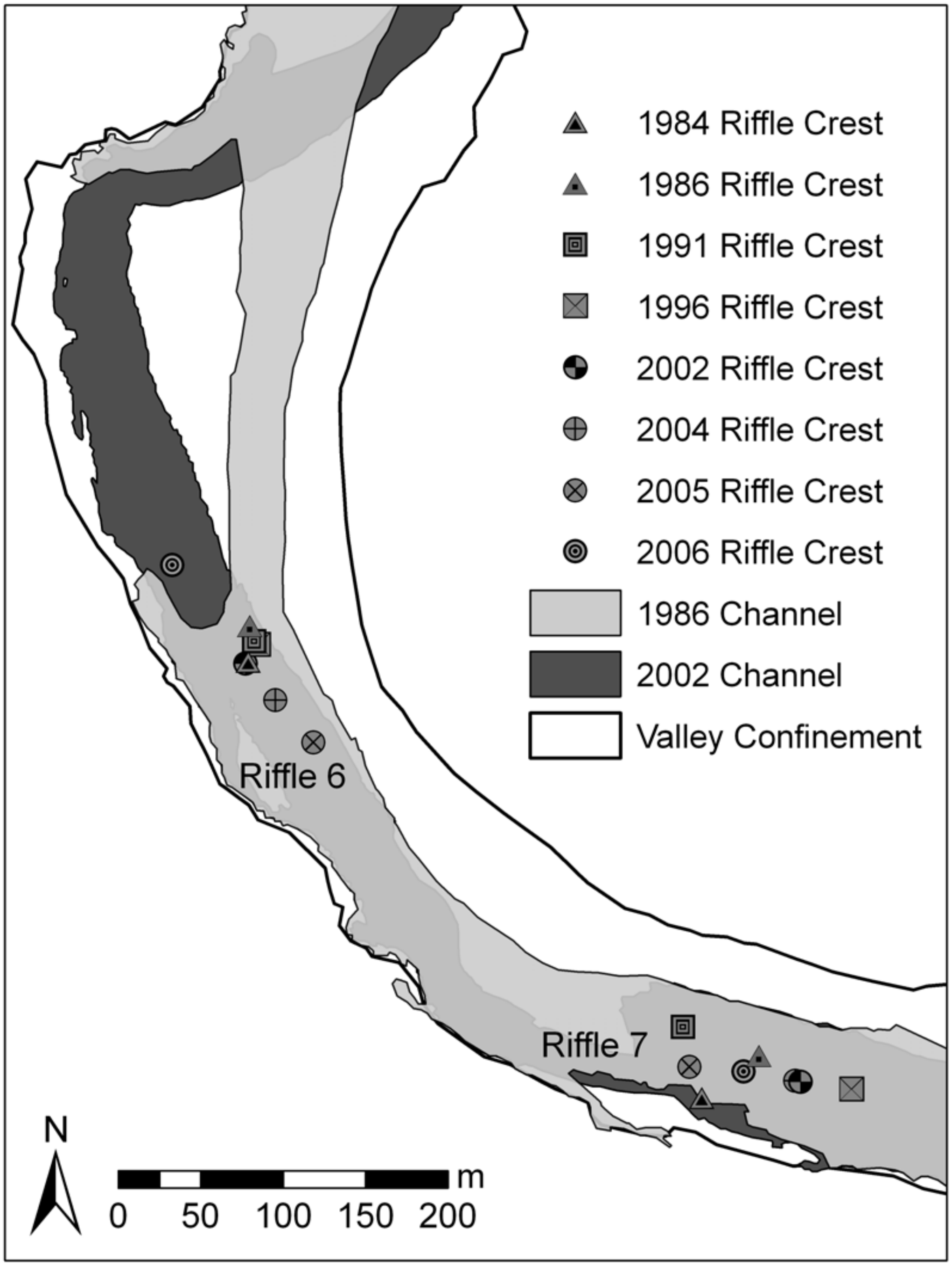
1984 Riffle Crest
1986 Riffle Crest
1991 Riffle Crest
1996 Riffle Crest
2002 Riffle Crest
2004 Riffle Crest
2005 Riffle Crest
2006 Riffle Crest
1986 Channel
2002 Channel
Valley Confinement
Riffle 6
Riffle 7
N
m
0
50
100
150
200

Figure 12. Riffle crest locations for the 1952 aerial photo. Riffle crests are located in the same general location as the mean riffle location of the 22 year study.

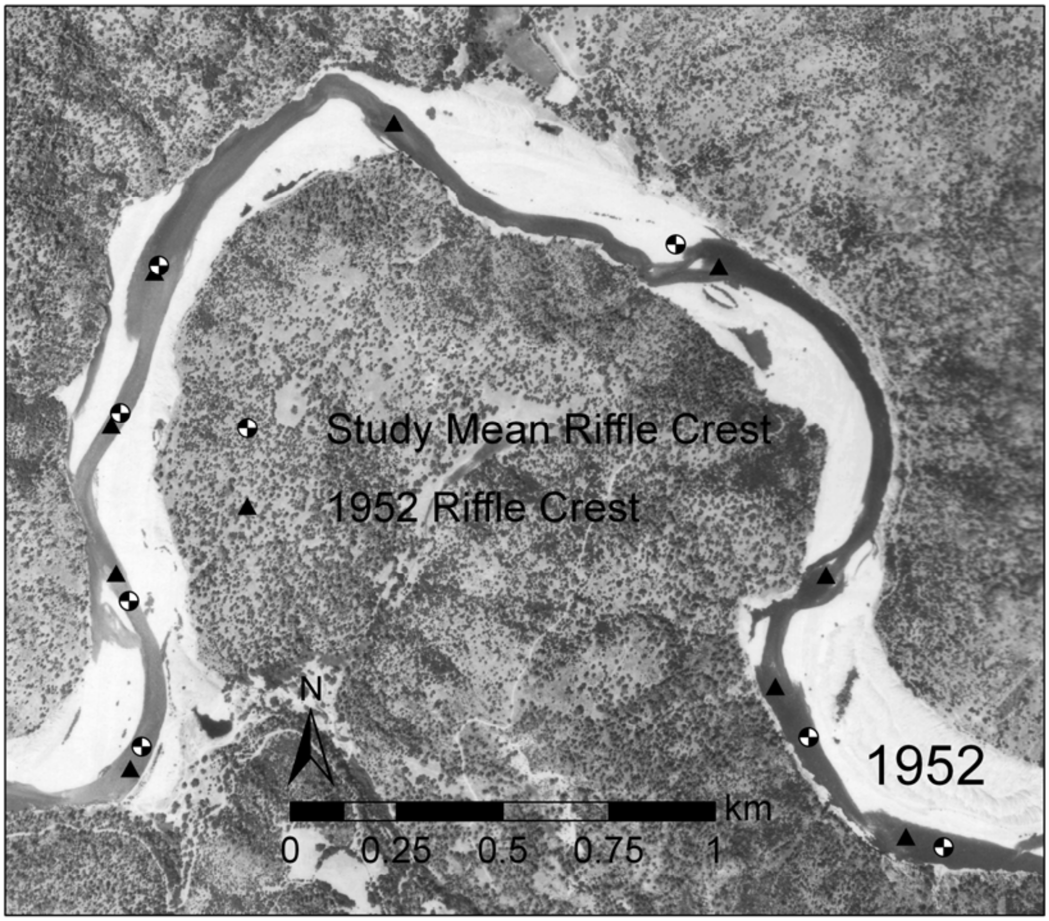

Figure 13. A longitudinal comparison of 1999 and 2006 slope-subtracted bed elevations and valley width, along with persistent riffle locations for all photosets. The dashed lines with up arrows show areas of valley width expansion coinciding with relative topographic highs (riffles). The dashed lines with down arrows show areas of valley width constriction coinciding with relative topographic lows (pools).

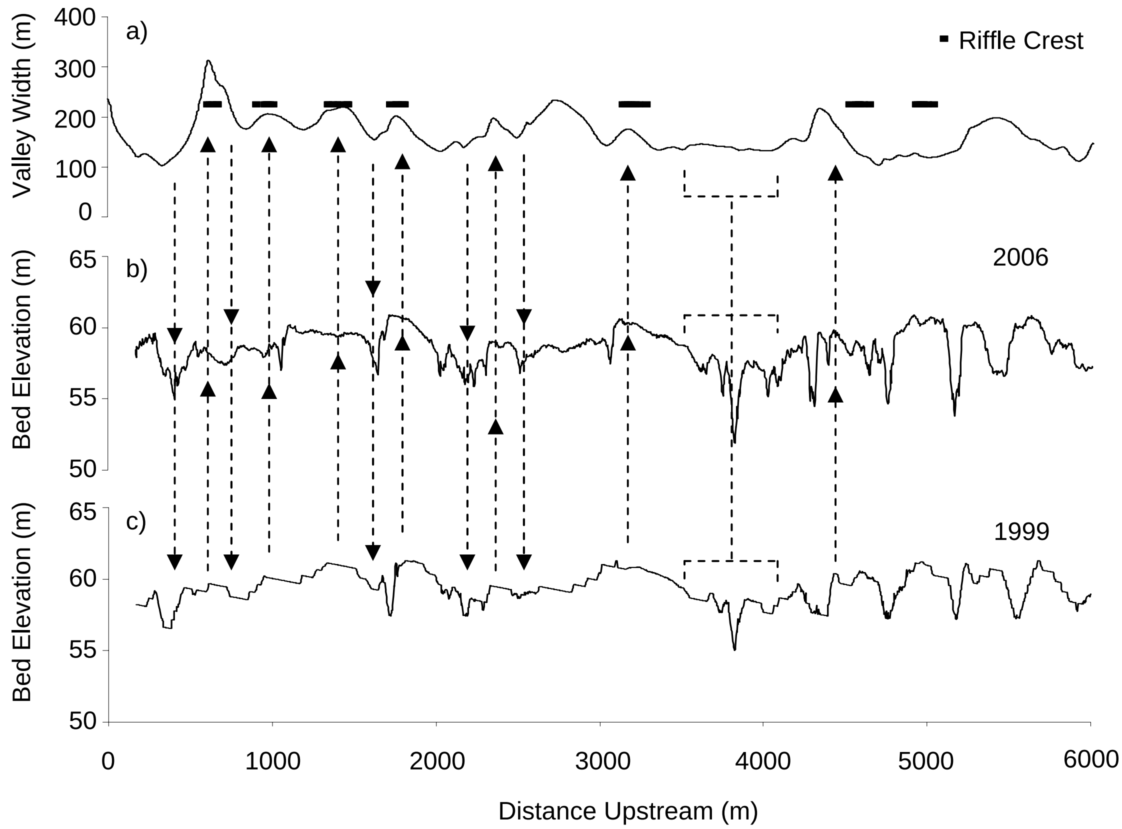

APPENDIX 3

Riffle-Pool Self-Maintenance and Flow Convergence Routing Confirmed on a Large Gravel Bed River

Title: Riffle-Pool Self-Maintenance and Flow Convergence Routing Confirmed on a Large Gravel Bed River

Authors:

April M. Sawyer[1], Gregory B. Pasternack[1*], Hamish J. Moir[2], and Aaron A. Fulton[1]

Addresses:

[1]Department of Land, Air, and Water Resources, University of California, One Shields Avenue, Davis, CA 95616-8626, USA;

[2]Macaulay Institute, Craigiebuckler, Aberdeen, AB15 8QH, UK.

*Corresponding Author

ABSTRACT

The processes responsible for riffle-pool self-maintenance in gravel-bed rivers have been sought after for decades. Most studies have focused on small wadable rivers, but even then they lack much evidence for overbank flood conditions or a spatially explicit characterization of morphodynamics. In this study, 1-m horizontal resolution digital elevation models (DEMs) were collected from a riffle-pool-run sequence before and after an overbank flood with a 7.7-year recurrence interval on the relatively large gravel-bed lower Yuba River, California. DEM differencing was used to quantify the magnitude and pattern of flood-induced change. Cross-section based analysis and 2D physics-based modeling were performed for discharges ranging from 0.147-7.63 times bankful discharge to evaluate the hydraulic mechanisms responsible for the observed changes. One key finding was that riffle-pool relief increased 0.42 m, confirming the occurrence of hydrogeomorphic self-maintenance. Spatially complex patterns of scour and deposition exceeding 0.15 m at the scale of sub-width morphological units were reasonably predicted by the 2D mechanistic model that accounts for convective acceleration, whereas a cross-section based method underperformed the 2D model significantly. Consequently, multiple scales of channel non-uniformity and a dynamic flow regime were interpreted to cause the observed self-maintenance, by the mechanism termed “flow convergence routing” by MacWilliams et al. (2006).

1. INTRODUCTION

Riffle-pool sequences are important morphological characteristics of low to moderate gradient gravel-bed streams. They are determined by complex interactions between hydraulic and sediment transport processes. Their formation has been attributed to local flow convergence and divergence in either freely formed (i.e. cross channel flow or sediment transport) or forced (i.e. channel bends, obstructions) channel patterns (Lisle, 1986; Montgomery and Buffington 1997). Generally, pools are topographic depressions covered with finer sediment, while riffles are topographic highs covered with coarser bed material; these two features are defined relative to each other (O'Neill and Abrahams, 1984; Montgomery and Buffington, 1997). Under low-flow conditions vertical variations in topography along the length of a river control hydraulics and sediment transport; pools having slow, divergent flow and low transport competence, determined by a low water-surface slope; and riffles having faster, convergent flow and moderate transport competence due to a steep water surface slope (Clifford and Richards, 1992). Riffle-pool morphology creates physical heterogeneity that promotes habitat diversity for instream species (Gorman and Karr, 1978; Brown and Brown, 1984; Palmer, 1997; Giller and Malmqvist, 1998; Woodsmith and Hassan, 2005).

A key question related to riffle-pool sequence is whether they are self-sustaining, and if so, how? Explanations for riffle-pool sequence self-maintenance have been debated for decades. Geomorphologists historically observed a reversal in mean flow parameters (e.g. mean velocity, near bed velocity and bed shear stress) as a possible explanation for riffle-pool self-maintenance in gravel-bed rivers. The velocity reversal hypothesis states that "at low flow the bottom velocity is less in the pool than in the adjacent riffles" and that "with increasing discharge the bottom velocity in pools increases faster than in riffles" (Keller, 1971, p. 754). Gilbert (1914) first described a reversal in bottom velocity but was unable to quantify this observation. Lane and Borland (1954) speculated that channel hydraulic conditions in riffle-pool sequences and channel geometry both affect scour and deposition patterns during high flow events. Actual velocity measurements were not taken to support these observations until Keller's (1969, 1971) study on Dry Creek near Winters, California. Keller measured near-bed velocity at pool and riffle cross sections at several discharges that were safe to wade into. He showed that the velocities became similar as flow increased, but not that the near-bed velocity in the pool actually became higher than that in the riffle. Thus, he coined the "hypothesis of velocity reversal" (Clifford and Richards, 1992; MacWilliams et al. 2006).

The velocity reversal hypothesis has been highly contentious in the scientific community. Uncertainty mainly arises from different approaches to describing this phenomenon (Woodsmith and Hassan, 2005). Early studies, such as Teleki (1971) and Whitaker and Jaeggi (1982), refuted Keller's velocity reversal hypothesis due to inconsistency with hydraulic principles and lack of a description of water-sediment interface conditions. Other studies aimed to describe the velocity reversal hypothesis using alternative parameters, such as mean boundary shear stress (Lisle, 1979), section-averaged velocity (Keller and Florsheim, 1993; Clifford and Richards, 1992) and section-averaged shear velocity (Carling, 1991).

Increasingly, field-validated computational models are being used to describe and evaluate hydraulic phenomena (Keller and Florsheim, 1993; MacWilliams et al., 2006; Pasternack et al., 2008). These models are capable of characterizing high flows under which field measurement are impractical. MacWilliams et al. (2006) stated that the velocity reversal hypothesis was not adequate to describe processes responsible for riffle-pool maintenance on

Dry Creek in a re-examination of Keller's original study using 2D and 3D models. They did not reject Keller's (1969, 1971) original proposed ideas but, rather, they proposed the concept of flow-convergence routing as a "new working hypothesis" to describe these processes. It states that flow converges in riffles at low flows, causing armoring, gradual incision and diminishing relief, but that during high magnitude, infrequent floods, flow converges in pools, causing rapid scour that enhances relief. MacWilliams et al. (2006) also reviewed all studies of velocity reversal (incorporating a range of flow parameters) and stated that these should be viewed as a "suite of multiple working hypotheses for explaining riffle-pool morphology" based on different maintenance mechanisms present in varying channel conditions. This flow-convergence routing hypothesis is further explored in conjunction with the velocity reversal hypothesis in this study to qualify riffle-pool maintenance mechanisms in a large, dynamic gravel-bed river system.

A key gap in the existing knowledge of riffle-pool maintenance is the lack of studies in larger gravel-bed rivers, defined as those with a non-dimensional base-flow width to median bed material size ratio $>10^3$ and a width too large to be spanned by the length of a fallen riparian tree. Most previous studies have sought to observe pool and riffle hydraulics over a wide range of flows, necessitating safe and practical wadable conditions or a narrow channel that can be spanned by a simple bridge for measurement during floods (e.g. Keller, 1969, 1971; Richards, 1976a, b; Clifford and Richards, 1992), both situations requiring relatively small streams. Wood, boulders and bedrock outcrops often force channel constriction and alter channel hydraulics in small streams (Thompson et al. 1998, 1999). In such circumstances, pool geometry is controlled by constrictions where flow and sediment convergence encourages scour and pool maintenance, while exit slopes control deposition at the pool tail (Thompson et al., 1998). However, the degree of impact of such localized features on large gravel-bed rivers is unknown.

The overall goal of this study was to address this critical research gap by investigating the mechanisms of riffle-pool self-maintenance on a large river meeting the above criteria. Two key factors enabled the characterization of the response of a riffle-pool unit on a large river to an infrequent flood: 1) a uniquely managed river basin (as described in section 2) in a Mediterranean climate in a water year with two long periods of low flow punctuated by a single high-magnitude, short duration flood that enabled detailed pre- and post-flood channel characterization and 2) high-resolution, two-dimensional (2D) hydrodynamic modeling that simulated the effect of vertical and lateral channel non-uniformity on bed scour during the peak of the flood. Thus, the specific objectives of this study were to a) quantify riffle-pool reversals in depth-averaged velocity and bed shear stress as well as section-averaged velocity and bed shear stress at an ecologically important riffle-pool unit on a large river subjected to an overbank flood, b) compare cross-section based hydraulic geometry analysis and 2D hydrodynamic modeling for their ability to predict channel conditions such as width, depth, velocity, and discharge-slope relations, c) relate the pattern of scour and deposition caused by the flood to non-dimensional shear stress predictions made using a 2D hydrodynamic model, and d) re-assess whether the flow-convergence routing hypothesis is suitable to describe processes responsible for riffle-pool morphology maintenance for a large river. By combining field data, cross-section analyses, and mechanistic modeling, it was possible to obtain a new and unique perspective on riffle-pool maintenance for large rivers. Although this study does not end debate on the topic, it confirms the existence and geomorphic significance of flow convergence routing in a large gravel-bed river for the first time.

2. STUDY AREA

The Yuba River basin has a Mediterranean climate with hot, dry summers and cool, wet winters. Relative to other basins draining the Sierra Nevada range, the Yuba has among the highest mean annual precipitation, with more than 1,500 mm in the upper basin (WRCC, 2003). On average, snowmelt comprises approximately 50% of the annual runoff into the Yuba River except for during wet years when winter storm runoff augments annual runoff (YCWA *et al.* 2000). The Yuba River flows southwest from the western slope of the Sierra Nevada in northern California and drains a 3,490 km^2 watershed in Sierra, Placer, Yuba and Nevada counties (CALFED, 1999) (Fig. 1). It has a 2,610 m elevation drop from the upper basin to the confluence with the Feather River close to Marysville and Yuba City at ~10 m above mean sea level. The North, Middle and South Forks of the Yuba River converge in a canyon above Englebright Dam, and then Deer Creek, a sizable regulated tributary draining ~220 km^2, joins the Yuba ~1.2 miles downstream in the canyon.

The Yuba River basin has been developed for hydropower production, water supply, flood regulation, gold mining and sediment control (James, 2005). During the California Gold Rush of the mid- to late 1800's, gold-bearing terrace sediments were hydraulically mined after the readily available placer deposits were exhausted. Miners used mercury sluice boxes to wash and extract gold. As a result, mercury laden hydraulic mine tailings from tributaries substantially increased the sediment supply to the Yuba River. Before hydraulic mining, hillslope erosion naturally dominated sediment production (James, 2005). According to G. K. Gilbert (1917), unlicensed hydraulic mining supplied ~522 million m^3 of sediment to the Yuba River until the Sawyer Decision of 1884 ended such large-scale operations (Curtis et al., 2005).

Englebright Dam was built in 1941 to serve as a debris barrier on the main stem Lower

Yuba River (LYR). With a relatively small water storage capacity of 82.6 million m^3, the reservoir generates some hydroelectric power and contributes to irrigation-based agriculture. In 1970, New Bullards Bar Reservoir was completed at a site ~10 km upstream from Englebright on the North Fork Yuba River. It has a total storage capacity of 1.19 billion m^3 and functions as the dominant flood control and water supply reservoir in the Yuba River basin (LYRFTWG, 2005). Given that the Middle and South Forks do not have large reservoirs, it is common for large rainstorms and spring snowmelt to produce uncontrolled floods that overtop Englebright. Historically, the natural hydrograph of the Yuba River was characterized by rapid flow fluctuations in November through March due to direct storm runoff from large rain storms, a sustained snowmelt flow from April through June, and a stable summer base flow from July to October (LYRFTWG, 2005). Large natural inter-annual variations also occurred (Fig. 2). Streamflow data are recorded at the United States Geological Survey (USGS) Smartville gage (#11418000) 0.5 km downstream of Englebright Dam in the bedrock canyon. During the period between the completion of Englebright Dam in 1942 and New Bullards Bar in 1971, the statistical bankful discharge (Q_b, 1.5 year recurrence interval) at the Smartville gage was 328.5 m^3s^{-1}. In the period since 1971, the gage's Q_b is 159.2 m^3s^{-1}.

Present-day channel conditions are fundamentally governed by past and present human activities. Dams, bank alteration, and in-channel mining are common activities occurring simultaneously that alter the natural state of many rivers. These activities often cause narrowing, incision, changes to channel pattern and coarsening of bed sediments as a result of reduction in bedload sediment supply and increased transport capacity (Williams and Wolman, 1984; Kondolf, 1997). California's regulated rivers draining the Sierra Nevada have narrowed by ~50-70%, lost most active gravel bars, incised ~1-10 m and become armored with cobbles since dams were built (e.g. Kondolf, 1997; Edwards, 2004). However, even though Englebright Dam blocks all bedload, the LYR remains a wandering gravel bed river with a valley-wide active zone due to the gravel-rich hydraulic-mining deposits. The absence of a bedload influx drives a rapid valley-wide incision rate on the order of ~10 m over 65 years. Yet, based on a comparison of photographs taken by G. K. Gilbert in 1906 and a series of aerial and ground-based photographs taken from 1937 to 2006, a sequence of pools and riffles has persisted for decades despite the rapid rate of long-term incision (Fig. 3). Other historical channel changes in the lower valley include some anthropogenic bank and meander bend stabilization with large dredger tailings from hydraulic-mining in the late 1930s, channel activation and abandonment, riparian vegetation growth cycles and natural levee stabilization. In summary, the geomorphology of the modern LYR is heavily impacted, but an abundant supply of coarse bed material and a relatively natural flow regime (especially bedload mobilizing flood flows) have enabled riffles and pools to maintain themselves in the same locations for 30-100 years. These factors make this river an appropriate and interesting case for investigating pool-river self-maintenance in dynamic gravel-bed rivers.

2.1 Timbuctoo Bend study site

Downstream of Englebright Dam after the bedrock canyon ends, a valley-wide wandering gravel-bed river exists (Fig. 1). This study focuses on a ~ 450 m long by ~ 200 m wide riffle-pool-run unit of the LYR 6.25 river-km downstream of Englebright Dam at the apex of a large meander bend in the valley called "Timbuctoo Bend" (39°13'56"N, 121°18'48"W). Timbuctoo Bend is characterized by active gravel bars, a well-connected floodplain, secondary and tertiary flood channels and non-uniform channel geometry. Specifically, the study site has a large and dynamic island/bar complex that defines a riffle-pool-run morphology (upstream to downstream). Below Q_b, a perennial side channel exists along the river-right bank of the study site; above Q_b the island and part of the floodplain are submerged. The bankful channel in 2004 and 2005 was defined by moderately steep alluvial banks lined by non-encroaching, semi-permanent, low-growing woody riparian vegetation (mostly *Salix* spp.) (LYRFTWG, 2005). At $\sim 2 \cdot Q_b$ there are locations with valley-wide flow, and then at $\sim 3\text{-}4 \cdot Q_b$ there is widespread valley-wide flow. Isolated, streamlined bedrock outcrops with localized scour holes exist on both sides of the valley in the study area. According to Moir and Pasternack (2008), the bed material at the site was a gravel and cobble mixture (D_{50} of 60 mm, and D_{90} of 123 mm) with very little sand present near the bed surface and a heavily armored riffle crest. The channel bed slope at Timbuctoo Bend in 2004 was 0.0054.

The Yuba River historically hosted large runs of fall and spring run Chinook salmon (*Oncorhynchus tshawytscha*) (Yoshiyama et al., 1996). According to the California Department of Fish and Game (1993), the Yuba River "historically supported up to 15% of the annual run of fall-run chinook salmon in the Sacramento River system". The spring-run chinook population is now present in very low numbers due to habitat loss after dam construction and hydraulic mining, causing genetic homogenization with the fall-run chinook (Yoshiyama et al., 1996). This study site within Timbuctoo Bend on the LYR was reported by local fisheries biologists to be one of the most heavily used by fall-run spawners since Englebright Dam's construction. The number of redds counted at the study site in 2004 was 434.

In May 2005 a flood occurred on the Yuba River due to a large rainstorm beginning on 15 May, which abated after 2 pm on 16 May and then resumed again after 6 pm on 17 May. Rainfall stopped at 5 pm on 19 May. In the upper Yuba watershed at Lake Spaulding (1572 m amsl) the total rainfall during the event was 218.19 mm, with a peak intensity of 7.87 mm/hr in the evening of 18 May. Prior to the flood the river was at a base flow of ~30 m^3s^{-1} for 6 months with spring snowmelt elevating flows throughout April 2005. The flood peaked at 1,215.8 m^3s^{-1} during the night of May 21, 2005. Using log-normal flood frequency analysis on the 1971-2004 dataset, this corresponded to a 7.7 year recurrence interval. By May 31 the flow had receded off the floodplain and it was evident that the channel had changed significantly, warranting investigation. Three weeks later the flow had reduced to 85 m^3s^{-1}. During September 2005 managers reduced the flow to 19.5-24 m^3s^{-1} for the annual inspection and maintenance of the powerhouse at Englebright Dam.

3. METHODS

The key data that was collected to characterize channel change at the study site involved a high-resolution, feature-based topographic survey shortly before and shortly after the May 2005 flood. Digital elevation models (DEMs) from these surveys were used to drive at-a-station hydraulic geometry analysis, 2D hydrodynamic models, and DEM differencing. Hydraulic field data collected before, during, and after the flood were used to help prepare and validate the models. The four discharges that were analyzed were the autumn low flow (23.4 m^3s^{-1}), present-day Q_b (159.2 m^3s^{-1}), the 1942-1971 Q_b (328.5 m^3s^{-1}), and the peak of the 7.7 year event (1,215.8 m^3s^{-1}). These discharges represent the low to middle range of the natural flood hydrograph of the Yuba River at Timbuctoo Bend.

3.1 Field Methods

3.1.1 Topography

Detailed topographic data was collected before and after the May 2005 flood. For the pre-flood condition, data was collected during low flows from September 2004 to March 2005 using a similar method to Brasington et al. (2000), Pasternack et al. (2004, 2006), and Elkins et al. (2007). A Trimble 5700 was used to perform static surveys to establish three permanent benchmarks in geographic coordinates, NAD83. Corpscon 6.0 was used to convert those coordinates to California State Plane Zone 2 (NAD83) coordinates. Working from these benchmarks, a Topcon GTS-802A robotic total station measured bed positions on a staggered grid with supplemental points as needed to resolve bed features (e.g., boulders, slope breaks, redd dunes, etc). The few unwadable locations were mapped from a small inflatable raft. After quality checks, the survey yielded 28,008 points. The mean sampling density in the channel was 0.617 points/ m^2. A lower sampling density was used on the relatively flat floodplain, yielding an overall sampling density for the whole study area of 0.418 points/ m^2. Surveying accuracy was assessed using 98 control network checks and was found to average 0.013 m in the horizontal and 0.011 m in the vertical, which is significantly smaller than the natural error induced by the bed material, typically ranging in size between 0.05-0.2 m.

For the post-flood condition, site bathymetry was surveyed using a boat-based approach on the falling limb of the flood shortly after bedload transport had abated. The survey was performed on June 10 and 11, 2005 over which period flows attenuated from 167 to 116 m^3s^{-1}. A private hydrography firm (Environmental Data Solutions, San Rafael, CA) was contracted to partner in this effort to produce a map meeting U.S Army Corps of Engineers' rigorous Class 1 standard (±0.15m vertical accuracy; USACE, 2002). A customized 6-m long Boston Whaler was outfitted with an Odom Hydrotrack survey-grade fathometer with a 3°, 200-kHz transducer.

Position data for the fathometer were collected using a Trimble 5700 real-time kinematic GPS receiving corrections by radio from an on-site base station located on one of the pre-established benchmarks. Both streams of data were recorded onto a laptop running Hypack Max 4.3 (Hypack, Inc., Middletown, CT). Where depth permitted, the boat made cross sections on a ~3-m interval and did six longitudinal transects approximately evenly spaced across the channel. To account for the water surface slope and its changes through time, four Mini Troll 400 vented pressure transducers (In-situ, Inc., Fort Collins, CO) were placed in the river along the study site and their elevations were surveyed using a total station. An algorithm within Hypack (tide adjustments) was used to interpolate water surface slopes based on the distance between the pressure transducers. In post-processing, a radial filter was applied to the boat-based data to ensure a 0.25-m spacing between points. Quality assurance and quality control information beyond the scope of this summary is on file with the contractor. The floodplain was subsequently surveyed with a Leica TPS 1200 robotic total station using the same approach as described above. In September and October 2005 when flow was at its lowest, the Leica total station was used to map all remaining gaps in the dataset. In addition, two regions where the boat had been used were re-surveyed with the Leica total station as a quality check to compare the results of the two methods. Accounting for both data collection methods and quality checks, a total of 48,914 points were collected to characterize the post-flood surface. The mean sampling density in the channel was 1.141 points/ m^2 and that for the entire site including the floodplain was 0.734 points/ m^2. Topographic data from each survey were imported into Autodesk Land Desktop 3 to create a DEM of the study site pre- and post-flood using a standard TIN-based approach with breaklines (Wheaton et al., 2004; Pasternack et al., 2004, 2006; Elkins et al., 2007).

3.1.2 Hydraulics

Cross-sectional depth and velocity data were collected along three transects (Fig. 4) on February 13, 2005 using standard methods appropriate for validating a 2D hydrodynamic model (Wheaton et al., 2004; Pasternack et al. 2004, 2006; Brown and Pasternack, 2008). The only modification of the method for this study (on a much wider river) was to use the Topcon GTS-802A to survey the exact position of each paired measurement of depth and velocity, which were collected an average of 2.87-m along a transect. This allowed field data to be precisely compared to model predictions for the same location. Transects 1 and 2 span the mainstem channel and were used to also estimate total discharge (Q), whereas transect 3 spanned only the side channel. Measurement errors were ±1 cm for depth using a stadia rod and ±33 mm s^{-1} root mean square for velocity using a Marsh-McBirney Flo-Mate 2000. Velocity was sampled at 30 Hz and averaged over 30 seconds at 0.6×depth from the water surface to obtain a measure of the depth-averaged velocity. Measuring velocity at one position within the water column was appropriate given the uniform flow conditions and low relative bed roughness (water depth was 10-20 × local D_{50}) in the location of the three transects. Studies of flow around individual large grains and pebble clusters demonstrate that point measurements of velocity at arbitrary locations on a gravel-bed will be strongly influenced by these features at the 0.1-0.5 m scale (Acarlar and Smith, 1987; Paola et al., 1986; Kirkbride and Ferguson, 1995; Buffin-Belanger and Roy, 1998; Lawless and Robert, 2001a, b).

In addition, the water surface elevation (WSE) along the edge of the channel was mapped using the Topcon total station for three of the four discharges modeled in this study (23.4, 328.5, and 1,215.8 m^3s^{-1}). Because it was impossible to know in advance or during the event when the flood peak would occur, physical indicators of the 1,215.8 m^3s^{-1} peak were surveyed with the Topcon total station the following day during the falling limb. The peak stage was clearly delineated by bank scour and a line of debris.

3.1.3 Sedimentary analysis

The general sedimentary characteristics across the entire site were visually assessed and mapped prior to the flood (Moir and Pasternack, 2008). In this procedure, sediment character was defined in terms of the dominant and sub-dominant size classes (i.e., boulder > 256 mm, cobble 64 – 256 mm, gravel 2 – 64 mm, sand and finer < 2 mm, all sizes being intermediate axis diameter). In addition, the 'Wolman-walk' procedure (Wolman, 1954) was used to conduct 32 pebble counts at the study site in autumn 2004. Although they were all carried out under low discharge conditions, flows at certain regions of the site was too deep and/or fast to permit sampling using this technique. Visual assessment of those areas was performed. Thus, samples were not evenly distributed throughout the site or across all morphological units; they tended to be biased towards accessible channel margin locations. At each location, a minimum of 100 particles (mean = 120, range = 100-219) were sampled across a ~3 m × 3 m section of the bed. The position of the center point of each sampling location was surveyed using the Topcon total station.

3.2 At-a-station Analysis

Traditionally, analysis of hydraulics and channel change at cross-sections has been the dominant method used to characterize fluvial geomorphology. This standard method was employed here to promote inter-comparison with historical studies and provide results for those most comfortable with this classic approach. WinXSPRO version 3.0, a resistance equation-based channel cross-section analyzer available through the United States Forest Service (Hardy et. al, 2005), was used to obtain at-a-station hydraulic geometry relationships for these cross sections over a wide range of flows. Pool, riffle crest and run cross sections were extracted from the pre- and post- flood DEMs using Land Desktop 3 (Fig. 4). WinXSPRO assumes uniform flow so that bed slope, water surface slope (S_w), and the total energy grade line are parallel at the individual channel cross-section location (Hardy et. al, 2005). The program computes hydraulics at increments between specified low and high WSEs. Data inputs for each range of flows investigated include low and high WSE values along with their corresponding Manning's n roughness coefficients and S_w values. Outputs include cross-sectional area (m), wetted perimeter (m), width (m), hydraulic depth (m), S_w (m/m), average velocity from Manning's equation (ms^{-1}), Q (m^3s^{-1}), and shear stress (Pa). These outputs were then used to calculate width, depth and velocity at-a-station hydraulic geometry relations for each cross section. Width, depth, velocity and shear stress were also non-dimensionalized using D_{50} (Pitlick and Cress, 2002) to obtain results intercomparable across a wide range of spatial scales, but are not reported due to similarities between dimensional and non-dimensional results.

In order to take advantage of available S_w observations at some stages and optimize the performance of WinXSPRO, each cross section was analyzed incrementally in three sub-sets by Q: (1) 0 to 159.2 m^3s^{-1}, (2) 159.2 m^3s^{-1} to 328.5 m^3s^{-1}, and (3) 328.5 m^3s^{-1} to 1,215.8 m^3s^{-1}. In each flow range, Manning's n values were selected to match those from the calibrated 2D model simulations that are described later. First, the WSE at 0 m^3s^{-1} and that estimated for 159.2 m^3s^{-1} were specified along with a constant corresponding Manning's n value of 0.043 for the low discharge and 0.042 for the high discharge (Moir and Pasternack, 2008). The water surface slope for 159.2 m^3s^{-1} was fixed at 0.0047, but that for 0 m^3s^{-1} was adjusted to yield the field-observed water surface slope of 0.0055 at 23.4 m^3s^{-1}. In WinXSPRO, S_w decreases linearly as Q increases. Once that was solved for, the WSE for 159.2 m^3s^{-1} was adjusted to yield a model-estimated discharge as close to 159.2 m^3s^{-1} as possible, while holding the S_w for that WSE constant. For the next Q increment (159.2 -328.5 m^3s^{-1}), the obtained parameters for 159.2 m^3s^{-1} were used as the low WSE values and the S_w for 328.5 m^3s^{-1} was set to the observed value of 0.003. Manning's n was set at 0.042 and 0.041 for the low and high discharges, respectively. The WSE for 328.5 m^3s^{-1} was adjusted to yield a Q as close to 328.5 m^3s^{-1} as possible. The same approach was repeated again for the highest range of Q, given the observed S_w for 1,215.8 m^3s^{-1}. Manning's n was set at 0.041 and 0.039 for the low and high discharges, respectively. In summary, the use of WinXSPRO was optimized to take advantage of the available field observations and back-calculate unknowns.

3.2.1 WinXSPRO Validation

Recognizing that WinXSPRO- a tool commonly used for gravel river analysis and management- assumes steady, uniform flow and that this assumption does not hold well for gravel-bed rivers whose riffle-pool relief by definition is non-uniform (MacWilliams et al., 2006), the output data were compared against the same values obtained from 2D models that do resolve non-uniform hydraulics for the four specific discharges investigated. Details of the 2D modeling procedure are presented in the next section. To obtain intercomparable cross-sectional averages, cross section locations were imported into each 2D model, results were extracted at ~2-m intervals, and these values were averaged. Wetted width was also obtained for each cross section. The percent deviation between WinXSPRO and 2D model results was calculated for each variable. Hydraulic data were used to compare both models against field observations, though the size of the river and the danger posed by the flood limited the flow range of that data.

3.3 2D Yuba Model

Two-dimensional (depth-averaged) hydrodynamic (2D) models have existed for decades and have been used to study a variety of hydrogeomorphic processes (Bates et al., 1992; Leclerc et al., 1995; Miller and Cluer, 1998; Cao et al., 2003). Recently, they have been evaluated for use in regulated river rehabilitation emphasizing spawning habitat rehabilitation by gravel placement (Pasternack et al. 2004, 2006; Wheaton et al. 2004; Elkins et al., 2007) and to better understand the relative benefits of active river rehabilitation versus flow regime modification (Jacobson and Galat, 2006; Brown and Pasternack, 2008) on regulated rivers. In this study, the long-established 2D model Finite Element Surface Water Modeling System 3.1.5 (FESWMS), implemented within the Surface-water Modelling System (SMS) graphical interface (Environmental Modeling Systems, Inc.), was used to predict hydrodynamics and characterize mean and local velocity reversals at the described cross sections using the pre-flood topography. FESWMS solves the vertically integrated conservation of momentum and mass equations to acquire depth-averaged 2D velocity vectors and water depths at each node in a finite element mesh (Froehlich, 1989). A mesh element is "dry" when depth is below a user-defined threshold (set at $1 \times D_{90}$ ~0.12 m here), but to the extent possible, the mesh area was trimmed to closely match the observed wetted area. FESWMS is capable of simulating steady, unsteady, subcritical and supercritical flows. The full equations and other details of the model have been widely reported in the past (Froehlich, 1989; MacWilliams et al., 2006) and need not be reproduced here. Details on the validation procedure used to characterize model uncertainty in this study follow the explanation of model development.

3.3.1 2D Model Development

Refined topographic point and breakline data used to produce the pre-flood DEM were exported to SMS for use in the 2D model. A unique computational mesh was developed for each flow investigated and the density of computational nodes was higher relative to the density of the 2004 pre-flood topographic data used to run the models (Table 1). Each mesh was generated using a built-in paving algorithm without reference to the independently located depth and velocity measurement points. Node elevations were interpolated from imported DEM data using a TIN-based linear interpolation algorithm.

To run FESWMS, discharge and downstream boundary water surface elevation are necessary. The discharge at the base flow was obtained by velocity-area flow gaging. Since that was not possible at the three higher flows that occurred during the rising limb of the flood, discharge was obtained by combining the discharges from the U.S. Geological Survey gaging stations on the Yuba River near Smartville (station #11418000) and on Deer Creek (station #11418500), the one significant tributary between Englebright Dam and the study site. The gaging stations are too close together to necessitate accounting for propagation time of the flood wave to the Deer Creek confluence. The water surface elevation at the downstream flow boundary of the study site was measured using a total station.

The two primary model parameters in FESWMS include bed roughness as approximated using Manning's n for a gravel/cobble bed and isotropic kinematic eddy viscosity (E). The effect of channel roughness on flow was addressed two ways in the model. Roughness associated with resolved bedform topography (e.g. rock riffles, boulders, gravel bars, etc) was explicitly represented in the detailed channel DEM. 2D model predictions are highly sensitive to DEM inaccuracies (Bates et al., 1997; Hardy et al., 1999; Lane et al., 1999; Horritt et al., 2006), which is why high-resolution topographic mapping was carried out in this study. For unresolved roughness, Manning's coefficient (*n*) was initially estimated as 0.043 for the gravel bed area with $D_{50} \sim 60$ mm and 0.06 for the armoured cobble/boulder bed over the highest velocity section of the riffle crest using a standard linear summation method (McCuen, 1989) and based on 2D modelling studies of similar gravel rivers (Pasternack et al., 2004, 2006). Although it is possible to spatially vary the bed-roughness parameter in a 2D model to try to account for variable bed sediment facies, measurement accuracy in gravel-bed rivers constrains justification of small (<0.005) local deviations relative to 2D-model and field-measurement accuracy in gravel-bed rivers. After performing simulations at each discharge with the initial n-value, Manning's n was calibrated in intervals of 0.001 for each modeled discharge using the available field-measured WSE data (except 159.2 m^3s^{-1} for which there was no WSE data) to obtain the smallest deviation between observed and modeled WSE longitudinal profiles. 2D models have been reported to be sensitive to large (>0.01) variations in n values (Bates et al., 1998; Lane and Richards, 1998; Nicholas and Mitchell, 2003), and the validation approach described in the next section would reveal that scale of deficiency.

In a study of 2D model sensitivity for a bedrock channel, Miller and Cluer (1998) showed that 2D models are particularly sensitive to the eddy viscosity parameterization used to cope with turbulence. In the model used in this study, eddy viscosity (E) was a variable in the system of model equations, and it was computed using the following standard additional equations developed based on many studies of turbulence in rivers (Fischer et al., 1979; Froehlich, 1989):

$$E = 0.6H \cdot u_* + E_o \qquad (1)$$

$$u_* = U\sqrt{C_d} \tag{2}$$

$$C_d = 9.81\frac{n^2}{H^{1/3}} \tag{3}$$

where H is water depth, u_* is shear velocity, U is depth-averaged water velocity, C_d is a drag coefficient, n is Manning's n, and E_0 is a minimized constant (0.033 m^2s^{-1}) necessary for model stability. These equations allow E to vary throughout the channel, which yields more accurate transverse velocity gradients. However, a comparison of 2D and 3D models for a shallow gravel-bed river demonstrated that even with this spatial variation, it is not enough to yield as rapid lateral variations in velocity as occurs in natural channels, presenting a fundamental limitation of 2D models like FESWMS (MacWilliams et al., 2006).

3.3.2 2D Model Validation

2D models have inherent strengths and weaknesses, thus uncertainty in modelled results needs to be understood and accepted (Van Asselt and Rotmans, 2002). Previous studies using FESWMS for comparable gravel-bed rivers like the lower Yuba River have validated the model for this application and provide valuable information regarding model utility and uncertainty (Pasternack et al., 2004, 2006; Wheaton et al., 2004; MacWilliams et al., 2006; Elkins et al., 2007; Brown and Pasternack, 2008). Although Manning's n was calibrated to minimize the deviation between the observed and predicted longitudinal profile of water surface elevation, values remained in the physically realistic realm. A comparison of predicted and observed conditions at independent locations was used to provide an assessment of model capability and uncertainty.

Three different validation tests were used to evaluate model performance. First, to validate model calculated eddy viscosity (E), these values were checked against field-based estimates at 23.4 m^3s^{-1} (summer low flow) for the three observational cross sections. Recognizing that E is not a real physical quantity, but an artificial model parameter, the difference between field-based estimates and model-calculated values is within the range typically reported for this type of 2D model (MacWilliams et al., 2006; Pasternack et al., 2006).

Second, even though the field-measured WSE longitudinal profiles were used to calibrate Manning's n for each simulation, the final deviations between observed and predicted profiles were non-zero. Thus, the deviations between observed and predicted WSE profiles for the final calibrated simulations were used as one metric to characterize the uncertainty in depths and water surface slopes.

Third, recognizing that lateral and longitudinal variation in velocity in a river is highest at low discharge and low during large floods (Clifford and French, 1998), model validation of depth and velocity on the LYR was performed at a low discharge of 23.4 m^3s^{-1} using observed depths and velocities from cross sections 1, 2 and 3 (Fig. 4). Raw statistical metrics were calculated using all data and comparisons were made on a cross-sectional basis. Models such as FESWMS should be viewed as presenting likely outcomes, but with uncertainty. In combination with field collected empirical data that helps characterize model uncertainty, such models can help researchers obtain process-based understanding of hydraulic phenomena.

3.4. Scour Pattern Analysis

Whereas many previous studies have evaluated channel hydraulics over a range of discharges to ascertain whether a velocity reversal existed, few have reported the details of topographic change due to overbank floods, as recorded using comprehensive digital elevation modeling and DEM differencing. In this study the pre- and post-flood surveys enabled a comprehensive characterization of flood-induced channel change as well as interpretation of the change in terms of any riffle-pool relief maintenance. Also, the depth and velocity predictions from the 2D model of the flood's peak discharge along with the bed material data enabled prediction of the Shields stress pattern of the river during the flood. A comparison of the Shields stress pattern against the actual pattern of channel change permitted a mechanistic interpretation of flood processes.

3.4.1 Channel Change

The pre- and post-flood DEMs were imported into ArcGIS 9.2 and a differencing analysis was performed to characterize the spatial pattern of net scour and deposition due to the May 2005 flood at Timbuctoo Bend. The DEM difference was calculated by subtracting the 2004 surface from the 2005 surface. Coincident rasters (cell size 0.023 m^2) were generated from TIN elevation models in 3D Analyst and then differenced using Spatial Analyst. The raw differenced surface was then classified to identify areas of scour and deposition. To assess uncertainty in DEM differencing caused by various sources of error, a sensitivity analysis was performed in which different minimum thresholds (0 m, ±0.0254 m, ±0.0508 m, ±0.15 m, and ±0.3 m) were set below which the difference values were forced to be zero. The zonal statistics tool was then used to calculate the gross and net volumetric difference for the DEM difference outcome using each threshold value. To convert volumes to masses for this loose gravel and cobble, a density estimate of 1.645 tonnes m^{-3} was used based on the quarry tests of Merz et al. (2006).

The spatial pattern of scour and deposition was inspected to determine whether there was any indication of riffle-pool maintenance. First, the pattern of channel change was evaluated considering the whole domain of the river corridor to determine if there existed foci of change and to qualitatively infer the mechanism responsible for the change. Second, at each cross-section, the mean bed elevation of the modern bankful channel was calculated using the pre- and post- flood cross-sectional datasets. Then the change in mean bankful bed elevation due to the flood was computed for each cross-section and the direction and magnitude of change were used as the key test metrics. Based on the flow convergence routing hypothesis, maintenance would be confirmed by net scour in the upstream pool and net deposition in the riffle. Less corroboration would be provided if the whole channel scoured, as might be expected in a reach lacking sediment supply from upstream. Topographic change in other morphological units was also assessed.

3.4.2 Shields Stress Prediction

Shear velocity (U^*), bed shear stress (τ_b), and non-dimensional Shields stress (τ^*) were calculated at each node in the 2D model according to

$$U^* = U/\left(5.75\log\left(12.2H/2D_{90}\right)\right) \tag{4}$$

$$\tau_b = \rho_w\left(U^*\right)^2 \tag{5}$$

$$\tau^* = \tau_b/\left(\rho_s - \rho_w\right)gD_{50} \tag{6}$$

where U is depth-averaged velocity magnitude at a point, H is water depth, ρ_w is water density, ρ_s is bed particle bulk density, g is gravitational acceleration, and D_{90} and D_{50} are the bed material sizes that 90% and 50% of the bed material is smaller than, respectively (Pasternack et al. 2006). Shields stress values were categorized based on transport regimes defined by Lisle et al. (2000), where values of $\tau^*<0.01$ correspond to no transport, $0.01< \tau^* <0.03$ correspond to intermittent entrainment, 0.03< τ^* <0.06 corresponds to partial transport (Wilcock et al., 1996), and τ^* >0.06 corresponds to full transport.

To evaluate the role of the flood peak hydraulics on channel change, a comparison was made between 2D model results and DEM difference residuals. DEM difference residuals were interpolated to the 2D model's computational mesh nodes to obtain comparable values. A scatter plot was made between residuals and τ^* to determine the nature of the relation between the data sets. Also, a box and whisker plot was made to evaluate the distributions of τ^* for erosional (residuals <-0.15 m), no change (residuals within ±0.15 m), and depositional zones (residuals >0.15 m).

Recognizing that hydraulics and channel change may vary between morphological units, a separate analysis was done isolating the data at the pool, riffle and run cross sections. Also, to distinguish between in-channel and floodplain dynamics, the cross-sectional data was further subdivided relative to the known bankful elevation. It was hypothesized that τ^* data extracted from the 2D model that exceeded the threshold for partial transport (τ^*>0.03) should corresponded to observed scour locations. Conversely, locations with low transport capacity (i.e., τ^*<0.03) should correspond to no change or deposition. This was assessed throughout the whole study site at meso-scale morphological units which play a key role in integrating stream ecology, geomorphology and hydrology (Moir and Pasternack, 2008).

4. RESULTS

The May 2005 flood caused significant geomorphic change to the study site. According to both models, the locations of highest depth-averaged velocity and τ^* shift multiple times with increasing discharge. To describe the shifts, results from the cross section analyzer (WinXSPRO) and the 2D hydrodynamic model (FESWMS) will first be reported independently and without scrutiny. Then the two will be inter-compared. Finally, the geomorphic change results will be reported and related to the τ^* pattern predicted by the 2D model. It is important to be mindful that the point in a morphological unit with the local peak velocity and τ^* as predicted by the 2D model does not necessary occur on the cross-section taken for each unit and used for the WinXSPRO analysis, since cross-sections were chosen morphologically according to the standard method. As a result, independent evaluations of peak magnitudes is necessary for the two methods.

4.1 WinXSPRO Results

WinXSPRO analyzed the pool, riffle and run cross-sections and produced at-a-station hydraulic geometry relationships for all discharges 0 - 1,218 m^3s^{-1} (Fig. 5). Five velocity reversals were predicted by WinXSPRO among the three cross-sections, as indicated by arrows on Figure 5c. The key results of the analysis are described below. In this subsection, all hydraulic variables are reported as cross-sectional averages.

4.1.1 Summer Low Flow to Modern Q_b

At discharges below the typical autumn salmon-spawning flow of 23.4 m^3s^{-1}, WinXSPRO predicted that the pool has the lowest velocity and τ^* as well as the widest and shallowest cross section. Conversely, up to 23.4 m^3s^{-1}, WINXSPRO predicted that the highest velocity and τ^* occurred at the run, where the river was the narrowest and deepest. A velocity reversal occurred at ~23.4 m^3s^{-1}, where pool velocity, depth and τ^* surpassed those of the riffle, but not the run (Fig. 5c; Table 2).

For all discharges between the typical autumn salmon-spawning flow of 23.4 m^3s^{-1} and modern Q_b at 159.2 m^3s^{-1}, the run continued to have the highest predicted velocity and τ^*. As discharge approached modern Q_b, the run became wider. Also, the pool had a higher predicted velocity than the riffle, but at Q_b the velocity and width at the riffle became slightly higher than those at the pool yielding a slight reversal (Fig. 5c). Over a very narrow flow range, the velocity and width at the riffle decreased as discharged increased thereafter, so the pool was restored as the wider and faster cross-section after the brief range of riffle ascendancy. These fluctuations are minor responses to differential topography.

4.1.2 Modern Q_b to pre-Bullards Bar Dam Q_b

At discharges above present day Q_b, the locations of velocity and τ^* peaks were predicted by WinXSPRO to change and two velocity reversals were predicted at the cross sections analyzed in this study (Fig. 5). From 159.2 m^3s^{-1} to 328.5 m^3s^{-1}, the width at the run doubled leading to a slight decrease in depth. At ~200 m^3s^{-1}, the pool velocity and τ^* surpassed those of the run. At these discharges the pool had the deepest cross section. A second reversal was predicted to occur at ~ 300 m^3s^{-1}, at which point the velocity in the run became lower than the riffle. At this flow the riffle had the widest cross section.

4.1.2 Pre-Bullards Bar Dam Q_b to Peak Flood Flow

At all discharges above 328.5 m^3s^{-1}, the pool cross section was predicted to have the highest velocity magnitude (> 2 m s^{-1}), while the riffle had higher velocities than the run. The pool was deepest and the run shallowest, while the run became the widest cross section for all analyzed discharges above ~700 m^3s^{-1}. Shield stress values for the three cross-sections showed the same relative magnitudes and trends with increasing discharge as was predicted for velocity.

4.2 2D Model Results

The results of 2D modeling also show velocity reversals in Timbuctoo Bend on the lower Yuba River (Fig. 6; Table 2), but the velocity reversal patterns predicted by the 2D model differ significantly from those predicted by WinXSPRO (Fig. 5, points versus lines). In addition to characterizing shifts in the location of peak velocity on the rising limb of the 1,215.8 m^3s^{-1} flood, the 2D model assisted in illustrating the relationship between hydraulics and sediment transport dynamics responsible for maintaining the topography at Timbuctoo Bend.

4.2.1 2D Model Validation

Measured E values ranged from 0.001 m^2s^{-1} to 0.043 m^2s^{-1}, with a mean of 0.023 m^2s^{-1} (SD = 0.010 m^2s^{-1}). The minimum value of E_0 that could achieve model stability was 0.0355 m^2s^{-1}. Resulting modeled E values were higher than field estimates, ranging from 0.034 m^2s^{-1} to 0.075 m^2s^{-1} with a mean of 0.057 m^2s^{-1} (SD = 0.010 m^2s^{-1}). This shift to higher eddy viscosity values causes greater transference of momentum and more smoothing of velocity values across the channel (MacWilliams et al., 2006; Pasternack et al., 2006).

Manning's n calibration yielded final values for each flow. For 23.4 m^3s^{-1} final n = 0.043; due to low flow hydraulics causing model instability this value was unable to be changed. At 328.5 m^3s^{-1}, main channel final n = 0.047, left bank floodplain n = 0.045, and willow levee n = 0.1. For the flood peak, 1,215.8 m^3s^{-1}, main channel and floodplain n = 0.039, but after analysis of roughness caused by willows during this specific flood event, *n* in each line of willows was set at 0.057. The iterative calibration of Manning's n by relating predicted and observed water surface slopes yielded deviations of <0.15 % error in water surface elevations showing overall good longitudinal predictions. To put these percentages into more meaningful absolute values, in the model runs with the calibrated Manning's n values, mean absolute values of the deviations of predicted WSE at 23.4 m^3s^{-1}, 328.5 m^3s^{-1}, and 1,215.8 m^3s^{-1} were 0.051 m (SD = 0.04 m), 0.07 m (SD =0.05 m), and 0.10 m (SD = 0.09 m) respectively. However, mean raw WSE deviations (observed – modeled) were 0.031 m (SD = 0.06), 0.01 m (SD = 0.09), and -0.02 m (SD = 0.14), respectively for the above discharges. Thus, at the two lower discharges the model slightly under-predicted WSE and at the flood flow the model slightly over-predicted WSE. The calibration process helped increase the model's performance in this study and resulted in physically realistic values with acceptable deviations from field observed water surface elevations.

Hydraulic measurements made at 83 points along 3 cross sections (Fig. 7) showed moderately accurate model predicted versus observed depth and velocity values at low flow conditions, 23.4 m^3s^{-1} (Fig. 7). A coefficient of determination of 0.929 for depth and 0.768 for velocity was observed for predicted versus observed values over all cross sections ($p<0.001$ for both tests). Average absolute deviation between predicted and observed depth and velocity was 10% and 22% respectively. One abnormally low velocity measurement at ~80 m in cross section 1 (Fig. 7) was excluded from the previous value, but typical of stream-measurement variability. Cross section 1 showed that predicted depth and velocity very closely matched the observed smoothed best-fit curve. At cross section 2, more lateral variation in depth and velocity occurred, but the general pattern of predicted and observed measurements remained intact. The 2D model under-predicted depth and over-predicted velocity at cross section 3, but the patterns match. This validation was only performed at low flow because high flow velocity measurements were not feasible for practical and safety reasons. However, as illustrated by the model results, velocity fields at higher flows have less variability at high discharges (Fig. 6).

Model validation for Timbuctoo Bend described the capabilities and limitations of a 2D model for this application as stated by previous studies (Lane et al., 1999; Pasternack et al., 2004, 2006; MacWilliams et al., 2006; Brown and Pasternack, 2008; Moir and Pasternack, 2008). Predicted spatial patterns in depth and velocity can be considered accurate with reasonable confidence, but a 3D model that does not assume a constant eddy viscosity would best capture lateral velocity variation. However, the 2D model is practical for this application and valuable if the inherent uncertainties in the simulation process are acknowledged.

4.2.2 Model Predictions

The 2D model predicted velocity and τ^* reversals at four discharges, gave results for comparison with WinXSPRO output at each cross section (Fig. 5), and provided a visual representation of the entire modeled reach to better understand spatial results. At summer low flow, the pool was the widest morphological unit and it had the greatest cross-sectional area (Table 2, Fig. 6a). Cross-sectional average velocity at the pool was low (0.36 ms^{-1}, SD ±0.10) and τ^* was negligible. The riffle cross section was divided by the mid-channel island (Fig. 6), with the highest velocity flow (mean column 1.12 ms^{-1}, SD=0.58 ms^{-1}) located in the main channel. Shields stress in the riffle at low flow (cross-sectional mean τ^*=0.04, SD=0.010) was within the partial transport domain (0.03< τ^*<0.06). The run cross section was narrow, with moderately high velocity within the channel, but τ^* relatively remained low within the intermittent transport range ($0.01 < \tau^* < 0.03$).

At present day Q_b, cross-sectional width and area began to converge at the pool and riffle cross sections (Fig. 5a, 6b). The depth in the pool and riffle also converged at this discharge (Table 2). The velocity in the riffle remained higher than that in the pool due to the funneling effects of the island topography on the shallow flow over this cross section. However, the run cross section concentrated flow through a relatively narrow cross section, so that location had the highest velocity at present day Q_b, yielding a velocity reversal between the riffle and run (Table 2). Even though a velocity reversal was predicted, τ^* was still slightly higher at the exact location of the riffle cross-section compared to that of the run (0.048 versus 0.044). However, further downstream in the run at the model outlet, the velocity and τ^* cross-sectional averages were higher than at the riffle. Both the run and riffle mean τ^* values were within the partial transport domain.

The Pre-Bullards Bar Dam Q_b model results showed that cross-sectional width had mostly equalized between units (Fig. 6c, Table 2). However, the width in the run was still narrowest, so the constricted flow induced acceleration and yielded the highest velocity there. The zone of highest velocity at the run extended further upstream compared to the present day Q_b, so the selected cross-section location better represented flow conditions in the run at this discharge (Fig. 6c). Velocity remained higher in the run than in the riffle, and τ^* became slightly higher in the run than riffle at this discharge, though both were lower than their corresponding values at present day Q_b.

Finally, at the peak flood flow, valley walls constricted flow in the pool, so wetted width was narrowest there and a major velocity reversal occurred. Velocity (mean=2.33 ms^{-1}, SD=0.081 ms^{-1}) and τ^* (mean=0.041, SD=0.020) were highest in the pool relative to other cross sections (Table 2). Downstream at the run cross section, the floodplain was less constricted and wider, allowing flow to spread out more between the valley walls (Fig. 6d). Compared with the lower discharges, downstream variation in velocity was significantly lower, while cross-channel variation was higher.

4.3 WinXSPRO versus 2D model

Overall, WinXSPRO overestimated values compared to 2D model predictions of width, depth, velocity, and τ^* (Fig. 5). Given the theoretical assumptions, WinXSPRO was unable to characterize backwater effects caused by topographic highs. In contrast, the 2D model predicted deeper and slower conditions in the pool at low flows and in the run at high flows as a result of lateral and vertical channel constrictions. At 23.4 m^3s^{-1}, the 2D model predicted depth 50% greater and velocity 149% slower than those predicted by WinXSPRO for the pool cross section. While the riffle exhibited similarity in the predictions of the two methods suggesting approximately uniform flow conditions, the run showed a slight backwater effect with a 4% higher depth and a 23% lower velocity in the 2D model (Fig. 5). At present day Q_b, the 2D model predicted a backwater effect in the pool, with a 28% higher depth and a 58% lower velocity. However, a slight acceleration occurred at the riffle, while the run showed approximately uniform conditions at Q_b. Once again, the 2D model predicted velocity 40% lower than WinXSPRO in the pool at 328.5 m^3s^{-1}, indicating the backwater effect of the riffle crest on pool hydraulics. At this discharge approximately uniform flow conditions existed at the riffle and run units. At 1,215.8 m^3s^{-1}, the trend was reversed with the pool showing a slightly higher velocity in the 2D model relative to WinXSPRO. The riffle maintained approximately uniform flow conditions, while the 2D model predicted velocity 15% lower than WinXSPRO in the run at this flow.

An analysis of cross-sectional area, width and depth with increasing discharge can help explain the velocity reversals evident at Timbuctoo Bend. On average WinXSPRO slightly overestimated width by 7% compared to the 2D model. Recognizing that the 2D model turned off near-bank mesh elements whose depth was <0.12 m, this difference is not significant. On average for both methods, the pool was ~70% and ~130% wider than the riffle and run cross-sections at 23.4 m^3s^{-1}, respectively (Table 2). In addition, the pool had the greatest cross-sectional area and the lowest velocity at summer low flow. At present day Q_b, WinXSPRO predicted that mean width, depth and velocity values in the riffle were similar to those in the pool, but the run had the narrowest cross section. Also, the average velocity in the run peaked at present day Q_b and thus was a function of a low width to depth ratio and the smallest relative area of all cross sections (Table 2).

The 2D model deviated from the WinXSPRO estimates because it accounts for channel non-uniformity and the associated flow accelerations and backwater effects. According to the 2D model, the pool had the lowest predicted velocity at 328.5 m^3s^{-1}, while WinXSPRO predicted that the pool and run had approximately the same cross-sectional area and velocity at this discharge (Fig. 5, Table 2). This is consistent with a backwater effect in the 2D model associated with vertical and lateral channel non-uniformity that is absent from WinXSPRO. At 1,215.8 m^3s^{-1}, WinXSPRO predicted that the run had the widest cross section with the largest cross-sectional area. Both methods predicted average velocity was lowest in the run and highest in the pool, though they differed on the exact value (Fig. 5c, Table 2). According to the 2D model, velocity was greater in the pool than predicted by WinXSPRO due to a smaller cross-sectional area. The pool had the narrowest, deepest cross section at this discharge (Fig. 5), because it was bounded by steep bedrock valley walls that resist widening. The flow was fastest through the pool and then diverged and slowed down exiting the pool. This hydraulic effect was primarily associated with lateral channel non-uniformity.

Shields stress predictions also varied between the two models, corresponding to the differences in velocity described above. For example, at summer low flow, WinXSPRO overestimated velocity at the pool cross section due to inability to predict backwater effects. Shields stress here was 0.020 as predicted by WinXSPRO and close to 0.000 (±0.001) for the 2D model (Table 2). The same occurred at the run, but WinXSPRO underestimated τ^* on the riffle (0.026 compared to 0.040, SD=0.010) at low flow. Shields stress incongruence between the two methods corresponds to that between velocity predictions for all cross sections (Table 2). Notably, τ^* was predicted to be the highest at the pool at peak flood flow by both methods (Table 2, Fig. 5)

4.4 Flood Scour And Deposition

On 21 May, 2005 a high flow changed the topography of Timbuctoo Bend. An evaluation was made to determine if these changes yielded “maintenance” (i.e. pool scour and riffle deposition) of the morphological units. The DEM difference between the 2004 and 2005 topographies resulted in six major locations of scour and deposition (Table 3). Starting from upstream, the pool and pool exit (i.e., riffle entrance) units scoured up to ~1 m (location 1, Fig. 8). Downstream of that, the horseshoe-shaped, armored crest of the riffle shifted upstream and incised, indicative of knickpoint migration (location 2, Fig. 8). On the right of the riffle migration area, up to 1.2 m of deposition occurred in the side channel on river right (location 4,

Fig. 8). Deposition up to 2.3 m occurred on the downstream end of the island/bar complex, mostly along the right side of the main channel (location 5, Fig. 8). Flanking the riffle on either side of the valley, local scour holes adjacent to bedrock outcrops incised 1.8 - 2.4 m (location 3, Fig. 8). Deposition along the bankful channel margins enhanced the relief of natural levees covered with willows. This zone of deposition represented the largest combined area of deposition during the flood (location 6, Fig. 8).

When the bed-elevation change within the bankful channel caused by the flood was analyzed on a cross-section basis, the pool was the only one to show net scour. The mean bed-elevation changes for the pool, riffle, and run cross-sections were -0.35 m (i.e. net scour), 0.07 m (i.e. net deposition), and 0.04 m (i.e. net deposition), respectively. The magnitude of net scour at the pool cross-section is a strong signal beyond the level of noise in the DEM differencing analysis, whereas the magnitudes of net deposition in the riffle and run are within the noise and may thus be indicative of no net change. Nevertheless, the relief between the riffle and pool cross-sections increased by 0.42 m.

4.5 Accuracy of Sediment Transport Regime Predictions

A key objective of this study was to test the predictive ability of the 2D model to characterize sediment transport capacity when related to observed scour and deposition patterns. A regression analysis of raw elevation change versus predicted τ^* at the flood's peak discharge (n=1001) yielded a coefficient of determination (r^2) value of 0.03. When model-predicted Shields stress data for the flood peak were stratified by direction of channel change (i.e. scour, no change, or deposition), then significant differences were apparent (Fig. 9). Areas of no significant change had the lowest values for the 25th, 50th, 75th, and 90th percentiles of τ^*, while areas of significant scour had the highest of all of those values. Areas of deposition had higher τ^* at the flood peak than those with no significant topographic change.

Unlike the bulk analysis of the raw τ^* and topographic change data, when stratified by morphological unit (i.e., the pool, riffle, and run cross sections), scour and deposition showed a strong systemic response to model-predicted τ^* at the flood peak (Fig. 10), with the observed pattern in line with the underlying mechanisms indicated by the 2D model. Where the 2D model predicted $\tau^*>0.045$, scour dominated (Fig. 10). Where the model predicted $\tau^*<0.03$, deposition dominated. In between those thresholds is the domain of partial transport in which both deposition or scour are possible, but in very small amounts overall. The one exception being in the lines of willows, where significant deposition will take place during partial transport (Fig. 10).

The majority of the pool cross section was characterized by 0.15-0.5 m of scour and $\tau^*>$ 0.045 (Figs. 10c, 11a). The location of deepest scour (~1 m) along the left bank of the bankful channel corresponded with a τ^* of 0.049 and decreased toward the bank. Some bank scour was associated with intermediate τ^*, possibly facilitated by smaller particle sizes and bank undercutting. In addition, deposition occurred on the vegetated floodplain adjacent to the pool's left cutbank in shallower areas (~ 2-3 m deep) with moderately low velocity (~1.5 m s^{-1}) and τ^* (0.01-0.02) (Figs. 10c, 11a). Together these factors increased bank steepness and sharpened the delineation between channel and floodplain (Figs. 8, 11). Equivalent bank scour did not occur on river right since the bank there was composed of bedrock.

At the riffle cross section there were three distinct zones of matching bed change and τ^* (Figs. 10b, 11b). Knickpoint migration of the horseshoe riffle crest scoured 0.15-1 m down through the riffle, in which location the model-predicted τ^* was between 0.046-0.052. Over the island and side channel (evident below contemporary bankful discharge), deposition occurred and τ^* were between 0.02-0.034. The rest of the cross section showed no significant change in bed elevation and had intermediate τ^* of 0.034-0.045. Relative to the other two cross sections, the floodplain adjacent to the riffle experienced no significant elevation change.

The run cross section was predominantly depositional due to a wide, deep cross section and low mean cross-sectional velocity during the flood peak. The mean velocity including the delineated floodplain was the lowest at the run as predicted by both modeling methods (Table 3), with an active zone of relative highest velocity (Fig. 6d) and a local τ^* maximum of 0.04 (Fig. 11c) mid-channel. This cross section experienced 0.15-0.8 m of deposition, with the most occurring along both vegetated banks (Fig. 11c) where τ^* were 0.02-0.04. On the floodplain adjacent to the run, deposition occurred over the vegetated levees where Shields stresses were ~0.04 (Figs. 8,11). At these locations, floodplain deposition occurred in relatively deep (up to ~4 m) and fast (up to ~2.5 m^3s^{-1}) water (Fig. 10). Some scour also occurred on the floodplain left of the willow levee on river left (Fig. 8), possibly caused by flow re-routing around vegetation. In summary, DEM differencing results demonstrate a threshold-like differentiation of Shields stress values between areas dominated by scour versus deposition, when data are stratified by morphological unit.

5. DISCUSSION

5.1 Riffle-Pool Self-Maintenance Confirmed

An overbank flood with a 7.7 year recurrence interval occurred on the regulated, gravel-bed lower Yuba River, causing geomorphically significant changes. High-resolution DEMs and

DEM differencing found that the upstream pool scoured, the riffle scoured and aggraded in different sub-units (e.g. knickpoint, exposed bar, and side channel features), the run aggraded, and the floodplain aggraded. Cross-section analysis confirmed that the net channel change caused by the flood accentuated pool-riffle relief by 0.42 m. That outcome is consistent with the definition of "self-maintenance" of riffle and pool morphology as meaning that over time riffles remain topographically high and pools remain topographically low. Thus, the presence of self-maintenance is confirmed at the study site for this one flood event.

Because this study focuses on evaluating the mechanism of self-maintenance, it is beyond the scope to demonstrate that the observed riffle-pool maintenance is not a fluke of the particular flood that was investigated. However, aerial photos of the site exist going back to 1937. A companion historical analysis of channel change in Timbuctoo Bend based on those aerial photos confirms that from 1937-2008 there has been a pool-riffle unit at the study site (White, 2008). The exact morphology and longitudinal position of the riffle have changed within a narrow limit over decades, but the pool has always been a pool and the riffle has always been a riffle. Consequently, both detailed quantitative metrics over a single flood event and photo-based analysis spanning decades agree that the study site exhibits riffle-pool self-maintenance.

5.2 Velocity and Shields Stress Reversals Confirmed

The results of this study are consistent with past studies reporting reversals in maximum hydraulic parameters from riffles at low flow to pools at high flow. Despite inherent model uncertainties, the field validated computational methods used in this study adequately described a reversal in section-averaged velocity and non-dimensional bed shear stress from riffle to pool with increasing discharge. Further, where the 2D model predicted $\tau^* > 0.045$, the measurable channel change was net scour. Conversely, where τ^* was <0.03, the channel change was net deposition. Although there was not a simple, continuous function defining the τ^* versus scour depth relation, the directionality of model predictions and observations did match, providing strong evidence of the validity and utility of the 2D model.

Clifford and Richards (1992) stated that competence reversal occurs at 50-90 % Q_b based on cross section studies at relatively low discharge in the River Quarme, UK, a small lowland stream channel. In the present study, a double competence reversal occurred in a contiguous riffle-pool sequence in a much larger river channel, with those reversals occurring at $Q \geq Q_b$. First, velocity and τ^* (a surrogate for sediment transport competence) were highest in the riffle for discharges up to Q_b, at which point there are velocity and τ^* reversals. Under this low-flow regime, bankful channel morphology and a large island created the non-uniformity that controlled hydraulic convective acceleration. Second, from $1\text{-}2{\cdot}Q_b$ the run had highest relative competence. In this flow range, willow-influenced natural levees and the wide floodplain served as hydraulic controls constricting the run much more so than the riffle or pool. Finally, at the highest discharge analyzed in this study ($7.63{\cdot}Q_b$), the pool had highest relative competence, indicating that a second reversal occurred between those two modeled flows. Pool dimensions during the flood peak were constrained by the valley walls. This overall linked morphologic-hydraulic behavior can be described as a series of “transient reversals” (Clifford and Richards, 1992) with competence reversals occurring dependent on the expression of different scales of channel constrictions and expansions at different discharges. Contrary to Lisle and Hilton (1992), there is an apparent dependence of sediment transport competence on depth where deposition occurs in the shallowest cross section (run). However, mean cross-sectional depth and width are inversely related at high flows due to valley wall constrictions in each cross section. Under discharges where the pool was the deepest and narrowest cross section, the most scour occurred. In a 3D modeling experiment, Booker et al. (2001) concluded that near-bed flow direction routes sediment away from the deepest part of pools; therefore, riffle-pool morphology is maintained by a lack of sediment input into pools rather than increased erosion within pools due to convergent flow. The results from this study, though based on a 2D model, indicate that erosion occurred in the deepest part of the pool due to convergent flow at a constricted location and deposition occurred alongside the active transport zones in the riffle and run downstream. Thus, the hypothesis of "flow convergence routing" (MacWilliams et al., 2006) in conjunction with low-intermediate maintenance flows and persistent bank vegetation describe mechanisms responsible for riffle-pool morphology maintenance at the study site on the LYR.

5.3 WinXSPRO Limitations

WinXSPRO is a standard cross-section analyzer of the type commonly used in practice to evaluate and design river channels. It is only accurate when channels are "approximately" uniform. How does one know if a channel is in fact "approximately" uniform for any given reach? By definition, riffles and pools in gravel-bed rivers are significant topographic highs and lows, respectively. Over a wide range of discharges, riffle crests impose a backwater effect on upstream morphological units and experience non-uniform flow acceleration over and downstream of themselves (Pasternack et al., 2008). Therefore, WinXSPRO should not be expected to accurately predict hydraulics in riffle-pool sequences. It is possible that a channel can become submerged to such a large depth that vertical bed variability becomes an insignificant fraction of total depth, but under that condition lateral variability in channel and valley widths imposes significant channel non-uniformity, still violating the key assumption of

WinXSPRO. For example, in this study it was found that the domain of poor performance of WinXSPRO in predicting velocity and τ^* ranged from 0 – 7.6·Q_b. Over that domain, WinXSPRO predicted five velocity reversals, but the validity of that assessment is questionable. Brown and Pasternack (in press) performed thorough inter-comparisons of hydraulic geometry methods, 1D numerical modeling, and 2D modeling at predicting hydraulics for two different configurations of pool-riffle-pool sequences lacking velocity reversals and found that even under that condition hydraulic geometry methods performed poorly.

5.4 2D Model Limitations

2D models account for channel non-uniformity associated with morphological units and predict local depth to within ~10% and local depth-averaged velocity to within ~25%. However, because most 2D models use a constant eddy viscosity to address turbulence closure, they underestimate the lateral variability in velocity magnitude relative to 3D models (MacWilliams et al., 2006). Also, bed scour is caused by near-bed velocity, not depth-averaged velocity (Keller, 1969, 1971; Clifford and Richards, 1992; MacWilliams et. al, 2006). Near-bed velocity is a good approximation of local sediment transport competence (Rubey, 1938; Keller, 1971; Clifford and Richards, 1992). However, field collection of such data is not practical at high flows that mobilize the bed. 2D models tend to overestimate τ^* (Lane et al., 1999), though two studies have shown that the overestimation can be corrected for (MacWilliams et al., 2006; Pasternack et al., 2006).

5.5 Spatially Variable Sediment Competence

The common perception of how sediment transport works is that during low flows there is little to no sediment transport in a gravel-bed river and thus no significant channel change occurs. Further, it is commonly postulated that a minimum threshold exists, commonly defined as $\tau^*=0.03$ or 0.045, above which "partial transport" occurs (Wilcock et al., 1996). When $\tau^*>0.06$, it is believed that a sheet of sediment is in transport with a thickness of 1-2 times D_{90} (Lisle et al., 2000). The implication of this framework is that the primary goals in evaluating sediment transport and channel change are to determine the discharge at which sediment transport begins, the "effective discharge" at which annualized sediment transport is maximized in light of the frequency distribution of the flow regime, and the discharge that is responsible for controlling channel morphology on the decadal time scale (Andrews and Nankervis, 1995).

Previous studies have questioned the existence and measurability of a minimum threshold in τ^* before sediment transport begins. Paintal (1971) performed long-duration sediment-transport flume experiments and found that "…a distinct condition for the beginning of movement does not exist" and that defining such an arbitrary threshold is of "no practical importance". Wilcock (1988) described the conundrum of significantly different threshold values being obtained by different measurement methods. Using special bedload traps in gravel-bed rivers, Bunte and Abt (2005) found a similar result as Paintal (1971) did in the flume in that observed bedload transport rates were different depending on the duration of observation. Finally, a common aspect of flume and field studies of bedload transport is that they are almost always done on stable morphological units with simple cross-sections and simple morphological controls yielding a simple, one-to-one functional relation between Q and τ^*. The relevance of such simplicity to naturally complex channels is debatable.

This study contributes a new significant finding relevant to this issue; in fact large gravel-bed rivers have significant channel non-uniformity at multiple spatial scales, and consequently exhibit spatially variable sediment transport competence as a function of discharge (Fig. 6). Velocity and τ^* at any point in a river generally goes up as a function of discharge as long as hydraulics are governed by the same morphologic control, as assumed by many sediment-transport studies. However, when the morphologic control at a site shifts from a smaller scale feature of channel non-uniformity to a different, larger scale one, then the shape of the Q versus τ^* function changes and τ^* can go down or stay the same, as exhibited by the lines and points in Figure 5d. The stronger the channel non-uniformity and the more scales over which it changes, the more spatially and temporally variable the sediment transport function will become. Thompson et al. (1996, 1998) recognized the effects of higher local velocity at a pool head due to channel constriction. Also, Cao et al. (2003) noted that constricted channel conditions can lead to competence reversal in some cases depending on combinations of channel geometry, flow discharge and sediment properties. In this study, the single highest local velocity and τ^* on the riffle was predicted by the 2D model to occur at the lowest discharge (Fig. 6). Thus, bedload transport rate and the greatest potential for localized riffle change should occur at a low discharge when channel non-uniformity causes the riffle to act as a weir (Clifford and French, 1998; Brown and Pasternack, 2008) and exhibit transcritical or supercritical hydraulic conditions. This process of riffle scour is enhanced by the long durations of low flow common to most rivers. Even though the sediment eroded off riffles will not transport far, given the low τ^* in downstream morphological units during low flow, we have observed on several gravel-bed rivers in the western United States that the local channel change that occurs is highly ecologically significant, since it creates graded sedimentary deposits with local hydraulic complexity that can serve many species' different needs at different lifestages. In contrast to riffles, this study finds that pools tend to show the expected function of increasing τ^* with increasing discharge (Figs. 5,6).

6. CONCLUSION

A study combining field measurements, cross-section analysis, and mechanistic numerical modeling has revealed that a large gravel-bed river exhibited self-maintenance of a riffle-pool unit during a flood with a 7.7-year recurrence interval and a peak magnitude of $7.63 \cdot Q_{bf}$. Comparing the topography before and after the flood, riffle-pool relief increased 0.42 m. Further, multiple scales of channel non-uniformity and a dynamic flow regime were found to be ultimately responsible for the observed self-maintenance, because they drive the mechanism termed "flow convergence routing" by MacWilliams et al., (2006). Spatially complex patterns of scour and deposition at the scale of sub-width morphological units were reasonably predicted by the 2D mechanistic model that accounts for convective acceleration, whereas the cross-section base method underperformed the 2D model considerably. The 2D model failed to accurately predict the magnitude of point-scale channel change, likely because that is governed by highly localized bed material properties, sub-grid scale gravel-cobble structures, and bank vegetation dynamics. Flow convergence routing and the ability of 2D models to capture it will be useful to guide more process-based river restoration projects (e.g, Elkins et al., 2007).

ACKNOWLEDGEMENTS

Financial support for this work was provided by the U.S. Fish and Wildlife Service Anadromous Fish Restoration Program (Agreement #113323J011). The authors gratefully acknowledge Carlos Alvarado, Blake Andrews, Mary Berta, Mike Bezemek, Evan Buckland, Eve Elkins, Marisa Escobar, Kari Fish, Aaron Fulton, Dave Van Herrick, Lauren Hilliard, Ryan Keating, Donald Moir, Scott Morford, Cameron Poya, Carrie Simms, Nakul Thomas, Ben Torchia, Julie Tuck, Conner Voss, and Jason White for their assistance in collection of field data and performing data analyses.

REFERENCES

Acarlar, M.S., Smith, C.R., 1987. A study of hairpin vortices in a laminar boundary layer: Part 1. Hairpin vortices generated by a hemispherical protuberance. Journal of Fluid Mechanics 175, 1–41.

Andrews, E.D., Nankervis, J.M. 1995. Effective discharge and the design of channel maintenance flows for gravel-bed rivers. In Natural and Anthropogenic Influences in Fluvial Goemorphology. (eds. Costa, J.E., Miller, A.J., Potter, K.W., Wilcock, P.R.). American Geophysical Union, Geophysical Monograph 89, pp. 151–164.

Bates, P.D., Anderson, M.G., Baird, L., Walling, D.E., Simm, D., 1992. Modelling floodplain flow with a two dimensional finite element scheme. Earth Surface Processes and Landforms 17, 575-588.

Bates, P.D., Anderson, M.G., Hervouet, J. M., Hawkes, J.C., 1997. Investigating the behaviour of two-dimensional finite element models of compound channel flow. Earth Surface Processes and Landforms, 22(1), 3-17.

Bates, P.D., Horritt, M.S., J.M. Hervouet. 1998. Investigating two-dimensional, finite element predictions of floodplain inundation using fractal generated topography. Hydrological Processes 12(8):1257-1277.

Bhowmik, N.G., and M. Demissie. 1983. Bed material sorting in pools and riffles. Journal of the Hydraulics Division, American Society of Civil Engineers 108:1227-1231.

Booker, D.J., Sear, D.A., Payne, A.J. 2001. Modelling three-dimensional flow structures and patterns of boundary shear stress in a natural pool-riffle sequence. Earth Surface Processes and Landforms 26: 553-576.

Brasington, J., Rumsby, B.T., McVey, R.A., 2000. Monitoring and modelling morphological change in a braided gravel-bed river using high resolution GPS-based survey, Earth Surface Processes and Landforms 25, 973–990.

Brown, A.V., Brown, K.B., 1984. Distribution of insects within riffles of streams. Freshwater Invertebrate Biology 3, 2–11.

Brown, R. A. and Pasternack, G. B. 2008. Engineered Channel Controls Limiting Spawning Habitat Rehabilitation Success on Regulated Gravel-bed Rivers. Geomorphology 97:631-654.

Brown, R. A. and Pasternack, G. B. in press. Comparison of Methods for Analyzing Salmon Habitat Rehabilitation Designs For Regulated Rivers. River Research and Applications.

Buffin-Belanger, T., and Roy, A.G. 1998. Effects of a pebble cluster on the turbulent structure of a depth-limited flow in a gravel-bed river. Geomorphology 25, 249-267.

Bunte, K., and Abt, S. R. 2005. Effect of sampling time on measured gravel bed load transport rates in a coarse-bedded stream, Water Resources Research 41:W11405, doi:10.1029/2004WR003880.

California Department of Fish and Game (CDFG). 1993. Restoring Central Valley streams; a plan for action. Compiled by F.L. Reynolds, T.J. Mills, R. Benthin and A. Low. Report for public distribution, November 10, 1993. Inland Fisheries Division, Sacramento. 129 pp.

Cao, Z., Carling, P., Oakey, R., 2003. Flow reversal over a natural riffle-pool sequence: a computational study. Earth Surface Processes and Landforms 28, 689-705.

Carling, P.A. 1991. An appraisal of the velocity reversal hypothesis for stable riffle-pool sequences in the River Severn, England. Earth Surface Processes and Landforms 16: 19-31.

Cherkauer, D.S. 1973. Minimization of power expenditure in a riffle-pool alluvial channel. Water Resources Research 9: 1612-1627.

Clifford N.J. and K.S. Richards. Chapter 2: Maintenance of Riffle-Pool Sequences: A Review and Field Appraisal. In Lowland Floodplain Rivers: Geomorphological Perspectives. (eds. Carling, P.A. and Petts, G.E.). John Wiley and Sons Ltd, 1992.

Clifford, N. J., French, J. R., 1998. Restoration of channel physical environment in smaller, moderate gradient rivers: geomorphological bases for design criteria. In: Bailey, R. G., Jose, P. V., Sherwood, B. R. (Eds.), United Kingdom Floodplains. Westbury Academic & Scientific Publishing, Westbury, pp. 72-76.

Curtis, J.A., Flint, L.E., Alpers, C.N., Yarnell, S.M. 2005. Conceptual model of sediment processes in the upper Yuba River watershed, Sierra Nevada, CA. Geomorphology 68, 149-166.

Edwards, B.R., 2004. Historical assessment of the ecological condition and channel dynamics of the lower Mokelumne River: 1910-2001, Humboldt State University, 62 pp.

Elkins, E.E., Pasternack, G.B., Merz, J.E., 2007. The use of slope creation for rehabilitating incised, regulated, gravel-bed rivers. Water Resources Research 43, W05432, doi:10.1029/2006WR005159.

Fischer, H.B., List, E.J., Koh, R.C.Y., Imberger, J., Brooks, N.H., 1979. Mixing in Inland and Coastal Waters. Academic Press, Inc., New York, 483 pp.

Froelich, D.C. 1989. Finite Element Surface-water Modeling System: Two-dimensional Flow in a Horizontal Plane User's Manual. US Department of Transportation, Publication #FHWA-RD-88-177.

Gilbert, G.K. 1914. The transportation of debris by running water. U.S. Geological Survey, Professional Paper 86, 263 p.

Gilbert, G.K., 1917. Hydraulic-mining debris in the Sierra Nevada. U.S. Geol. Survey Prof. Paper vol. 105. 154 pp.

Giller, S., Malmqvist, B., 1998. The Biology of Streams and Rivers. Oxford University Press, Oxford, pp. 296.

Gorman, O.T., Karr, J.R., 1978. Habitat structure and stream fish communities. Ecology 59 (3), 507–515.

Hardy, R.J., Bates, P.D., Anderson, M.G., 1999. The importance of spatial resolution in hydraulic models for floodplain environments. Journal of Hydrology, 216(1-2), 124-136.

Hardy, T., Panja, P., and D. Mathias. 2005. WinXSPRO, A Channel Cross Section Analyzer, User's Manual, Version 3.0. Gen. Tech. Rep. RMRS-GTR-147. Fort Collins, CO: U.S. Department of Agriculture, Forest Service, Rocky Mountain Research Station. 94 p.

Horritt, M.S., Bates, P.D., Mattinson, M.J., 2006. Effects of mesh resolution and topographic representation in 2D finite volume models of shallow water fluvial flow. Journal of Hydrology, 329(1-2), 306-314.

James, L.A., 2005. Sediment from hydraulic mining detained by Englebright and small dams in the Yuba basin. Geomorphology 71, 202-226.

Jacobson, R.B., Galat, D.L., 2006. Flow and form in rehabilitation of large-river ecosystems – an example from the Lower Missouri River. Geomorphology 77, 249-269.

Keller, E.A. 1969. Form and fluvial processes of Dry Creek, near Winters California, M.S. thesis, University of California, Davis.

Keller, E.A. 1971. Areal sorting of bed-load material: The hypothesis of velocity reversal. Geological Society of America Bulletin 82:753-756.

Keller, E. A. 1972. Development of alluvial stream channels: A five stage model, Geological Society of America Buletin 83: 1531– 1536.

Keller, E.A. and Florsheim, J.L. 1993. Velocity reversal hypothesis: A model approach. Earth Surface Processes and Landforms 18: 733-740.

Kirkbride, A.D., Ferguson, R.I., 1995. Turbulent flow structure in a gravel-bed river: Markov chain analysis of the fluctuating velocity profile. Earth Surfaces Processes and Landforms 20, 721–733.

Kondolf, G.M. 1997. Hungry water: Effects of dams and gravel mining on river channels. Environmental Management 21 (4): 533-551.

Lane, E.W. and W.M. Borland. 1954. River-bed scour during floods. American Society of Civil Engineers Transactions 119: 1069-1080.

Lane, S.N., Bradbrook, K.F., Richards, K.S., Biron, P.A., Roy, A.G., 1999. The application of computational fluid dynamics to natural river channels: three-dimensional versus two dimensional approaches. Geomorphology, 29(1-2), 1-20.

Lane, S.N., and Richards, K.S., 1998. High resolution, two-dimensional spatial modelling of flow processes in a multi-thread channel. Hydrological Processes, 12(8), 1279-1298.

Lawless, M., and Robert, A. 2001a. Scales of boundary resistance in coarse-grained channels: turbulent velocity profiles and implications. Geomorphology 39, 221-238.

Lawless, M., and Robert, A. 2001b. Three-dimensional flow structure around small-scale bedforms in a simulated gravel-bed environment. Earth Surface Processes and Landforms 26, 507-522.

Leclerc M., Boudreault, A., Bechara, J.A., Corfa, G., 1995. Two-dimensional hydrodynamic modeling: a neglected tool in the instream flow incremental methodology. Transactions of the American Fisheries Society 124, 645–662.

Lisle, T.E. 1979. A sorting mechanism for a riffle-pool sequence. Geological Society of America 90(11): 1142-1157.

Lisle, T.E. 1986. Stabilization of a gravel channel by large streamside obstructions and bedrock bends, Jacoby Creek, northwestern California. Geological Society of America Bulletin 97:999-1011.

Lisle, T. E., and S. Hilton. 1992. The volume of fine sediment in pools: An index of sediment supply in gravel-bed streams, Water Resources Bulletin 28: 371– 383.

Lisle, T. E., J.M. Nelson, J. Pitlick, M.A. Madej, and B.L. Barkett. 2000. Variability of bed mobility in natural, gravel-bed channels and adjustments to sediment load at local and reach scales, Water Resources Research 36(12): 3743-3755.

Lower Yuba River Fisheries Technical Working Group (LYRFTWG). "Draft Implementation Plan for Lower Yuba River Anadromous Fish Habitat Restoration: Multi-Agency Plan to Direct Near-Term Implementation of Prioritized Restoration and Enhancement Actions and Studies to Achieve Long-Term Ecosystem and Watershed Management Goals" October, 2005.

MacWilliams, M.L., Wheaton, J.M., Pasternack, G.B., Kitanidis, P.K., Street, R.L., 2006. The flow convergence-routing hypothesis for riffle-pool maintenance in alluvial rivers. Water Resources Research. 42, W10427, doi:10.1029/2005WR004391.

McCuen, R.H. 1989. Hydrologic Analysis and Design. Prentice Hall: Englewood Cliffs.

Merz, J. E., Pasternack, G. B., Wheaton, J. M. 2006. Sediment Budget for Salmonid Spawning Habitat Rehabilitation in the Mokelumne River. Geomorphology 76:1-2:207-228.

Miller, A. J., Cluer, B. L., 1998. Modeling considerations for simulation of flow in bedrock channels. In: Wohl, E. E., Tinkler, K.J. (Eds.), Rivers over rock: fluvial processes in bedrock channels. American Geophysical Union, Geophysical Monograph Series #107, Washington, DC, USA, 61-104.

Milne, J,A. 1982. Bed-material size and the riffle-pool sequence. Sedimentology 29: 267-278.

Moir, H. J. and G.B. Pasternack, 2008. Interactions between meso-scale morphological units, stream hydraulics and chinook salmon (*Oncorhynchus tshawytscha*) spawning habitat on the Lower Yuba River, California. Geomorphology doi:10.1016/j.geomorph.2008.02.001.

Montgomery, D.R. and J.M. Buffington. 1997. Channel reach morphology in mountain drainage basins. Geological Society of America Bulletin 109(5): 596-611.

Nicholas, A.P., Mitchell, C.A., 2003. Numerical simulation of overbank processes in topographically complex floodplain environments. Hydrological Processes, 17, 727-746.

O'Neill, M.P., and Abrahams, A.D. 1984. Objective identification of pools and riffles. Water Resources Research 20: 921-926.

Palmer, M.A., Ambrose, R.F., Poff, N.L. 1997. Ecological Theory and Community Restoration Ecology. Restoration Ecology 5: 291-300.

Paintal, A.S., 1971. Concept of critical shear stress in loose boundary open channels. Journal of Hydraulic Research 9(1): 91–113.

Paola, C., Gust, G., Southard, J.B., 1986. Skin friction behind isolated hemispheres and the formation of obstacle marks. Sedimentology 33, 279–293.

Pasternack, G.B., Bounrisavong, M.K., Parikh, K.K. 2008. Backwater Control on Riffle-Pool Hydraulics, Fish Habitat Quality, and Sediment Transport Regime in Gravel-Bed Rivers. Journal of Hydrology. doi:10.1016/j.jhydrol.2008.05.014

Pasternack, G.B., Wang, C.L., Merz, J., 2004. Application of a 2D hydrodynamic model to reach-scale spawning gravel replenishment on the lower Mokelumne River, California. River Research and Applications 20(2), 205-225.

Pasternack, G.B., Gilbert, A.T., Wheaton, J.M., Buckland, E.M., 2006. Error propagation for velocity and shear stress prediction using 2d models for environmental management. Journal of Hydrology, 328, 227-241.

Pitlick, J., and R. Cress. 2002. Downstream changes in the channel geometry of a large gravel bed river, Water Resources Research, 38(10), 1216, doi:10.1029/2001WR000898.

Richards, K.S. 1976a. Channel width and the riffle-pool sequence. Geological Society of America Bulletin 87: 883-890.

Richards, K.S. 1976b. The morphology of riffle-pool sequences. Earth Surface Processes and Landforms 1: 71-88.

Rubey, W.W. 1938. The force required to move particles in a stream bed. U.S. Geological Survey Professional Paper 189-E: 121-141.

Teleki, P.G. 1971. Areal Sorting of bed load material: The hypothesis of velocity-reversal:

Discussion. Geological Society of America Bulletin 83: 911-914.

Thompson, D.M., Wohl, E.E. and Jarrett, R.D. 1996. A revised velocity reversal and sediment-sorting model for a high-gradient, pool–riffle stream. Physical Geography 17: 142–156.

Thompson, D.M., Nelson, J.M., and E.E. Wohl. 1998. Interactions between pool geometry and hydraulics. Water Resources Research 34(12):3673-3681.

U.S. Army Corps of Engineers. 2002. Hydrographic Survey Manual, Engineering and Design Manual No. EM-1110-2-1003, Washington D.C.

Van Asselt, M. B. A., Rotmans, J., 2002. Uncertainty in integrated assessment modelling – From positivism to pluralism. Climatic Change 54, 75-105.

Western Regional Climate Center (WRCC), 2003. Western U.S. Historical Summaries by State, Annual Precipitation Averages And Extremes, http://www.wrcc.dri.edu/htmlfiles/ca/ca.ppt.ext.html.

Wheaton, J.M., Pasternack, G.B., Merz, J.E., 2004. Spawning habitat rehabilitation - 2. Using hypothesis development and testing in design, Mokelumne River, California, U.S.A. International Journal of River Basin Management 2(1), 21-37.

Whittaker, J.G. and Jaeggi M.N.R. 1982. Origin of step-pool systems in mountain streams. Journal of the Hydraulics Division, ASCE 108:758-773.

Wilcock, P.R., Barta, A.F., Shea, C.C., Kondolf, G.M., Matthews, W.V.G, Pitlick, J.C. 1996. Observations of flow and sediment entrainment on a large gravel-bed river. Water Resources Research 32: 2897–2909.

Williams, G. and M.G. Wolman. Downstream effects of dams on alluvial rivers, US Geological Survey Professional Paper, 1286. 1984.

Wolman, M. G., 1954. A method of sampling coarse river-bed material. Transactions of the American Geophysical Union 35, 951-956.

Woodsmith, R.D. and Hasssan, M.A.. Chapter 10: Maintenance of an obstruction-forced pool in a gravel-bed channel: streamflow, channel morphology, and sediment transport. Catchment Dynamics and River Processes: Mediterranean and Other Climate Regions (eds. Garcia, C., Batalla, R.J.). Elsevier B.V. 2005.

Yoshiyama, R.M., Gerstung, E.R., Fisher, F.W., Moyle, P.B. 1996. Historical and present distribution of chinook salmon in the Central Valley drainage of California. Appendix I, Chapter 7, Sierra Nevada Ecosystem Project vol. 3, pp. 309– 362.

Yuba County Water Agency (YCWA), Surface Water Resources, Inc., and Jones & Stokes Associates. 2000. Draft Environmental Evaluation Report. Yuba River Development Project (FERC No. 2246). Submitted to the Federal Energy Regulatory Commission. December 2000.

FIGURES

Figure 1. Map and aerial photo of the Yuba River showing the location of the study site in Tumbuctoo Bend below Englebright Dam.

Figure 2. Typical annual hydrographs for the A) unregulated period (1904-1942), B) post Englebright Dam period (1942-1971), and C) post New Bullards Bar construction (1971 – present). Actual water years shown are 1922, 1950 and 1991, respectively.

Figure 3. Photographs of the same downstream 1-km straight-away in Timbuctoo Bend taken in A) 1906 by G.K. Gilbert and B) 2006 by authors illustrating incision on the order of 15 m and persistence of similar morphological units.

Figure 4. Topographic map of the wetted channel at the study site at 23.4 m^3s^{-1} prior to the May 2005 flood showing the cross section locations where depths and velocities were measured (XS1, XS2, and XS3) as well as locations of cross sections for hydraulic geometry analysis (pool, riffle, and run).

Figure 5. Hydraulic geometry relationships, WinXSPRO results compared to SMS results.

Figure 6. SMS velocity magnitude results for all discharges A) summer low flow (23.4 m^3s^{-1}), B) present-day Q_b (159.2 m^3s^{-1}), C) pre-Bullards Bar Dam Q_b (328.5 m^3s^{-1}) and D) and a 7.7 year event (1,215.8 m^3s^{-1}).

Figure 7. A) Depth and B) velocity validation best fit curves for 3 cross sections, see Fig. 4 for

cross section location.

Figure 8. Simplified visualization of DEM difference illustrating areas of scour (shaded dots) and deposition (shaded hatch marks) by morphological unit. Locations indicate 1) pool scour, 2) upstream knickpoint migration, 3) bedrock outcrop constriction corresponding to scour, 4) side channel deposition, 5) island/bar complex elongation by deposition and 6) deposition on willow levee and floodplain.

Figure 9. Box and whisker plot of 2D model predicted Shields stress data related to the occurrence of scour (elevation change <-0.15m), no change (-0.15 m $< x <0.15$ m) and deposition (>0.15m) on a point-by-point basis.

Figure 10. Comparison of 2D-model predicted τ^* for the flood peak discharge and elevation change 2004-2005 stratified by bankful wetted cross sections and the floodplain. Shaded area is region of uncertain channel change.

Figure 11. Cross sections from 2004 to 2005 showing locations of scour and deposition with corresponding 2D model output Shields stresses for A) pool, B) riffle and C) run cross sections. View is looking upstream.

Table 1. 2D FESWMS model characteristics

Discharge Modeled (m^3 s^{-1})	Mesh Area (m^2)	# Mesh Nodes	In-Channel Node Density (nodes/m^2)	Floodplain Node Density (nodes/m^2)
23.4	24483	51000	2.083	NA
159.2	38262	69490	1.816	NA
328.5	59779	25917	0.428	0.445
1215.8	74304	47799	0.660	0.661

Table 2. Cross section averaged 2D model (SMS) and WinXSPRO parameter comparison at four discharges.

Cross section	Wetted width (m)		Depth (m)		Area (m^2)		Velocity (ms^{-1})		Shields stress	
	2D	Win-XSPRO	2D Mean (±SD)	Win-XSPRO	2D	Win-XSPRO	2D Mean (±SD)	Win-XSPRO	2D Mean (±SD)	Win-XSPRO
Q=23.4 m^3s^{-1}										
Pool	81.0	71.0	0.74 (±0.27)	0.37	59.6	26.2	0.36 (± 0.10)	0.89	0.000 (±0.001)	0.02
Riffle	42.1	46.8	0.44 (±0.36)	0.47	18.3	22.0	1.12 (±0.58)	1.06	0.040 (±0.010)	0.026
Run	33.4	34.0	0.60 (±0.27)	0.58	20.0	19.6	0.98 (±0.37)	1.20	0.016 (±0.007)	0.032
Q=159.2 m^3s^{-1}										
Pool	98.5	95.8	1.40 (±0.46)	1.01	137.5	96.9	1.04 (±0.31)	1.64	0.012 (±0.004)	0.048
Riffle	101.0	107.6	0.82 (±0.50)	0.94	82.8	100.6	1.66 (±0.60)	1.58	0.048 (±0.053)	0.043
Run	50.0	61.1	1.38 (±0.57)	1.32	69.1	80.9	2.03 (±0.50)	1.97	0.044 (±0.011)	0.063
Q=328.5 m^3s^{-1}										
Pool	124.7	121.6	1.77 (±0.74)	1.53	221.1	185.6	1.27 (±0.56)	1.77	0.016 (±0.009)	0.046
Riffle	135.6	141.7	1.32 (±0.72)	1.40	179.5	198.0	1.59 (±0.65)	1.66	0.030 (±0.014)	0.042
Run	106.9	121.4	1.43 (±1.03)	1.53	153.3	185.3	1.65 (±0.80)	1.77	0.031 (±0.015)	0.046
Q=1215.8 m^3s^{-1}										
Pool	135.9	143.7	3.44 (±1.00)	3.78	467.2	543.2	2.33 (±0.81)	2.24	0.041 (±0.020)	0.049
Riffle	177.1	173.5	3.03 (±1.23)	3.39	535.8	587.3	1.94 (±0.75)	2.07	0.029 (±0.016)	0.044
Run	205.2	206.6	3.06 (±1.48)	3.03	628.3	626.0	1.69 (±0.67)	1.94	0.023 (±0.013)	0.040

Table 3. Results of DEM difference of 2004 and 2005 surfaces.

Metric	Minimum Δz (m)	Maximum Δz (m)	Mean Δz (m)	Standard deviation Δz (m)	Volumetric change (m^3)	Mass change* (tonnes)
Gross Scour	-2.62	0.00	-0.20	0.25	-7,728	-12,710
Gross Deposition	0.00	2.31	0.20	0.24	7,669	12,614
Raw Difference	-2.62	2.31	0.00	0.32	-58	-96
2.54-cm threshold	-2.62	2.31	0.00	0.32	-72	-118
5.08-cm threshold	-2.62	2.31	0.00	0.32	-129	-213
15-cm threshold	-2.62	2.31	-0.01	0.48	-416	-684
30-cm threshold	-2.62	2.31	-0.01	0.63	-215	-353

*Using a bulk density of 1.645 tonnes m^{-3} (Merz et al., 2006)

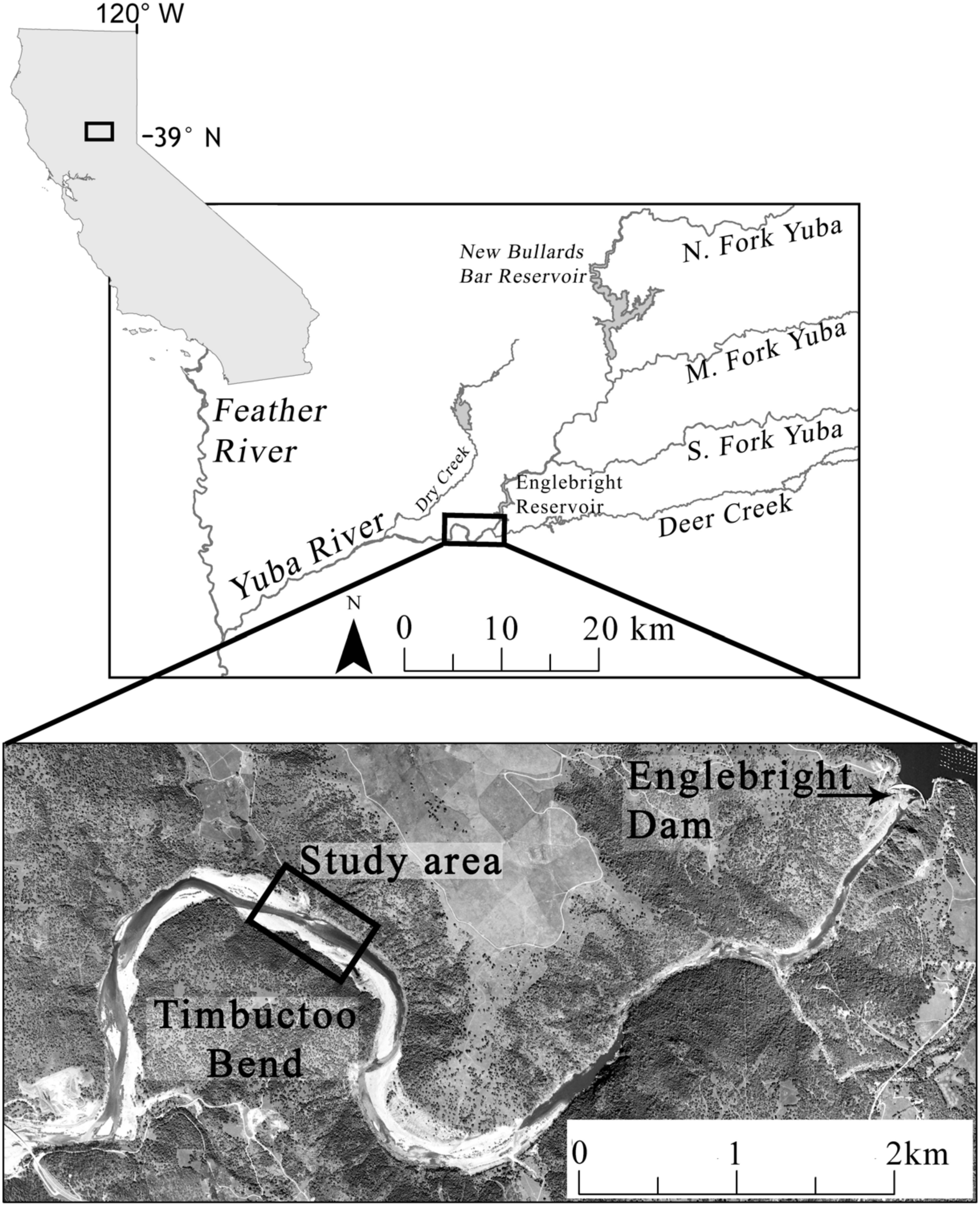
120° W
39° N
New Bullards
Bar Reservoir
N. Fork Yuba
M. Fork Yuba
S. Fork Yuba
Feather
River
Dry Creek
Englebright
Reservoir
Deer Creek
Yuba River
N
0
10
20 km
Englebright
Dam
Study area
Timbuctoo
Bend
0
1
2km

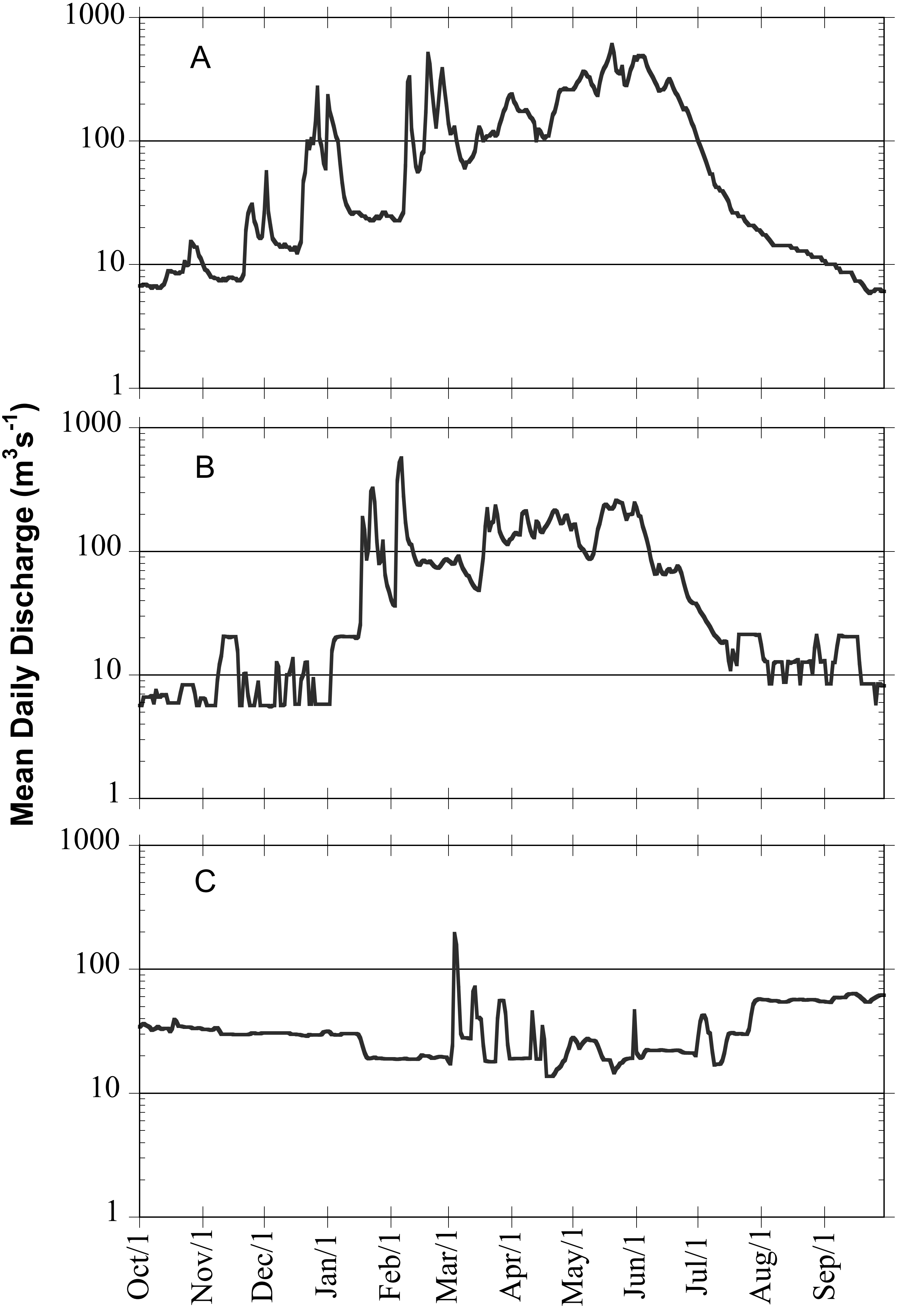

Mean Daily Discharge (m^{3}s^{-1})
A
B
C
1000
100
10
1
Oct/1
Nov/1
Dec/1
Jan/1
Feb/1
Mar/1
Apr/1
May/1
Jun/1
Jul/1
Aug/1
Sep/1

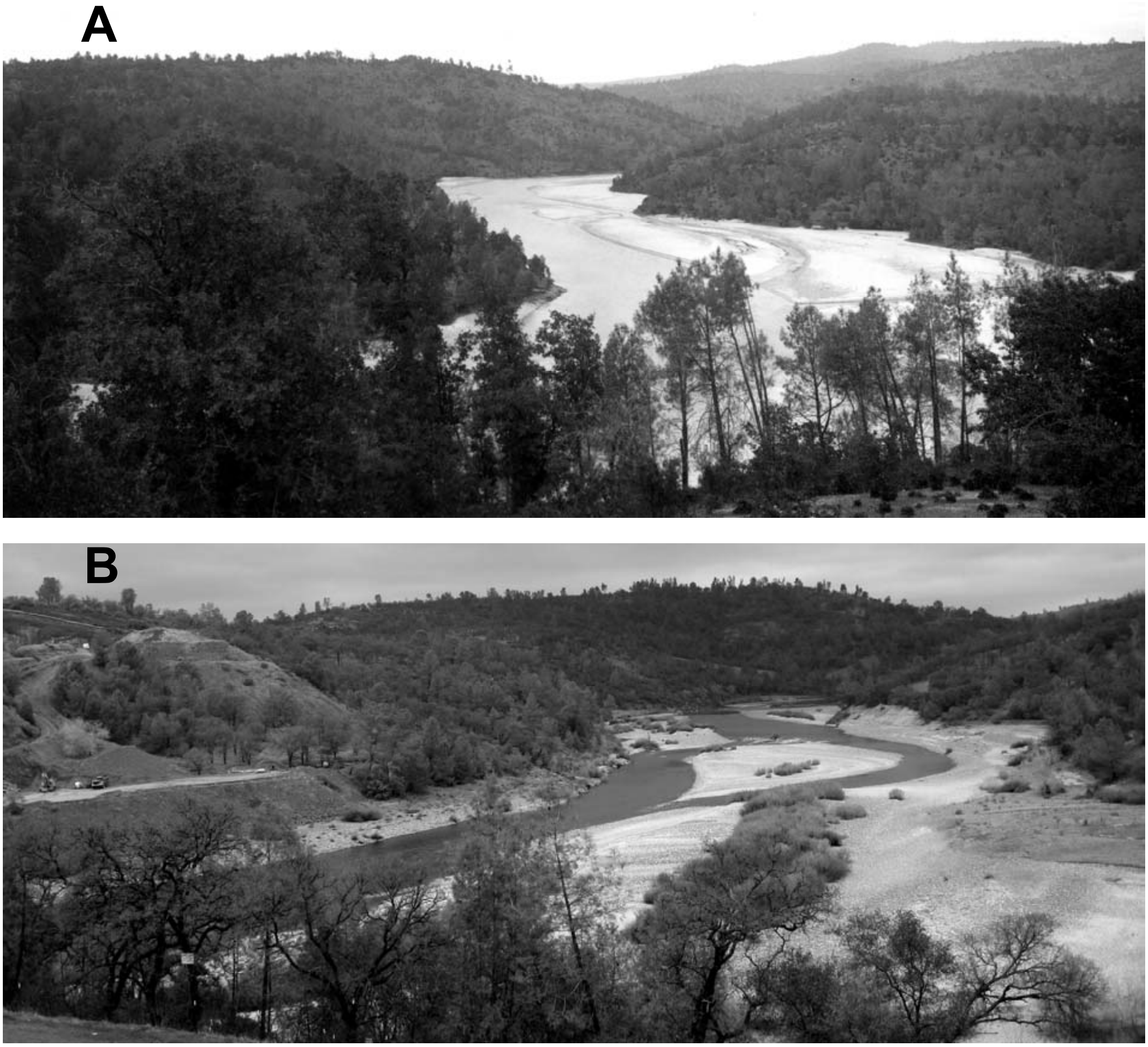
A
B

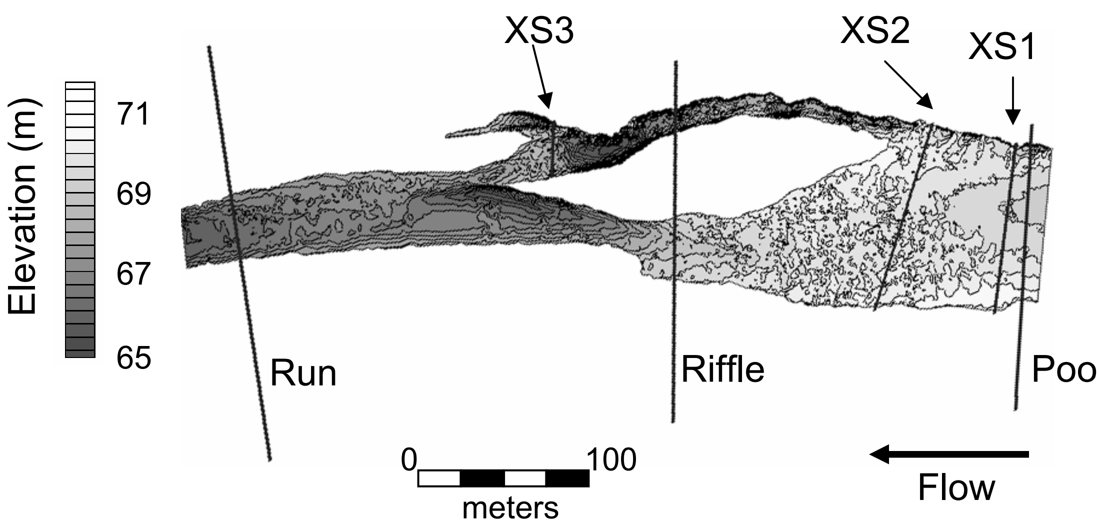

XS3
XS2
XS1
Elevation (m)
71
69
67
65
Run
Riffle
Pool
0
100
meters
Flow

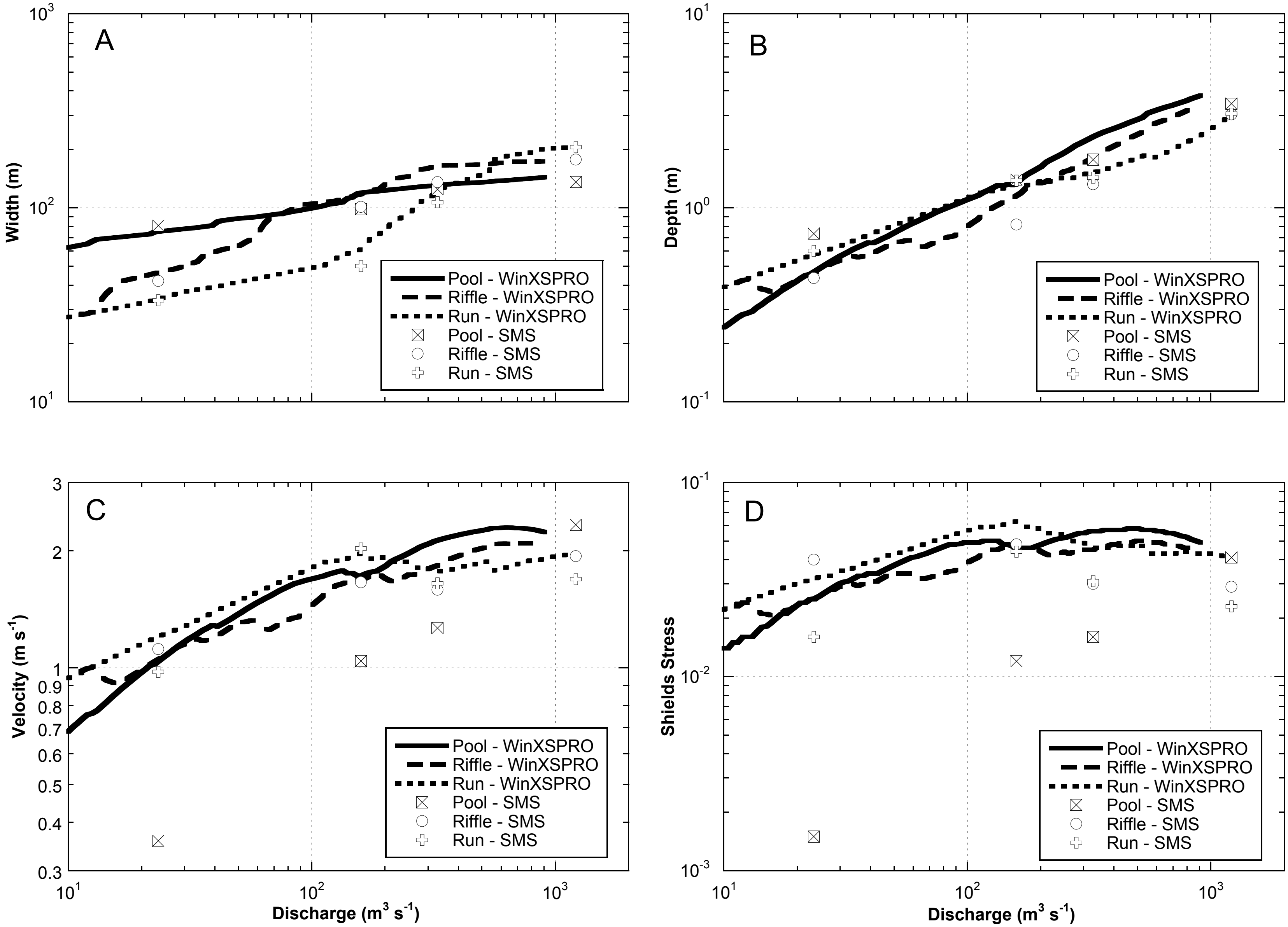

A
B
C
D
Width (m)
Depth (m)
Velocity (m s-1)
Shields Stress
Discharge (m3 s-1)
Discharge (m3 s-1)
Pool - WinXSPRO
Riffle - WinXSPRO
Run - WinXSPRO
Pool - SMS
Riffle - SMS
Run - SMS

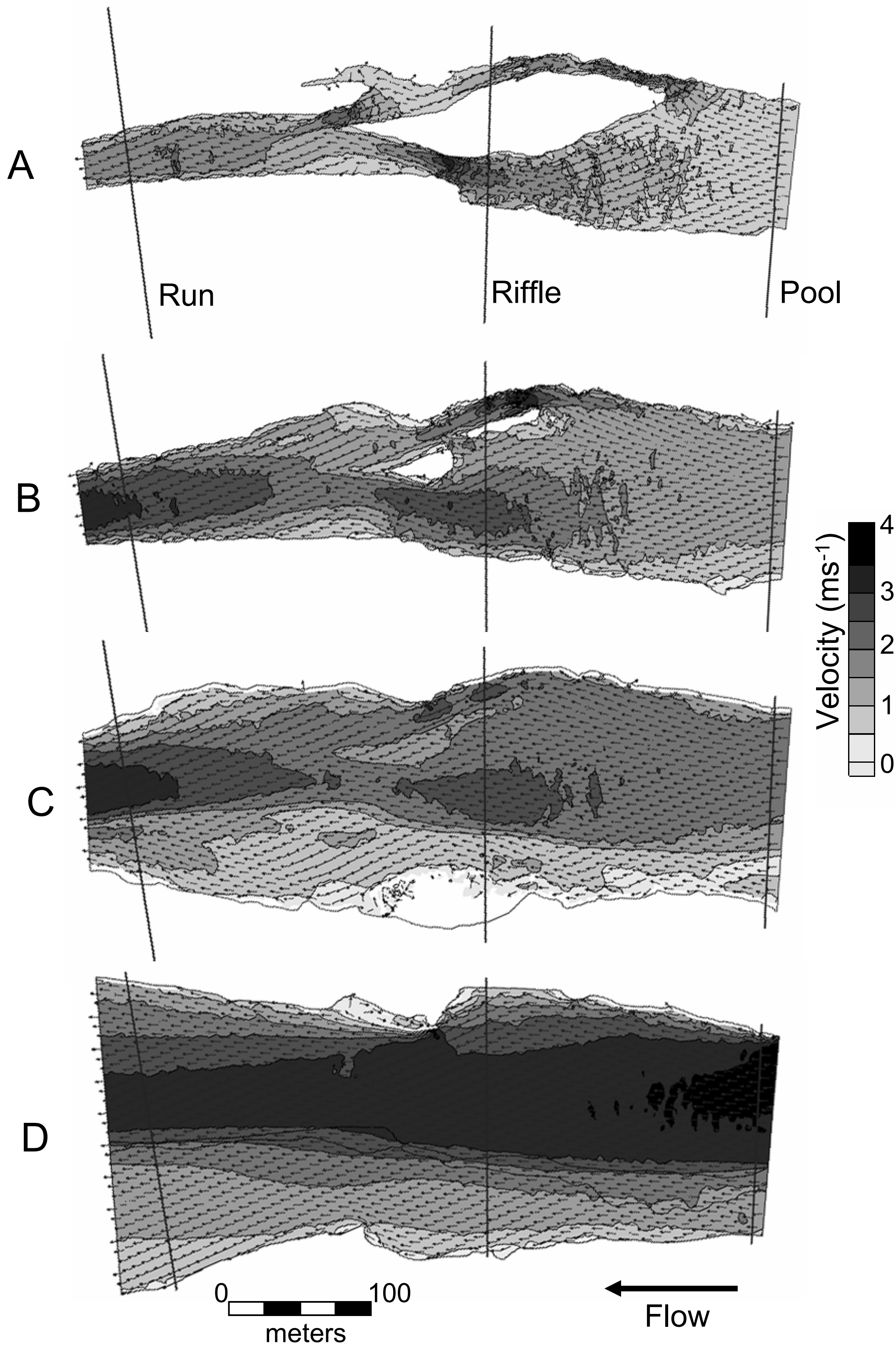
A
B
C
D
Run
Riffle
Pool
Velocity (ms-1)
4
3
2
1
0
0
100
meters
Flow

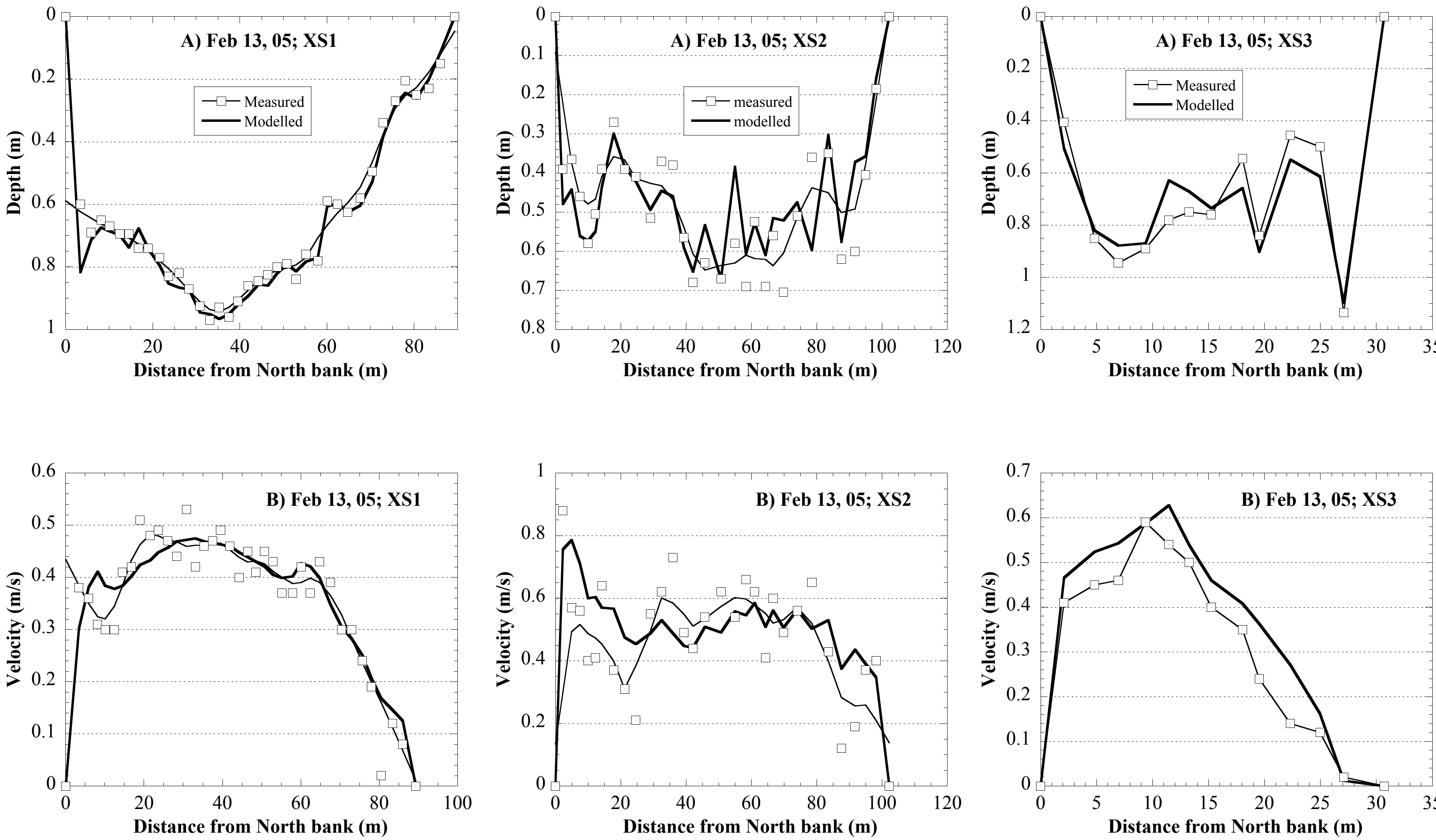

A) Feb 13, 05; XS1
Measured
Modelled
Depth (m)
Distance from North bank (m)
A) Feb 13, 05; XS2
measured
modelled
A) Feb 13, 05; XS3
B) Feb 13, 05; XS1
Velocity (m/s)
B) Feb 13, 05; XS2
B) Feb 13, 05; XS3

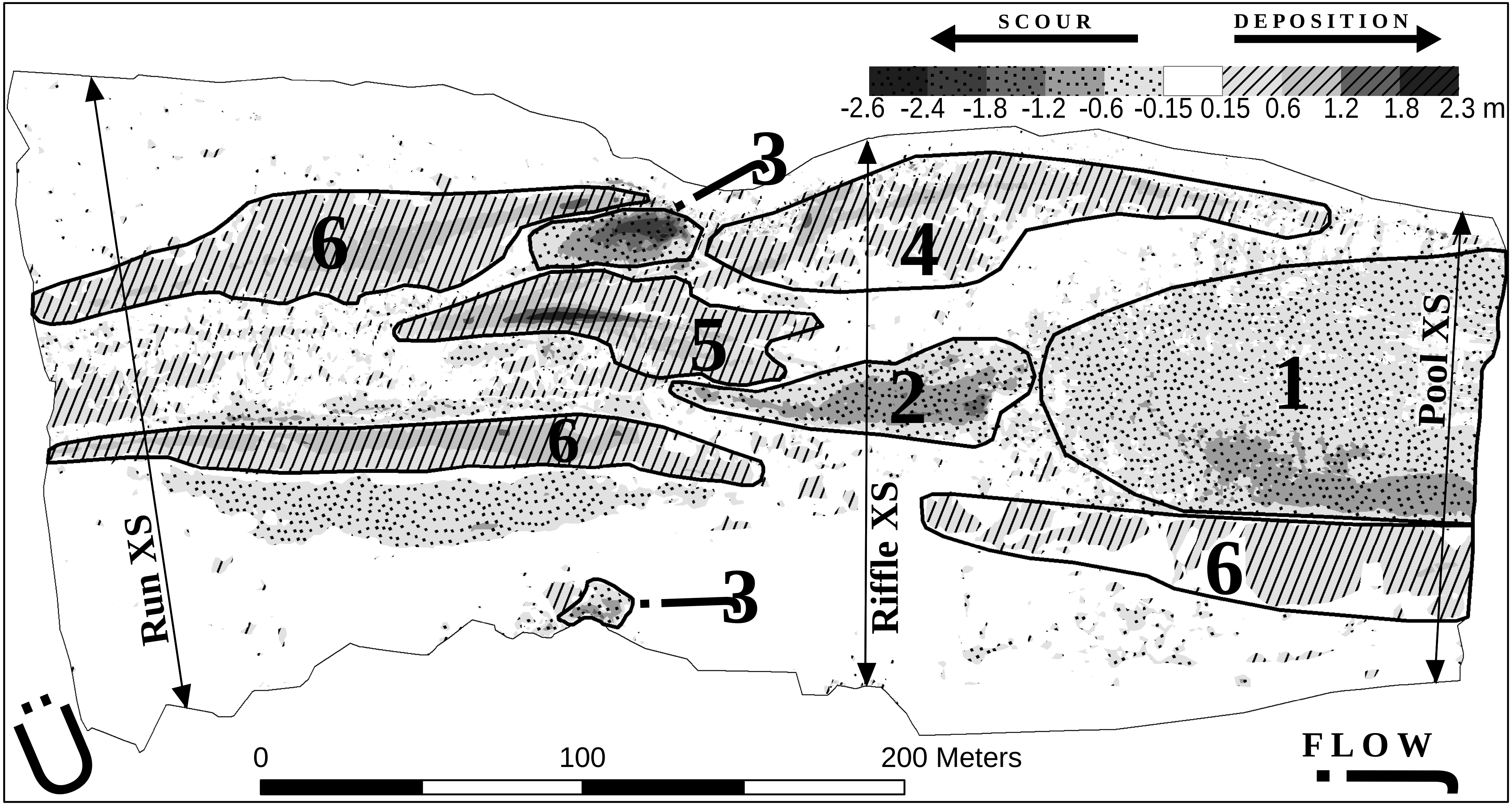
SCOUR
DEPOSITION
-2.6 -2.4 -1.8 -1.2 -0.6 -0.15 0.15 0.6 1.2 1.8 2.3 m
1
2
3
3
4
5
6
6
6
Run XS
Riffle XS
Pool XS
0
100
200 Meters
FLOW

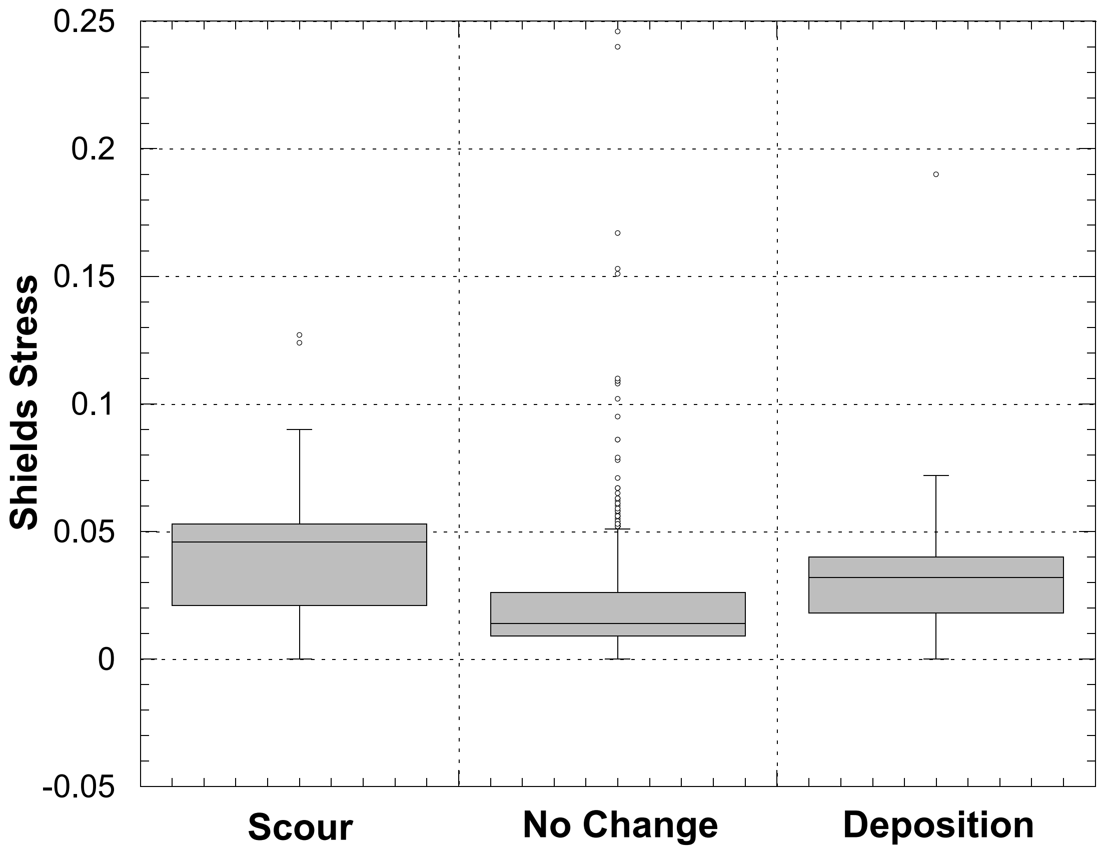
Shields Stress
0.25
0.2
0.15
0.1
0.05
0
-0.05
Scour
No Change
Deposition

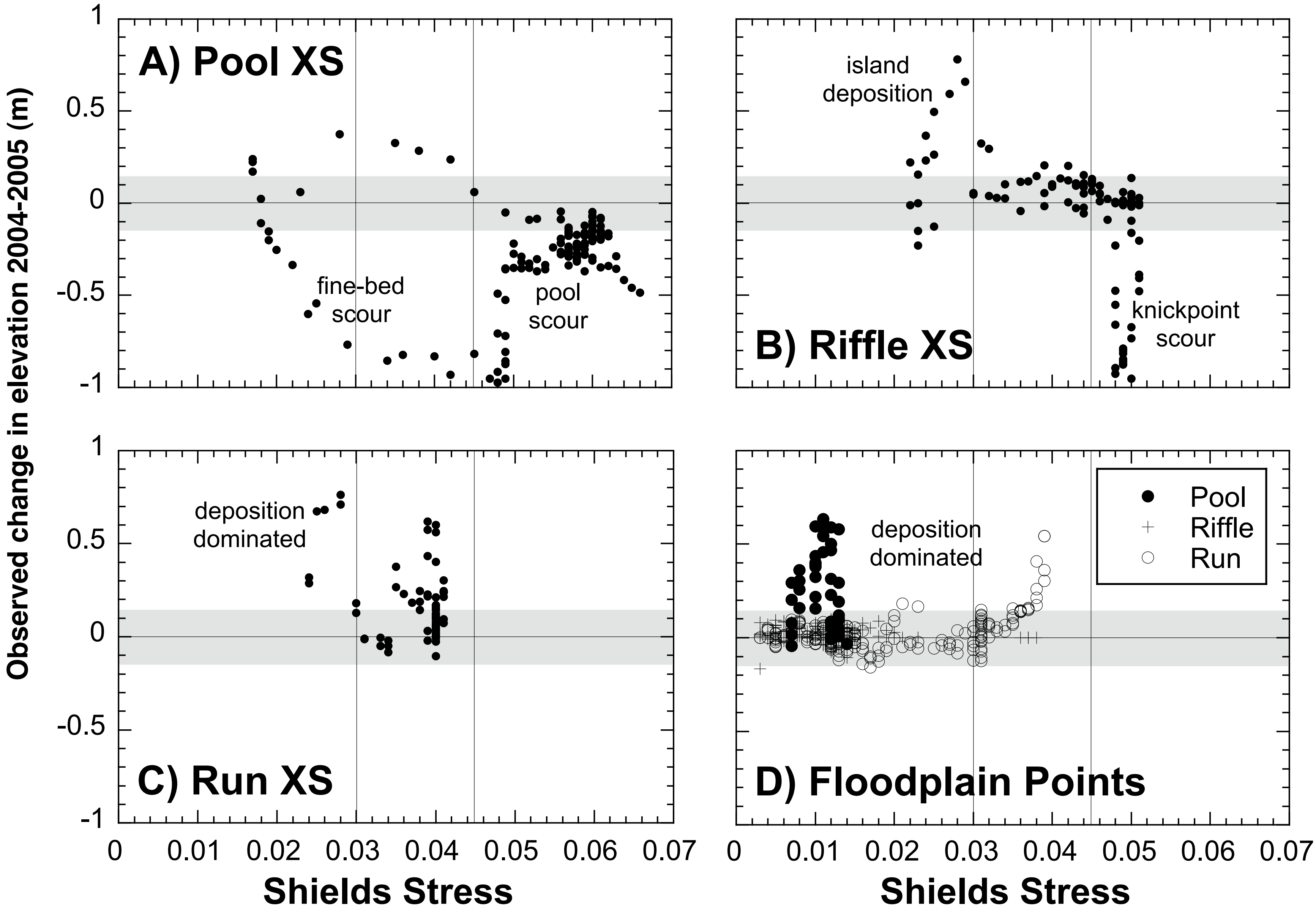

A) Pool XS
fine-bed
scour
pool
scour
B) Riffle XS
island
deposition
knickpoint
scour
C) Run XS
deposition
dominated
D) Floodplain Points
deposition
dominated
Pool
Riffle
Run
Observed change in elevation 2004-2005 (m)
Shields Stress
Shields Stress
1
0.5
0
-0.5
-1
0
0.01
0.02
0.03
0.04
0.05
0.06
0.07

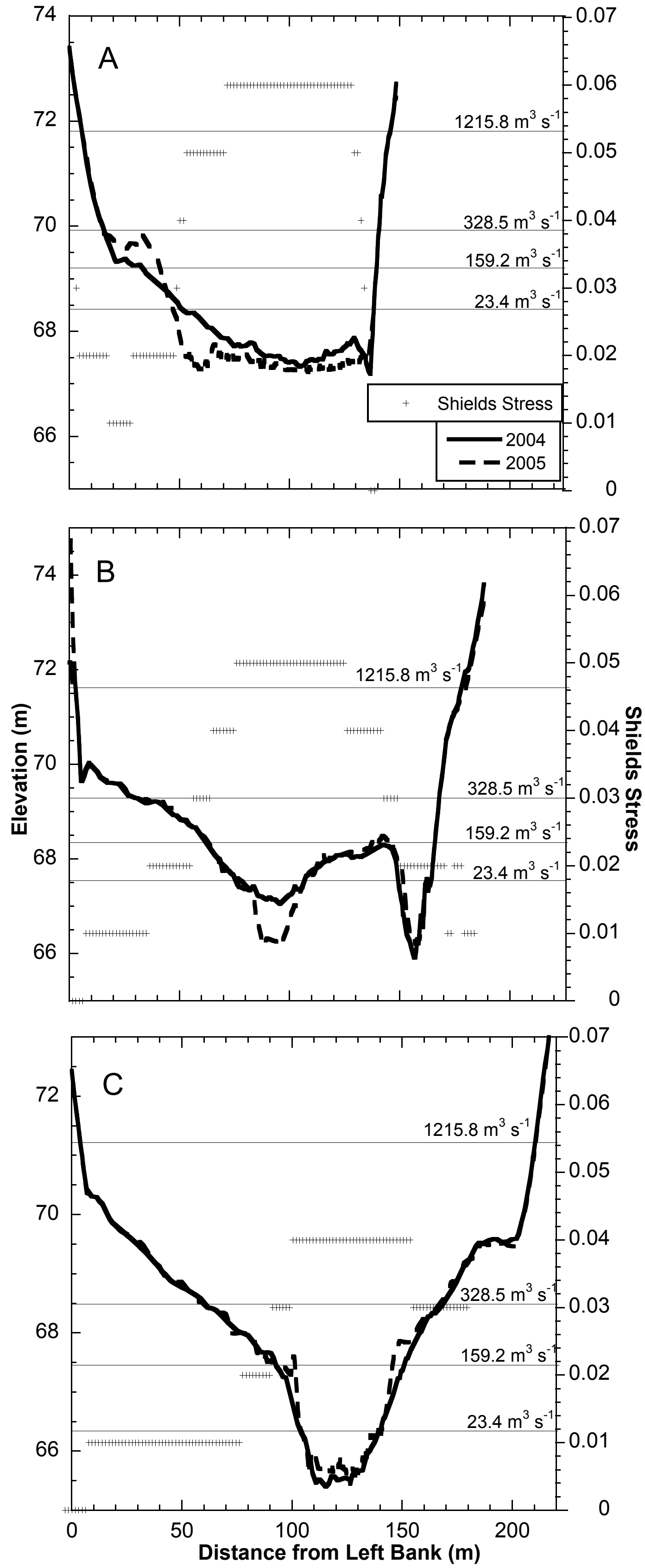

A
B
C
1215.8 m3 s-1
328.5 m3 s-1
159.2 m3 s-1
23.4 m3 s-1
Shields Stress
2004
2005
Elevation (m)
Shields Stress
Distance from Left Bank (m)

APPENDIX 4

Relationships between mesoscale morphological units, stream hydraulics and Chinook salmon (Oncorhynchus tshawytscha) spawning habitat on the Lower Yuba River, California

Available online at www.sciencedirect.com
ScienceDirect
Geomorphology 100 (2008) 527 – 548
GEOMORPHOLOGY
www.elsevier.com/locate/geomorph

Relationships between mesoscale morphological units, stream hydraulics and Chinook salmon (*Oncorhynchus tshawytscha*) spawning habitat on the Lower Yuba River, California

Hamish J. Moir *, Gregory B. Pasternack

Department of Land, Air, and Water Resources, University of California, One Shields Avenue, Davis, CA 95616-8626, USA

Received 8 October 2006; received in revised form 31 January 2008; accepted 1 February 2008
Available online 14 February 2008

Abstract

An expert-based approach was used to identify 10 morphological unit types within a reach of the gravel bed, regulated Yuba River, California, that is heavily utilized by spawning Chinook salmon (*Oncorhynchus tshawytscha*). Analysis of these units was carried out using two-dimensional hydrodynamic modeling, field-based geomorphic assessment, and detailed spawning surveying. Differently classified morphological units tended to exhibit discrete hydraulic signatures. In most cases, the Froude number adequately differentiated morphological units, but joint depth–velocity distributions proved the most effective hydraulic classification approach. Spawning activity was statistically differentiated at the mesoscale of the morphological unit. Salmon preferred lateral bar, riffle, and riffle entrance units. These units had moderately high velocity (unit median >0.45 m s^{-1}) and low depth (unit median <0.6 m), but each exhibited a unique joint depth–velocity distribution. A large proportion of redds (79%) were associated with conditions of convective flow acceleration at riffle and riffle entrance locations. In addition to reflecting microhabitat requirements of fish, it was proposed that the hydraulic segregation of preferred from avoided or tolerated morphological units was linked to the mutual association of specific hydraulic conditions with suitable caliber sediment that promotes the provision and maintenance of spawning habitat.

Keywords: Chinook salmon; Spawning; Morphological units; Hydraulics; Two-dimensional modeling; Fluvial geomorphology

1. Introduction

When viewed in terms of their role supporting ecological functions, fluvial processes may be differentiated by spatial scale relative to channel width (w) into those occurring at micro (0.01–1.0 w), meso (1.0–10 w), and larger spatial scales >10 w commonly referred to as reaches and/or segments depending on the classification system (e.g., Grant and Swanson, 1995; Montgomery and Buffington, 1997; Thompson et al., 2001). The term "microhabitat" is defined as the localized depth, velocity, temperature, and substrate at a point in a river without regard to the surrounding conditions. It is often possible to empirically relate ecological function to microhabitat variables (Bovee, 1986), but doing so provides a limited understanding of how and why fluvial–ecological linkages are spatially related. The term "mesohabitat" is defined as the interdependent set of the same physical variables over a discernible landform known as a morphological unit (e.g., scour pool, riffle, and lateral bar). There is a general lack of studies that nest the microscale requirements of instream species within the mesoscale context of an assemblage of morphological units. Consequently, in this study it is hypothesized that by linking the mesoscale of morphological units to microhabitat characteristics, it would be possible to explain fluvial–ecological linkages better.

Previous studies have provided justification why morphological units should be able to explain fluvial–ecological relations. First, they are considered to be the "fundamental building blocks of rivers systems" (Brierly and Fryirs, 2000). Also at the mesoscale, the concept of physical biotopes has been proposed as a framework for classifying streams based on their physical characteristics that is typically linked to instream habitats

* Corresponding author. The Macaulay Institute, Craigiebuckler, Aberdeen, AB15 8QH, UK. Fax: +44 1224 311556.
E-mail addresses: h.moir@macaulay.ac.uk (H.J. Moir), gpast@ucdavis.edu (G.B. Pasternack).

0169-555X/$ - see front matter © 2008 Elsevier B.V. All rights reserved.
doi:10.1016/j.geomorph.2008.02.001

(Padmore et al., 1998). Newson and Newson (2000) stated that a "biotope approach represents an important linking scale between the detail of microscale habitat hydraulics and the need for network-scale appraisals for management of channels and flows." Second, some studies have found that mesohabitat is a good predictor of fish utilization patterns (Geist and Dauble, 1998; Hanrahan, 2007). Finally, the type and distribution of morphological units have been found to be sensitive to landuse within the watershed (Beechie et al., 2003). In terms of practicality, the mesoscale provides a manageable resolution of analysis that balances scientific detail with the potential for catchment-scale application (Padmore et al., 1998); the study of the form, function and distribution of morphological units is therefore useful both in terms of scaling-up to watershed scale estimates of habitat capacity and for assessing how this might be impacted by human activity (Reeves et al., 1989; Beechie et al., 2001).

Although more general mesoscale research of habitat-types has been undertaken (Jowett, 1993; Orth, 1995), this has rarely involved specific studies of salmonid spawning habitat in anything but small streams (e.g., Moir et al., 2006). In many river systems spawning habitat has been identified as a key limiting factor controlling salmonid population sizes. Because salmonids spawn in gravel beds with heterogeneous features (Wheaton et al., 2004b), habitat availability and distribution depend on the physical character of stream channels at the mesoscale (Moyle, 1994; Montgomery et al., 1999; Brown, 2000). Yet most salmonid spawning studies have characterized microhabitats (e.g., Burner, 1951; Beland et al., 1982; Moir et al., 2002) or made more general and qualitative links to geomorphic form and process (e.g. Shirvell, 1989; Magee et al., 1996; Montgomery et al., 1996; Payne and Lapointe, 1997; Geist and Dauble, 1998; Knapp and Preisler, 1999; Dauble and Geist, 2000; Fukushima, 2001; Moir et al., 2002). Montgomery et al. (1999) and Moir et al. (2004) linked salmonid spawning habitat to a qualitative characterization of channel morphology, although both studies were explicitly reach scale, too coarse to resolve unit-specific geomorphic–biotic relationships. Few have explicitly examined the mesoscale, made quantitative physical–biotic linkages or assessed across spatial scales (e.g., characterized microscale hydraulic patterns nested within mesoscale units). Furthermore, the majority of studies examining salmonid spawning habitat have been conducted in relatively small streams where biological assessment (e.g., redd counts and spawning observation) and physical measurements (hydraulics and sediments) are less logistically demanding.

Moir et al. (2006) adopted a mesoscale approach to study the relationships between channel morphology, hydraulics, and Atlantic salmon spawning activity over a range of discharges at six study sites in an upland Scottish stream. Statistically significant differences in discharge–hydraulic relationships between the contrasting morphological unit types were identified. However, only morphological units utilized for spawning were studied; no comparison was made between spawning and non-spawning units. Also, instream hydraulics were sampled at a relatively low resolution (average of 0.081 points·m^{-2}) that may not have been sufficient to identify complex hydraulic patterns that are potentially important to habitat selection by spawning salmonids. Indeed, due to the inherent difficulties involved in representatively characterizing such phenomena, few studies have considered nonuniform hydraulic patterns (e.g., convergence, divergence, vorticity) at the mesoscale, factors that are known to be important geomorphic (Pasternack et al., 2006; MacWilliams et al., 2006; Brown and Pasternack, in press) and biological (Crowder and Diplas, 2002, 2006; Elkins et al., 2007) agents.

This study aimed to identify specific mesoscale morphological units associated with Chinook salmon (*Oncorhynchus tshawytscha*) spawning habitat in a large gravel-bed river and link them explicitly to microscale hydraulic patterns, sedimentary characteristics, and the geomorphic processes that control their character and distribution. Specifically, the objectives of the study were to (i) identify and map the distribution of morphological units, (ii) report their microhabitat characteristics, (iii) relate patterns of Chinook salmon spawning activity to the spatial distribution of morphological units and their hydraulic characteristics, and, (iv) describe the association between Chinook salmon spawning habitat, nonuniform hydraulics, and geomorphic processes.

The study was carried out at a site on the mainstem Yuba River, California adopting a combination of high-resolution topographic surveys, two-dimensional hydrodynamic modeling, and field-based biological and geomorphic analyses. Compared to other methods of assessment (e.g., one-dimensional models, cross-sectional assessments), the application of a two-dimensional hydrodynamic model allowed a closer representation of the resolution at which salmon select spawning sites and a better characterization of the broader scale flow patterns (e.g., convective acceleration, turbulent eddies, shear zones) that may be important in providing habitat. Understanding the geomorphic processes that control the ecological functioning and evolution of salmonid habitats is essential to determine the likely ecological effects of changes to the sediment and water budgets of a river system (through river management, landuse or climate change) and to guide science-based sustainable habitat rehabilitation.

2. Study area

The Yuba River is a tributary of the Sacramento River in the northern central valley of California (Fig. 1). It drains 3480 km^2 from the crest of the Sierra Nevada (highest elevation is Mount Lola at 2774 m amsl) to the confluence of the Feather River near Marysville and Yuba City (~10 m amsl). Flowing in a southwesterly direction, it grades from mountainous and forested in the headwaters to foothill terrain and then to a wide-open valley. Annual precipitation ranges from >1500 mm at the Sierra Nevada crest to ~500 mm at Marysville, ~85% of which falls between November and April (Curtis et al., 2005). In the upper regions of the catchment, much of this accumulates as snow pack that contributes significantly to spring runoff April–July.

The Yuba basin has been highly manipulated for hydropower, water supply, flood regulation, gold mining, and sediment control (James, 2005). Although two small dams exist on the South and

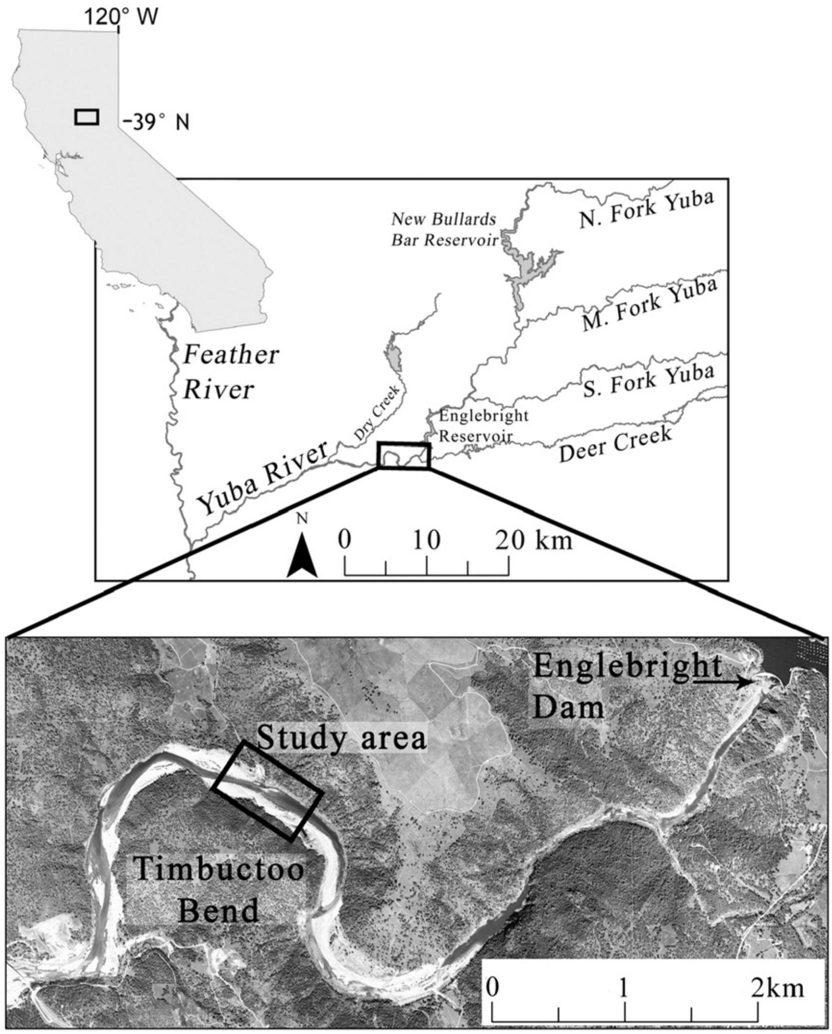

Fig. 1. Study area: Timbuctoo Bend on the Lower Yuba River, northern California, USA.

Middle Forks (Spaulding Dam and Jackson Meadows Reservoir), they are situated high enough in the watershed that their effects on flows (particularly during floods) in lower river locations are minimal. In contrast, New Bullards Bar Dam (operational in 1969) captures nearly the entire runoff of the North Fork Yuba and has a large reservoir capacity of 1.2 billion m^3 (6.7 times the combined total capacity of Spaulding and Jackson Meadows). Englebright Dam is an older concrete arch dam built in 1941 on the mainstem Yuba ~38 km upstream from the confluence with the Feather and ~16 km downstream from New Bullards Bar. It stands 85 m high in a narrow canyon, has a reservoir capacity of 86 million m^3, and primarily serves as a sediment barrier blocking export of hydraulically mined, gold-depleted sedimentary deposits. Although a smaller structure with limited impact to flood flows, it is very important to geomorphic and ecologic processes on the Yuba, being a complete barrier to the passage of sediment downstream and anadromous fish migration upstream. The section of the mainstem river from Englebright Dam downstream to the confluence with the Feather is defined as the Lower Yuba River (LYR). Although Englebright Dam was built with the purpose of trapping sediment liberated during hydraulic-mining operations, by the time it was built large volumes of material had already infilled the lower river valley to depths of up to 25 m. This large storage of sediment in the LYR is frequently reworked and provides a long-term template of channel incision.

The statistical "bankfull" discharges (~1.5-yr return interval of annual peak series) recorded at the U.S. Geological Survey (USGS) Smartville gauge (#11418000) located 0.5 km downstream of Englebright Dam for the periods 1942–2004 and for 1971–2004 are 330 and 160 $m^3\ s^{-1}$, respectively, illustrating the significant impact to hydrology of New Bullards Bar. Englebright Dam has a controlled flow release potential of 135 $m^3\ s^{-1}$, although uncontrolled flows over Englebright Dam occur frequently. One hundred flow events have exceeded bankfull discharge and overtopped Englebright Dam between the construction of New Bullards Bar Dam in 1970 and the beginning of October 2005. Over the 1971–2004 period, the median daily discharge at the Smartville gauge was 43.6 $m^3\ s^{-1}$. The 5-, 10-, and 50-yr return interval discharge for 1971–2004 are 1050, 1450, and 4025 $m^3\ s^{-1}$, respectively. Therefore, despite some flow regulation, the Yuba River below Englebright Dam experiences a dynamic flood regime. The combination of a near-natural flood hydrology and a plentiful supply of locally stored sediment in the LYR provides a dynamic geomorphic environment that produces a sequence of active bar complexes and a heterogeneous channel and floodplain morphology normally associated with a wandering gravel-bed river.

2.1. Timbuctoo Bend study site

The specific site examined in the present study is located 6.3 km downstream from Englebright Dam within 'Timbuctoo Bend', a highly dynamic and active gravel/cobble zone of the river (Figs. 1 and 2). Timbuctoo Bend has a well-connected floodplain with large active gravel bars, secondary and tertiary flood channels, limited vegetation encroachment, and nonuniform channel geometry. Based on aerial photographs from 1937 to 2006, historical channel change has been dramatic, including emplacement of large dredger tailings on the floodplain, activation and abandonment of channels, and cycles of willow growth and natural levee stabilization. The study site is 460 m long and extends laterally ~300 m to include the entire valley floor up to the 50-yr return interval water surface elevation. In 2004 it was dominated by an island/bar complex that generally defined a pool-riffle-run sequence of morphological units in the downstream direction. Sediments are dominantly in the cobble (64–256 mm) and gravel (2–64 mm) size classes and exhibit spatial patterns that indicate hydraulic sorting during a period of few high flow events following a large flood in 1997 (~42-yr return interval). In recent years, this site is the most heavily utilized area of spawning habitat by Chinook salmon on the Yuba River.

Between the Smartville gage and the study site, a tributary (Deer Creek, USGS station #11418500) enters the river, contributing direct runoff during rain events and little otherwise. Deer Creek drains ~220 km^2 on the southeast margins of the Yuba Basin. Therefore, flood hydrographs at the study site during rainstorm events reflect the combined flow of the mainstem Yuba and Deer Creek.

3. Methods

3.1. Field methods

Field data were collected between April 2004 and April 2005, a period characterized by relatively stable flows (see Section 3.1.5). Conditions in the channel were documented using a combination of detailed topographic data, morphological classification, hydraulic measurements, sediment analysis (visual assessments and pebble counts), and spawning utilization surveys. Field data were used to develop and validate a two-dimensional hydrodynamic model, and then model results were used to characterize high-resolution hydraulic patterns at the mesoscale and how this relates to spawning activity.

3.1.1. Topography

A detailed map of channel topography was used to aid geomorphic interpretation and to describe the bottom boundary for the two-dimensional hydrodynamic model. The map was obtained using a similar method to Brasington et al. (2000), Pasternack et al. (2004) and Elkins et al. (2007); a Topcon GTS-802A robotic total station measured bed positions on a staggered grid with supplemental points as needed to resolve bed features (e.g., boulders, slope breaks, etc.). The mean sampling density in the channel was 0.61 points m^{-2}, with a lower density on the

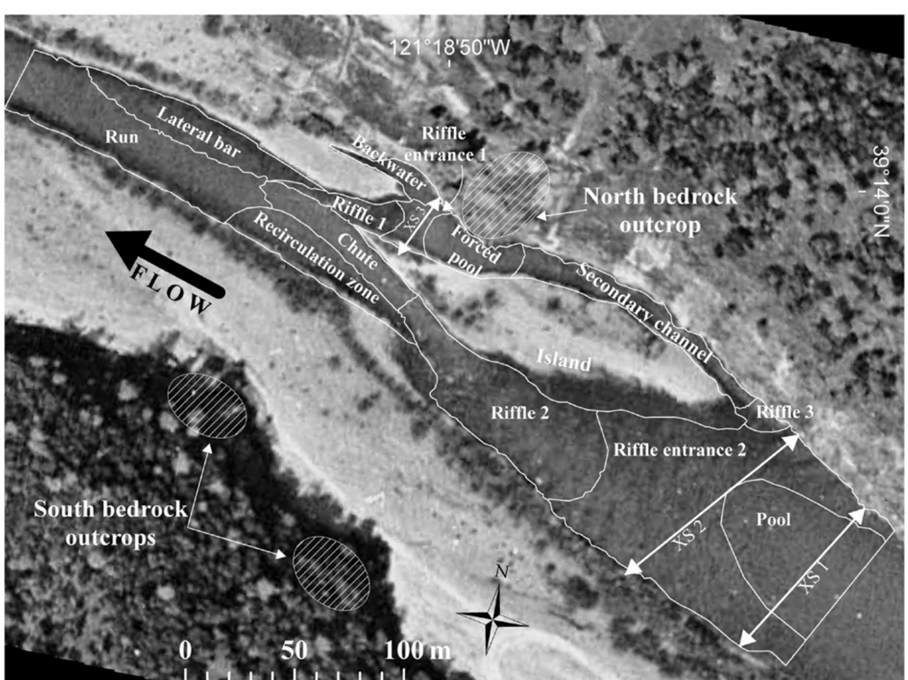

Fig. 2. Aerial photograph of the study site showing the extent of the modelled reach, the identified morphological units and the location of the hydraulic validation cross-sections. The mismatch between the modelled and photograph water edge reflects different discharges (23.4 m^3 s^{-1} modelled, ~30 m^3 s^{-1} photo).

relatively flat floodplain. Surveying accuracy was assessed using 98 control network checks and was found to average 0.013 m in the horizontal and 0.011 m in the vertical, which is significantly smaller than the natural error induced by the bed material, typically ranging in size between 0.05 and 0.2 m.

3.1.2. Morphological units

Morphological units were identified by expert-based reconnaissance of the site during detailed topographic surveying and through interpretation of features evident in the Digital Elevation Model (DEM, discussed in Section 3.2). No definitive morphological unit classification scheme was identified in the literature. Therefore, the scheme adopted represented a combination of morphological definitions (e.g., Montgomery and Buffington, 1997; Padmore et al., 1998; Thompson et al., 2001) specifically adapted for the characteristics of the study site. The geomorphic unit classifications used at the site were pool, riffle, run, riffle entrance, forced pool, chute, lateral bar, recirculation zone, backwater, and secondary channel, each of which are described in Table 1. Only two unit types were replicated at the study site; there were three riffles and two riffle entrances. For statistical purposes it would have been preferable to have had a number of replicates of each unit type. However, this would have meant modeling a much larger section of the river to obtain even one replicate of every unit type, especially since the study site had a highly diverse morphology within the context of the LYR. This would not have been practical given the resolution of data required for the objectives of the study.

Clearly, classification procedures that integrate underlying topography with surface flow are intrinsically linked to hydrological regime. As discharge increases, the spatial distribution of relative hydraulic conditions will vary. Hydraulic heterogeneity also tends to decrease with increasing discharge (Stewardson and McMahon, 2002; Moir et al., 2006; Brown and Pasternack, in press) with the associated merging and simplification of morphological/habitat units. However, the classification of morphological units in this study was carried out during the spawning season and therefore represents a relatively narrow discharge range (see Section 3.1.5) with little potential for variation in the spatial distribution and classification of morphological units.

Table 1
Description of morphological unit types identified at the study site

Morphological unit	Description
Pool	A region of relatively deep and slow flow with low water surface slope.
Riffle	Relatively fast and shallow flow with high water surface slope and rough water surface texture. Such units may be associated with the downstream face of a transverse (alternate) bar feature.
Riffle entrance	A transitional zone between an upstream pool and downstream riffle. Water depth is relatively low and velocity characterized by a downstream convective acceleration toward the riffle crest that is often associated with lateral and vertical flow convergence. The upstream limit is at the approximate location where there is a transition from a divergent to convergent flow pattern. The downstream limit is at the slope break of the channel bed termed the riffle crest.
Run	Exhibits a moderate flow velocity, low to moderate depth, and moderate water surface slope. Such units typically exhibit a moderate to high roughness of water surface texture and tend not to be associated with transverse bar features that riffles may be.
Forced pool	A subclass of pool in which a localized area of the bed is "over-deepened" from local convective acceleration and scour associated with static structures such as woody debris, large boulders, or bedrock outcrops (Montgomery and Buffington, 1997; Thompson et al., 2001).
Chute	Characterized by the moderate flow velocity and relatively high depth of the channel thalweg. Chutes are often located in a constriction downstream of a riffle as it transitions into a run. Chutes typically have relatively coarse sediment.
Lateral bar	A depositional unit that is located at the channel margins and orientated longitudinally to the direction of flow. The feature slopes toward the channel thalweg with an associated increase in both flow depth and velocity. Sediment size tends to be lower than in adjacent sections of the channel.
Recirculation zone	Characterized by low-velocity or recirculating flow, often bound by a hydraulic shear zone toward the channel thalweg that controls flow separation and the shedding of turbulent eddy structures. These units are usually the associated with an abrupt transition in the topography of the channel (e.g., the downstream extent of a bar feature or bedrock outcrop) that results in lateral flow separation.
Backwater	An area of low-velocity flow adjacent to the main channel but connected at the downstream or upstream end of the unit.
Secondary channel	A smaller channel active under normal flow conditions that is connected at both upstream and downstream ends to the mainstem channel. In reality such features may incorporate a range of morphological characteristics, but in order to be classified at the same absolute resolution as is necessary for mainstem units, a single unit is defined. These units therefore tend to extend over a greater dimensionless length (i.e., number of channel widths) than others.

3.1.3. Hydraulics

Cross-sectional depth and velocity data were collected along three transects (Fig. 2) on February 13, 2005 using standard methods appropriate for validating a two-dimensional hydrodynamic model (Wheaton et al., 2004a; Pasternack et al., 2004, 2006; Brown and Pasternack, in press). The only modification of the method for this study (on a much wider river) was to use the Topcon GTS-802A to survey the exact position of each paired measurement of depth and velocity, which were collected an average spacing of 2.87-m along a transect. This allowed field data to be precisely compared to model predictions for the same location. Transects 1 and 2 span the mainstem channel and were also used to estimate total discharge, whereas transect 3 spanned only the side channel. Measurement errors were ±1 cm for depth using a stadia rod and ±33 mm s^{-1} root mean square for velocity using a Marsh-McBirney Flo-Mate 2000. Velocity was sampled at 30 Hz and averaged over 30 s at 0.6 × depth from the water surface to obtain a measure of the depth-averaged velocity. Measuring velocity at one position within the water column was appropriate given the uniform flow conditions and low relative bed roughness (water depth was 10–20 × local median substrate size, d_{50}) in the location of the three transects. Studies of flow around individual large grains and pebble clusters demonstrate that point measurements of velocity at arbitrary locations on a gravel bed will be strongly influenced

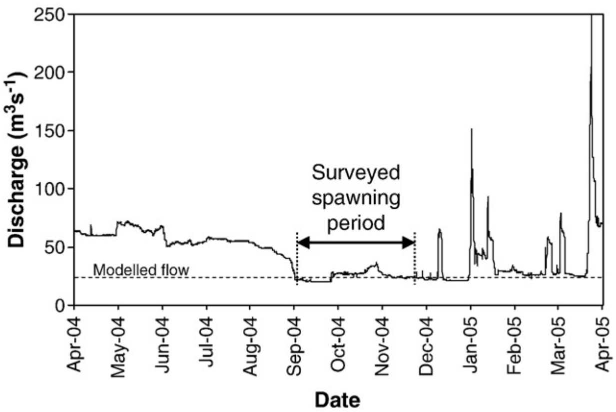

Fig. 3. Hydrograph for the study period (i.e., April 2004 to April 2005). The period over which spawning analyses were carried out is highlighted. The horizontal dashed line represents the modeled discharge (25.7 m^3 s^{-1} as indexed to combined USGS flow data from the Yuba River and Deer Creek).

by these features at the 0.1–0.5 m scale (Acarlar and Smith, 1987; Paola et al., 1986; Kirkbride and Ferguson, 1995; Buffin-Belanger and Roy, 1998; Lawless and Robert, 2001a,b).

3.1.4. Sedimentary analysis

The general sedimentary characteristics across the entire site were visually assessed and mapped. This data was subsequently linked to the individual morphological units identified at the site (Section 3.3.1). In this procedure, sediment character was defined in terms of the dominant and subdominant size classes (i.e., boulder > 256 mm, cobble 64–256 mm, gravel 2–64 mm, sand and finer < 2 mm, all sizes being intermediate axis diameter).

Using the "Wolman-walk" procedure (Wolman, 1954), 32 pebble counts were also conducted at the study site. Although they were all carried out under low discharge conditions, flows at certain regions of the site were too deep and/or fast to permit sampling using this technique. Thus, samples were not evenly distributed throughout the site or across all morphological units; they tended to be biased toward accessible channel margin locations. Therefore, only backwater, recirculation zone, riffle entrance and run units were sampled. At each location, a minimum of 100 particles (mean = 120, range = 100–219) were sampled across a ~3 × 3 m section of the bed. The position of the center point of each sampling location was surveyed using a Topcon GTS-802A robotic total station.

3.1.5. Redd mapping

The location of individual redds (cumulative total = 451) were surveyed on 52 days between September 17 and November 16 inclusive during the 2004 spawning season by experienced observers. The location of the deepest part of the redd "pit" was surveyed in each case using a Topcon GTS-802A robotic total station. Redds that had been previously surveyed were identified by a painted marker stone that was placed in the pit. If the marker stone was buried by subsequent redd excavation, the position of the modified pit was re-surveyed. There are 'spring' and 'fall' runs of Chinook spawn in the LYR, with both spawning in the fall. Some local experts identify spring run fish as those that spawn September 1–30 and fall run from October 1 to December 31 in the Yuba, while others disagree with this delineation and report overlap in timing so that it is difficult to tell with certainty that a given redd was constructed by spring or fall fish. In relation to the period of spawning surveying undertaken in this study, the nominal "spring run" could be considered to have been sampled September 17 to 30 and the "fall run" from October 1st to November 16. However, the first survey carried out on September 17 mapped all the redds that had been constructed prior to that date. During this initial survey there were still relatively few redds at the site and it was apparent that each was a discrete feature (i.e., there was no evidence that superimposition had occurred by that point). It was therefore unlikely that many redds constructed prior to September 17 were not identified. Thus, redds were effectively mapped between the onset of the 2004 spawning season and November 16. Although fall spawning is regarded to continue until December 31, the cumulative number of redds was so high in the 2004 spawning season that by mid-November it was very difficult to distinguish between new and previously constructed redds, despite the use of markers to identify previously mapped features. Therefore, to avoid bias through re-sampling, the final redd survey was conducted on November 16. The number of redds surveyed by that date (i.e., 451) was sufficient to conduct subsequent statistical analyses. Subsequent visits to the study site after November 16 revealed that no new locations had been utilized so that the spatial cover of the surveys conducted was representative. Over the period September 1 to November 16, discharge was well below bankfull (160 m^3 s^{-1}) and relatively stable compared to the variation over the period April 2004 to April 2005 (Figs. 3 and 4). Spawning period non-exceedence probability values for daily discharge, Q_{10}, Q_{50}, and Q_{90}, were 30.2, 25.4, and 20.0 m^3 s^{-1}, respectively (Fig. 4). Flow variations were due to dam releases that delivered water to downstream users. There was some variation in flows between the periods September 1 to 30 and October 1 to November 16, with median and mean discharge values of 20.6 and 21.7; and 26.8 and 27.3 m^3 s^{-1}, respectively.

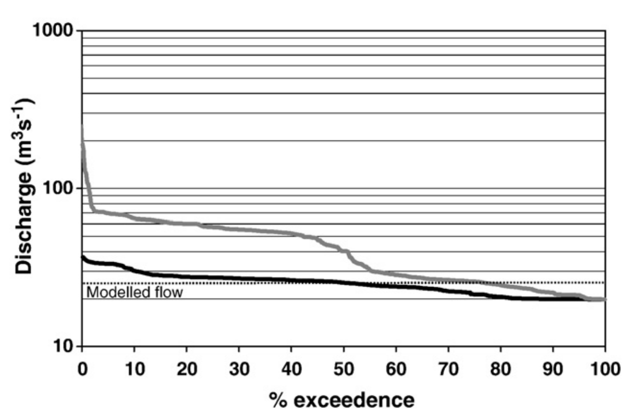

Fig. 4. Flow duration curves for the study period (i.e., April 2004 to April 2005; solid grey line) and spawning analysis period (solid black line). The horizontal dashed line represents the modeled discharge (25.7 m^3 s^{-1} as indexed to combined USGS flow data from the Yuba River and Deer Creek).

3.2. Two-dimensional Yuba model

Two-dimensional (depth-averaged) hydrodynamic models have existed for decades and have been used to study a variety of hydrogeomorphic processes (Bates et al., 1992; Leclerc et al., 1995; Miller and Cluer, 1998; Cao et al., 2003). Recently, they have been evaluated for use in regulated river rehabilitation emphasizing spawning habitat restoration by gravel placement (Pasternack et al., 2004, 2006; Wheaton et al., 2004b; Elkins et al., 2007) and to better understand the relative benefits of active river rehabilitation versus flow regime modification (Jacobson and Galat, 2006; Brown and Pasternack, in press) on regulated rivers. In this study, the long-established two-dimensional model known as Finite Element Surface Water Modeling System 3.1.5 (FESWMS), implemented within the Surface-water Modelling System (SMS) graphical interface (Environmental Modeling Systems, Incorporated), was used to simulate site hydrodynamics at the 1-m scale relevant to microhabitat utilization by fish that are ~1 m long. FESWMS solves the vertically integrated conservation of mass and momentum equations using a finite element method to acquire depth-averaged two-dimensional velocity vectors and water depths at each node in a finite element mesh (Froehlich, 1989). A mesh element is "dry" when depth is below a user-defined threshold (set at $1 \times d_{90} \sim 0.12$ m here), but to the extent possible, the mesh area was trimmed to closely match the observed wetted area.

FESWMS is a long-established model best viewed as a conceptual guide of likely outcomes, rather than literal truth. Application of FESWMS to gravel-bed rivers has been extensively validated on the Lower Mokelumne River (four basins south of the Yuba and having similar spawning period discharge and bed material conditions) using observed velocity and depth at 35 cross-sections. This indicated good predictions for the gravel bed and poor predictions around large woody debris or complex banks (Pasternack et al., 2004, 2006; Wheaton et al., 2004a; Elkins et al., 2007). Pasternack et al. (2006) reported details regarding FESWMS model uncertainty when used for gravel-bed rivers. They found that FESWMS could predict local shear stress over gravel-bed riffles as accurately as five common field estimation methods. MacWilliams et al. (2006) compared FESWMS with one-dimensional and three-dimensional models of gravel-bed river hydrodynamic and found that the two-dimensional model was capable of simulating key stage-dependent processes responsible for riffle-pool maintenance. Details on the validation procedure used in this study follow the explanation of model development.

3.2.1. Model development

Topographic data were imported into Autodesk Land Desktop 3 to create a digital elevation model (DEM) of the study site using a standard approach (Wheaton et al., 2004a; Pasternack et al., 2004, 2006; Elkins et al., 2007). Refined topographic point and break-line data used to produce the DEM were exported to SMS for use in the two-dimensional model. The two-dimensional mesh was generated using a built-in paving algorithm without reference to the independently located depth and velocity measurement points. This independence provided a fair test of the accuracy of a two-dimensional model without special attention to the mesh in the vicinity of validation locations. Node elevations were interpolated from imported DEM data using a Triangulated Irregular Network (TIN)-based scheme. The wetted mesh covered 24,483 m^2 of channel with 51,000 computational nodes comprising 24,847 elements, with the highest density near boulder clusters. The node density of the mesh varied but averaged 2.1 points m^{-2}, which was higher than that for the DEM.

To run FESWMS, discharge and downstream boundary water surface elevation were obtained from velocity–area flow gauging and by surveying the water surface edge, respectively. Based on an analysis of combined USGS gage data from the Yuba at Smarville and Deer Creek, simulations were made for the minimum, median, and maximum discharges during the spawning period. For sake of brevity and recognizing from preliminary comparisons of model output that the median flow was representative of the discharge range over the spawning season, only results associated with the median flow simulation are presented and analyzed. For that median flow, the field-measured discharge was 23.4 $m^3\ s^{-1}$, which is the mean of discharges calculated at the two channel-wide cross-sections measured in this study. This corresponded to a combined flow of 25.7 $m^3\ s^{-1}$ from the upstream USGS gages (Smartville and Deer Creek). The 9% difference is thought to be due to transmission losses between the USGS gages located in bedrock reaches and the study site located on thick hydraulic-mining deposits of permeable gravel. The water surface elevation corresponding to the modeled discharge at the downstream end of the site was surveyed by total station with a vertical accuracy of ±2 cm and found to be 66.25 m relative to the NAVD88 vertical datum.

Rather than calibrating the model to obtain optimal parameters that might be physically unrealistic, the approach taken was to estimate parameters using field data and then validate the resulting model predictions to assess the resulting accuracy. The two primary model parameters in FESWMS are bed roughness (as approximated using Manning's n for a gravel/cobble bed) and isotropic kinematic eddy viscosity (E). The effect of channel roughness on flow was addressed two ways in the model. Roughness associated with resolved bedform topography (e.g., rock riffles, boulders, gravel bars, etc.) was explicitly represented in the detailed channel DEM. Two-dimensional model predictions are highly sensitive to DEM inaccuracies (Bates et al., 1997; Hardy et al., 1999; Lane et al., 1999; Horritt et al., 2006), which is why detailed topographic mapping was done in this study. For unresolved roughness, Manning's coefficient (n) was estimated as 0.043 for the gravel-bed area with $d_{50} \sim 50$ mm and 0.06 for the coarse cobble/boulder bed over the highest velocity section of the riffle using a standard linear summation method (McCuen, 1989). Although it is possible to vary the bed-roughness parameter spatially in a two-dimensional model to try to account for variable bed sediment facies, it is difficult to justify small (<0.005) local deviations relative to two-dimensional model and measurement accuracy in gravel-bed rivers. Two-dimensional models have been reported to be sensitive to large (>0.01) variations in n values (Bates et al., 1998; Lane and Richards, 1998; Nicholas and Mitchell, 2003), and the validation approach used here would reveal that scale of deficiency.

Miller and Cluer (1998) showed that two-dimensional models could be particularly sensitive to the eddy viscosity parameterization used to cope with turbulence. In the model used in this study, eddy viscosity (E) was a variable in the system of model equations, and it was computed using the following standard additional equations developed based on many studies of turbulence in rivers (Fischer et al., 1979; Froehlich, 1989):

$$E = 0.6H \cdot u_* + E_0 \tag{1}$$

$$u_* = U\sqrt{C_\mathrm{d}} \tag{2}$$

$$C_\mathrm{d} = 9.81\frac{n^2}{H^{1/3}} \tag{3}$$

where H is water depth, u_* is shear velocity, U is depth-averaged water velocity, C_d is a drag coefficient, n is Manning's n, and E_0 is a minimized constant (0.033 $\mathrm{m^2\ s^{-1}}$) necessary for model stability These equations allow E to vary throughout the channel, which yields more accurate transverse velocity gradients. However, a comparison of two and three-dimensional models for a shallow gravel-bed river demonstrated that even with this spatial variation, it is not enough to yield as rapid lateral variations in velocity as occurs in natural channels, presenting a fundamental limitation of two-dimensional models like FESWMS (MacWilliams et al., 2006).

3.2.2. Model validation

Recognizing that two-dimensional models, like all models, have inherent strengths and weaknesses, some amount of uncertainty in model results must be understood and accepted (Van Asselt and Rotmans, 2002). Since model parameters were set to physically realistic values and not numerically calibrated to match observations, comparisons of predicted and observed conditions provide a meaningful assessment of model parameter uncertainty. Three different types of validation testing were done to evaluate model performance at 23.4 $\mathrm{m^3\ s^{-1}}$, making use of the depth and velocity data collected at three cross-sections as well as water edge elevations collected around the perimeter of the site.

First, to test the suitability of the selected Manning's n values of 0.043 and 0.06, the Topcon total station was used to measure the longitudinal profile of water surface elevation along the reach at 23.4 $\mathrm{m^3\ s^{-1}}$. Over the 460 m length of channel, 113 measurements were made at a ~4-m interval. The deviations between the observed and model-predicted values were calculated and statistically described.

Second, to validate model performance with regard to the key model parameter of eddy viscosity, the range of E values in model output was checked against field-based estimates. Field estimates of E were calculated using Eqs. (1)–(3) with observed depth and velocity measurements at the study's cross-sections, except that no E_0 value was needed. The mean and range of E values were compared between model predictions and field-based estimates. Also, a qualitative evaluation was made to determine if the model correctly predicted flow recirculations behind boulders and bedrock outcrops where they were visually evident during field observations, which is controlled by the model's E values.

Third, to quantify the accuracy of depth and velocity predictions at points and across the three cross-sections, total station surveyed coordinates of each field measurement of depth and velocity were imported into SMS, and then model depths and velocities at those exact locations were obtained using TIN-based interpolation of model result at computational nodes. For a simple point-scale comparison, matching data and predictions were statistically evaluated without any spatial context. To better comprehend the spatial pattern of observed versus model-predicted velocities across a channel, it is helpful to discern sub-grid scale spatial fluctuations from grid-resolvable trends. This was achieved by fitting a cross-sectional smoothing curve to the data using the locally weighted Least Squared error method and then comparing the two-dimensional model predictions to the smoothed curve. The fraction of the data considered during each smoothing step was set to 20%, thus for cross-section 3 where there were fewer measurement points, smoothing was minimal.

3.3. Data analysis

3.3.1. Morphological unit hydraulics

After characterizing model accuracy, depth and velocity were extracted from the two-dimensional model output and used to characterize morphological units. Depth and velocity data were not non-dimensionalized (e.g., by grain size) since this would likely have obscured important relationships linked to the absolute sedimentary and hydraulic habitat requirements of spawning salmonids that are linked to their body size (Crisp and Carling, 1989). Rather, the Froude number was adopted as a non-dimensional parameter to test for differences in the hydraulic characteristics between morphological units. It was calculated from the basic model output data at each node from the relationship:

$$\mathrm{Fr} = \frac{U}{(H \cdot g)^{0.5}} \tag{4}$$

where g is gravitational acceleration (9.81 $\mathrm{m\ s^{-2}}$). Since it is dimensionless, the Froude number provided a scale-independent means to discriminate between morphological unit classes in terms of their hydraulic character. Hydraulic data were returned to the spatial resolution of the surveyed data (i.e., 0.61 points $\mathrm{m^{-2}}$) from that of the higher point density of the model grid (i.e., 2.1 points $\mathrm{m^{-2}}$). This was done by employing a random filter of the data that reflected the proportional difference in the spatial point densities. The predicted depth, velocity, and Froude number values for all model nodes were distributed into subsets corresponding to the classified morphological units (Fig. 2).

Between-subset differences in the overall distribution of the Froude number (i.e., the shape of cumulative frequency distributions rather than just comparing the variance or mean) were carried out using the Kolmogorov–Smirnov (K–S) test. The values of the K–S statistic were used to provide an indication of the relative similarity/difference in hydraulic (Froude number) characteristics between morphological unit pairings at the study site. The 10th and 90th percentiles of the K–S values were arbitrarily used to define hydraulically similar and different morphological unit pairings, respectively. In this way it could be examined whether morphological units with the same classification exhibited more similar Froude number distributions than differently classified units and if differently classified unit types had similar Froude number characteristics.

To summarize the joint depth–velocity distribution of the identified morphological units, a statistical classification procedure (Kernel Discriminant Analysis, KDA) was used. Since the hydraulic data for each unit tended not to be normally distributed, a confidence limit based contouring approach could not be adopted. KDA objectively assessed the hydraulic character of the identified morphological units by comparing each data point to every other data point (i.e., using a cross-validation method) and determining which morphological unit it was most likely to be associated with, via a probabilistic measure. The data are summarized by actual unit class (i.e., the morphological unit that model output data was assigned to based on their spatial distribution, Fig. 2) in terms of the proportion of points within each morphological unit class as predicted by KDA. In effect the procedure calculates the morphological unit classes that are most probable to occur across the entire depth–velocity hydraulic space.

3.3.2. Abiotic–biotic integration

Individual surveyed redds were assigned to subsets corresponding to the classified morphological units. The depth, velocity, and Froude number values at the location of each redd were obtained from two-dimensional model output using ArcGIS 9.0. Utilization frequency was standardized by the area of respective morphological units to produce mean redd density within a unit (redds·m^{-2}). A morphological unit suitability index (MUSI) was calculated by employing the relativized electivity index (Vanderploeg and Scavia 1979; Lechowicz, 1982). This index discriminates equally between selection and avoidance (in this case of morphological unit types) and is calculated with the equation:

$$E^* = \frac{\left(\frac{R}{\sum R}\right) - \frac{1}{n}}{\left(\frac{R}{\sum R}\right) + \frac{1}{n}} \qquad (5)$$

where R is the ratio of the proportions of utilization to availability for each unit type and n is the number of unit types. E^* varies between −1 (avoidance) and +1 (selection) with 0 representing indifference. A value of MUSI > 0 indicates a greater proportional utilization than availability of a particular unit and therefore “selected” or “preferred” by spawning fish. A MUSI value of 0 indicates utilization proportional to availability, between −1 and 0 indicate “tolerated” conditions (i.e., fish utilize the unit but at a proportion lower than that unit's availability) and values of −1 (i.e., no utilization), “avoided”. MUSI values of all the morphological units were regressed against each of the median hydraulic descriptors (i.e., H_{50}, U_{50}, and Fr_{50}).

4. Results

4.1. DEM and morphological units

Within the general pool-riffle-run pattern of the study site, transitional units (riffle entrances and a chute) and laterally discrete units (lateral bar, recirculation zone, secondary channel and backwater) were identified that added heterogeneity (Fig. 2). Only the center section of the secondary channel was provided with that specific classification (i.e., secondary channel) because more discretely defined units were identified at the upstream (riffle) and downstream (forced pool, riffle entrance, and riffle) margins. At this resolution it is apparent that the large bedrock outcrop at the north channel margin near the centre of the modeled reach (Fig. 2) is likely responsible for the development of the adjacent forced pool

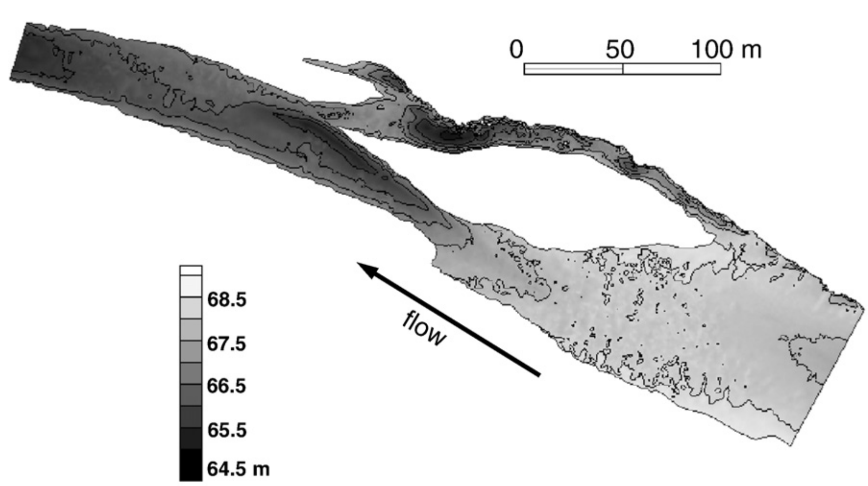

Fig. 5. DEM of the Timbuctoo Bend study site, Lower Yuba River.

unit (Fig. 5). The DEM highlights the variation in channel geometry through the study site. The channel initially widened from 80 m at the pool at the upstream limit of the site to 100 m at the head of the island feature where the mainstem and secondary channels diverge. The mainstem channel then narrowed sharply (85 m wide at the channel split to 15 m at the narrowest point of the riffle) before widening again towards the tail of the island (30 m at the island terminus). Once the secondary channel rejoined the mainstem downstream of the island, width increase to a maximum of 40 m before reducing to 30 m at the downstream limit of the study site.

4.2. Model validation

Three types of validation were carried out to understand the uncertainty in the two-dimensional model. The first validation test was a comparison of observed and predicted longitudinal water surface profiles to assess the validity of the Manning's n values used. The modeled water surface elevation was slightly lower than observed for 76% of the test points. Of these, the median deviation was 0.046 m. For those 24% of points whose predicted water surface elevation was higher than the observed value, the median deviation was only 0.023 m. Among all points, half were within 0.04 m and 90% within 0.11 m. Given water depths ranged from 0–2.6 m and an observational measurement error at control point checks of 0.011 m, the deviation between model predictions and observations was considered acceptable.

The second validation test was an assessment of E values between model predictions and field-based estimates. The resulting mean (0.057 m^2 s^{-1}) and range (0.034–0.075 m^2 s^{-1}) of model E values were higher than the field-based estimates (0.023 and 0.001–0.043 m^2 s^{-1}), but proved low enough to yield recirculating eddies in the model behind boulders and bedrock outcrops. The difference in modeled and measured values of E introduces extra momentum transfer and decreases velocity gradients in model results, as reported in a comparison of two and three-dimensional models by MacWilliams et al. (2006).

The third validation test was an assessment of the accuracy of depth and velocity predictions at points and across the three cross-sections. Hydraulic conditions at all of the points (n=83) along three cross-sections showed reasonable matching of predicted versus observed depths and velocities, typical of two-dimensional models (Fig. 6). First, consider only the raw observations and model predictions. An overall comparison of raw observed versus predicted values among all 83 points found a coefficient of determination of 0.929 for depth and 0.768 for velocity (P<0.001 for both tests). The average absolute deviation between raw observed and predicted depth was 10%, which is consistent with the deviations in water surface elevations reported above. Excluding one anomalously low measured value at the 80 m mark of cross-section 1 (Fig. 6), the average absolute deviation between raw observed and predicted velocity was 22%, which is typical given the variability inherent in stream measurements. The maximum error observed between an individual raw observation and corresponding model-predicted value was 66% for depth and 213% for velocity, highlighting the importance of sub-grid scale spatial fluctuations to field measurements.

Since the scale of an adult spawner and a redd is at the grid-scale or larger, it is valuable to filter out spatial measurement "noise" (i.e., sub-grid scale fluctuations) and see how the model performed in matching grid-resolvable cross-channel trends in depth and velocity compared to the smoothed observational trends. For cross-section 1, both depth and velocity predictions closely match the smoothed best-fit curve of the observed data. Depth and velocity values at cross-section 2 show more lateral variation than at cross-section 1, with the predicted pattern following the observed pattern, but not matching it as tightly (e.g., deviation of 0–40% for velocity). At cross-section 3, the model under-predicted depth in the north half of the channel and over-predicted it in the south while generally over-predicting velocity, but the spatial patterns matched closely. No statistically significant correlation existed between the magnitudes of depth and velocity errors across all data, indicating that the high-resolution DEM was very high quality and not responsible for the resulting errors, as previously reported for such models (Pasternack et al., 2004, 2006). Similarly, since depth is not consistently over or under-predicted across the section, uncertainty in Manning's n cannot be responsible. Based on a comparison study of one, two, and three-dimensional models of a different gravel-bed river (MacWilliams et al., 2006), the most likely explanation is that eddy viscosity is not varying enough spatially, causing too much momentum transfer across the channel and thus smoothing the velocity field. Further decreasing E_0 to enhance spatial variability in eddy viscosity causes model instability, so this ultimately is the limiting factor in the accuracy of two-dimensional models. Overall, the two-dimensional Yuba model using realistic parameters provided good depth and velocity prediction and performance comparable to or better than the accuracies reported for other two-dimensional modeling studies (e.g., Lane et al., 1999; Rathburn and Wohl, 2003; Gard, 2006; Pasternack et al., 2006; Elkins et al., 2007; Brown and Pasternack, in press).

4.3. Model output and hydraulics of morphological units

Model predictions of the spatial distribution and magnitude of depth, mean column velocity, and Froude number are provided in Fig. 7A–C, respectively; summaries of hydraulic output by morphological unit type are given in Table 2. Although hydraulic conditions were highly variable across the entire site, broad flow patterns reflected underlying channel topography. A general sequence of flow divergence–convergence–divergence–convergence is observed in a downstream direction through the site, the pattern reflecting variations in channel cross-sectional area described in Section 4.1. Flow accelerated and shallowed between the upstream limit of the site and the topographic high of the riffle crest. Further convective acceleration occurred through the relatively steep riffle 1 unit, accentuated by the lateral constriction of the channel in this region and resulting in the highest velocities throughout the site for the modelled flow (mean column velocity = 3.1 m s^{-1}).

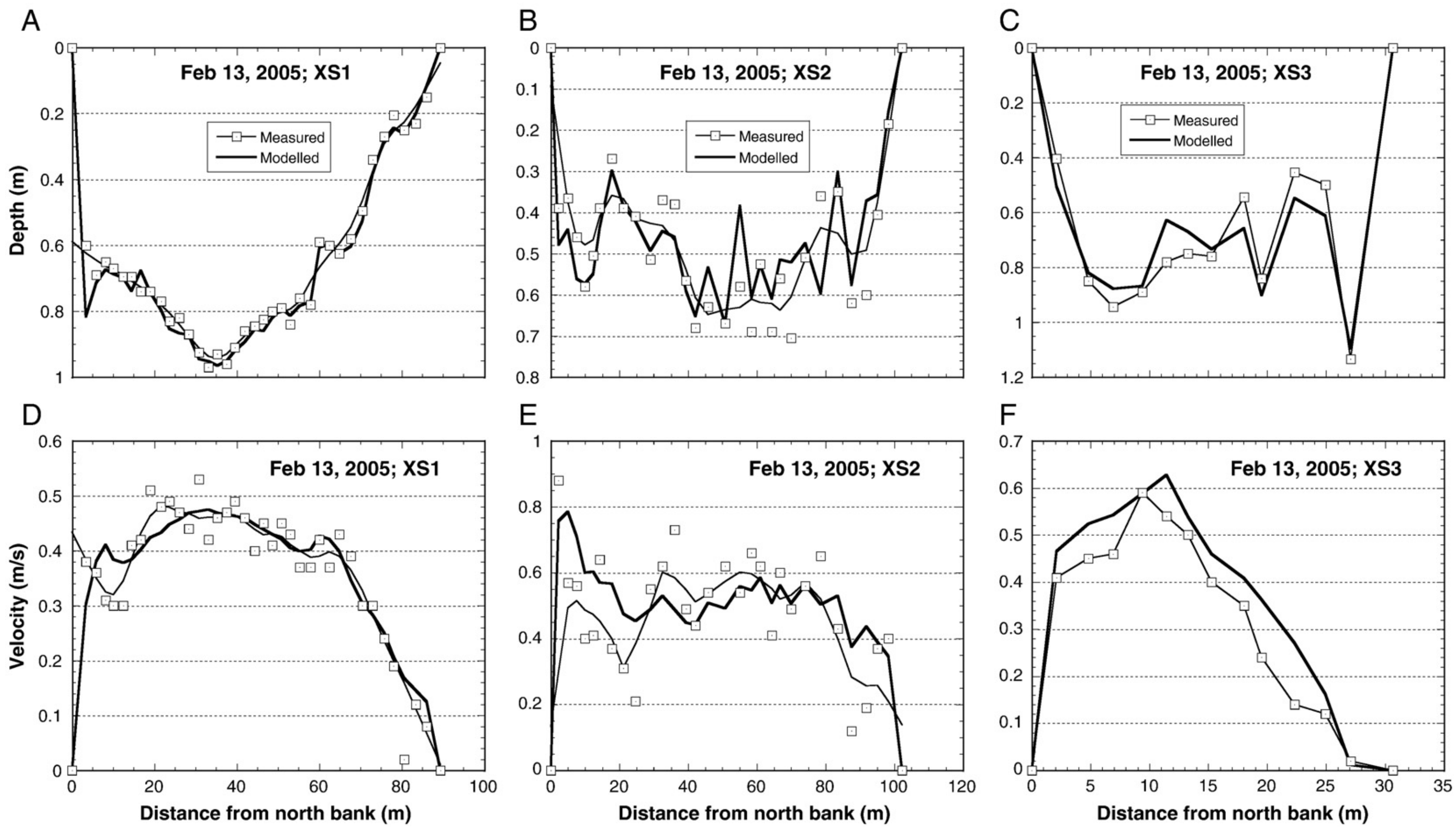

Fig. 6. Comparisons of observed versus predicted (A) depths and (B) velocities at three representative cross-sections. Field observations were fit with a curve using the locally weighted least squared error method to reduce measurement noise.

Downstream of the location where the mainstem and secondary channels rejoin the flow again shallowed and subsequently deepened (with mutual increases and decreases in velocity) as it passed the topographic high associated with the lateral bar unit, the feature also forcing the thalweg towards the south bank.

4.3.1. Froude number characteristics of morphological units

The Froude number distributions of the morphological units show a wide range, with median values varying from 0.001 in the backwater to 0.63 in riffle 1 (Fig. 8; Table 2). Table 2 also shows that specific units exhibited a wide range in Froude number (e.g., riffles 1,2 and 3 had a 5th to 95th percentile Fr range, Fr_{5-95}, of 0.73, 0.82 and 1.08, respectively, with a mean of 0.88) while others of a similar geographical area had small ranges (e.g., the pool unit had $Fr_{5-95}=0.06$). Similar morphological units had similar Fr characteristics. The three riffle and two riffle entrance units had similar within-type Fr_{50} values and 25th to 75th percentile ranges (Fig. 8, Table 2).

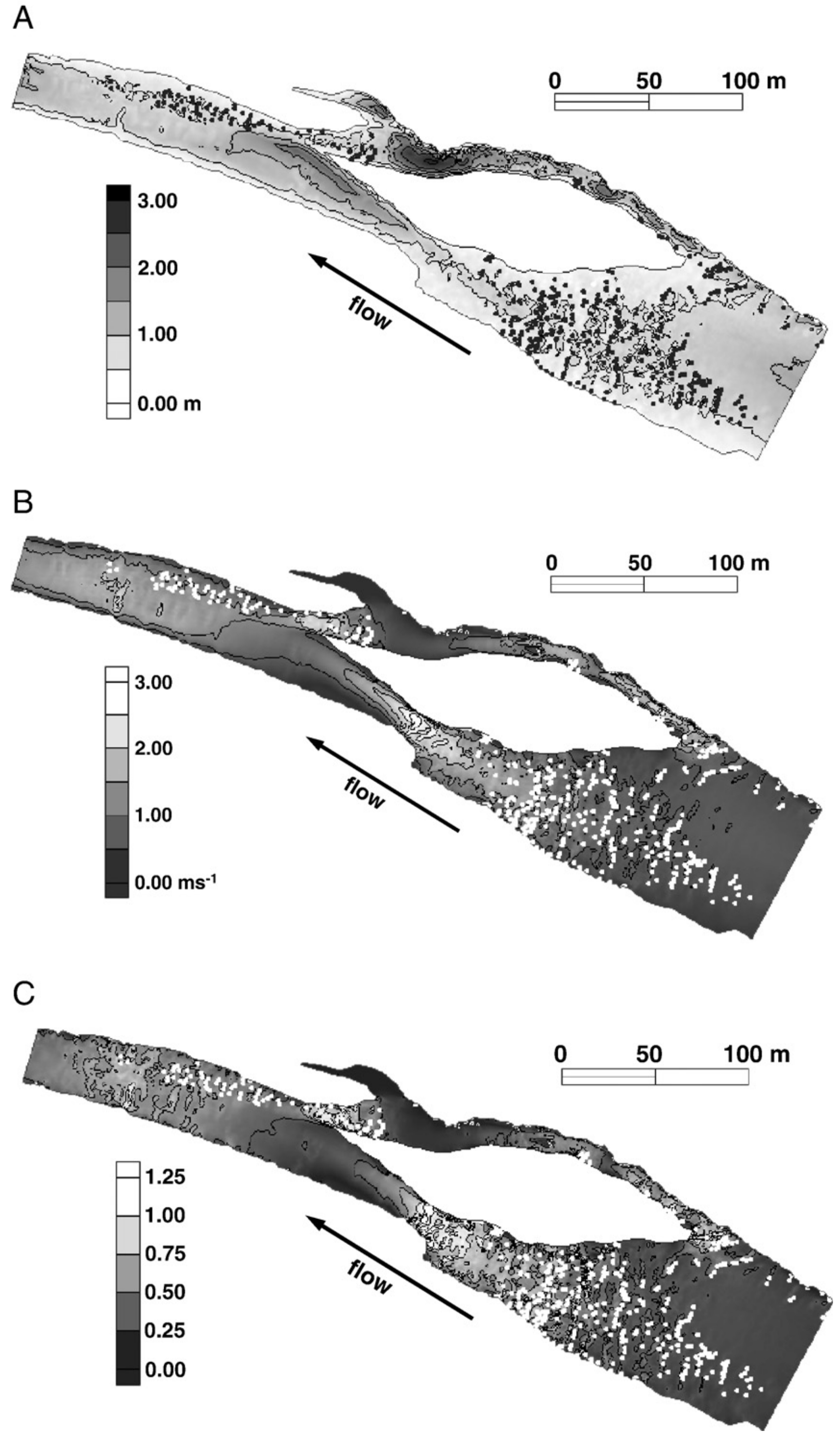

Fig. 7. Model output at the representative spawning period flow (23.4 m^3 s^{-1}): (A) depth, (B) mean column velocity, (C) Froude number. Solid circles indicate the location of surveyed redds.

However, riffle entrances 1 and 2 versus chute and lateral bar versus run units display little difference in Fr_{50} and 25th to 75th percentile ranges despite having contrasting morphological classifications.

The results of the K–S test comparing the Froude number distributions of all the pairing combinations of morphological units are given in Table 3. The unit pairs that were most hydraulically similar and different to one another (defined by the 10th and 90th percentiles of the distribution of the K–S statistic values, respectively), are highlighted in Table 3 by bold and italic text, respectively. These data correspond with that presented graphically in Fig. 8; (i) units with the same morphological classification (i.e., the three riffle units and the two riffle head units) had similar Froude number characteristics, (ii) certain differently classified units (e.g., riffle entrance 1 and chute, run and lateral bar) appear hydraulically similar in terms of Froude number, and (iii) pool and forced pool units are consistently the most hydraulically different to other morphologies (including each other).

4.3.2. Depth–velocity hydraulic domain characteristics of morphological units

Fig. 9A–C summarizes the hydraulic domain of the morphological units, plotting the results of the KDA. The plots represent the regions of the hydraulic domain that can be probabilistically assigned to a specific morphological unit class. To aid visualization, the plots are divided into: a) averaged "preferred" versus "avoided" hydraulic domains (as defined by the MUSI statistic, Table 2), b) individual "preferred" morphological units, and c) individual "avoided" morphological units. In order to highlight the contrasting hydraulics between units exhibiting different utilization regimes by spawning salmon, the plots do not incorporate "tolerated" morphological units (i.e., pool and secondary channel units, Section 4.5). There is a very clear delineation between "preferred" and "avoided" morphological units; "preferred" units occupy a wide velocity range but relatively low depths while the opposite is the case for "avoided" units. In terms of the within-unit spread, riffles (collectively) and forced pool units are most heterogeneous (i.e., they cover a larger area of the depth–velocity space). In contrast, riffle entrance units (which combined accounted for the largest geographical area at the site, Table 2) extended over a relatively limited depth–velocity space; i.e., they exhibited relatively homogeneous hydraulic characteristics. It is also apparent that certain units exhibited discontinuous distributions across the depth–velocity space (e.g., lateral bar, Fig. 9B; run, Fig. 9C). The relative proximity of the hydraulic domains of different units generally agrees well with the K–S statistic used to indicate similarity in Froude number characteristics (Table 3). However, the two-dimensional nature of the plot allows the units that appear hydraulically similar in terms of Froude number characteristics (e.g., lateral bar and run, chute and riffle entrances, Fig. 8) to plot in discrete locations. Moreover, units that have the same morphological classification (i.e., riffles 1–3 and riffle entrances 1 and 2) remain within similar locations of the hydraulic domain.

The results of the KDA are also summarized in Table 4. In each case, the unit with the highest proportion of predicted points corresponds to the actual unit those points occur within (i.e., the morphological unit they were assigned to from the spatial unit classification, Fig. 2). Also, in five out of the ten types, the unit

Table 2
Summary of hydraulic, sedimentary and spawning data by morphological unit type

Descriptor	Backwater	Recirculation zone	Chute	Lateral bar	Pool	Riffle 1	Riffle 2	Riffle 3	Riffle entrance 1	Riffle entrance 2	Run	Forced pool	Secondary channel
H_{50} (m)	0.48	0.73	1.18	0.39	0.75	0.42	0.42	0.41	0.57	0.44	0.69	1.46	0.79
H_{5-95} (m)	1.40	1.04	1.42	0.55	0.40	0.58	0.77	0.95	0.69	0.56	0.87	2.10	1.36
U_{50} (m s^{-1})	0.002	0.44	0.73	0.85	0.45	1.19	1.06	1.32	0.53	0.46	1.13	0.29	0.86
U_{5-95} (m s^{-1})	0.10	0.81	1.14	1.02	0.12	1.35	1.67	1.58	0.81	0.85	1.15	0.50	1.54
Fr_{50}	0.001	0.17	0.21	0.43	0.16	0.63	0.53	0.56	0.22	0.22	0.43	0.08	0.33
Fr_{5-95}	0.05	0.29	0.32	0.41	0.06	0.73	0.82	1.08	0.41	0.53	0.37	0.13	0.63
Avail. area (m^2)	374	1542	1072	1557	3215	529	3537	195	395	6981	3114	797	1335
% avail. area	1.5	9.3	4.0	5.8	12.8	2.1	14.1	0.8	1.6	27.9	12.7	3.3	5.5
Redds (n)	0	0	0	46	31	14	94	7	19	209	0	0	14
% redds	0	0	0	10.6	7.1	3.2	21.7	1.6	4.4	48.2	0	0	3.2
Redds/m^2	0	0	0	0.032	0.010	0.027	0.027	0.037	0.049	0.030	0	0	0.011
MUSI	−1	−1	−1	0.28	−0.26	0.23	0.23	0.37	0.29	0.49	−1	−1	−0.28
Sediment class	Gravel/cobble	Cobble/sand	Boulder/cobble	Gravel/cobble	Gravel/cobble	Gravel/cobble–boulder/cobble	Gravel/cobble–cobble/gravel	Gravel/cobble–cobble/gravel	Gravel/cobble	Gravel/cobble	Cobble/boulder	Gravel/cobble	Cobble/gravel/boulder
Pebble counts (n)	9	6	0	7	0	0	0	0	6	3	10	0	0
d_{50} (mm) mean, range	64.2, 59.7–71.5	74.1, 59.3–92.2	n/a	66.2, 57.3–74.0	n/a	n/a	n/a	n/a	60.9, 53.4–68.1	43.0, 32.2–52.7	83.2, 72.5–97.7	n/a	n/a
d_{90} (mm) mean, range	117.9, 90.6–157.6	178.7, 139.1–212.3	n/a	120.8, 91.8–157.6	n/a	n/a	n/a	n/a	102.9, 88.0–113.0	106.0, 63.1–152.2	165.4, 144.0–199.5	n/a	n/a

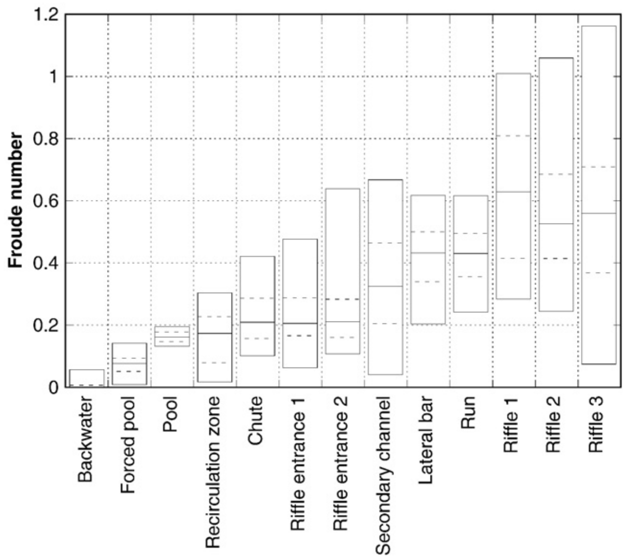

Fig. 8. Percentile plots of model-derived Froude number distributions for individual morphological units. The central line within the box represents the median value of the distribution, the top and bottom of the box are the 5th and 95th percentiles, respectively. Internal dashed lines are the upper and lower quartiles (i.e., 25th and 75th percentiles).

with the second highest proportion of predicted points was adjacent to the actual unit in terms of their geographical distributions (Fig. 2). Although 60.4% of its points were correctly classified, the secondary channel accounts for a substantial proportion of the error in classification in other units (e.g., 27.9% in the recirculation zone). When data from this unit was taken out of the analysis, the proportion of correctly predicted points increased in all units (the mean prediction across all units improved from 57.8% to 67.1%).

4.4. Sedimentary character of morphological units

The qualitative assessment of sedimentary characteristics across the study site showed that the majority of morphological units (9 out of 13) had gravel as the dominant size class (Table 2). The recirculation zone, chute, run and secondary channel had coarser dominant size classes (boulder for chute, the remainder cobble).

As discussed in Section 3.1.4, pebble counts were not carried out at all morphological units due to unwadeable conditions (i.e., too deep and/or fast flowing water). However, the units for which data was obtained show agreement between the qualitative and quantitative assessments; the average d_{50} and d_{90} values of units classified as gravel-dominated (i.e., backwater, lateral bar, and riffle entrances 1 and 2) is 61.3 and 114.6 mm, respectively, compared to 79.8 and 170.4 mm, respectively, for cobble-dominated units (i.e., recirculation zone, run). Of the gravel-dominated units, only the backwater was not 'preferred' (i.e., MUSI > 0) by spawning fish.

4.5. Morphological units and Chinook salmon spawning activity

The locations of redds surveyed in the 2004 season indicate that spawning was concentrated at predictable points (Fig. 7A–C). Spawning tended to occur in locations exhibiting relatively low depth (Fig. 7A), moderate velocity (Fig. 7B) and low to moderate Froude number (Fig. 7C). However, there were also locations meeting these general hydraulic criteria that were not utilized by fish due to unsuitable substrate sizes in those locations (e.g., cobble-dominated material at the channel margin adjacent to the south bank, downstream of the island).

In terms of morphological units, spawning was concentrated at lateral bar, riffle, and riffle entrance locations with sporadic incidents also located in the secondary channel and pool. Raw spawning frequency data reveal that riffle entrance units were the most utilized followed by riffle, lateral bar, pool, and then secondary channel (Table 2). This pattern remained much the same when spawning in morphological units was standardized by area. Only six morphological units had MUSI values > 0 (i.e., "preferred"), these being riffle entrances 1 and 2, riffles 1–3, and the lateral bar. Pool and secondary channel units had MUSI values between −1 and 0 (i.e., "tolerated") while backwater, recirculation zone, chute, run, and forced pool units had no observed spawning/redds and therefore MUSI values of −1 (i.e., "avoided").

The riffle entrance, lateral bar, and riffle units that were preferred by spawners were relatively variable in terms of Froude

Table 3
Results of Kolmogorov–Smirnov test comparing Froude number distribution data for each combination of morphological unit pairs

Unit type	Recirculation zone	Chute	Lateral bar	Pool	Riffle 1	Riffle 2	Riffle 3	Riffle entrance 1	Riffle entrance 2	Run	Forced pool	Secondary channel
Backwater	17.91	24.26	24.68	26.74	22.30	26.98	20.51	21.94	27.10	26.75	**5.29**	24.53
Recirculation zone		8.02	11.34	24.66	9.20	12.92	8.03	**6.02**	10.38	13.90	20.16	20.86
Chute			12.40	24.24	10.89	15.84	8.98	**1.70**	**2.61**	15.16	30.94	14.44
Lateral bar				*36.41*	6.66	**5.25**	6.91	8.63	13.40	**2.01**	30.70	12.45
Pool					29.78	*47.61*	27.65	20.64	*34.60*	*45.30*	*37.53*	*38.85*
Riffle 1						**6.15**	**4.72**	10.06	11.15	7.94	24.60	16.75
Riffle 2							**3.07**	13.47	19.74	8.50	*39.68*	24.20
Riffle 3								8.34	10.85	8.21	22.07	13.85
Riffle entrance 1									**3.58**	12.98	25.29	11.28
Riffle entrance 2										18.28	*42.69*	20.49
Run											*38.08*	19.43
Forced pool												*41.32*

Entries are the Kolmogorov–Smirnov test statistic (XD); those in bold are less than the 90th percentile of XD values (i.e., most similar Froude number distributions), entries in italics are greater than the 10th percentile of XD values (i.e., least similar Froude number distributions).

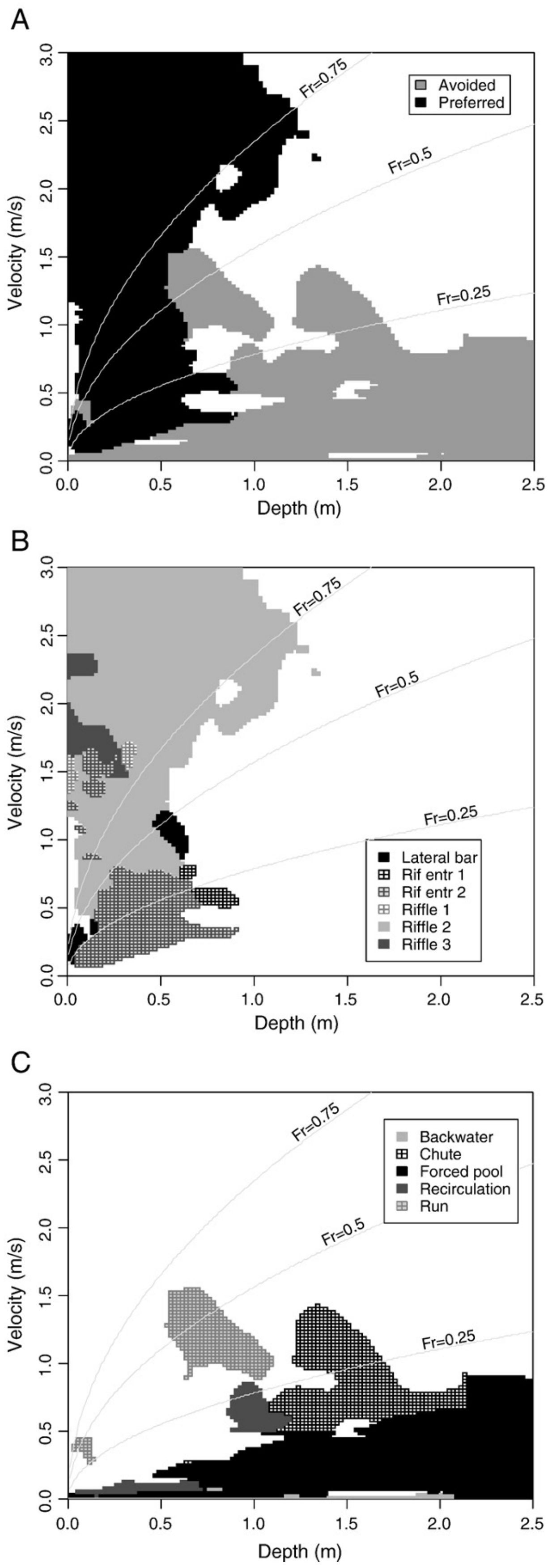

number characteristics (Figs. 7C, 8 and 9B, Table 2); Fr_{50} values range from 0.22 (riffle entrance 1) to 0.63 (riffle 1) and Fr_{5-95} values from 0.41 (lateral bar) to 1.08 (riffle 3). Velocity characteristics (Figs. 7B and 9B) also covered a relatively large range (i.e., U_{50}=0.46 m s^{-1} at riffle entrance 2 to 1.32 m s^{-1} at riffle 3), therefore explaining the relatively wide Froude number range. However, in contrast to their divergent Froude numbers and velocities, median depths were all similarly low for the preferred units (Figs. 7A and 9B, Table 2). The only non-preferred morphological unit to also have a median depth <0.6 m is the backwater class. In summary, all units with MUSI>0 exclusively had H_{50}<0.60 m and U_{50}>0.45 m s^{-1}. In correspondence with these findings, median depth showed the strongest relationship with MUSI among all the morphological units (H_{50}: R^2=0.444, P=0.013; U_{50}: R^2=0.192, P=0.134; Fr_{50}: R^2=0.336, P=0.038).

A higher resolution plot of the hydraulic characteristics of the three types of unit 'preferred' by spawning fish (i.e., riffle, riffle entrance, and lateral bar) is shown in Fig. 10. Given the within-unit hydraulic similarity amongst the three riffles and two riffle entrances apparent in Figs. 7–9 and from the K–S statistic (Table 3), the data from each unit type are combined in Fig. 10. Although there is considerable scatter associated with all three units, a general trend of increasing velocity with depth is evident for the riffle and lateral bar classes. However, the riffle entrance unit exhibits the opposite general relationship with a pattern of decreasing velocity with increasing depth.

5. Discussion

Spawning site characteristics and their spatial distributions are controlled by processes operating at multiple scales (Beechie et al., in press). The physical characteristics of river systems are organized in a nested hierarchy, with physical processes operating at larger scales influencing those at successively finer resolutions (Frissell et al., 1986), ultimately controlling the microscale distribution of instream habitats. The micro and mesoscales are therefore both equally critical elements within this hierarchy with different geomorphic and ecological processes being relevant at these resolutions. For instance, microscale factors will dictate the specific location that a fish selects to spawn while the spatial distribution of mesoscale features will control the locations within a reach where such conditions will exist. An important aspect of the present study was nesting microscale hydraulic data within the larger and ecologically significant scale of the morphological unit. Understanding the mechanistic linkages between the hierarchically organized scales within a river system is necessary to fully understand ecological processes at the catchment scale.

This study has also extended the understanding of mesoscale habitat utilization by spawning salmonids to a larger river system

Fig. 9. Plots of results of KDA: (A) preferred (i.e., MUSI>1) and avoided (i.e., MUSI<1) unit groups, (B) individual preferred units, (C) individual avoided units. Individual hydraulic domains (of individual units or unit groups) are determined by comparing each model output data point to every other data point, identifying which morphological unit it was most probabilistically associated with.

Table 4
Summary of the results of the KDA showing the percentages of data points predicted in each unit type compared to the actual unit type they occurred in (based on field and DEM delineation of the morphological units)

Unit type	Backwater (predicted)	Chute (predicted)	Forced pool (predicted)	Lateral bar (predicted)	Pool (predicted)	Recirculation zone (predicted)	Riffle entrance 1 (predicted)	Riffle entrance 2 (predicted)	Riffle 1 (predicted)	Riffle 2 (predicted)	Riffle 3 (predicted)	Run (predicted)	Secondary channel (predicted)
Backwater (actual)	65.8	0.0	2.4	0.0	0.0	1.7	0.0	0.1	0.0	0.0	0.0	0.0	0.1
Chute (actual)	0.9	61.1	2.4	2.0	3.7	8.0	4.8	2.7	0.0	0.6	0.0	3.2	11.5
Forced pool (actual)	20.6	1.7	69.7	0.0	1.7	8.2	4.8	1.6	0.0	0.0	0.0	0.0	0.7
Lateral bar (actual)	0.3	0.0	0.1	36.8	0.0	0.2	1.3	5.0	0.0	9.9	0.0	4.1	0.6
Pool (actual)	0.0	0.0	0.0	0.0	70.4	0.0	0.0	3.0	0.0	0.0	0.0	0.0	0.0
Recirculation zone (actual)	6.7	8.8	6.1	1.7	3.5	39.1	18.1	3.8	0.0	0.5	0.0	0.4	4.2
Riffle entrance 1 (actual)	0.9	0.2	1.3	1.7	3.6	5.0	45.8	5.1	0.0	2.6	0.0	0.1	2.3
Riffle entrance 2 (actual)	1.7	0.0	4.4	3.7	14.0	4.8	2.2	56.9	4.3	12.5	11.9	0.2	0.2
Riffle 1 (actual)	0.0	0.0	0.0	4.7	0.0	0.0	1.3	0.8	26.1	9.2	21.4	2.1	1.6
Riffle 2 (actual;)	0.3	0.0	0.2	18.0	0.2	1.9	4.0	6.9	30.4	39.9	26.2	8.2	8.1
Riffle 3 (actual)	0.3	0.7	0.1	1.7	0.1	2.6	0.0	1.7	17.4	5.4	35.7	2.5	4.0
Run (actual)	0.3	0.0	0.1	18.0	0.0	0.6	1.3	3.9	4.3	6.8	0.0	57.8	6.1
Secondary channel (actual)	2.3	27.5	13.4	11.6	2.7	27.9	16.3	8.5	17.4	12.6	4.8	21.4	60.4

Cells highlighted grey compare like with like morphological units.

than has typically previously been examined. The application of two-dimensional hydrodynamic modeling enabled a high-resolution quantification of the hydraulic characteristics of the different units present at the spatial scale experienced by fish. Most studies that have attempted to assess the hydraulic characteristics of channel units at the mesoscale have been conducted at a relatively low spatial resolution (e.g., Jowett, 1993; Padmore et al., 1998; Emery et al., 2003). In order that mesoscale physical–biotic linkages can be properly assessed, the resolution of hydraulic information needs to more closely represent that which instream species experience (i.e., <1 m).

5.1. Site-scale distribution of morphological units and interactions with general flow patterns

The study site exhibited a highly heterogeneous channel topography, exemplified by the identification of ten discrete morphological unit types within a section ~8 channel widths in length. The longitudinal and lateral sequences of morphological units across the site provided a wide range of hydraulic and sedimentary conditions. Although heterogeneous across the entire site, hydraulic conditions were well ordered by the underlying topography at the modeled immobile bed low flow. Spatial variation in relative bed elevation and channel width as a consequence of the diverse morphology controlled the mutual adjustment of depth and velocity and was responsible for strong patterns of nonuniform flow (e.g., convergence, divergence, and recirculation). These morphology–flow interactions have important implications for the direct provision of suitable microscale hydraulic conditions and for providing sedimentary characteristics within the mesoscale units that support Chinook salmon spawning, discussed in Sections 5.3.

5.2. Hydraulic characteristics of morphological units

There were considerable differences in hydraulic characteristics between morphological unit types. In most cases the Froude number alone is an adequate hydraulic descriptor to differentiate and group morphological unit types. Indeed, the median and 25th–75th percentile range of Froude number of riffles 1, 2, and 3 are similar despite their very different physical dimensions (e.g., riffle 2 is ~3 times wider and transmits ~2.5 times the discharge under modeled conditions than riffle 1). These data suggest that the dimensionless character of the Froude number may permit the quantitative and generic differentiation between and grouping within certain morphological units types across a range of channel magnitudes or stream orders. A number of other studies have demonstrated that the Froude number is the single best hydraulic parameter to differentiate between morphological units/biotopes (e.g., Jowett, 1993; Rowntree and Wadeson, 1996; Padmore et al., 1998). However, certain units exhibiting contrasting morphologies had very similar Froude number characteristics. Whereas the lateral bar and run units could be argued as being part of the same overall unit (the lateral bar being a subunit of the run located at the channel margins), the chute and riffle entrance units are clearly morphologically and spatially discrete. The

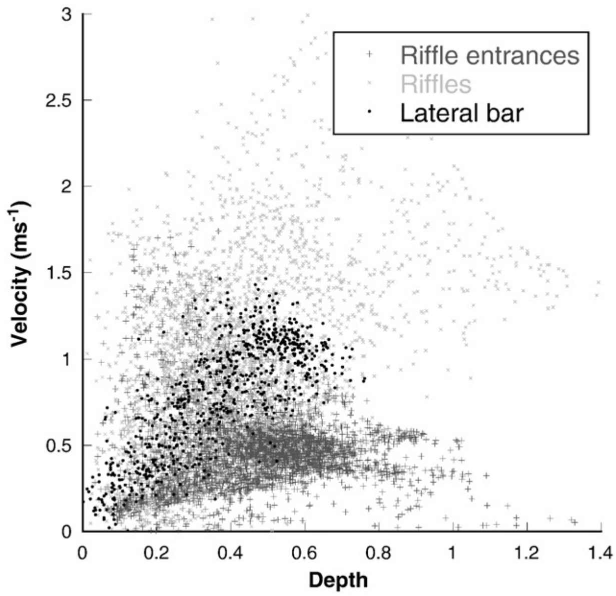

Fig. 10. High-resolution depth–velocity scatter plot for the 'preferred' (i.e., MUSI > 1) spawning units (i.e., riffles, riffle entrances, and lateral bar).

chute unit, although having very similar Froude number characteristics, was associated with much deeper flow (and therefore faster mean column velocities) and coarser sediments (from visual assessment) than the riffle entrance units. Therefore, while the dimensionless character of the Froude number may aid in grouping like units in channels of differing magnitude, it also meant that some locations that were very different in terms of geomorphic context and absolute hydraulic characteristics had very similar Froude number values. Moreover, since the sample sizes for each morphological unit are large (ranging between 280 and 3320 data points per unit with a mean of 1,179) the Froude number distributions of all pairings were significantly different (K–S test at $P<0.01$). However, although statistically significant, small differences in the Froude number characteristics between certain units are unlikely to be geomorphically or ecologically significant. For example, the chute and the riffle entrance units are statistically different ($P=0.0084$) but had Fr_{50} values of 0.21 and 0.22, respectively. Therefore, statistical testing with a recognized confidence level was not able to discriminate between Froude number attributes of morphological units. Rather, the 10th and 90th percentiles of the K–S statistic values of test pairings were more useful in identifying the most similar and different morphological units in terms of Froude number. These results showed that, although units with the same classification (i.e., riffles and riffle entrances) were relatively similar to one another, certain unit types that had clearly different physical characters (e.g., chute and riffle entrances) could not be differentiated (i.e., they had relatively low K–S statistic values).

The bivariate plot of the simplified depth–velocity "hydraulic domain" of the "preferred" and "avoided" morphological units (Fig. 9A–C) provided a more detailed insight of the hydraulic functioning at the site. Although not depicting the entire hydraulic scatter across the site, plotting the data in this way offered a compromise between high data resolution and a simplified pattern that aided in identifying the general hydraulic similarities and differences between morphological units exhibiting contrasting levels of spawning utilization. All of the morphological unit types that were identified at the initial survey of the site (and subsequently determined to be "preferred" or "avoided" by spawning Chinook) appeared justified as they were each associated with unique "most probable" locations within the depth–velocity space from the KDA (although, to aid visualization, pool and secondary channel units were not included in the plots). In reality there was considerable overlap in the depth–velocity scatter between morphological units but centers of the distributions were generally discretely located (as identified from the median hydraulic statistics in Table 2). The KDA defined sharp boundaries between morphological units since the procedure predicts the most probable single unit type throughout the available depth–velocity space. This produced discontinuous depth–velocity distributions for certain morphological units; where units overlapped in the depth–velocity space, the unit with the highest density of points in that region was classified as the most probable. In a number of cases (e.g., lateral bar, recirculation zone), this divided a unit type into different regions of the plot. Different morphological units tended to plot in discrete Froude number zones, with riffles being highest and backwater and forced pool lowest (Figs. 8 and 9). However, the depth–velocity plot distinguished between morphological units within the same Froude number zone; riffle entrance, chute, run, and lateral bar units all plotted in discrete locations within the depth–velocity space. Therefore, by plotting hydraulic characteristics on two axes there is a greater ability to differentiate between morphological units.

The KDA results (Fig. 9A–C, Table 4) provided quantitative validation of the morphological unit classifications; in all cases the unit class with the highest proportion of predicted hydraulic data corresponded with the actual unit type as initially identified in the field. However, a large proportion of data points within each unit were misclassified (mean = 42.2% including the secondary channel, 32.9% excluding the secondary channel), representing considerable overlap in the depth–velocity scatter between unit types. This is an inevitable situation given that there is a continuum of hydraulics at the site; defining sharp boundaries between morphological units, although necessary for delineation, is at odds with the natural "fuzzy" transition between units. The fact that the KDA results show that the unit type with the second highest proportion of prediction was more likely to be geographically adjacent to the actual unit served to reiterate the influence of "fuzzy" hydraulic boundaries in the segregation of the data.

5.3. Relationships between spawning activity and morphological units

The results of this study demonstrate that Chinook salmon spawning activity was clustered at the mesoscale of specific morphological units. Riffle, riffle entrance, and lateral bar units were found to be "preferred", whereas backwater, recirculation zone, chute, run, and forced pool units were entirely avoided. Although there are inconsistencies in the definition of morphological units between studies, this finding corresponded with observations made by previous researchers (Geist and Dauble, 1998; Groves and Chandler, 2002; Moir et al., 2002; Hanrahan, 2007). Groves and Chandler (2002) found that most fall Chinook spawning in the Snake River, Idaho occurred in riffles, although this may also incorporate what is defined as riffle entrance in the present study. In the same river system, Hanrahan (2007) found that the upstream and downstream sides of riffles crests (corresponding to riffle entrance and riffle units, respectively, as defined in the present study) accounted for 31% and 53% of Chinook salmon redds, respectively. In the present study, the combined proportion of redds in the equivalent units was similar (79.1%), although individually the fractions were almost exactly reversed (52.6% for riffle entrance and 26.5% for riffle). Some of this difference is likely related to contrasting definitions of morphological units. For instance, Hanrahan (2007) states that 10% of redds occurred in the "downstream end of pools", a region that would likely be incorporated within the riffle entrance in the present study. However, the larger proportion of redds in riffle units reported by Hanrahan (2007) cannot be explained in this way and must be related to other factors (e.g., differing geomorphic controls producing contrasting hydraulic and sedimentary characteristics within riffles; differences in size structure of fish populations, influencing habitat suitability requirements).

In terms of broader scale geomorphic considerations, the highest frequency of spawning utilization at the riffle entrance unit was likely related to the topographic high of the bar/island structure that controls the location of the main riffle crest. The persistence of a riffle at this location is apparent from a sequence of 14 aerial photographs of the study site between 1937 and 2006. Although this topic is the focus of other investigations currently underway, it appears that a valley constriction immediately downstream of the riffle yields a backwater effect during floods that decreases the velocity at the riffle-island location by ~30% when discharge is approximately double bankfull. During low flow, the bar/island feature acts as the hydraulic control for a region of relatively low bed slope, rectangular channel shape and little cross-sectional topographic variation upstream, producing moderate depths and velocities across the entire width of the channel in this area (Stewardson and McMahon, 2002). These hydraulic conditions provide spawning habitat through the direct provision of suitable depth and velocity combinations and by promoting the maintenance of appropriately sized sediments under all but morphology resetting flows.

Although mesoscale Froude number characteristics tend to differentiate between individual morphological unit types and group those given the same classification, they do not discriminate well between those exhibiting contrasting degrees of spawning utilization. The Froude number characteristics of the morphological units "preferred" by spawners covered a relatively wide range. Only at $Fr_{50}<0.2$ do "preferred" morphological units not occur, although the pool unit is "tolerated" ($Fr_{50}=0.16$, MUSI $=-0.27$). Furthermore, there was only a marginally significant relationship between median Froude number and the MUSI value of morphological units ($R^2=0.336$, $P=0.038$). Although salmonid spawning habitat has been shown to be associated with specific Froude number characteristics (Moir et al., 2002), the assessment of this variable at the mesoscale will incorporate locations within a morphological unit that are not suitable (i.e., not all locations within a specific morphological unit will have suitable microhabitat conditions despite that unit being utilized by spawners), thereby reducing the level of explanation. At this spatial resolution, median depth was most closely linked to spawning preference of morphological units by spawning fish ($R^2=0.444$, $P=0.013$ with $R^2=0.192$ and $P=0.134$ for median velocity) and the possible reasons for this are discussed below. The depth–velocity hydraulic domain plot (Fig. 9A–C) better discriminates between morphological units exhibiting different proportional rates of utilization. The bivariate character of the plot allows for the hydraulic differentiation of units that have similar Froude number characteristics but contrasting relative spawning frequencies (i.e., lateral bar and run, riffle entrance, and chute).

The observation that the morphological units associated with the highest relative spawning frequencies occur exclusively in the lower depth region of the hydraulic domain cannot be explained simply in terms of the provision of suitable microscale hydraulic conditions. Although median depths differ between units exhibiting varying rates of relative utilization (i.e., MUSI), there is still sufficient intersection in the depth–velocity space to provide suitable spawning conditions in preferred, tolerated, and certain avoided units (i.e., run and recirculation zone). Two different concepts are proposed to explain the segregation of the "preferred" morphological units to the lower depth region of the hydraulic domain. First, two of the preferred unit types (riffle and riffle entrance) were observed to be hydraulically constricted (both laterally and vertically), and this may provide desirable surface and subsurface hydraulics not captured in the model but recognized and preferred by spawners. Such constrictions provide not only higher surface flow velocities but also stronger velocity gradients. Such gradients may enable spawners to swim over to low-velocity resting habitat quicker and with less effort and have been shown to be especially important in locations lacking cover (Abbe et al., 2002). Previous studies have also reported that flow constrictions force well-oxygenated water into the bed, providing high quality hyporheic conditions for embryo survival that spawners may instinctually recognize (Couloumbe-Pontbriand and Lapointe, 2004). However, no morphological constriction was apparent at the lateral bar unit (also preferred by spawning Chinook) and flow convergence was not as apparent. It is therefore unclear from the results of the present study whether nonuniform flow characteristics are explicitly a condition that spawning Chinook actively select. Nevertheless, the results show that nonuniform flow characteristics as dictated by a heterogeneous channel morphology are important at the mesoscale and the nature of these interactions affect the spatial distribution of suitable microhabitat conditions for spawning Chinook salmon. This distinction between preferred units based on presence/absence of significant nonuniform flow conditions may suggest two discrete types of spawning habitat that are associated with contrasting hydraulic pattern.

Second, characteristic geomorphic conditions (i.e., shear stress/channel competence/transport capacity) at the preferred morphological units promote the maintenance of suitable spawning sediment, a factor not directly accounted for in the hydraulic analysis. Although limited in extent and detail, the sedimentary data in the present study indicate that spawning Chinook select relatively small substrate sizes within the study site (Table 2). This in itself is not a novel finding; it is widely accepted that spawning salmonids select specific substrate sizes (Crisp and Carling, 1989; Kondolf and Wolman, 1993; Moir et al., 2002). Sedimentary factors appear to explain why certain units that provided suitable hydraulic conditions were not utilized by spawning Chinook. The most notable example was the run unit where near ideal combinations of depth and velocity were provided near the channel margins adjacent to the south bank and downstream of the island (Fig. 7). In this location substrate was too coarse for spawning, with cobble-sized material being the dominant size class. The 10 pebble counts conducted within the run unit had mean d_{50} and d_{90} values of 79.8 mm (range = 72.5–97.7 mm) and 165.4 mm (range = 144.0–199.5 mm), respectively, coarser than that quoted as suitable for spawning Chinook salmon (Kondolf and Wolman, 1993). The pertinent question in relation to the present study is therefore not whether spawning Chinook were selecting a certain caliber of sediment (which they clearly did) but, rather, why specific morphological units supported a suitable sedimentary character while others did not?

Large magnitude flood events (i.e., $Q \gg Q_{\text{bankfull}}$) re-set channel morphology and the spatial pattern of sediments, which, in conjunction with river flow, dictate the spatial and temporal distribution of subsequent geomorphic forces. Over time, the mutual adjustment of these factors will result in a quasi-equilibrium state being achieved, with sediments at the site being hydraulically sorted until the next major channel morphology resetting event occurs. The survey of the study site was carried out between April 2004 and April 2005, with the previous large magnitude event (~3800 m^3 s^{-1}, ~42-yr return interval) occurring on January 1, 1997. Based on aerial photos, a 1999 topographic map from the U.S. Army Corps of Engineers, and field observations, sediments and site morphology appear to have been well adjusted to "normal" geomorphic forces at the time of the study. The only notable site changes 1999 to 2004 were bank erosion on the south side of the island adjacent to the chute and armoring on the main riffle. Spawning habitat can only occur in locations where suitably sized sediment is maintained (i.e., not transported) at flows down to that which spawning occurs (which, in the case of the study site, are the lowest flows in the annual hydrograph). In a large gravel-bed river like the Yuba, the forces acting on the bed near the channel thalweg (where velocity tends to be greatest within a cross-section) are too great even at low flows to permit the maintenance of the mix of gravel and cobble-sized material required by spawning Chinook salmon (Kondolf and Wolman, 1993); thus, areas promoting the preservation of spawning caliber sediment tend to occur in relatively low depth regions of the study site i.e., at channel margins (e.g., lateral bar) and areas with relatively high width:depth ratio (e.g., riffles and riffle entrances). Patterns of shear stress at spawning flows (as could be estimated from the model output) are unlikely to be closely related to mesoscale sedimentary pattern since these are more closely linked to higher flow conditions that are responsible for resetting channel morphology ($Q > 9 \times Q_{\text{bankfull}}$ as observed at the study site). Not all low depth regions are associated with suitable spawning sediment; some locations (e.g., backwater) are also associated with low velocities that promote the deposition of material too fine for spawning (and may also be hydraulically unsuitable for spawning) and, in others, antecedent conditions have provided too high a proportion of large sized material (e.g., recirculation zone). The sedimentary data presented in Table 2 generally support this hydraulic sorting assertion; morphological units with relatively low median depths tend to be associated with smaller sediment sizes.

The high-resolution output from the two-dimensional model identifies that the morphologically-distinct mesoscale units preferentially utilized for spawning (i.e., lateral bar, riffle, and riffle entrance) have distinct hydraulic characteristics (Fig. 10). The riffle entrance locations exhibit a general pattern of decreasing mean column velocity with increasing depth, characteristic of a rectangular channel shape that has little cross-sectional difference in bed elevation but with longitudinal variation in bed slope (Stewardson and McMahon, 2002). Specifically, a downstream topographic high (the riffle crest) acts as a vertical constriction to the flow reducing the cross-sectional area of the channel. Flow continuity dictates that this is associated with an increase in mean velocity, producing a condition of convective acceleration towards the riffle crest and a general pattern of decreasing depth and increasing velocity. The converse pattern of generally co-varying mean column velocity with depth evident for the lateral bar and riffle units indicate a prismatic channel shape with relatively high cross-sectional variation in bed topography but little along the longitudinal axis. In these locations, in the absence of a downstream topographic high, velocity increased with depth towards the channel thalweg as relative roughness and, therefore, flow resistance diminishes. However, despite a similar general depth–velocity trend, important differences in the hydraulic characteristics of riffle and lateral bar units were apparent. The riffle units encompassed a large spatial area and spanned the entire width of the main and secondary channels, producing a broad range of depth–velocity conditions. Also, the tapered constriction of the riffle units produces a convective acceleration effect with velocity increasing in a downstream direction but without an equivalent reduction in the rate of change of depth (as in the riffle entrance units), adding scatter to the plot. The lateral bar unit covered a smaller spatial area and did not extend to the channel thalweg; the associated hydraulic characteristics were therefore over a more restricted range compared to the riffle units. Also, since this unit is not laterally constricted, there is minimal downstream convective acceleration and less scatter in velocity values for a given depth. Furthermore, due to the generally lower energy slope and larger cross-sectional area in the vicinity of the lateral bar unit, velocity tended to be less for a given depth in lateral bar than riffle units.

There was limited opportunity to test whether hydraulic characteristics were consistent by morphological unit type in the present study due to insufficient replication (for the practical reasons described in Section 3.1.2). Only two unit types had replicates (three riffles and two riffle entrances) and, although these exhibited similar dimensionless hydraulic characteristics (median and range of Froude number; general depth–velocity trends), it is not reasonable to extend this assumption to all unit types. However, since hydraulic patterns are governed by channel geometry and universal river mechanics theory (Stewardson and McMahon, 2002), it is likely that similar types of morphological units as those identified in this study (using the classification described in Section 3.1.2) would at least display the same general trend in joint depth–velocity distribution and approximately equivalent Froude number characteristics, even given differences in stream size. Furthermore, the general character of the unit-specific hydraulic relationships (although not absolute hydraulic parameter values) are likely to be relatively consistent with increasing discharge until a significant channel geometry threshold is breached. This is likely to occur initially at bankfull stage where there is typically an abrupt change in channel cross-sectional shape in alluvial channels as lateral gradient sharply decreases.

Employing an “at-a-station” hydraulic geometry-type approach, Moir et al. (2006) showed that the character of discharge versus depth and velocity relationships were statistically different in mesoscale units of contrasting morphology utilized by spawning Atlantic salmon. Therefore, varying discharge is also likely to be met with contrasting absolute hydraulic responses between different types of preferred morphological units identified in this study. Units that exhibit rapid hydraulic change will show relatively large variation in quantity and/or spatial distribution of habitat availability as flow varies. Other units with more stable hydraulics will provide a more consistent quantity and spatial distribution of suitable habitat over a relatively wide flow range. Webb et al. (2001) demonstrated how individual sites on the Girnock Burn, Scotland were utilized by spawning Atlantic salmon over very specific discharge ranges in three consecutive years (despite contrasting availability of discharge) and speculated that the interaction of discharge with the particular morphology of a site controlled this. These and the findings of the present study suggest that the cumulative effect of a diverse assemblage of morphological units within a section of river will be to provide suitable spawning habitat (and, indeed, habitat for all species and life stages present) over a range of flows; morphological heterogeneity can therefore be regarded as a natural mechanism by which habitat availability can be maintained under a variable discharge regime.

6. Conclusion

The study showed that different morphological units exhibited contrasting characteristics that together provided highly variable conditions across the site for the modeled flow. Despite presumably constant microscale habitat requirements, spawning Chinook salmon preferentially selected specific mesoscale morphological units (lateral bar, riffles, and riffle entrances) that were shown to exhibit opposing depth–velocity relationships (i.e., positive relationship for riffles and lateral bar and negative for riffle entrance) that were controlled by generic nonuniform components of channel geometry. However, all preferred spawning units were shown to display relatively low depth characteristics within that available between all units. In addition to providing appropriate microscale hydraulics, this was thought related to the provision of suitable sedimentary conditions that were hypothesized to be linked to higher flow geomorphic conditions specific to the morphology of these units. Plotting the joint depth–velocity distribution provided the greatest degree of differentiation between unit types although, in most cases, Froude number characteristics alone gave adequate segregation. However, consideration of the joint depth–velocity distribution is essential to capture the specific nature of the relationships between these variables, something the Froude number can only crudely accomplish.

Classic studies by Richards (1976a,b, 1978) demonstrated that riffle and pool units commonly have different channel widths and that variable channel geometry is an implicit condition in gravel-bed rivers. More recent studies have shown that such variations drive nonuniform hydraulics (e.g., convective acceleration, turbulent eddies) that are important to a more complete understanding fluvial and, therefore, ecological processes (Crowder and Diplas, 2006; MacWilliams et al., 2006). The benefits of employing a two-dimensional hydrodynamic modeling approach to resolve mesoscale hydraulics in relation to specific morphological characteristics was demonstrated in this study. The ability of the two-dimensional model to continuously predict hydraulic conditions across the study at the resolution (~1 m) that fish experience them is a clear benefit (Elkins et al., 2007). Also, the resolution of the secondary (lateral) components of stream flow is essential to characterizing convective acceleration, shear zones, and turbulent structures. Such processes play a key role in morphology–flow–sedimentary–hydraulic interactions and are important agents dictating geomorphic character in dynamic gravel-bed systems. Therefore, characterizing these types of channel at the mesoscale using conventional cross-sectional and analytical or pseudo one-dimensional approaches (such as those used in PHABSIM) will fail to capture these nonuniform physical processes that contribute to providing the template for instream habitats.

Restoration of spawning habitat often involves the design of a uniform channel providing suitable microhabitat conditions over a particular range of discharges. This does not explicitly consider morphological complexity, a factor that this study has shown to be closely linked to Chinook salmon spawning habitat and nonuniform geomorphic processes (e.g., convective acceleration) that may be important direct components of habitat and mechanisms for maintaining a quasi-stable channel morphology. This study has shown that a range of unit types promote morphological and hydraulic complexity and it is suggested that this condition provides the template for temporal and spatial habitat dynamics that support suitable microscale conditions for a variety of species and life stages over a range of flows.

Acknowledgements

Financial support for this work was provided by the U.S. Fish and Wildlife Service Anadromous Fish Restoration Program

(Agreement #113323J011). The authors gratefully acknowledge Carlos Alvarado, Blake Andrews, Mary Berta, Mike Bezemek, Evan Buckland, Eve Elkins, Marisa Escobar, Kari Fish, Dave Van Herrick, Lauren Hilliard, Ryan Keating, Cameron Poya, April Sawyer, Carrie Simms, Nakul Thomas, Ben Torchia, Julie Tuck, Conner Voss, and Jason White for their assistance in collection of field data and laboratory analysis.

References

Abbe, T.B., Pess, G.R., Montgomery, D.R., Fetherston, K., 2002. Integrating engineered log jam technology into reach-scale river restoration. In: Montgomery, D.R., Bolton, S., Booth, D.B. (Eds.), Restoration of Puget Sound Rivers. University of Washington Press, Seattle, WA, pp. 443–482.

Acarlar, M.S., Smith, C.R., 1987. A study of hairpin vortices in a laminar boundary layer: Part 1. Hairpin vortices generated by a hemispherical protuberance. Journal of Fluid Mechanics 175, 1–41.

Bates, P.D., Anderson, M.G., Baird, L., Walling, D.E., Simm, D., 1992. Modelling floodplain flow with a two dimensional finite element scheme. Earth Surface Processes and Landforms 17, 575–588.

Bates, P.D., Anderson, M.G., Hervouet, J.M., Hawkes, J.C., 1997. Investigating the behaviour of two-dimensional finite element models of compound channel flow. Earth Surface Processes and Landforms 22 (1), 3–17.

Bates, P.D., Horritt, M.S., Hervouet, J.M., 1998. Investigating two-dimensional, finite element predictions of floodplain inundation using fractal generated topography. Hydrological Processes 12, 1257–1277.

Beechie, T.J., Collins, B.D., Pess, G.R., 2001. Holocene and recent geomorphic processes, land-use and fish habitat in two Puget Sound watersheds. In: Dorava, J.M., Montgomery, D.R., Palcsak, B., Fitzpatrick, F. (Eds.), Geomorphic Processes and River Habitat. American Geophysical Union, Washington D.C., pp. 37–54.

Beechie, T.J., Pess, G., Beamer, E., Lucchetti, G., 2003. Role of watershed assessments in recovery planning for salmon. In: Montgomery, D.R., Bolton, S., Booth, D.B., Wall, L. (Eds.), Restoration of Puget Sound Rivers. University of Washington Press, Seattle, WA, pp. 194–225.

Beechie, T., Moir, H., Pess, G., in press. Hierarchical physical controls on salmonid spawning location and timing. In: DeVries, P., Sear, D. (Eds.), Salmon spawning habitat in rivers: physical controls, biological responses, and approaches to remediation. American Fisheries Society, Bethesda, MD.

Beland, K.F., Jordan, R.M., Meister, A.L., 1982. Water depth and velocity preferences of spawning Atlantic salmon in Maine rivers. North American Journal of Fisheries Management 2, 11–13.

Bovee, K.D., 1986. Development and evaluation of habitat suitability criteria for use in the instream flow incremental methodology. Instream Flow Information Paper 21, U. S. Fish and Wildlife Service Biological Report 86(7), U. S. Fish and Wildlife Service.

Brasington, J., Rumsby, B.T., McVey, R.A., 2000. Monitoring and modelling morphological change in a braided gravel-bed river using high resolution GPS-based survey. Earth Surface Processes and Landforms 25, 973–990.

Brierly, G.J., Fryirs, K., 2000. River styles, a geomorphic approach to catchment characterization: implications for river rehabilitation in Bega catchment, New South Wales, Australia. Environmental Management 25, 661–679.

Brown, L.R., 2000. Fish communities and their associations with environmental variables, lower San Joaquin River drainage, California. Environmental Biology of Fishes 57, 251–269.

Brown, R.A., Pasternack, G.B., in press. Engineered channel controls limiting spawning habitat rehabilitation success on regulated gravel-bed rivers. Geomorphology. doi:10.1016/j.geomorph.2007.09.012.

Buffin-Belanger, T., Roy, A.G., 1998. Effects of a pebble cluster on the turbulent structure of a depth-limited flow in a gravel-bed river. Geomorphology 25, 249–267.

Burner, C.J., 1951. Characteristics of spawning nests of Columbia River salmon. U.S. Fish and Wildlife Service Bulletin 61, 97–110.

Cao, Z., Carling, P., Oakey, R., 2003. Flow reversal over a natural pool-riffle sequence: a computational study. Earth Surface Processes and Landforms 28, 689–705.

Couloumbe-Pontbriand, M.C., Lapointe, M., 2004. Landscape controls on the availability of coarse substrate and winter habitat and their effects on Atlantic salmon (*Salmo salar*) parr abundance patterns along two rivers in the Gaspe Peninsula, Quebec. Canadian Journal of Fisheries and Aquatic Sciences 61, 648–658.

Crisp, D.T., Carling, P.A., 1989. Observations on siting, dimensions and structure of salmonid redds. Journal of Fish Biology 34, 119–134.

Crowder, D.W., Diplas, P., 2002. Vorticity and circulation: Spatial metrics for evaluating flow complexity in stream habitats. Canadian Journal of Fisheries and Aquatic Sciences 59, 633–645.

Crowder, D.W., Diplas, P., 2006. Applying spatial hydraulic principles to quantify stream habitat. Rivers Research and Applications 22, 79–89.

Curtis, J.A., Flint, L.E., Alpers, C.N., Yarnell, S.M., 2005. Conceptual model of sediment processes in the upper Yuba River, Sierra Nevada, CA. Geomorphology 68, 149–166.

Dauble, D.D., Geist, D.R., 2000. Comparisons of mainstem spawning habitats for two populations of fall Chinook salmon in the Columbia River basin. Regulated Rivers 16, 345–361.

Elkins, E.E., Pasternack, G.B., Merz, J.E., 2007. The use of slope creation for rehabilitating incised, regulated, gravel-bed rivers. Water Resources Research 43. doi:10.1029/2006WR005159 W05432.

Emery, J.C., Gurnell, A.M., Clifford, N.J., Petts, G.E., Morrissey, I.P., Soar, P.J., 2003. Classifying the hydraulic performance of riffle-pool bedforms for habitat assessment and river rehabilitation design. River Research and Applications 19, 533–549.

Fischer, H.B., List, E.J., Koh, R.C.Y., Imberger, J., Brooks, N.H., 1979. Mixing in Inland and Coastal Waters. Academic Press, Inc., New York.

Frissell, C.A., Liss, W.J., Warren, C.E., Hurley, M.D., 1986. A hierarchical framework for stream habitat classification: viewing streams in a watershed context. Environmental Management 10, 199–214.

Froehlich, D.C., 1989. Finite Element Surface-Water Modelling Systems: Two-Dimensional Flow in a Horizontal Plane User's Manual. U.S. Department of Transportation, Washington, D.C. Publication #FHWA-RD-88-177.

Fukushima, M., 2001. Salmonid habitat–geomorphology relationships in low gradient streams. Ecology 82, 1238–1246.

Gard, M., 2006. Modeling changes in salmon spawning and rearing habitat associated with river channel restoration. International Journal of River Basin Management 4, 1–11.

Geist, D.R., Dauble, D.D., 1998. Redd site selection and spawning habitat use by fall Chinook salmon: the importance of geomorphic features in large rivers. Environmental Management 22, 655–669.

Grant, G.E., Swanson, F.J., 1995. Morphology and processes of valley floors in mountain streams, Western Cascades, Oregon. Geophysical Monograph 89, 83–101.

Groves, P.A., Chandler, J.A., 2002. The Quality and Availability of Fall Chinook Salmon (*Oncorhynchus tshawytscha*) Spawning and Incubation Habitat Downstream of the Hells Canyon Complex. Idaho Power Company, Boise, ID. Technical Report Appendix E.3.1.3 to FERC Relicensing Application.

Hanrahan, T.P., 2007. Bedform morphology of salmon spawning areas in a large gravel-bed river. Geomorphology 86, 529–536.

Hardy, R.J., Bates, P.D., Anderson, M.G., 1999. The importance of spatial resolution in hydraulic models for floodplain environments. Journal of Hydrology 216, 124–136.

Horritt, M.S., Bates, P.D., Mattinson, M.J., 2006. Effects of mesh resolution and topographic representation in 2D finite volume models of shallow water fluvial flow. Journal of Hydrology 329, 306–314.

Jacobson, R.B., Galat, D.L., 2006. Flow and form in rehabilitation of large-river ecosystems — an example from the Lower Missouri River. Geomorphology 77, 249–269.

James, L.A., 2005. Sediment from hydraulic mining detained by Englebright and small dams in the Yuba basin. Geomorphology 71, 202–226.

Jowett, L.G., 1993. A method of objectively identifying pool, run and riffle habitats from physical measurements. New Zealand Journal of Marine and Fisheries Research 27, 241–248.

Kirkbride, A.D., Ferguson, R.I., 1995. Turbulent flow structure in a gravel-bed river: Markov chain analysis of the fluctuating velocity profile. Earth Surface Processes and Landforms 20, 721–733.

Knapp, R.A., Preisler, H.K., 1999. Is it possible to predict habitat use by spawning salmonids? A test using California golden trout (*Oncorhynchus mykiss aguabonita*). Canadian Journal of Fisheries and Aquatic Science 56, 1576–1584.

Kondolf, G.M., Wolman, M.G., 1993. The sizes of salmonid spawning gravels. Water Resources Research 29, 2275–2285.

Lane, S.N., Richards, K.S., 1998. High resolution, two-dimensional spatial modelling of flow processes in a multi-thread channel. Hydrological Processes 12, 1279–1298.

Lane, S.N., Bradbrook, K.F., Richards, K.S., Biron, P.M., Roy, A.G., 1999. The application of computational fluid dynamics to natural river channels: three-dimensional versus two-dimensional approaches. Geomorphology 29, 1–20.

Lawless, M., Robert, A., 2001a. Scales of boundary resistance in coarse-grained channels: turbulent velocity profiles and implications. Geomorphology 39, 221–238.

Lawless, M., Robert, A., 2001b. Three-dimensional flow structure around small-scale bedforms in a simulated gravel-bed environment. Earth Surface Processes and Landforms 26, 507–522.

Lechowicz, M.J., 1982. The sampling characteristics of electivity indices. Oecologia 52, 22–30.

Leclerc, M., Boudreault, A., Bechara, J.A., Corfa, G., 1995. Two-dimensional hydrodynamic modeling: a neglected tool in the instream flow incremental methodology. Transactions of the American Fisheries Society 124, 645–662.

MacWilliams, M.L., Wheaton, J.M., Pasternack, G.B., Kitandis, P.K., Street, R.L., 2006. The flow convergence-routing hypothesis for pool-riffle maintenance in alluvial rivers. Water Resources Research 42, W10427. doi:10.1029/2005WR004391.

Magee, J.P., McMahon, T.E., Thurow, R.F., 1996. Spatial variation in spawning habitat of cutthroat trout in a sediment-rich stream basin. Transactions of the American Fisheries Society 125, 768–779.

McCuen, R.H., 1989. Hydrologic Analysis and Design. Prentice Hall, Englewood Cliffs, NJ.

Miller, A.J., Cluer, B.L., 1998. Modeling considerations for simulation of flow in bedrock channels. In: Wohl, E.E., Tinkler, K.J. (Eds.), Rivers over Rock: Fluvial Processes in Bedrock Channels. Geophysical Monograph Series. American Geophysical Union, Washington DC, USA, pp. 61–104. #107.

Moir, H.J., Soulsby, C., Youngson, A.F., 2002. Hydraulic and sedimentary controls on the availability and use of Atlantic salmon (*Salmo salar*) spawning habitat in the River Dee system, north-east Scotland. Geomorphology 45, 291–308.

Moir, H.J., Gibbins, C.N., Soulsby, C., Webb, J.H., 2004. Linking channel geomorphic characteristics to spatial patterns of spawning activity and discharge use by Atlantic salmon (*Salmo salar* L.). Geomorphology 60, 21–35.

Moir, H.J., Gibbins, C.N., Soulsby, C., Webb, J.H., 2006. Discharge and hydraulic interactions in contrasting channel morphologies and their influence on site utilization by spawning Atlantic salmon (*Salmo salar*). Canadian Journal of Fisheries and Aquatic Science 2568–2586.

Montgomery, D.R., Buffington, J.M., 1997. Channel reach morphology in mountain drainage basins. Geological Society of America Bulletin 109, 596–611.

Montgomery, D.R., Buffington, J.M., Peterson, N.P., Schuett-Hames, D., Quinn, T.P., 1996. Steam-bed scour, egg burial depths, and the influence of salmonid spawning on bed surface mobility and embryo survival. Canadian Journal of Fisheries and Aquatic Science 53, 1061–1070.

Montgomery, D.R., Beamer, E.M., Pess, G.R., Quinn, T.P., 1999. Channel type and salmonid spawning distribution and abundance. Canadian Journal of Fisheries and Aquatic Science 56, 377–387.

Moyle, P.B., 1994. The decline of anadromous fishes in California. Conservation Biology 8, 869–870.

Newson, M.D., Newson, C.L., 2000. Geomorphology, ecology and river channel habitat: mesoscale approaches to basin-scale challenges. Progress in Physical Geography 24, 195–217.

Nicholas, A.P., Mitchell, C.A., 2003. Numerical simulation of overbank processes in topographically complex floodplain environments. Hydrological Processes 17, 727–746.

Orth, D.J., 1995. Food web influences on fish population responses to instream flow. Bulletin Francais de la Peche et de la Pisciculture 337/338/339, 317–318.

Padmore, C.L., Newson, M.D., Charlton, M.E., 1998. Instream habitat in gravel bed rivers: identification and characterisation of biotopes. In: Klingeman, P.C., Beschta, R.L., Komar, P.D., Bradley, J.B. (Eds.), Gravel Bed Rivers in the Environment. Water Resources Publications, Highlands Ranch, CO, pp. 345–364.

Paola, C., Gust, G., Southard, J.B., 1986. Skin friction behind isolated hemispheres and the formation of obstacle marks. Sedimentology 33, 279–293.

Pasternack, G.B., Wang, C.L., Merz, J.E., 2004. Application of a 2D hydrodynamic model to design of reach-scale spawning gravel replenishment on the Mokelumne River, California. Rivers Research and Applications 20, 205–225.

Pasternack, G.B., Gilbert, A.T., Wheaton, J.M., Buckland, E.M., 2006. Error propagation for velocity and shear stress prediction using 2D models for environmental management. Journal of Hydrology 328, 227–241.

Payne, B.A., Lapointe, M.F., 1997. Channel morphology and lateral stability: effects on distribution of spawning and rearing habitat for Atlantic salmon in a wandering cobble-bed river. Canadian Journal of Fisheries and Aquatic Science 54, 2627–2636.

Rathburn, S.L., Wohl, E.E., 2003. Predicting fine sediment dynamics along a pool-riffle mountain channel. Geomorphology 55, 111–124.

Reeves, G.H., Everest, F.H., Nickelsen, T.E., 1989. Identification of physical habitats limiting the production of coho salmon in western Oregon and Washington. U.S. Forest Service General Technical Report PNW-GTR-245, Boise, ID.

Richards, K.S., 1976a. Channel width and the pool-riffle sequence. Bulletin of the Geological Society of America 87, 877–896.

Richards, K.S., 1976b. The morphology of pool-riffle sequences. Earth Surface Processes and Landforms 1, 87–95.

Richards, K.S., 1978. Channel geometry in the pool-riffle sequence. Geografiska Annaler. Series A 60, 23–27.

Rowntree, K.M., Wadeson, R.A., 1996. Translating channel geomorphology into hydraulic habitat: application of the hydraulic biotope concept to an assessment of discharge related habitat changes. In: Leclerc, M., Boudreault, A., Capra, H., Côté, Y., Valentin, S. (Eds.), Proceedings of the 2nd International Symposium on Habitat Hydraulics, Quebec City. INRS-EAU, Quebec, pp. 342–351.

Shirvell, C.S., 1989. Ability of PHABSIM to predict Chinook salmon spawning habitat. Regulated Rivers Research and Management 3, 277–289.

Stewardson, M.J., McMahon, T.A., 2002. A stochastic model of hydraulic variations within stream channels. Water Resources Research 38, 1–14.

Thompson, J.R., Taylor, M.P., Fryirs, K.A., Brierley, G.J., 2001. A geomorphological framework for river characterization and habitat assessment. Aquatic Conservation: Marine and Freshwater Ecosystems 11, 373–389.

Van Asselt, M.B.A., Rotmans, J., 2002. Uncertainty in integrated assessment modelling — from positivism to pluralism. Climatic Change 54, 75–105.

Vanderploeg, H.A., Scavia, D., 1979. Two electivity indices for feeding with special reference to zooplankton grazing. Journal of the Fisheries Research Board of Canada 36, 362–365.

Webb, J., Moir, H.J., Gibbins, C.N., Soulsby, C., 2001. Flow requirements of spawning Atlantic salmon (*Salmo salar*) in an upland stream: implications for water resources management. Journal of the Institute of Water and Environmental Management 15, 1–8.

Wheaton, J.M., Pasternack, G.B., Merz, J.E., 2004a. Spawning Habitat Rehabilitation-II. Using hypothesis testing and development in design, Mokelumne River, California, U.S.A. International Journal of River Basin Management 2, 21–37.

Wheaton, J.M., Pasternack, G.B., Merz, J.E., 2004b. Use of habitat heterogeneity in salmonid spawning habitat rehabilitation design. In: Garcia, D., Martinez, P.V. (Eds.), Fifth International Symposium on Ecohydraulics: Aquatic Habitats: Analysis and Restoration, IAHR-AIRH: Madrid, Spain, pp. 791–796.

Wolman, M.G., 1954. A method of sampling coarse river-bed material. Transactions of the American Geophysical Union 35, 951–956.

APPENDIX 5

Differences in River Ecological Functions Due to Differences in Rapid Channel Alteration Processes and Channel Morphology in Two California Rivers

Title: Differences in River Ecological Functions Due to Differences in Rapid Channel Alteration Processes and Channel Morphology in Two California Rivers

Authors: Marisa I. Escobar Arias[1,2*], Gregory B. Pasternack[1]

* Corresponding Author

Addresses:

[1] Department of Land, Air, and Water Resources, University of California, One Shields Avenue, Davis, CA 95616

[2] Stockholm Environment Institute, 133 D Street Suite F, Davis; CA 95616

Phone: 916-3250960, Fax: 530-7568670, e-mail: marisa.escobar@sei-us.org

Send proofs to Marisa I. Escobar Arias, marisa.escobar@sei-us.org, Stockholm Environment Institute, 133 D Street Suite F, Davis; CA 95616

1 Abstract

This study presents the conceptual development and applications of the functional flows model that integrates the role of hydrogeomorphic processes and ecological functions to assess stream physical habitat. Functional flows are discharge values that serve ecological functions. The model was adjusted to evaluate functionality for fall-run Chinook salmon at spawning sites located in riffles that have been rehabilitated with gravel augmentation in the Mokelumne River, and riffles that have changed due to floods in the Yuba River. The overall hypothesis of this

study is that differences in geomorphic conditions before and after rapid morphologic changes, among sites within a river reach, and among rivers, are reflected in differences in ecological performance of the physical habitat. Ecological functions studied were bed occupation, or periods when fish interact with the river bed (i.e. spawning, incubation, and emergence), and bed preparation, or periods when there is river bed surface reworking by the river. Model outputs were the number of days within a water year that present functional flows, the ranges of functional flows that provide sediment transport stages favorable for each ecological function, and the efficiency of a site to produce functional flows from available flows. Statistical significance of the results was tested using non-parametric methods. Functional flows analyses at habitat units that were monitored in detail before and after geomorphic alteration indicate that river rehabilitation below Camanche Dam on the Mokelume River increased the number of days with functional flows, while the May 2005 flood in the Timbuctoo bend of the Yuba River increased the functional ranges of flows. Reach scale analyses indicated similar ecological performance of reference habitat units with respect to sites that were monitored in detail. A comparison between both rivers showed that despite an overall greater geomorphic potential of the Mokelumne River sites, Yuba River sites present better ecological performance for fall-run Chinook salmon freshwater life stages due to greater ranges of flows available. The functional flows analysis provided an objective tool to assess changes in ecological functionality at hydrogeomorphically dynamic sites.

2 Introduction

Hydrogeomorphic processes in rivers determine the conditions of physical habitat where organisms perform their ecological functions, which include interactions with their physical habitat (Knighton 1998, Marcot and Heyden 2001, Moyle and Check 2004). Hydrologic and geomorphologic processes at the watershed scale, such as climate change and landscape evolution, determine the amount of water and sediment that move through catchments and into streams (Poff et al. 1997, Richards et al. 2002). Streamflow and sediment interact at the reach scale (i.e. defined as a portion of the river with length > 10^2 channel widths) through hydrologic, hydraulic, and sediment transport processes changing local water depth, velocity, bed form, and substrate composition (Fig. 1) (Lisle et al. 2000, Parker et al. 2003). The rate at which hydrogeomorphic processes at the watershed and reach scales happen vary from long term geologic trends to rapid alterations of water and/or sediment supply (Major and Mark 2006, Gibbins et al. 2007, May 2007). Watershed scale events that induce rapid hydrogeomorphic alterations include river engineering projects and convulsive natural events such as floods, volcanic eruptions, storms, hurricanes, wildfires, mass wasting, volcanic eruptions and earthquakes (Knighton 1998, Major and Mark 2006, Moody and Kinner 2006) (Fig. 1). Such events are likely to determine local hydrologic, hydraulic, and geomorphic changes, however the conditions of physical habitat units that make them suitable to be used by organisms to perform their ecological functions have the potential to persist (Maddock et al. 2004, Tipton et al. 2004, Ito et al. 2006).

The overall objective of this paper is to apply the functional flows model developed in Chapter 1 to analyze ecological functionality under two different types of rapid hydrogeomorphic change and under different morphologies. The model was adjusted tuned for fall-run Chinook salmon (*Oncorhynchus tshawytscha*), a key endangered Pacific Northwest salmon species that is an indicator of ecosystem functionality (Merz et al. 2004, Augerot et al. 2005, Merz and Chan 2005). The application of the model is performed in two significantly different rivers supporting fall-run Chinook salmon to observe the effects of hydraulic and morphologic differences on ecological functionality: the narrow, sediment starved, low-flow Mokelumne River which has undergone river rehabilitation through gravel augmentation projects, and the wide Yuba River, with an abundance of hydraulic mining sediment in the floodplain and a diverse flow regime, which has undergone rapid morphologic changes due to flood (Fig. 2).

Events that cause rapid hydrogeomorphic changes have dramatic impacts on local habitat conditions (May 2007). Gravel augmentation and natural floods change channel morphology, substrate composition, hydraulics, and floodplain connectivity (Wheaton et al. 2004a, Major and Mark 2006). These alterations affect ecological functionality of physical habitat for organisms that interact with the water column and the river bed (Tipton et al. 2004, Ito et al. 2006). Before a morphologic alteration, specific flow magnitudes generate certain water depths and velocities causing specific bed mobility stages that may be functional for an organism life stage. After a morphologic alteration, the same flow magnitude may generate higher or lower water depths and velocities causing a dissimilar bed mobility stage changing its functionality. Consequently, the functionality of a specific hydrograph can change in river sections where rapid hydrogeomorphic changes occur. Likewise, sites with different morphologies may behave different in terms of their hydraulics and sediment transport stages, causing differences in ecological functionality.

Assessments of flow functionality before and after changes in physical characteristics of the habitat and at sites with different morphologies within a reach allow the identification of the effect of hydrogeomorphic processes and morphology on ecological functionality. The functional flows model is used to address fundamental research questions to analyze differences in habitat functionality due to gravel augmentation, natural floods, and differences in channel morphology. The overall hypothesis of this study is that differences in hydrogeomorphic conditions due to rapid alterations in channel morphology and due to differences in channel form induce changes in ecological performance of the physical habitat. Research questions 1 to 3 are formulated to test the hypothesis by comparing functional flows before and after morphologic alterations caused by events that induce rapid hydrogeomorphic changes for specific ecological functions occurring at habitat units defined as zones with characteristic physical attributes where organisms perform ecological functions, which are the ways in which organisms interact with their physical habitat (Knighton 1998, Marcot and Heyden 2001, Moyle and Check 2004).. Additional research questions 4 and 5 are posited to compare functional flows among sites within the same river reach and between rivers for specific streamflow timeseries:

1) What are the ranges of flows that are potentially functional?
2) What is the number of days that flows are functional?
3) What is the efficiency of a habitat unit in producing functional flows?
4) What is the overall functionality of habitat units within a river reach as measured by the ranges of functional flows, number of days with functional flows, and efficiency to produce functional flows?
5) How does functionality of a reach as measured by the ranges of functional flows, number of days with functional flows, and efficiency to produce functional flows compare to

other reaches in the river and to other rivers?

In order to answer the research questions, specific objectives of this study are to 1) perform functional flows analyses for theoretical and actual water years to study the effects of gravel augmentation on ecological functionality in the Mokelumne River and to study the effects of flood-induced morphologic changes on ecological functionality in the Yuba River, 2) compare results of the functional flows analyses before and after morphologic alteration, among different habitat units within the same river reach, and between the rivers compare to observe the utility of applying the model in habitat units with different hydrologic regimes and morphologies. The analyses presented in this paper are an example of the use of the functional flows model. The application presented shows that the functional flows analysis provides a uniform measure that can be used to assess and compare ecological functionality among habitat units on a single river and among rivers.

3 Functional Flows Analysis

The functional flows model uses assessments of geomorphic dynamics achieved using discharge and channel data to estimate the temporal pattern of shear stress, which is a key factor determining physical habitat for several ecological functions. A functional flow is defined as a discharge that interacts with river bed morphology through hydraulic processes providing a shear stress value that serves an ecological function. Depending on the specificity of a given ecological function, functional flows may occur over a range of discharges.

To classify ranges of flows that are functional, the initial step is to identify relevant ecologic functions for the target species, in this case, fall-run Chinook salmon. The next step is to identify habitat units in order to perform the analysis to calculate temporal patterns of shear stress for the selected habitat units for which it is necessary to gather the input data (i.e. discharge time series, cross-section geometry, water surface slope, and grain size distribution). The next step is to build a table of functionality to specify the dependence of ecological functions on river bed sediment transport stages determined by shear stress thresholds and to assign functionality to shear stress time series and their correspondent streamflow time series. The next subsections present a summary of the procedure to perform functional flows analysis.

3.1 Ecological Functions

Ecological functions are defined as the ways in which organisms interact with and use their physical habitat (Marcot and Heyden 2001). Ecological functions related to physical habitat happening during the freshwater life stage of salmon include upstream migration of adults, spawning, embryo incubation, fry emergence, and juvenile rearing. Every year salmon migrate to upstream reaches to spawn in foothill and mountain cold water streams (Reiser and Bjornn 1979). They initiate the construction of the nest, called redd, by digging a hole to depths that vary depending on the size classes of the females for each species (DeVries 1997, Montgomery et al. 1999). After females lay their eggs and males fertilize them, the females finish the redd construction by covering the embryos with gravel (Groot and Margolis 1991, DeVries 1997). During incubation, the embryos remain buried within the gravel. After a period that ranges 8 months, the just-hatched fish, called fry, emerge through the gravel to begin their rearing life in freshwater (Groot and Margolis 1991, Merz et al. 2004, Augerot et al. 2005). To simplify the analysis, ecological functions of interest are grouped as 1) bed occupation functions that occur in periods when the fish interact with the river bed (i.e. spawning, incubation, and emergence), and 2) bed preparation functions that modify river bed surface conditions for the next spawning season (Fig. 3A). High and low flows may be functional or not depending on the timing with respect to the selected ecological functions (Fig. 3B).

3.2 Habitat Units

Physical habitat units in rivers are zones with characteristic physical attributes where organisms perform ecological functions (Knighton 1998, Marcot and Heyden 2001, Moyle and Check 2004). The selection of sites for functional flows applications concentrates on sites where the ecological functions under analysis are expected to occur. Preferred spawning habitat units are areas with low water depths, moderate velocities, and gravel that fish can move for redd construction (Lisle and Lewis 1992, Kondolf and Wolman 1993, DeVries 1997, Gallagher and Gard 1999, Lapointe et al. 2000). Flow, bed topography, and sediment sorting at the pool tail provide the bed form and water depth and velocity that salmon seek to carry out their reproductive life stage (Emery et al. 2003). Consequently, pool tail/riffle entrance is one preferred location for spawning (Montgomery et al. 1999, Coulombe-Pontbriand and LaPointe 2004, Moir et al. 2004, Moyle and Check 2004). Other locations include side channels and lateral bars (Webb et al. 2001, Moir et al. 2004, Morley et al. 2005).

3.3 Equations for Shear Stress Calculation

Shear stress is the key parameter that represents the force available to scour the river bed and can be used to delimit ecological functions that are highly dependent on sediment transport regimes at selected habitat units (Montgomery et al. 1999). An equation to estimate shear stress can be derived from the 1D Saint Venant Eq. that comes from balance of momentum for non-steady and non-uniform flow conditions:

$$\tau_0 = \rho g R\left(S - \frac{\partial h}{\partial x} - \frac{U}{g}\frac{\partial U}{\partial x} - \frac{1}{g}\frac{\partial U}{\partial t} \right) \tag{1}$$

where ρ is the water density, g is gravity, R is the hydraulic radius (wetted area/ wetted perimeter). The first term in the brackets, S, is the bed surface slope at the control volume being analyzed (i.e. slope of river bed) and $\rho g R S$ represent the steady component of the shear stress due to gravity forces acting on the fluid mass. The second term, $\partial h / \partial x$, is the change in cross section averaged depth with respect to downstream distance, and the third term, $U \partial U / g \partial x$, is the cross section averaged velocity of the control volume multiplied by the change in cross section averaged velocity with respect to downstream distance; these two terms represent the non-uniformity of the control volume. The fourth term in the brackets, $\partial U / g \partial t$, is the change in velocity between two timesteps divided by gravity, and represents the temporal change of the shear stress.

In addition to the 1D Saint Venant equation for non-steady non-uniform flow, at least 9 other methods can be used to estimate boundary shear stress from field measurements as summarized in Table 1 of Dietrich and Whiting (1989). Any of those methods could be used to estimate boundary shear stress for functional flows analysis. For the application presented in this study, the simplified depth-slope product was selected to calculate boundary shear stress

$$\tau_0 = \rho g R S \quad \text{or}$$

$$\tau_0 = \rho g h S \quad \text{for wide channels} \tag{2}$$

This method assumes conditions of uniform and steady flow that need to be checked for actual applications. Eq. 2 is used as a first cut approach that incorporates the dominant hydraulic interactions controlling channel sediment transport (Konrad et al. 2002, Buffington et al. 2004, Murray 2007). Such assumptions are discussed in Appendix 1 for the particular application presented in this paper. Using this simplified expression for shear stress focuses the study on exploring the interactions among physical processes and ecological functions without necessitating calculating shear stress in detail, which is a valuable effort that has been the focus of several studies (Booker 2003, Rodriguez et al. 2004, Wilson et al. 2006).

"At-a-station" cross section geometry relations can be used to evaluate depth at a range of discharge values

$$h = cQ^f \tag{3}$$

where c and f are empirical values that control the water depth response to discharge increments at the cross section (Leopold and Maddock 1953, Parker 1979). This approach is useful to obtain water depth time series necessary to estimate shear stress time series. Although this study use this approach, an alternative approach that provides water depth values for specific discharge values could be used.

Replacing Eq. 3 in Eq. 2, the shear stress becomes

$$\tau_0 = \rho_w g(cQ^f)S \tag{4}$$

Functional flows are expressed in terms of non-dimensional shear stress τ_o*, which allows a generalized definition of the model. Eq. 4 can be non-dimensionalized to obtain non-dimensional absolute values of shear stress

$$\tau_0{}^* = \frac{\tau_0}{g(\rho_s - \rho)D_{50}} \tag{5}$$

where ρ_s is the sediment density. Non-dimensional boundary shear stress can be compared to non-dimensional absolute values of τ_o* that represent the critical magnitude necessary to entrain gravel of a given size, τ_{crit}*, or Shields parameter (Buffington and Montgomery 1997, Wheaton et al. 2004a). Substituting Eq. 3 and 4 into Eq. 5, a new form of τ_o* is obtained

$$\tau_0{}^* = \frac{\rho g h S}{g(\rho_s - \rho)D_{50}} = \frac{\rho(cQ^f)S}{(\rho_s - \rho)D_{50}} \tag{6}$$

Eq. 6 can be used to evaluate $\tau_o{}^*$ for discharge time series and for a given cross section with a specific median grain size. The temporal pattern of shear stress represents geomorphic dynamics that are relevant to identify functional transport stages for fall-run Chinook salmon life stages (Fig. 4).

3.4 Shear Stress Thresholds

The functional flows model requires specification of bed mobility transport stages delimited by boundary shear stress thresholds for selected ecological functions (Table 1, Column 1) (Kondolf and Wilcock 1996, Lisle et al. 2000). Bed mobility categories are high flow/full mobility (FM), intermediate high flow/interstitial fines mobility (IFM), intermediate low flow/ superficial fines mobility (SFM), and low flow/stable bed (SB) (Fig. 4). Associated dimensionless critical shear stress values are used to delimit bed mobility stages for gravel-bed rivers according to values found in the literature (Table 1, Column 2B). Values of the Shields parameter for the median grain size, or mobility number

$$\tau_{c50}{}^* = \frac{\tau_{c50}}{g(\rho_s - \rho)D_{50}} \tag{7}$$

are an indicator of the initiation of motion in a non-uniform mix of grain sizes. Comparing the non-dimensional shear stress of the river bed $\tau_o{}^*$ to the Shields parameter $\tau_{c50}{}^*$ provides an indication of the degree of mobility of the river bed. On hydraulically rough beds, which is the common condition in gravel bed streams, the Shields parameter $\tau_{c50}{}^*$ ranges from ~0.03 to ~0.06 (Andrews 1984, Knighton 1998). Details on the variability of the thresholds for bed mobility stages are provided in Chapter 1. For the present application of functional flows analysis, a stable bed is assumed when $\tau_o^*<0.01$, intermittent transport when $0.01< \tau_o^*<0.03$, partial transport when $0.03<\tau_o^*<0.06$, and full mobility when $0.06<\tau_o^*<0.10$ (Buffington and Montgomery 1997, Lisle et al. 2000). The upper threshold for full mobility is set at 0.10 assuming that beyond this point there is intensive bed load transport that is non-functional to support spawning ecological functions (Lisle et al. 2000).

3.5 Model Structure and Table of Functionality

The algorithm for functional flows analysis integrates key relations between shear stress and ecological functions that have already been identified and are available in the literature such as the ones presented above. Estimating τ_o^* as a function of discharge time series it is possible to create the "table of functionality" to determine the functionality of sediment transport stages and flows serving ecological functions (Table 1).

In addition to temporal changes in bed mobility stages represented by Eq. 6, it is possible to observe the dependence of the geomorphic dynamics on streamflow. Q can be non-dimensionalized by a combination of variables with length and time dimensions (i.e. $L^{-3}T^{1}$). The formulation by Parker et al. (1979) is used

$$Q^* = \frac{Q}{\sqrt{gD_{50}}\,D_{50}^{\,2}} \tag{8}$$

Eqs. 6 and 8 can be used to produce curves of τ_o^* vs. Q^* to observe shear stress as a function of streamflow (Fig. 5). Curves of non-dimensional quantities allow comparison of channels with a wide range of characteristics and have been used to group and observe trends in data of rivers from different geographic regions (Parker et al. 2003). In this study, the resultant curve τ_o^* vs. Q^*, where τ_o^* is function of S, D_{50}, c and f; and Q^* is function of Q and D_{50}, depicts the variation in bed mobility stages for a cross section with a particular slope, median grain size, and geometry for a range of discharges. Each portion of the curve within thresholds of τ_{c50}^* (0.01, 0.03, 0.06, and 0.1) can be categorized as functional or non-functional. The model was programmed in Matlab to facilitate calculations. The Matlab code is available to the public to use and the manual to use the code constitutes Appendix 2 of this dissertation.

The functional flows model provides an approach to understand the relations among hydrogeomorphic parameters and ecological functions based on a representation of the natural system (Murray 2007). The analytical algorithm does not provide a predictive model, but an explanatory model conceived to explain abstract links among physical processes and biological systems (van Asselt and Rotmans 2002, Murray 2003). Inputs of the model include large scale parameterizations of the interactions among the most significant variables representing physical and ecological processes. Outputs of the model permit measuring such interactions under different sets of conditions resulting in data that adds to the existing knowledge about hydrogeomorphic and ecologic links. Functional ranges of Q*, number of days with functional flows, and percent efficiency for a habitat unit and for a water year are abstract results of the interactions based on relations among streamflow time series, water depth, and shear stress that have been tested. The validation of these results would require extensive concrete measures of discharge values, sediment transport stages, and ecological functions at all sites all days within a water year. The benefit of the model is that it is possible to obtain results about those interactions without having to embark on impractical field campaigns. Therefore, the functional flows model constitutes a theoretical analysis with scientific bases and its actual validation is beyond the objective of the present study (Murray 2003).

4 Field Sites

The Mokelumne and Yuba rivers flow generally west draining watersheds covering 1,624 km^2 and 3,480 km^2 respectively of the central Sierra Nevada of California (Figure 2). The Mokelumne River is a tributary to the San Joaquin River, while the Yuba River is a tributary to the Feather River. Their watersheds are ~110 km apart. The upstream reaches of both rivers receive ~ 1,200 mm of precipitation annually, while the central region of the watersheds receives ~510 mm (Mount 1995). Water feeds the rivers mostly as rain runoff in the late fall and winter, and as snowmelt in the spring. Historically, both rivers have been manipulated for dam construction, gold mining, gravel extraction, hydropower generation, water supply, and flood regulation (Elkins et al. 2007a, Moir and Pasternack Submitted). Such anthropogenic influence has caused in-stream physical habitat degradation (Mount 1995). Recently, both rivers have undergone morphological alterations produced by dissimilar causes: artificial gravel augmentation in the Mokelumne River, and natural floods in the Yuba River. These processes have modified channel form and have changed habitat conditions.

4.1 Gravel Augmentation in the Mokelumne River

The Mokelumne River has 16 major impoundments, Pardee Reservoir (259 million m^3) completed in 1929 and Camanche Reservoir (531 million m3) completed in 1963 being the two largest (Pasternack et al. 2004, Merz and Chan 2005, Elkins et al. 2007a). East Bay Municipality Utility District (EBMUD) manages both reservoirs for water supply serving 1.2 million people east of San Francisco Bay (Merz and Chan 2005). A statistical analysis of the flows from a gaging station downstream of Camanche Dam (USGS Station # 11323500) using the Indicators of Hydrologic Alteration (IHA) software shows the combined effect of both dams on the alteration of the natural flow regime (Richter et al. 1996, Richter et al. 1997) (Fig. 6A). For instance, median flows for the month of May when the highest spring snow-melt flows occur decrease on average from 95 m^3/s before Pardee Reservoir to 16 m^3/s after Camanche Reservoir (flow records 1905-1929, and 1964-2003 respectively). Since 1964, daily average flows have exceeded the post-dam 10 year return internal of 140 m^3/s in only three years: 1986, 1997, and 2006. In addition, the dams have acted as gravel traps, minimizing gravel recruitment downstream of Camanche Reservoir (Pasternack et al. 2004). The flow and sediment budget alterations in the Mokelumne River have degraded in-stream habitat and are viewed as main causes for fishery declines (Moyle 1994). Given the unavailability of flows and gravel, the Federal Energy Regulatory Commission recommended performing gravel replenishment projects to improve fish habitat (Pasternack et al. 2004).

River rehabilitation projects to improve habitat for spawning salmon using 8,357 m^3 of gravel and cobble have been built 1999-2006 in the 1-km reach downstream of Camanche Dam (Wheaton et al. 2004b, Elkins et al. 2007a). More are expected annually. The projects have counteracted channel degradation caused by flow regulation and gravel trapping. Positive ecological effects resulting from the projects include increases in the numbers of fish spawners using the reach, embryo survival to fry stage, macroinvertebrate diversity, and floodplain connectivity (Merz et al. 2004, Merz and Chan 2005, Elkins et al. 2007a).

By reducing water depth, increasing water velocity, and changing the morphology of the river bed, gravel augmentation changes the ecological functionality of the site providing appropriate hydraulic conditions to perform ecological functions despite the controlled hydrology of the river. The functional flows model provides a tool to assess the effect of gravel augmentation on the ranges of flows that are functional for theoretical and actual water years, and to assess the changes in the number of days that are functional for specific life stages in a given year. Also, the functional flows model provides a way to assess how gravel augmentation changes the efficiency of the sites in terms of their capacity to produce functional conditions from the available flows. Performing the analysis in several habitat units is useful to know the overall functionality of restored and un-restored sections of the river and might help explain how gravel augmentation has promoted hydrogeomorphic response and might provide directions on how to proceed in future projects

4.2 Natural Floods in the Yuba River

The largest dam of the North Fork Yuba River is New Bullards Bar Dam (1.2 billion m^3) completed in 1970, and the largest dam of the mainstem Yuba River is Englebright Dam (86 million m^3) built in 1941. The first is a flood control reservoir, while the latter acts as a sediment barrier that blocks downstream transport of sediment produced during hydraulic mining between 1850 and 1880 (Mount 1995). The IHA analysis for median monthly flows for the Yuba River (Smartville USGS Station # 11418000) shows a decrease in spring-snowmelt flows due to the dams (Fig. 6B). For the month of May flows decreased on average from 147 m^3/s before to 55 m^3/s after New Bullards Dam (flow records 1941969, and 1970-2003 respectively). The powerhouses at Englebright Dam can only pass a continued 125 m^3/s, so discharges greater than that flows flow over the top. Since 1970, daily average flows have exceeded the post-dam 10 year return interval of 2,700 m^3/s in only three years: 1986, 1997, and 2005. In May and Dec 2005 hourly high flows at Smartville peaked at 1,200 m^3/s (7.7 yr return interval) and 3,285 m^3/s (24 yr return interval) respectively. Despite the sediment trapping effect of Englebrigth Dam, millions of metric tons of gravel and cobble are stored in the Yuba River floodplain due to hydraulic mining (Mount 1995).

The combined effects of ample sediment present in the channel and floodplain as well as availability of high flows create conditions for the Yuba River to self-maintain salmon spawning habitat. The particular pool-riffle-run unit (500 m long x 250 m wide) located at the apex of Timcubtoo Bend, situated 5 km downstream of Englebright Dam, was mapped in 2004 and 2005 to assess morphological adjustments. Aerial photos going back to 1937 demonstrate that this feature has persisted for over 70 years. A cut-fill analysis of the pre- and post- May 2005 event indicated that the flood eroded 7,728 m^3 from the riffle and deposited 7,669 m^3 on an island and along the banks (Moir and Pasternack 2003).

By scouring and depositing new gravel, floods change the morphology and the substrate composition, thus altering local hydraulics. The functional flows analysis in the Yuba River provides a tool to analyze the flood-induced changes in 1) the ranges of functional flows, 2) the number of days with functional flows for a given water year, and 3) the efficiency of the sites to produce functional conditions. Performing the analysis in several sites is useful in order to observe the spatial distribution of ecological functionality conditions in this dynamic gravel bed river heavily used by fish spawners.

4.3 Selection of Habitat Units for Functional Flows Analysis

Habitat units were selected within river reaches corresponding to riffles that have undergone detailed topographic monitoring before and after the events, and from downstream riffles located at non-restored sites in the Mokelumne and at a reference site in the Yuba River (Wheaton et al. 2004a, Merz et al. 2006, Elkins et al. 2007a) (Fig. 7). In the Mokelumne River, sites were selected from riffles located at the furthest upstream reach between Camanche Dam and Mackville Road Bridge which spans 7.8 km and corresponds to 32% of total area of the lower Mokelumne River (Merz and Setka 2004). Habitat units identified for the analysis included three gravel-augmented and three reference riffles (Fig. 7A; 8A). Cross sections were made at each habitat unit. Cross section XS1 was located 237 m downstream of the dam. Initially, this habitat unit was a chute with fast current flowing through two obstructions; after the 1999 gravel addition it became a riffle with depths varying between 0.15 and 1.5 m for base flows of 11 m^3/s; after the 2004 gravel addition it became a shallower riffle with depths varying between 0.15 and 0.75 m (Fig. 7A). XS2 was located 607 m downstream of the dam. This habitat unit was a degraded deep riffle, and after 2001 gravel addition it was shaped into a shallow central bar with a downstream riffle. XS3 was located 295 m downstream of the dam, immediately downstream of XS1, and it became an extension of the XS1 riffle exit after gravel addition in 2005. The section of the river where XS1 and XS3 were located presents a steep right bank with encroached vegetation, and a low-slope left bank with a connected floodplain that has a recreational use. The section where XS2 was located has a vertical right bank formed by a rock outcrop. The reference sites XS4, XS5, and XS6 were located 1,175 m, 1,560 m, and 2,857 m downstream of the dam respectively and represent natural riffles that have not been restored (Fig. 7). All the downstream reference sites have a steep left bank and a gently sloping right bank (Fig. 8B).

In the Yuba River, habitat units were selected at the Timbuctoo bend: three habitat units were selected at the riffle located at the apex of the bend and a reference habitat unit was selected at the next wide riffle in the downstream direction (Fig. 7B, 8C). XS1 and XS2 were located at the riffle entrance and riffle crest respectively, and both eroded during the flood. XS3 was located at the downstream glide and accreted during the flood. This section of the river has a connected floodplain, with gravel bars, adjacent channels, small extent of vegetation encroachment, and variable morphology. A main feature of the site was a central bar/island that divides the flow into a main channel to the left and a secondary channel to the right. XS4 was located in a wide, shallow riffle that is heavily used by spawning fish located midway between the apex and the downstream end of the Timbuctoo bend (Fig. 8C).

5 Methods

The functional flows model calculations required ecological, geomorphic, hydrologic, and hydraulic input data. In order to use the algorithm, it was necessary to gather site-specific hydrogeomorphic data of cross section geometry, water surface slope, and grain size distribution. In addition, flow records from USGS stations (#11323500 at the Mokelumne River and #11418000 at the Yuba River) were used to isolate distinct water year types for both rivers and the event years, or the years pre- and post-gravel augmentation in the Mokelumne River and pre- and post- May 2005 flood in the Yuba River. The table of functionality, hydrogeomorphic data, and water year types were used as input to perform functional flows calculations.

5.1 Water Year Types

Two types of functional flows analysis were performed: a theoretical analysis using representative water year types for characteristic hydrologic conditions in each river, and an actual analysis using water year data corresponding to the years when events occurred (Table 2). Theoretical water year types were identified using the Flood Regime Characterization (FRC) Matlab code developed by Booth et al. (2006) (http://watershed.ucdavis.edu/pages/programs.html) (Booth et al. 2006). The code identifies distinct water year types from flow records by requesting a set of decisions isolating distinct flood types based on flood duration and magnitude. One output of the code is the daily flow for each Julian day averaged across all years of the same flood year class.

The flow record used for the Mokelumne River was 1963-2006 and for the Yuba River was 1941-2006. Two water year flood types identified with the FRC code for the Mokelumne River included WY1 that represents a scenario of highly regulated flows with maximum flow of 25 m^3/s in the snowmelt season and corresponds to the 1 yr return interval flood, and WY2 that represents a scenario with the highest flows that can be released from the dam with a max flow of 95 m^3/s in the rain season and corresponds to the 3 yr return interval flood. Two water year flood types identified with the FRC code for the Yuba River included WY1 that represents a scenario of regulated flows with a maximum discharge of 125 m^3/s in the snowmelt season and corresponds to the 1 yr return interval flood, and WY2 that represents a scenario with a max flow of 600 m^3/s in the rain season and represents a 3 yr return interval flood. For the second type of analysis involving actual water years, the daily average flow values were obtained from the USGS gauging stations for 1997-2005 for the Mokelumne River and for 2005-2006 for the Yuba River (Figs. 9A and 10A) (Note that WY1 and WY2 were not depicted for limited space).

5.2 Geomorphic Data

Campaigns to collect field data were performed before and after morphologic alterations between 1998-2005 in the Mokelumne River, between 2004-2005 in the Yuba River, and in November 2005 in both rivers for the reference sites (XS4, XS5, and XS6 in the Mokelmune River, and XS4 in the Yuba River). Detailed river bed topography data (i.e. 0.5-1.5 pt/m^2) was used to build annual channel DEMs using AutoCAD® as previously reported (Wheaton et al. 2004a, Merz et al. 2006, Elkins et al. 2007b). Cross sections through selected habitat units were sampled from the pre- and post-gravel augmentation surfaces in the Mokelumne River, and pre- and post- flood surfaces in the Yuba River. Cross section geometry and bed slope of the reference sites were surveyed with an autolevel, tape, and rod, and the coordinates of the sites were obtained with a Trimble Pathfinder Pro XRS, a with a real-time kinematic GPS. Water surface slope as an approximation of river bed slope and grain size distribution for XS1, XS2, and XS3 in both rivers was obtained from previous studies and from unpublished data (Pasternack et al. 2004, Wheaton et al. 2004b, Moir and Pasternack 2006, Elkins et al. 2007a) (Table 3). Since water surface slope was reported for a set discharge value, a unique value was obtained for each cross section and was used for the depth-slope product calculations and for stage-discharge geometry relations. This constitutes an assumption, since the water surface slope may change as discharge increases or decreases. Position and elevation data for each cross section was used to build stage-discharge relationships using a routine of the functional flows Matlab code. The routine calculates areas for incremental stage values using input cross section geometry and their corresponding velocities using Manning's equation with a typical value of n=0.043 for gravel bed rivers (Pasternack et al. 2004) and with their corresponding water surface slopes. The code was used to calculate hydraulic radius and discharge for incremental stage values to obtain the parameters of Eq. 3. Coefficients and exponents are summarized in Table 3.

5.3 Data Analysis

A total of 50 analyses were performed: 30 for the Mokelumne River corresponding to 6 cross sections analyzed for 5 distinct water year types and 20 for the Yuba River corresponding to the 5 cross sections analyzed for 4 distinct water year types. Functional flows analysis results were graphed to answer the research questions posited. Results depicted in graphs were grouped first by water year types and then by cross section in order to observe trends.

To answer research question 1, what are the ranges of flows that are potentially functional?, τ_o* vs. Q* curves were graphed indicating the ranges of flows that fell within predetermined bed mobility stages for each water year (Figs. 9B and 10B). In each τ_o* vs. Q* curve, shaded gray lines correspond to the available ranges of flows produced during the water year that fell within a specified bed mobility stages. Symbols such as circles, squares, or triangles superimposed on the shaded gray lines correspond to the days within a water year that had a functional discharge value that not only fell within specified bed mobility stages but also happened at the time when they were functional for the life stage according to Table 1. Arrows indicate the shift of one cross section from the initial to subsequent locations in the τ_o* vs. Q* space due to hydrogeomorphic changes (i.e. gravel augmentation in the Mokelumne River, flooding in the Yuba River). Functional ranges of Q* were calculated subtracting the minimum from the maximum functional Q* occurring in a given water year (Table 4). Cases with zero range of Q* corresponded to absence of ecological functionality, while cases with the highest values of functional ranges of Q* corresponded to the highest ecological functionality.

To answer research question 2, what is the number of days that flows are functional?, counts of the number of days that presented functional flows for each cross section were graphed (Figs. 9C and 10C; Table 4) . Higher number of days with functional flows corresponded to higher ecological functionality performance and viceversa.

To answer research question 3, what is the efficiency of a habitat unit in producing functional flows?, percentage efficiency was estimated as the ratio between functional ranges of Q* and available ranges of Q* (Figs. 11 and 12; Table 4). Higher values of efficiency indicated higher ecological functionality and viceveresa.

In order to find out if the results from addressing questions 1-3 were statistically significant, results were grouped to compared inputs and outputs of the functional flows model before and after gravel augmentation in the Mokelumne River (i.e. 15 before vs. 15 after), before and after May 2005 flood in the Yuba River (i.e. 9 before vs. 11 after), among sites within each river (i.e. 24 upstream vs. 6 downstream in the Mokelumne River and 18 upstream vs. 2 downstream in the Yuba River), and between rivers (i.e. 30 in the Mokelumne River vs. 20 in the Yuba River) (Table 5). Given that datasets presented differences in standard deviations, they were analyzed with non-parametric statistics. Non-parametric statistics have been widely applied trough earth sciences studies (Pasternack 1998). The non-parametric Kolmogorov-Smirnov (KS) two-sample test was performed to determine statistical significance of the difference between data groups to facilitate comparison in research questions to confirm or reject the hypothesis that differences in geomorphic variables caused differences in ecological functionality. This statistical procedure was appropriate to test the relationship between the data groups for the available sample size without making assumptions about the distribution of the data (Statsoft 1998). The threshold to determine that differences were statistical significant above the 95% confidence level was set at p-level <0.05 (Table 5).

KS test results for input variables vs. functional flows outputs were organized into matrices with 3 columns and 4 files that provided 4 tests of the hypothesis for each functional flows model result for a total of 12 tests of the hypothesis for each comparison group (Table 5). Confirmation or rejection of hypothesis was assigned following a set of rules. For instance, if statistical difference on geomorphic variables among datasets (T), represented by statistically different or similar geomorphic variables datasets respectively, resulted on statistical difference in functional flows outputs (T), represented by statistically different or similar functional flows results respectively as measured by functional ranges of Q*, number of days with functional flows, and % efficiency, then the hypothesis was confirmed (T), which corresponds to the rule T→T=T. Additional rules were T→F=F, F→F=T, and F→T =F.

Such lay out of results was used to answer research question 4, what is the overall functionality of habitat units within a river reach as measured by the ranges of functional flows, number of days with functional flows, and efficiency to produce functional flows?, by comparing results from upstream habitat units (XS1, XS2, and XS3 on both rivers) and downstream habitat units (XS4, XS5, and XS6 on the Mokelumne River and XS4 on the Yuba River) to assess overall trends within a river reach, and to answer research question 5, how does functionality of a reach as measured by the ranges of functional flows, number of days with functional flows, and efficiency to produce functional flows compare to other reaches in the river and to other rivers? by comparisons among overall functionality on both rivers.

6 Functional Flows Analysis Results

Each subsection of the functional flows analysis results corresponds to research questions 1 through 5. In addition to description of graphs and presentation of calculations outputs, each subsection refers to the KS test reported in Table 5 for confirmation or rejection of the overall hypothesis.

6.1 Change in functional ranges of Q*

For the Mokelumne River, results indicated that river rehabilitation caused a vertical shift in τ_o* vs. Q* curves for XS1 and XS3 from a non-functional domain to a functional domain for all water years. The τ_o* vs. Q* curves presented a vertical shift from a non-functional to a functional domain (Figs. 9B) increasing the range of functional flows for XS1 and XS3 for all water years, and for XS2 for WY1. The effect of gravel augmentation before and after gravel augmentation on geomorphic variables S, D_{50}, c, and f was statistically significant above the 99% confidence level ($p<0.01$, <0.05. <0.01, <0.005 respectively), and on functional ranges of

Q* and % efficiency was not statistically significant ($p<0.10$). The hypothesis was rejected for all 4 combinations of functional ranges of Q* and hydrogeomorphic variables (Table 5A).

For the Yuba River, results indicated that natural floods caused a lateral shift in τ_o* vs. Q* curves for XS1 and XS2 maintaining them within a functional domain. τ_o* vs. Q* curves for XS3 presented a diagonal shift (Figs. 10B). Lateral shifts to the right and a diagonal shift increased the ranges of functional flows for all cross sections for all water years. Changes before and after the flood on hydrogeomorphic variables S, D_{50}, c, and f and on the functional ranges of Q* was statistically significant above the 97.5 confidence level ($p<0.001$, <0.001, <0.025, <0.0025, <0.005 respectively). The hypothesis was accepted for all 4 combinations of functional ranges of Q* and geomorphic variables (Table 5A).

6.2 Change in the number of days that are functional

For the Mokelumne River, results indicated that river rehabilitation increased the number of days with functional flows for XS1 and XS3for all water years, while it increased the number of days with functional flows for XS2 for WY2 only (Figs. 9C). In the Mokelumne River, the mean value of days with functional flows was 60 before and 138 after gravel augmentation. The effect of gravel augmentation on the number of days with functional flows was statistically significant above the 95% confidence level ($p<0.05$). The hypothesis was accepted for all 4 combinations of number of days with functional flows and geomorphic variables (Table 5A).

For the Yuba River, results indicated the May 2005 natural flood maintained the number of days with functional flows for WY1 and WY2 while it increased the number of days with functional flows for the year when the event happened for XS1 and XS2 (Figs. 10C). Also, the flood increased the number of days with functional flows for all 4 water years for XS3. Even though the mean value of days with functional flows across all 4 water years was 157 before and

174 after the May 2005 flood, the change in the number of days with functional flows not statistically significant ($p>0.10$). The hypothesis was rejected for all 4 combinations of number of days with functional flows and geomorphic variables (Table 5A).

6.3 Change in efficiency of a habitat unit to produce functional flows

For the Mokelumne River, results indicated that after gravel augmentation XS1 and XS3 increased their efficiency to produce functional flows for all water years, while XS2 increased its efficiency to produce functional flows for WY2 only. The change in efficiency was not statistically significant ($p<0.10$). The hypothesis was rejected for all 4 combinations of % efficiency and geomorphic variables (Table 5A).

For the Yuba River, results indicated that the May 2005 natural flood maintained the efficiency to produce functional flows for XS1 and XS2 for WY1 and WY2, reduced the efficiency for XS3 for WY2, and increased the efficiency for all cross sections for the actual WY. The change in % efficiency was not statistically significant ($p>0.10$). The hypothesis was rejected for all 4 combinations of % efficiency and geomorphic variables (Table 5A).

6.4 Overall functionality of a river reach

The overall functionality of each river reach was analyzed by comparing the functionality of habitat units located at detailed monitoring and reference sites within the same river. The difference in the values of c and f between upstream and reference sites was statistically significant ($p<0.001$ and $p<0.05$ respectively), while the difference in values of S, D_{50}, and functional flows results was not statistically significant ($p>0.10$). Reference sites of the Mokelumne River presented some degree of functionality measured from the occurrence of days with functional flows and from the efficiency to produce functional flows. Curves of τ_o* vs. Q* for XS4 and XS6 were within the functional domain for WY1 and WY2, while the curve of τ_o* vs. Q* for XS5 presented a small section within the functional domain for WY2 only. XS4 and XS6 presented days with functional flows for both water years, while XS5 presented days with functional flows for WY2 only. XS4 and XS6 presented above average efficiency for WY1 and WY2, while XS5 presents above average efficiency for WY2 only (Table 4). The hypothesis was confirmed for 6 and rejected for 6 combinations of functional flows outputs and hydrogeomorphic variables inputs (Table 5B).

For the Yuba River, hydrogeomorphic variables and functional flows outputs of upstream and downstream sites were statistically similar ($p > 0.05$). XS4 located at the reference site presented lower functionality than upstream reaches for WY1 as shown by its lower section of the τ_o* vs. Q* curve within the functional domain and by the low number of days with functional flows. In contrast, XS4 presented functionality comparable to upstream reaches for WY2 represented by its high section of the τ_o* vs. Q* curve within the functional domain and by its high number of days with functional flows. XS4 presented lower than average efficiency for WY1 and higher than average efficiency for WY2 (Table 4). The hypothesis was confirmed for all 12 combinations of functional flows outputs and hydrogeomorphic variables inputs (Table 5B).

6.5 Comparison among rivers

The Yuba River presented better flow functionality than the Mokelumne River determined by the location of τ_o* vs. Q* curves for all cross sections within the functional domains and by a higher number of days with functional flows. In addition, the efficiency of the Yuba River sites was higher on average than that of the Mokelumne River sites. Slope, D_{50}, c, and functional flows outputs were statistically different ($p<0.001$) while f was statically similar (p>0.10). The hypothesis was accepted for 9 combinations of functional flows outputs and hydrogeomorphic variables inputs (Table 5C).

7 Discussion

The analysis of ecological functionality using functional flows reflects how changes of geomorphic variables due to hydrogeomorphic processes modify the suitability of in-stream physical habitat for fall-run Chinook Salmon. For each habitat unit, ranges of flows, number of days that flows are functional, and efficiency to produce functional flows were obtained from Eqs. 6 and 8. Rewriting Eq. 6 in terms of Q* yields:

$$\tau_0{}^* = \frac{\rho}{(\rho_s - \rho)} \frac{S}{D_{50}} c(g^{1/2} D_{50}{}^{5/2} Q^*)^f$$

where each input variable influences the final result depending on its effect on the value of $\tau_o{}^*$. the exponent f determines the slope of the curve $\tau_o{}^*$ vs. Q*, the D_{50} is related non-linearly to $\tau_o{}^*$, and S and c are related linearly to $\tau_o{}^*$. Overall, within the ranges found at the cross sections studied, lower values of f promoted lower depth response to depth increments that may be beneficial for spawning habitat (i.e. such response is found in shallow riffles), large values of D_{50} promoted higher upper thresholds of Q* incrementing the ranges of functional flows, and higher values of c and S promoted the vertical shift up of $\tau_o{}^*$ vs. Q* curves from stable bed to functional transport regimes (i.e. superficial fines mobility, interstitial fines mobility, and full mobility). The next subsections include a discussion of results obtained analyzing the effect of geomorphic variables on functional flows output.

7.1 Effect of geomorphic changes on functional ranges of Q*

The rejection of the hypothesis that changes in geomorphic variables due to gravel augmentation modified the ecological response as measured by the difference in functional ranges of flows in the Mokelumne River indicates that the alteration of the morphologic variables S, D_{50}, c and f did not cause an ecological improvement of the habitat. The positive change of S into higher values that caused a shift of the τ_o* vs. Q* curves from a stable bed into functional transport regimes together with the positive change of the variable f into lower values that signify a lower depth response to increments in discharge increased the functional ranges of flows to some level. The positive effects of S and f were counteracted by the negative change of D_{50} into a larger value that reduced the upper threshold of the ranges of Q observed in the lateral shift to the left of the τ_o* vs. Q* curves. The manipulation of the morphology of the channel alone was not sufficient to create a statistically significant difference after gravel augmentation of the functionality of the habitat as measured by the increase of functional ranges of flows and cannot substitute the need for larger flows that would increase the ranges of functional flows to a level that is statistically significant.

The confirmation of the hypothesis that changes in geomorphic variables due to the May 2005 flood modified the ecological response as measured by the difference in functional ranges of flows in the Yuba River indicates that the changes in the morphologic variables S, D_{50}, c and f were sufficient to improve the ecological conditions of the habitat. Despite the fact that the variable f increased changing into values that are theoretically less functional promoting greater depth increments to increments in discharge that may be negative to the habitat, the combined effect of a lower slope, smaller grain size, and available flows provided the conditions to increase the functional ranges of flows.

7.2 Effect of geomorphic changes on number of days with functional flows

The confirmation of the hypothesis that changes in geomorphic variables due to gravel augmentation modified the ecological response as measured by the difference in the number of days with functional flows in the Mokelumne River suggests that achievement of a lower depth response to increments in discharge by reducing the values of f and the achievement of a functional sediment transport stage by increasing the values of S allowed the available low flows to provide functional habitat conditions during some of the crucial spawning life stages.

The rejection of the hypothesis that changes in geomorphic variables due the May 2005 modified the ecological response as measured by the difference in the number of days with functional flows in the Yuba River indicates that the geomorphic improvements after the flood were not sufficient to modify to improve the number of days with functional flows. An explanation of this result is that sites presented a high count of days with functional flows even before the flood, and the geomorphic changes after the flood did not impact the results significantly. This suggest that there may be a threshold of number of days with functional flows for sites depending on hydrologic conditions above which it is unlikely to increase.

7.3 Effect of geomorphic changes on the efficiency to produce functional flows

The efficiency of a habitat unit to produce functional flows is a metric that combines the hydrologic and geomorphic response with the ecological requirements for life stages. The complex, non-linear interaction among variables yields a variety of hydrogeomorphic responses and the consequent variability in efficiency to produce functional flows. The available ranges of flows may fall within a non-functional domain causing the absence of functional ranges of flows or the available ranges of flow may fall within a functional domain in which case the presence of functional ranges of flows depends on the time series of flows that may or may not produce functional sediment transport regimes at the appropriate times for each life stage.

Despite the given conditions to increase efficiency at both rivers due to the increase of number of days with functional flows in the Mokelumne River and due to the increase of functional ranges of flows in the Yuba River, the hypothesis that changes in geomorphic variables modified the ecological response as measured by % efficiency was rejected, indicating that this metric did not reflect the habitat improvement shown by the other two functional flows outputs.

7.4 Functional flows analysis at the reach scale

In the context of comparing cross sections within the same reach, geomorphic similarity can be defined for cross sections with geomorphic variables that are statistically similar (i.e. the results of the KS statistical test are negative). Likewise, the similarity of the ecological performance can be defined for cross sections with functional flows outputs that are statistically similar. The confirmation of the hypothesis that similarity of the geomorphic variables S and D_{50} caused similarity of ecological performance as measured by functional ranges of flows, number of days with functional flows, and efficiency between restored and un-restored sites within the same river reach at the Mokelumne River indicates that un-restored sites may not need the same level of channel morphology modification that restored sites underwent. The rejection of the hypothesis for the geomorphic variables c and f indicates that un-restored sites may need channel geometry improvements such as reduction of f values to decrease depth response to discharge increments and decrease incision that generated positive effects on the restored sites.

The confirmation of the hypothesis that similarity of the all geomorphic variables analyzed caused similarity of ecological performance as measured by functional ranges of flows, number of days with functional flows, and efficiency between restored and un-restored sites within the same river reach at the Yuba River indicates that larger scale processes control the geomorphology of the reach, and that the ecological performance of the habitat in this section of the river may be controlled also by such larger scale processes.

7.5 Functional flows analysis at the regional scale

In the context of comparing rivers within the same region such as the Sierra Nevada, statistically differences of geomorphic variables and ecological performance reflect the importance of the geomorphology and history of each watershed. The confirmation of the hypothesis that differences of geomorphic variables S, D_{50}, and c cause differences of ecological performance as measured by the functional ranges of flows, number of days with functional flows, and efficiency between the Mokelumne River and the Yuba River indicates that processes at each watershed, such as geomorphic controls and local human impacts, rather than regional processes, such as climate, control the ecological performance of each river. Higher values of S and higher values of D_{50} have the potential to cause lower functionality at the Yuba River with respect to the Mokelumne River by reducing the span of τ_o* vs. Q* curves within functional sediment transport domains. However, values of functional ranges of Q*, number of days with functional flows, and % efficiency are larger at the Yuba River than at the Mokelumne River. Lower values of c may contribute partially to the effect of greater functionality at the Yuba River because they cause a higher span within functional sediment transport stages. Yet the largest factor contributing to better functional flows outputs at the Yuba River is larger flow availability, which promotes ecological functionality despite the overall lower geomorphic performance of the Yuba River with respect to the Mokelumne River.

7.6 Key Lessons

Gravel augmentation in the Mokelumne River between 1999-2006 has increased the number of days with functional flows for fall-run Chinook salmon for the study sites but has not impacted significantly the functional ranges of flows. Hydrogeomorphic variables have reached a functional stage after gravel augmentation as observed by the location of τ_o* vs Q* curves in functional domains. The next possible stage to increase ecological functionality in the restored sites is to increase available ranges of flows at the appropriate times during the year in order to increase functional ranges of flows.

The May 2005 flood in the Yuba River increased functional ranges of flows by shifting τ_o* vs Q* laterally. Although the May 2005 flood increased the number of days with functional flows at the study sites, there was a high occurrence of days with functional flows before the flood and the consequent effect of the flood on this analysis output is insignificant.

The metric of percentage efficiency did not reflect the ecological improvements of number of days with functional flows in the Mokelumne River and of functional ranges of Q* in the Yuba River. This is a complex metric that requires several steps for calculation and involves several variables that may counteract each other. According to the results of this study, the work invested in obtaining this metric does not provide additional information that is helpful for understanding ecological functionality in rivers.

Detailed monitoring sites and reference sites present similar ecological functionality in both rivers. Despite the local effects of gravel augmentation that have changed local geometry in the Mokelumne River sites, ecological functionality of reference sites is similar to that of restored sites indicating that reference sites may not need abrupt gravel augmentation projects to improve their habitat. In the Yuba River, study sites at the apex of the Timbuctoo bend and the reference site present similar ecological functionality, indicating the uniformity of conditions within the reach to provide habitat quality for fall-run Chinook salmon.

The Mokelumne River and the Yuba River in general present differences in ecological functionality. Overall, the Mokelumne River has a characteristic geomorphic functionality that comes from the combination of hydrogeomorphic variables such as slope, grain size distribution, and cross section geometry that produce ecological functionality despite low flow availability. On the other hand, the Yuba River also presents geomorphic functionality that is complemented by a hydrologic functionality that comes from ample flow availability for an optimal combination of hydrologic and geomorphologic conditions for ecological functionality.

8 Conclusions

In summary, this study supports the hypothesis that it is possible to measure the changes in ecological functionality of the habitat by measuring hydrogeomorphic changes. Rapid geomorphic changes have the capacity to alter hydraulics that in turn affect sediment transport stages and ecological response of the river bed. Depending on the direction of the morphologic change, such alterations may be positive for the physical habitat. When geomorphic change promotes the proper combination of geomorphic variables and hydrology it also induces the conditions for improved ecological functionality. Sites with suitable combinations of slope, grain size distribution, and cross section geometry may have the potential to create ecological functionality. However, ecological functionality will only be provided if there is ample availability of functional ranges of flows working with local morphology and hydraulics to provide sediment transport stages that are functional for fall-run Chinook salmon life stages. The application of the functional flows analysis presented in this study contributes to the current knowledge of interactions between hydraulics, geomorphology, and ecology indicating the pertinence of this approach to the crucial understanding of the effects of physical processes on ecological response.

9 References

Andrews, E. D. 1984. Bed-Material Entrainment and Hydraulic Geometry of Gravel-Bed Rivers in Colorado. Geological Society of America Bulletin **95**:371-378.

Augerot, X., C. Steinback, and N. Fobes. 2005. Atlas of Pacific Salmon. University of California Press, Portland, Oregon.

Booker, D. J. 2003. Hydraulic modelling of fish habitat in urban rivers during high flows. Hydrological Processes **17**:577-599.

Booth, E. G., J. F. Mount, and J. H. Viers. 2006. Hydrologic Variability of the Cosumnes River Floodplain. San Francisco Estuary and Watershed Science **4**.

Buffington, J. M., and D. R. Montgomery. 1997. A systematic analysis of eight decades of incipient motion studies, with special reference to gravel-bedded rivers. Water Resources Research **33**:1993-2029.

Buffington, J. M., D. R. Montgomery, and H. M. Greenberg. 2004. Basin-scale availability of salmonid spawning gravel as influenced by channel type and hydraulic roughness in mountain catchments. Canadian Journal of Fisheries and Aquatic Sciences **61**:2085-2096.

Coulombe-Pontbriand, M., and M. LaPointe. 2004. Geomorphic controls, riffle substrate quality, and spawning site selection in two semi-alluvial salmon rivers in the Gaspe Peninsula, Canada. River Research and Applications **20**:577-590.

DeVries, P. 1997. Riverine salmonid egg burial depths: review of published data and implications for scour studies. Canadian Journal of Fisheries and Aquatic Sciences **54**:1685-1698.

Elkins, E. M., G. B. Pasternack, and J. E. Merz. 2007a. Slope creation in regulated rivers. Water Resources Research **43(5)**.

Elkins, E. M., G. B. Pasternack, and J. E. Merz. 2007b. Use of slope creation for rehabilitating incised, regulated, gravel bed rivers. Water Resources Research **43**.

Emery, J. C., A. M. Gurnell, N. J. Clifford, G. E. Petts, I. P. Morrissey, and P. J. Soar. 2003. Classifying the hydraulic performance of riffle-pool bedforms for habitat assessment and river rehabilitation design. River Research and Applications **19**:533-549.

Gallagher, S. P., and M. F. Gard. 1999. Relationship between chinook salmon (Oncorhynchus tshawytscha) redd densities and PHABSIM-predicted habitat in the Merced and Lower American rivers, California. Canadian Journal of Fisheries and Aquatic Sciences **56**:570-577.

Gibbins, C., D. Vericat, R. J. Batalla, and C. M. Gomez. 2007. Shaking and moving: low rates of sediment transport trigger mass drift of stream invertebrates. Canadian Journal of Fisheries and Aquatic Sciences **64**:1-5.

Groot, C., and L. Margolis. 1991. Pacific salmon life histories. University of Columbia Press, Vancouver, B.C.

Ito, H., S. Ito, T. Matsui, and T. Marutani. 2006. Effect of fluvial and geomorphic disturbances on habitat segregation of tree species in a sedimentation-dominated riparian forest in warm-temperate mountainous region in southern Japan. Journal of Forest Research **11**:405-417.

Knighton, D. 1998. Fluvial Forms and Processess, A New Perspective, London.

Kondolf, G. M., and P. R. Wilcock. 1996. The flushing flow problem: Defining and evaluating objectives. Water Resources Research **32**:2589-2599.

Kondolf, G. M., and M. G. Wolman. 1993. The sizes of salmonid spawning gravels. Water Resources Research **29**:2275-2285.

Konrad, C. P., D. B. Booth, S. J. Burges, and D. R. Montgomery. 2002. Partial entrainment of gravel bars during floods. Water Resources Research **38**:9-1 - 9-16.

Lapointe, M., B. Eaton, S. Driscoll, and C. Latulippe. 2000. Modelling the probability of salmonid egg pocket scour due to floods. Canadian Journal of Fisheries and Aquatic Sciences **57**:1120-1130.

Leopold, L. B., and T. Maddock. 1953. The Hydraulic Geometry of Stream Channels and Some Physiographic Implications. Professional Paper 252, USGS, Washington.

Lisle, T. E., and J. Lewis. 1992. Effects of Sediment Transport on Survival of Salmonid Embryos in a Natural Stream - a Simulation Approach. Canadian Journal of Fisheries and Aquatic Sciences **49**:2337-2344.

Lisle, T. E., J. M. Nelson, J. Pitlick, M. A. Madej, and B. L. Barkett. 2000. Variability of bed mobility in natural, gravel-bed channels and adjustments to sediment load at local and reach scales. Water Resources Research **36**:3743-3755.

Maddock, I., M. Thoms, K. Jonson, F. Dyer, and M. Lintermans. 2004. Identifying the influence of channel morphology on physical habitat availability for native fish: application to the two-spined blackfish (Gadopsis bispinosus) in the Cotter River, Australia. Marine and Freshwater Research **55**:173-184.

Major, J. J., and L. E. Mark. 2006. Peak flow responses to landscape disturbances caused by the cataclysmic 1980 eruption of Mount St. Helens, Washington. Geological Society of America Bulletin **118**:938-958.

Marcot, B. G., and M. V. Heyden. 2001. Key ecological functions of wildlife species. Pages 168-186 *in* D. H. Johnson, T. A. O'Neil, and T. Coordinators, editors. Wildlife-habitat relationships in Oregon and Washington. Oregon State University Press, Corvallis OR.

May, C. 2007. Sediment and wood routing in steep headwater streams: An overview of geomorphic processes and their topographic signatures. Forest Science **53**:119-130.

Merz, J. E., and L. K. O. Chan. 2005. Effects of gravel augmentation on macroinvertebrate assemblages in a regulated California river. River Research and Applications **21**:61-74.

Merz, J. E., G. B. Pasternack, and J. M. Wheaton. 2006. Sediment budget for salmonid spawning habitat rehabilitation in a regulated river. Geomorphology **76**:207-228.

Merz, J. E., and J. D. Setka. 2004. Riverine habitat characterization of the lower Mokelumne River, California. East Bay Municipal Utility District, Lodi, CA.

Merz, J. E., J. D. Setka, G. B. Pasternack, and J. M. Wheaton. 2004. Predicting benefits of spawning-habitat rehabilitation to salmonid (Oncorhynchus spp.) fry production in a regulated California river. Canadian Journal of Fisheries and Aquatic Sciences **61**:1433-1446.

Moir, H., and G. B. Pasternack. Submitted. Interactions between meso-scale morphological units, stream hydraulics and chinook salmon (Oncorhynchus tshawytscha) spawning habitat on the Lower Yuba River, California. Geomorphology.

Moir, H. J., C. N. Gibbins, C. Soulsby, and J. Webb. 2004. Linking channel geomorphic characteristics to spatial patterns of spawning activity and discharge use by Atlantic salmon (Salmo salar L.). Geomorphology **60**:21-35.

Moir, H. J., and G. B. Pasternack. 2003. Implications of a Dynamic Hydromorphic Regime For Environmental Management on a Disturbed Large Gravel-Bed River. Eos Trans. AGU **57 (52)**.

Moir, H. J., and G. B. Pasternack. 2006. Implications of a Dynamic Hydromorphic Regime For Environmental Management on a Disturbed Large Gravel-Bed River. Eos Trans. AGU **57 (52)**.

Montgomery, D. R., E. M. Beamer, G. R. Pess, and T. P. Quinn. 1999. Channel type and salmonid spawning distribution and abundance. Canadian Journal of Fisheries and Aquatic Sciences **56**:377-387.

Moody, J. A., and D. A. Kinner. 2006. Spatial structures of stream and hillslope drainage networks following gully erosion after wildfire. Earth Surface Processes and Landforms **31**:319-337.

Morley, S. A., P. S. Garcia, T. R. Bennett, and P. Roni. 2005. Juvenile salmonid (Oncorhynchus spp.) use of constructed and natural side channels in Pacific Northwest rivers. Canadian Journal of Fisheries and Aquatic Sciences **62**:2811-2821.

Mount, J. 1995. California Rivers and Streams. University of California Press, Berkeley.

Moyle, P. B. 1994. The Decline of Anadromous Fishes in California. Conservation Biology **8**:869-870.

Moyle, P. B., and J. J. Check. 2004. Fishes : an introduction to ichthyology. 5th Ed edition. Pearson Prentice Hall, Upper Saddle River, NJ.

Murray, A. B. 2003. Contrasting goals, strategies, and predictions associated with simplified numerical models and detailed simulations.*in* P. R. Wilock and M. I. Richard, editors. Prediction in Geomorphology. American Geophysical Union, Washington D.C.

Murray, A. B. 2007. Reducing model complexity for explanation and prediction. Reduced-Complexity Geomorphological Modelling for River and Catchment Management **90**:178-191.

Parker, G. 1979. Hydraulic Geometry of Active Gravel Rivers. Journal of the Hydraulics Division-Asce **105**:1185-1201.

Parker, G., Toro-Escobar, R. C.M., and B. M., S. 2003. Effect of floodwater extraction on mountain stream morphology. Journal of hydraulic engineering ASCE:885-895.

Pasternack, G. B., C. L. Wang, and J. E. Merz. 2004. Application of a 2D hydrodynamic model to design of reach-scale spawning gravel replenishment on the Mokelumne River, California. River Research and Applications **20**:205-225.

Poff, N. L., J. D. Allan, M. B. Bain, J. R. Karr, K. L. Prestegaard, B. D. Richter, R. E. Sparks, and J. C. Stromberg. 1997. The natural flow regime. Bioscience **47**:769-784.

Reiser, D. W., and T. C. Bjornn. 1979. Influence of Forest and Rangeland Management on Anadromous Fish Habitat in Western North America -

Habitat Requirements of Anadromous Salmonids. U.S. Department of Agriculture.

Richards, K., J. Brasington, and F. Hughes. 2002. Geomorphic dynamics of floodplains: ecological implications and a potential modelling strategy. Freshwater Biology **47**:559-579.

Richter, B. D., J. V. Baumgartner, J. Powell, and D. P. Braun. 1996. A method for assessing hydrologic alteration within ecosystems. Conservation Biology **10**:1163-1174.

Richter, B. D., J. V. Baumgartner, R. Wigington, and D. P. Braun. 1997. How much water does a river need? Freshwater Biology **37**:231-249.

Rodriguez, J. F., F. A. Bombardelli, M. H. Garcia, K. M. Frothingham, B. L. Rhoads, and J. D. Abad. 2004. High-resolution numerical simulation of flow through a highly sinuous river reach. Water Resources Management **18**:177-199.

Statsoft. 1998. STATISTICA for Windows (Volume I). Tulsa, OK.

Tipton, J. A., H. L. Bart, and K. R. Piller. 2004. Geomorphic disturbance and its impact on darter (Teleostomi : Percidae) distribution and abundance in the Pearl River drainage, Mississippi. Hydrobiologia **527**:49-61.

van Asselt, M. B. A., and J. Rotmans. 2002. Uncertainty in integrated assessment modelling - From positivism to pluralism. Climatic Change **54**:75-105.

Webb, J. H., C. N. Gibbins, H. Moir, and C. Soulsby. 2001. Flow requirements of spawning Atlantic salmon in an upland stream: Implications far water-resource management. Journal of the Chartered Institution of Water and Environmental Management **15**:1-8.

Wheaton, J. M., G. B. Pasternack, and J. E. Merz. 2004a. Spawning Habitat Rehabilitation-I. Conceptual Approach and Models. International Journal of River Basin Management **2**:3-20.

Wheaton, J. M., G. B. Pasternack, and J. E. Merz. 2004b. Spawning habitat rehabilitation-II. Using hypothesis development and testing in design, Mokelumne River, California, U.S.A. International Journal of River Basin Management **2**:21-37.

Wilson, C., O. Yagci, H. P. Rauch, and N. R. B. Olsen. 2006. 3D numerical modelling of a willow vegetated river/floodplain system. Journal of Hydrology **327**:13-21.

Figures and Tables Captions

Figure 1. Interaction of hydrogeomorphic processes that control physical habitat conditions for ecological functionality.

Examples of each process or function are given inside each circle. Convulsive events are in italics.

Figure 2. Location of Mokelumne River and Yuba River study reaches

Figure 3. Life stages of Fall-run Chinook salmon in relation to flow magnitude

A) Bed occupation and bed preparation ecological functions timing for fall-run Chinook salmon freshwater life stage; B) Water year flow magnitudes at the Yuba River, CA and examples of functional flows for the ecological functions in A).

Figure 4. Functional flows classification for fall-run Chinook salmon ecological functions

Non-dimensional shear stress time series for riffle cross section in the Yuba River with S=0.046 and D_{50}= 0.068 for the water year depicted in 3B) with functional (solid line) and non-functional (dashed line) transport regimes according to Table 1. After day 330 BO stands for Bed Occupation, N-f stands for non-functional, and F stands for functional.

Figure 5. τ_o* vs Q* curve for example in Figure 4

Non-dimensional shear stress vs non-dimensional discharge for identification of functional ranges of flows using same example in Figs. 3 and 4. Available Q* (gray line) refers to ranges of flows within a water year that fall within specified bed mobility stages, Functional Q* (triangle symbol) refer to ranges of flow within a water year that fall within specified bed mobility stages and happen at the time when they are functional for the life stage. FM stands for full mobility, IFM stands for interstitial fines mobility, SFM stands for superficial fines mobility, and SB stands for stable bed

Figure 6. IHA-RVA analysis of flow records

A) Mokelumne River USGS Station # 11323500, B) Yuba River USGS Station # 11418000

Figure 7. Habitat units for functional flows analysis

Coordinates in meters for A) Mokelume River sites XS1 (1,953,735, 691,786), XS2 (1,953,739, 691,672), XS3 (1,953,383, 691,716), XS4 (1,953,435, 691,661), XS5 (1,953,697, 691,777), XS6 (1,953,696, 691,690); and B) Yuba River sites XS1 (2,059,431, 674,116), XS2 (2,059,388, 674,141), XS3 (2,059,179, 674,222), XS4 (1,928,546, 803,447)

Figure 8. Cross sections geometry

A) Mokelumne River cross sections at restored riffles before (dashed line) and after (solid line) gravel augmentation, B) Mokelumne River cross sections at reference riffles, C) Yuba River cross sections before (dashed line) and after (solid line) May 20005 natural flood and reference site (XS4).

Figure 9. Functional flows analysis of restored riffles for Actual WY at Mokelumne River

A) Julian water year discharge time series for water years before and after gravel augmentation, B) τ_o* vs Q* curves - gray lines correspond to the actual ranges of Q* produced by the water year and symbols correspond to the days with functional ranges of Q* that produced a functional sediment transport sage for a specific ecological function according to the table of functionality (Table 1), symbols are not depicted when days with functional ranges of Q* are absent for the specific site and ecological function, C) Count of number of days with functional flows for water year in A)

Figure 10. Functional flows analysis of all sites for Actual WY at Yuba River

A) Julian water year discharge time series for actual water years before and after May 2005 flood, B) and C) captions are the same as Fig. 9.

Figure 11. Efficiency of habitat units to produce functional flows for Mokelumne River

Empty circles indicate minimum and maximum available Q* for the water year, and solid circles indicate minimum and maximum functional Q* for the water year for A) Restored sites, B) Reference sites

Figure 12. Efficiency of habitat units to produce functional flows for Yuba River

Empty circles indicate minimum and maximum available Q* for the water year, and solid circles indicate minimum and maximum functional Q* for the water year.

Table 1. Table of functionality

Table 2. Summary of functional flows analysis

Table 3. Summary of physical parameters for functional flows analysis

Table 4. Summary of functional flows analysis comparison criteria and outputs

Table 5. Hypothesis testing and statistical significance of comparisons among hydrogeomorphic input variables and functional flows outputs datasets

Table 1. Table of functionality.

Flow magnitude and bed mobility stages delimited by Shields stress are used to determine functionality for bed occupation and bed preparation ecological functions during the spawning life stage. "Functional" refers to flow magnitudes associated with bed mobility stages that favor the life stage. "Non-functional" refers to flow magnitudes associated with bed mobility stages that hinder the life stage.

1	2A	2B	3	4	5	6
Flow Magnitude/ Bed Mobility Stage	**Functional Flows Delimiters**		**Bed Occupation**			**Bed Preparation**
	In terms of τ_o vs τ_{c50}	**In terms of τ_o* vs Shields #**	**Spawning**	**Embryo Incubation**	**Emergence**	
High/ Full mobility (FM)	$\tau_o > \tau_{c50}$	$0.06 < \tau_o^* < 0.1$	Non-functional	Non-functional	Non-functional	Functional
Intermediate High/ Interstitial fines mobility (IFM)	$\tau_o = \tau_{c50}$	$0.03 < \tau_o^* < 0.06$	Non-functional	Non-functional	Non-functional	Functional
Intermediate Low/ Superficial fines mobility (SFM)	$\tau_o < \tau_{c50}$	$0.01 < \tau_o^* < 0.03$	Functional	Functional	Functional	Non-functional
Low/ Stable bed (SB)	$\tau_o << \tau_{c50}$	$\tau_o^* < 0.01$	Functional	Non-functional	Functional	Non-functional

Table 2. Summary of functional flows analysis

Type of analysis is theoretical for WY1 and WY2, and Actual for water years when the events occurred. Timeline of events represent water years (horizontal arrows) and the approximate date of the events occurrence (vertical arrows). Sites marked with * are reference sites. Sites marked with ** were analyzed twice for WY1 and WY2 due to the occurrence of two different gravel augmentation projects at the same site. A total of 30 analysis were performed in the Mokelumne River, and a total of 20 analysis were performed in the Yuba River.

Type of Analysis		**Theoretical**				**Actual**							
Water Year		**1**	**1**	**2**	**2**	**97-98**	**98-99**	**99-00**	**00-01**	**02-03**	**03-04**	**04-05**	**05-06**
Timeline of Events		Gravel Augmentation/ Flood		Gravel Augmentation/ Flood		Gravel Augmentation		Gravel Augmentation		Gravel Augmentation	Gravel Augmentation		Flood
Mokelumne River	**XS1**	Pre**	Post**	Pre**	Post**	Pre	Post			Pre	Post		
	XS2	Pre	Post	Pre	Post			Pre	Post				
	XS3	Pre	Post	Pre	Post						Pre	Post	
	XS4*	Pre		Pre									
	XS5*	Pre		Pre									
	XS6*	Pre		Pre									
Yuba River	**XS1**	Pre	Post	Pre	Post							Pre	Post
	XS2	Pre	Post	Pre	Post							Pre	Post
	XS3	Pre	Post	Pre	Post							Pre	Post
	XS4*	Pre		Pre									

Table 3. Summary of physical parameters for functional flows analysis

Cross sections geometry, slope, and median grain size were obtained from data reported in previous studies as indicated next to each value and from data collected for this study. Data sources are (1) Merz et al 2005 , (2) Elkins et al 2007 , (3) Wheaton 2003, (4) This Study, (5) Moir and Pasternack Submitted. Parameters c and f were obtained from cross section geometry relations developed for each cross section geometry.

River	XS Name	Date Surface/ Surveyed	S	D_{50}	c	f
Mokelumne River	XS1	97-98	0.0001 (1)	40.0 (1)	0.38	0.45
		98-99	0.0038 (1)	50.0 (1)	0.22	0.39
		02-03	0.0020 (2)	50.4 (2)	0.18	0.43
		03-04	0.0080 (2)	50.4 (2)	0.17	0.39
	XS2	99-00	0.0003 (3)	68.0 (3)	0.35	0.41
		00-01	0.0006 (3)	55.0 (3)	0.30	0.39
	XS3	03-04	0.0003 (1)	47.5 (1)	0.34	0.46
		04-05	0.0018 (4)	71.0 (4)	0.22	0.39
	XS4	Fv 2005	0.0034 (4)	67.0 (4)	0.12	0.52
	XS5	Fv 2005	0.0012 (4)	53.0 (4)	0.16	0.38
	XS6	Fv 2005	0.0052 (4)	40.0 (4)	0.11	0.51
Yuba River	XS1	03-04	0.0069 (5)	101.1 (5)	0.16	0.37
		04-05	0.0046 (4)	60.7 (4)	0.09	0.47
	XS2	03-04	0.0069 (5)	101.1 (5)	0.18	0.35
		04-05	0.0046 (4)	78.0 (4)	0.15	0.39
	XS3	03-04	0.0046 (5)	179.8 (5)	0.13	0.41
		04-05	0.0039 (4)	69.3 (4)	0.14	0.42
	XS4	Fv 2005	0.0011 (4)	66.0 (4)	0.10	0.50

Table 4. Summary of functional flows analysis comparison criteria and outputs

Comparison criteria are river, before/after gravel augmentation in the Mokelumne River of flood in the Yuba River (B/A), and detailed monitoring sites or reference site (D/R). Functional flows outputs are available ranges of Q*, functional ranges of Q*, # days with functional flows, and % efficiency (100*functional ranges of Q*/available ranges of Q*).

Comparison Criteria						Functional Flows Analysis Outputs			
River	Water Year Type	XS	Site	Before/ After	Detailed monitoring site/ Reference site	Available Range Q*	Functional Range Q*	# Days with functional flows	% Efficiency
Mokelumne River	WY1	XS1	97-98	B	D	10,948	-	0	0
			98-99	A	D	10,948	10,948	248	100
			02-03	A	D	10,733	9,715	179	91
			03-04	A	D	10,733	8,176	185	76
		XS2	99-00	B	D	5,076	-	0	0
			00-01	A	D	8,627	-	0	0
		XS3	03-04	B	D	12,446	-	0	0
			04-05	A	D	4,557	2,290	75	52
		XS4	Nov05	B	R	5,267	4,768	179	91
		XS5	Nov05	B	R	9,464	-	0	0
		XS6	Nov05	B	R	19,126	19,126	250	100
	WY2	XS1	97-98	B	D	81,580	-	0	0
			98-99	A	D	46,699	31,461	190	67
			02-03	A	D	45,778	38,363	174	84
			03-04	A	D	45,778	25,687	185	56
		XS2	99-00	B	D	21,650	-	0	0
			00-01	A	D	36,798	16,450	50	45
		XS3	03-04	B	D	53,089	10,200	14	19
			04-05	A	D	19,435	18,853	174	97
		XS4	Nov05	B	R	22,467	15,136	200	67
		XS5	Nov05	B	R	40,369	20,605	73	51
		XS6	Nov05	B	R	81,580	45,777	185	56
	Actual WY	XS1	97-98	B	D	95,006	-	0	0
			98-99	A	D	45,064	15,129	232	34
			02-03	A	D	27,742	1,729	179	6
			03-04	A	D	35,626	23,809	155	67
		XS2	99-00	B	D	15,559	-	0	0
			00-01	A	D	3,608	-	0	0
		XS3	03-04	B	D	23,785	-	0	0
			04-05	A	D	15,125	5,600	43	36

Table 4. Summary of functional flows analysis comparison criteria and outputs (Continuation)

Comparison Criteria						Functional Flows Analysis Outputs			
River	Water Year Type	XS	Site	Before/ After	Detailed monitoring site/ Reference site	Available Range Q*	Functional Range Q*	# Days with functional flows	% Efficiency
Yuba River	WY1	XS1	03-04	B	D	10,160	10,054	184	99
			04-05	A	D	36,405	36,024	190	99
		XS2	03-04	B	D	10,160	10,054	179	99
			04-05	A	D	19,458	19,254	162	99
		XS3	03-04	B	D	2,409	1,219	86	51
			04-05	A	D	26,099	25,826	160	99
		XS4	Nov05	A	R	29,506	2,924	7	10
	WY2	XS1	03-04	B	D	58,405	21,645	177	37
			04-05	A	D	209,272	77,559	176	37
		XS2	03-04	B	D	58,405	21,645	177	37
			04-05	A	D	111,852	41,454	170	37
		XS3	03-04	B	D	13,847	13,136	112	95
			04-05	A	D	150,030	55,603	173	37
		XS4	Nov05	A	R	169,615	148,392	101	87
	Actual WY	XS1	03-04	B	D	10,944	4,954	182	45
			04-05	A	D	306,674	199,965	265	65
		XS2	03-04	B	D	10,944	4,954	216	45
			04-05	A	D	163,912	163,912	254	100
		XS3	03-04	B	D	2,595	1,874	99	72
			04-05	A	D	219,859	219,859	255	100

Table 5. Hypothesis testing and statistical significance of comparisons among geomorphic input variables and functional flows outputs datasets. Differences between datasets were considered statistically significant for p-level<0.05. Table contains p-level and Kolmogorov-Smirnov (KS) test results for each dataset comparison. A) Before and after rapid alteration of channel morphology, B) Detailed monitoring sites vs. reference sites, C) Mokelumne River vs. Yuba River. rQ* stands for functional ranges of Q*, #DFF stands for # days with functional flows, %Eff stands for % efficiency. Hypothesis: statistically significant differences in hydrogeomorphic conditions cause statistically significant differences in ecological performance of the physical habitat. Hypothesis confirmation or rejection is indicated at the crossing of inputs (left column) vs. outputs (top row) for datasets compared. Confirmation of the hypothesis is provided according to material conditional truth rules T→T=T, T→F=F, F→F=T. The combination F→T was considered F.

A. Mokelumne River (n=15 before vs. n=15 after)

	p-level	KS test	rQ*	#DFF	%Eff
			p < .10	p < .05	p < .10
			F	T	F
S	p < .01	T	F	T	F
D_{50}	p < .05	T	F	T	F
c	p < .01	T	F	T	F
f	p < .005	T	F	T	F

Yuba River (n=15 before vs. n=15 after)

	p-level	KS test	rQ*	#DFF	%Eff
			p < .005	p > .10	p > .10
			T	F	F
S	p < .001	T	T	F	F
D_{50}	p < .001	T	T	F	F
c	p < .025	T	T	F	F
f	p < .025	T	T	F	F

B. Mokelumne River (n=24 restored vs. n=6 reference)

	p-level	KS test	rQ*	#DFF	%Eff
			p > .10	p > .10	p > .10
			F	F	F
S	p > .10	F	T	T	T
D_{50}	p > .10	F	T	T	T
c	p < .001	T	F	F	F
f	p < .05	T	F	F	F

Yuba River (n=18 apex vs. 2 reference)

	p-level	KS test	rQ*	#DFF	%Eff
			p > .10	p > .10	p > .10
			F	F	F
S	p < .10	F	T	T	T
D_{50}	p > .10	F	T	T	T
c	p > .10	F	T	T	T
f	p < .10	F	T	T	T

C. Mokelumne River (n=30) vs. Yuba River (n=20)

	p-level	KS test	rQ*	#DFF	%Eff
			p < .05	p < .01	p < .025
			T	T	T
S	p < .001	T	T	T	T
D_{50}	p < .001	T	T	T	T
c	p < .001	T	T	T	T
f	p > .10	F	F	F	F

F1

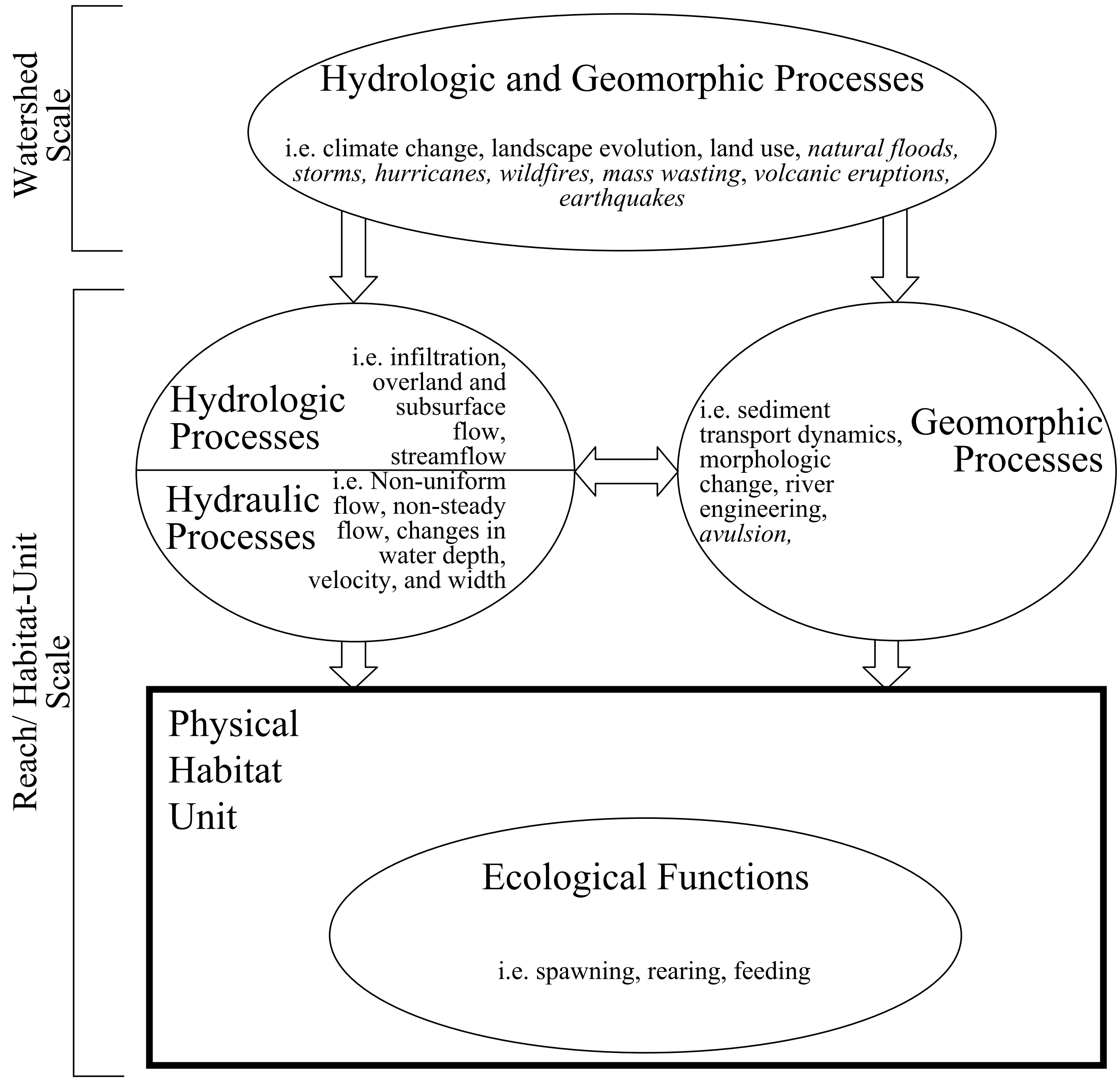
Watershed Scale
Hydrologic and Geomorphic Processes
i.e. climate change, landscape evolution, land use, *natural floods, storms, hurricanes, wildfires, mass wasting*, *volcanic eruptions, earthquakes*
Reach/ Habitat-Unit Scale
Hydrologic Processes
i.e. infiltration, overland and subsurface flow, streamflow
Hydraulic Processes
i.e. Non-uniform flow, non-steady flow, changes in water depth, velocity, and width
Geomorphic Processes
i.e. sediment transport dynamics, morphologic change, river engineering, *avulsion,*
Physical Habitat Unit
Ecological Functions
i.e. spawning, rearing, feeding

F2

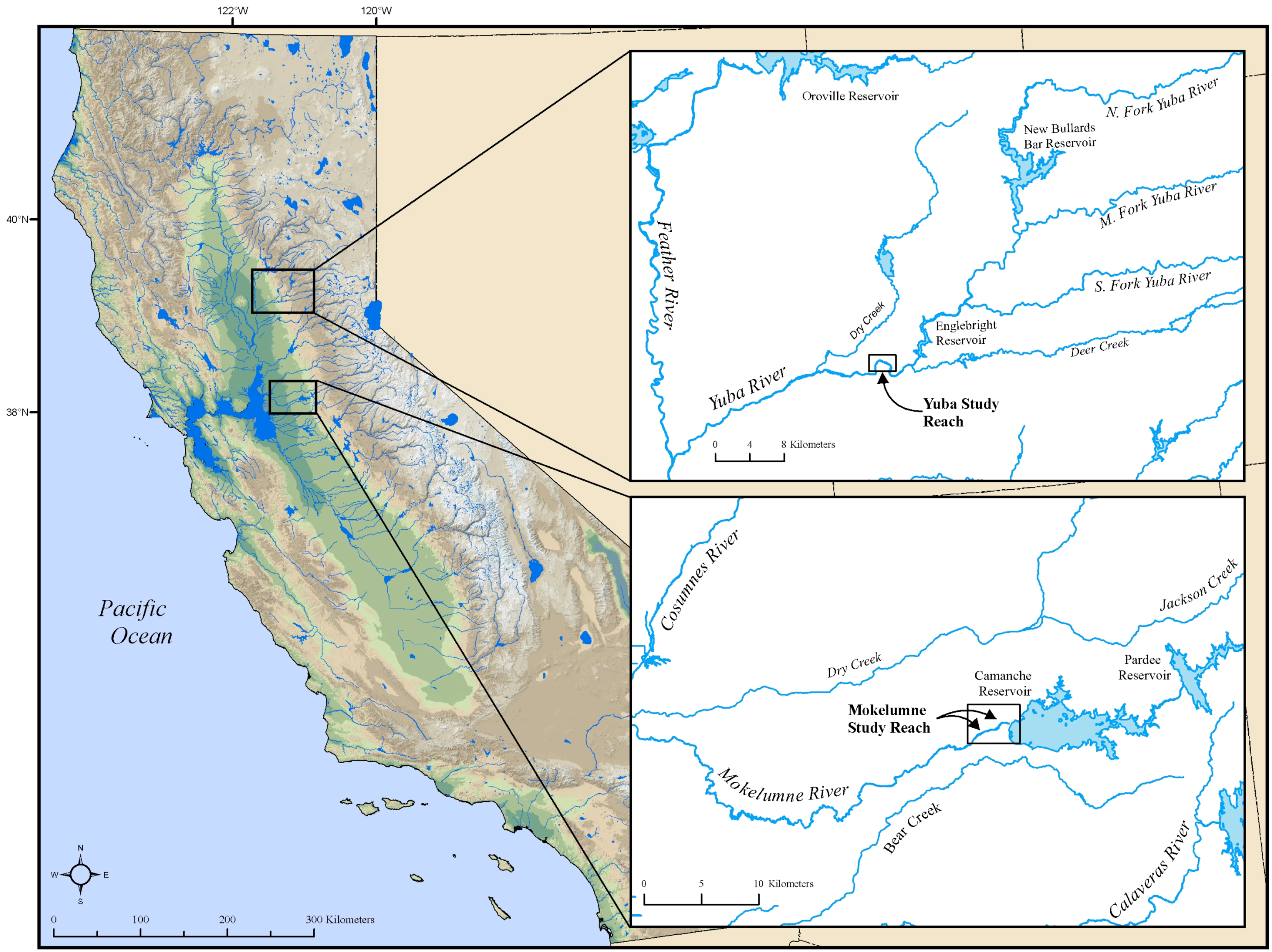

122°W
120°W
40°N
38°N
Pacific Ocean
N
W
E
S
0
100
200
300 Kilometers
Oroville Reservoir
N. Fork Yuba River
New Bullards Bar Reservoir
M. Fork Yuba River
Feather River
S. Fork Yuba River
Dry Creek
Englebright Reservoir
Deer Creek
Yuba River
Yuba Study Reach
0
4
8 Kilometers
Cosumnes River
Jackson Creek
Pardee Reservoir
Dry Creek
Camanche Reservoir
Mokelumne Study Reach
Mokelumne River
Bear Creek
Calaveras River
0
5
10 Kilometers

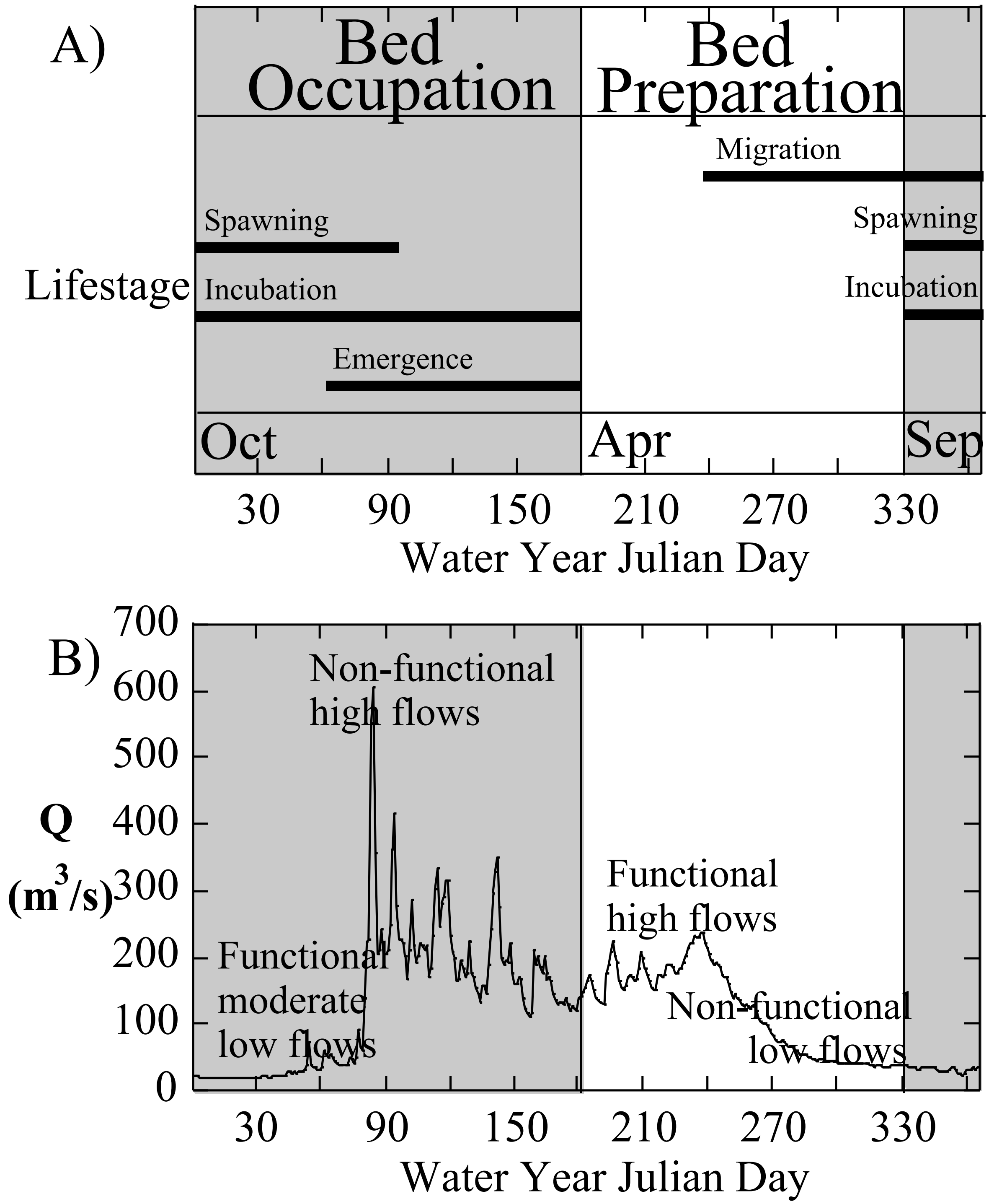

A)
Bed Occupation
Bed Preparation
Migration
Spawning
Spawning
Lifestage
Incubation
Incubation
Emergence
Oct
Apr
Sep
30
90
150
210
270
330
Water Year Julian Day
B)
700
600
500
400
300
200
100
0
Q
(m3/s)
Non-functional high flows
Functional high flows
Functional moderate low flows
Non-functional low flows
30
90
150
210
270
330
Water Year Julian Day

F3

F4

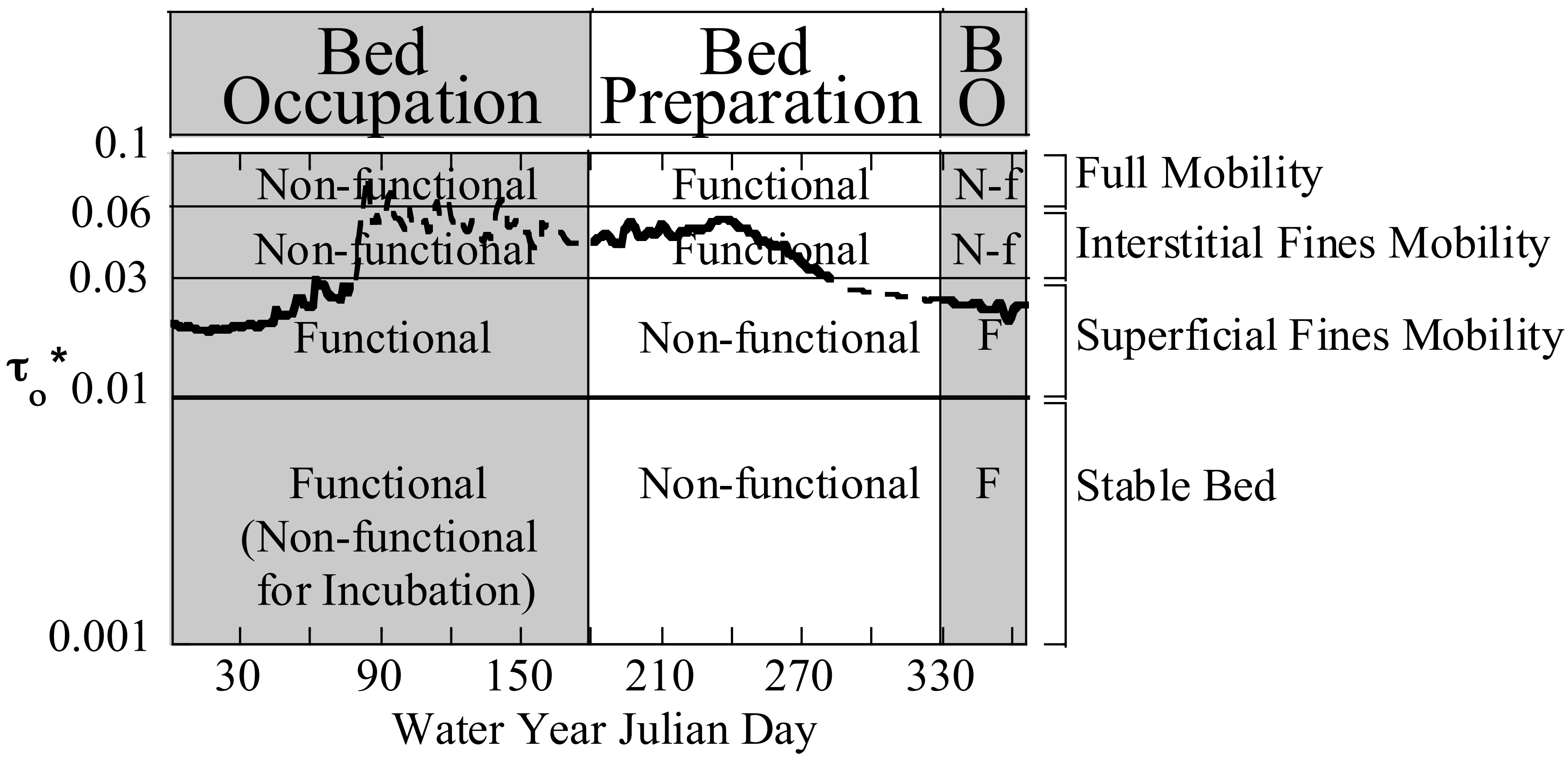
Bed Occupation
Bed Preparation
B O
0.1
0.06
0.03
τ_o^* 0.01
0.001
Non-functional
Functional
N-f
Non-functional
Functional
N-f
Functional
Non-functional
F
Functional (Non-functional for Incubation)
Non-functional
F
Full Mobility
Interstitial Fines Mobility
Superficial Fines Mobility
Stable Bed
30
90
150
210
270
330
Water Year Julian Day

F5

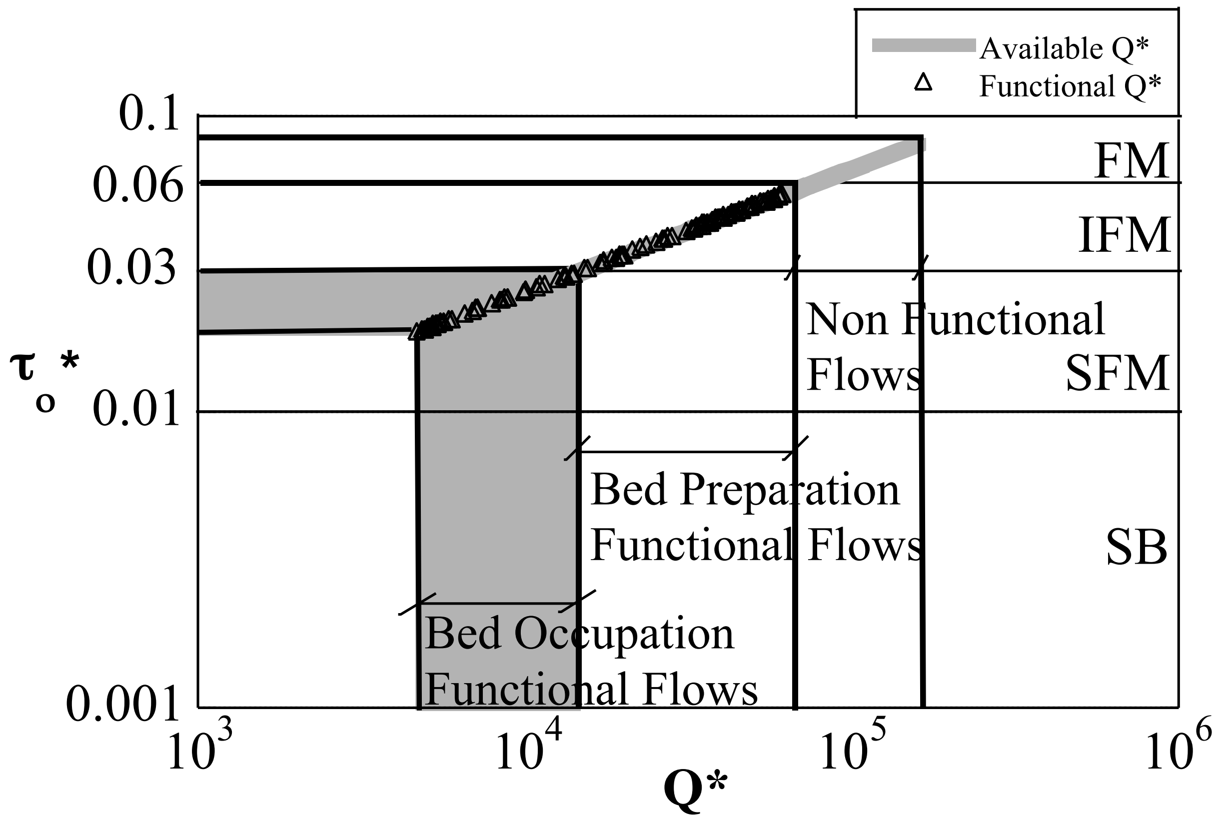
Available Q*
Functional Q*
0.1
0.06
0.03
0.01
0.001
τ_o*
FM
IFM
SFM
SB
Non Functional
Flows
Bed Preparation
Functional Flows
Bed Occupation
Functional Flows
10^3
10^4
10^5
10^6
Q*

F6

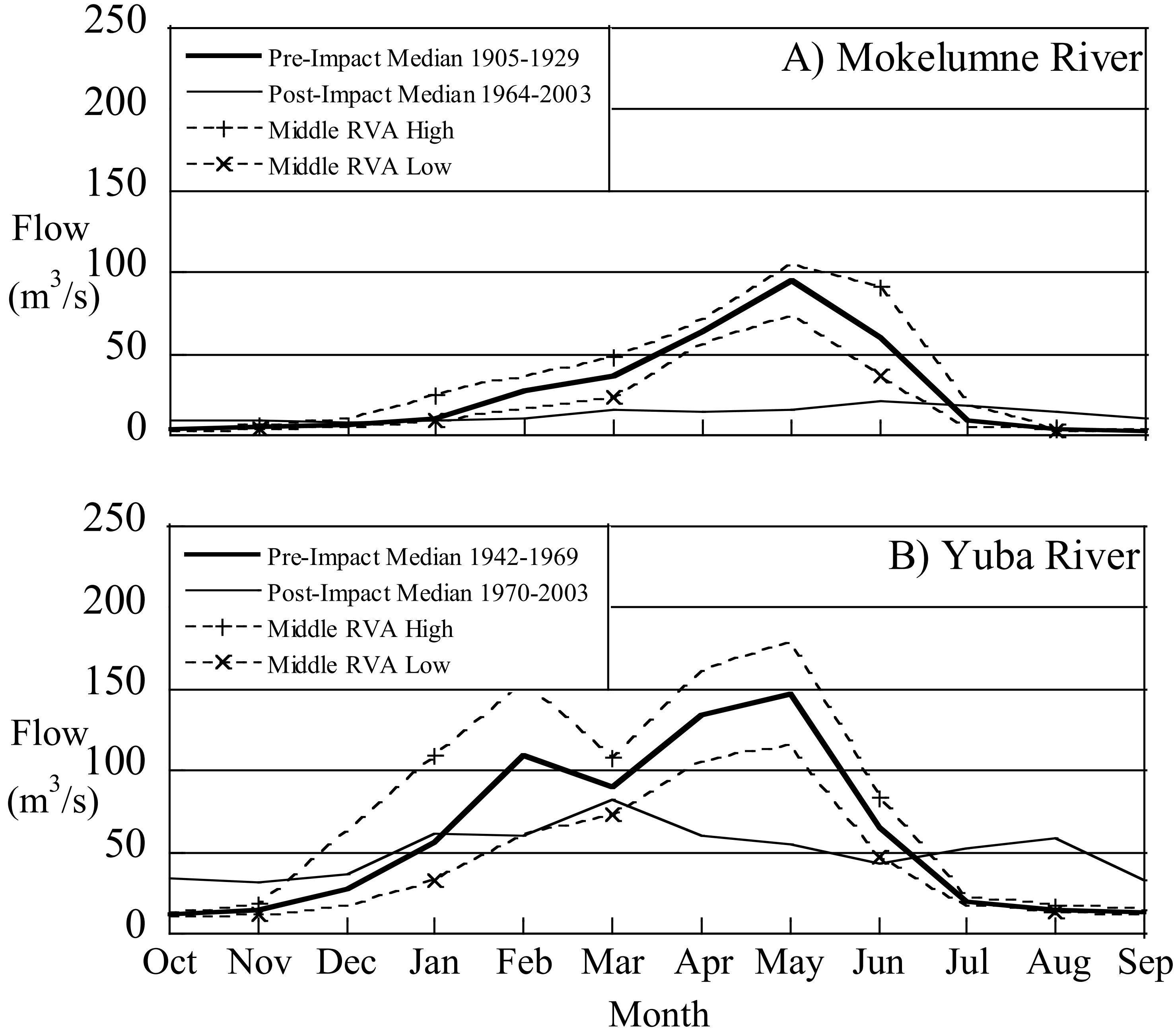
A) Mokelumne River
Pre-Impact Median 1905-1929
Post-Impact Median 1964-2003
Middle RVA High
Middle RVA Low
B) Yuba River
Pre-Impact Median 1942-1969
Post-Impact Median 1970-2003
Middle RVA High
Middle RVA Low
Flow (m^3/s)
250
200
150
100
50
0
Oct
Nov
Dec
Jan
Feb
Mar
Apr
May
Jun
Jul
Aug
Sep
Month

F7

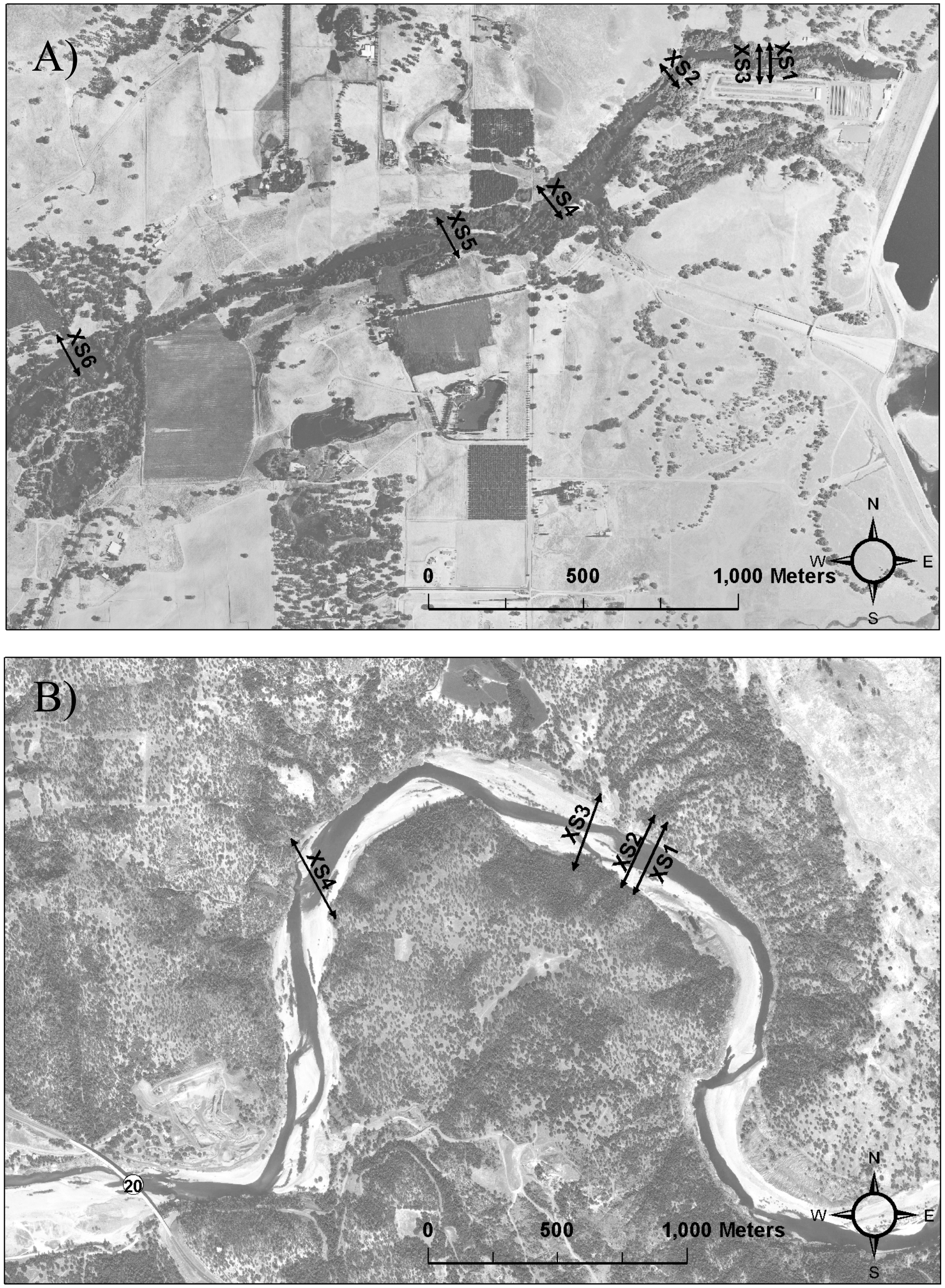
A)
XS1
XS2
XS3
XS4
XS5
XS6
N
S
W
E
0
500
1,000 Meters
B)
XS1
XS2
XS3
XS4
20
N
S
W
E
0
500
1,000 Meters

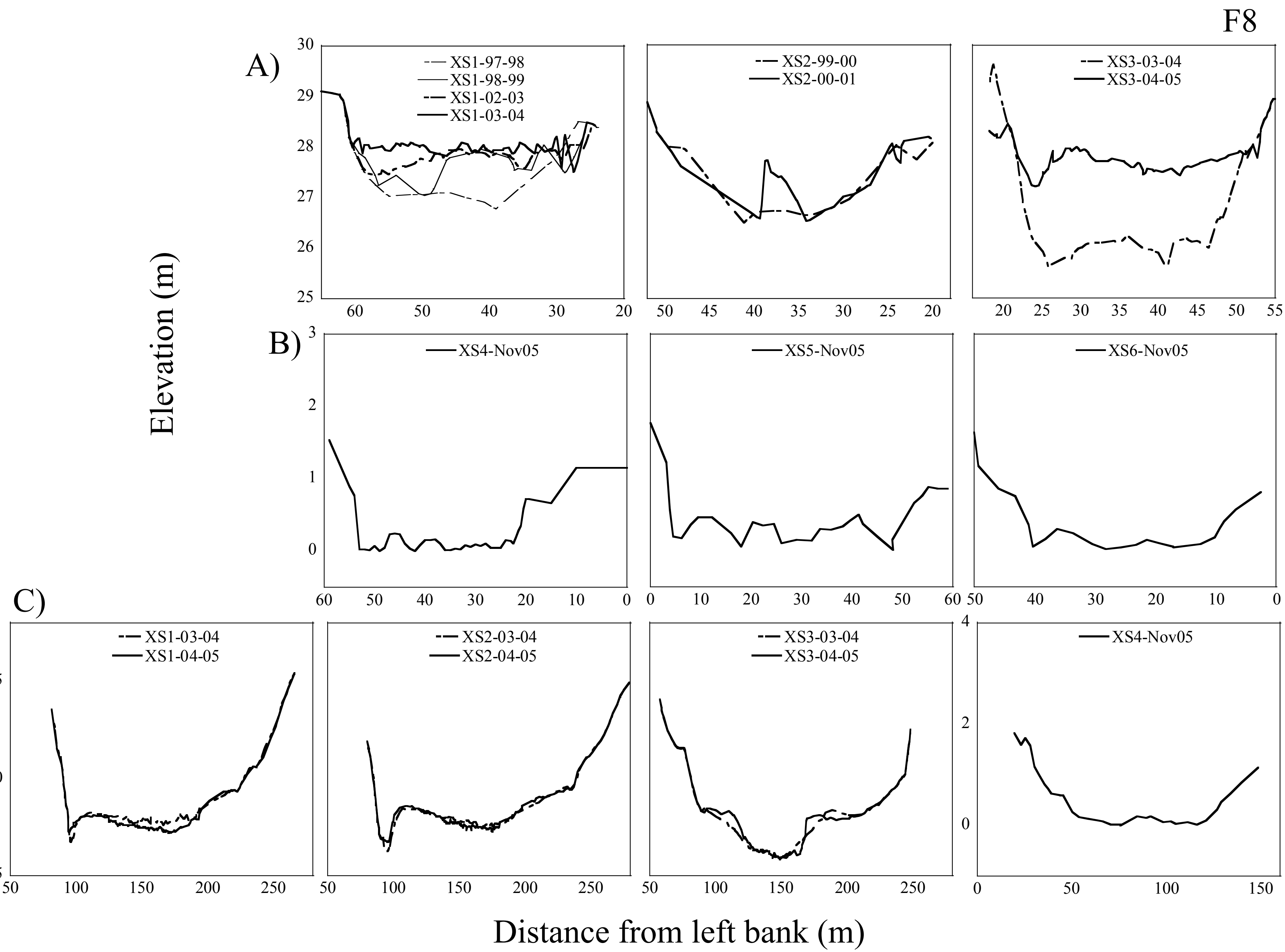

F8
A)
XS1-97-98
XS1-98-99
XS1-02-03
XS1-03-04
XS2-99-00
XS2-00-01
XS3-03-04
XS3-04-05
B)
XS4-Nov05
XS5-Nov05
XS6-Nov05
C)
XS1-03-04
XS1-04-05
XS2-03-04
XS2-04-05
XS3-03-04
XS3-04-05
XS4-Nov05
Elevation (m)
Distance from left bank (m)

F9

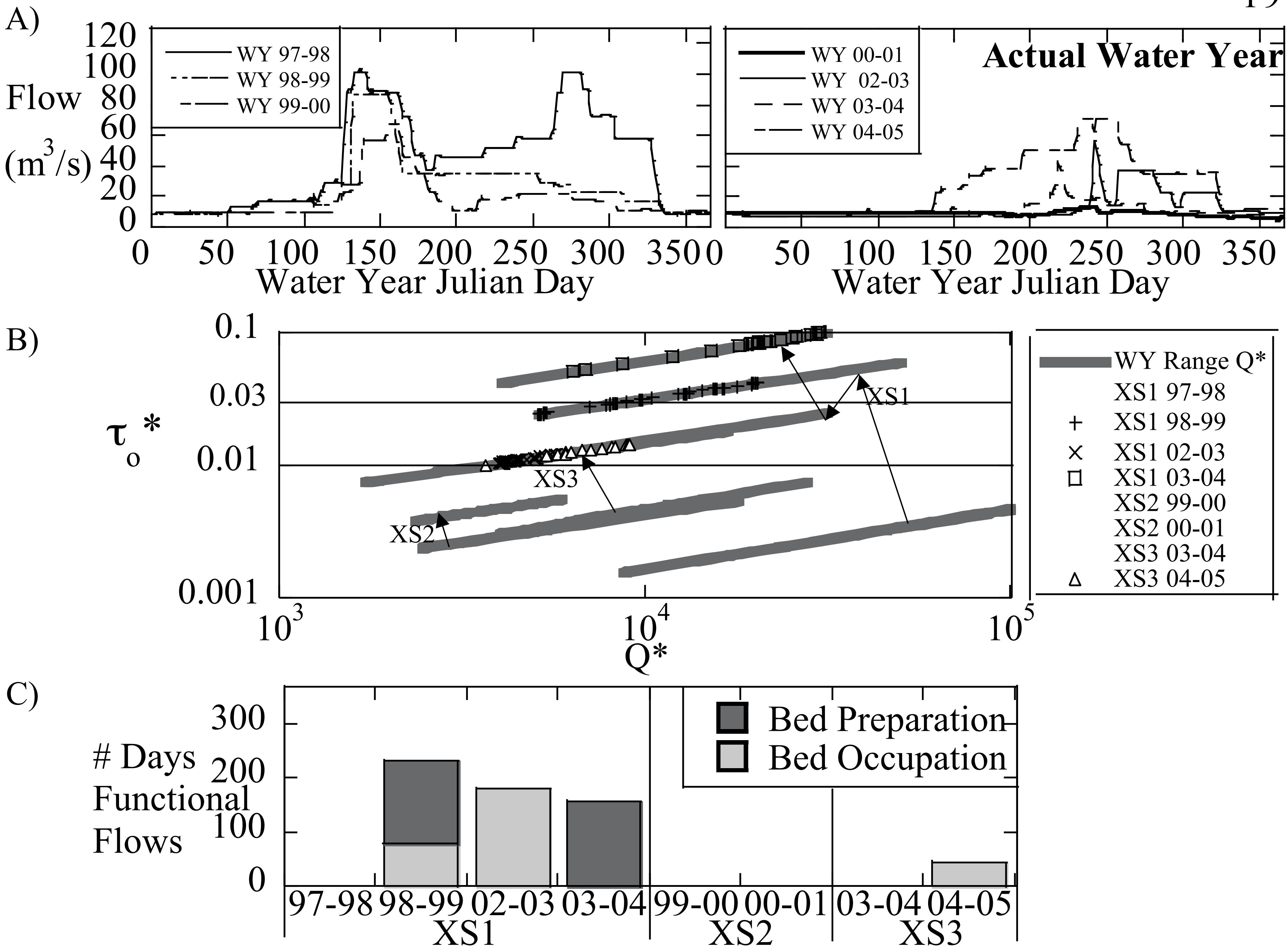

A)
Flow
(m3/s)
WY 97-98
WY 98-99
WY 99-00
WY 00-01
WY 02-03
WY 03-04
WY 04-05
Actual Water Year
Water Year Julian Day
Water Year Julian Day
B)
τo*
Q*
WY Range Q*
XS1 97-98
XS1 98-99
XS1 02-03
XS1 03-04
XS2 99-00
XS2 00-01
XS3 03-04
XS3 04-05
XS1
XS2
XS3
C)
Days
Functional
Flows
Bed Preparation
Bed Occupation
97-98
98-99
02-03
03-04
99-00
00-01
03-04
04-05
XS1
XS2
XS3

F10

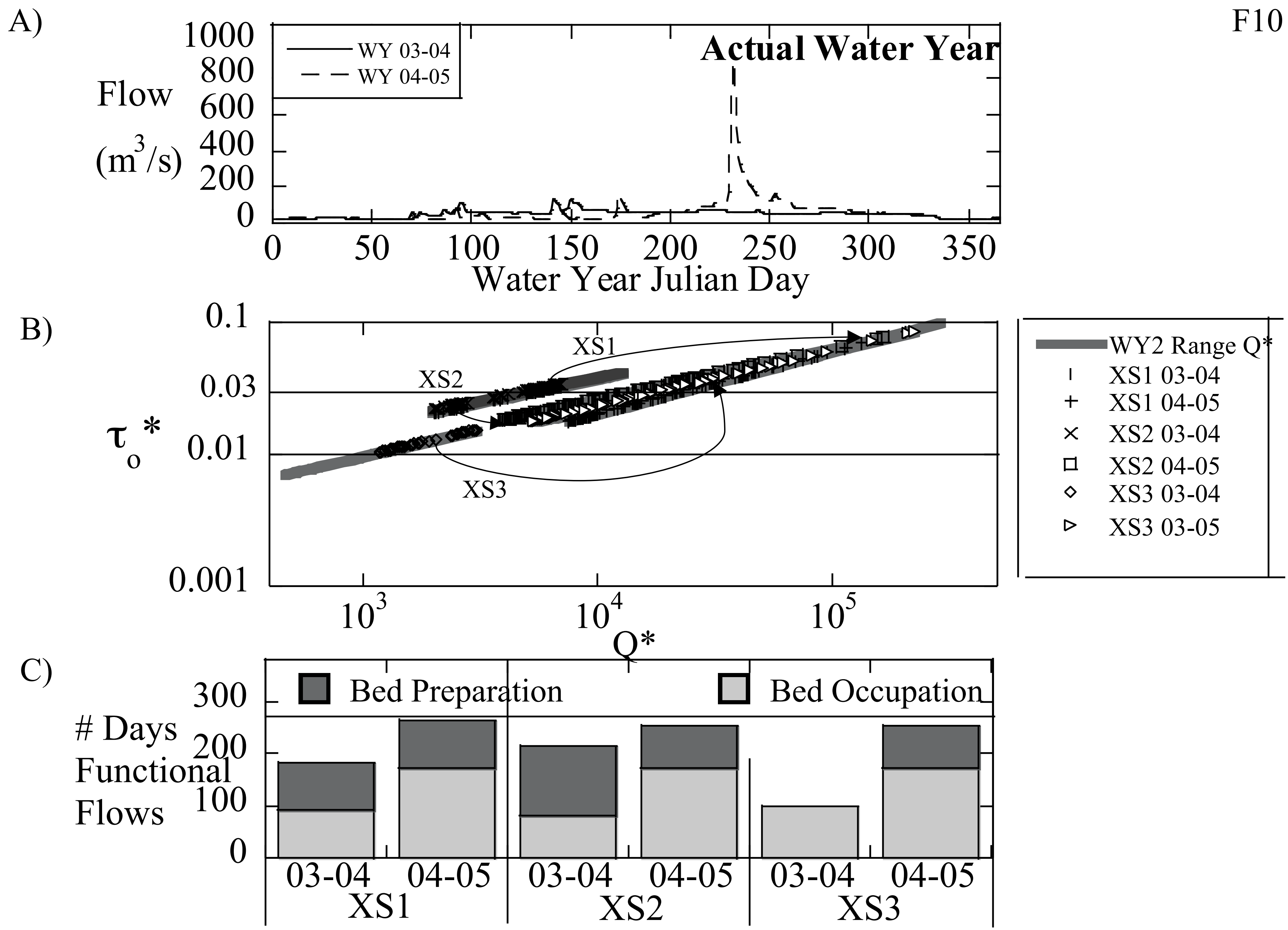

A)
Flow
(m3/s)
1000
800
600
400
200
0
WY 03-04
WY 04-05
Actual Water Year
0
50
100
150
200
250
300
350
Water Year Julian Day
B)
0.1
0.03
0.01
0.001
τo*
XS1
XS2
XS3
10^3
10^4
10^5
Q*
WY2 Range Q*
XS1 03-04
XS1 04-05
XS2 03-04
XS2 04-05
XS3 03-04
XS3 03-05
C)
Bed Preparation
Bed Occupation
Days
Functional
Flows
300
200
100
0
03-04
04-05
XS1
03-04
04-05
XS2
03-04
04-05
XS3

F11

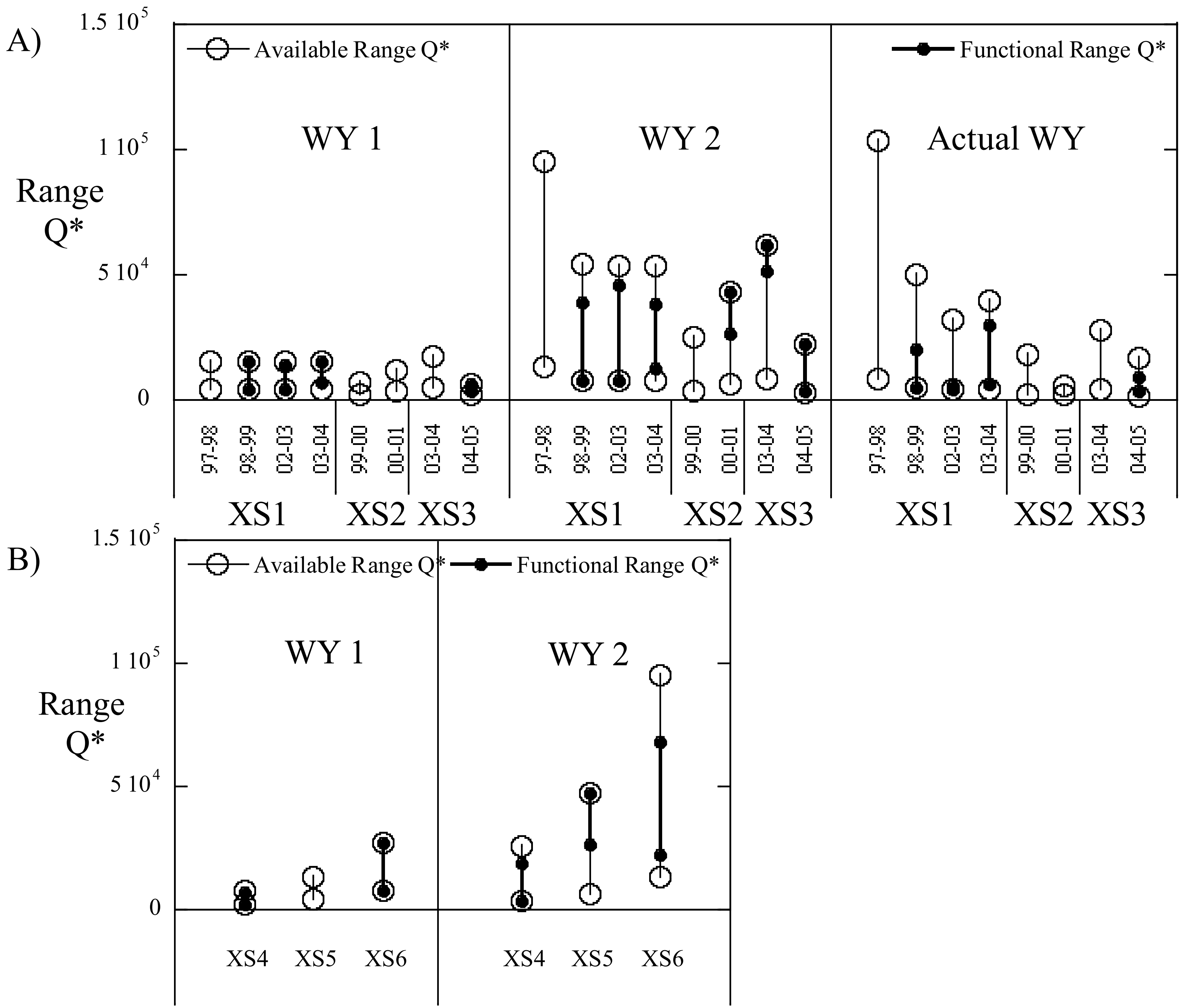

A)
1.5 10^5
1 10^5
5 10^4
0
Range Q*
Available Range Q*
Functional Range Q*
WY 1
WY 2
Actual WY
97-98
98-99
02-03
03-04
99-00
00-01
03-04
04-05
XS1
XS2
XS3
B)
WY 1
WY 2
XS4
XS5
XS6

F12

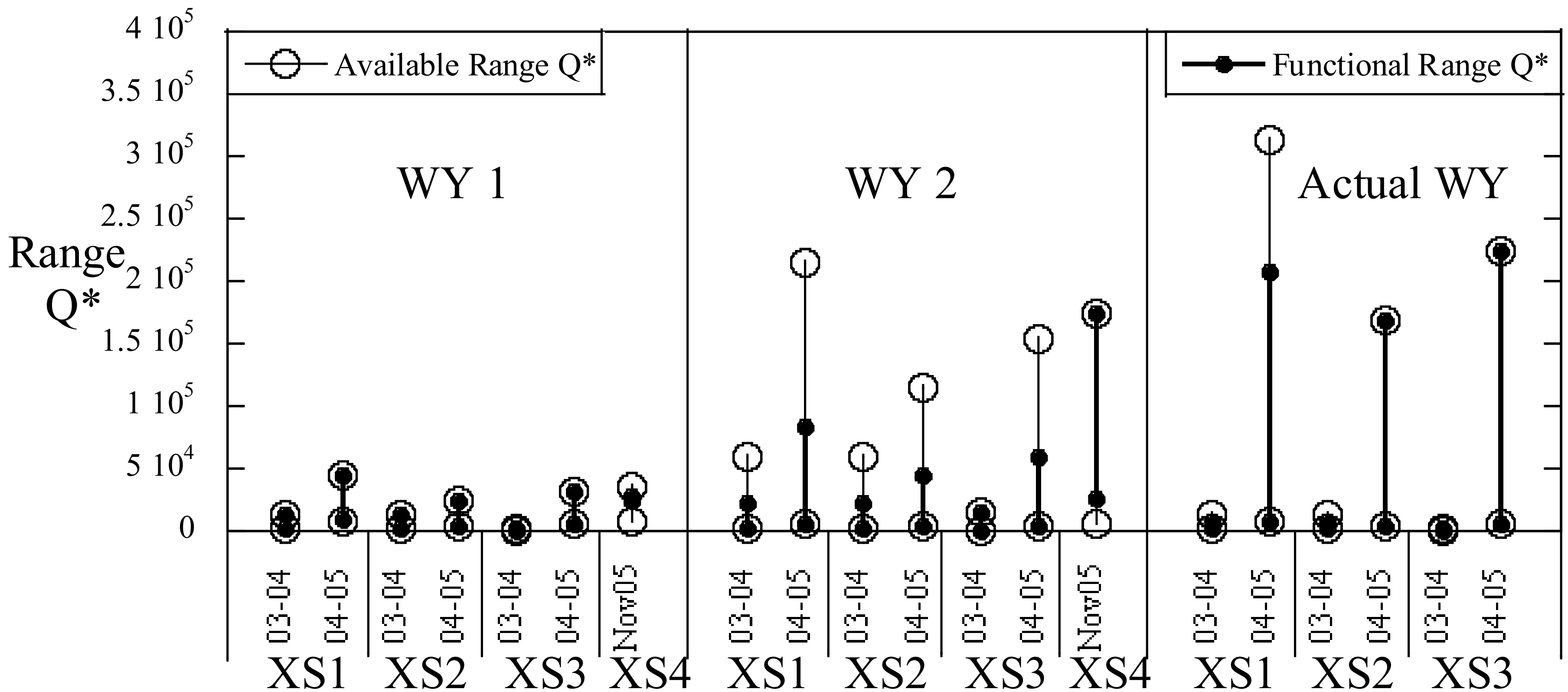

Available Range Q*
Functional Range Q*
WY 1
WY 2
Actual WY
Range Q*
4 10^5
3.5 10^5
3 10^5
2.5 10^5
2 10^5
1.5 10^5
1 10^5
5 10^4
0
03-04
04-05
Nov05
XS1
XS2
XS3
XS4